INFORMATION TO USERS

This manuscript has been reproduced from the microfilm master. UMI films the text directly from the original or copy submitted. Thus, some thesis and dissertation copies are in typewriter face, while others may be from any type of computer printer.

The quality of this reproduction is dependent upon the quality of the copy submitted. Broken or indistinct print, colored or poor quality illustrations and photographs, print bleedthrough, substandard margins, and improper alignment can adversely affect reproduction.

In the unlikely event that the author did not send UMI a complete manuscript and there are missing pages, these will be noted. Also, if unauthorized copyright material had to be removed, a note will indicate the deletion.

Oversize materials (e.g., maps, drawings, charts) are reproduced by sectioning the original, beginning at the upper left-hand corner and continuing from left to right in equal sections with small overlaps.

Photographs included in the original manuscript have been reproduced xerographically in this copy. Higher quality 6" x 9" black and white photographic prints are available for any photographs or illustrations appearing in this copy for an additional charge. Contact UMI directly to order.

ProQuest Information and Learning
300 North Zeeb Road, Ann Arbor, MI 48106-1346 USA
800-521-0600

Université d'Ottawa · University of Ottawa

Abstract

The body of work in this thesis is divided into *two main parts*; (I) the first being that of *the collision-induced emission (CIE) spectroscopy study* of small polyatomic molecules; and (II) the second being a *tandem mass spectrometry study of a series of perfluorinated organics.*

(I) Collision-Induced Emission (CIE)Spectroscopy Studies

Over the past thirty years, many gas-phase optical emission studies (carried out under conditions of thermal kinetic energy and controlled electron-impact excitation) have shown that several groups (e.g., linear, conjugated, or aromatic, etc...) of *large polyatomic* radical-cation species possess unique and characteristic optical emission spectra of their intact-parent $M_1^{+\bullet}$ species. These optical emission spectra may serve as a "fingerprint" to aid in the identification of their presence and the elucidation of their inherent structure. This being the case, one may use an alternative method (that is used here is this thesis) to attempt to obtain an optical emission spectrum of the intact-parent $M_1^{+\bullet}$ species, known as collision-induced emission (CIE) spectroscopy, and this technique will be discussed below.

Thus, the original motivation for the CIE studies presented here in this thesis, was the recording of novel optical emission spectra of large polyatomic intact-parent $M_1^{+\bullet}$ species and their corresponding fragments. The intent was the utilization of this optical emission data as an aid in their identification and structural elucidation in a complimentary fashion to their mass spectrometric information.

To this end, a series of *small* polyatomic linear molecules, N≡N, C≡O, O=C=O, O=C=C=O, were selected for study. As well, a series of *larger* polyatomic aromatic molecules,

C_6H_6, C_6F_6, and C_4H_4O, were selected in an attempt to extend and explore the capabilities of the CIE technique.

The CIE studies presented in Chapter 2 consisted of a source generated fast moving 8 keV projectile-ion, $M_1^{+\bullet}$, undergoing a collision encounter with a stationary target gas, G_1, under single collision conditions (i.e., ≈ 90%T). During the collision event, a non-momentum transfer occurs, that deposits an amount of internal excitation energy, $\Delta(\Delta E_{int})$, into the projectile-ion, producing an excited electronic state $(M_1^{+\bullet})^*$ species. Thus the $(M_1^{+\bullet})^*$ species may now exhibit optical emission and/or fragment into ground, $M_2^+ + M_3^\bullet$; or excited, $(M_2^+)^\bullet + M_3^\bullet$, $M_2^+ + (M_3^\bullet)^\bullet$, $(M_2^+)^\bullet + (M_3^\bullet)^\bullet$, electronic state dissociation products. Additionally, if the charge exchange process between $M_1^{+\bullet}$ and G_1 is present, a ground M_1, or excited $(M_1)^*$ electronic state parent neutral may be produced. Thus, again the $(M_1)^*$ species may now exhibit optical emissions and/or fragment into ground or excited electronic state dissociation products. As well, with respect to the stationary target gas the $(G_1)^*$ and $(G_1^{+\bullet})^*$ species and/or their fragments may be produced.

The target gases used here were He, Ar, and O_2. There were no CIE signals observed corresponding to radical-cation atomic target gases. In contrast, for the O_2 molecule there were intense CIE signals observed for the radical-cation and neutral target gas species (as well as its dissociation products). The ratio of the intensity of the total emission counts for the He, Ar, and O_2 target gases were typically 1 : 1.5 : 3. This trend parallels the neutralization efficiency of He, Ar, an O_2 that are ineffective, moderately effective, and strongly effective, respectively, in the neutralization of $M_1^{+\bullet}$ to produce $(M_1)^*$.

Previously, other monochromated CIE spectra studies of lower sensitivity, were recorded in the UV-VIS wavelength region of 190-680 nm, under *multiple collision conditions*,

via the use of a TE cooled PMT. The *new work presented here in this thesis*, were comprised of monochromated CIE spectra studies of higher sensitivity, and were over a greater wavelength range that was extended into the NIR (i.e., 700-1020nm). The monochromated CIE spectra were recorded over a calibrated wavelength range in the UV-VIS-NIR of 190-1020 nm, via a liquid nitrogen cooled charge-coupled device (CCD) camera. The CIE experiments were also carried out under *single-collision conditions*. This was done to maximize the possibility of the observation of intact-parent projectile-ion $M_1^{+\bullet}$ species optical emission over that of their respective fragments, whilst minimizing the possible production of overpowering interfering stationary target gas emissions.

For the *small* polyatomic projectile-ions studied here of the $N{\equiv}N^{+\bullet}$, $C{\equiv}O^{+\bullet}$, $O{=}C{=}O^{+\bullet}$, $O{=}C{=}C{=}O^{+\bullet}$ systems, intact parent-ion emissions were observed for all of them, except for the *latter* species. As well, intact parent neutral emissions were only observed for $N{\equiv}N$, $C{\equiv}O$. The Wigner-Witmer correlation Rules were utilized to correlate the observed CIE signals of the fragments to that of the proposed respective neutral and radical-cation parents. For the *larger* polyatomic projectile-ions studied here of the $C_6H_6^{+\bullet}$, $C_6F_6^{+\bullet}$, and $C_4H_4O^{+\bullet}$ systems, *no intact-parent emissions were observed*, only those of weak atomic and diatomic fragment emissions.

Thus, the above CIE studies of the series of small and larger polyatomic molecules would appear to suggest that as the size of the fast moving projectile-ion $M_1^{+\bullet}$ increases, quasi-equilibrium dissociation becomes dominant over that of optical emission. Thus, the present CIE technique is unsuitable for the study of large polyatomic molecules. *However*, if there were a modification made to the present CIE experimental set up, such as the addition of a *"deceleration-zone"* prior to the optical observation cell, the *controlled reduction of the*

translational kinetic energy of the projectile-ion $M_1^{+\bullet}$, may result in the tilting-of-the-balance in *favour* of optical emission over that of quasi-equilibrium dissociation.

(II) Tandem Mass Spectrometry Studies of Perfluorinated Organics

Over the past half-century, the gas-phase ion-chemistry of hydrogen containing organics has by far been the dominant species of choice for study, owing originally to the interest of the petroleum industry. A wealth of information on their reaction mechanisms, mass spectral characteristics, ion energetics and thermodynamic properties has been amassed on these compounds to the point that, generally, they are well understood and their behaviour well established.

However, the same can not be generally said of their (per)fluorinated analogues. The field of fluorine chemistry has always been a smaller, less studied, and more self-contained area of study within the chemistry community as a whole. Their primary industrial interest was in their use as solvents and coolants, widely known as perfluorochlorocarbons. Due to their difficult syntheses, somewhat toxic qualities, and chemical instability, halogen containing compounds are generally more difficult to obtain and are less studied. As well, with the discovery in the 1970's of their ozone-depleting characteristics a new interest in their gas-phase ion-chemistry was created at the same time as their use began to be curtailed. In the 1990's, the Montreal Protocols set out a timetable for the complete phasing out of many halogenated compounds by the early twenty-first century. Thus, a systematic study of some halogen containing compounds, prior to their possible future unavailability, is of interest to the gas-phase ion-chemistry community as a whole.

Thus, the principal motivation of these tandem mass spectrometry studies of perfluorinated compounds (in which all hydrogens are replaced by fluorines, a term known as perfluorination) was to present in one location a comprehensive qualitative gas-phase ion-chemistry study, that may inspire other studies which may pull the field of fluorine chemistry further into the mainstream milieu of the gas-phase ion chemistry community.

The tandem mass spectrometry studies of perfluorinated organics, presented in Chapters 3 and 4, were conducted on a series of iodo, oxo and unsaturated compounds.

In particular, the perfluoro iodo compounds *were hoped* (with iodine being such a good leaving group) to be possible ideal sources of *unrearranged* fragment perfluorocarbocations, $C_nF_m^+$. However, unfortunately this did not always prove to be the case.(e.g., the primary metastable loss from $(CF_3)_3CI^{+\bullet}$ was unexpectedly FI and not $I^\bullet$). For the perfluoro iodo compounds, the isomers of perfluorobutyl, C_4F_9I, and perfluoropropyl, C_3F_7I, iodides were utilized as precursors. (As well, $(CF_3)_3C–C(CF_3)_3$ was utilized as a precursor for $(CF_3)_3C^+$). Specifically, it was proposed here that the (fragment) perfluorocarbocations, $C_nF_m^+$ possessed a *reserved cation stability order (i.e., primary > secondary > tertiary)*; $CF_3CF_2CF_2CF_2^+ > (CF_3)_3CFCF_2^+ > (CF_3)_3C^+$; that is *not* seen in their respective hydrocarbon counterparts.

For the perfluoro unsaturated compounds, perfluor-2-butyne, $CF_3–C{\equiv}C–CF_3$, and perfluoropropene, $CF_2{=}CFCF_3$, were utilized as precursors.

Lastly for the perfluoro oxo compounds, the C_3F_6 isomers of perfluoroacetone $(CF_3)_2C{=}O$, perfluoromethylvinyl ether, $CF_2{=}CFOCF_3$, and perfluoromethyloxirane, c-$F_2(COC)FCF_3$, were utilized as precursors. The normal mass spectra, metastable ion (MI), and collision induced dissociation (CID) mass spectra of the various isomers were catalogued and analyzed. *Several isomeric structures and their order of stability were proposed on the basis of*

the perfluoro and perfluorination effects that result upon the replacement of all hydrogen atoms by that of fluorines. This resulted in novel and sometimes unpredictable gas-phase ion-chemistry to be exhibited in the perfluorinated species, whose behaviour sometimes paralleled that of its hydrogen analogue, and otherwise was completely unique.

Most importantly, the *perfluoroketene neutral* CF_2=C=O, produced in the neutralization step of the neutralization-reionization (NR) study of CF_2=C=O$^{+\bullet}$ presented in Chapter 4, was shown to be *indeed a stable species* possessing a lifetime on the order of the transit time between the neutralization and reionization cells (i.e., $\approx$ 1μs) via the presence of an extremely strong recovery peak in its NR mass spectrum. *This represents the first direct experimental evidence for the existence of the long sought after elusive* CF_2=C=O *neutral.*

Acknowledgements

I would like to gratefully thank my supervisor Dr. J.L. Holmes for his wise guidance, encouragement, patience, and financial support throughout the completion of this work. As well I am very thankful to Dr. A.A. "Sander" Mommers for always being there to keep the VG ZAB-3F running and for his helpful suggestions on trouble-shooting the CCD camera. I would also like to thank Andrew Zlotorynski for writing the Microsoft Excel 95 macro delete.xls that made possible the signal processing of the CIE spectra. As well, I would thank Dr. J. Krause for allowing me to photocopy his copy of Turner's book Molecular Photoelectron Spectroscopy that was of immeasurable help over the years in understanding the CIE work, and Dr. Clem Kazakoff for his enjoyable discussions of the "challenges" involved in operating a mass spectrometer, and the science fiction show Babylon 5 ("Mr. Garibaldi").

To Hongwen Chen, I wish to express my hearty thanks for always taking the time to help me on those (16 hour CIE) days when the ZAB was about to give out and for your encouragement and kind words of friendship. (Thanks for writing out the Chinese good luck symbol "How-Yoon" that was placed on ZAB during the CIE experiments and the loan of the "Energizer Bunny" that was placed atop the magnet.) As well, to Dr. Michael "Myke" Polce, thanks a lot for those ever enjoyable discussions about life, work and the X-Files (The truth is out there Myke!), and for the many fruitful discussions of my CIE spectra.

I would also like to thank the other students and post-docs: Ya Ping, Christiane Aubry, David Harnish, Yan An, Jie Cao, Richard Ochran, and Julie McCormack, for making the lab an enjoyable place to work.

To my parents, Norman and Frances Dawson, I thank you so much for all of the constant love, support, and encouragement, and for always helping whenever I needed it over

the years, and who will no doubt be overjoyed that I've completed my graduate work. As well, the Hughes family is thanked for their constant encouragement and generous opening of their home to me.

Finally, I would like to thank my beloved wife, Dianne Hughes, whose constant love, support, understanding, and never ending encouragement have always been so important and a great source of strength for me, which kept me going all the way through my journey in graduate school. And last but not least, to our little white poodle, Arthur ("the baby"), thanks for always being a constant source of happiness and love and providing those "head-clearing" breaks when we go on your "w-a-l-k-s".

Table of Contents

List of Tables

Chapter 2

List of Figures

Chapter 1

Chapter 2

Comments on gas-Phase Ion-Chemistry Thermochemical Data

In this thesis, the majority of the relevant thermochemical data (i.e., the heat of formation of the neutral, $\Delta_f H^0[M_1]$, the adiabatic ionization energy of the neutral, $IE_a[M_1]$, and the heat of formation of the ion, $\Delta_f H^0[M_1^{+\bullet}]$) were quoted from "the standard" literature source, known as the compilation of S.G. Lias, J.E. Bartmess, J.F. Liebman, J.L. Holmes, R.D. Levin, and W.G. Mallard, *Gas-Phase Ion and Neutral Thermochemistry*, J. Phys. Chem. Ref. Data, 17, (1988). As well, any other thermochemical data from outside this source was specifically quoted.

There were *no theoretical ab initio calculations* of any kind (i.e., $\Delta_f H^0[M_1]$, $IE_a[M_1]$, or $\Delta_f H^0[M_1^{+\bullet}]$) performed in this thesis, and they are *beyond its' scope*. Any instance of a pre-existing theoretical ab initio result that was utilized in the text for discussion, or placed in an energy level diagram (e.g., the ab initio value of $\Delta_f H^0[O{=}C{=}C{=}O[\tilde{X}\,^3\Sigma_g^-]] = 55$ kJ•mol^{-1}) was *explicitly indicated*. Save these rare instances, all thermochemical data discussed in the text, and/or used to construct the proposed energy level diagrams of the perfluorinated species was taken from "the standard" literature compilation of Lias et. al., other experimental literature sources, empirically estimated Benson's Additivity values, or qualitatively estimated values, *explicitly discussed* in the body of the text.

The heat of formation of the ionic species was calculated as given below;

$$\Delta_f H^0[M_1^{+\bullet}] = IE_a[M_1] + \Delta_f H^0[M_1]$$

where $\Delta_f H^0[M_1]$, $IE_a[M_1]$, and $\Delta_f H^0[M_1^{+\bullet}]$ denote the neutral heat of formation, the adiabatic ionization energy of the neutral, and the ionic heat of formation, respectively. In the majority

of the cases, theses above values were taken from " the standard" compilation of Lias. et. al.. Otherwise, the $\Delta_fH^0[M_1^{+\bullet}]$ value was determined via the utilization of a *known experimental* (e.g., photoelectron spectroscopy) $IE_a[M_1]$ value and an empirically estimated Benson's Additivity $\Delta_fH^0[M_1]$ value. (One noted exception being usage of the *explicitly discussed estimated* $IE_a[CF_2{=}C{=}O] \approx 11$ eV value in the determination of the proposed $\Delta_fH^0[CF_2{=}C{=}O^{+\bullet}]$ value).

The Benson's Rules of Additivity are first presented in Chapter 3, Section 3.2. They are also *covered in more detail in Appendix C, and the reader is referred to them.*

Generally, the error limits on the Δ_fH^0 values listed in "the standard" compilation of Lias et. al., for hydrogen compounds are about $\pm$ 0.8 kJ•mol^{-1} (i.e., $\pm$ 0.2 kcal•mol^{-1}), and are somewhat greater for fluorine compounds of about $\geq$ 4.2 kJ•mol^{-1} (i.e., $\geq$ 0.5 kcal•mol^{-1}). As well, *all Δ_fH^0 values quoted in the tables and elsewhere in this thesis are given to three or four significant figures. The error limits are shown where available. The Δ_fH^0 values calculated by Benson's Additivity are, in general, likely to be no better than about $\pm$ 2.1 kJ•mol^{-1} (i.e., $\pm$ 0.5 kcal•mol^{-1}), even though they may be quoted to four significant figures.*

At this point, one further matter deserves emphasis. The proposed energy level diagrams of the perfluoro compounds are meant to serve as qualitative guides to the order of the dissociation products for which there were no available Δ_fH^0 values in the literature. Thus, they are not to be seen as static constructs. The author hopes that upon their inspection, they will serve as a source of inspiration for others to continue their own future work, and bring the field of fluorine chemistry further into the mainstream milieu of gas-phase ion-chemistry as a whole (this being the original intent of their construction).

Chapter 1 Introduction to Gas-Phase Ion-Chemistry and Mass Spectrometry

1.1 Introduction

This chapter will deal with the basic principles of gas-phase ion-chemistry [1-8] and tandem mass spectrometry [9-20] that will be utilized in the rest of the work presented here in this thesis. The gas-phase ion-chemistry (see section 1.2.1) topics will cover the thermodynamic quantities, such as $\Delta_f H^0[M_1]$, $IE_a[M_1]$, $IE_v[M_1]$, $\Delta_f H^0[M_1^{+\bullet}]$, $AE[M_2^+]$, and $\Delta_f H^0[M_2^+]$, which denote the (standard) heat of formation of the neutral M_1, the adiabatic, and the vertical ionization energies of the neutral M_1, the heat of formation of the radical-cation $M_1^{+\bullet}$, the appearance energy, and the heat of formation of the fragment-ion M_2^+, respectively [1-3]. These quantities are vital to the elucidation of molecular structure (i.e., atom connectivity within the molecular framework) and the explanation of trends in dissociation behaviour in a series of structurally related compounds.

Next, the tandem mass spectrometry section (see section 1.2.2) will cover the essentials of the functioning of the VG ZAB-3F reverse geometry (magnetic B, electric E, and electric E) three sector (BEE) mass spectrometer and the experimental techniques which were utilized here as follows; the normal mass spectrum, the metastable ion (MI), collision induced dissociation (CID), the neutralization-reionization (NR) mass spectra, and the Kinetic Energy Release ($T_{0.5}$) measurements. It should be noted here that the normal mass spectrum *alone does not contain structurally unique information*, but it is the combination of the MI, CID, $T_{0.5}$ measurements and sometimes the NR mass spectra, that allows the complete assignment of the ion's structure.

1.2 Mass Spectral Instrumentation and Experimental Techniques

1.2.1 Gas-Phase Ion-Chemistry

The dissociation behaviour of an ion $M_1^{+\bullet}$, for the purposes of this thesis, will be considered to be governed by quasi-equilibrium theory (QET) [1, 10, 12, 13]. Now for the polyatomic $M_1^{+\bullet}$ species with N atoms in the molecular framework, there are 3N–5 and 3N–6 vibrational modes (i.e., internal degree of freedom) for linear and non-linear molecules, respectively. Thus, the larger the molecule the greater the number of vibrational modes into which the internal energy, E_{int}, may be partitioned. Therefore, the unimolecular dissociation of the parent ion $M_1^{+\bullet}$ into the fragment ion M_2^+ and the neutral $M_3^\bullet$, maybe expressed as follows;

$$M_1^{+\bullet} \xrightarrow{\bullet} M_2^+ + M_3^\bullet$$

there are four basic assumptions of quasi-equilibrium theory that are listed below as follows:

(I) The time required for dissociation of a polyatomic ion is long compared to the time required for its formation and excitation.

(II) The rate of dissociation of an ion is slower than the rate of redistribution of E_{int} among all of the internal degrees of freedom.

(III) The ion achieves a condition of E_{int} equilibrium in which the energy is distributed over all internal degrees of freedom with equal probability.

(IV) The observed dissociation products result from a series of consecutive and competing reactions.

Now, at the heart of QET is the internal energy dependant rate constant, k(E), which characterizes each possible dissociation reaction and is expressed below as follows;

$$k(E) = \left[\frac{\prod_{i=1}^{S} \nu_i}{\prod_{j=1}^{S-1} \nu_j}\right]\left(1-\frac{\varepsilon_0}{E}\right)^{S-1} = \left(10^{15}\, s^{-1}\right)\left(1-\frac{\varepsilon_0}{E}\right)^{S-1}$$

where E, k(E), ν_i, ν_j, γ_0, and S denote the internal energy, the unimolecular dissociation rate constant, the vibration energies of the molecular ion $M_1^{+\bullet}$, the activated complex $[M_1^{+\bullet}]^*$, the minimum critical energy for fragmentation, and the effective number of vibrational modes (i.e., $S \leq N$), respectively. The unimolecular dissociation rate constant, k(E), is equal to the reciprocal of the dissociation lifetime (i.e., $k(E)=1/\tau$).

On inspection of the above equation, fast dissociations, with one or very few vibrations coupled, possess k(E) values on the order of $10^{13}-10^{15}$ s^{-1}, and slower dissociations, with several or all vibrations coupled, possess k(E) values of $< 10^{12}$ s^{-1}.

There are three types of molecular ions, $M_1^{+\bullet}$, produced in a mass spectrometer (see section 1.2.2) and are known as stable, metastable, and fragment ions. Stable ions exit the ion source and travel all the way through the mass spectrometer without fragmenting and possess k(E) values of $\approx 10^0-10^4$ s^{-1}. Metastable ions exit the ion source intact and then fragment at some point later on and possess k(E) values of $\approx 10^4-10^7$ s^{-1}. Lastly, fragment ions possess the highest k(E) values of $\approx 10^7-10^{15}$ s^{-1} are formed from parent ions in the ion source. Thus, the time scale of events may be listed as follows: ionization, 10^{-16} s, collisional excitation $10^{-14}-10^{-15}$ s, vibration $10^{-12}-10^{-14}$ s, rotation 10^{-8} s, and ion flight time through the mass spectrometer $10^{-4}-10^{-6}$ s.

Now, one will discuss the thermodynamic terms known as the (standard) heat of formation, $\Delta_f H^0$, of the neutral and its ion, and the adiabatic, IE_a, and vertical, IE_V, ionization energies [1-8], and they are illustrated in Figure 1.1. The conditions under which the $\Delta_f H^0$ values are measured is known as standard ambient temperature and pressure (SATP) and consists of a pressure of p = 1 atm and a Kelvin temperature of T = 298 K (i.e., a t_c =25°C) where T = 0 K is taken as absolute zero. Thus at SATP, the standard heat of formation of a

Figure 1.1 The Determination of the Heats of Formation of Gaseous Ions

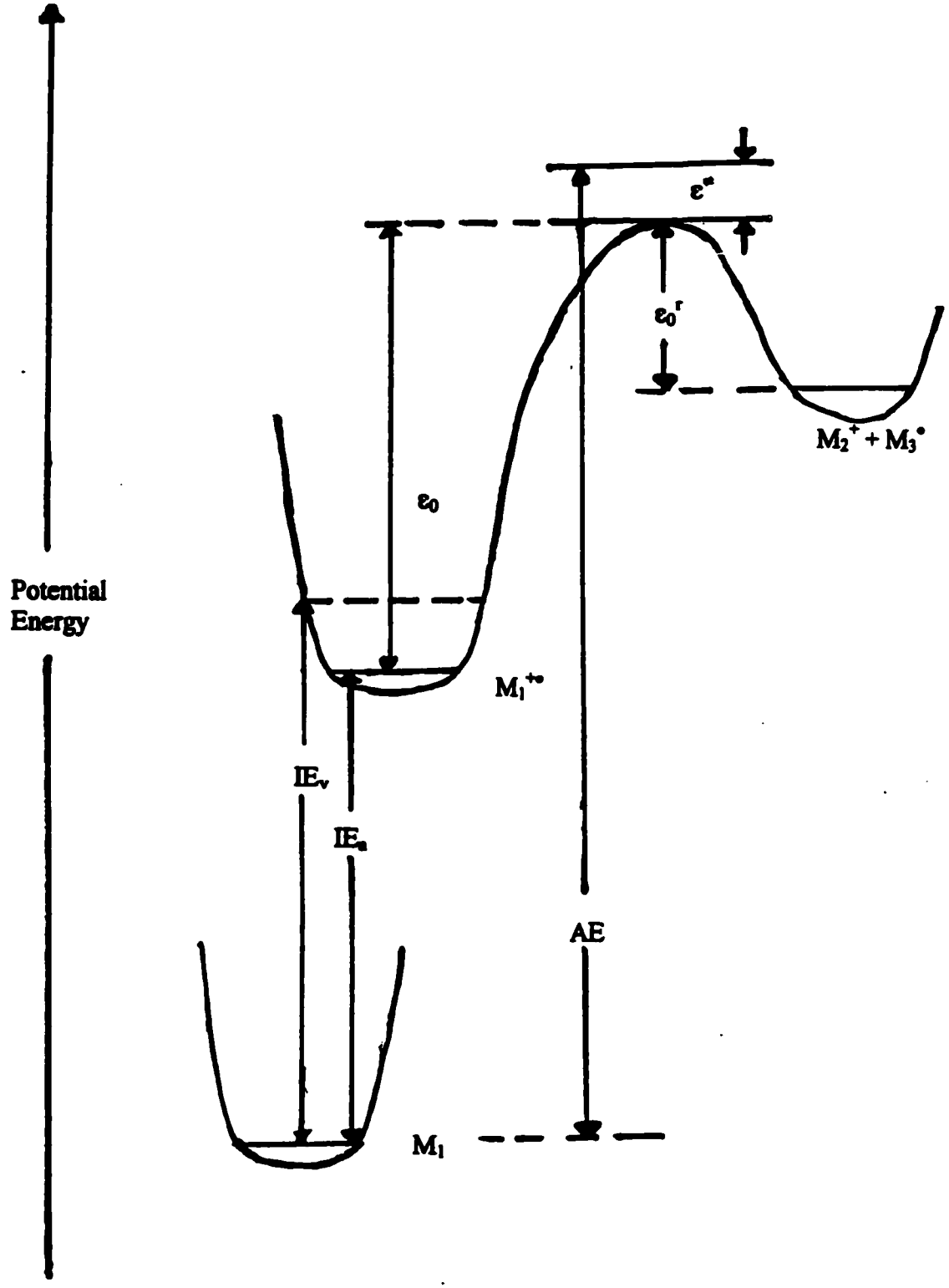

neutral molecular species $\Delta_f H^0[M_1]$, is defined as the heat released (or required) on its formation from its constituent atoms and has units of ($kJ \bullet mol^{-1}$) [1]. (Note, the standard conversion factors are 96.487 $kJ \bullet mol^{-1}$ = 23.061 $kcal \bullet mol^{-1}$ = 8065.5 cm^{-1}=1.00 eV [1]). The $\Delta_f H^0$ values range from endothermic (heat required), to thermoneutral (no heat), and exothermic (heat released) in nature and are expressed as positive, zero, and negative quantities.

Most closed shell (even election) molecular species have exothermic $\Delta_f H^0$ values for their neutrals, whereas the diatomics (e.g. H_2, N_2, O_2, F_2, etc.) have their $\Delta_f H^0$ values defined as zero due to them representing the most stable form of their atomic constituents [1].

Now, on inspection of Figure 1.1, one may see that the minimum energy required to remove an electron, e^-, from the highest occupied orbital of the neutral molecule M_1 is known as the first ionization energy, IE [1]. The IE values are quoted in units of electron volts, eV. Thus, in the production of a molecular ion, $M_1^{+\bullet}$, by electron impact ionization may be expressed as follows;

$$M_1 + e^- \rightarrow M_1^{+\bullet} + 2e^-$$

and may be seen to occur by a vertical (i.e., Franck-Condon type) process [1, 9-14] in which the inter-nuclear distances of $M_1^{+\bullet}$ remain the same as M_1 due to the ionization time (10^{-16} s) being much shorter than the vibrational periods (10^{-12}–10^{-14} s). Thus, the minimum energy required to produce molecular ions, via electron impact, is usually the vertical ionization energy, IE_V, which may (depending on the potential energy curves of M_1 and $M_1^{+\bullet}$) be greater than the adiabatic ionization energy, IE_a, which is the minimum energy the lowest between vibrational ($v = 0$) levels of M_1 and $M_1^{+\bullet}$.

Additionally, on inspection of Figure 1.1 one should note the following terms. For the dissociation process of,

neutral molecular species $\Delta_f H^0[M_1]$, is defined as the heat released (or required) on its formation from its constituent atoms and has units of ($kJ \bullet mol^{-1}$) [1]. (Note, the standard conversion factors are 96.487 $kJ \bullet mol^{-1}$ = 23.061 $kcal \bullet mol^{-1}$ = 8065.5 cm^{-1}=1.00 eV [1]). The $\Delta_f H^0$ values range from endothermic (heat required), to thermoneutral (no heat), and exothermic (heat released) in nature and are expressed as positive, zero, and negative quantities.

Most closed shell (even election) molecular species have exothermic $\Delta_f H^0$ values for their neutrals, whereas the diatomics (e.g. H_2, N_2, O_2, F_2, etc.) have their $\Delta_f H^0$ values defined as zero due to them representing the most stable form of their atomic constituents [1].

Now, on inspection of Figure 1.1, one may see that the minimum energy required to remove an electron, e^-, from the highest occupied orbital of the neutral molecule M_1 is known as the first ionization energy, IE [1]. The IE values are quoted in units of electron volts, eV. Thus, in the production of a molecular ion, $M_1^{+\bullet}$, by electron impact ionization may be expressed as follows;

$$M_1 + e^- \rightarrow M_1^{+\bullet} + 2e^-$$

and may be seen to occur by a vertical (i.e., Franck-Condon type) process [1, 9-14] in which the inter-nuclear distances of $M_1^{+\bullet}$ remain the same as M_1 due to the ionization time (10^{-16} s) being much shorter than the vibrational periods (10^{-12}–10^{-14} s). Thus, the minimum energy required to produce molecular ions, via electron impact, is usually the vertical ionization energy, IE_v, which may (depending on the potential energy curves of M_1 and $M_1^{+\bullet}$) be greater than the adiabatic ionization energy, IE_a, which is the minimum energy the lowest between vibrational ($v = 0$) levels of M_1 and $M_1^{+\bullet}$.

Additionally, on inspection of Figure 1.1 one should note the following terms. For the dissociation process of,

$$M_1^{+\bullet} \rightarrow M_2^{+} + M_3^{\bullet}$$

according to QET, ε_0, ε_0^r, ε^* denote the minimum critical energy for the forward dissociation reaction to occur, the minimum critical energy for the reverse (re-association) reaction to occur, and the non-fixed internal energy (also known as the kinetic shift) necessary to yield an observable fragment M_2^+ on the timescale of the experiment, respectively.

Therefore, one may see the appearance energy of the fragment ion M_2^+, $AE[M_2^+]$, can be expressed as follows;

$$AE[M_2^+] = IE_a[M_1] + \varepsilon_0 + \varepsilon^* = (\Delta_f H^0[M_2^+] + \Delta_f H^0[M_3^\bullet]) - (\Delta_f H^0[M_1]) + (\varepsilon_0^r + \varepsilon^*)$$

Additionally, the heat of formation of the molecular ion $M_1^{+\bullet}$ is expressed as follows;

$$\Delta_f H^0[M_1^{+\bullet}] = IE_a[M_1] + \Delta_f H^0[M_1]$$

and the heat of formation of the fragment ion M_2^+ is expressed as follows;

$$\Delta_f H^0[M_2^+] = AE[M_2^+] - \Delta_f H^0[M_3^\bullet] + \Delta_f H^0[M_1] - (\varepsilon_0^r + \varepsilon^*)$$

Therefore, one may see that the experimentally measured value of $AE[M_2^+]$ and thus $\Delta_f H^0[M_2^+]$ will be close to its "true" value if the fragmentation of $M_1^{+\bullet}$ possesses a ε^* of little or no significant value, and there is no reverse activation energy barrier ε_0^r. As such, the experimental $AE[M_2^+]$ values, obtained either by monochromated electron impact or photoion-photoelectron coincidence (PIPECO) spectroscopy [1] should be taken as upper limits.

Therefore, with the experimentally measured $IE[M_1]$ and $AE[M_2^+]$, one still needs to have $\Delta_f H^0$ values for M_1 and $M_3^\bullet$ to be able to calculate $\Delta_f H^0$ values for $M_1^{+\bullet}$ and M_2^+. The $\Delta_f H^0$ values for the neutral and ionic species are contained in the standard compilations [1-3]. If $\Delta_f H^0[M_1]$ and $\Delta_f H^0[M_3^\bullet]$ are not found in the literature, one may estimate them empirically via Benson's Additivity Rules [4-8]. This scheme breaks the molecule down into its constituent groups, based on the most reliable thermochemical data, and the $\Delta_f H^0$ value of the whole

molecule is derived from the sum of the $\Delta_f H^0$ values of the individual groups. This is explored more in depth in Chapter 3.

Next, one needs to discuss the factors involved in conversion of the $M_1^{+\bullet}$ isomer into a different $(M_1')^{+\bullet}$ isomer, and this is illustrated in Figure 1.2. At this point, one should emphasize that the ions produced in the ion source cover a wide range of internal energies, and they may not only fragment, but they may isomerize as well.

On inspection of Figure 1.2, one may note the following terms. The minimum critical energy necessary for the isomerization of $M_1^{+\bullet}$ into $(M_1')^{+\bullet}$ is denoted by ε_0^i. At the summit of the barrier between $M_1^{+\bullet}$ and $(M_1')^{+\bullet}$ there is located a species whose structure is known as the transition state (or activated complex) of the isomerization process. As well, $\varepsilon_0[M_2^+]$ and $\varepsilon_0[M_2^+]$ denote the minimum critical energies necessary for the independent $M_1^{+\bullet} \rightarrow M_2^+ + M_3^\bullet$, and $(M_1')^{+\bullet} \rightarrow M_4^+ + M_5^\bullet$ dissociation processes to occur, respectively.

On the timescale of the event occurring in the ion-source, both of the processes of fragmentation and isomerization shall occur at E_{int} values that are in excess of their respective minimum critical energies. Thus, source generated ions possess a relatively large range of E_{int} values and are very likely to contain various isomeric species. In contrast, metastable ions that are generated later outside the ion-source, are produced at or very near the fragmentation threshold. Therefore, they possess only a very narrow range of E_{int} values, and may likely be seen to represent a single ion structure. Thus, if one compares the CID mass spectra of a source generated ion to its metastably generated counterpart, and they are the same, then one may suggest that they are representative of one ion structure. However, if they are significantly different, then one may suggest that the source generated ion is composed of several isomeric ions (see Section 1.2.2).

Figure 1.2 The Isomerization of $M_1^{+\bullet}$ into $(M_1')^{+\bullet}$. (I) No Isomerization and Independent Fragmentation, (II) Equal Isomerization and Fragmentation, and (III) Favoured Isomerization and its Fragmentation

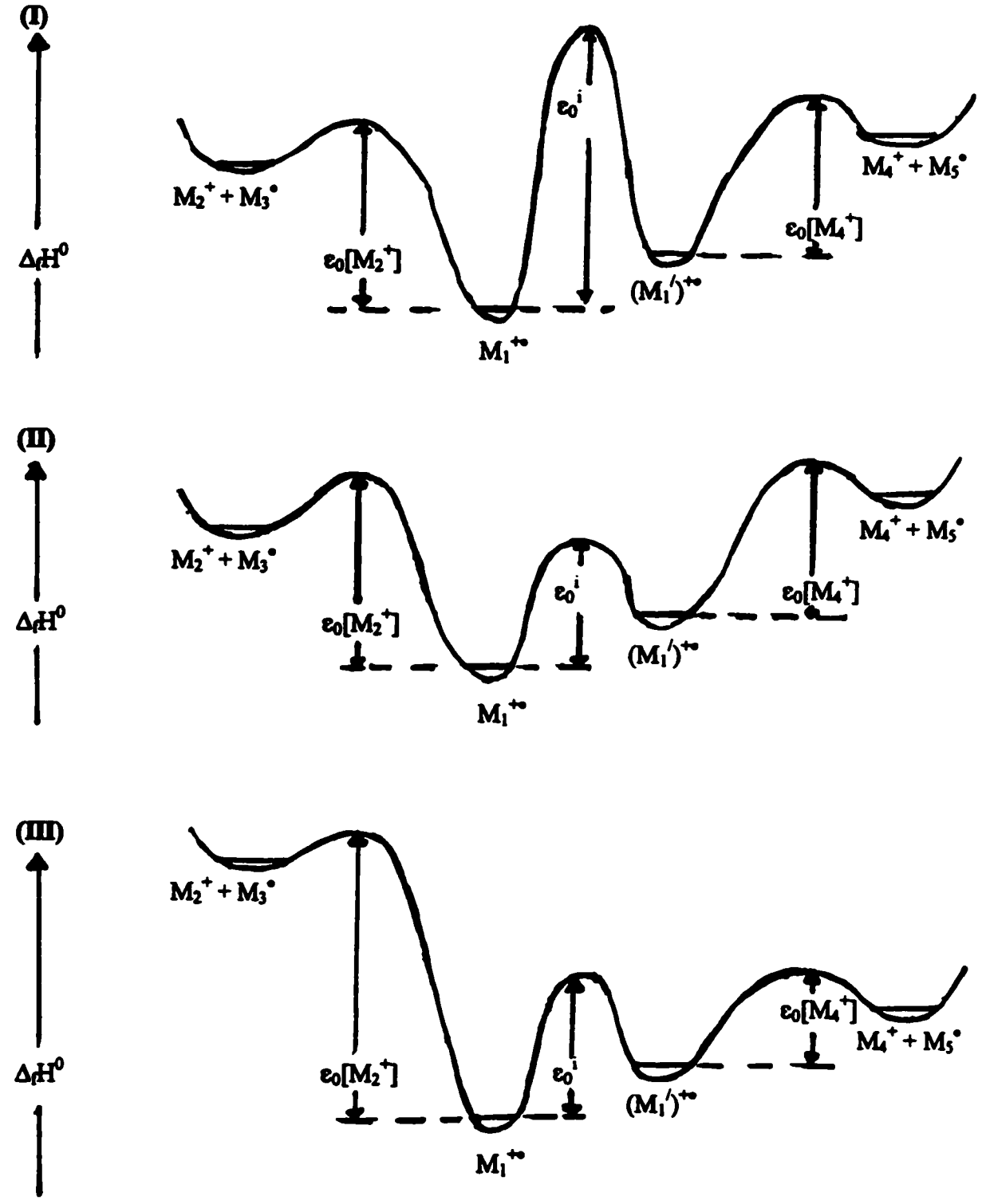

Therefore, the competition between the fragmentation and isomerization processes shall depend on their respective k(E) values and the following three general cases may result as follows:

(I) If $\varepsilon_0^i >> \varepsilon_0[M_2^+]$ and $\varepsilon_0^i >> \varepsilon_0[M_4^+]$; then the isomerization process of $M_1^{+\bullet}$ into $(M_1')^{+\bullet}$ *can not* take place. Thus, the MI mass spectra will yield *unique* structural information for each isomer.

(II) If $\varepsilon_0^i < \varepsilon_0[M_2^+]$ and $\varepsilon_0[M_2^+] \approx \varepsilon_0[M_4^+]$; then the isomerization process of $M_1^{+\bullet}$ into $(M_1')^{+\bullet}$ *may* take place. However, this prevents one from being able to distinguish between the $M_1^{+\bullet}$ and $(M_1')^{+\bullet}$ isomers as they may freely interconvert prior to fragmentation and thus produce *identical* MI spectra.

(III) If $\varepsilon_0[M_2^+] >> \varepsilon_0^i$ and $\varepsilon_0[M_2^+] >> \varepsilon_0[M_4^+]$; then the $M_1^{+\bullet}$ isomer cannot easily access (under MI conditions) its $M_2^+ + M_3^\bullet$ dissociation limit. The isomerization of $M_1^{+\bullet}$ into $(M_1')^{+\bullet}$ shall be strongly favoured prior to the accessing of the $M_4^+ + M_5^\bullet$ dissociation limit. Thus, $(M_1')^{+\bullet}$ may be considered to be the reacting configuration of $M_1^{+\bullet}$ (i.e., the structure that leads directly to the activated complex without further rearrangement [18]). This will result in the MI mass spectra of $M_1^{+\bullet}$ and $(M_1')^{+\bullet}$ to be very *similar* and further experimental information, such as CID mass spectra, will be required to distinguish the isomers.

Thus, the field of gas-phase ion-chemistry is an immense one, and the basic concepts that will be utilized later in Chapters 2 through 4 have been illustrated here. The next section will briefly discuss the experimental apparatus and techniques used in the tandem mass spectrometry studies presented in Chapters 3 and 4.

1.2.2 Components of a Mass Spectrometer

This section will deal with the reverse geometry three sector VG ZAB-3F mass spectrometer, and the experimental techniques of the metastable ion (MI), collision induced discussion (CID), the neutralization-reionization (NR) mass spectrometry and the kinetic energy release $T_{0.5}$ measurements utilized here [9-20].

The VG ZAB-3F Mass Spectrometer

The principal function of a mass spectrometer is to measure the mass spectrum of an ion in order to identify it. The mass spectrum is a plot of ion intensity (Y-axis) versus mass to charge ratio, m/z, (X-axis) of the molecular ion and its fragments. The mass to charge ratio can be determined by measuring the ions momentum (via a magnetic analyzer, B) and also its energy (via an electric analyzer, E). The reverse geometry three sector VG ZAB-3F (BEE) mass spectrometer used in this thesis is illustrated in Figure 1.3.

The general operating conditions of the VG ZAB-3F will now be briefly discussed. The entire instrument, from the ion source all the way to the end, is kept at a background pressure of $\approx 10^{-9}$ Torr via roughing, and diffusion pumps. For the MI and CID experiments, the typical ion source gas pressures are $\approx 10^{-7}$ Torr. Whereas, for the NR experiments they are at somewhat higher pressures of $\approx 10^{-6}$ Torr. For all MI, CID, and NR experiments, the collision gas pressures in the collision cells were sufficient to reduce the ion beam intensity by 10% (i.e., 90%T beam transmission, thus producing single collision conditions [18]) and were on the order of 10^{-6}–10^{-7} Torr measured pressure.

Next, there were three sample inlet systems which were used to introduce the neutral M_1 species, in its gaseous form, in the ion source. The first was the gas inlet system that allowed

Figure 1.3 The Reverse Geometry Three Sector VG ZAB-3F (BEE) Mass Spectrometer

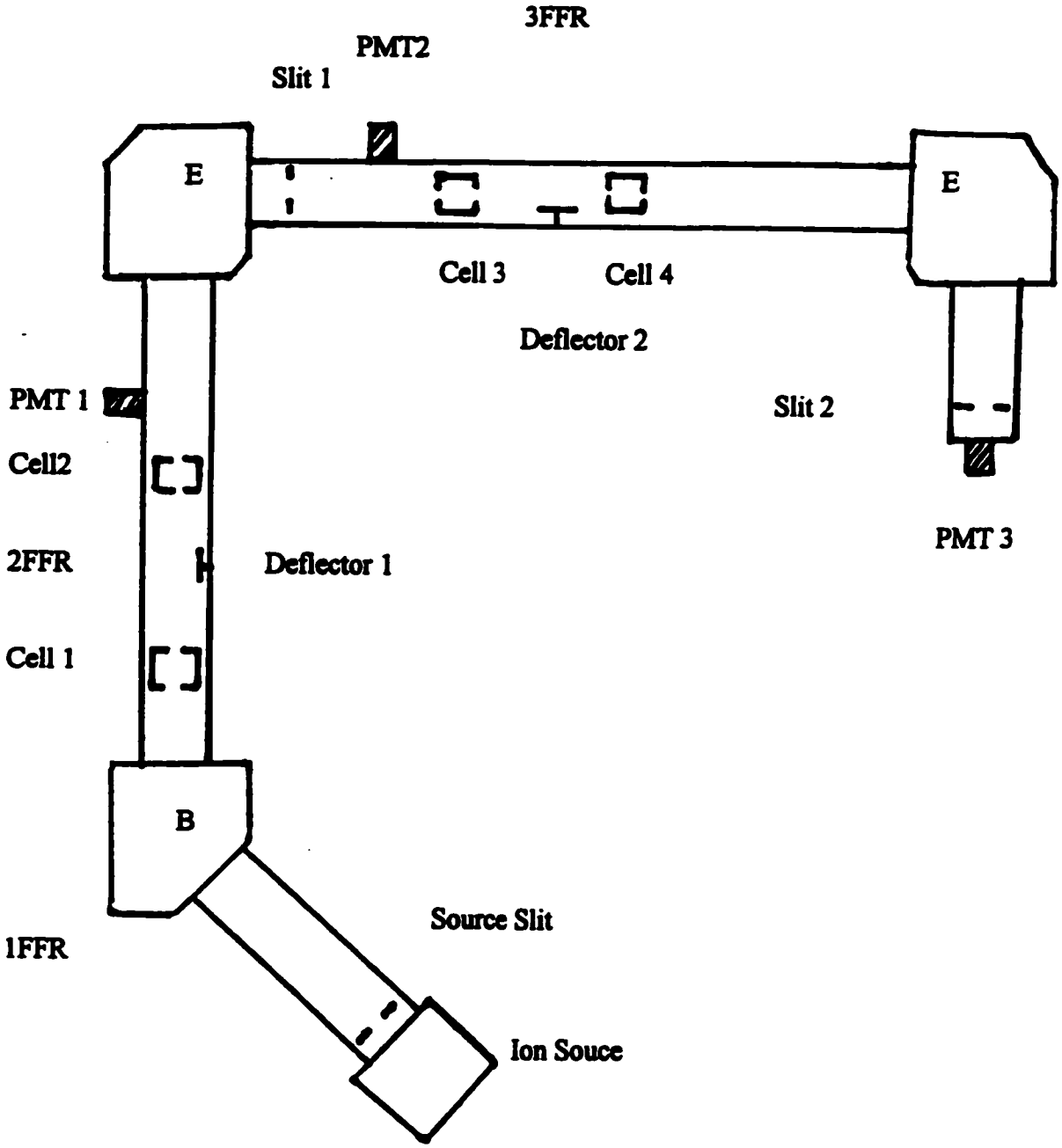

gaseous compounds to be admitted directly into the source. The second was the septum inlet which consisted of an inner glass capillary apparatus that was heated to 180 °C and into which non-viscous liquids could be injected via a syringe. The liquids would then be volatilized and entered the ion source in a gaseous form. Lastly, was the Granville-Philips inlet system which consisted of an external glass line that fed directly into the ion source via a capillary leak. The opposite end consisted of a detachable glass bulb; an ice bath maintained the temperature of the liquid or volatile solid contained within at $\approx 0\ ^{0}C$.

Pirani ion gauges monitored the gas pressures throughout the mass spectrometer (i.e., in the ion source, the sample inlets, and the collision cells). The beam of fast positive ions impinged upon a plate at –5 kV, and thus was annihilated. During the process, the released electrons were accelerated onto a scintillator plate (which upon electron impact emitted photons). Three photomultiplier tubes (PMT1, PMT2, and PMT3, see Figure 1.3) measured the emitted photons, which amplified the signal by $\approx 10^{6}$ (the resultant intensity was displayed on the oscilloscope of the ZAB control console).

On inspection of Figure 1.3, one will now trace the path of the molecular ion $M_1^{+\bullet}$ through the mass spectrometer. Upon ionization of M_1 in the ionization source $M_1^{+\bullet}$ exits into the first field-free region, 1FFR, with an acceleration voltage of V_{acc}. The $M_1^{+\bullet}$ passes through the (beam defining) source slit and enters the mass selecting magnetic sector, B. On passing through the magnetic sector $M_1^{+\bullet}$ enters the second field-free region, 2FFR, which contains collision cells 1 and 2 with deflector 1 sandwiched between them, after which comes PMT1. To collect a normal mass spectrum of $M_1^{+\bullet}$, one may simply perform a mass scan of the magnetic sector B, which will be recorded in PMT1.

Next, as $M_1^{+\bullet}$ exits the 2FFR and passes through the first electric sector, E, it is energy selected and enters the third field-free region, 3FFR. The 3FFR contains the (energy resolving) slit 1, PMT2, collision cells 3 and 4 with deflector 2 sandwiched in between them. To collect a MI, CID, or NR 2FFR mass spectrum, as well as a $T_{0.5}$ measurement, one may mass select $M_1^{+\bullet}$ with the magnetic sector, transmit it through the2FFR and perform an energy scan of the first electric sector E, which will be recorded by PMT2.

Finally, as $M_1^{+\bullet}$ exits the 3FFR and passes through the second electric sector, E, it is energy selected and enters into the fourth field-free region, 4FFR, which contains the (energy resolving) slit 2, and PMT3.

Now that the components of the three sector VG ZAB-3F (BEE) mass spectrometer have been illustrated, one will now specifically discuss the function of the ion source, the magnetic analyzer (i.e., the magnetic sector), and the electrostatic analyzer (i.e., the electric sector).

The Ion Source

The ion source consists of an electrically insulated hollowed out source block, containing a small inner ionization chamber, into which the neutral M_1 species is leaked and then ionized via electron impact;

$$M_1 + e^- \rightarrow M_1^{+\bullet} + 2e^-$$

The process is rapid (10^{-16} s) and is considered to be a vertical Franck-Condon process (see section 1.2.1). The source block is kept at a constant electric voltage, known as the accelerating voltage V_{acc}, whose standard value is 8000 V (i.e., 8 kV). The source of electrons is a tungsten alloy filament placed in front of a small aperture. An electric current passed through the

filament heats it and causes the ejection of free electrons into the ionization chamber. The electrons are then drawn towards the trap (anode) on the other side of the ionization chamber. As a result, the electrons are forced through the central space of the ion source in travelling 15 to 20 mm from the filament to the trap. A pair of small magnets generate a weak magnetic field that causes the electrons to follow a helical path of a small diameter. This is to increase the probability of interaction with the neutral M_1 molecules.

The filament can be set at an electric potential below (e.g., 7930 V) that of the source block (e.g., 8000 V) and this difference (e.g., 70 V) determines the translation kinetic energy of the electrons (e.g., 70 eV). The standard electron energy used in the electron impact source is 70 eV. Since most hydrogen containing organics have IE value of ≈ 8–10 eV, and their perfluorinated organics have IE values ≈ 10–12 eV, the excess energy (of the 70 eV) may contribute to the internal energy of the $M_1^{+\bullet}$ radical-cations. Thus, the $M_1^{+\bullet}$ radical-cations with enough internal energy may then undergo the fragmentation process in the ion source;

$$M_1^{+\bullet} \rightarrow M_2^{+} + M_3^{\bullet}$$

Now, any positive ions (e.g., $M_1^{+\bullet}$, M_2^{+}, etc.) produced in the ion source shall be forced out of the ion source, via a repeller (at about 8010 V), placed under the electron path, and under the exit slit. Upon passing through the exit slit, the ions enter the acceleration zone, located between the ion source block (at 8000 V) and a grounded pair of plates (at 0 V), close to the block. Therefore, over a very small region of space all ions fall through the very large electric potential gradient of V_{acc} (i.e., 8000 V) and are accelerated to a translational kinetic energy, E_{trans}, expressed as follows;

$$E_{trans} = mv^2/2 = zV_{acc}$$

where m, v, and z, denote the mass velocity, and charge of the ion, respectively. Thus one may note that all ions, regardless of mass receive the same E_{trans} on exiting the source.

The Magnetic Analyzer

On inspection of Figure 1.3, the magnetic analyzer separates the 1FFR and 2FFR. The magnetic analyzer (i.e., the magnetic sector) separates ions according to their m/z, values via their momentum. Positive ions that pass through a magnetic field of magnitutde, B, perpendicular to their path of motion, will travel in a circular arc in a plane and this path may be expressed as follows;

$$mv^2/r_B = zvB$$

where r_B denotes the radius of the flight tube. Therefore the momentum to charge ratio, mv/z, may be expressed as follows;

$$mv/r_B = zB$$

One may note that ions of different mass, but possessing the same E_{trans}, originating from the same point, shall therefore follow different trajectories through a stationary magnetic field. Thus, for given values of magnetic field strength, B, only ions with a selected m/z value will traverse successfully the allowed trajectory along the circular path of the magnetic analyzer (i.e., along r_B). Thus, on substitution of $E_{trans} = mv^2/2 = zV_{acc}$ into the previous equation, one obtains the following;

$$m/z = (r_B^2 B^2)/(2V_{acc})$$

for the allowed trajectory at the selected m/z value. The standard units for m, z, r_B, B, and V_{acc} are the kilogram, coulomb, metre, tesla, and volt, respectively.

At this point, the characteristics of the metastably generated ions in the 1FFR, prior to entering the magnetic analyzer deserve mention. When the parent $M_1^{+\bullet}$ ion fragments into $M_2^+ + M_3^\bullet$ the law of conservation of momentum dictates that the total momentum of $M_1^{+\bullet}$ is proportionally partitioned between M_2^+ and $M_3^\bullet$. As well the velocity of M_2^+ is unchanged the following expression holds;

$$E_{trans} = (1/2)m_2v_1^2 = (1/2)m_2\left(\frac{m_2}{m_1}\right)v_2^2 = (1/2)\left(\frac{(m_2)^2}{(m_1)}\right)v_2^2$$

Therefore, the M_2^+ ion metastable generated in the 1FFR appears in the magnetic analyzer at a non-integral effective mass, m^*, expressed as follows;

$$m^* = (m_2)^2/(m_1)$$

The Electrostatic Analyzer

On inspection of Figure 1.3, one may see there are two electrostatic analyzers; the first one separates the 2FFR from the 3FFR, and second one separates the 3FFR from the 4FFR. The electrostatic analyzer separates ions according to their translational energy to charge ratios. The equation of motion for the circular arc of an ion in an electric field of magnitude, E, is expressed as follows;

$$mv^2/r_E = zE$$

where r_E denote the radius of the circular path and the electric field E is in units of volt/meter. Thus, the translational energy to charge ratio may be expressed as follows;

$$mv^2/z = r_EE$$

At this point, the characteristics of the metastably generated ions in the 2FFR, prior to entering the first electrostatic analyzer deserve mention. When the parent ion $M_1^{+\bullet}$ fragments

ion $M_2^+ + M_3^\bullet$, the law of conservation of momentum dictates that the momentum of $M_1^{+\bullet}$ is proportionally partitioned between $M_2^+ + M_3^\bullet$. Thus, one has the following;

$$(m/z)_{fragment} = (V_{fragment}/V_{parent}) \bullet (m/z)_{parent}$$

where $V_{fragment}$ and V_{parent} denote the observed sector voltages (i.e., energies) which transmit the fragment, and the parent (i.e., V_{acc}), respectively. Thus, one may determine the effective mass of fragment by dividing its observed voltage by the accelerating voltage, and then multiplying by the mass of the parent.

Now, one will discuss the experimental techniques of the kinetic energy release, $T_{0.5}$, measurement, the metastable ion (MI), collision induced dissociation (CID), and the neutralization-reionization (NR) mass spectra.

Kinetic Energy Release ($T_{0.5}$) Measurement

Now, the two mass spectral peaks for M_1^+ and M_2^+, with masses of m_1 and m_2, each of equal peak height, H, are considered to be adequately resolved if the height of their background overlap, h, is less than or equal to 10 % (i.e., $h/H \leq 0.10$). The mass resolution is defined by $R = m/\Delta m$, where m is the nominal (unit) mass and $\Delta m = m_2 - m_1$ is the actual difference between the masses. For example, $CO^{+\bullet}$ and $N_2^{+\bullet}$ have m/z values of 27.994915 and 28.006148 respectively, may be separated by a resolution, R, expressed as follows,

$$R = (28)/((28.006148) - (27.994915)) = 2493$$

As well, in terms of energy resolution, ΔE, is taken the full width at half height (i.e., the width at H/2) of the peak measured in the electrostatic analyzer.

Now, when the parent ion $M_1^{+\bullet}$ undergoes the fragmentation process, $M_1^{+\bullet} \rightarrow M_2^+ + M_3^\bullet$, some of the excess internal energy of the transition state (non-fixed excess internal energy,

ε^{*}), and the reverse activation energy ε_0^{r} (see Figure 1.1), will released as translational kinetic energy. This shall result in the broadening of the metastable fragment ion M_2^+ peak. The degree of the broadening of the peak depends of the magnitudes of ε^{*} and ε_0^{r} for the dissociation.

The kinetic energy release $T_{0.5}$ measurements are commonly reported in terms of their peak width at half height. Thus, for the metastable dissociation $M_1^{+\bullet} \rightarrow M_2^+ + M_3^{\bullet}$, the $T_{0.5}$ measurement associated with the metastable fragment ion M_2^+ peak may be expressed as follows;

$$T_{0.5} = \frac{1}{16}\left(\frac{(m_1)^2}{(m_2)(m_3)^2}\right)\left(\frac{(\Delta E_2)^2-(\Delta E_1)^2}{V_{acc}}\right)$$

where m_1, m_2, m_3, ΔE_1, ΔE_2, and V_{acc} denote the masses of $M_1^{+\bullet}$, M_2^+, $M_3^{\bullet}$, the peak widths at half height for the main beam $M_1^{+\bullet}$, the metastable M_2^+ peak, and the accelerating voltage, respectively. The $T_{0.5}$ values are quoted in units of meV. As well, *low* $T_{0.5}$ values (e.g., about 10 meV and less) are generally associated with *direct bond scission*, whereas high $T_{0.5}$ values (e.g., on the order of $\approx$ 100 meV) are generally associated with a *rearrangement* occurring before fragmentation.

The conditions of high resolution for the $T_{0.5}$ measurements are facilitated via the narrowing of the source slit and slit 1 (see Figure 1.3), such that the intensity of the main ion beam is reduced about 50% in intensity for each slit. This typically results in ΔE values of less than or equal to 4 eV.

In addition to the above $T_{0.5}$ values, under conditions of high resolution one may also gain information from the peak shapes. There are general types of peak shapes known as; (I) Gaussian, (II) Flat and Dish-topped, and (III) composite.

ε^*), and the reverse activation energy ε_0^r (see Figure 1.1), will released as translational kinetic energy. This shall result in the broadening of the metastable fragment ion M_2^+ peak. The degree of the broadening of the peak depends of the magnitudes of ε^* and ε_0^r for the dissociation.

The kinetic energy release $T_{0.5}$ measurements are commonly reported in terms of their peak width at half height. Thus, for the metastable dissociation $M_1^{+*} \rightarrow M_2^+ + M_3^\bullet$, the $T_{0.5}$ measurement associated with the metastable fragment ion M_2^+ peak may be expressed as follows;

$$T_{0.5} = \frac{1}{16}\left(\frac{(m_1)^2}{(m_2)(m_3)^2}\right)\left(\frac{(\Delta E_2)^2-(\Delta E_1)^2}{V_{acc}}\right)$$

where m_1, m_2, m_3, ΔE_1, ΔE_2, and V_{acc} denote the masses of M_1^{+*}, M_2^+, $M_3^\bullet$, the peak widths at half height for the main beam M_1^{+*}, the metastable M_2^+ peak, and the accelerating voltage, respectively. The $T_{0.5}$ values are quoted in units of meV. As well, *low* $T_{0.5}$ values (e.g., about 10 meV and less) are generally associated with *direct bond scission*, whereas high $T_{0.5}$ values (e.g., on the order of $\approx$ 100 meV) are generally associated with a *rearrangement* occurring before fragmentation.

The conditions of high resolution for the $T_{0.5}$ measurements are facilitated via the narrowing of the source slit and slit 1 (see Figure 1.3), such that the intensity of the main ion beam is reduced about 50% in intensity for each slit. This typically results in ΔE values of less than or equal to 4 eV.

In addition to the above $T_{0.5}$ values, under conditions of high resolution one may also gain information from the peak shapes. There are general types of peak shapes known as; (I) Gaussian, (II) Flat and Dish-topped, and (III) composite.

The (I) Gaussian peaks are symmetric and may be roughly approximated by a triangle. They are generally associated with small $T_{0.5}$ values.

The (II) Flat and Dish-topped peaks are very wide and have large $T_{0.5}$ values. The observed dish is instrument dependent and results from Z-axial discrimination against the ion beam by one or more of the resolving slits.

The (III) composite peaks generally have a narrow (Gaussian) peak atop a wide hump background (Flat-topped) and are an indication of the production of more than one isomeric ions and/or the presence of more than one transition state. For example, the metastable CF_3^+ peak for the $C_2F_3O^+ \rightarrow CF_3^+ + C{\equiv}O$ dissociation reaction possesses a *composite* shape (see Chapter 3, $C_2F_3O^+$ (m/z 97) section). The narrow component may be proposed to be associated with the *direct bond scission* $CF_3{-}C{\equiv}O^+ \rightarrow CF_3^+ + C{\equiv}O$ process. However, the wide hump background component may be proposed to be associated with the *rearrangement* $^+CF_2{-}CF{=}O \rightarrow CF_3^+ + C{\equiv}O$, and $CF_2{=}C^+{-}OF \rightarrow CF_3^+ + C{\equiv}O$ processes.

Metastable Ion (MI) Mass Spectra

The metastable ion (MI) mass spectra result from the spontaneous dissociation process illustrated below;

$$M_1^{+\bullet} \rightarrow M_2^+ + M_3^\bullet$$

The MI 2FFR mass spectra were recorded by mass selecting the parent ion $M_1^{+\bullet}$, transmitting it into the 2FFR, and scanning the first electrostatic analyzer from low voltages to just below V_{acc}. As with all energy scans, the masses of fragment ions were determined by dividing their observed voltage by V_{acc} and multiplying it by the mass of the parent-ion.

Collision Induced Dissociation (CID) Mass Spectra

The collision induced dissociation (CID) mass spectra were obtained by admitting collision gas, G_1, into a collision cell in the projectile-ion $M_1^{+\bullet}$ beam path. A non-momentum energy transfer collision event between $M_1^{+\bullet}$ and G_1 may occur, and converts some amount of the translational energy of $M_1^{+\bullet}$ into internal energy, thus opening up other dissociation processes as expressed below;

$$M_1^{+\bullet} + G_1 \rightarrow M_2^{+} + M_3^{\bullet} + G_1$$

The collision gas pressures generally utilized here were those sufficient to create single collision conditions (i.e., ≈ 90%T beam transmission).

The CID mass spectra may be collected for source and metastably generated ions. If the metastably and source generated CID mass spectra of an ion are the same, one may propose that they represent the same ion structure (see section 1.2.1).

The source generated (CID) 2FFR mass spectra were recorded by mass selecting the parent ion $M_1^{+\bullet}$, transmitting it into the 2FFR with G_1 present in cell 1, and the first electrostatic sector performing an energy scan.

The metastably generated (CID) mass spectra may be recorded in one of two ways. Firstly, the metastable dissociation ($M_1B^{+\bullet} \rightarrow M_1^{+\bullet} + B$) may occur in the 1FFR. The magnetic sector can transmit $M_1^{+\bullet}$ into the 2FFR at the non-integral effective of mass of $m^* = (m[M_1^{+\bullet}])^2/(m[M_1B^{+\bullet}])$. For example, the 1FFR metastably generated $C_2F_4^{+\bullet}$ ion, from the $C_3F_6^{+\bullet} \rightarrow C_2F_4^{+\bullet} + CF_2$ dissociation, may be transmitted to the 2FFR at an effective mass of $m^* = (100)^2/(150) = 66.7$. Secondly, the metastable dissociation ($M_1B^{+\bullet} \rightarrow M_1^{+\bullet} + B$) may occur in the 2FFR. The first electrostatic analyzer may transmit the fragment ion $M_1^{+\bullet}$ into the 3FFR at a voltage of $V[M_1^{+\bullet}] = (m[M_1^{+\bullet}])/(m[M_1B^{+\bullet}])\bullet V_{acc}$. In the 3FFR with G_1 present in cell 3, the

CID mass spectra may be recorded by the second electrostatic energy analyzer performing an energy scan from low values to just below V[$M_1^{+\bullet}$].

Neutralization-Reionization (NR) Mass Spectra

The neutralization-reionization (NR) mass spectra were obtained by admitting neutralization gas into a collision cell in the projectile-ion $M_1^{+\bullet}$ beam path. In addition to collisional excitation, there is some charge exchange between $M_1^{+\bullet}$ and G_1, resulting in $G_1^{+\bullet}$ and the neutralization of $M_1^{+\bullet}$ into M_1 (and its fragments $M_2^{\bullet} + M_3^{\bullet}$, etc.). Next, a deflector with a strong positive voltage (i.e., + 1000 V) deflects all positive ions from the beam path allowing only the neutral species (i.e., M_1, $M_2^{\bullet}$, $M_3^{\bullet}$, etc.) to be transmitted into a second collision cell containing the reionization gas, G_2. There the neutral M_1 species is collisional reionized into $M_1^{+\bullet}$ (and its fragments $M_2^{+} + M_3^{\bullet}$, etc.). The neutralization (N) and reionization (R) steps are expressed below;

$$M_1^{+\bullet} + G_1 \rightarrow M_1 + G_1^{+\bullet} \qquad ; (N)$$

$$M_1 + G_2 \rightarrow M_1^{+\bullet} + G_2 + e^{-} \qquad ; (R)$$

The neutralization and reionization target gas pressures utilized here were those sufficient to create single collision conditions (i.e., ≈ 90% T beam transmission) for each step. The usual neutralization gas used here was Xe, and the reionization gas was O_2.

As was the case with the CID mass spectra, if the metastably and source generated NR mass spectra of an ion are the same, one may propose that they represent the same ion structure.

The metastably and source NR mass spectra are collected in the same fashion as the CID mass spectra were, except now the energy scan must in each case go somewhat past the expected position of the $M_1^{+\bullet}$ parent-ion so that one may observe the recovery signal.

The *absence* of a recovery signal may be due to two possibilities. Firstly, the geometry differences between $M_1^{+\bullet}$ and M_1 may be so great that upon vertical neutralization no stable M_1 is produced (i.e., only its fragments $M_2^{\bullet} + M_3^{\bullet}$, etc.). Secondly, some stable neutral M_1 may have been upon vertical neutralization and survived the trip from the neutralization cell to the reionization cell intact, only to undergo dissociative vertical reionization.

A more conclusive observation is the *presence* of a (strong) recovery peak for $M_1^{+\bullet}$ in the NR mass spectrum. This may be interpreted as the successful production of the M_1 neutral in the neutralization step, such that it is a stable species with a lifetime on the order of the transit time between the neutralization and reionization cells (i.e., $\approx$ 1μs). For example, presented in Chapter 4, via the NR spectra of $CF_2{=}C{=}O^{+\bullet}$ produced from ionized $CF_2{=}CFOCF_3$, the presence of a recovery signal for $CF_2{=}C{=}O^{+\bullet}$ (m/z 78) was interpreted as representing the first direct experimental observation of the elusive neutral perfluoroketene, $CF_2{=}C{=}O$, as a stable species.

1.3 References

[1] S.G. Lias, J.F. Liebman, J.L. Holmes, R.D. Levin, and W.G. Malland, J. Phys. Chem. Ref. Data, 17, (1988).

[2] M.W. Chase, Jr., NIST-JANAF Thermochemical Tables, 4th Ed., J. Phys. Ref. Data Monogr., 9, (1998).

[3] H.E. O'Neal, and S.W. Benson, Natl. Stand. Ref. Data Ser. Natl. Bur. Stand., 21, (1970).

[4] S.W. Benson, and J.H. Buss, J. Chem. Phys. 29(3), 546-572, (1958).

[5] N. Cohen, and S.W. Benson, Chem. Rev., 2419-2438, (1993).

[6] S.W. Benson, F.R. Cruickshank, D.M. Golden, G.R. Haugen, H.E. O'Neal, A.S. Rodgers, R. Shaw, and R. Walsh, Chem. Rev., 29, 279-324, (1969).

[7] S.W. Benson, Thermochemical Kinetics, 2nd,John Wiley and Sons, New York, New York, USA, (1976).

[8] H.E. O'Neal, and S.W. Benson, J. Phys. Chem., (6)72, 1866-1877, (1968).

[9] J.T. Watson, Introduction to Mass Spectrometry, 2nd Ed., Raven Press, New York, New York, USA, (1985).

[10] R.G. Cooks, J.H. Beynon, R.M. Caprioli, and R.R. Lester, Metastable Ions, Elsevier, Amsterdam, (1973).

[11] C.F. Clark, Ed., Encyclopedia of Spectroscopy, Reinhold, New York, New York, USA, pp. 628-647, (1960).

[12] W.A. Chupka, J. Chem. Phys., 30(1), 191-211, (1959).

[13] H.M. Rosenstock, M.B. Wallenstein, A.L. Wahrhafig, and H. Eyring, Proc. Natl. Acad. Sci. U.S., 38, 667, (1952).

[14] J.A. Hipple, and E.U. Condon, Phys. Rev., 68, 54, (1945).

[15] W.A. Hadden, and F.W. McLafferty, J. Am. Chem. Soc., 90, 4745, (1968).

[16] K.R. Jennings, Int. J. Mass Spectrom. Ion Phys., 1, 227, (1968).

[17] P.C. Burgers, and J.L. Holmes, Int. J. Mass Spectrom. Ion Proc., 58, 15, (1984).

[18] J.L. Holmes, and J.K. Terlouw, Org. Mass Spectrom., 15(8) 383-396, (1980).

[19] J.L. Holmes, Org. Mass Spectrom., 20(3), 169-183, (1985).

[20] (a) C. Wesdemiotis, and F.W. McLafferty, Chem. Rev., 87, 405, (1985).

(b) J.K. Terlouw, and H. Schwarz, Angew. Chem. Int. Ed. Engl., 26, 805, (1987).

(c) J.L. Holmes, Mass Spectrom. Rev., 8, 513, (1989).

Chapter 2 Collision-Induced Emission Spectroscopy of Small Polyatomic Molecules

2.1 Introduction

This chapter will discuss the optical emissions observed in the ultraviolet-visible-near infrared (UV-VIS-NIR) 190-1020nm Collision-Induced Emission (CIE) spectra that monitored the collision encounter between a fast moving (8 keV) projectile-ion, $M_1^{+\bullet}$, and a stationary target gas, G_1. The analysis of the optical emissions of the $M_1^{+\bullet}/G_1$ encounter is quite complex. This process involves the consideration of the gas-phase ion-chemistry of $M_1^{+\bullet}$ and G_1 given in the standard thermochemical data compilations [1-3], Bensons Rules of Additivity [4-8], the underlying mass spectrometry [9-20], previous CIE studies [21-25], the Wigner-Witmer Correlation Rules [26-30], the electronic spectroscopy and emission spectroscopy [31-42], and the photoelectron spectroscopy [29, 30, 43-61].

The stationary target gases utilized here were He [31, 33, 36, 37, 43], Ar [31, 33, 38, 62-66], and O_2 [29-31, 34-37, 67, 68, 70]. The fast moving projectile-ions studied here were $N{\equiv}N^{+\bullet}$ [29-31, 34-37, 40, 43, 69-75], $C{\equiv}O^{+\bullet}$ [29-31, 34-36, 40, 43, 71, 76-79], $O{=}C{=}O^{+\bullet}$ [29-31, 34-36, 40-43, 75, 80-90], and $O{=}C{=}C{=}O^{+\bullet}$ [29-31, 34-36, 40-43, 91-114].

The original aim of this project was to extend the CIE technique, based on the pervious work of Holmes et. al. [21-25], to large polyatomic molecules. The parent-ion and neutral emission for the N≡N, C≡O, and O=C=O species studied here were observed, however those for the O=C=C=O species were not. In addition, the parent-ion emissions for the aromatic species, benzene C_6H_6, perfluorobenzene C_6F_6, and furan C_4H_4O were not observed here, via the CIE technique. Specifically, for the C_6F_6 case this was surprising as the $C_6F_6^{+\bullet}[\tilde{B}\,^2A_{2u} \rightarrow \tilde{X}\,^2E_{1g}]$ emission has been previously observed by Maier et. al. [32,

115], and possessed a strong intensity over a wide wavelength range. Thus, the inability to realize the goal of extending the CIE technique to large polyatomics may be proposed to be a result of the large amounts of internal energy, E_{int}, that were deposited in $M_1^{+\bullet}$ travelling at 8 keV, thus favouring dissociation over emission. This will be further discussed and some modifications to the present CIE experiment suggested later in section 2.6.

2.1.1 Collision-Induced Emission (CIE) Spectrscopy Experimental

All of the gases utilized in these experiments for the projectile-ions $N{\equiv}N^{+\bullet}$, $C{\equiv}O^{+\bullet}$, and $O{=}C{=}O^{+\bullet}$, and the stationary target gases He, Ar, and O=O, were of the chemically pure grade (> 99%). The $O{=}C{=}C{=}O^{+\bullet}$ projectile-ion was obtained from the oxalyl choride $(Cl\text{-}C{=}O)_2$ parent (purity 99%) and was used as received.

All of the CIE spectra, from 190-1020 nm, were obtained under single collision conditions (i.e., ≈ 90%T)[18-20] to maximize the probability of the observation parent ion/neutral emissions. The CIE spectra were observed in a collision cell (denoted as the observations cell (OC)) in the 3FFR of the VG-ZAB 3F mass spectrometre (see Figure 2.1). On top of the OC cell there was a quartz window (fused silica-WU Optikon Corp. Waterloo Ontario, Canada) that allows the optical emissions to enter the entrance slit of the scanning wavelength monochromator (Acton Spectra Pro 275, 275 cm focal length, 1200 groove/mm holographic grating) and acted to wavelength resolve the light. The entrance slit was set at a value of 2000 μm to obtain a compromise between an experimentally usable signal intensity and a moderate wavelength resolution (i.e., an average uncertainty of $\lambda \pm 0.5$ mn). A liquid nitrogen cooled ($t_c = -120^0C$) charge-couple device (CCD) camera (LN/CCD-1152 EUV, 152 x 298

Figure 2.1 The Collision-Induced Emission (CIE) Experimental Set Up of the VG-ZAB-3FMagnetic Sector/Electric Sector/ Electric Sector (BEE) Tandem Mass Spectrometer

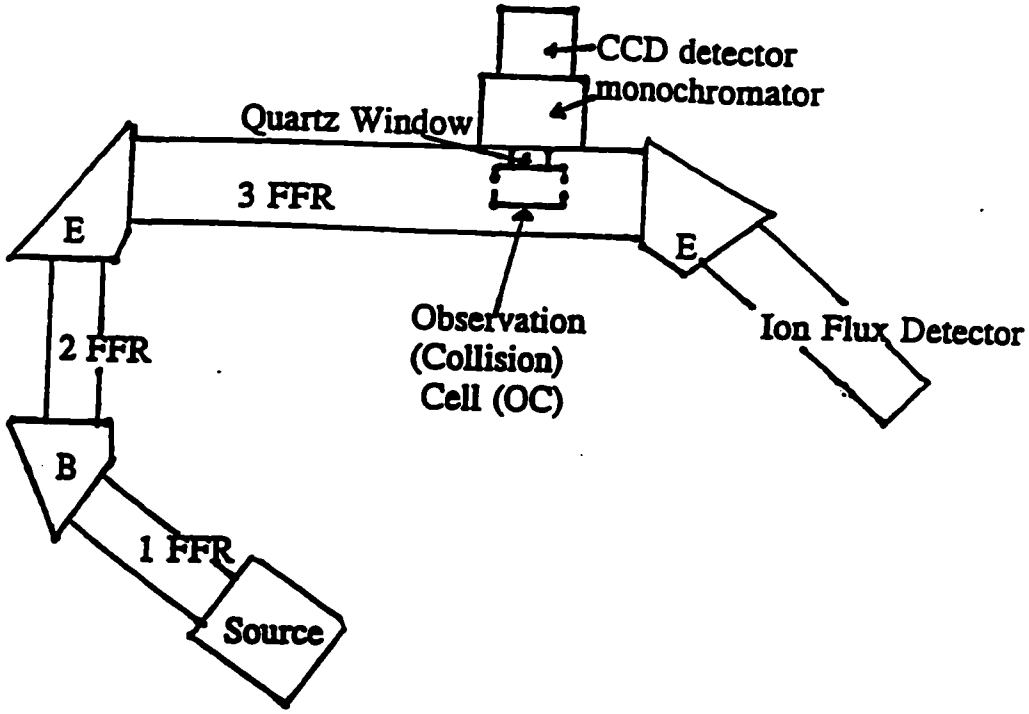

Typical CID-CIE Experimental Conditions

Electron Energy	: ≈60 eV
Acceleration Voltage	: 8 keV
Source Gas Pressure	: ≈10^{-5} Torr
Target Gas Pressure	: ≈10^{-7} Torr
Beam Transmission	: ≈90 %T
Source Ion Slit	: EI Slit
CCD Dewar Temperature	: -120°C
Monochromator Slitwidth	: 2000 μm
Wavelength Range	: 190-1020 nm
Wavelength Regions	: Fourteen, 70 nm sections
Accumulations	: one 30 min (i.e., 1/2 hour/section)

pixels, 190-1080 nm range, Princeton Instruments, Trenton, N.J., USA) was placed atop the exit slit of the monochromator and used to detect the optical emissions.

The optical emissions from 190-1020 nm were recorded in 14 sections, each ≈ 70 nm in width, for an accumulation of 30 minutes (i.e., a 7 hour total accumulation time per CIE spectrum). The optimal emissions were digitally recorded utilizing the CSMA program provided by Princeton Instruments. Each of the 14 sections were background subtracted from a background subtraction file (centred at 225 nm and ≈ 70 nm wide) which was recorded under "dark conditions" (i.e. an empty collision cell, with the ion gauges in the 3FFR turned off). Additionally each section underwent a cosmic background subtraction step to remove any signal spikes. The next step was to convert all of the digital data in the 14 sections by the CSMA program into ASC II format for export.

The converted ASC II files of the 14 sections were then imported into and processed by an Excel 95 macro called delete.xls from Microsoft Office 95. The Excel 95 macro consisted of three parts. The first part of the macro dealt with the first 7 sections of data in the UV-VIS range of 190-650 nm (each centred on 225, 295, 365, 435, 500, 560 and 620 nm respectively). The macro reads the first section and deletes every second point of data. Then it reads the second section of data, deletes every second point of data, and then joins it to the first section and averages any overlap. This process is sequentially repeated until a continuous CIE spectrum was produced from 190-650 nm. The second part of the macro dealt with the last 7 sections of data in VIS-NIR range of 650-1020 nm (each centred on 680, 740, 795, 845, 945, and 995 nm respectively). It performed the same operations as the data of the first part, until a continuous CIE spectrum from was produced from 650-1020 nm. The third part of the macro read the data from the 190-650 nm range and deleted every second point of data. It then read the

data in the 650-1020 nm range, deleted every second part of data. Then it joined the 190-650 nm range to the 650-1020 nm range (averaging any overlap), thus producing a continuous UV-VIS-NIR 190-1020 nm CIE spectrum. The Y-axis was presented in units of intensity (ion-counts) and the X-axis was presented in units of wavelength, λ(nm), and consisted of $\approx$ 4000 data points (Excel 95 cannot display more than 4000 data points).

The liquid nitrogen dewar jacket surrounding the CCD chip in the camera was maintained at a temperature of $t_c = -120$ °C to obtain an extremely low dark current (i.e., an absolutely flat baseline) with an experimentally usable signal intensity. The CCD camera is a very sensitive device that detects photons striking its chip surface, which are then converted into an electric current and a digital signal. Thus the standard 3 to 1 ratio of signal to background is circumvented here and one-count above baseline can be taken as a valid datum. (However, the CCD camera is very sensitive to background cosmic radiation, e.g. solar flares, so that it is experimentally fruitless to obtain a usable background on days of such activity).

The wavelength scale (the X-axis) was calibrated using the CSMA program. The entrance slit of the monochromater was set at 50 μm and fitted with a pinhole aperture. A mercury lamp was placed in line with the aperture and the whole apparatus (i.e., the mercury lamp, the monochromater, and the CCD camera) was completely covered by a large thick black cloth to block out all room light. The wavelength scale (the X-axis) was then standardized (from 190-1020 nm) using the CSMA program with the Hg (I) wavelengths of 253.652 nm and 1013.975 nm (R.C. Weast. Ed., Handbook of Chemistry and Physics, 67th Ed., (1986-1987), CRC Press, Boca Raton, Florida, U.S.A., p. E257 (1987)) used as the standard reference.

After wavelength standardization, the camera was centred over the quartz window above the OC cell. This was accomplished by setting the monochromator wavelength to 0 nm (i.e., no

wavelength resolution, allowing the grating to act as a window and letting all wavelengths to enter), and with the monochromater slits at 3000 μm (fully open)). The CCD camera was then slowly moved back and forth across the quartz window (the emission axis) until a square shaped signal of maximum intensity from the background emission from the 3FFR ion gauge was obtained. The camera was then firmly secured to the 3FFR region of the VGZAB-3F mass spectrometer and covered with a large thick black cloth to block out all room light.

It should be noted that during the collection of the CIE spectra, the ion-gauge in the 3FFR must be turned off. As well, due to the build up of vacuum pump oil on the quartz window and on the inner polished surface of the entrance and exit slits of the OC cell, [21-25], one should clean them about every four to six months.

Next, to achieve an experimentally usable ion-flux a constant source gas pressure reading of $\approx 10^{-5}$ Torr should be used, as well as an amplifier setting of 10^{-7}/1 and photo multiplier setting in the 2FFR and 3FFR of $\approx$ 0.40 - 0.80 (the loss in the ion-flux from the 2FFR to the 3FFR cannot be more than $\approx$ 10 %). The target gas pressure readings are typically on the order of $\approx 10^{-7}$ Torr, and results in a beam reduction of 10% (i.e., a beam transmission $\approx$ 90 %T). Under these (constantly maintained) conditions, the background subtracted total-ion emission count (i.e. undispersed at $\lambda = 0$ nm) spectrum must have an intensity of greater than 500 counts per a 30 minute accumulation time in order to obtain an experimentally observable CIE spectrum.

Thus, the CIE experiment is steady-state measurement on a large ensemble of molecules, rather than a transient measurement of a single event. Therefore, all things being equal, during the 30 minute accumulation time, an emitting excited electronic state with a nanosecond (ns) radiative lifetime would emit more often and thus would be more intense than

those of microsecond (μs), and millisecond (ms) radiative lifetimes, respectively. As well the intensity of the total-ion count for the target gases He, Ar, and O_2 is 1 : 1.5 : 3 , respectively.

At this point, one should emphasize that after M_1 is ionized into $M_1^{+\bullet}$ it spends roughly 1μs in the source; once $M_1^{+\bullet}$ exits the source at 8 keV, it takes a transit time of the order of ≈ 10^1–10^2 μs to reach the OC cell. Thus, in the absence of the stationary target gas G_1 in the OC cell, essentially one should expect all of the $M_1^{+\bullet}$ species to be in their *ground electronic state and thus no emission should be observed.*

For the $N{\equiv}N^{+\bullet}$ species, the radiative lifetimes, τ_{rad}, are as follows; $\tau_{rad}[\tilde{B}\,^2\Sigma_u^+] \approx 70$ ns and $\tau_{rad}[\tilde{A}\,^2\Pi_u] \approx 17$ μs, for the $\tilde{B}\,^2\Sigma_u^+ \rightarrow \tilde{X}\,^2\Sigma_g^+$ and $\tilde{A}\,^2\Pi_u \rightarrow \tilde{X}\,^2\Sigma_g^+$ transitions, respectively [69, 72, 75]. For the $C{\equiv}O^{+\bullet}$ species, the radiative lifetimes, τ_{rad}, are as follows; $\tau_{rad}[\tilde{B}\,^2\Sigma^+] \approx 50$ ns and $\tau_{rad}[\tilde{A}\,^2\Pi] \approx 4$ μs, for the $\tilde{B}\,^2\Sigma^+ \rightarrow \tilde{X}\,^2\Sigma^+$, and $\tilde{A}\,^2\Pi \rightarrow \tilde{X}\,^2\Sigma^+$ transitions, respectively [75, 76, 78, 79]. For the $O{=}C{=}O^{+\bullet}$ species, the radiative lifetimes, τ_{rad}, are as follows: $\tau_{rad}[\tilde{B}\,^2\Sigma_u^+] \approx 145$ ns, and $\tau_{rad}[\tilde{A}\,^2\Pi_u] \approx 120$ ns for the $\tilde{B}\,^2\Sigma_u^+ \rightarrow \tilde{X}\,^2\Pi_g$, and $\tilde{A}\,^2\Pi_u \rightarrow \tilde{X}\,^2\Pi_g$, transitions, respectively [75, 85]. However, for the $O{=}C{=}C{=}O^{+\bullet}$ species, there are no known radiative lifetime, τ_{rad}, values. Nevertheless, if one may compare by analogy this tetra-atomic species to that that of the triatomic $O{=}C{=}O^{+\bullet}$ species one may propose that the τ_{rad} values of $O{=}C{=}C{=}O^{+\bullet}$ are likely to be in the ns regime. Now with the above listed τ_{rad} values at hand, it is not surprising that in the absence of a target gas in the OO cell, there was no experimental observation of any optical emissions from the ion-beam. Thus one may conclude that all of the projectile-ions entered the OC cell in their ground electronic states (i.e., $N{\equiv}N^{+\bullet}[\tilde{X}\,^2\Sigma_g^+]$, $C{\equiv}O^{+\bullet}[\tilde{X}\,^2\Sigma^+]$, $O{=}C{=}O^{+\bullet}[\tilde{X}\,^2\Pi_g]$, and $O{=}C{=}C{=}O^{+\bullet}[\tilde{X}\,^2\Pi_u]$).

Thus, in conclusion, a protocol for the experimental criteria of the successful observation of Collision-Induced Emission (CIE) spectra for $M_1^{+\bullet}$ parent-radicals is listed below as follows;

(I) A minimum (threshold) ion concentration must be present in the observation collision cell to produce experimentally observable emissions.

(II) There must be some electric-dipole allowed electronic transitions possible for $M_1^{+\bullet}$ (e.g., predicted by photoelectron spectra, low temperature absorption spectra in a solid moble gas matrix, or ab initio SPINDO calculations).

(III) The $M_1^{+\bullet}$ species must possess emission rate constants (i.e., $k_{rad} = 1/\tau_{rad}$) that can effectively compete against non-radiative and (pre) dissociative processes.

(IV) The controlled collision conditions (single collision, 10% beam reduction, 90% T) of the projectile ion $M_1^{+\bullet}$ and the stationary target gas G_1 must be maintained throughout the collection of the dispersed (monochromated) emission spectra (i.e., constant background, identifiable excitation energy).

2.1.2 The Shapes and Characteristics of Molecular-Orbitals

This section will deal with the shapes and characteristics of the molecular-orbitals formed from the s and p atomic-orbitals [29-43] (see Appendix A and B for additional details). The analysis presented here is based on the qualitative discussion of the separability of the symmetry of the (2s)-type and (2p)-type molecular-orbital and the single-electron configurations that may be produced from them. The addition of multiple-electron configuration interaction (used in quantum-mechanical ab initio studies [30, 48-55] into the following analysis of this section and does not appreciably alter the conclusions proposed here.

Orbitals that have electron density of positive-amplitude are drawn white in colour, whereas those that have electron density of negative-amplitude are drawn black in colour. The s-orbitals are drawn as spheres, whereas the p-orbitals are drawn as double lobes, one lobe of positive-amplitude, one lobe at negative-amplitude, zero amplitude (i.e., a node) at the centre of the atom.

Next, at this point, one should discuss types of bonding in the molecular-orbitals. The qualitative types of molecular-orbitals are bonding, anti-bonding and non-bonding. Additionally, there are two main types of bonds to be discussed here. They are σ-, and π-bonds. For σ-bonds, the electron density is centred along the axis that joins the two adjacent atoms in the molecular framework. For π-bonds, the electron density is located above and below, but not along the axis joining the two adjacent atoms in the molecular framework. Now, these individual bond types are combined to make up the bonding, anti-bonding, and non-bonding orbitals. For a bonding-molecular orbital, there are constructive (i.e., additive) overlaps of electron density of positive-amplitude (denoted by white lobes) with another of positive-amplitude, or alternatively overlaps of electron density of negative-amplitude (denoted by black lobes) with another of negative-amplitude (i.e., increased electron density), plus forming an increased overlap of electron density (i.e., a bond). In contrast, for an anti-bonding molecular-orbital, there are destructive (i.e., substractive) overlaps of electron density of positive-amplitude with that of negative-amplitude, thus forming an overall absence of electron-density (i.e., a node, or anti-bond). Finally, for a non-bonding molecular-orbital, there is a gap of electron density somewhere in the molecular framework that completely separates any two regions of electron-density (i.e., of positive and negative-amplitude). This results in there being

no interaction (i.e., no additive or subtractive overlap) at all between the regions of electron-density (i.e., a non-bond).

Thus, the physical characteristics (e.g. its adiabatic ionization energy, IE_a, its heat of formation $\Delta_f H^0$, etc.) of a molecule are dictated by the symmetry of the molecular framework and the identity of the atoms in it. The atomic-orbitals merge together within the molecular framework to form the molecular- orbitals. There are two general classes of molecular-orbitals and they are known as core and valence orbitals.

Core-orbitals are basically the (1s)-type atomic-orbitals associated only with the atom on which it is centred (i.e., it is essentially an isolated atomic-orbital unassociated of the molecular framework. The (1s)-type core-orbital of all atoms (save that of $H^{\bullet}$) possess very high ionization energies in the range of ≈ 100-700 eV and require X-ray sources of X-ray photoelectron spectroscopy (XPS) to remove them [29,30,40,44]. Thus, they are considered as non-participants in determining the unique physical characteristics of the molecule. This task is considered to be left to that of the valence orbitals which may be accessed via ultraviolet photoelectron spectroscopy (UPS) [29,30,40].

Now the atoms of interest with their ground state electron configurations are as follows: $H^{\bullet}$, (1s); C, $(1s)^2(2s)^2(2p)^2$; $N^{\bullet}$, $(1s)^2(2s)^2(2p)^3$; O, $(1s)^2(2s)^2(2p)^4$, and $F^{\bullet}$, $(1s)^2(2s)^2(2p)^5$. For these species, save $H^{\bullet}$, $(1s)^2$ is a core-orbital, and (2s) and (2p) are valence-orbitals. Any atomic-orbitals (i.e., (ns), (np), (nd)) composed of higher principal quantum numbers n, (e.g., for $H^{\bullet}$, (2s), (2p), (3s), (3p), (3d), (4s), ..., and for the others, (3s), (3p), (3d), (4s), ...) are known as Rydberg atomic-orbitals [26-31, 33-35, 40]. Similarly, the molecular Rydberg-orbitals [34] are those which are composed of higher principal quantum numbers, n, (eg., (3s), (3p), (3d), (4s),...) and are atomic-like in shape (i.e., s, p, d-like), very diffuse in nature (i.e., large) and may extend

over large regions of the molecular framework. Rydberg-orbitals act as intermediaries between the neutral M_1 and its radical-cation $M_1^{+\bullet}$ (see Chapter 2, Section 2.2).

The CIE spectra presented later in sections 2.2-2.5, are those of the linear molecular projectile-ions, $N{\equiv}N^{+\bullet}$, $C{\equiv}O^{+\bullet}$, $O{=}C{=}O^{+\bullet}$, and $O{=}C{=}C{=}O^{+\bullet}$. Thus, one will examine their characteristics presented in Table 2.1, and Figures 2.2, 2.3, 2.4, and 2.5, which illustrate the classes of the molecular orbitals for the linear centrosymmetric A≡A, B=A=B, and B=A=A=B species, the qualitative molecular orbitals of A≡A, B=A=B, B=A=A=B, and vibrational modes of linear polyatomic molecules respectively (for the A≡B, A=A=B, A=A=A=B species the YYY subscripts are dropped.). The salient features illustrated by the above mentioned Table and Figures will now be discussed.

Firstly, the core-orbitals of $(1\sigma_g)^2(1\sigma_u)^2$, $(1\sigma_g)^2(1\sigma_u)^2(2\sigma_g)^2$, and $(1\sigma_g)^2(1\sigma_u)^2(2\sigma_g)^2(2\sigma_u)^2$, of the A=A, B=A=B, and B=A=A=B species are examples of N≡N (and C≡O), O=C=O, and O=C=C=O, respectively. For N≡N the core-orbitals are arrangements of N(1s) orbitals and for the oxides of carbon C≡O, O=C=O, and O=C=C=O, they are arrangements of the O(1s) and C(1s) orbitals, respectively.

Secondly, on inspection of Figure 2.2, (i.e., N≡N and C≡O) one may see that the (2s)-type valence orbitals, $(2\sigma_g)^2(2\sigma_u)^2$, are σ-bonding and anti-bonding, respectively. Next, the (2p)-type valence orbitals, $(1\pi_u)^4(3\sigma_g)^2$, are π-bonding; and σ-bonding, respectively. Lastly, the unoccupied (2p)-type valence orbitals, $(1\pi_g)^0(3\sigma_u)^0$, are π-antibonding, and σ-antibonding, respectively.

Thirdly, on inspection of Figure 2.3, (i.e., O=C=O) one may see that the (2s)-type valence orbitals, $(3\sigma_g)^2(2\sigma_u)^2(4\sigma_g)^2$, are σ-bonding, σ-nonbonding, and σ-antibonding, respectively. Next, for the (2p)-type valence orbitals, $(3\sigma_u)^2(1\pi_u)^4(1\pi_g)^4$, are σ-bonding; π-

Table 2.1 Classes of Molecular Orbitals for the Linear Centrosymmetric A≡A, B−A−B, and B−A−A−B Species[a]

Species	
	(1s)-type Core Orbitals
A≡A	$(1\sigma_g)^2(1\sigma_u)^2$
B−A−B	$(1\sigma_g)^2(1\sigma_u)^2(2\sigma_g)^2$
B−A−A−B	$(1\sigma_g)^2(1\sigma_u)^2(2\sigma_g)^2(2\sigma_u)^2$
	(2s)-type Valence Orbitals
A≡A	$(2\sigma_g)^2(2\sigma_u)^2$
B−A−B	$(3\sigma_g)^2(2\sigma_u)^2(4\sigma_g)^2$
B−A−A−B	$(3\sigma_g)^2(3\sigma_u)^2(4\sigma_g)^2(4\sigma_u)^2$
	(2p)-type Valence Orbitals
A≡A	$(1\pi_u)^4(3\sigma_g)^2$
B−A−B	$(3\sigma_u)^2(1\pi_u)^4(1\pi_g)^4$
B−A−A−B	$(5\sigma_g)^2(1\pi_u)^4(1\pi_g)^4(2\pi_u)^2$
	Unoccupied (2p)-type Valence Orbitals
A≡A	$(1\pi_g)^0(3\sigma_u)^0$
B−A−B	$(2\pi_u)^0(3\sigma_g)^0(4\sigma_u)^0$
B−A−B	$(2\pi_g)^0(5\sigma_u)^0$

[a]For the linear non-centrosymmetric A≡B, A−A−B, A−A−A−B species, the subscripts g and u are not applicable.

Figure 2.2 The Qualitative Molecular Orbitals of the A≡A Species

A≡A[$\tilde{X}\,^1\Sigma_g^+$] (e.g., N≡N)

(1s)-type Core	$(1\sigma_g)^2(1\sigma_u)^2$
(2s)-type Valence	$(2\sigma_g)^2(2\sigma_u)^2$
(2p)-type Valence	$(1\pi_u)^4(3\sigma_g)^2$
(2p)-Unoccupied	$(1\pi_g)^0(3\sigma_u)^0$

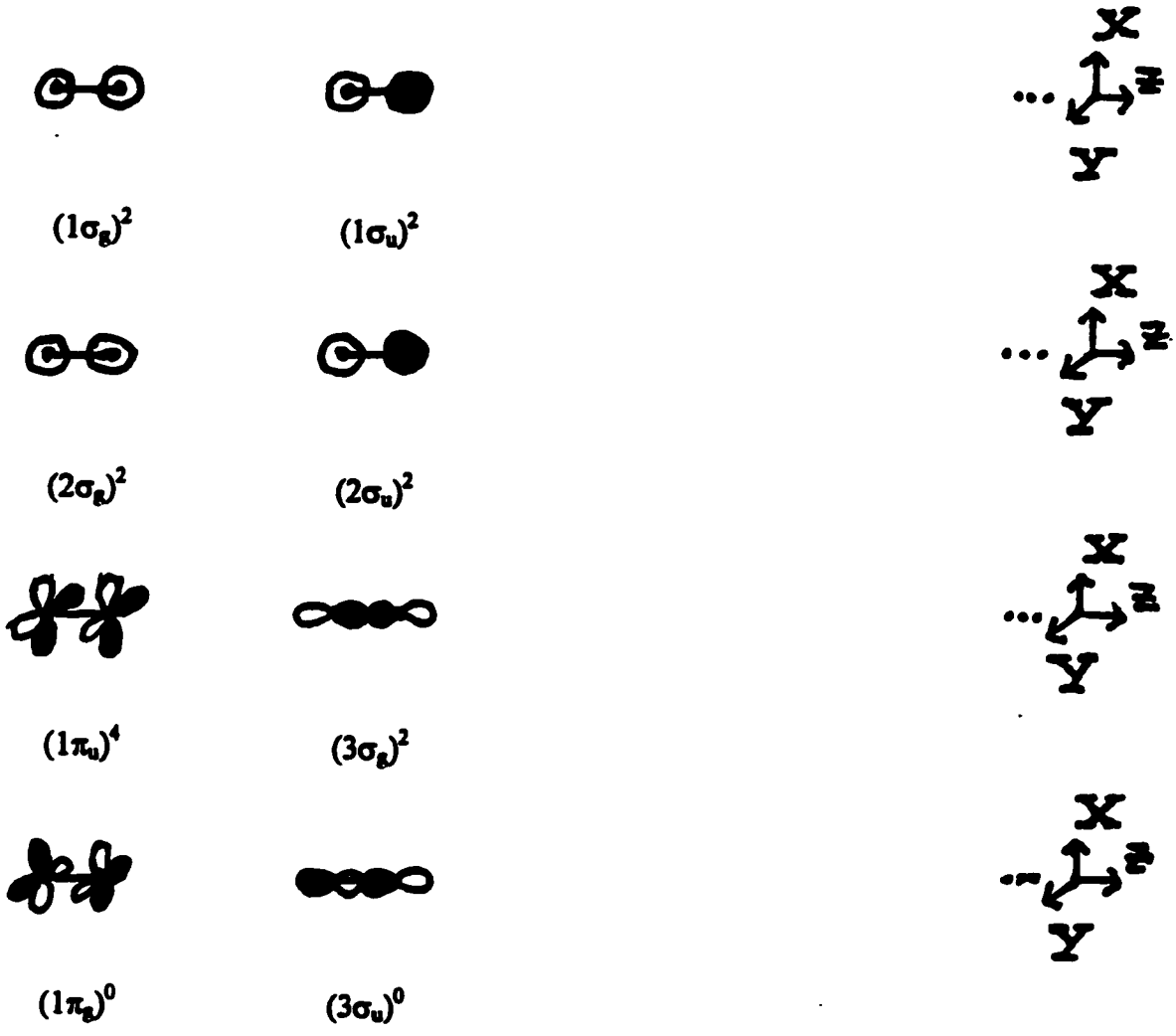

Figure 2.3 The Qualitative Molecular Orbitals of the B=A=B Species

B=A=B[$\tilde{X}\,^1\Sigma_g^+$] (e.g., O=C=O)

(1s)-type Core	$(1\sigma_g)^2(1\sigma_u)^2(2\sigma_g)^2$
(2s)-type Valence	$(3\sigma_g)^2(2\sigma_u)^2(4\sigma_g)^2$
(2p)-type Valence	$(3\sigma_u)^2(1\pi_u)^4(1\pi_g)^4$
(2p)-Unoccupied	$(2\pi_g)^0(5\sigma_g)^0(4\sigma_u)^0$

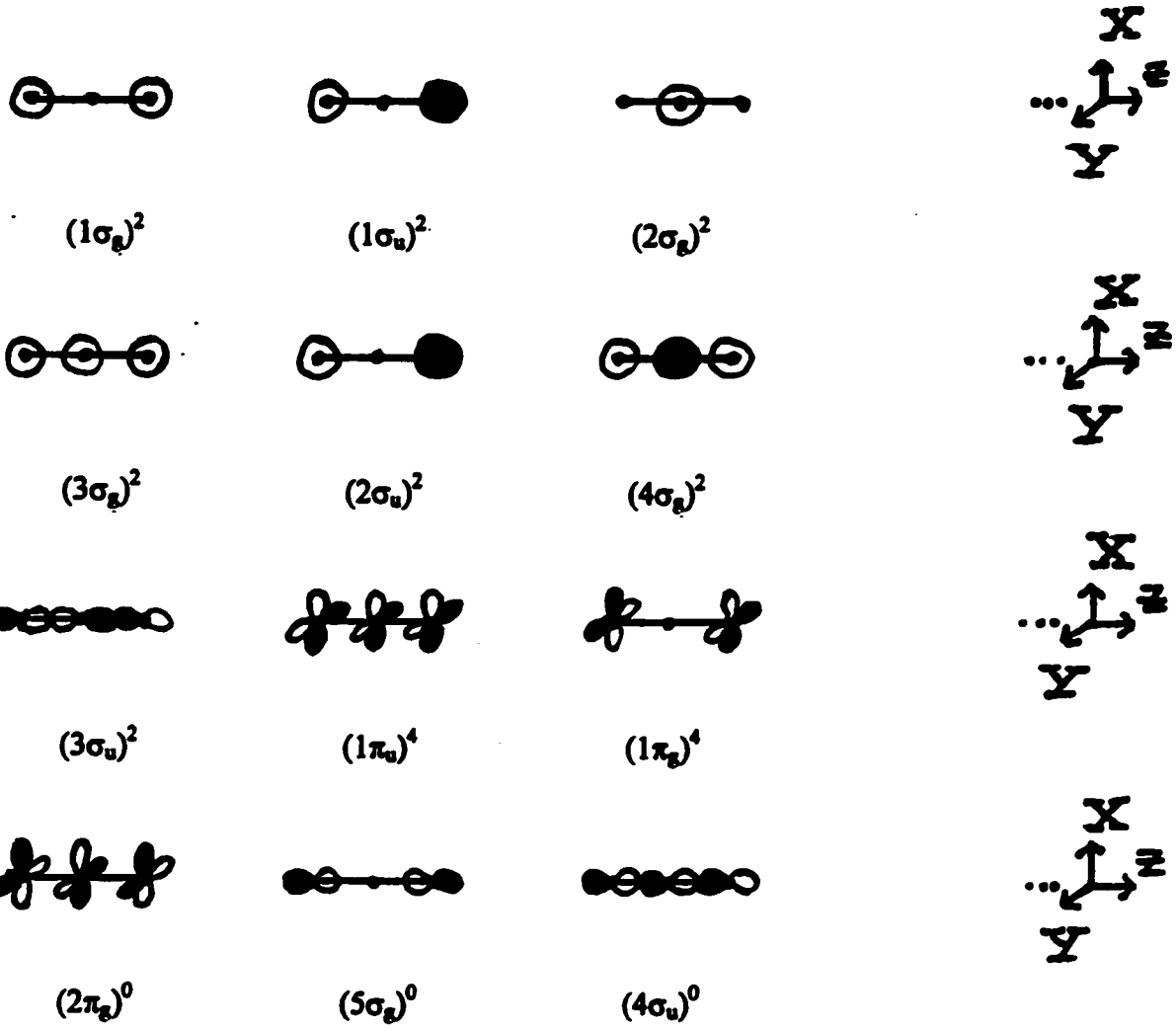

Figure 2.4 The Qualitative Molecular Orbitals of the B=A=A=B Species

B=A=A=B[$\tilde{X}\,^3\Sigma_g^-$] (e.g., O=C=C=O)

(1s)-type Core	$(1\sigma_g)^2(1\sigma_u)^2(2\sigma_g)^2(2\sigma_u)^2$
(2s)-type Valence	$(3\sigma_g)^2(3\sigma_u)^2(4\sigma_g)^2(4\sigma_u)^2$
(2p)-type Valence	$(5\sigma_g)^2(1\pi_u)^4(1\pi_g)^4(2\pi_u)^2$
(2p)-Unoccupied	$(2\pi_g)^0(5\sigma_u)^0$

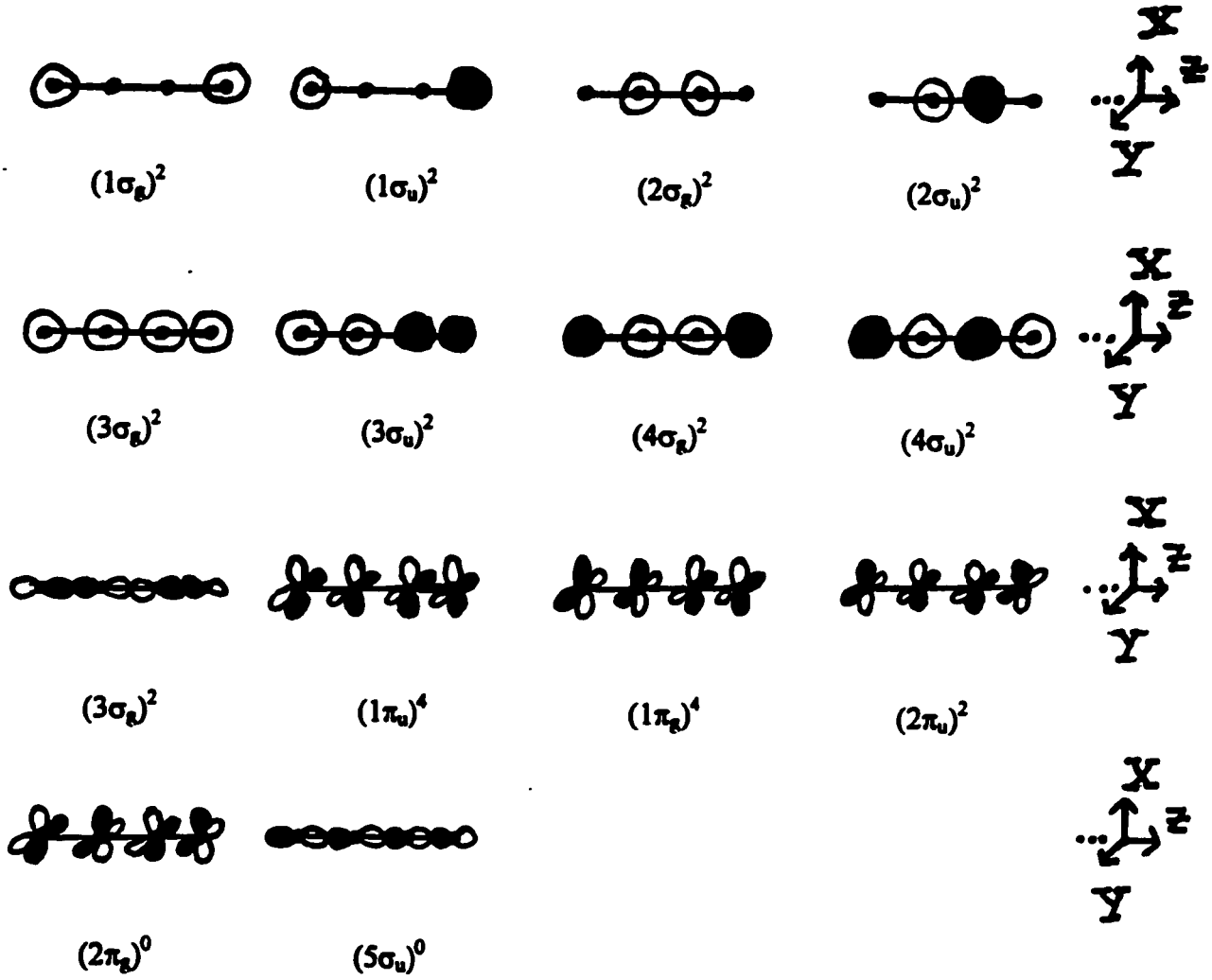

Figure 2.5 The Vibrational Modes of Linear Polyatomic Molecules

Total Vibrations	:	3N-5	(N = number of atoms)
Stretching Vibrations	:	N-1	
Bending Vibrations	:	2N-4	

Diatomic Molecules (N≡N , C≡O , O=O)

$\nu_1(\Sigma_g^+)$  sym. stretch

Linear Triatomic Molecules (O=C=O)

$\nu_1(\Sigma_g^+)$  CO sym. stretch

$\nu_2(\Pi_u)$  sym. bend

$\nu_3(\Sigma_u^+)$  CO asym. stretch

Linear Tetraatomic Molecules (O=C=C=O)

$\nu_1(\Sigma_g^+)$  CO sym. stretch

$\nu_2(\Sigma_g^+)$ 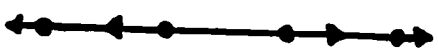 CC sym. stretch

$\nu_3(\Sigma_u^+)$  CO, CC asym. stretch

$\nu_4(\Pi_g)$ 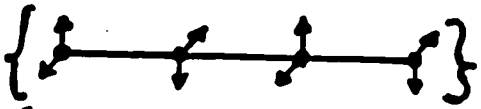 trans-bend

$\nu_5(\Pi_u)$  cis-bend

bonding; and π-nonbonding; respectively. Lastly, the unoccupied (2p)-type valence orbitals, $(2\pi_u)^0(5\sigma_g)^0(4\sigma_u)^0$, are π-antibonding; σ-nonbonding; and σ-antibonding; respectively.

Fourthly, on inspection of Figure 2.4, (i.e., O=C=C=O) one may see that the (2s)-type valence orbitals, $(3\sigma_g)^2(3\sigma_u)^2(4\sigma_g)^2(4\sigma_u)^2$, are; CC and CO σ-bonding; CC σ-antibonding and CO σ-bonding; CC σ-bonding and CO σ-antibonding; and CC and CO σ-antibonding, respectively. Next, the (2p)-type valence orbitals, $(5\sigma_g)^2(1\pi_u)^4(1\pi_g)^4(2\pi_u)^2$, are; CC and CO σ-bonding; CC and CO π-bonding; CC π-antibonding and CO π-bonding; and CC π-bonding and CO π-antibonding, respectively. Lastly, the unoccupied (2p)-type valence orbitals, $(2\pi_g)^0(5\sigma_u)^0$, are ; CC and CO π-antibonding; and CC and CO σ-antibonding, respectively.

Additionally, the relationship to the molecular-orbitals of N≡N (and C≡O), O=C=O, and O=C=C=O, illustrated in Figures 2.3-2.4, of their corresponding vibrational modes is illustrated in Figure 2.5. The vibrational energy of these modes can indicate certain changes in geometry between the neutral M_1 and radical-cation $M_1^{+\bullet}$ species, and is manifested experimentally in their infrared (IR), untraviolet photoelection spectra (UPS), and optical emission spectroscopy (e.g. CIE spectra). The above mentioned information is of critical productive value, not only in the vibrational analysis of UPS spectra of molecular and dimeric species, but it will be utilized to support the qualitative arguments (via Walsh's Rules and the Renner-Teller Theorem, see Appendix B) presented in later sections. These will be that the lower excited electron states of neutral O=C=O are mainly dissociative to bending and more importantly that both $O=C=C=O^{+\bullet}[\tilde{X}\,^2\Pi_u(^2B_u)]$ and $O=C=C=O^{-\bullet}[\tilde{X}\,^2\Pi_u(^2A_u)]$ are strongly quasi-linear species (e.g., Renner-Teller dynamically-linear, see Appendix B).

2.1.3 Mechanisms of the Production of $(M_1^+)^*$ and $(M_1)^*$

This section will deal with the mechanisms of the production of $(M_1^{+*})^*$ and $(M_1)^*$ due the collision event between the mast moving projectile-ion M_1^{+*} and the stationary target gas G_1. It should be emphasized that the process is a large ensemble of collision events, during which there are two concomitant processes that are collision-excitation (via a non-momentum transfer of internal energy, E_{int}, into M_1^{+*}) and charge-exchange neutralization, [19-25].

The salient topics of discussion are presented in Figure 2.6, and Tables 2.2 and 2.3 that illustrate the competitive processes for the fate of M_1^+, the proposed Rydberg states accessed during the M_1^+ to M_1 neutralization process, and the charge-exchange process and neutralization-energy balance Q_N, respectively.

Firstly, on inspection of Figure 2.6, one may note the following trends. The behaviour of M_1^+ is governed by the simultaneous competition of (I) unimolecular-dissociation, (II) radiative, and (III) non-radiative processes, each with rate constants denoted by k, k_{rad}, and k_{nrad}, respectively.

The (I) direct unimolecular dissociation of small symmetric molecules is governed by the Wigner-Witmer Correlation Rules [26-30] (see Appendix A). Briefly, they are as follows: (1) there is a conservation of symmetry such that the direct product of the electronic states of the dissociation products must contain that of the parent; and (2) there is a conservation of spin such that the sum of the spins of the dissociation products must contain that of the parent.

The (II) allowed optical emission shall occur if the direct product of the upper and lower electronic states contains a component of the transition electric-dipole operator (X, Y, Z), their multiplicites, (2S +1), must be the same (i.e., $\Delta S = 0$) and the transition must be gerade (even) $\leftrightarrow$ ungerade (odd), (see Appendix A). The ground electronic state is denoted by $\tilde{X}$ and the successive excited electric states of the same multiplicity of $\tilde{X}$ are denoted $\tilde{A}$, $\tilde{B}$, $\tilde{C}$, ...,

Figure 2.6 The Competitive Processes for the Fate of $M_1^{+\bullet}$

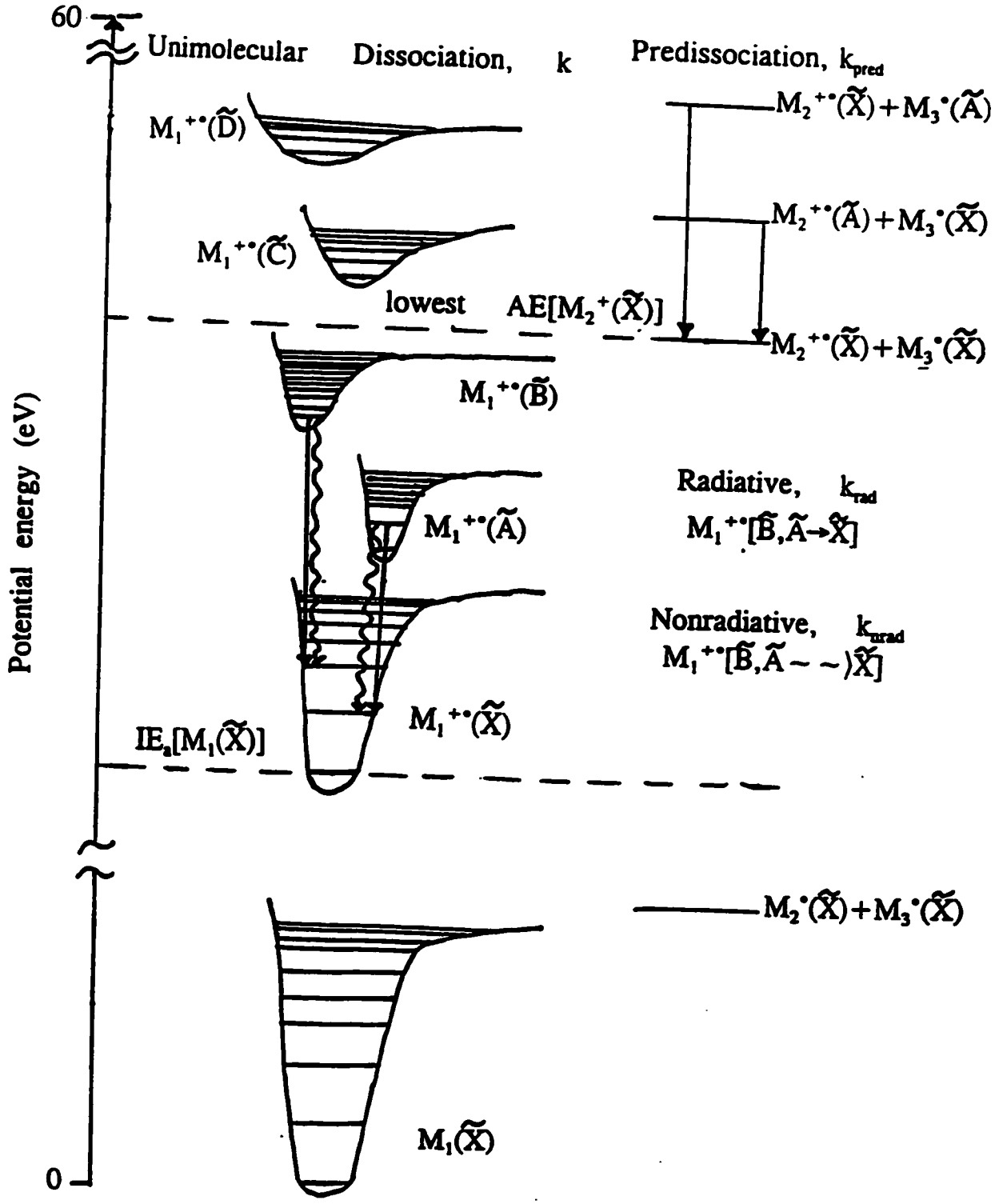

Table 2.2 The Proposed Rydberg States Accessed During the $M_1^{+\bullet}$ to M_1 Neutralization Process.

$M_1^{+\bullet}$ Valence	M_1^{*} Rydberg	M_1 Valence
N≡N		
$\tilde{X}\,^2\Sigma_g^+$	$(3s\sigma_g)\ \tilde{e}\,^3\Sigma_g^+$	$\tilde{c}\,^3\Pi_u$
C≡O		
$\tilde{X}\,^2\Sigma^+$	$(3p\pi)\ \tilde{c}\,^3\Pi$	$\tilde{a}\,^3\Pi$
$\tilde{A}\,^2\Pi$	$(3p\pi)\ ^3\Sigma^+$	$\tilde{a}\,'^3\Sigma^+,\ \tilde{d}\,^3\Delta,\ \tilde{e}\,^3\Sigma^-$
$\tilde{B}\,^2\Sigma^+$	$(3p\sigma)\ ^1\Sigma^+$	$\tilde{X}\,^2\Sigma^+,\ ^1\Sigma^+$
O=C=O		
$\tilde{X}\,^2\Pi_g$	$(3s\sigma_g)\ ^3\Pi_g$	$^3\Sigma_u^+,\ ^3\Sigma_u^-,\ ^3\Delta_u,\ ^3\Pi_u$
O=C=C=O		
$\tilde{X}\,^2\Pi_u$	$(3s\sigma_g)\ ^3\Pi_u$	$^3\Sigma_g^+,\ ^3\Sigma_g^-,\ ^3\Delta_g,\ ^3\Pi_g$

Table 2.3 The Charge-Exchange Process and the Neutralization Energy Balance, Q_N

Projectile-Ion, $M_1^{+\bullet}$ Ionization Energy $IE_v[M_1]$ (eV)[b]		Target Gas, G_1 Ionization Energy $IE_v[G_1]$ (eV)[b]	
N≡N	15.58	He	24.59
C≡O	14.01	Ar	15.76
O=C=O	13.77	O_2	12.07
O=C=C=O	≈9.2[c]		

	Neutralization Energy Balance Q_N ($M_1^{+\bullet}/G_1$) (eV)[a]		
	Target Gas, G_1		
Projectile-Ion $M_1^{+\bullet}$	He	Ar	O_2
$N{\equiv}N^{+\bullet}$	9.01	0.18	−3.51
$C{\equiv}O^{+\bullet}$	10.58	1.75	−1.94
$O{=}C{=}O^{+\bullet}$	10.82	1.99	−1.70
$O{=}C{=}C{=}O^{+\bullet}$	≈15.4	–	≈2.9

[a] $Q_N = IE_v[G_1] - NE_v[M_1^{+\bullet}]$, $NE_v[M_1^{+\bullet}] \leq IE_v[M_1]$. [b] Ref. [1], assume $IE_a[M_1] \approx IE_v[M_1]$. [c] Estimated IE_a[O=C=C=O], see text.

respectively. These excited electronic states of different multiplicity than $\tilde{X}$ are successively denoted $\tilde{a}$, $\tilde{b}$, $\tilde{c}$, ..., respectively.

The (II) quasi-equilibrium unimolecular dissociation of $M_1^{+\bullet}$ occurs via rapid de-excitation of all the excited electronic states to the ground electronic state followed by vibrational (pre)dissociation (i.e., as the size of the molecule increases quasi-equilibrium dissociation starts to become favoured over emission)..

Next, on inspection of Table 2.3, one may note the proposed Rydberg states that may act as intermediaries (either radiatively and/or non-radiatively) between $M_1^{+\bullet}$ and M_1 during the neutralization process. For example, for nitrogen the following process may occur, $N{\equiv}N^{+\bullet}[\tilde{X}\,^2\Sigma_g^+] + e^- \rightarrow N{\equiv}N[(3s\sigma_g)\,\tilde{e}\,^3\Sigma_g^+] \rightarrow N{\equiv}N[\tilde{c}\,^3\Pi_u]$. This may be proposed to allow the following radiative cascade $N{\equiv}N[\tilde{c}\,^3\Pi_u \rightarrow \tilde{b}\,^3\Pi_g]$ and $N{\equiv}N[\tilde{b}\,^3\Pi_g \rightarrow \tilde{a}\,^3\Sigma_u^+]$ emissions.

Now, during the charge-exchange process between the stationary target gas G_1 and the projectile-ion M_1^+, the neutralization energy balance, Q_N, is defined as follows;

$$Q_N = IE_v[G_1] - NE_v[M_1^{+\bullet}]$$

where, $IE_v[G_1]$, and $NE_v[M_1^{+\bullet}]$ denotes the vertical ionization energy of G_1, and the vertical neutralization energy of M_1^+ ($NE_v[M_1^{+\bullet}] \leq IE_v[M_1]$), respectively. Thus, Q_N provides a measure of the internal energy, E_{int}, required (endothermic, $Q_N > 0$), not required (thermoneutral, $Q_N \approx 0$), or deposited (exothermic, $Q_N < 0$) in M_1 (whilst formed from $M_1^{+\bullet}$) during the collision event. Table 2.3 lists the IE values of M_1 and G_1 and the respective $Q_N(M_1^{+\bullet}/G_1)$ values (see section 2.5 for the estimated $IE_a[O{=}C{=}C{=}O] \approx 9.2$ eV value). On inspection of Table 2.3, one may note the following trends. He is an extremely poor neutralization agent as Q_N is very endothermic,

and thus neutralization is an extremely remote event. Now, Ar is a better neutralization agent as Q_N varies from almost thermoneutral to slightly endothermic. Lastly, O_2 is markedly the best neutralization agent as Q_N is strongly exothermic (save for $O{=}C{=}C{=}O^{+\bullet}$) and is very likely to produce some excited electronic state neutral (i.e., $(M_1^{+\bullet})^*$). Thus, one would expect the likelihood of the observation of the neutral parent M_1 emissions in the CIE spectra to be negligible for He, present for Ar, and markedly strong for O_2, as was experimentally observed (see sections 2.2-2.5).

2.1.4 The Photoelectron Spectra of N≡N, C≡O, O=C=O, and O=O

This section deals with the photoelectron spectra of the projectiles N≡N, C≡O, O=C=O, and the target O=O [29, 30, 43]. Briefly, a photoelectron spectrum of M_1 is produced via its photoionization by a photon of excitation energy, $h\nu_0$, and is governed by the following expression [29, 30,43];

$$IE = h\nu_0 - KE(e^-)$$

where IE is the observed ionization energies corresponding to the respective kinetic energies of the ejected electron, $KE(e^-)$. The experimental setup [29, 30, 43] is basically an ionization chamber connected to a (127° 17') electric sector that kinetic energy resolves and focuses the beam of ejected electrons into the detector apparatus (typical a photomultipler (PMT). Thus, on the measurement of all the $KE(e^-)$ values and subtracting it from $h\nu_o$ one obtains a plot of electron intensity (Y-axis) verus the ionization energy IE (footnote: In the traditional British

system one reads the IE axis increasing from right to left, and in the newer American system on reads the IE axis increasing from left to right.).

There are two main excitation sources for UPS. The first being the He (Iα) line at 58.4 nm providing 21.22 eV, and the second being the He (IIα) line at 30.4 nm providing 40.81 eV.

The essence of this type of fixed wavelength UPS spectrum is it provides a "snap-shot" of the ground electronic state $\tilde{X}$, and the excited electronic states $\tilde{A}$, $\tilde{B}$, $\tilde{C}$, ..., Franck-Condon ionization profiles that contain the IE_e, IE_v and vibrational spacing values at the moment of ionization of M_1. The utility of this information is its predictive value in determining the wavelengths (of the vibrationless; 0_0^0) emission transitions in the radical-cation M_1^+, simply by calculating the proposed ΔIE_e values of the respective electronic states.

Table 2.4 presents the ultraviolet photoelectron spectroscopy (UPS) adiabatic ionization energy values for N≡N, C≡O, O=C=O, and O=O, and the productive relationship to the vibrationless electronic transitions of their radical-cations. On inspection, on Table 2.4, one may see the utility of identifying the electronic states, their electronic transitions, and that the match between the ΔIE_e values and the optical known 0_0^0 is very accurate indeed.

Therefore, such information is invaluable in the identification and analysis of the optical emission spectra of polyatomic molecules. The lion's share of that research has been carried out by the group of J.P. Maier et.al. [32, 115]. Briefly, the experiment consisted of an observation chamber into which the gaseous M_1 species was leaked (along the X-axis) and was excited and ionized by an energy controlled (≈ 20 eV) electron beam (along the Y-axis). The resulting optical emissions from M_1^+ were recorded above (along the Z-axis) through a quartz window atop of which stood a monochromator and a PMT detector. The J.P. Maier group was

Table 2.4 The Ultraviolet Photoelectron Spectroscopy (UPS) Adiabatic Ionization Energy Values for N≡N, C≡O, O=C=O, and O=O and the Predictive Relationship to the Vibrationless Electronic Transitions of their Radical-Cations.

Adiabatic Ionization Energy, IE_a(eV)[a]	Radical-Cation Vibrationless Electronic Transition	Vibrationless Wavelength ΔIE_a in UPS λ(nm)[a]	Vibrationless Wavelength Known Emission λ(nm)[b]
N≡N			
$\tilde{X}^2\Sigma_g^+$ 15.58	$\tilde{B}^2\Sigma_u^+ \rightarrow \tilde{X}^2\Sigma_g^+$, (0,0)	389.9	391.4
$\tilde{A}^2\Pi_u$ 16.69	$\tilde{A}^2\Pi_u \rightarrow \tilde{X}^2\Sigma_g^+$, (0,0)	1117.0	1108.8
$\tilde{B}^2\Sigma_u^+$ 18.76			
C≡O			
$\tilde{X}^2\Sigma^+$ 14.01	$\tilde{B}^2\Sigma^+ \rightarrow \tilde{X}^2\Sigma^+$, (0,0)	218.7	219.0
$\tilde{A}^2\Pi$ 16.53	$\tilde{B}^2\Sigma^+ \rightarrow \tilde{A}^2\Pi$, (0,0)	393.6	397.7
$\tilde{B}^2\Sigma^+$ 19.68	$\tilde{A}^2\Pi \rightarrow \tilde{X}^2\Sigma^+$, (0,0)	492.0	490.0
O=C=O			
$\tilde{X}^2\Pi_g$ 13.78	$\tilde{B}^2\Sigma_u^+ \rightarrow \tilde{X}^2\Pi_g$, 0_0^0	288.3	289.0
$\tilde{A}^2\Pi_u$ 17.32	$\tilde{A}^2\Pi_u \rightarrow \tilde{X}^2\Pi_g$, 0_0^0	350.2	350.3
$\tilde{B}^2\Sigma_u^+$ 18.08			
$\tilde{C}^2\Sigma_g^+$ 19.40			
O=O			
$\tilde{X}^2\Pi_g$ 12.07	$\tilde{A}^2\Pi_u \rightarrow \tilde{X}^2\Pi_g$, (0,0)	249.0	–[c]
$\tilde{a}^4\Pi_u$ 16.10	$\tilde{b}^4\Sigma_g^- \rightarrow \tilde{a}^4\Pi_u$, (0,0)	599.0	602.6
$\tilde{A}^2\Pi_u$ 17.05			
$\tilde{b}^4\Sigma_g^-$ 18.17			
$\tilde{B}^2\Sigma_g^-$ 20.30			
$\tilde{c}^4\Sigma_u^-$ 24.58			

[a]Ref. [43, 68]. [b]Ref. [35, 71]. [c]Not resolved.

successful in recording and analyzing many symmetric (poly) ene, (poly) yne and (per)fluorinated aromatic type polyatomics [32, 115].

Thus, for one wishing to carry out CIE studies of polyatomics, the experimental consultation of UPS data banks [45-56], and the productive calculations of their peaks by the Green's Function [57, 114], and HAM/3 [58-61], methods are essential to the selection of suitable candidates for CIE study and the analysis of any observed CIE spectra.

2.1.5 Atomic Fragment Emission Features

This section will deal with the experimentally observed atomic fragment emission features of N, N^+, C, C^{+*}, O, and O^{+*}, [31,33,34,36-38] in the CIE spectra presented in sections 2.2-2.5. Now, Tables 2.5, 2.6, 2.7 and 2.8, illustrate the electronic states of the N^*, and N^+ species ; C and C^{+*} species; O and O^{+*}species; and the wavelengths of the observed emissions of the atomic fragments produced from the nitrogen, N≡N, and the oxides of carbon C≡O, O=C=O, O=C=C=O, systems; respectively.

Now, on inspection of Table 2.8, one may note the following trends, where the partner target gas column indicates in which CIE spectrum the atomic fragment may be found. One may observe the N^+ emission trend to be in UV-VIS range, whereas the N^* emissions trend to be in the NIR range. As well, the same may be said of the O^{+*} and O emissions, respectively. The C^{+*} emissions are in the UV-VIS range, whereas the C emissions are in the UV. All of the observed emissions (save those of $N^+[(2p)\ ^1D \rightarrow (2p)\ ^3P]$ and $O[(2p)\ ^1D \rightarrow (2p)\ ^3P]$) may be proposed to be produced via concomitant bond scission and subsequent excitation. The O^{+*} emissions and O emission at 616.3 nm and 927.3 nm are present only on utilization of the O_2

Table 2.5 The Electronic States of the N^* and N^+ Species

Valence Electron Configuration[a]	Electronic States
N^*	
$(2s)^2(2p)^3$	$(2p)\ ^4S^0$, $(2p)\ ^2D^0$, $(2p)\ ^2P^0$
$(2s)^2(2p)^2(ns)$	$(ns)\ ^2D$, $(ns)\ ^4P$, $(ns)\ ^2P$, $(ns)\ ^2S$
$(2s)^2(2p)^2(np)$	$(np)\ ^2F^0$, $(np)\ ^4D^0$, $(np)\ ^2D^0(2)$, $(np)\ ^4P^0$, $(np)\ ^2P^0$, $(np)\ ^4S^0$, $(np)\ ^2S^0$
$(2s)^2(2p)^2(nd)$	$(nd)\ ^2G$, $(nd)\ ^4F$, $(nd)\ ^2F(2)$, $(nd)\ ^4D$, $(nd)\ ^2D(3)$, $(nd)\ ^4P$, $(nd)\ ^2P(2)$, $(nd)\ ^2S$
N^+	
$(2s)^2(2p)^2$	$(2p)\ ^3P$, $(2p)\ ^1D$, $(2p)\ ^1S$
$(2s)^2(2p)(ns)$	$(ns)\ ^3P^0$, $(ns)\ ^1P^0$
$(2s)^2(2p)(np)$	$(np)\ ^3D$, $(np)\ ^1D$, $(np)\ ^3P$, $(np)\ ^1P$, $(np)\ ^3S$, $(np)\ ^1S$
$(2s)^2(2p)(nd)$	$(nd)\ ^3F^0$, $(np)\ ^1F^0$, $(nd)\ ^3D^0$, $(nd)\ ^1D^0$, $(nd)\ ^3P^0$, $(np)\ ^1P^0$

[a]The principal quantum number, n = 3, 4, 5, ...

Table 2.6 The Electronic States of the C and C^{+n} Species

Valence Electron Configuration[a]	Electronic States
C	
$(2s)^2(2p)^2$	$(2p)\ ^3P$, $(2p)\ ^1D$, $(2p)\ ^1S$
$(2s)(2p)^3$	$(2s2p^3)\ ^3D^0$, $(2s2p^3)\ ^1D^0$, $(2s2p^3)\ ^3P^0$, $(2s2p^3)\ ^1P^0$, $(2s2p^3)\ ^5S^0$, $(2s2p^3)\ ^3S^0$
$(2s)^2(2p)(ns)$	$(ns)\ ^3P^0$, $(ns)\ ^1P^0$
$(2s)^2(2p)(np)$	$(np)\ ^3D$, $(np)\ ^1D$, $(np)\ ^3P$, $(np)\ ^1P$, $(np)\ ^3S$, $(np)\ ^1S$
$(2s)^2(2p)(nd)$	$(nd)\ ^3F^0$, $(nd)\ ^1F^0$, $(nd)\ ^3D^0$, $(nd)\ ^1D^0$, $(nd)\ ^3P^0$, $(nd)\ ^1P^0$
C^{+n}	
$(2s)^2(2p)$	$(2p)\ ^2P^0$
$(2s)(2p)^2$	$(2s2p^2)\ ^2D$, $(2s2p^2)\ ^4P$, $(2s2p^2)\ ^2P$, $(2s2p^2)\ ^2S$
$(2s)^2(ns)$	$(ns)\ ^2S$
$(2s)^2(np)$	$(ns)\ ^2P^0$
$(2s)^2(nd)$	$(ns)\ ^2D$

[a]The principal quantum number, n = 3, 4, 5, ...

Table 2.7 The Electronic States of the O and $O^{+\bullet}$ Species

Valence Electron Configuration[a]	Electronic States
O	
$(2s)^2(2p)^4$	$(2p)\ ^3P$, $(2p)\ ^1D$, $(2p)\ ^1S$
$(2s)^2(2p)^3(ns)$	$(ns)\ ^3D^0$, $(ns)\ ^1D^0$, $(ns)\ ^3P^0$, $(ns)\ ^1P^0$
$(2s)^2(2p)^3(np)$	$(np)\ ^3F$, $(np)\ ^1F$, $(np)\ ^3D(2)$, $(np)\ ^1D(2)$, $(np)\ ^5P$, $(np)\ ^3P(3)$, $(np)\ ^1P(2)$, $(np)\ ^3S$, $(np)\ ^1S$
$(2s)^2(2p)^3(nd)$	$(nd)\ ^3G^0$, $(nd)\ ^1G^0$, $(nd)\ ^3F^0(2)$, $(nd)\ ^1F^0(2)$, $(nd)\ ^5D^0$, $(nd)\ ^3D^0(3)$, $(nd)\ ^1D^0(2)$, $(nd)\ ^3P^0(2)$, $(nd)\ ^1P^0(2)$, $(nd)\ ^3S^0$, $(nd)\ ^1S^0$
$O^{+\bullet}$	
$(2s)^2(2p)^3$	$(2p)\ ^4S^0$, $(2p)\ ^2D^0$, $(2p)\ ^2P^0$
$(2s)^2(2p)^2(ns)$	$(ns)\ ^2D$, $(ns)\ ^4P$, $(ns)\ ^2P$, $(ns)\ ^2S$
$(2s)^2(2p)^2(np)$	$(np)\ ^2F^0$, $(np)\ ^4D^0$, $(np)\ ^2D^0(2)$, $(np)\ ^4P^0$, $(np)\ ^2P^0$, $(np)\ ^4S^0$, $(np)\ ^2S^0$
$(2s)^2(2p)^2(nd)$	$(nd)\ ^2G$, $(nd)\ ^4F$, $(nd)\ ^2F(2)$, $(nd)\ ^4D$, $(nd)\ ^2D(3)$, $(nd)\ ^4P$, $(nd)\ ^2P(2)$, $(nd)\ ^2S$

[a]The principal quantum number, n = 3, 4, 5, ...

Table 2.8 The Observed Emissions of the Atomic Fragments Produced from the Nitrogen, N≡N, and the Oxides of Carbon, C≡O, O=C=O, and O=C=C=O, Systems

Electronic Transition	Observed Wavelength λ(nm)[a]	Partner Target Gas
N^+		
$(4d)\ ^3D^0 \rightarrow (3p)\ ^3D$	226.7	He, Ar
$(4d)\ ^3D^0 \rightarrow (3p)\ ^3P$	250.2	He, Ar
$(3d)\ ^3F^0 \rightarrow (3p)\ ^3D$	567.9	He, Ar, O_2
$(2p)\ ^1D \rightarrow (2p)\ ^3P$	658.1	He, Ar, O_2
N°		
$(3p)\ ^4P^0 \rightarrow (3s)\ ^4P$	819.8	He, , O_2
$(3p)\ ^4D^0 \rightarrow (3s)\ ^4P$	868.1	He, Ar, O_2
$(3d)\ ^2P \rightarrow (3s)\ ^2S^0$	905.6	He, Ar, O_2
$(3p)\ ^2D^0 \rightarrow (3s)\ ^2P$	939.5	He, Ar, O_2
$(3d)\ ^4P \rightarrow (3s)\ ^4D^0$	1001.2	He, , O_2
C^{+*}		
$(3p)\ ^2P^0 \rightarrow (2s2p^2)\ ^2S$	283.7	He, Ar, O_2
$(3p)\ ^2P^0 \rightarrow (3s)\ ^2S$	657.8	He, Ar, O_2
C		
$(3s)\ ^1P^0 \rightarrow (2p)\ ^1D$	193.1	He, Ar, O_2
$(3s)\ ^1P^0 \rightarrow (2p)\ ^1S$	247.9	He, Ar, O_2
O^{+*}		
$(3d)\ ^4F \rightarrow (3p)\ ^4D^o$	408.4	O_2
$(3p)\ ^4D^o \rightarrow (3s)\ ^4P$	463.9	O_2
O		
$(4d)\ ^5D^o \rightarrow (3p)\ ^5P$	616.3	O_2
$(2p)\ ^1D \rightarrow (2p)\ ^3P$	630.2	He, Ar, O_2
$(3p)\ ^5P \rightarrow (3s)\ ^5S^o$	777.4	He, Ar, O_2
$(3p)\ ^3P \rightarrow (3s)\ ^3S^o$	844.6	He, Ar, O_2
$(3d)\ ^5D^o \rightarrow (3p)\ ^5P$	927.3	O_2

[a]Average Uncertainty, $\lambda \pm 0.5$ nm.

target gas, and these most likely result from the dissociation O_2 and of $O_2^{+\bullet}$ and the concomitant excitation of the fragments.

The O emissions at 630.2, 777.4, and 844.6 nm are grouped together in that they are all present (sometimes with further magnification of 630.2 nm) regardless of the identity of the target gas. Thus, one may propose that they are most likely produced by bond scission in the oxides of carbon, followed by subsequent excitation.

The $N^+[(2p)\ ^1D \rightarrow (2p)\ ^3P]$ and $O[(2p)\ ^1D \rightarrow (2p)\ ^3P]$ at 658.1, and 630.2 nm are special and deserve emphasis. Firstly, they are both forbidden transitions (see Appendix A) and thus should be of low (or near-zero intensity). Whereas, the $O[(2p)\ ^1D \rightarrow (2p)\ ^3P]$ emission is of low intensity (and sometimes requires further inspection to be seen), the $N^+[(2p)\ ^1D \rightarrow (2p)\ ^3P]$ is quite intense [31] (and is known as an auroral line). The two emissions are low energy ones (i.e., non-Rydberg) which are associated with certain known dissociation limits of the parent molecules that are studied here.

Therefore, the two above emissions allow one to estimate the minimum observable internal energy deposited in M_1^+ (and/or M_1) during the collision event monitored by the CIE experiment, and is denoted by $\Delta(\Delta E_{int})$. Thus, $\Delta(\Delta E_{int})$ may be defined as being equal to the difference between the internal excitation energy of the observed dissociation limit, $(\Delta E_{int}[M_2^+] + \Delta E_{int}[M_3^\bullet])$, and the ground state parent, $\Delta(\Delta E_{int}[M_1^{+\bullet}])$ and is expressed as follows;

$$\Delta(\Delta E_{int}) = (\Delta E_{int}[M_2^+] + \Delta E_{int}[M_3^\bullet]) - \Delta(\Delta E_{int}[M_1^{+\bullet}]) = (\Delta_f H^0[M_2^+] + [M_3^\bullet]) - (\Delta_f H^0[M_1^{+\bullet}])$$

for $M_1^{+\bullet} \rightarrow M_2^+ + M_3^\bullet$ where the dissociation limit, $M_2^+ + M_3^\bullet$, may be reached directly and/or indirectly via an excited intermediate $(M_1^+)^*$.

Thus, the $N^+[(2p)\ ^1D \rightarrow (2p)\ ^3P]$ transition allows one to analyze the N≡N system [69, 70]. Now, for $N{\equiv}N^{+\bullet}$ one may calculate a value of $\Delta(\Delta E_{int}) = (\Delta E_{in}[N^+[(2p)\ ^1D] + N^\bullet[(2p)\ ^3P]) - (\Delta E_{in}\ [N{\equiv}N^{+\bullet}[\ \tilde{X}\ ^2\Sigma_g^+])) = (26..19\ eV) - (15.58\ eV) = 10.61\ eV$. Therefore, one may propose that at least 10.61 eV of internal excitation energy was deposited in $N{\equiv}N^{+\bullet}$ during the single collision event with He, Ar, and O_2.

Similarly, the $O[(2p)\ ^1D \rightarrow (2p)\ ^3P]$ transition allows one to analyze the target gas O=O system and the projectile C≡O, and O=C=O systems.

For the O=O system [67, 70], for the O=O system one may calculate a value of $\Delta(\Delta E_{int}) = (\Delta E_{in}[O\ [(2p)\ ^1D] + O[(2p)\ ^3P]) - (\Delta E_{in}\ [O{\equiv}O[\ \tilde{X}\ ^3\Sigma_g^-])) = (7.13\ eV) - (0.00\ eV) = 7.13\ eV$. Similiarly, for the radical-cation $O{=}O^{+\bullet}$ one may calculate a value of $\Delta(\Delta E_{int}) = (\Delta E_{in}(O^{+\bullet}[(2p)\ ^4S^0] + O\ [(2p)\ ^1D]) - (\Delta E_{in}\ [O{\equiv}O^{+\bullet}[\ \tilde{X}\ ^2\Pi_g])) = (20.70\ eV) - (12.07\ eV) = 8.63\ eV$.

For the C≡O system [76, 77], for the radical-cation $C{\equiv}O^{+\bullet}$ one may calculate a value of $\Delta(\Delta E_{int}) = (\Delta E_{in}(C^{+\bullet}[(2p)\ ^2P^0] + [O\ [(2p)\ ^1D]) - (\Delta E_{in}\ [C{\equiv}O^{+\bullet}[\ \tilde{X}\ ^2\Sigma^+])) = (24.33\ eV) - (14.01\ eV) = 7.13\ eV$.

For the O=C=O system [86, 87, 91], for the neutral O=C=O, one may calculate a value of $\Delta(\Delta E_{int}) = (\Delta E_{in}(C{\equiv}O[\ \tilde{X}\ ^2\Sigma^+] + [O\ [(2p)\ ^1D]) - (\Delta E_{in}\ [O{=}C{=}O[\ \tilde{X}\ ^1\Sigma_g^+])) = (7.42\ eV) - (0.00\ eV) = 7.42eV$. Similarly, for the radical-cation $O{=}C{=}O^{+\bullet}$ one may calculate a value of $\Delta(\Delta E_{int}) = (\Delta E_{in}(C{\equiv}O^{+\bullet}[\ \tilde{X}\ ^2\Sigma^+] + [O\ [(2p)\ ^1D]) - (\Delta E_{in}\ [O{=}C{=}O^{+\bullet}[\ \tilde{X}\ ^2\Pi_g])) = (21.43\ eV) - (13.77\ eV) = 7.66\ eV$.

Thus, one may propose that during the CIE experiment there was a minimum of, 10.61, 7.13, 7.65, 10.32, 7.42, and 7.66 eV, of internal excitation energy deposited in $N{\equiv}N^{+\bullet}$, O=O, $O{=}O^{+\bullet}$, $C{\equiv}O^{+\bullet}$, C=C=O, and $O{=}C{=}O^{+\bullet}$, respectively.

2.1.6 Target Gas G_1 Emissions

This section will deal with the target emissions of He, Ar, and O_2 [31,33-38,62-68]. The electronic states and the observed emissions are listed in Tables 2.9, and 2.10, for He; Tables 2.11, and 2.12 for Ar; and Tables 2.13, and 2.14, for O_2, respectively. The partner target gas column in Tables 2.10, 2.12 and 2.14, indicate in which CIE spectrum their emissions are to found.

All of the atomic and molecular species discussed here follow the traditional Russell-Saunders LS, and ΛS coupling schemes, respectively, save that of Ar. The Ar species follows the j-l coupling scheme and the Racah term symbol notation (nl) $[K]_J$, (see Appendix A). In the CIE experiments, only neutral He and Ar emissions were observed in contrast to the O_2 case, where both those of the neutral and radical-cation were observed.

For the O=O system [35, 67, 70], on inspection Table 2.14 one may note the following trends. The $O{=}O^{+\bullet}$ emissions $\tilde{A}\,^2\Pi_u \rightarrow \tilde{X}\,^2\Pi_g$ and $\tilde{b}\,^4\Sigma_g^- \rightarrow \tilde{a}\,^4\Pi_u$, consist of a continuum for 190-610 nm, and a series of vibrational peaks in the range of ≈ 526-637 nm, respectively. Underneath the former emission, the neutral O=O species processes an emission $\tilde{B}\,^3\Sigma_u^- \rightarrow \tilde{X}\,^3\Sigma_g^-$ which is also a continuum, for 190-510 nm. Now, the radiative lifetimes [67], τ_{rad}, For the neutral $\tilde{B}\,^3\Sigma_u^-$ and the radical-cation electronic states $\tilde{b}\,^4\Sigma_g^-$ and $\tilde{A}\,^2\Pi_u$ are > 1 ms, ≈ 1.2 μs, and ≈ 0.7 μs, respectively. Thus one may propose that the continuum in the UV-VIS region is composed mainly of the radical-cation emission with some contribution from the neutral.

Table 2.9 The Electronic States of the He Species

Valence Electron Configuration[a]	Electronic States
$(1s)^2$	$(1s)\ ^1S$
(1s)(ns)	$(ns)\ ^3S$, $(ns)\ ^1S$
(1s)(np)	$(np)\ ^3P$, $(np)\ ^1P$
(1s)(nd)	$(nd)\ ^3D$, $(nd)\ ^1D$

[a]The principal quantum number, n = 2, 3, 4, 5, ...

Table 2.10 The Observed Emissions of the Neutral He Target Gas

Electronic Transition	Observed Wavelength λ(nm)[a]	Partner Projectile Ion
$(4p)\,^3P^0 \rightarrow (2s)\,^2S$	317.2	N_2^{+*}
$(5d)\,^3D \rightarrow (2p)\,^3P^0$	402.4	N_2^{+*}
$(4d)\,^3D \rightarrow (2p)\,^3P^0$	447.3	N_2^{+*}
$(3d)\,^3D \rightarrow (2p)\,^3P^0$	587.6	N_2^{+*}, CO^{+*}, CO_2^{+*}, $C_2O_2^{+*}$
$(3d)\,^1D \rightarrow (2p)\,^1P^0$	668.4	N_2^{+*}, CO^{+*}, CO_2^{+*}, $C_2O_2^{+*}$

[a]Average Uncertainty, $\lambda \pm 0.5$ nm.

Table 2.11 The Electronic States of the Ar Species

Valence Electron Configuration[a]	Electronic States	$Ar^{+*}(^2P^0_{3/2}, {}^2P^0_{1/2})$ Coupled Core
$(3s)^2(3p)^6$	$(3p)\ {}^1S_0$	
$(3s)^2(3p)^5(ns)$	$(ns)\ [3/2]^0_{(2,1)}$	$^2P^0_{3/2}$
	$(ns')\ [1/2]^0_{(0,1)}$	$^2P^0_{1/2}$
$(3s)^2(3p)^5(np)$	$(np)\begin{bmatrix}5/2\\3/2\\1/2\end{bmatrix}\begin{matrix}(3,2)\\(2,1)\\(1,0)\end{matrix}$	$^2P^0_{3/2}$
	$(np')\begin{bmatrix}3/2\\1/2\end{bmatrix}\begin{matrix}(1,2)\\(0,1)\end{matrix}$	$^2P^0_{1/2}$
$(3s)^2(3p)^5(nd)$	$(nd)\begin{bmatrix}7/2\\5/2\\3/2\\1/2\end{bmatrix}^0\begin{matrix}(4,3)\\(3,2)\\(2,1)\\(1,0)\end{matrix}$	$^2P^0_{3/2}$
	$(nd')\begin{bmatrix}5/2\\3/2\end{bmatrix}^0\begin{matrix}(2,3)\\(1,2)\end{matrix}$	$^2P^0_{1/2}$

[a]The j–l coupling. [b]The term symbol is $(nl)\ [K]_J$, $(nl')\ [K]_J$, when there is an even number of odd l; $(nl)\ [K]^0_J$, $(nl')\ [K]^0_J$, when there is an odd number of odd l; and (nl) and (nl') are coupled to $^2P^0_{3/2}$, and $^2P^0_{1/2}$, respectively (i.e., $^2P^0_J$).

Table 2.12 The Observed Emissions of the Neutral Ar Target Gas

Electronic Transition	Observed Wavelength λ(nm)[a]	Partner Projectile Ion
$(7d)\ [3/2]^0_2 \rightarrow (4p)\ [1/2]_1$	488.5	N_2^{+*}
$(5d)\ [7/2]^0_4 \rightarrow (4p)\ [5/2]_3$	603.1	N_2^{+*}, , CO_2^{+*}
$(4p')\ [1/2]_1 \rightarrow (4s)\ [3/2]^0_2$	696.7	N_2^{+*}, CO^{+*}, CO_2^{+*}
$(4p)\ [1/2]_1 \rightarrow (4s)\ [3/2]^0_2$	706.7	N_2^{+*}, CO^{+*}, CO_2^{+*}
$(4d)\ [7/2]^0_4 \rightarrow (4p)\ [5/2]_3$	738.6	N_2^{+*}, CO^{+*}, CO_2^{+*}
$(4p)\ [1/2]_0 \rightarrow (4s)\ [3/2]^0_2$	751.3	N_2^{+*}, CO^{+*}, CO_2^{+*}
$(4p)\ [3/2]_2 \rightarrow (4s)\ [3/2]^0_2$	763.5	N_2^{+*}, CO^{+*}, CO_2^{+*}
$(4p)\ [3/2]_1 \rightarrow (4s)\ [3/2]^0_2$	772.2	N_2^{+*}, CO^{+*}, CO_2^{+*}
$(4p')\ [3/2]_1 \rightarrow (4s')\ [1/2]^0_0$	795.4	N_2^{+*}, CO^{+*}, CO_2^{+*}
$(4p)\ [5/2]_2 \rightarrow (4s)\ [3/2]^0_2$	802.0	N_2^{+*}, CO^{+*}, CO_2^{+*}
$(4p)\ [5/2]_3 \rightarrow (4s)\ [3/2]^0_2$	811.6	N_2^{+*}, CO^{+*}, CO_2^{+*}
$(4p)\ [5/2]_2 \rightarrow (4s)\ [3/2]^0_1$	842.6	N_2^{+*}, CO^{+*}, CO_2^{+*}
$(4p')\ [3/2]_1 \rightarrow (4s')\ [1/2]^0_1$	852.8	N_2^{+*}, CO^{+*}, CO_2^{+*}
$(4d)\ [1/2]^0_1 \rightarrow (4p')\ [1/2]_1$	907.2	N_2^{+*}
$(4p)\ [1/2]_1 \rightarrow (4s)\ [3/2]^0_2$	912.2	N_2^{+*}, CO^{+*}, CO_2^{+*}

[a]Average Uncertainty, $\lambda \pm 0.5$ nm.

Table 2.13 The Electronic States of the Neutral and Radical-Cation O=O Species

Valence Electron Configuration	Electronic States
O=O	
$(2\sigma_g)^2(2\sigma_u)^2(3\sigma_g)^2(1\pi_u)^4(1\pi_g)^2$	$\tilde{X}\,^3\Sigma_g^-$, $\tilde{a}\,^1\Delta_g$, $\tilde{b}\,^1\Sigma_g^+$
$(2\sigma_g)^2(2\sigma_u)^2(3\sigma_g)^2(1\pi_u)^3(1\pi_g)^3$	$\tilde{A}\,^3\Sigma_u^+$, $\tilde{B}\,^3\Sigma_u^-$, $\tilde{C}\,^3\Delta_u$, $^1\Sigma_u^+$, $\tilde{c}\,^1\Sigma_u^-$, $^1\Delta_u$
$(2\sigma_g)^2(2\sigma_u)^2(3\sigma_g)^2(1\pi_u)^4(1\pi_g)(3\sigma_u)$	$^3\Pi_u$, $^1\Pi_u$
$(2\sigma_g)^2(2\sigma_u)^2(3\sigma_g)(1\pi_u)^4(1\pi_g)^2(3\sigma_u)$	$^5\Sigma_u^-$, $^3\Sigma_u^+$, $^3\Sigma_u^-(2)$, $^3\Delta_u$, $^1\Sigma_u^+$, $^1\Sigma_u^-$, $^1\Delta_u$
$(2\sigma_g)^2(2\sigma_u)^2(3\sigma_g)^2(1\pi_u)^4(1\pi_g)(3s\sigma_g)$	$^3\Pi_g$, $^1\Pi_g$ (Ryd.)
$O{=}O^{+\bullet}$	
$(2\sigma_g)^2(2\sigma_u)^2(3\sigma_g)^2(1\pi_u)^4(1\pi_g)$	$\tilde{X}\,^2\Pi_g$
$(2\sigma_g)^2(2\sigma_u)^2(3\sigma_g)^2(1\pi_u)^3(1\pi_g)^2$	$\tilde{a}\,^4\Pi_u$, $\tilde{A}\,^2\Pi_u$, $^2\Pi_u(2)$, $^2\Phi_u$
$(2\sigma_g)^2(2\sigma_u)^2(3\sigma_g)(1\pi_u)^4(1\pi_g)^2$	$\tilde{b}\,^4\Sigma_g^-$, $^2\Sigma_g^+$, $\tilde{B}\,^2\Sigma_g^-$, $\tilde{C}\,^2\Delta_g$
$(2\sigma_g)^2(2\sigma_u)(3\sigma_g)^2(1\pi_u)^4(1\pi_g)^2$	$\tilde{c}\,^4\Sigma_u^-$, $^2\Sigma_u^-$, $^2\Delta_u$, $^2\Sigma_u^+$

Table 2.14 The Observed Emissions of the Neutral and Radical-Cation O=O Target Gas

Electronic Transition	Observed Wavelength λ(nm)[a]	Partner Projectile Ion
$O{=}O^{+\bullet}$		
$\tilde{A}^2\Pi_u \rightarrow \tilde{X}^2\Pi_g$	190–610[c]	$N_2^{+\bullet}$, $CO^{+\bullet}$, $CO_2^{+\bullet}$, $C_2O_2^{+\bullet}$
$\tilde{b}^4\Sigma_g^- \rightarrow \tilde{a}^4\Pi_u$		
Δv[b]		
+2	526.1	$N_2^{+\bullet}$, $CO^{+\bullet}$, $CO_2^{+\bullet}$, $C_2O_2^{+\bullet}$
+1	560.0	$N_2^{+\bullet}$, $CO^{+\bullet}$, $CO_2^{+\bullet}$, $C_2O_2^{+\bullet}$
0	599.8	$N_2^{+\bullet}$, $CO^{+\bullet}$, $CO_2^{+\bullet}$, $C_2O_2^{+\bullet}$
−1	637.3	$N_2^{+\bullet}$, $CO^{+\bullet}$, $CO_2^{+\bullet}$, $C_2O_2^{+\bullet}$
O=O		
$\tilde{B}^3\Sigma_u^- \rightarrow \tilde{X}^3\Sigma_g^-$	190–500[c]	$N_2^{+\bullet}$, $CO^{+\bullet}$, $CO_2^{+\bullet}$, $C_2O_2^{+\bullet}$

[a]Average Uncertainty, $\lambda \pm 0.5$ nm. [b]$\Delta v = (v',v'') = v' - v''$. [c]Overlapping continuum.

At this point, one should mention that O_2 is the most effective neutralization (and reionization) target gas of those used here in the CIE experiments discussed in the following sections 2.2-2.5. As one will see, trend towards neutral parent emissions is that there is none, some, and then a marked increased occurrence, on the utilization of He, Ar, and O_2, respectively, as a target gas. As well, if one steady state population of O=O[$\tilde{B}\,^3\Sigma_u^-$] with its long radiative lifetime is proposed to build up, it may in certain instances (see the $C_2F_4^{+\bullet}$ section of Chapter 3) interact differently with certain isomers and yield collision gas dependent CID mass spectra.

2.2 The Nitrogen N≡N System

This section will deal with the CIE studies of the N≡N system, the observed emissions of the parent and its fragments, and discuss its behaviour and the processes occurring during the collision event [29-31, 34-37, 40, 43, 69-75].

At this point, one should note that the radiative lifetimes [69, 72, 75], τ_{rad}, for the radical-cation $\tilde{B}\,^2\Sigma_u^+$, $\tilde{A}\,^2\Pi_u$ and neutral $(3s\sigma_g)$ $\tilde{e}\,^3\Sigma_g^+$, $\tilde{c}\,^3\Pi_u$, and $\tilde{b}\,^3\Pi_g$ electronic states are ≈ 70ns, ≈ 17 μs, ≈ 190 μs, ≈ 37 ns, and ≈ 8 μs, respectively. Now, Table 2.15, Figure 2.7 [69], and Table 2.16, illustrate the electronic states of the neutral and radical-cation N≡N species, the potential energy curves of the N≡N and $N{\equiv}N^{+\bullet}$ species, and the expected emissions of the $N{\equiv}N^{+\bullet}$/He, Ar, O_2 systems, respectively. As well, Figures 2.8, 2.9, and 2.10, illustrate the experimental CIE spectra of $N{\equiv}N^{+\bullet}$ with the target gases, He, Ar, and O_2, respectively; whilst Table 2.17 catalogues their observed wavelengths (see Appendix A for additional information on the selection rules, and the Wigner-Witmer Correlation Rules). The partner target gas column of Table 2.17 indicates in which of the CIE spectra (i.e., Figure 2.8, 2.9, or 2.10) the emissions were observed.

Now, for the N≡N system the heat of formation values of interest are $\Delta_f H^0[N{\equiv}N[\,\tilde{X}\,^1\Sigma_g^+]] = 0.0$ kJ•mol^{-1} and $\Delta_f H^0[N{\equiv}N^{+\bullet}[\,\tilde{X}\,^2\Sigma_g^+]] = 1503.3$ kJ•mol^{-1} [1]. The adiabatic ionization energy values [1, 43] (see Section 2.1.4, Table 2.4) to reach the $\tilde{X}\,^2\Sigma_g^+$, $\tilde{A}\,^2\Pi_u$, and $\tilde{B}\,^2\Sigma_u^+$ electronic states of $N{\equiv}N^{+\bullet}$ are 15.58, 16.69, and 18.76 eV, respectively. For the neutral manifold, on inspection of Figure 2.7 [69, 70], the dissociation limits of interest are,

Table 2.15 The Electronic States of the Neutral and Radical-Cation N≡N Species

Valence Electron Configuration	Electronic States
N≡N	
$(2\sigma_g)^2(2\sigma_u)^2(1\pi_u)^4(3\sigma_g)^2$	$\tilde{X}\,^1\Sigma_g^+$
$(2\sigma_g)^2(2\sigma_u)^2(1\pi_u)^3(3\sigma_g)^2(1\pi_g)$	$\tilde{a}\,^3\Sigma_u^+$, $\tilde{w}\,^3\Delta_u$, $\tilde{b}'\,^3\Sigma_u^-$, $\tilde{A}'\,^1\Sigma_u^-$, $\tilde{W}\,^1\Delta_u$, $\tilde{B}'\,^1\Sigma_u^+$
$(2\sigma_g)^2(2\sigma_u)^2(1\pi_u)^4(3\sigma_g)(1\pi_g)$	$\tilde{b}\,^3\Pi_g$, $\tilde{B}\,^1\Pi_g$
$(2\sigma_g)^2(2\sigma_u)(1\pi_u)^4(3\sigma_g)^2(1\pi_g)$	$\tilde{c}\,^3\Pi_u$, $^1\Pi_u$
$(2\sigma_g)^2(2\sigma_u)^2(1\pi_u)^4(3\sigma_g)(3s\sigma_g)$	$\tilde{e}\,^3\Sigma_g^+$, $^1\Sigma_g^+$ (Ryd.)
$N\equiv N^{+\bullet}$	
$(2\sigma_g)^2(2\sigma_u)^2(1\pi_u)^4(3\sigma_g)$	$\tilde{X}\,^2\Sigma_g^+$
$(2\sigma_g)^2(2\sigma_u)^2(1\pi_u)^3(3\sigma_g)^2$	$\tilde{A}\,^2\Pi_u$
$(2\sigma_g)^2(2\sigma_u)(1\pi_u)^4(3\sigma_g)^2$	$\tilde{B}\,^2\Sigma_u^+$
$(2\sigma_g)^2(2\sigma_u)^2(1\pi_u)^3(3\sigma_g)(1\pi_g)$	$^4\Sigma_u^+$, $^4\Delta_u$, $^4\Sigma_u^-$, $\tilde{C}\,^2\Sigma_u^+$, $^2\Sigma_u^+$, $^2\Delta_u(2)$, $^2\Sigma_u^-(2)$
$(2\sigma_g)^2(2\sigma_u)^2(1\pi_u)^2(3\sigma_g)^2(1\pi_g)$	$^4\Pi_g$, $^2\Phi_g$, $\tilde{D}\,^2\Pi_g$, $^2\Pi_g(2)$

Figure 2.7 The Potential Energy Curves of the N≡N and N≡N$^{+\bullet}$ Species

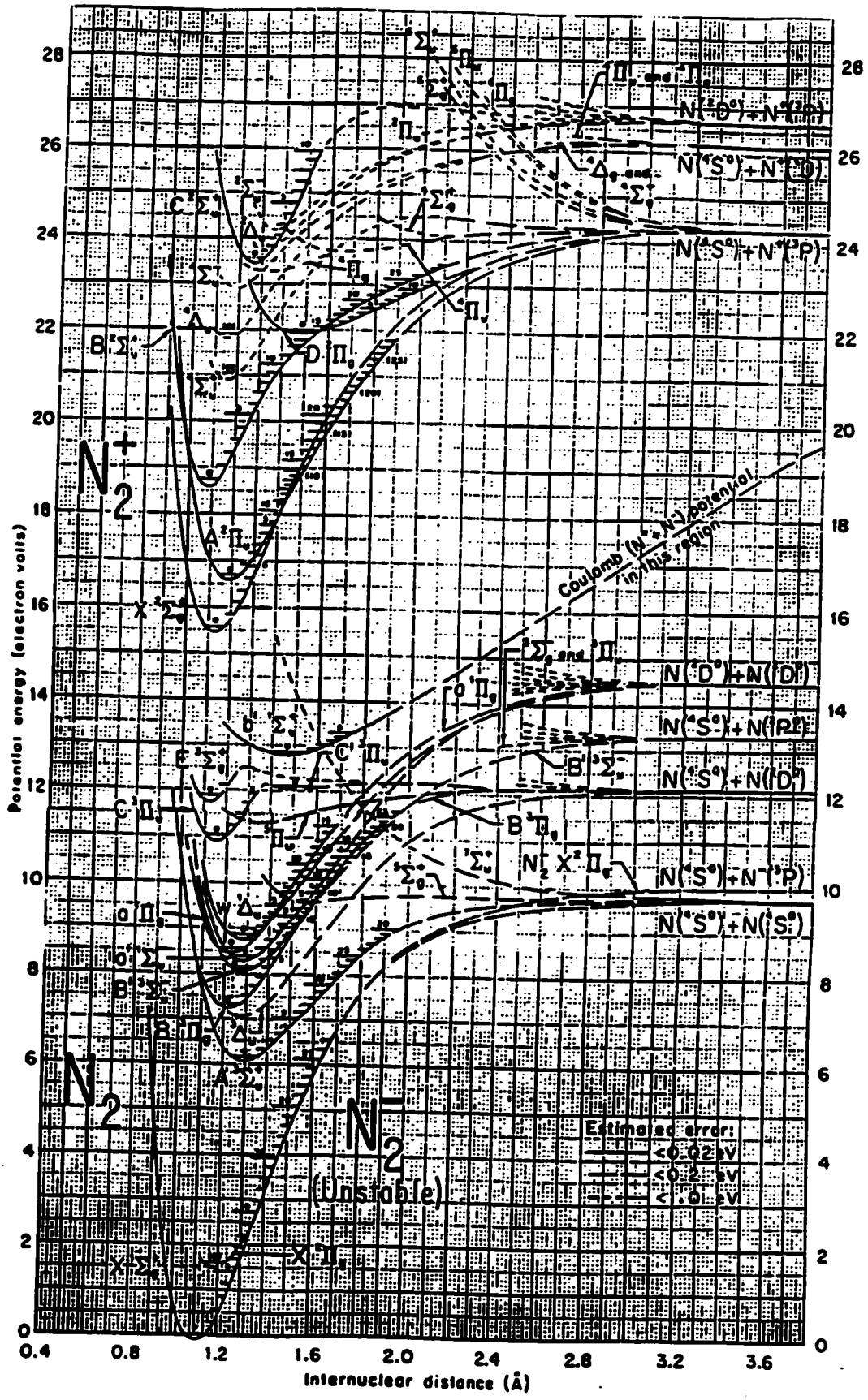

Table 2.16 The Expected Emissions of the $N{\equiv}N^{+*}$/He, Ar, O_2 Systems

Electronic Transition	Comment
$N{\equiv}N^{+*}$	
$\tilde{C}^2\Sigma_u^+ \rightarrow \tilde{X}^2\Sigma_g^+$	He
$\tilde{D}^2\Pi_g \rightarrow \tilde{A}^2\Pi_u$	He
$\tilde{B}^2\Sigma_u^+ \rightarrow \tilde{X}^2\Sigma_g^+$	dominant, UV
$\tilde{A}^2\Pi_u \rightarrow \tilde{X}^2\Sigma_g^+$	VIS-NIR
$N{\equiv}N$	
$\tilde{c}^3\Pi_u \rightarrow \tilde{b}^3\Pi_g$	Ar, O_2 UV-VIS
$\tilde{b}^3\Pi_g \rightarrow \tilde{a}^3\Sigma_u^+$	O_2, NIR

Important Atomics	
N^+	
$(2p)\ ^1D \rightarrow (2p)\ ^3P$	$N_2^{+*}[^4\Delta_u] \rightarrow N^+[(2p)\ ^1D] + N^*[(2p)\ ^4S^0]$

Figure 2.8 The Collision-Induced Emission (CIE) Spectrum of the N≡N$^{+\bullet}$/He System

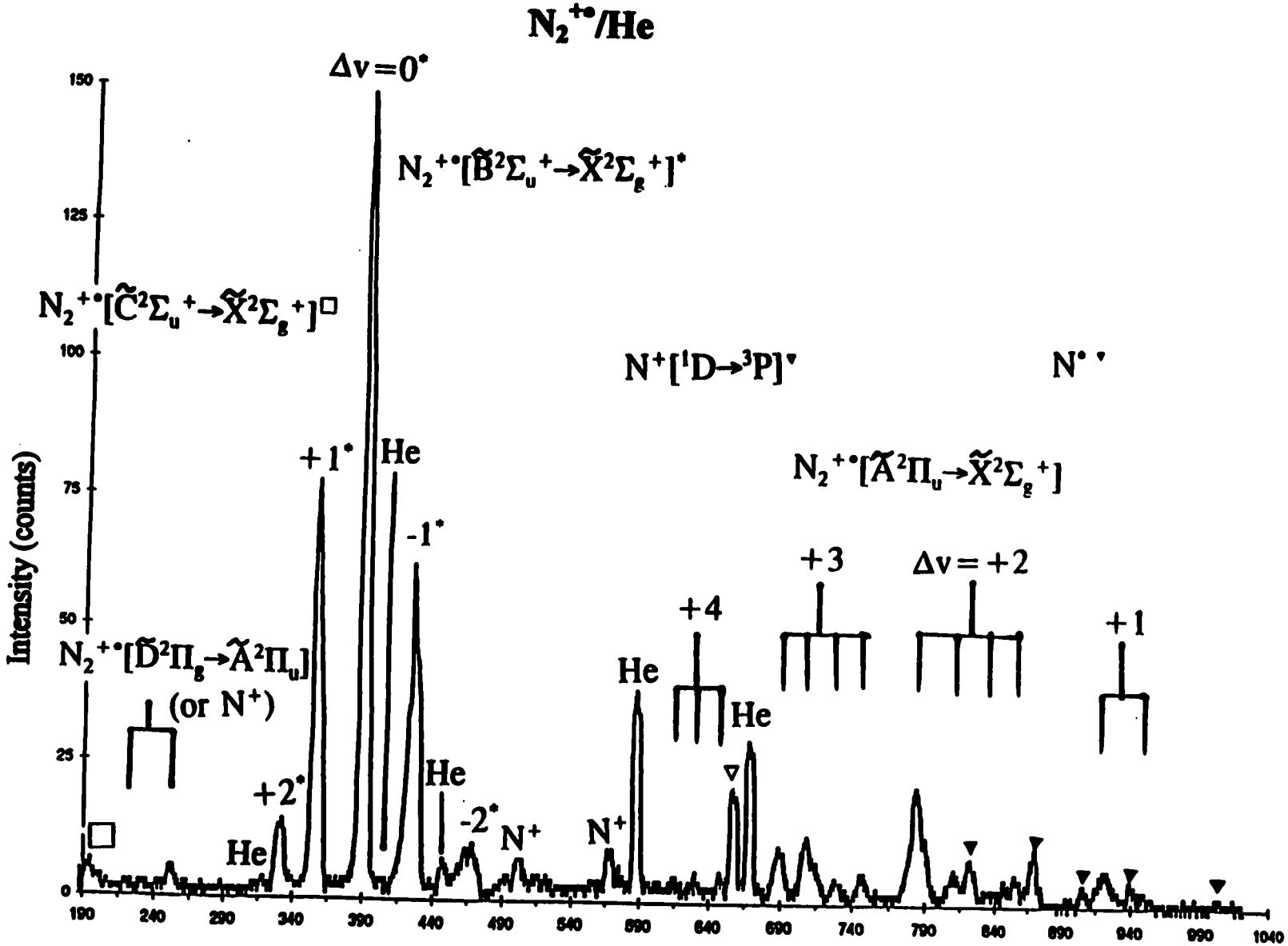

Figure 2.9 The Collision-Induced Emission (CIE) Spectrum of the N≡N$^{+\bullet}$/Ar System

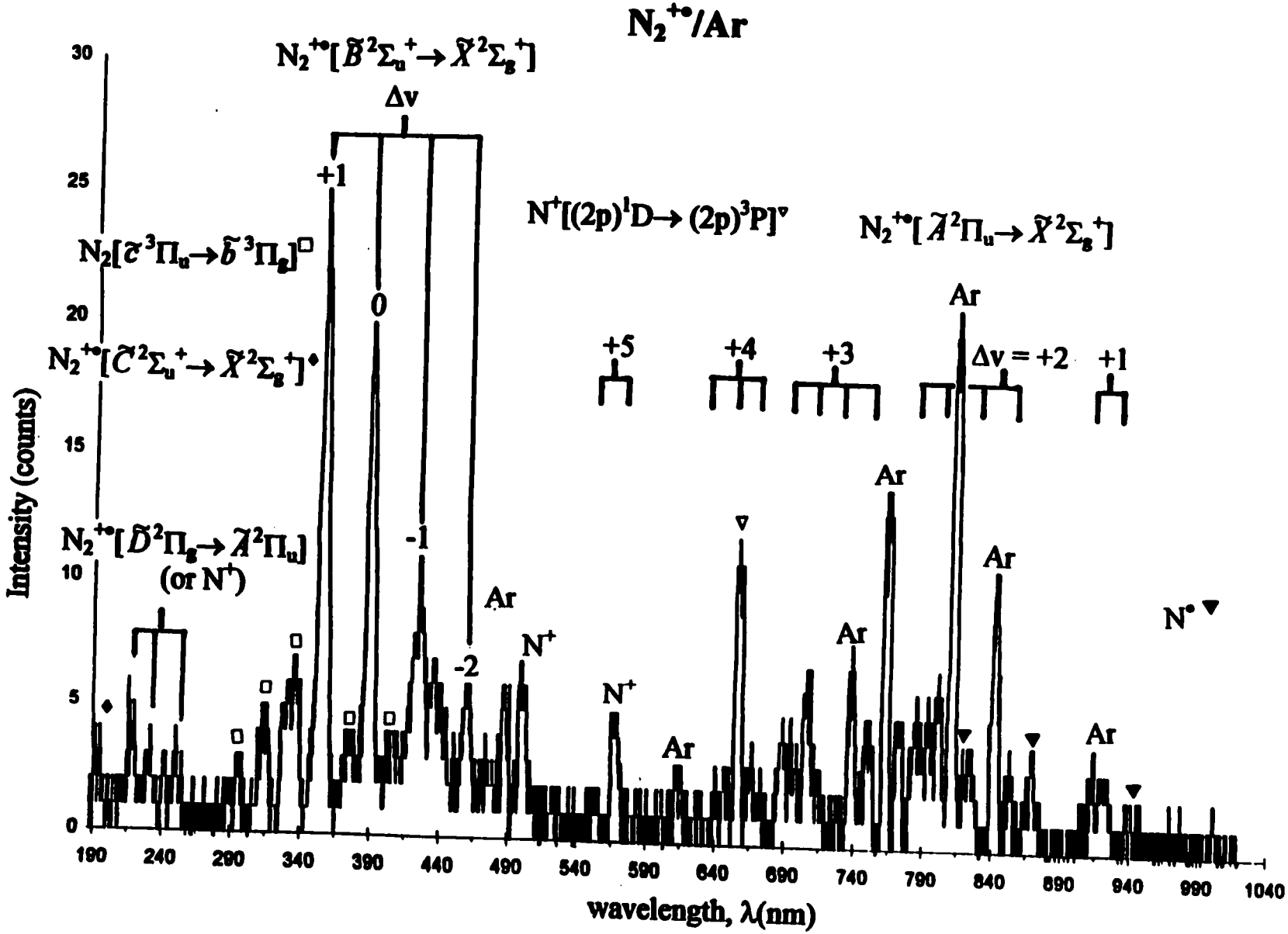

Figure 2.10 The Collision-Induced Emission (CIE) Spectrum of the N≡N$^{+\bullet}$/O_2 System

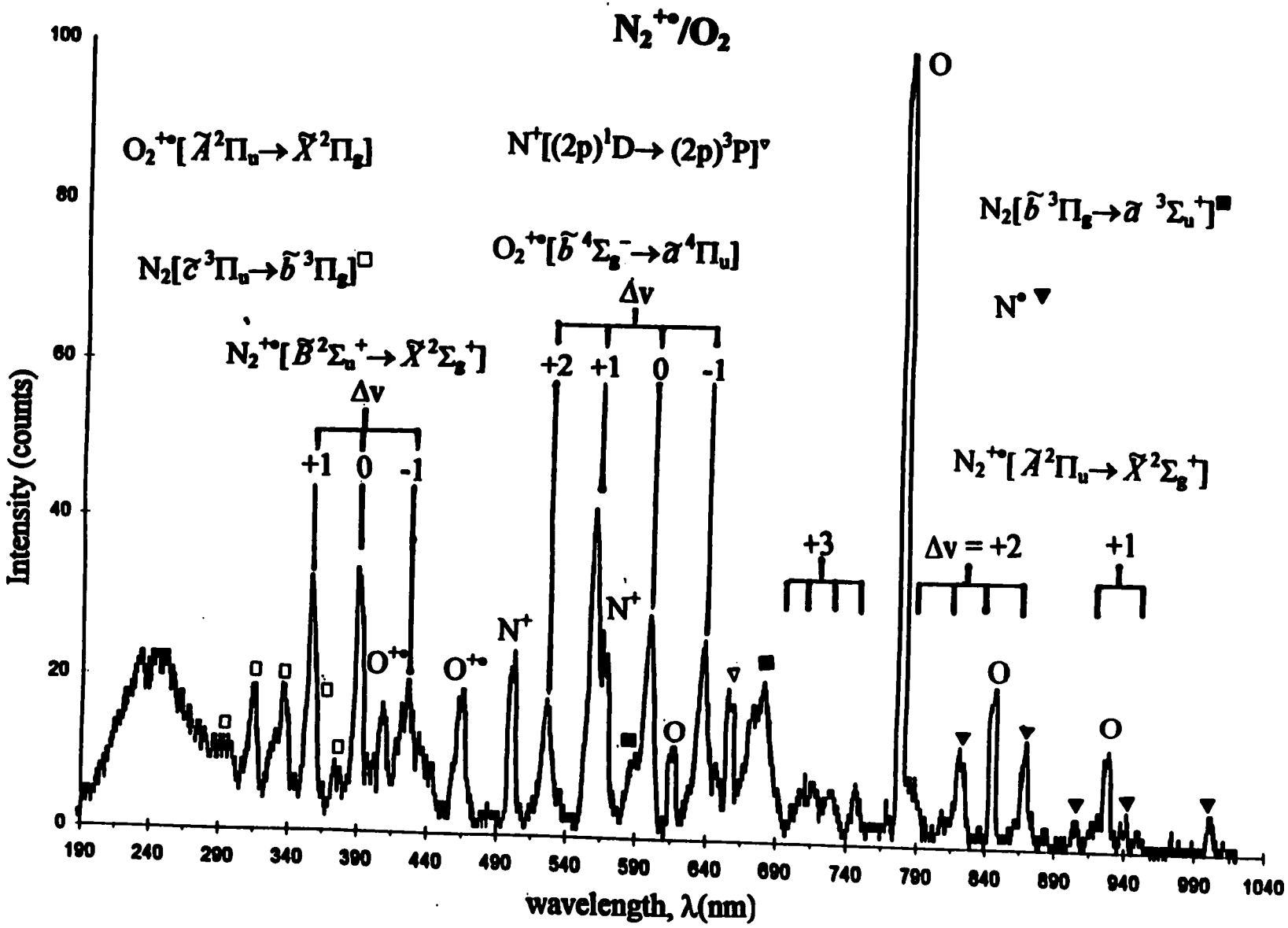

Table 2.17 The Observed Emissions of the Neutral and Radical-Cation N≡N Projectile

Electronic Transition	Observed Wavelength λ(nm)[a]	Partner Target Gas
$N{\equiv}N^{+\bullet}$		
$\tilde{C}^2\Sigma_u^+ \rightarrow \tilde{X}^2\Sigma_g^+$		
Δv[b]		
−6, (3,9)	191.2	He, Ar
−7, (5,12)	197.1	He
, (3,10)	198.6	He
$\tilde{D}^2\Pi_g \rightarrow \tilde{A}^2\Pi_u$		
Δv		
+7, (9,2)	216.7	He, Ar
+5, (7,2)	223.3	He, Ar
+3, (5,2)	231.1	He, Ar
+1, (5,4)	252.4	He, Ar
$\tilde{B}^2\Sigma_u^+ \rightarrow \tilde{X}^2\Sigma_g^+$		
Δv		
+2, (2,0)	329.6	He
+1, (1,0)	358.4	He, Ar, O_2
0, (0,0)	391.9	He, Ar, O_2
−1, (0,1)	427.6	He, Ar, O_2
−2, (0,2)	469.9	He, Ar

[a]Average Uncertainty, λ ± 0.5 nm. [b]$\Delta v = (v',v'') = v' - v''$.

Table 2.17 The Observed Emissions of the Neutral and Radical-Cation N≡N Projectile (Continued)

Electronic Transition	Observed Wavelength λ(nm)[a]	Partner Target Gas
$N{\equiv}N^{+\bullet}$		
$\tilde{A}^2\Pi_u \rightarrow \tilde{X}^2\Sigma_g^+$		
Δv[b]		
+5, (5,0)	552.7	Ar
, (6,1)	567.1	Ar
+4, (4,0)	612.7	He, Ar
, (5,1)	628.6	He, Ar
, (6,2)	645.7	He, Ar
+3, (3,0)	687.5	He, Ar, O_2
, (4,1)	706.8	He, Ar, O_2
, (5,2)	726.6	He, Ar, O_2
, (6,3)	747.5	He, Ar, O_2
+2, (2,0)	785.2	He, Ar, O_2
, (3,1)	808.2	He, Ar, O_2
, (4,2)	832.6	He, Ar, O_2
, (5,3)	857.4	He, Ar, O_2
+1, (1,0)	918.3	He, Ar, O_2
, (2,1)	947.1	He, Ar, O_2
N≡N		
$\tilde{c}^3\Pi_u \rightarrow \tilde{b}^3\Pi_g$		
Δv		
+2, (2,0)	297.4	Ar, O_2
+1, (1,0)	316.2	Ar, O_2
0, (0,0)	336.9	Ar, O_2
−1, (0,1)	358.0	Ar, O_2
−2, (0,2)	380.6	Ar, O_2
$\tilde{b}^3\Pi_g \rightarrow \tilde{a}^3\Sigma_u^+$		
Δv		
+4, (9,5)	590.5	O_2
+3, (3,0)	678.9	O_2

[a]Average Uncertainty, λ ± 0.5 nm. [b]$\Delta v = (v',v'') = v' - v''$.

$N^*[(2p)\ ^4S^0] + N^*[(2p)\ ^4S^0]$, and $N^*[(2p)\ ^2D^0] + N^*[(2p)\ ^4S^0]$ at excitation energies of 9.76, and 12.14 eV, respectively, above $\Delta_f H^0[N{\equiv}N[\ \tilde{X}\ ^1\Sigma_g^+]]$. The N≡N electronic states $\tilde{X}\ ^1\Sigma_g^+$, $\tilde{a}\ ^3\Sigma_u^+$ converge to the first; and $\tilde{b}\ ^3\Pi_g$, $\tilde{c}\ ^3\Pi_u$, $(3s\sigma_g)\ \tilde{e}\ ^3\Sigma_g^+$ converge to the second dissociation limit, respectively.

Similarly, for the radical-cation manifold [69, 70], the dissociation limits of interest are, $N^+[(2p)\ ^3P] + N^*[(2p)\ ^4S^0]$, $N^+[(2p)\ ^1D] + N^*[(2p)\ ^4S^0]$, and $N^+[(2p)\ ^3P] + N^*[(2p)\ ^2D^0]$, at excitation energies of 24.29, 26.19, and 26.68 eV, respectively, above $\Delta_f H^0[N{\equiv}N[\ \tilde{X}\ ^1\Sigma_g^+]]$. The $N{\equiv}N^{+\bullet}$ electronic states $\tilde{X}\ ^2\Sigma_g^+$, $\tilde{A}\ ^2\Pi_u$, $\tilde{B}\ ^2\Sigma_u^+$, $\tilde{D}\ ^2\Pi_g$ converge to the first; $^2\Delta_u$ converges to the second; and $\tilde{C}\ ^2\Sigma_u^+$ converges to the third dissociation limit, respectively. As previously discussed (see section 2.1.5), for radical-cation species the minimum observed internal excitation energy deposited, $\Delta(\Delta E_{int})$, during the dissociative excitation, $N^+[(2p)\ ^1D] + N^*[(2p)\ ^4S^0] \leftarrow N{\equiv}N^{+\bullet}[\ \tilde{X}\ ^2\Sigma_g^+]$, is 10.61 eV.

Now, for the mass spectrometry processes, both the metastable ion (MI), and collision induced dissociation (CID) mass spectra of $N{\equiv}N^{+\bullet}$ (m/z 28) exhibit only one peak for N^+ (m/z 14).

Thus, in summary, on inspection of the CIE spectra illustrated in Figure 2.8, 2.9, and 2.10, and Table 2.17, one may note the following trends. The $N{\equiv}N^{+\bullet}$ emissions of $\tilde{B}\ ^2\Sigma_u^+ \rightarrow \tilde{X}\ ^2\Sigma_g^+$, and $\tilde{A}\ ^2\Pi_u \rightarrow \tilde{X}\ ^2\Sigma_g^+$ are always present regardless of target gas. Whereas, for the N≡N emissions of $\tilde{c}\ ^3\Pi_u \rightarrow \tilde{b}\ ^3\Pi_g$, and $\tilde{b}\ ^3\Pi_g \rightarrow \tilde{a}\ ^3\Sigma_u^+$ only the former is observed with the Ar target gas. However, both are observed when O_2 is the target gas. This may be proposed to be due to their differences in radiative lifetimes (i.e., the $\tilde{b}\ ^3\Pi_g$ being longer lived) and/or the

greater neutralization effectiveness (see section 2.1.3, Table 2.3) of O_2 relative to Ar (as well the intense Ar emissions may have swamped out the latter emissions).

2.3 The Carbon Monoxide C≡O System

This section will deal with the CIE studies of the C≡O system, the observed emissions of the parent and its fragments, and discusses its behaviour and the processes occurring during the collision event [29-31, 34-37, 40, 43, 71, 74-79, 91].

At this point, one should note that the radiative lifetimes, [71, 75, 76, 78, 79] for the radical-cation $\tilde{B}\,^2\Sigma^+$, and $\tilde{A}\,^2\Pi$ electronic states are ≈ 50 ns, and ≈ 4 μs, respectively. Now, Table 2.18, Figure 2.11 [76, 77], and Table 2.19, illustrate the electronic states of the neutral and radical-cation C≡O species, the potential energy curves for the C≡O and $C{\equiv}O^{+\bullet}$ species, and the expected emissions of the $C{\equiv}O^{+\bullet}$/He, Ar, O_2 systems, respectively. As well, Figures 2.12, 2.13, 2.14, illustrate the experimental CIE spectra of $C{\equiv}O^{+\bullet}$ with target gas, He, Ar, and O_2, respectively; whilst Table 2.20 catalogues their observed wavelengths (see Appendix A for additional information the selection rules, and the Wigner-Witmer Correlation Rules). The partner target gas column of Table 2.20 indicates in which of the CIE spectra (i.e., Figure 2.12, 2.13, or 2.14) the emissions were observed.

Now, for the C≡O system the heat of formation values of interest are $\Delta_f H^0[C{\equiv}O[\tilde{X}\,^1\Sigma^+]]$ = −110.5 kJ•mol^{-1} and $\Delta_f H^0[C{\equiv}O^{+\bullet}[\tilde{X}\,^2\Sigma^+]]$ = 1241.6 kJ•mol^{-1} [1]. The adiabatic ionization energy values [1, 43] (see section 2.1.4, Table 2.4) to reach the $\tilde{X}\,^2\Sigma^+$, $\tilde{A}\,^2\Pi$, and $\tilde{B}\,^2\Sigma^+$ electronic states of $C{\equiv}O^{+\bullet}$ are 14.01, 16.53, and 19.68 eV, respectively.

For the neutral manifold, on inspection of Figure2.11 [76, 77], the dissociation limit of interest is C[(2p) ^{3}P] + O[(2p) ^{3}P] at an excitation energy of 11.09 eV above $\Delta_f H^0[C{\equiv}O[\tilde{X}\,^1\Sigma^+]]$. The C≡O electronic states of $\tilde{X}\,^1\Sigma^+$, $\tilde{a}\,^3\Pi$, $\tilde{a}'\,^3\Sigma^+$, $\tilde{d}\,^3\Delta$, $\tilde{e}\,^3\Sigma^-$, $\tilde{A}\,^1\Pi$, $\tilde{I}\,^1\Sigma^-$, $^1\Delta$, and $^1\Sigma^+$ converge to this dissociation limit.

Table 2.18 The Electronic States of the the Neutral and Radical-Cation C≡O Species

Valence Electron Configuration	Electronic States
C≡O	
$(3\sigma)^2(4\sigma)^2(1\pi)^4(5\sigma)^2$	$\tilde{X}\,^1\Sigma^+$
$(3\sigma)^2(4\sigma)^2(1\pi)^4(5\sigma)\,(2\pi)$	$\tilde{a}\,^3\Pi$, $\tilde{A}\,^1\Pi$
$(3\sigma)^2(4\sigma)^2(1\pi)^3(5\sigma)^2(2\pi)$	$\tilde{a}\,'^3\Sigma^+$, $\tilde{d}\,^3\Delta$, $\tilde{e}\,^3\Sigma^-$, $\tilde{I}\,^1\Sigma^-$, $^1\Delta$, $^1\Sigma^+$
$(3\sigma)^2(4\sigma)^2(1\pi)^4(5\sigma)\,(3s\sigma)$	$\tilde{b}\,^3\Sigma^+$, $\tilde{B}\,^1\Sigma^+$ (Ryd.)
$(3\sigma)^2(4\sigma)^2(1\pi)^4(5\sigma)\,(3p\sigma)$	$\tilde{j}\,^3\Sigma^+$, $\tilde{C}\,^1\Sigma^+$ (Ryd.)
$(3\sigma)^2(4\sigma)^2(1\pi)^4(5\sigma)\,(3p\pi)$	$\tilde{c}\,^3\Pi$, $\tilde{E}\,^1\Pi$ (Ryd.)
$(3\sigma)^2(4\sigma)^2(1\pi)^3(5\sigma)^2(3p\pi)$	$^3\Sigma^+$, $^3\Delta$, $^3\Sigma^-$, $^1\Sigma^+$, $^1\Delta$, $^1\Sigma^-$ (Ryd.)
C≡O$^{+\bullet}$	
$(3\sigma)^2(4\sigma)^2(1\pi)^4(5\sigma)$	$\tilde{X}\,^2\Sigma^+$
$(3\sigma)^2(4\sigma)^2(1\pi)^3(5\sigma)^2$	$\tilde{A}\,^2\Pi$
$(3\sigma)^2(4\sigma)\,(1\pi)^4(5\sigma)^2$	$\tilde{B}\,^2\Sigma^+$
$(3\sigma)^2(4\sigma)^2(1\pi)^2(5\sigma)^2(2\pi)$	$\tilde{a}\,^4\Pi$, $^2\Phi$, $^2\Pi(3)$
$(3\sigma)^2(4\sigma)^2(1\pi)^2(5\sigma)^2(6\sigma)$	$^4\Sigma^-$, $^2\Sigma^-$, $^2\Sigma^+$, $^2\Delta$

Figure 2.11 The Potential Energy Curves of the C≡O and C≡O$^{+\bullet}$ Species

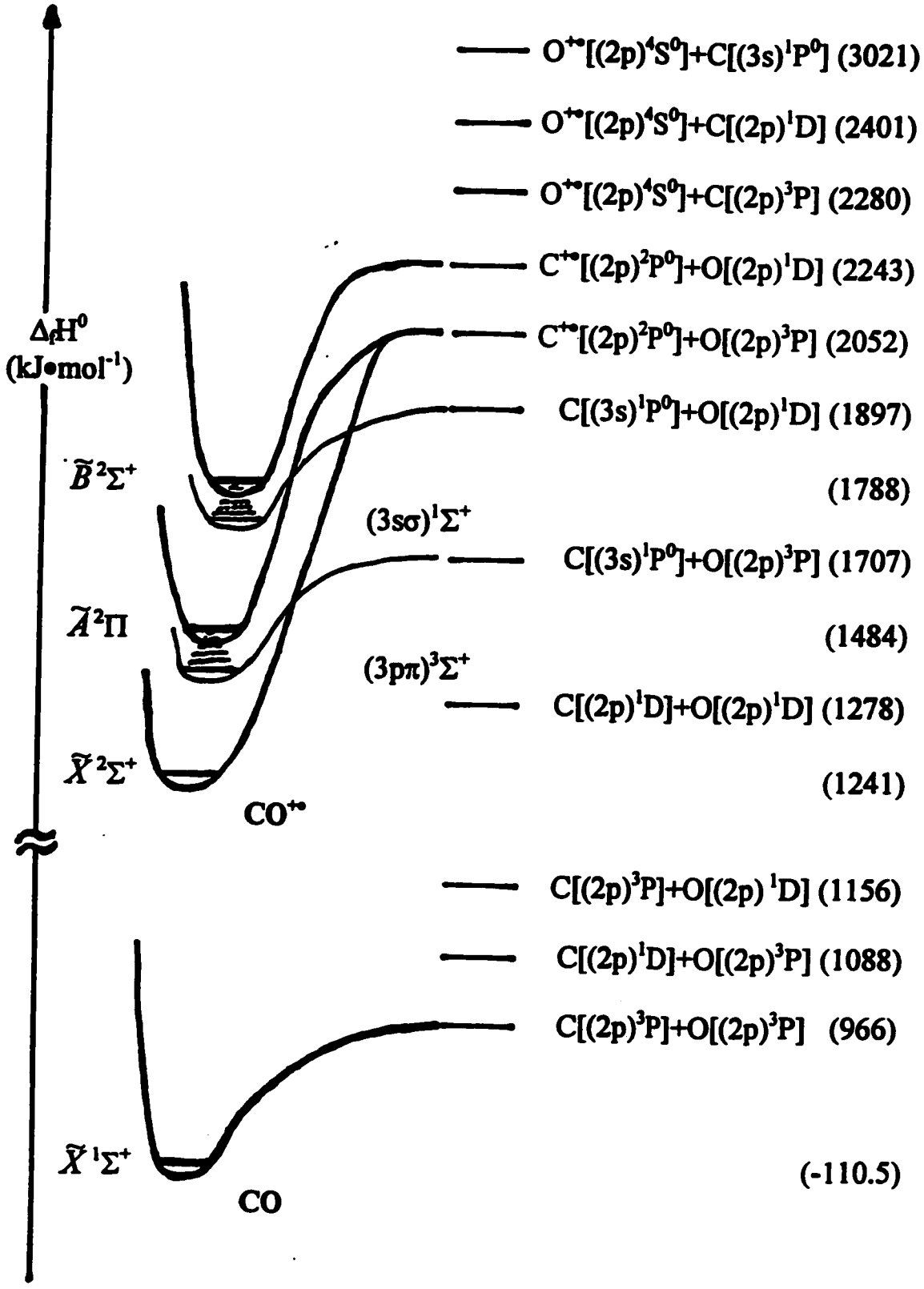

Table 2.19 The Expected Emissions of the C≡O$^{+\bullet}$/He, Ar, O_2 Systems

Electronic Transition	Comment
C≡O$^{+\bullet}$	
$\tilde{B}\,^2\Sigma^+ \rightarrow \tilde{X}\,^2\Sigma^+$	dominant, UV
$\tilde{B}\,^2\Sigma^+ \rightarrow \tilde{A}\,^2\Pi$	not observed
$\tilde{A}\,^2\Pi \rightarrow \tilde{X}\,^2\Sigma^+$	VIS
C≡O	
$\tilde{e}\,^3\Sigma^- \rightarrow \tilde{a}\,^3\Pi$	O_2, VIS
$\tilde{d}\,^3\Delta \rightarrow \tilde{a}\,^3\Pi$	O_2, VIS
$\tilde{a}\,'^3\Sigma^+ \rightarrow \tilde{a}\,^3\Pi$	O_2, NIR

Important Atomics	
O	
(2p) ^{1}D → (2p) ^{3}P	$CO^{+\bullet}[\tilde{B}\,^2\Sigma^+] \rightarrow C^{+\bullet}[(2p)\,^2P^0] + O[(2p)\,^1D]$

Figure 2.12 The Collision-Induced Emission (CIE) Spectrum of the C≡O$^{+\bullet}$/He System

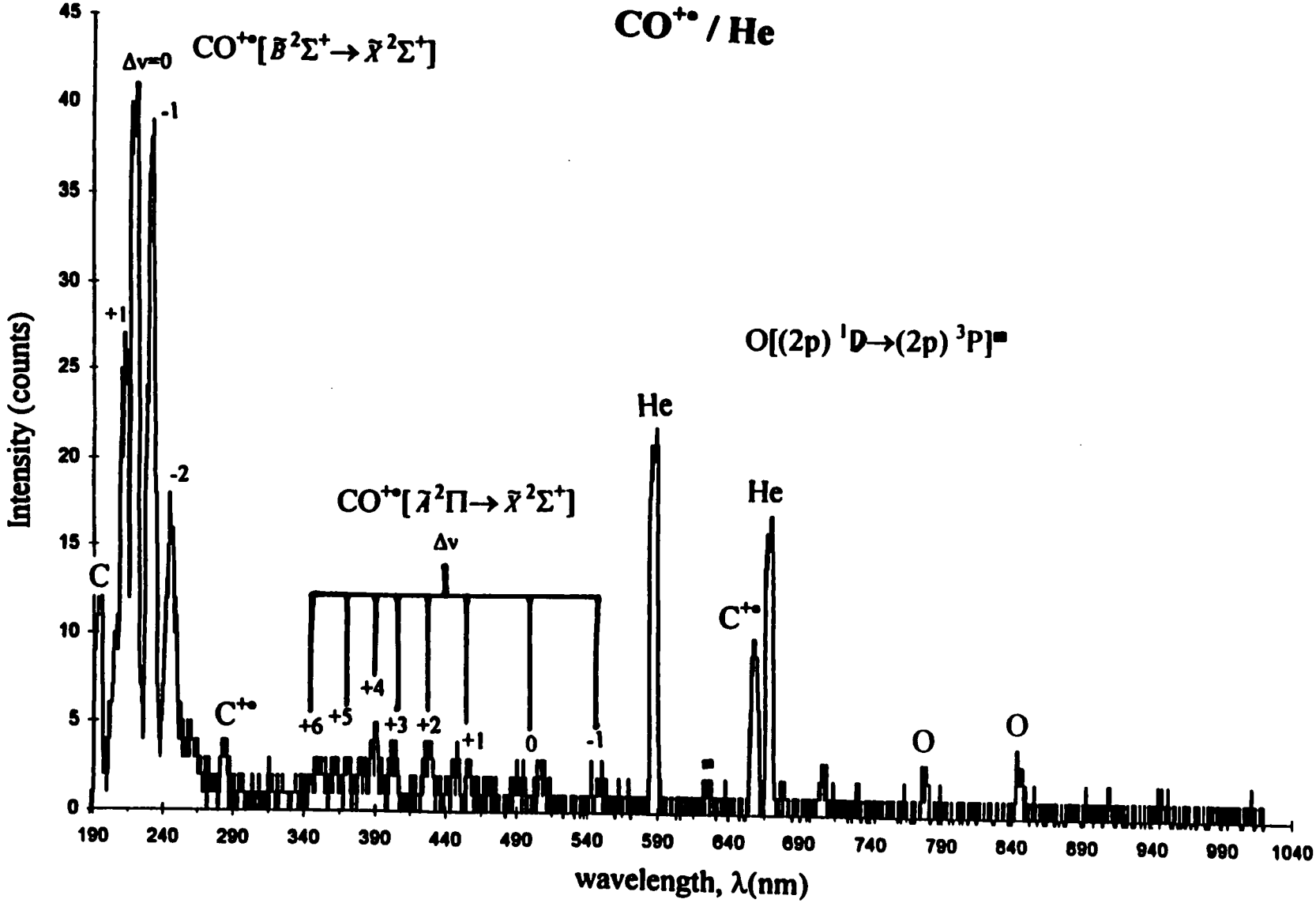

Figure 2.13 The Collision-Induced Emission (CIE) Spectrum of the C≡O$^{+\bullet}$/Ar System

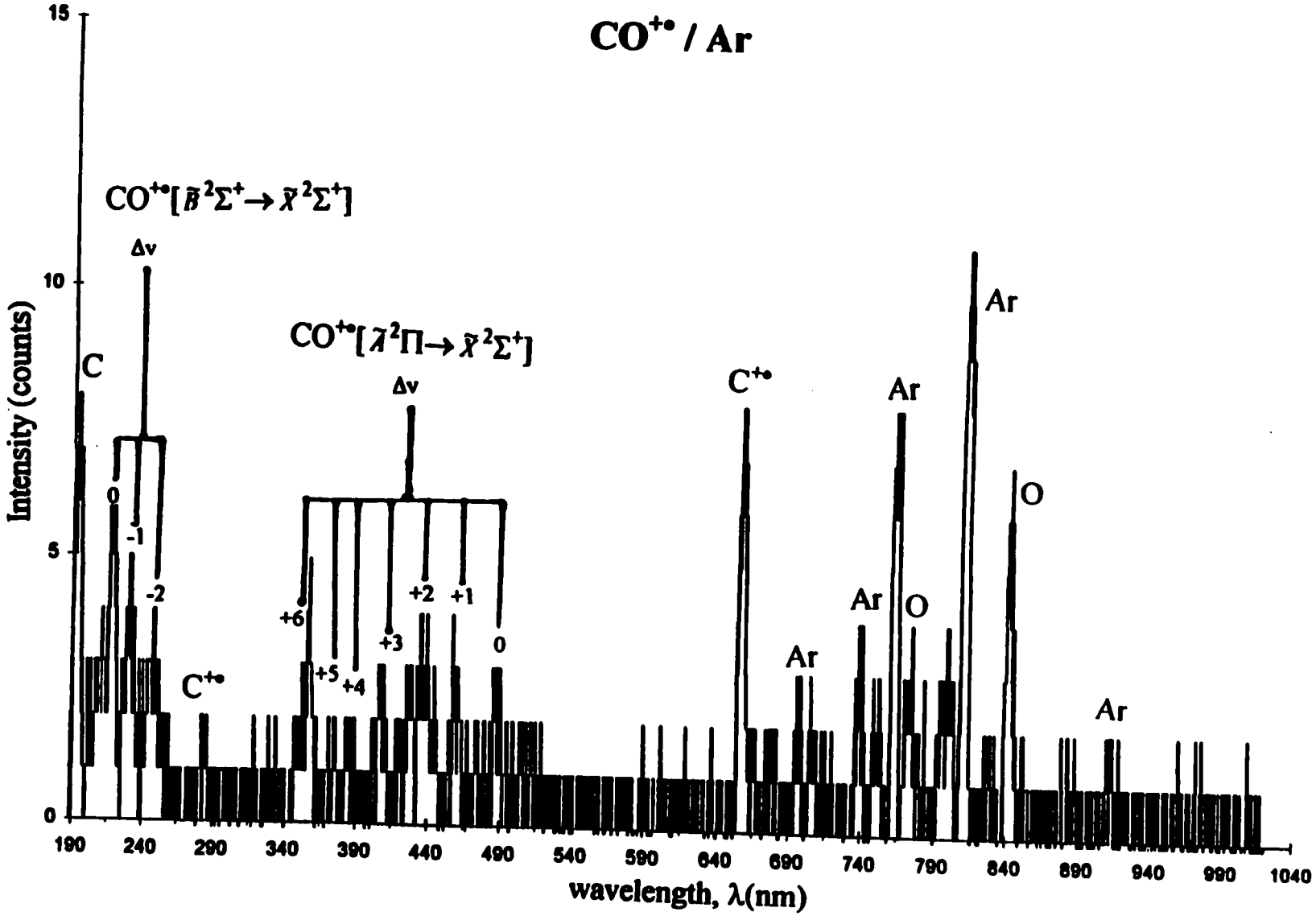

Figure 2.14 The Collision-Induced Emission (CIE) Spectrum of the C≡O$^{+\bullet}$/O_2 System

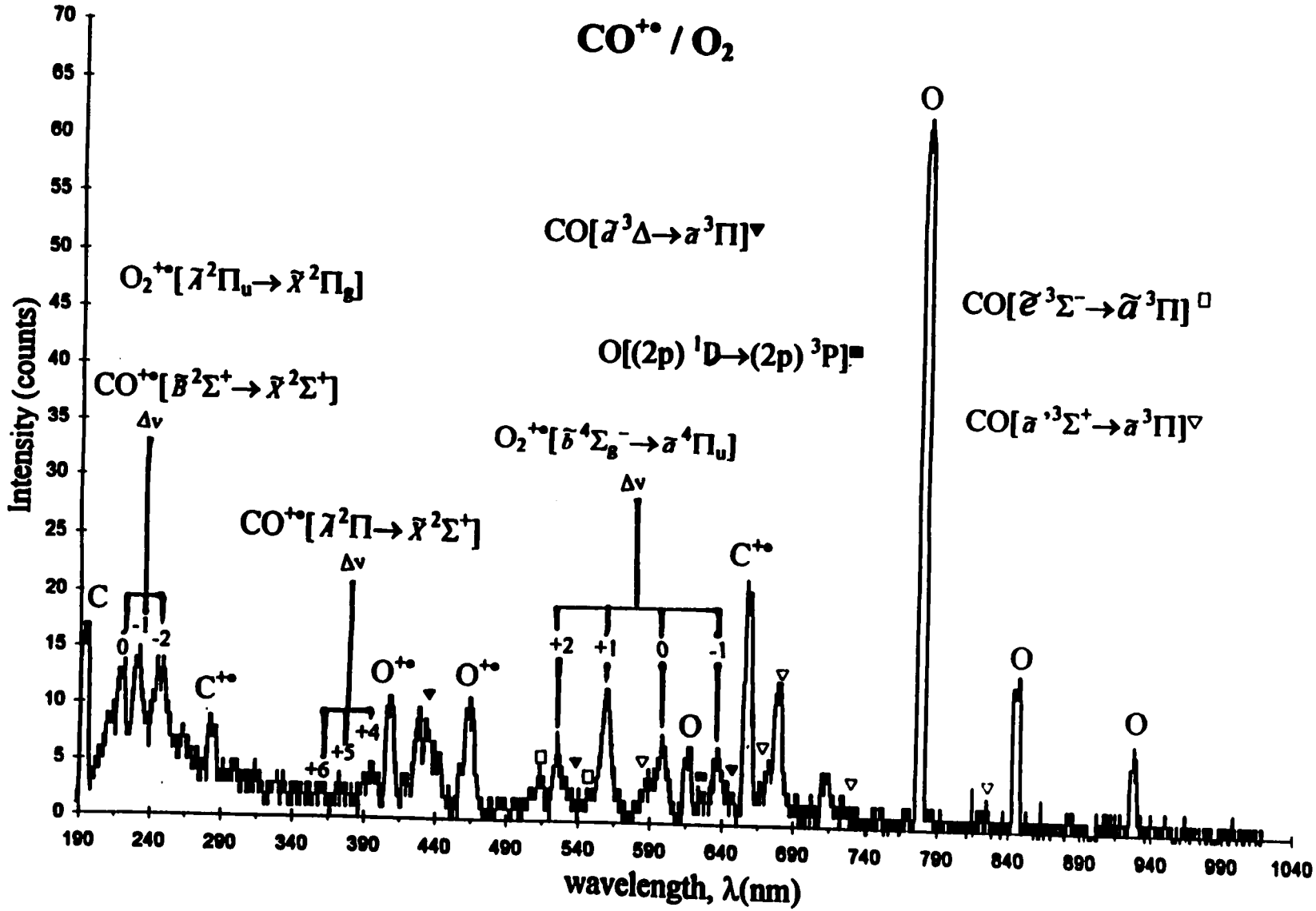

Table 2.20 The Observed Emissions of the Neutral and Radical-Cation C≡O Projectile

Electronic Transition	Observed Wavelength λ(nm)[a]	Partner Target Gas
$C{\equiv}O^{+\bullet}$		
$\tilde{B}^2\Sigma^+ \rightarrow \tilde{X}^2\Sigma^+$		
Δv^b		
+1, (1,0)	211.6	He
0, (0,0)	218.9	He, Ar, O_2
−1, (0,1)	230.0	He, Ar, O_2
−2, (2,4)	247.3	He, Ar, O_2
$\tilde{A}^2\Pi \rightarrow \tilde{X}^2\Sigma^+$		
Δv		
+6, (6,0)	342.4	He, , O_2
, (7,1)	352.3	He, Ar
+5, (5,0)	359.3	He, Ar, O_2
, (6,1)	369.8	He, , O_2
+4, (4,0)	378.8	He, Ar, O_2
, (5,1)	390.4	He, , O_2
+3, (3,0)	401.4	He, Ar
+2, (2,0)	426.4	He, Ar
, (3,1)	439.2	He, Ar
+1, (1,0)	455.5	He, Ar
, (2,1)	470.3	He
0, (0,0)	490.5	He, Ar
, (1,1)	506.6	He, Ar
−1, (0,1)	548.8	He

[a]Average Uncertainty, λ ± 0.5 nm. [b]$\Delta v = (v',v'') = v' - v''$.

Table 2.20 The Observed Emissions of the Neutral and Radical-Cation C≡O Projectile (Continued)

Electronic Transition	Observed Wavelength λ(nm)[a]	Partner Target Gas
C≡O		
$\tilde{d}\,^3\Delta \rightarrow \tilde{a}\,^3\Pi$		
Δv[b]		
+9, (11,2)	432.7	O_2
+3, (3,0)	533.1	O_2
0, (0,0)	643.4	O_2
$\tilde{e}\,^3\Sigma^- \rightarrow \tilde{a}\,^3\Pi$		
Δv		
+3, (3,0)	512.6	O_2
+2, (2,0)	541.3	O_2
$\tilde{a}\,'^3\Sigma^+ \rightarrow \tilde{a}\,^3\Pi$		
Δv		
+9, (9,0)	586.3	O_2
+8, (10,2)	680.5	O_2
, (11,3)	711.8	O_2
+7, (7,0)	668.8	O_2
+6, (6,0)	721.0	O_2
+5, (6,1)	822.3	O_2

[a]Average Uncertainty, $\lambda \pm 0.5$ nm. [b]$\Delta v = (v',v'') = v' - v''$.

Similarly, for the radical-cation manifold [76, 77], the dissociation limits of interest are, $C^{+\bullet}[(2p)\ ^2P^0] + O[(2p)\ ^3P]$, and $C^{+\bullet}[(2p)\ ^2P^0] + O[(2p)\ ^1D]$ at excitation energies of 23.36, and 24.33 eV, respectively above $\Delta_f H^0[C{\equiv}O[\ \tilde{X}\ ^1\Sigma^+]]$. The $C{\equiv}O^{+\bullet}$ electronic states $\tilde{X}\ ^2\Sigma^+$, $\tilde{A}\ ^2\Pi$, $\tilde{a}\ ^4\Pi$, converge to the first; and $\tilde{B}\ ^2\Sigma^+$ converges to the second dissociation limit, respectively. As previously discussed (see section 2.1.5) for the radical-cation species the minimum observed internal excitation energy deposited, $\Delta(\Delta E_{int})$, during the dissociative excitation, $C^{+\bullet}[(2p)\ ^2P^0] + O[(2p)\ ^1D] \leftarrow C{\equiv}O^{+\bullet}[\ \tilde{X}\ ^2\Sigma_g^+]$, is 10.32 eV.

At this point, the intensity of the $C[(3s)\ ^1P^0 \rightarrow (2p)\ ^1D]$ emission at 193.1 nm deserves mention. On inspection of Figures 2.12, 2.13, and 2.14, one may note that its relative intensity increases as one goes across the series of target gases, He, Ar, and O_2 respectively. The explanation for this is found on inspection of Figure 2.11, the potential energy curves of the C≡O and $C{\equiv}O^{+\bullet}$ species. For He, the possibility that the neutralization process occurring is remote and thus the dissociation limit of $O^{+\bullet}[(2p)\ ^4S^0] + C[(3s)\ ^1P^0]$ at an excitation energy of 18.44 eV above $\Delta_f H^0[C{\equiv}O[\ \tilde{X}\ ^1\Sigma^+]]$ must be accessed. However, when Ar, and O_2 are utilized and neutralization becomes more favourable, a lower energy route becomes available. There are two auto-ionizating Rydberg states of neutral C≡O denoted as $(3p\pi)\ ^3\Sigma^+$, and $(3s\sigma)\ ^1\Sigma^+$ that auto-ionizes to the $C{\equiv}O^{+\bullet}$ electronic state of $\tilde{A}\ ^2\Pi$, and $\tilde{B}\ ^2\Sigma^+$, respectively, and they converge to the dissociation limits of $C[(3s)\ ^1P^0] + O[(2p)\ ^3P]$ ($\Delta_f H^0$; 1707 kJ•mol^{-1}), and $C[(3s)\ ^1P^0] + O[(2p)\ ^1D]$ ($\Delta_f H^0$; 1897 kJ•mol^{-1}), respectively [76]. Therefore, one now has the possibility of two lower energy routes for the production of $C[(3s)\ ^1P^0 \rightarrow (2p)\ ^1D]$ that are at excitation energies of 4.82, and 6.79 eV, respectively above $\Delta_f H^0[C{\equiv}O[\ \tilde{X}\ ^1\Sigma^+]]$, thereby increasing its relative emission intensity.

Now, for the mass spectrometry processes of $C{\equiv}O^{+\bullet}$ (m/z 28), the MI mass spectrum exhibits a single peak for $C^{+\bullet}$ (m/z 12), and the CID mass spectra exhibits a base peak for $C^{+\bullet}$ (m/z 12), and a very weak for $O^{+\bullet}$ (m/z 16) peak.

In summary, on inspection of the CIE spectra illustrated in Figures 2.12, 2.13, and 2.14 and Table 2.20, one may note the following trends. Firstly, the fragment $O[(2p)\ ^1D \rightarrow (2p)\ ^3P]$ emission is always present (discernible for Ar upon closer magnification) and may be attributed to coming from the dissociation of the parent projectile species. As well, the $C{\equiv}O^{+\bullet}$ emissions of $\tilde{B}\,^2\Sigma^+ \rightarrow \tilde{X}\,^2\Sigma^+$, and $\tilde{A}\,^2\Pi \rightarrow \tilde{X}\,^2\Sigma^+$, are also always present. The C≡O emissions of $\tilde{e}\,^3\Sigma^- \rightarrow \tilde{a}\,^3\Pi$, $\tilde{d}\,^3\Delta \rightarrow \tilde{a}\,^3\Pi$, and $\tilde{a}\,'^3\Sigma^+ \rightarrow \tilde{a}\,^3\Pi$, are only present when O_2 is the target gas. This may be proposed to be due to the greater neutralization effectiveness (see section 2.13. Table 2.3) of O_2 relative to Ar.

2.4 The Carbon Dioxide O=C=O System

This section will deal with the CIE studies of the O=C=O system, the observed emissions of the parent and its fragments, and discusses its behaviour and the processes occuring during the collision event [29-31, 34-37, 40-43, 75, 80-91].

At this point, one should note that the radiative lifelines [75, 85], τ_{rad}, for the radical-cation $\tilde{B}\,^2\Sigma_u^+$, and $\tilde{A}\,^2\Pi_u$ electronic states are, ≈ 145 ns and ≈ 120 ns, respectively. Now, Table 2.21, Figure 2.15 [86, 87], and Table 2.22, illustrate the electronic states of the neutral and radical-cation O=C=O species, the potential energy surfaces, states, and lowest dissociation limits of the $O{=}C{=}O^{+\bullet}$ species, and the expected emissions of the $O{=}C{=}O^{+\bullet}$/He, Ar, O_2 systems, respectively. As well, Figures 2.16, 2.17, and 2.18, illustrate the experimental CIE spectra of $O{=}C{=}O^{+\bullet}$ with the target gases He, Ar, and O_2, respectively, whilst Table 2.23 catalogues their observed wavelengths (see Appendix A for additional information on the selection rules, and Wigner-Witmer Correlation Rules). The partner target gas column of Table 2.23 indicates in which of the CIE spectra (i.e., Figure 2.16, 2.17 or 2.18) the emissions were observed.

Now, for the O=C=O system the heat of formation values of interest are $\Delta_f H^0[O{=}C{=}O[\,\tilde{X}\,^1\Sigma_g^+]] = -393.5$ kJ•mol^{-1} and $\Delta_f H^0[O{=}C{=}O^{+\bullet}[\,\tilde{X}\,^2\Pi_g]] = 935.4$ kJ•mol^{-1} [1]. The adiabatic ionization energy value [1, 43] (see section 2.1.4, Table 2.4) to reach the $\tilde{X}\,^2\Pi_g$, $\tilde{A}\,^2\Pi_u$, and $\tilde{B}\,^2\Sigma_u^+$, and $\tilde{C}\,^2\Sigma_g^+$ electronic states of $O{=}C{=}O^{+\bullet}$ 13.77, 17.32, 18.08, and 19.40 eV, respectively.

For the neutral manifold, an extensive *absorption* spectroscopy study was carried out by Filseth [91] which found that all of the lower excited electronic states of O=C=O to be strong dissociative towards the $\nu_2(\Pi_u)$ vibrational bonding mode (see section 2.1.2, Figure 2.5; and see Appendix B). This results in there being *no observed emissions* from intact excited electronic

Table 2.21 The Electronic States of the Neutral and Radical-Cation O=C=O Species

Valence Electron Configuration	Electronic States
O=C=O	
$(4\sigma_g)^2(3\sigma_u)^2(1\pi_u)^4(1\pi_g)^4$	$\tilde{X}\,^1\Sigma_g^+$
$(4\sigma_g)^2(3\sigma_u)^2(1\pi_u)^4(1\pi_g)^3(2\pi_u)$	$^3\Delta_u$, $^3\Sigma_u^+$, $^3\Sigma_u^-$, $^1\Delta_u$, $^1\Sigma_u^+$, $^1\Sigma_u^-$
$(4\sigma_g)^2(3\sigma_u)(1\pi_u)^4(1\pi_g)^4(2\pi_u)$	$^3\Pi_g$, $^1\Pi_g$
$(4\sigma_g)^2(3\sigma_u)^2(1\pi_u)^4(1\pi_g)^3(3s\sigma_g)$	$^3\Pi_g$, $^1\Pi_g$ (Ryd.)
$(4\sigma_g)^2(3\sigma_u)^2(1\pi_u)^4(1\pi_g)^3(3p\pi_u)$	$^3\Delta_u$, $^3\Sigma_u^+$, $^3\Sigma_u^-$, $^1\Delta_u$, $^1\Sigma_u^+$, $^1\Sigma_u^-$ (Ryd.)
O=C=O$^{+\bullet}$	
$(4\sigma_g)^2(3\sigma_u)^2(1\pi_u)^4(1\pi_g)^3$	$\tilde{X}\,^2\Pi_g$
$(4\sigma_g)^2(3\sigma_u)^2(1\pi_u)^3(1\pi_g)^4$	$\tilde{A}\,^2\Pi_u$
$(4\sigma_g)^2(3\sigma_u)(1\pi_u)^4(1\pi_g)^4$	$\tilde{B}\,^2\Sigma_u^+$
$(4\sigma_g)(3\sigma_u)^2(1\pi_u)^4(1\pi_g)^4$	$\tilde{C}\,^2\Sigma_g^+$
$(4\sigma_g)^2(3\sigma_u)^2(1\pi_u)^4(1\pi_g)^2(2\pi_u)$	$\tilde{a}\,^4\Pi_u$, $^2\Pi_u(3)$, $^2\Phi_u$
$(4\sigma_g)^2(3\sigma_u)^2(1\pi_u)^4(1\pi_g)^2(5\sigma_g)$	$^4\Sigma_g^-$, $^2\Sigma_g^-$, $^2\Sigma_g^+$, $^2\Delta_g$

Figure 2.15 The Potential Energy Surfaces, States, and Lowest Dissociation Limits of the $O{=}C{=}O^{+*}$ Species

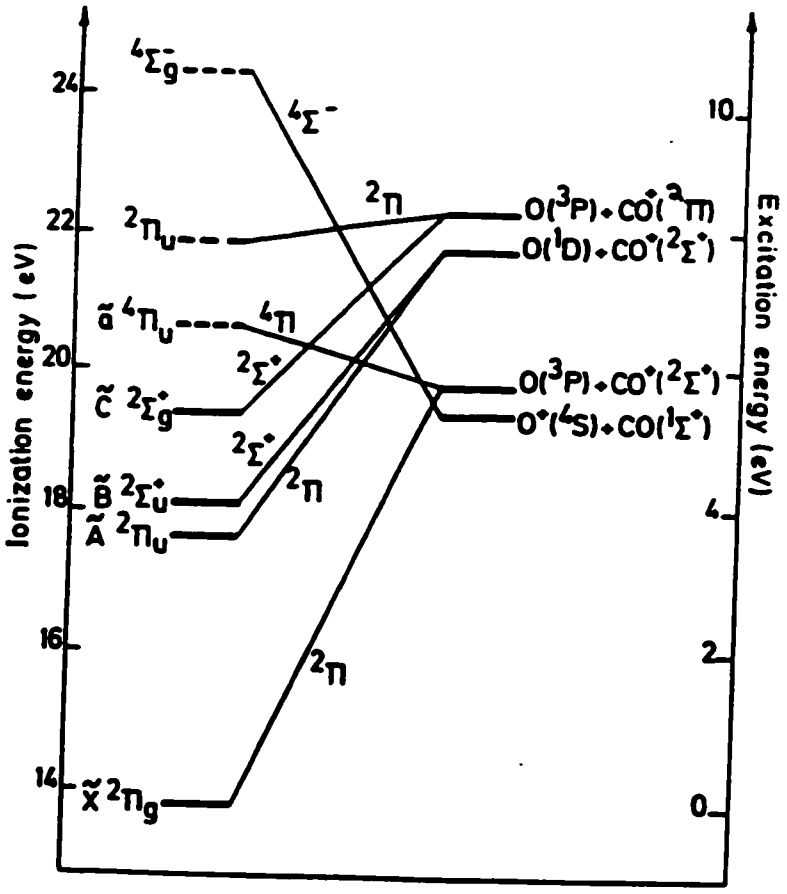

States and lowest dissociation limits of CO_2^+.

Energy/eV	Species	Symmetry
13.778	$CO_2^+(\tilde{X})$	$^2\Pi_g$
17.31	$CO_2^+[\tilde{A}(0,0,0)]$	$^2\Pi_u$
18.07	$CO_2^+[\tilde{B}(0,0,0)]$	$^2\Sigma_u^+$
19.071	$O^+(^4S_u)+CO(^1\Sigma^+)$	$^4\Sigma^-$
19.391	$CO_2^+[\tilde{C}(0,0,0)]$	$^2\Sigma_g^+$
19.466	$CO^+(^2\Sigma^+)+O(^3P_g)$	$^{2,4}\Sigma^-$, $^2\Pi$, $^4\Pi$
21.433	$CO^+(^2\Sigma^+)+O(^1D_g)$	$^2\Sigma^+$, $^2\Pi$, $^2\Delta$
21.976	$CO^+(^2\Pi)+O(^3P_g)$	$^{2,4}\Sigma^+$, $^{2,4}\Sigma^-$, $^{2,4}\Pi$, $^{2,4}\Delta$

Table 2.22 The Expected Emissions of the O=C=O$^{+\bullet}$/He, Ar, O_2 Systems

Electronic Transition	Comment
O=C=O$^{+\bullet}$	
$\tilde{B}\,^2\Sigma_u^+ \rightarrow \tilde{X}\,^2\Pi_g$	0_0^0 only, UV
$\tilde{A}\,^2\Pi_u \rightarrow \tilde{X}\,^2\Pi_g$	$1_{v'}^{v''}$ dominant, VIS
O=C=O	
none	All dissociative (save $\tilde{X}\,^1\Sigma_g^+$) O=C=O$^{\bullet} \rightarrow$ O + C≡O$^{\bullet}$
C≡O$^{+\bullet}$	
$\tilde{B}\,^2\Sigma^+ \rightarrow \tilde{X}\,^2\Sigma^+$	He, Ar, O_2
$\tilde{A}\,^2\Pi \rightarrow \tilde{X}\,^2\Sigma^+$	$CO_2^{+\bullet}[\tilde{C}\,^2\Sigma_g^+] \rightarrow CO^{+\bullet}[\tilde{A}\,^2\Pi]$ + O[(2p) ^{3}P]
C≡O	
$\tilde{e}\,^3\Sigma^- \rightarrow \tilde{a}\,^3\Pi$	O_2, VIS
$\tilde{d}\,^3\Delta \rightarrow \tilde{a}\,^3\Pi$	O_2, VIS
$\tilde{a}\,'^3\Sigma^+ \rightarrow \tilde{a}\,^3\Pi$	O_2, NIR

Important Atomics	
O	
(2p) ^{1}D $\rightarrow$ (2p) ^{3}P	$CO_2^{+\bullet}[\tilde{A}\,^2\Pi_u, \tilde{B}\,^2\Sigma_u^+] \rightarrow CO^{+\bullet}[\tilde{X}\,^2\Sigma^+]$ + O[(2p) ^{1}D]

Figure 2.16 The Collision-Induced Emission (CIE) Spectrum of the O=C=O$^{+\bullet}$/He System

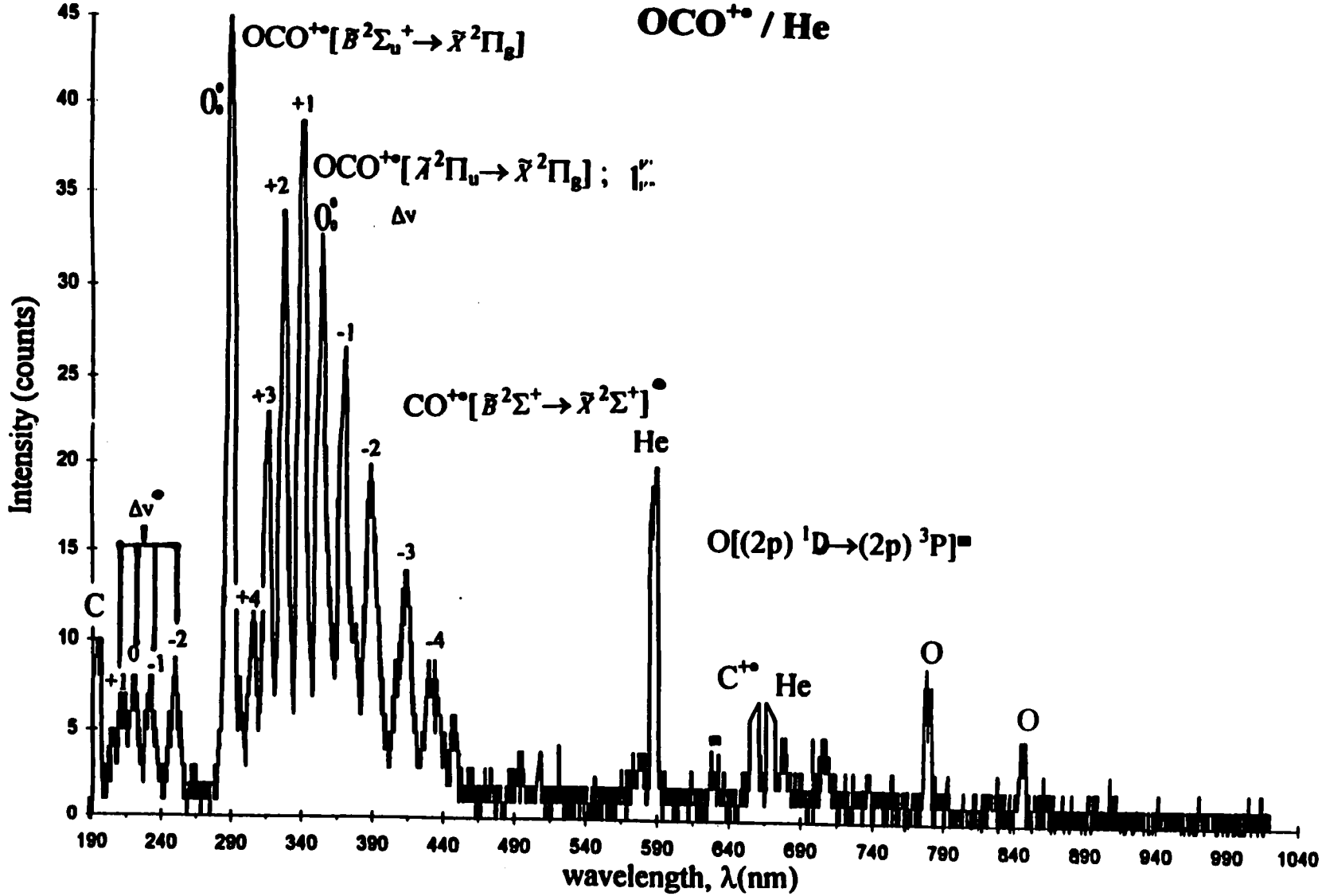

Figure 2.17 The Collision-Induced Emission (CIE) Spectrum of the O=C=O$^{+\bullet}$/Ar System

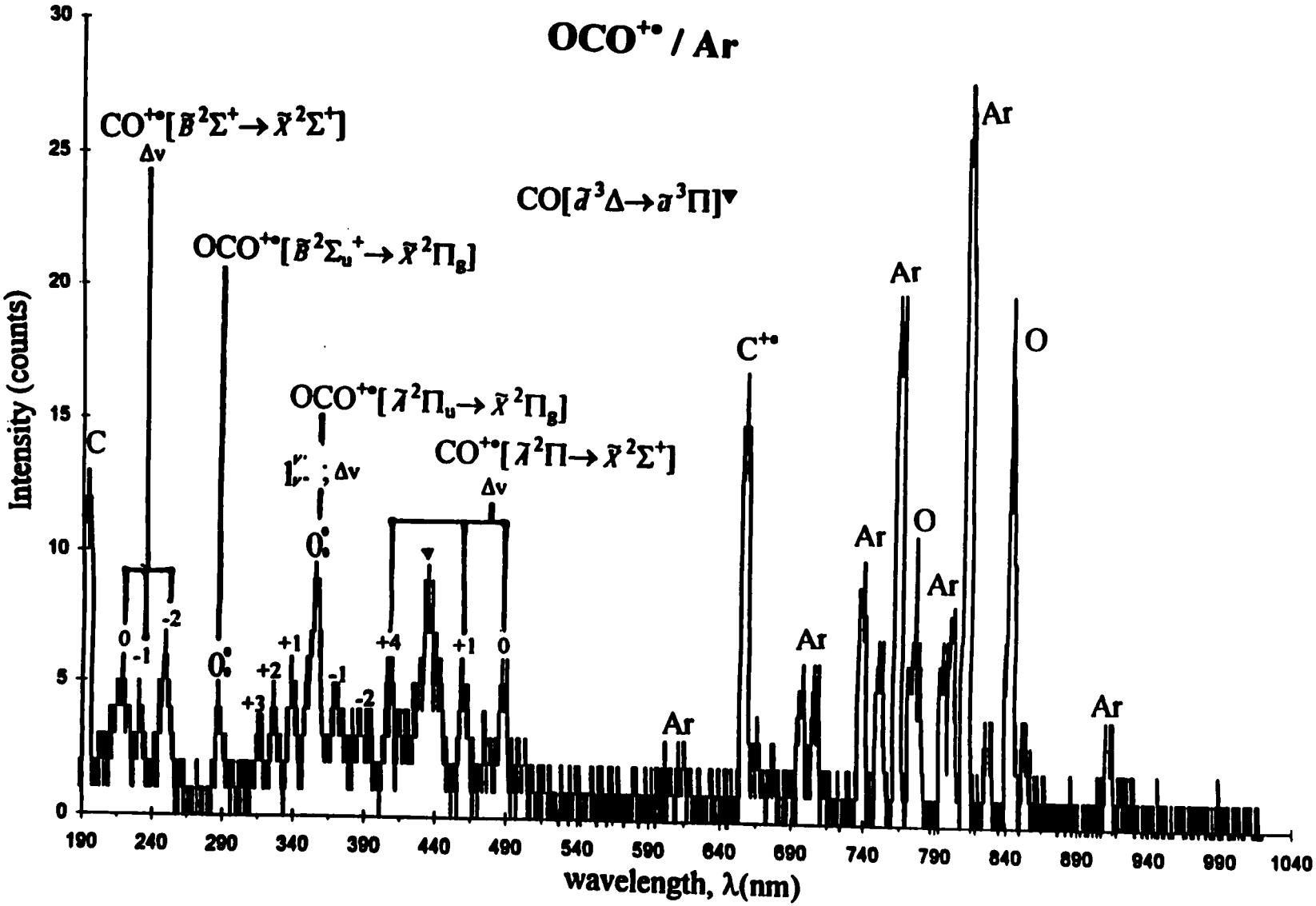

Figure 2.18 The Collision-Induced Emission (CIE) Spectrum of the O=C=O$^{+\bullet}$/O_2 System

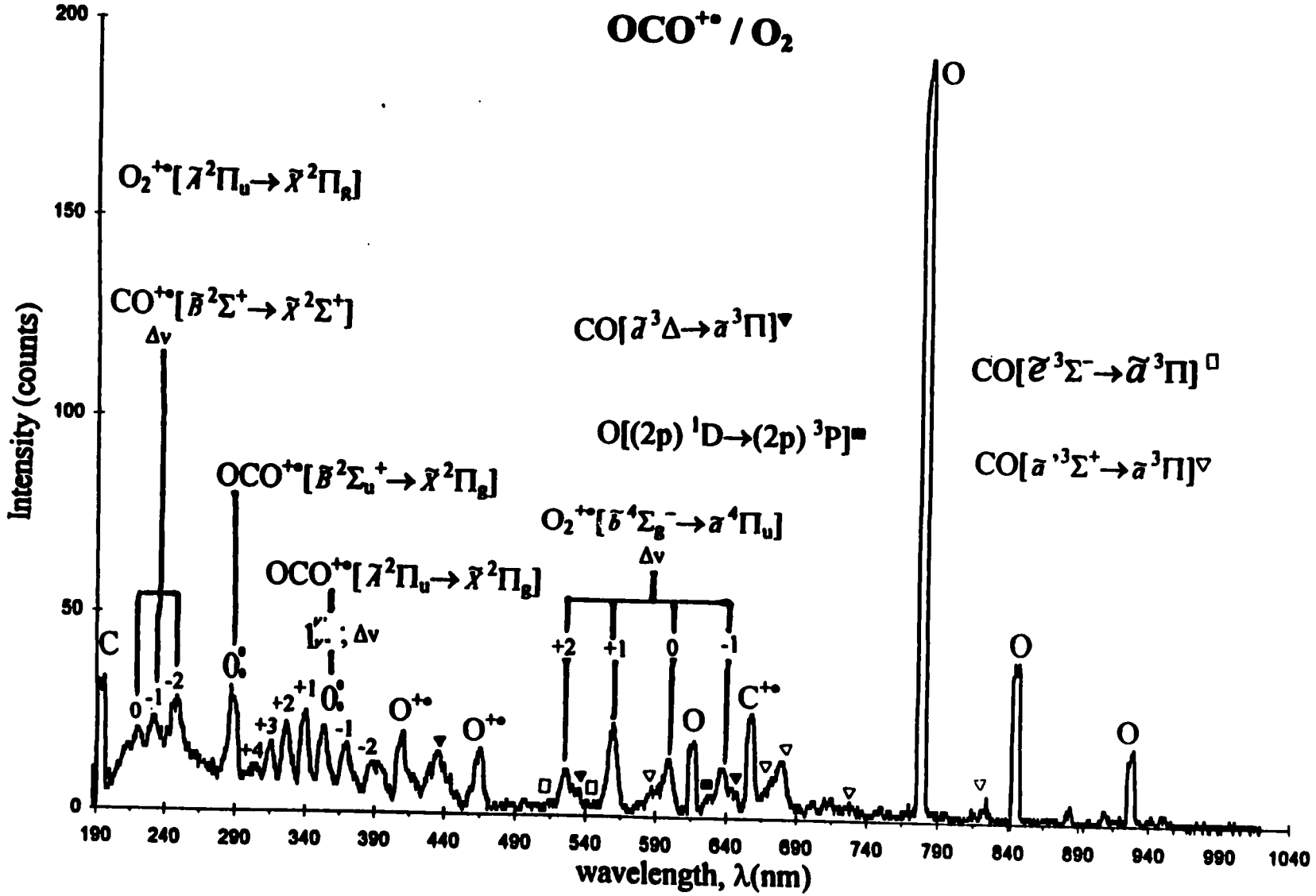

Table 2.23 The Observed Emissions Produced from the Neutral and Radical-Cation O=C=O Projectile

Observed Transition	Observed Wavelength λ(nm)[a]	Partner Target Gas
O=C=O$^{+\bullet}$		
$\tilde{B}\,^2\Sigma_u^+ \rightarrow \tilde{X}\,^2\Pi_g$		
Δv		
0_0^0	288.7	He, Ar, O_2
$\tilde{A}\,^2\Pi_u \rightarrow \tilde{X}\,^2\Pi_g$; $1_{v''}^{v'}$		
Δv		
+4	305.4	He, , O_2
+3	315.4	He, Ar, O_2
+2	326.9	He, Ar, O_2
+1	340.0	He, Ar, O_2
0_0^0	350.2	He, Ar, O_2
−1	368.6	He, Ar, O_2
−2	388.2	He, Ar, O_2
−3	414.0	He
−4	432.5	He
C≡O$^{+\bullet}$		
$\tilde{B}\,^2\Sigma^+ \rightarrow \tilde{X}\,^2\Sigma^+$		
Δv[b]		
+1, (1,0)	211.6	He
0, (0,0)	219.0	He, Ar, O_2
−1, (0,1)	230.3	He, Ar, O_2
−2, (2,4)	247.4	He, Ar, O_2
$\tilde{A}\,^2\Pi \rightarrow \tilde{X}\,^2\Sigma^+$		
Δv		
+4, (5,1)	379.0	Ar
+1, (1,0)	455.9	Ar
0, (0,0)	490.5	He, Ar, O_2

[a]Average Uncertainty, λ ± 0.5 nm. [b]$\Delta v = (v',v'') = v' - v''$.

Table 2.23 The Observed Emissions Produced from the Neutral and Radical-Cation O=C=O Projectile (Continued)

Electronic Transition	Observed Wavelength λ(nm)[a]	Partner Target Gas
C≡O		
$\tilde{d}\,^3\Delta \rightarrow \tilde{a}\,^3\Pi$		
Δv[b]		
+9, (11,2)	433.3	O_2
+3, (3,0)	531.3	O_2
0, (0,0)	643.8	O_2
$\tilde{e}\,^3\Sigma^- \rightarrow \tilde{a}\,^3\Pi$		
Δv		
+3, (3,0)	512.7	O_2
+2, (2,0)	541.3	O_2
$\tilde{a}\,'^3\Sigma^+ \rightarrow \tilde{a}\,^3\Pi$		
Δv		
+9, (9,0)	585.7	O_2
+8, (10,2)	680.7	O_2
, (11,3)	712.2	O_2
+7, (7,0)	668.5	O_2
+6, (6,0)	721.3	O_2
+5, (6,1)	822.4	O_2

[a]Average Uncertainty, λ ± 0.5 nm. [b]$\Delta v = (v',v'') = v' - v''$.

state O=C=O [35]. However, via the utilization of the Wigner-Witner Correlation Rules (see Appendix A) on bending, one may propose that the ground electronic state $\tilde{X}\,^1\Sigma_g^+$ may undergo vibronic coupling with the excited electronic (non-Rydberg) state $^3\Pi_g$, and thus undergo an avoided crossing resulting in the concomitant O=C=O[$\tilde{X}\,^1\Sigma_g^+$] → C≡O[$\tilde{X}\,^1\Sigma^+$] + O[(2p) ^{3}P], and O=C=O[$^3\Pi_g$] → C≡O[$\tilde{X}\,^1\Sigma^+$] + O[(2p) ^{1}D] dissociation processes. Thus for the neutral manifold, one may propose [91] the dissociation limits of interest to be C≡O[$\tilde{X}\,^1\Sigma^+$] + O[(2p) ^{3}P], C≡O[$\tilde{X}\,^1\Sigma^+$] + O[(2p) ^{1}D], C≡O[$\tilde{a}\,^3\Pi$] + O[(2p) ^{3}P], C≡O[$\tilde{a}\,'^3\Sigma^+$] + O[(2p) ^{3}P], C≡O[$\tilde{d}\,^3\Delta$] + O[(2p) ^{3}P], and C≡O[$\tilde{e}\,^3\Sigma^-$] + O[(2p) ^{3}P], at excitation energies of 5.45, 7.42, 11.46, 12.31, 12.97 and 13.35 eV, respectively, above $\Delta_f H^0$[O=C=O[$\tilde{X}\,^1\Sigma_g^+$]]. Thus, via the Wigner-Witner Correlation Rules (see Appendix A), one may propose that the O=C=O electronic states, $\tilde{X}\,^1\Sigma_g^+$, $^3\Sigma_u^-$ converge to the first; $^3\Pi_g$, $^1\Delta_u$, $^1\Sigma_u^+$ converge to the second; $^3\Delta_u$, $^3\Sigma_u^+$, $^1\Sigma_u^-$ converge to the third; (3pπ_u) $^3\Sigma_g^-$, (3pπ_u) $^1\Sigma_g^-$ converge to the fourth; (3pπ_u) $^3\Delta_g$, (3pπ_u) $^1\Delta_g$ converge to the fifth; and (3pπ_u) $^3\Sigma_g^+$, (3pπ_u) $^1\Sigma_g^+$ converge to the sixth dissociation limit, respectively.

Similarly, for the radical-cation manifold [86, 87] the dissociation limits of interest are C≡O$^{+\bullet}$[$\tilde{X}\,^2\Sigma^+$] + O[(2p) ^{3}P], C≡O$^{+\bullet}$[$\tilde{X}\,^2\Sigma^+$] + O[(2p) ^{1}D], and C≡O$^{+\bullet}$[$\tilde{A}\,^2\Pi$] + O[(2p) ^{3}P], at excitation energies of 19.47, 21.43, and 21.98 eV, respectively above $\Delta_f H^0$[O=C=O[$\tilde{X}\,^1\Sigma_g^+$]]. The O=C=O$^{+\bullet}$ electronic states $\tilde{X}\,^2\Pi_g$, $\tilde{a}\,^4\Pi_u$ converge to the first; $\tilde{A}\,^2\Pi_u$, and $\tilde{B}\,^2\Sigma_u^+$ converge to the second; and (the predissociated) $\tilde{C}\,^2\Sigma_g^+$ converges to the third dissociation limit, respectively.

As previously discussed (see section 2.1.5) for the neutral species, the minimum observed internal excitation energy deposited, $\Delta(\Delta E_{int})$, during the dissociative excitation,

$C{\equiv}O^{+\bullet}[\tilde{X}\,^2\Sigma^+] + O[(2p)\,^1D] \leftarrow O{=}C{=}O[\tilde{X}\,^1\Sigma_g^+]$, is 7.42 eV; whereas for the radical-cation species, the $\Delta(\Delta E_{ai})$ during, $C{\equiv}O^{+\bullet}[\tilde{X}\,^2\Sigma^+] + O[(2p)\,^1D] \leftarrow O{=}C{=}O^{+\bullet}[\tilde{X}\,^2\Pi_g]$, is 7.66 eV.

Now, for the mass spectrometry processes of $O{=}C{=}O^{+\bullet}$ (m/z 44), the MI mass spectrum exhibits a single peak for $CO^{+\bullet}$ (m/z 28), and the CID mass spectra exhibits weak peaks for $C^{+\bullet}$(m/z 12), $O^{+\bullet}$(m/z 16), CO_2^{2+} (m/z 22), and a strong base peak $CO^{+\bullet}$ (m/z 28).

Thus, in summary on inspection of the CIE spectra illustrated in Figures 2.16, 2.17, and 2.18 and Table 2.23, one may note the following trends. Firstly, the fragment emissions $O[(2p)\,^1D \rightarrow (2p)\,^3P]$ (discernible for Ar upon closer magnification), and $C{\equiv}O^{+\bullet}[\tilde{A}\,^2\Pi \rightarrow \tilde{X}\,^2\Sigma^+]$; (0,0) (discernible for He, and O_2 upon closer magnification) are always present and may be attributed to the dissociation of the parent projectile species. As well, the $O{=}C{=}O^{+\bullet}$ emissions of $\tilde{B}\,^2\Sigma_u^+ \rightarrow \tilde{X}\,^2\Pi_g$, and $\tilde{A}\,^2\Pi_u \rightarrow \tilde{X}\,^2\Pi_g$ are also always present. The C≡O emissions of $\tilde{e}\,^3\Sigma^- \rightarrow \tilde{a}\,^3\Pi$, $\tilde{d}\,^3\Delta \rightarrow \tilde{a}\,^3\Pi$, and $\tilde{a}\,'^3\Sigma^+ \rightarrow \tilde{a}\,^3\Pi$, are only present when O_2 is the target gas. This may be proposed to be due to the greater neutralization effectiveness (see section 2.1.3. Table 2.3 of O_2 relative to Ar.

2.5 The Ethenedione O=C=C=O System

This section will deal with the CIE studies of the O=C=C=O system, the observed emissions of the fragments, and discuss its proposed behaviour and the proposed processes occurring during the collision event [29-31, 34-37, 40-43, 91-114].

At this point, one should note that the radiative lifetimes, τ_{rad}, for the neutral and radical-cation O=C=C=O species are unknown. The existence of the stable neutral O=C=C=O as a genuine cumulene type linear molecule has been proposed theoretically in ab initio calculation studies [96, 97, 100, 102, 104]. As well, experimentally the existence of the stable neutral cumulene O=C=C=O species was proposed in the chemiluminescence optical emission study of Backer et. al., [95], in which the excited O=C=C=O* species was suggested as an intermediate in the $O + C_2O \rightarrow CO^* + CO$ reaction (where the asterisk denotes an excited species). In addition, the recent neutralization-reionization (NR) mass spectrometry studies of Holmes et. al., [108, 109], proposed that during the neutralization process of $O=C=C=O^{+\bullet}$ there was produced a stable neutral O=C=C=O species with a lifetime (relative to the CO + CO dissociation products) on the order of the transit time between the neutralization and reionization cells (i.e., $\approx$ 1 μs).

However, the above mentioned point of view *supporting* the existence of a stable neutral O=C=C=O is disputed experimentally and theoretically by Schwarz et. al., [105, 106]. These objections will be explored later in this section after the discussion of the CIE study of $O=C=C=O^{+\bullet}$ presented here below. For the sake of discussion, the author will now present and discuss the view *supporting* the existence of genuine stable cumulene neutral $O=C=C=O[\tilde{X}\,^3\Sigma_g^-]$, and radical-cation $O=C=C=O^{+\bullet}[\tilde{X}\,^2\Pi_u(^2B_u)]$as a linear, and a (quasi-)linear species, respectively (see Appendix B).

Now, Table 2.24, Figure 2.19, and Table 2.25, illustrate the (proposed) electronic states of the neutral and radical-cation O=C=C=O species, their (proposed) potential energy surfaces, and the expected emissions of the $O=C=C=O^{+\bullet}$/He, O_2 systems, respectively. As well, Figures 2.20 and 2.21, illustrate the experimental CIE spectra of $O=C=C=O^{+\bullet}$ with target gases, He, and O_2 respectively; whilst Table 2.26 catalogues their observed wavelengths (see Appendix A for additional details on the selection rules, and Wigner-Witner Correlation Rules). The partner target gas column of Table 2.26 indicates in which of the CIE Spectra (i.e., Figure 2.20 or 2.21) the emissions were observed.

Now for the neutral linear O=C=C=O species the lowest energy electron figuration, $(5\sigma_g)^2(1\pi_u)^4(1\pi_g)^4(2\pi_u)^2$, is related to the $\tilde{X}\,^3\Sigma_g^-$, $\tilde{a}\,^1\Delta_g$, and $\tilde{b}\,^1\Sigma_g^+$ electronic states. Korkin et. al, [104] calculated the energies of $\tilde{a}\,^1\Delta_g$, and $\tilde{b}\,^1\Sigma_g^+$ to be 39.8 kJ•mol^{-1} (0.412 eV), and 50.6 kJ•mol^{-1} (0.525 eV), respectively, above the ground $O=C=C=O[\tilde{X}\,^3\Sigma_g^-]$ state, which is in turn 276 kJ•mol^{-1} above $C\equiv O[\tilde{X}\,^1\Sigma^+] + C\equiv O[\tilde{X}\,^1\Sigma^+]$ (Δ_fH^0; −221 kJ•mol^{-1}) making $\Delta_fH^0[O=C=C=O[\tilde{X}\,^3\Sigma_g^-]] \approx 55$ kJ•mol^{-1}. Thus, along with the experimental value of $\Delta_fH^0[O=C=C=O^{+\bullet}[\tilde{X}\,^2\Pi_u(^2B_u)] = 940$ kJ•mol^{-1} [105], one may estimate an IE_a value of $O=C=C=O[\tilde{X}\,^3\Sigma_g^-]$ to be 885 kJ•mol^{-1} or 9.17 eV (i.e., ≈ 9.2 eV).

Thus, on the utilization of the Wigner-Witner Correlation Rules [26-30] (see Appendix A), and the pertinent thermodynamic [1] and spectroscopic [36, 37, 91-94] data, one may construct Figure 2.19, the proposed potential energy surfaces of the O=C=C=O and $O=C=C=O^{+\bullet}$ species.

At this point, the following studies on the neutral and radical-cation O=C=C=O species deserve emphasis. Raine et.al. [97] calculated (at the DZ + PSCF level) the vibrational modes of $O=C=C=O[\tilde{X}\,^3\Sigma_g^-]$ to be those of the $\nu_1(\Sigma_g^+)$, CO sym. str.; $\nu_2(\Sigma_g^+)$, CC str.; $\nu_3(\Sigma_u^+)$, CO

Table 2.24 The Electronic States of the Neutral and Radical-Cation O=C=C=O Species

Valence Electron Configuration	Electronic States
O=C=C=O	
$(4\sigma_u)^2(5\sigma_g)^2(1\pi_u)^4(1\pi_g)^4(2\pi_u)^2$	$\tilde{X}\,^3\Sigma_g^-$, $\tilde{a}\,^1\Delta_g$, $\tilde{b}\,^1\Sigma_g^+$
$(4\sigma_u)^2(5\sigma_g)^2(1\pi_u)^4(1\pi_g)^3(2\pi_u)^3$	$\tilde{A}\,^3\Sigma_u^+$, $\tilde{B}\,^3\Sigma_u^-$, $\tilde{C}\,^3\Delta_u$, $^1\Sigma_u^+$, $^1\Sigma_u^-$, $^1\Delta_u$
$(4\sigma_u)^2(5\sigma_g)(1\pi_u)^4(1\pi_g)^4(1\pi_u)^2(2\pi_g)$	$^3\Phi_g$, $^1\Phi_g$, $^5\Pi_g$, $^3\Pi_g(4)$, $^1\Pi_g(3)$
$(4\sigma_u)^2(5\sigma_g)^2(1\pi_u)^4(1\pi_g)^4(2\pi_u)(3s\sigma_g)$	$^3\Pi_u$, $^1\Pi_u$ (Ryd.)
O=C=C=O$^{+\bullet}$	
$(4\sigma_u)^2(5\sigma_g)^2(1\pi_u)^4(1\pi_g)^4(2\pi_u)$	$\tilde{X}\,^2\Pi_u$
$(4\sigma_u)^2(5\sigma_g)^2(1\pi_u)^4(1\pi_g)^3(2\pi_u)^2$	$\tilde{a}\,^4\Pi_g$, $\tilde{A}\,^2\Pi_g$, $^2\Pi_g(2)$, $^2\Phi_g$
$(4\sigma_u)^2(5\sigma_g)^2(1\pi_u)^3(1\pi_g)^4(2\pi_u)^2$	$\tilde{b}\,^4\Pi_u$, $\tilde{B}\,^2\Pi_u$, $^2\Pi_u(2)$, $^2\Phi_u$
$(4\sigma_u)^2(5\sigma_g)(1\pi_u)^4(1\pi_g)^4(2\pi_u)^2$	$\tilde{c}\,^4\Sigma_g^-$, $\tilde{C}\,^2\Sigma_g^-$, $\tilde{D}\,^2\Sigma_g^+$, $^2\Delta_g$
$(4\sigma_u)(5\sigma_g)^2(1\pi_u)^4(1\pi_g)^4(2\pi_u)^2$	$^4\Sigma_u^-$, $^2\Sigma_u^-$, $^2\Sigma_u^+$, $^2\Delta_u$

Figure 2.19 The Potential Energy Surfaces of the O=C=C=O and O=C=C=O$^{+\bullet}$ Species

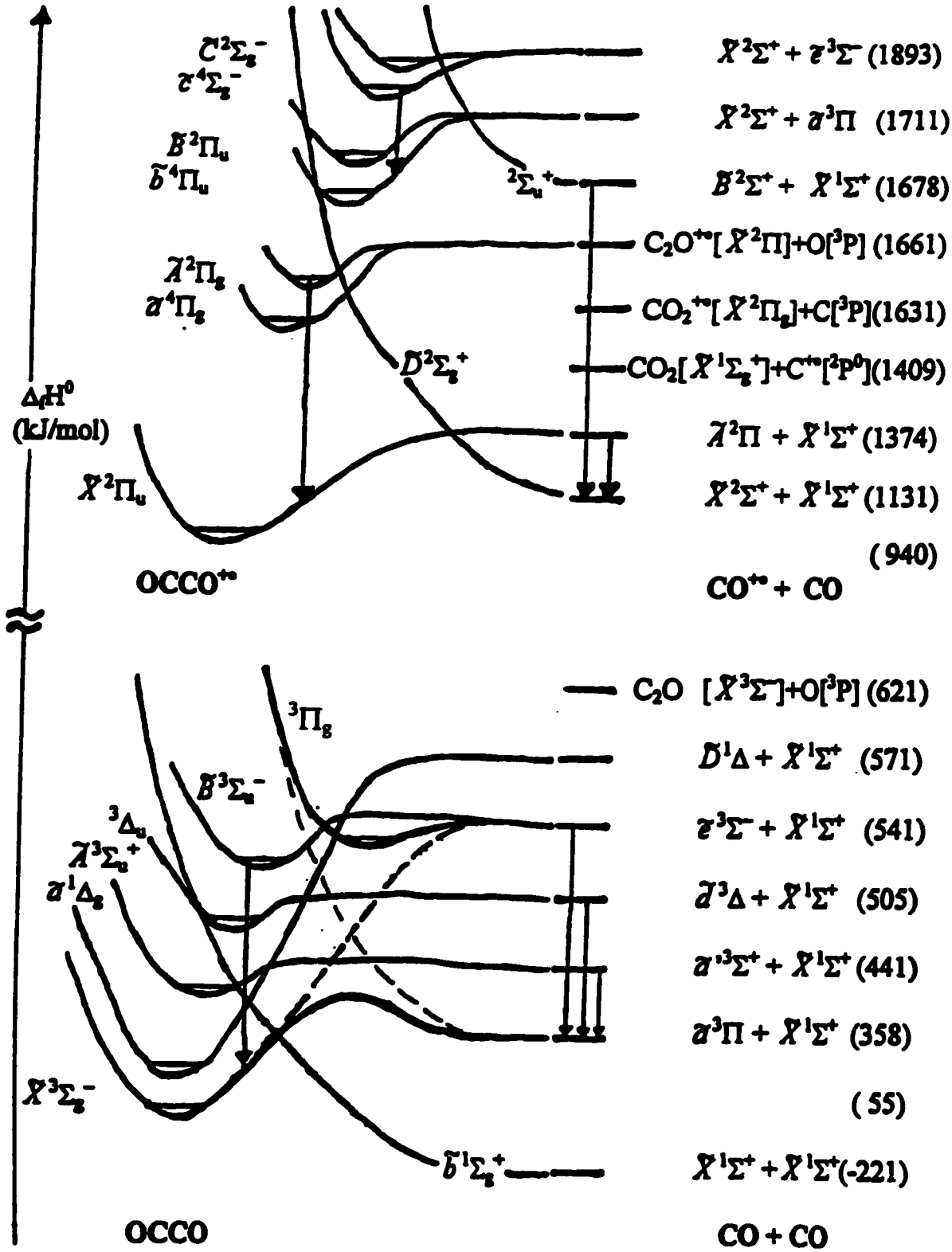

Table 2.25 The Expected Emissions of the $O{=}C{=}C{=}O^{+\bullet}$/He, O_2 Systems

Electronic Transition	Comment
$O{=}C{=}C{=}O^{+\bullet}$	
$\tilde{c}\,^4\Sigma_g^- \rightarrow \tilde{b}\,^4\Pi_u$	unobserved
$\tilde{b}\,^4\Pi_u \rightarrow \tilde{a}\,^4\Pi_g$	unobserved
$\tilde{B}\,^2\Pi_u \rightarrow \tilde{A}\,^2\Pi_g$	unobserved
$\tilde{A}\,^2\Pi_g \rightarrow \tilde{X}\,^2\Pi_u$	unobserved
$O{=}C{=}C{=}O$	
$\tilde{B}\,^3\Sigma_u^- \rightarrow \tilde{X}\,^3\Sigma_g^-$	unobserved
$C{\equiv}O^{+\bullet}$	
$\tilde{B}\,^2\Sigma^+ \rightarrow \tilde{X}\,^2\Sigma^+$	$C_2O_2^{+\bullet}[^2\Sigma_u^+] \rightarrow CO^{+\bullet}[\tilde{B}\,^2\Sigma^+] + CO[\tilde{X}\,^1\Sigma^+]$
$\tilde{A}\,^2\Pi \rightarrow \tilde{X}\,^2\Sigma^+$	$C_2O_2^{+\bullet}[\tilde{X}\,^2\Pi_u] \rightarrow CO^{+\bullet}[\tilde{A}\,^2\Pi] + CO[\tilde{X}\,^1\Sigma^+]$
$C{\equiv}O$	
$\tilde{e}\,^3\Sigma^- \rightarrow \tilde{a}\,^3\Pi$	$C_2O_2[\tilde{B}\,^3\Sigma_u^-, {}^3\Pi_g] \rightarrow CO[\tilde{e}\,^3\Sigma^-] + CO[\tilde{X}\,^1\Sigma^+]$
$\tilde{d}\,^3\Delta \rightarrow \tilde{a}\,^3\Pi$	$C_2O_2[{}^3\Delta_u] \rightarrow CO[\tilde{d}\,^3\Delta] + CO[\tilde{X}\,^1\Sigma^+]$
$\tilde{a}\,'^3\Sigma^+ \rightarrow \tilde{a}\,^3\Pi$	$C_2O_2[\tilde{A}\,^3\Sigma_u^+] \rightarrow CO[\tilde{a}\,'^3\Sigma^+] + CO[\tilde{X}\,^1\Sigma^+]$

Figure 2.20 The Collision-Induced Emission (CIE) Spectrum of the O=C=C=O$^{+\bullet}$/He System

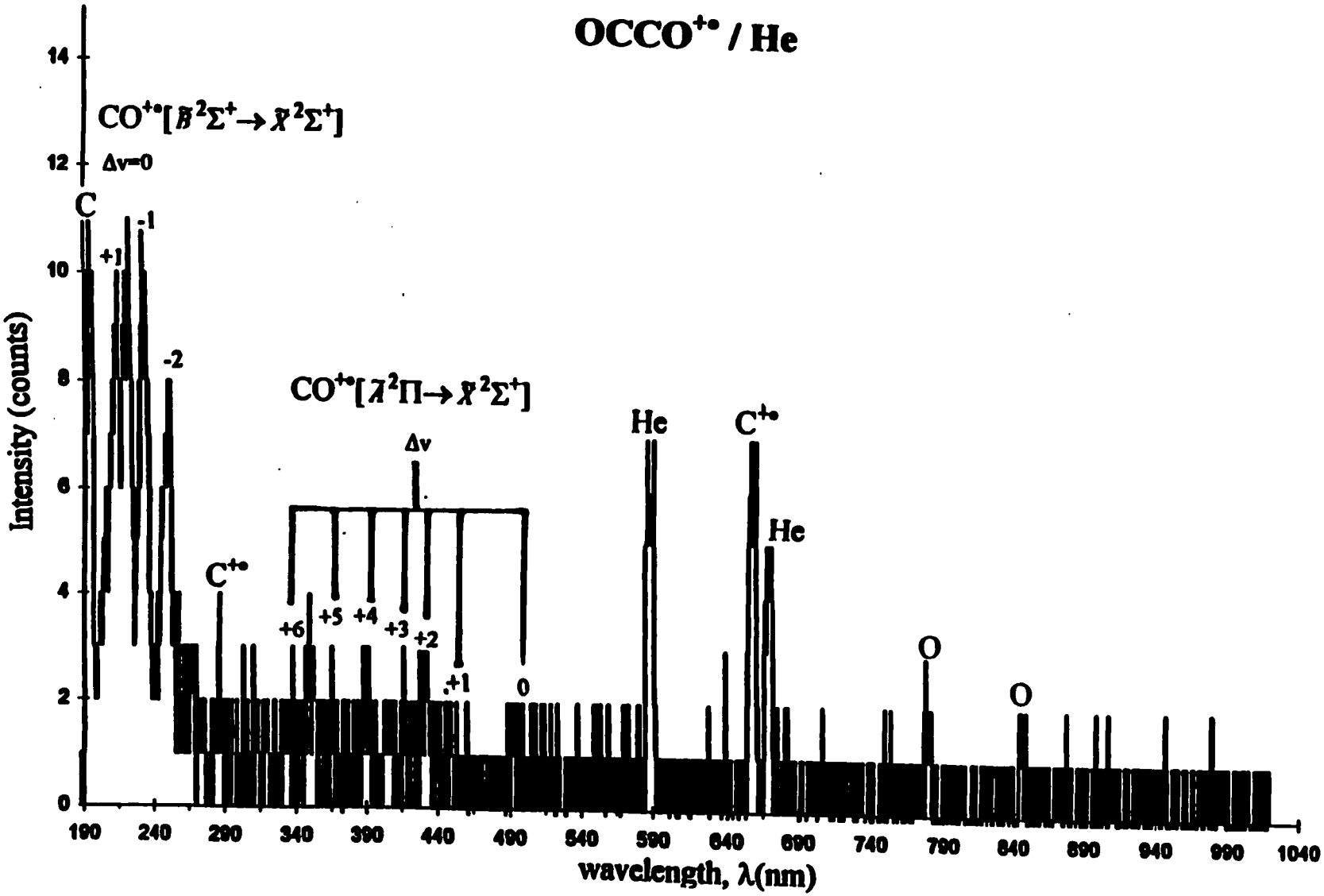

Figure 2.21 The Collision-Induced Emission (CIE) Spectrum of the O=C=C=O$^{+\bullet}$/O_2 System

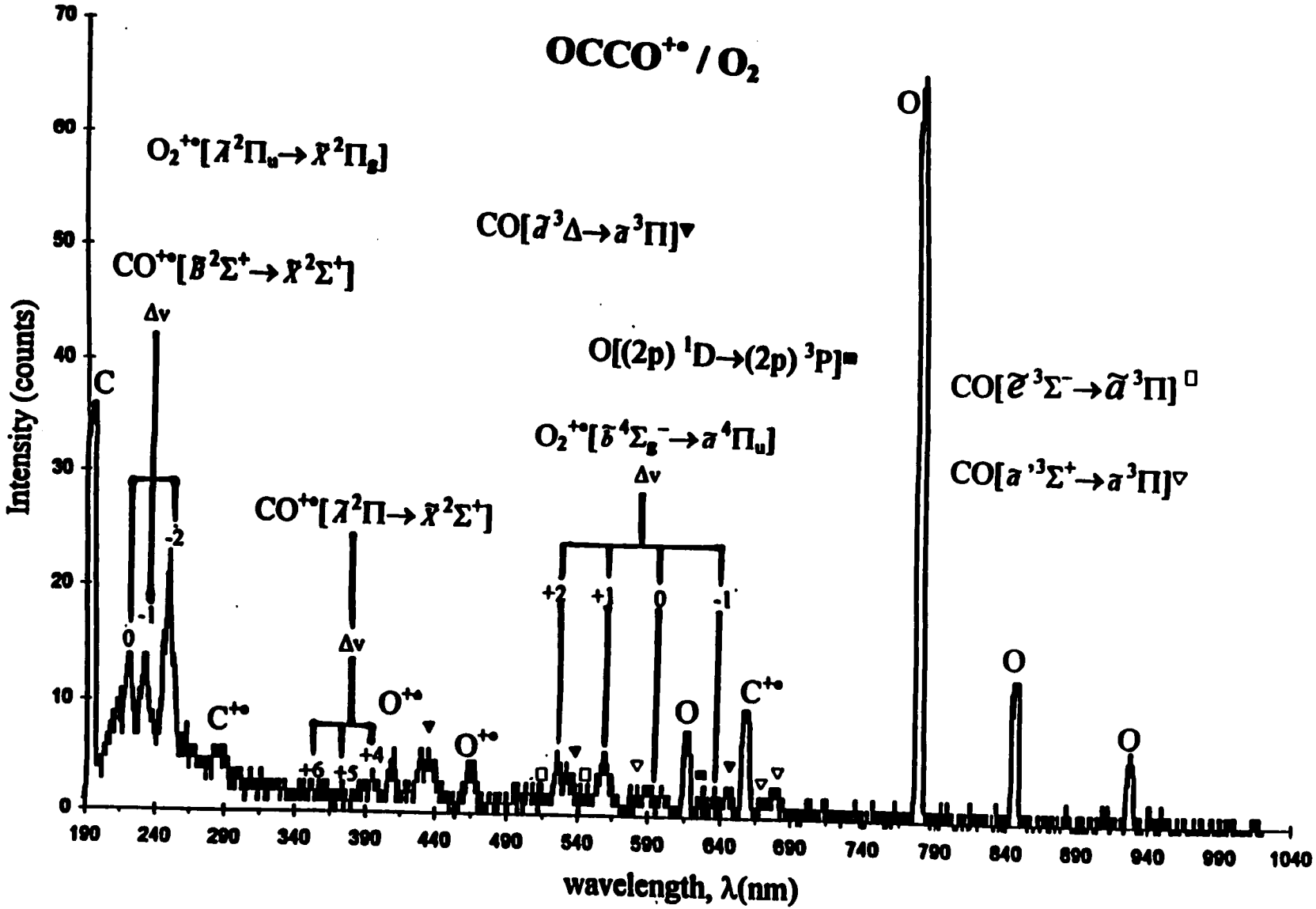

Table 2.26 The Observed Emissions Produced from the Neutral and Radical-Cation O=C=C=O Projectile

Electronic Transition	Observed Wavelength λ(nm)[a]	Partner Target Gas
$C{\equiv}O^{+\bullet}$		
$\tilde{B}\,^2\Sigma^+ \rightarrow \tilde{X}\,^2\Sigma^+$		
Δv^b		
+1, (1,0)	211.9	He
0, (0,0)	219.4	He, O_2
−1, (0,1)	230.3	He, O_2
−2, (2,4)	247.3	He, O_2
$\tilde{A}\,^2\Pi \rightarrow \tilde{X}\,^2\Sigma^+$		
Δv		
+6, (7,1)	352.4	He, O_2
+5, (6,1)	369.7	He, O_2
+4, (5,1)	389.8	He, O_2
+3, (3,0)	401.8	He
+2, (3,1)	438.7	He
+1, (1,0)	455.4	He
0, (0,0)	490.1	He
, (1,1)	506.7	He

[a]Average Uncertainty, λ ± 0.5 nm. [b]$\Delta v = (v',v'') = v' - v''$.

Table 2.26 The Observed Emissions Produced from the Neutral and Radical-Cation O=C=C=O Projectile (Continued)

Electronic Transition	Observed Wavelength λ(nm)[a]	Partner Target Gas
C=O		
$\tilde{d}\,^3\Delta \rightarrow \tilde{a}\,^3\Pi$		
Δv[b]		
+9, (11,2)	432.9	O_2
+3, (3,0)	533.3	O_2
0, (0,0)	643.2	O_2
$\tilde{e}\,^3\Sigma^- \rightarrow \tilde{a}\,^3\Pi$		
Δv		
+3, (3,0)	512.9	O_2
+2, (2,0)	541.2	O_2
$\tilde{a}\,'^3\Sigma^+ \rightarrow \tilde{a}\,^3\Pi$		
Δv		
+9, (9,0)	586.1	O_2
+8, (10,2)	680.4	O_2
+7, (7,0)	668.3	O_2

[a]Average Uncertainty, λ ± 0.5 nm. [b]$\Delta v = (v',v'') = v' - v''$.

asym. str.; $\nu_4(\Pi_u)$, trans-bend; and $\nu_5(\Pi_g)$, cis-bend to have energies of 913 cm^{-1}, 2369 cm^{-1}, 1745 cm^{-1}, 247 cm^{-1}, and 308 cm^{-1}, respectively. Therefore, at an internal energy of ≈ 1.47 eV (13, 5, and 48 vibrations of the $\nu_1(\Sigma_g^+)$, CO sym. str.; $\nu_2(\Sigma_g^+)$, CC str.; and $\nu_4(\Pi_u)$, trans-bend) the previously linear ground electronic state O=C=C=O[$\tilde{X}\,^3\Sigma_g^-$], via near (vibrational) resonance, experiences the $\tilde{X}\,^3\Sigma_g^-$ and $^3\Pi_g$ ($...(5\sigma_g)(1\pi_u)^4(1\pi_g)^4(2\pi_u)^2(2\pi_g)$) allowed vibronic mixing. This results in an avoided crossing of trans-bent C_2O_2 and the concomitant O=C=C=O[$\tilde{X}\,^3\Sigma_g^-$] → C≡O[$\tilde{a}\,^3\Pi$] + C≡O[$\tilde{X}\,^1\Sigma^+$], and O=C=C=O[$^3\Pi_g$] → C≡O[$\tilde{e}\,^3\Sigma^-$] + C≡O[$\tilde{X}\,^1\Sigma^+$]. Additionally, for the radical-cation O=C=C=O$^{+\bullet}$ [98], and the radical-anion O=C=C=O$^{-\bullet}$ [102] species the *relatively low barriers* of 10.2, and 0.9 kJ•mol^{-1} (i.e., 3567 cm^{-1} at UMP2//6-31G*, and 315 cm^{-1} at TZ2PP/CCSD(T) (and linear ≈ 0 cm^{-1} at UMP2//6-31G*)), respectively, of the trans-bent ^2B_u, and ^2A_u states to that of the linear $^2\Pi_u$ state allows one to propose that they to *both experience moderate Renner-Teller distortions* (see Appendix B, Figure 8.5) and thus may both be considered *dynamically-linear* (i.e. quasi-linear) O=C=C=O$^{+\bullet}$[$\tilde{X}\,^2\Pi_u(^2B_u)$], and O=C=C=O$^{-\bullet}$[$\tilde{X}\,^2\Pi_u(^2A_u)$] species.

Now, on inspection of Figure 2.19, with the proposed qualitative potential energy surfaces of O=C=C=O and O=C=C=O$^{+\bullet}$ on the left, dissociating to the products (with $\Delta_f H^0$ values) on the right, one may note the following trends. For the neutral manifold, the accessing of the C≡O[$\tilde{a}\,^3\Pi$] + C≡O[$\tilde{X}\,^1\Sigma^+$], C≡O[$\tilde{a}\,'^3\Sigma^+$] + C≡O[$\tilde{X}\,^1\Sigma^+$], C≡O[$\tilde{d}\,^3\Delta$] + C≡O[$\tilde{X}\,^1\Sigma^+$], C≡O[$\tilde{e}\,^3\Sigma^-$] + C≡O[$\tilde{X}\,^1\Sigma^+$] dissociation limits results from an internal excitation energy deposition, $\Delta(\Delta E_{int})$, into O=C=C=O[$\tilde{X}\,^3\Sigma_g^-$] of 3.14, 4.00, 4.66, and 5.04 eV respectively. Similarly, for the radical-cation manifold, the accessing of the C≡O$^{+\bullet}$[$\tilde{A}\,^2\Pi$] + C≡O[$\tilde{X}\,^1\Sigma^+$],

and $C{\equiv}O^{+\bullet}[\tilde{B}\,^2\Sigma^+] + C{\equiv}O[\tilde{X}\,^1\Sigma^+]$, dissociation limits results from an internal excitation energy deposition, $\Delta(\Delta E_{int})$, into $O{=}C{=}C{=}O^{+\bullet}[\tilde{X}\,^2\Pi_u]$ of 4.50, and 7.65 eV, respectively.

Thus, now on inspection of the experimental CIE spectra illustrated in Figures 2.20, and 2.21, and their wavelengths listed in Table 2.26, one may note the following trends. Firstly, no parent radical-cation and/or parent neutral O=C=C=O species expected allowed emissions, listed in Table 2.25 were observed. Only the fragment $C{\equiv}O^{+\bullet}$ and C≡O emissions were observed.

The lack of parent projectile emissions may be due to a number of reasons. Firstly, the vibrationless wavelengths, 0_0^0, for the O=C=C=O and $O{=}C{=}C{=}O^{+\bullet}$ are unknown (i.e., no experimental photoelectron spectrum). Thus, not having this information in hand, one could not run a multiple accumulation CIE spectrum centred on a small wavelength range containing 0_0^0. Thus, if any weak intensity $O{=}C{=}C{=}O^{+\bullet}$ and/or O=C=C=O emissions were present in the full range (190-1020nm) CIE spectra, they were too weak to be detected (but may perhaps be there).

Secondly, the amount of internal excitation energy deposited, $\Delta(\Delta E_{int})$, in $O{=}C{=}C{=}O^{+\bullet}$ upon collisional excitation, and in O=C=C=O upon neutralization of the 8KeV projectile may be simply too large and thus favour quasi-equilibrium dissociation over that of emission. Thus, on inspection of the CIE spectra illustrated in Figures 2.20 and 2.21, one may note that the $C{\equiv}O^{+\bullet}$ emissions of of $\tilde{B}\,^2\Sigma^+ \rightarrow \tilde{X}\,^2\Sigma^+$, and $\tilde{A}\,^2\Pi \rightarrow \tilde{X}\,^2\Sigma^+$, are always present, however the C≡O emissions of $\tilde{e}\,^3\Sigma^- \rightarrow \tilde{a}\,^3\Pi$, $\tilde{d}\,^3\Delta \rightarrow \tilde{a}\,^3\Pi$, and $\tilde{a}\,'^3\Sigma^+ \rightarrow \tilde{a}\,^3\Pi$, are only present when O_2 is the target gas. Thus, for the $O{=}C{=}C{=}O^{+\bullet}[\tilde{X}\,^2\Pi_u]$ species this may be interpreted as an internal excitation energy deposited, $\Delta(\Delta E_{int})$, of 4.50 and 7.65 eV, respectively; whilst for the $O{=}C{=}C{=}O[\tilde{X}\,^3\Sigma_g^-]$ this may be interpreted as $\Delta(\Delta E_{int})$ values of 4.00, 4.66, and 5.04 eV,

respectively. Thus, via the CIE spectra of $O{=}C{=}C{=}O^{+\bullet}$ one may propose that during the single collision event, the internal excitation energy deposited, $\Delta(\Delta E_{int})$, in the neutral and radical-cation species lie in the range of 4.00-5.04, and 4.50-7.65eV, respectively.

To further clarify the above-proposed analysis, consider the three possible sources of excited electronic state carbon monoxide, $C{\equiv}O^{\bullet}$. The $C{\equiv}O^{\bullet}$ species may originate as follows; from (I) a collisionally excited pre-existing neutral $C{\equiv}O$ from metastable $C_2O_2^{+\bullet}$ ions passing through the collision cell, or from (II) the dissociative collisional excitation process of $O{=}C{=}C{=}O^{+\bullet} \rightarrow C{\equiv}O^{+\bullet} + C{\equiv}O^{\bullet}$, or from (III) the dissociative neutralization process of $O{=}C{=}C{=}O \rightarrow C{\equiv}O + C{\equiv}O^{\bullet}$. Thus, due to the weak intensity of these CIE emissions, they are most likely to originate from the main beam $O{=}C{=}C{=}O^{+\bullet}$ (m/z 56) peak. As well, combined with the large neutralization effeciency of O_2 (over that of collision excitation), one may propose that the latter process, (III), is the major contributor to $C{\equiv}O^{\bullet}$ production, and the neutral $O{=}C{=}C{=}O$ is formed. Now, under the single collision conditions and gas pressures present here, one may estimate there are about 10^6 collisions per second between M_1^+ and G_1. Thus, the lifetime of $O{=}C{=}C{=}O[\tilde{X}\,^3\Sigma_g^-]$ may be proposed to be on the μs timescale (perhaps as high as the ms timescale).

Thirdly, the lack of $O{=}C{=}C{=}O$ and $O{=}C{=}C{=}O^{+\bullet}$ emissions may be the result of the disruption in their potential energy surfaces. The radical-cation emissions may be disrupted via predissociations, and by spin-orbit coupling (i.e., allowing curve jumping) to the $\tilde{D}\,^2\Sigma_g^+$, and $^2\Sigma_u^+$, and the rearrangement $CO_2 + C^{+\bullet}$, and $CO_2^{+\bullet} + C$ potential energy surfaces, respectively. Similarly, the neutral emissions may be disrupted if there is a high spin-orbital coupling of $\tilde{X}\,^3\Sigma_g^-$ to $\tilde{b}\,^1\Sigma_g^+$ (i.e., ≈ 0.525 eV) present, or if predissociation is completely dominant.

Thus, as far as the O=C=C=O$^{+\bullet}$ CIE spectra are concerned, on balance the author here is persuaded that some stable neutral O=C=C=O[$\tilde{X}\,^3\Sigma_g^-$] was indeed generated, however the deposition of too much $\Delta(\Delta E_{int})$ in the 8 keV neutral projectile likely produced some dissociative excited state O=C=C=O* species.

At this point, before we discuss the NRMS spectra of O=C=C=O$^{+\bullet}$, the distinction between the carbon monoxide dimer, $(CO)_2$, the cumulene ethenedione, O=C=C=O, and their ionized forms deserve emphasis. For the neutral species, the former is considered to be a weakly (physically) associated van der Waals complex of a diatomic monomer. It is devoid of a fixed structure [111, 112] and processes a tiny association energy of the order of $\approx$ 1 kJ$\bullet$mol^{-1} [111]. Whereas the latter is seen to exist as a strongly (chemically) bonded genuine tetra-atomic linear molecule O=C=C=O, with a large dissociation energy (in the absence of strong spin-orbital coupling) of 303 kJ$\bullet$mol^{-1} [104] (i.e., O=C=C=O[$\tilde{X}\,^3\Sigma_g^-$] $\rightarrow$ C$\equiv$O[$\tilde{a}\,^3\Pi$] + C$\equiv$O[$\tilde{X}\,^1\Sigma^+$], see Figure 2.19).

In the radical-cation manifold, the (C$\equiv$O$^{+\bullet}$)$\bullet$(C$\equiv$O) ion molecule-complex is still devoid of a fixed structure, but now processes a higher association energy of 125 kJ$\bullet$mol^{-1} [113], which is within the expected order of magnitude for a charge-induced dipole attraction at a monomer separation of 5 Å. In contrast O=C=C=O$^{+\bullet}$ is quasi-linear and possesses a larger dissociation energy of 256 kJ$\bullet$mol^{-1} (i.e., O=C=C=O$^{+\bullet}$[$\tilde{X}\,^2\Pi_u$] $\rightarrow$ C$\equiv$O$^{+\bullet}$[$\tilde{A}\,^2\Pi$] + C$\equiv$O[$\tilde{X}\,^1\Sigma^+$], see Figure 2.19). Thus, the $(CO)_2$ van der Waals dimer can be seen as occupying an unbound position on the ethenedione O=C=C=O hyper surface close to the O=C=C=O $\rightarrow$ O$\equiv$C + C$\equiv$O dissociation limit. This does not relate to the proposed generation [108, 109] of stable neutral O=C=C=O (discussed below), via the neutralization of a $C_2O_2^{+\bullet}$ fragment-ion (whose parent oxalyl halide X(O=C)–(C=O)X$^{+\bullet}$ ion possesses a pre-existing C-C chemical bond), only to then undergo

mainly dissociative reionization yielding no recovery NR signal at m/z 56 (i.e., $O{=}C{=}C{=}O^{+\bullet}$ + $G_1 \rightarrow O{=}C{=}C{=}O + G_1^{+\bullet}$, (N); $O{=}C{=}C{=}O + G_2 \rightarrow O{=}C{=}C{=}O^{+\bullet} + G_2 + e^-$, (R)).

Now, for the NRMS Xe 90%T / O_2 90%T study of $O{=}C{=}C{=}O^{+\bullet}$ by Holmes et. al, [108, 109] produced from several precursors, the best of which being oxalyl chloride, the NR 3FFR mass spectrum showed peaks for $C^{+\bullet}$ (m/z 12), $O^{+\bullet}$ (m/z 16), $C_2^{+\bullet}$ (m/z 24), $CO^{+\bullet}$ (m/z 28), $C_2O^{+\bullet}$ (m/z 40), and $CO_2^{+\bullet}$ (m/z 44), in a ratio of about 7.2: 2.6: 0.6: 100: 0.4: 0.15, respectively, with the absence of a recovery signal for $C_2O_2^{+\bullet}$ (m/z 56). Additionally, the CID mass spectrum of $O{=}C{=}C{=}O^{+\bullet}$ was very similar to the above NR mass spectrum [108, 109].

These results are essentially the same as those of Schwarz et. al., [105, 106], the first study being that of $O{=}C{=}C{=}O^{+\bullet}$ produced from squaric acid [105], and the second study being that of $O{=}C{=}C{=}O^{+\bullet}$ produced from $O{=}C{=}C{=}O^{-\bullet}$, via charge-reversal (i.e., $O{=}C{=}C{=}O^{-\bullet} + G \rightarrow O{=}C{=}C{=}O^{+\bullet} + G + 2e^-$) from the dimethylsquaric acid, croconic acid, and rhodizonic acid hydrate (which gave identical results for $O{=}C{=}C{=}O^{-\bullet}$ within experimental error; croconic acid gave the highest yield) [106].

In the first study, Schwarz et. al. [105] used extreme collision conditions (e.g. Xe ≈40 %T / O_2 ≈ 40 %T) which would involve [19] significant multiple (i.e., triple, quartuple,...) collision processes. In agreement with the $O{=}C{=}C{=}O^{+\bullet}$ NRMS studies of Holmes et. al. [108, 109] no recovery signal for $O{=}C{=}C{=}O^{+\bullet}$ (m/z 56) was detected. However in contrast [106], on the basis of the calculated difference in geometry (at the MCSCF//6-31G level) between the trans-bent $O{=}C{=}C{=}O^{+\bullet}[^2B_u]$ ion [98] (it was linear $O{=}C{=}C{=}O^{+\bullet}[\tilde{X}\,^2\Pi_u]$ at the lower UMP2//6-31G* level) and the linear $O{=}C{=}C{=}O[\tilde{X}\,^3\Sigma_g^-]$ neutral [96,97] it was proposed that *all* $O{=}C{=}C{=}O^{+\bullet}$ ions should undergo *neutralization to a dissociative* (i.e., $^1\Sigma_g^+$) [96] *state* of the

neutral O=C=C=O molecule (presumably the O=C=C=O[$\tilde{b}\,^1\Sigma_g^+$] state) leading to *barrier free dissociation* into C≡O[$\tilde{X}\,^1\Sigma^+$] + C≡O[$\tilde{X}\,^1\Sigma^+$]. The presence of peaks in their NR spectra assigned to :C=C$^{+\bullet}$ and C=C=O$^{+\bullet}$, *otherwise structure indicative fragments* were dismissed as having other explanations (but unstated) for their possible genesis [105].

In their second study, Schwarz et. al., [106] used charge-reversal (i.e., charge-stripping) of O=C=C=O$^{-\bullet}$ to generate O=C=C=O$^{+\bullet}$ and once again obtained basically the same results for their NR Xe 80%T/O_2 80%T mass spectrum (i.e., no recovery signal for O=C=C=O$^{+\bullet}$ (m/z 56)), as their first study [105], and the other studies of Holmes et.al. [108, 109]. Those results are not surprising as the charge-reversal process in general may be viewed as a single event which removes $2e^-$ in one step (i.e., thus making the possible momentary presence of the intermediate neutral O=C=C=O a non-issue). As well, now that one has charge-stripped O=C=C=O$^{-\bullet}$ of $2e^-$, via a collision with a target gas G, the O=C=C=O$^{+\bullet}$ ion produced may have deposited in it more internal excitation energy than would have been the case if it was produced from the oxalyl chloride precursor of the Holmes et.al., [108, 109] studies. Thus, this could result in an even lower possibility of observing a NR recovery signal for O=C=C=O$^{+\bullet}$ (m/z 56).

Additionally, Schwarz et.al., [106] performed some theoretical ab initio calculations (at the CCSD(T)/cc-pVDZ level) to detect the minimum energy crossing point (MECP) of the $\tilde{X}\,^3\Sigma_g^-$ and $\tilde{b}\,^1\Sigma_g^+$ surfaces to estimate the (dissociation) lifetime of the O=C=C=O[$\tilde{X}\,^3\Sigma_g^-$] (v = 0) species. Their results placed the MECP *at or near* the v = 0 level of O=C=C=O[$\tilde{X}\,^3\Sigma_g^-$] and thus gave an *extremely short lifetime value* in the range of 200fs - 20 ns [109]. However, they qualify this estimate with the following *caveats*; "the precise value of the presently derived $C_2O_2(^3\Sigma_g^-, v = 0)$ should not be taken too literally, owing to the rather simple model used to derive it and the remaining uncertainties about the potential energy surfaces", and "of course, no

experiment can ever prove the non-existence of long lived C_2O_2", (p. 2555 of [106]). The above mentioned work [106] *does not therefore add any new information* towards the experimental resolution of the question of the production of stable neutral O=C=C=O from $O{=}C{=}C{=}O^{+\bullet}$ during the neutralization step of the NR experiment and will not be considered further.

At this point, one will now re-emphasize the proposal of Holmes et. al., [108,109], on consideration of the similarity between the CID and NR mass spectra, of $O{=}C{=}C{=}O^{+\bullet}$, and that under the experimental conditions [108, 109] the collision frequency may be estimated to be about 10^6 collisions per second (i.e., one about every μs), we are persuaded the stable neutral O=C=C=O was likely generated by the NRMS experiment (having a lifetime on the order of the transit time between the neutralization and reionization cells, (i.e., ≈ 1 μs) but that its vertical reionization leads only to dissociative $O{=}C{=}C{=}O^{+\bullet}$ ions (and are compatible with the $O{=}C{=}C{=}O^{+}$ CIE experiments presented here).

Now, further possible experiments which may in the future aid in the gathering of information on the electronic energy levels of the neutral and radical-cation O=C=C=O species will be discussed below. For the neutral O=C=C=O species, the determination of its electronic energy levels may be indeed possible on consideration of the work of Zengin et.al, [94]. In this study a radical-anion $C{=}C{=}O^{-\bullet}$ species was mass selected and introduced into a photo-ionization chamber that produced a vibrational resolved photoelectron spectrum of the $C{=}C{=}O^{-\bullet}$ $\rightarrow$ C=C=O + e^- process. This photoelectron spectrum provided the excitation energy values for the C=C=O excited electronic states $\tilde{a}\,^1\Delta$, $\tilde{b}\,^1\Sigma^+$, and $\tilde{A}\,^3\Pi$, of 0.658, 1.015, and 1.468 eV, respectively, above that of the ground electronic state $\tilde{X}\,^3\Sigma^-$ [94]. These results showed strong agreement with the experimental value for C=C=O[$\tilde{A}\,^3\Pi \rightarrow \tilde{X}\,^3\Sigma^-$]; 0_0^0 of 1.444 eV of Devillers et. al. [93]. Therefore, if one introduced a suitable source of $O{=}C{=}C{=}O^{-\bullet}$ in the

apparatus of Zengin et. al., [94], one may possibly produce an experimental photoelectron spectra of the $O{=}C{=}C{=}O^{-*} \rightarrow O{=}C{=}C{=}O + e^-$ that would yield information on the electronic energy levels of neutral O=C=C=O.

Additionally, for the electronic energy levels of the states of the radical-cation $O{=}C{=}C{=}O^{+*}$, one may suggest an application of the Green's Function method to calculate its theoretical photoelectron spectrum, as was carried out in the study cyanogen molecule, N≡C–C≡N, by Cederbaum et. al., [114]. This study calculated the theoretical photoelectron spectrum of N≡C–C≡N, matching it to the known experimental result [43], and calculated quite accurate IE_a values for the $\tilde{X}\,^2\Pi_g$, $\tilde{A}\,^2\Sigma_g^+$, $\tilde{B}\,^2\Sigma_u^+$, and $\tilde{C}\,^2\Pi_u$ electronic states of the known outer valence electron configuration of $(4\sigma_g)^2(1\pi_u)^4(4\sigma_u)^2(5\sigma_g)^2(1\pi_g)^4$. However, this method can be *very sensitive* to the input parameters and can yield *erroneous results* (i.e., the *incorrect* $(4\sigma_g)^2(4\sigma_u)^2(5\sigma_g)^2(1\pi_u)^4(1\pi_g)^4$ orbital-order) and *must* always be compared against an experimental photoelectron spectrum (p.466 of [114]).

Thus, in conclusion it is the opinion of the author here that the neutral $O{=}C{=}C{=}O[\tilde{X}\,^3\Sigma_g^-]$ is indeed a genuinely linear stable species with a lifetime at least in the μs regime (perhaps as high as the ms regime) and in the future direct experimental evidence of this assertion will someday come to light. (The same sentiments are "colourfully" expressed in the review by Berson, Dirney, Dailey III, and Liebman, [100], where they refer to O=C=C=O as "being a veritable Till Eulenspiegel of a molecule". They then clarify this by stating that this term refers to "a notorious rapscallion of medieval Germany, the protagonist of Richard Strauss' tone poem Till Eulenspiegel's Merry Pranks. He managed to stay one step ahead of the authorities until his last adventure, which ended in his apprehension and hanging".)

2.6 Comments on Large Polyatomics

To select a suitable polyatomic candidate for an optical emission study, it is critical that the following terms are met in order for one to form a basis for its choice. The polyatomic candidate should possess a relatively intense peak (preferably the base peak) for the molecular ion in its normal mass spectrum, possess a known photoelectron spectrum (to assign its radical-cation electronic states), and possess some electric-dipole symmetry allowed (see Appendix A) electronic transitions. Now, Table 2.27, illustrates the ultraviolet photoelectron spectroscopy (UPS) adiabatic ionization energy values for the large polyatomic molecules O=C=C=C=O, CH_2=C=O, C_6H_6, C_6F_6, C_4H_4O and the predictive relationship to the proposed vibrationless, 0_0^0, electronic transitions at their radical-cations. On inspection of Table 2.27, one may note the following trends.

For O=C=C=C=O, there are three predicted allowed emissions in the UV, VIS, and NIR regions. However, Turner et.al, [43, 46] proposed that the rapid loss of vibrational structure in the $\tilde{A}^2\Pi_g$, and $\tilde{B}^2\Pi_u$ peaks is due to the predissociation of these electronic states by the crossing of the dissociative states which lead to C=C=$O^{+\bullet}$ and C=C=C=$O^{+\bullet}$ at appearance energy, AE, values of 15.1, and 15.9 eV, respectively. Thus, one should not expect O=C=C=C=$O^{+\bullet}$ emission to any significant extent.

For CH_2=C=O, there are three predicted emissions, two allowed and one forbidden. Maier et.al., [47] noted that no observable $\tilde{A}^2B_2 \rightarrow \tilde{X}^2B_1$ emissions (nor should it be expected as it is forbidden) or any others from higher electronic states were observed. Maier et.al., [47] proposed that the rapid loss of vibrational structure in the $\tilde{A}^2B_2$ was due to predissociation and bonding producing the $CH_2^{+\bullet}[\tilde{X}^2A_1]$ + C≡O[$\tilde{X}^1A_1(^1\Sigma^+)$] dissociation products. Thus, again one should not expect CH_2=C=$O^{+\bullet}$ emission to any significant extent.

Table 2.27 The Ultraviolet Photoelectron Spectroscopy (UPS) Adiabatic Ionization Energy Values for the Large Polyatomic Molecules O=C=C=C=O, CH_2=C=O, C_6H_6, C_6F_6, and C_4H_4O and the Predictive Relationship to the Proposed Vibrationless Electronic Transitions of their Radical-Cations.

Adibatic Ionization Energy, IE_a(ev)[a]		Radical-Cation Vibrationless Electronic Transition	Vibrationless ΔIE_a in UPS λ(nm)[a]	Wavelength Known Emission λ(nm)[b]
O=C=C=C=O				
$\tilde{X}^2\Pi_u$	10.60	$\tilde{A}^2\Pi_g \rightarrow \tilde{X}^2\Pi_u$, 0_0^0	322.0	–[d]
$\tilde{A}^2\Pi_g$	14.45	$\tilde{C}^2\Sigma_u^+ \rightarrow \tilde{A}^2\Pi_g$, 0_0^0	490.1	–[d]
$\tilde{B}^2\Pi_u$	15.68	$\tilde{B}^2\Pi_u \rightarrow \tilde{A}^2\Pi_g$, 0_0^0	1008.8	–[d]
$\tilde{C}^2\Sigma_u^+$	16.98			
$\tilde{D}^2\Sigma_g^+$	17.25			
CH_2=C=O				
$\tilde{X}^2B_1$	9.63	$\tilde{B}^2B_1 \rightarrow \tilde{X}^2B_1$, 0_0^0	249.5	–[d]
$\tilde{A}^2B_2$	13.84	$\tilde{A}^2B_2 \rightarrow \tilde{X}^2B_1$, 0_0^0	294.5[c]	–[d]
$\tilde{B}^2B_1$	14.60	$\tilde{C}^2B_2 \rightarrow \tilde{A}^2B_2$, 0_0^0	553.5	–[d]
$\tilde{C}^2B_2$	16.08			
$\tilde{D}^2A_1$	16.7			
C_6H_6				
$\tilde{X}^2E_{1g}$	9.25	$\tilde{C}^2A_{2u} \rightarrow \tilde{X}^2E_{1g}$, 0_0^0	393.6	–[d]
$\tilde{B}^2E_{2g}$	11.49	$\tilde{B}^2E_{2g} \rightarrow \tilde{X}^2E_{1g}$, 0_0^0	553.5[c]	–[d]
$\tilde{C}^2A_{2u}$	12.4			
C_6F_6				
$\tilde{X}^2E_{1g}$	9.906	$\tilde{B}^2A_{2u} \rightarrow \tilde{X}^2E_{1g}$, 0_0^0	464.2	462.9
$\tilde{B}^2A_{2u}$	12.577			
$\tilde{C}^2B_{2u}$	13.847			
C_4H_4O				
$\tilde{X}^2A_2$	8.89	$\tilde{A}^2B_1 \rightarrow \tilde{X}^2A_2$, 0_0^0	911.7	–[d]
$\tilde{A}^2B_1$	10.25			
$\tilde{B}^2A_1$	13.0			

[a]Ref. [43 , 45-48, 51, 55], [b]Ref. [32, 115], [c]Forbidden, [d]Unobserved.

Next, the three aromatic molecules C_6H_6, C_6F_6, and C_4H_4O make up a group on which the author here attempted CIE studies. It was observed that they each possessed total emission counts (i.e., at 0 nm per a 30 minute accumulation) of 100, 120, and 80 counts, respectively. Unfortunately, no intact parent projectile-ion emissions for any of these species were observed (only some weak non-informative atomic fragment emissions). The C_6F_6 case is especially surprizing and deserves further comment. The only discernible non-atomic emission feature was that of weak $FC{\equiv}CF^{+\bullet}[\tilde{A}\,^2\Pi_g \rightarrow \tilde{X}\,^2\Pi_u]$ emission in the UV (at about 200 nm [51]). The previously observed $C_6F_6^{+\bullet}[\tilde{B}\,^2A_{2u} \rightarrow \tilde{X}\,^2E_{1g}]$ emission by Maier et.al., [32, 115] that possesses very strong intensity in the 440-520 nm region, *was completely absent*. This observation may allow one to conservatively propose that *too much internal excitation energy* was likely deposited in the 8 keV $C_6F_6^{+\bullet}$ projectile-ion during the collision event and *thus quasi-equilibrium dissociation dominated* over (the expected) emission. Therefore, this would tend to suggest that the present CIE technique, with a 8 keV projectile-ion, is simply unsuitable for the successful experimental observation of emissions from large polyatomic molecules.

One possible remedy for this apparent problem is *to slow the projectile-ion down* just prior to entry of the collision cell, to a low enough translational kinetic energy that just enough internal excitation energy is deposited in $M_1^{+\bullet}$ to *allow emission to dominate* over that of quasi-equilibrium dissociation. However, this is not a simple matter of an electrostatic plate with a (deceleration) voltage applied to it. This proposed "deceleration-zone" apparatus would have to maintain the focus of the ion-beam uniformly along its transit axis with little or no loss, and then maintain a constant flux. As well, the degree of deceleration would have to be adjustable and maintained constant throughout the CIE experiment. Thus, one may tentatively propose that a hexapole apparatus may perhaps be able to fulfil the above mentioned characteristics of the

"deceleration-zone" prior to the collision (OC) cell. Therefore, if such a modification was made to the present CIE apparatus, perhaps in the future the CIE technique could be successfully extended to larger polyatomic molecules.

2.7 Conclusions

The parent projectile-ion CIE emissions for $N{\equiv}N^{+\bullet}$, $C{\equiv}O^{+\bullet}$, $O{=}C{=}O^{+\bullet}$, species were observed, however only those of the fragments were present for the $O{=}C{=}C{=}O^{+\bullet}$ species. As well, the neutral CIE emissions for the $N{\equiv}N$ and $C{\equiv}O$ species were observed, however those of the $O{=}C{=}O$ and $O{=}C{=}C{=}O$ species were not. The excited electronic state emissions of $C{\equiv}O$ were correlated to the dissociation of the proposed respective excited electronic states of $O{=}C{=}C{=}O$. As well, the ground electronic state of linear $O{=}C{=}C{=}O[\,\tilde{X}\,^3\Sigma_g^-]$ was proposed to be indeed a (relatively) stable species with a lifetime estimated to be on the order of the μs regime (perhaps as high as the ms regime). As well, it was proposed that if the Franck-Condon Factors of the neutral $O{=}C{=}C{=}O[\,\tilde{X}\,^3\Sigma_g^-]$ can be accessed at or below an internal excitation energy of ≈ 1.5 eV (i.e., via neutralization-reionization mass spectrometry) a stable linear species should be produced.

Also, the lack of any observable experimental CIE spectra from the larger polyatomic 8 keV projectile-ions, is proposed to illustrate the beginning of the onset of the dominance of quasi-equilibrium unimolecular dissociation as the size of the molecular system under consideration is increased. However, if the projectile-ion is slowed down in a "deceleration-zone" prior to entering the collision cell (see section 2.6), perhaps in the future it may be possible to extend the CIE technique to polyatomic species.

2.8 References

[1] S.G. Lias, J.F. Liebman, J.L. Holmes, R.D. Levin, and W.G. Mallard, J. Phys. Chem. Ref. Data, 17, (1988).

[2] M.W. Chase, Jr., NIST-JANAF Thermochemical Tables, 4th Ed., J. Phys. Ref. Data Monogr., 9, (1998).

[3] H.E. O'Neal, and S.W. Benson, Natl. Stand. Ref. Data Ser. Natl. Bur. Stand., 21, (1970).

[4] S.W. Benson, and J.H. Buss, J. Chem. Phys. 29(3), 546-572, (1958).

[5] N. Cohen, and S.W. Benson, Chem. Rev., 2419-2438, (1993).

[6] S.W. Benson, F.R. Cruickshank, D.M. Golden, G.R. Haugen, H.E. O'Neal, A.S. Rodgers, R. Shaw, and R. Walsh, Chem. Rev., 29, 279-324, (1969).

[7] S.W. Benson, Thermochemical Kinetics, 2nd,John Wiley and Sons, New York, New York, USA, (1976).

[8] H.E. O'Neal, and S.W. Benson, J. Phys. Chem., (6)72, 1866-1877, (1968).

[9] J.T. Watson, Introduction to Mass Spectrometry, 2nd Ed., Raven Press, New York, New York, USA, (1985).

[10] R.G. Cooks, J.H. Beynon, R.M. Caprioli, and R.R. Lester, Metastable Ions, Elsevier, Amsterdam, (1973).

[11] C.F. Clark, Ed., Encyclopedia of Spectroscopy, Reinhold, New York, New York, USA, pp. 628-647, (1960).

[12] W.A. Chupka, J. Chem. Phys., 30(1), 191-211, (1959).

[13] H.M. Rosenstock, M.B. Wallenstein, A.L. Wahrhaftig, and H. Eyring, Proc. Natl. Acad. Sci. U.S., 38, 667, (1952).

[14] J.A. Hipple, and E.U. Condon, Phys. Rev., 68, 54, (1945).

[15] W.A. Hadden, and F.W. McLafferty, J. Am. Chem. Soc., 90, 4745, (1968).

[16] K.R. Jennings, Int. J. Mass Spectrom. Ion Phys., 1, 227, (1968).

[17] P.C. Burgers, and J.L. Holmes, Int. J. Mass Spectrom. Ion Proc., 58, 15, (1984).

[18] J.L. Holmes, and J.K. Terlouw, Org. Mass Spectrom., 15(8) 383-396, (1980).

[19] J.L. Holmes, Org. Mass Spectrom., 20(3), 169-183, (1985).

[20] (a) C. Wesdemiotis, and F.W. McLafferty, Chem. Rev., 87, 405, (1985).
(b) J.K. Terlouw, and H. Schwarz, Angew. Chem. Int. Ed. Engl., 26, 805, (1987).
(c) J.L. Holmes, Mass Spectrom. Rev., 8, 513, (1989).

[21] J.L. Holmes, and P.M. Mayer, Eur. Mass Spectrom., 1, 23-31, (1995).

[22] J.L. Holmes, and P.M. Mayer, J. Mass Spectrom., 30, 52-56, (1995).

[23] J.L. Holmes, P.M. Mayer, and A.A. Mommers, Int. J. Mass Spectrom. Ion Proc., 135, 213-2228, (1994).

[24] J.L. Holmes, P.M. Mayer, and A.A. Mommers, Org. Mass Spectrom., 27, 537-539, (1992).

[25] J.L. Holmes, P.M. Mayer, and A.A. Mommers, J. Am. Chem. Soc., 113, 9405-9406, (1991).

[26] G. Herzberg, Molecular Spectra and Molecular Structure I. Spectra of Diatomic Molecules., Van Nostrand Reinhold Company, New York, New York, USA, (1950).

[27] G. Herzberg, Molecular Spectra and Molecular Structure II. Infrared and Raman Spectra of Polyatomic Molecules., D. Van Nostrand Company Inc., New York, New York, USA, (1945).

[28] G. Herzberg, Molecular Spectra and Molecular Structure III. Electron Spectra and Electronic Structure of Polyatomic Molecules., Van Nostrand Company, New York, New York, USA, (1966).

[29] J.H.D. Eland, Photoelectron Spectroscopy. An Introduction to Ultraviolet Photoelectron Spectroscopy in the Gas Phase, Butterworths, London, U.K., (1974).

[30] J.H.D. Eland, Photoelectron Spectroscopy. An Introduction to Ultraviolet Photoelectron Spectroscopy in the Gas Phase, 2nd Ed., Butterworths, London, U.K., (1984).

[31] P.F. Bernath, Spectra of Atoms of Molecules, Oxford University Press Inc., New York, New York, USA, (1995).

[32] T.A. Miller, Ed., and V.E. Bondybey, Ed., Molecular Ions: Spectroscopy, Structure and Chemistry, North-Holland Publishing Company, New York, New York, USA, (1983).

[33] G. Herzberg, Atomic Spectra and Atomic Structure, Dover Publications, New York, New York, USA, (1944).

[34] A.B.F. Duncan, Rydberg Series in Atoms and Molecules, Academic Press Inc., New York, New York, USA, (1971).

[35] R.W.B. Pearse, and A.G. Gaydon, The Identification of Molecular, 4th Ed., John Wiley and Sons, New York, New York, USA, (1976).

[36] S. Bashkin, and J.O. Stoner, Jr., Atomic Energy Levels and Grotrian Diagrams 1. Hydrogen I – Phosphorous XV, American Elsevier Publishing Company Inc., New York, New York, USA, (1975).

[37] S. Bashkin, and J.O. Stoner, Jr., Atomic Energy Levels and Grotrian Diagrams 1. Hydrogen I – Phosphorous XV, Addenda, North-Holland Publishing Company Inc., New York, New York, USA, (1978).

[38] S. Bashkin, and J.O. Stoner, Jr., Atomic Energy Levels and Grotrian Diagrams 2. Sulphur I – Titanium XXII, North-Holland Publishing Company Inc., New York, New York, USA, (1978).

[39] M.T. Bowers, Ed., Gas Phase Ion Chemistry, Ions and Light, Vol. 3, Academic Press Inc., New York, New York, USA, (1984).

[40] F.A. Cotton, Chemical Applications of Group Theory, 3rd Ed., John Wiley and Sons, New York, New York, USA, (1990).

[41] A.D. Walsh, J. Chem. Soc., 2260-2331, (1953).

[42] T.J. Lee, D.J. Fox, H.F. Schaefer III, and P.M. Pitzer, J. Chem. Phys., 81(1), 356-361, (1984).

[43] D.W. Turner, C. Baker, A.D. Baker, and C.R. Brundle, Molecular Photoelectron Spectroscopy, John Wiley and Sons, New York, New York, USA, (1970).

[44] F.C. Tompkins, Ed., The Photoelectron Spectroscopy of Molecules, Faraday Discuss. Chem. Soc., 54, 1-306, (1972).

[45] A.G. Ginsberg, and C.R. Brundle, J. Chem. Phys., 68(11), 5231-5243, (1978).

[46] C. Baker, and D.W. Turner, Chem. Commun., 400-401, (1968).

[47] D. Hall, and J.P. Maier, Chem. Phys., 24, 373-378, (1977).

[48] G. Bieri, and L. Asbrink, J. Electron Spectrosc. Rel. Phenom., 20, 149-167, (1980).

[49] L. Asbrink, W. Von Niessen, and G. Bieri, J. Electron Spectrosc. Rel. Phenom., 21, 93-101, (1980).

[50] W. Von Niessen, G. Bieri, and L. Asbrink, J. Electron Spectrosc. Rel. Phenom., 21, 175-191, (1980).

[51] G. Bieri, L. Asbrink, and W. Von Niessen, J. Electron Spectrosc. Rel. Phenom., 23, 281-322, (1981).

[52] J. Bastide, D. Hall, E. Heilbronner, J.P Maier, and R.G. Plevey, J. Electron Spectrosc. Rel. Phenom., 16, 205-208, (1979).

[53] L. Asbrink, A. Svensson, W. Von Niessen, and G. Bieri, J. Electron Spectrosc. Rel. Phenom., 24, 293-314, (1981).

[54] W. Von Niessen, L. Asbrink, and G. Bieri, J. Electron Spectrosc. Rel. Phenom., 26, 173-201, (1982).

[55] G. Bieri, L. Asbrink, and W. Von Niessen, J. Electron Spectrosc. Rel. Phenom., 27, 129-178, (1982).

[56] G. Bieri, F. Burger, E. Heilbronner, and J.P. Maier, Helv. Chim. Acta, 60, 2213-2233, (1977).

[57] W. Von Niessen, L.S. Cederbaum, J. Schirmer, G.H.F. Diercksen, and W.P. Kraemer, J. Electron Spectrosc. Rel. Phenom., 28, 45-78, (1982).

[58] L. Asbrink, C. Fridh, and E. Lindholm, Chem. Phys. Lett., 52(1), 63-68, (1977).

[59] L. Asbrink, C. Fridh, and E. Lindholm, Chem. Phys. Lett., 52(1), 69-71, (1977).

[60] L. Asbrink, C. Fridh, and E. Lindholm, Chem. Phys. Lett., 52(1), 72-75, (1977).

[61] D.P. Chong, Theoret. Chim. Acta (Berl.), 51, 55-64, (1979).

[62] W.L. Wiese, M.W. and B.N. Miles, Atomic Transition Probabilities, Vol.II, NSRDS-NBS 22, US Government Printing Office, Washington, DC, USA, (1969).

[63] W.C. Martin, R. Zalubas, and L. Hagan, Atomic Energy Levels-The Rare Earth Elements, NSRDS-NBS 60, US Government Printing Office, Washington, DC, USA, (1972).

[64] P. Erman, and I. Martinson, Physica Scripta., 8, 269-273, (1973).

[65] H.H. Lui, and C.J. Humphreys, J. Opt. Soc. Am., 64(8), 1072-1082, (1974).

[66] G. Norlan, Physica Scripta., 8, 249-268, (1973).

[67] P.H. Krupenie, "The Spectrum of Molecular Oxygen", J. Phys. Chem. Ref. Data, 1(2), 423-534, (1972).

[68] C.Y.R Yu, J. Quant. Spectrosc. Radiat. Transfer, 37(1), 1-15, (1987).

[69] A. Lofthus, and P.H. Krupenie, "The Spectrum of Molecular Nitrogen", J. Phys. Chem. Ref. Data, 6(1), 113-307, (1977).

[70] F.R. Gilmore, J. Quant. Spectrosc. Radiat. Transfer, 5, 369-390, (1965).

[71] R.F. Holland, and W.B. Maier II, J. Chem. Phys., 56(11), 5229-5246, (1972).

[72] W.B. Maier II, J. Chem. Phys., 61(8), 3459-3470, (1974).

{73] W.B. Maier II, and R.F. Holland, J. Chem. Phys., 59(8), 4501-4534, (1973).

[74] J.L. Gardner, and J.A.R. Samson, 62(4), 1447-1452, (1975).

[75] M. Bloch, and D.W. Turner, Chem. Phys. Lett., 30(3), 344-346, (1975).

[76] P.H. Krupenie, "The Band Spectrum of Carbon Monoxide", NSRDS-NBS 5, US Government Printing Office, Washington, DC, 1-87, (1966).

[77] S.G. Tilford, and J.D. Simmons, "Atlas of the Observed Absorption Spectrum of Carbon Monoxide between 1060 and 1900 Å", J. Phys. Chem. Ref. Data, 1(1), 147-187, (1972).

[78] J. Danon, G. Manclaire, T.R. Govers, and R. Marx, J. Chem. Phys., 76(3), 1255-1262, (1982).

[79] V.E. Bondybey, and T.A. Miller, J. Chem. Phys., 69(8), 3597-3602, (1978).

[80] D.L. Judge, G.S. Bloom, and L. Morse, Can. J. Phys., 47, 489-497, (1969).

[81] L.C. Lee, and D.L. Judge, J. Chem. Phys., 57(10), 4443-4445, (1972).

[82] D. Gauyaeq, M. Horani, S. Leach, and J. Rostas, Can. J. Phys., 53, 2040-2059, (1975).

[83] D.L. Judge, L.C. Lee, and M.J. Haugh, Can. J. Phys., 53, 1472-1476, (1975).

[84] J.M. Ajello, J. Chem. Phys., 55(7), 3169-3177, (1971).

[85] J.P. Maier, and F. Thommen, Chem. Phys., 51 319-327, (1980).

[86] M. Th. Praet, J.C. Lorquet, and G Raseev, J. Chem. Phys., 77(9), 4611-4618, (1982).

[87] J.H.D. Eland, and J. Berkowitz, J. Chem. Phys., 67(6), 2782-2787, (1977).

[88] M. Wu, D.P. Taylor, and P.M. Johnson, J. Chem. Phys., 95(2), 761-770, (1991).

[89] H. Bregman-Reisler, and J.P. Doering, J. Chem. Phys., 62(8), 3109-3117, (1975).

[90] J.E. Parker, R.G. Milner, and A.M. Robertson, Int. J. Mass Spectrom. Ion. Phys., 24, 429-445, (1977).

[91] S.V. Filseth, Adv. Photochem., 10, 1-57, (1977).

[92] S.P. Walch, J. Chem. Phys., 72(10), 5670-5686, (1980).

[93] C. Devillers, and D.A. Ramsay, Can. J. Phys., 49, 2839-2858, (1971).

[94] V. Zengin, B.J. Persson, and K.M. Strong, and R.E. Continetti, J. Chem. Phys., 105(22), 9740-9747, (1996).

[95] K.H. Becker, and K.D. Bayes, J. Chem. Phys., 48(2), 653-661, (1968).

[96] R.C. Haddon, D. Poppinger, and L. Radom, J. Am. Chem. Soc., 97(7), 1645-1649, (1975).

[97] G.P. Raine, H.F. Schaefer III, and R.C. Hadden, J. Am. Chem. Soc., 105, 194-198, (1983).

[98] J.T. Blair, J.C. Weisshaar, and Weinhold, J. Chem. Phys., 87(1), 392-410, (1987).

[99] J.T. Blair, J.C. Weisshaar, and Weinhold, J. Chem. Phys., 88(2), 1467-1468, (1988).

[100] J.A. Berson, D.M. Dirney, W.P. Dailey III, and J.F. Liebman, Molecular Structure and Energies, "Ethenedione: Its Ions and Analogues", Springer-Verlag, New York, New York, USA, pp. 391-441, (1987).

[101] S.C. Ostrander, L. Sanders, and J.C. Weisshaar, J. Chem. Phys., 84(1), 529-530, (1985).

[102] J.R. Thomas, D.J. Deleeuw, H.F. Schaefer III, B.J. Duke, and B. O'Leary, J. Chem. Phys., 102(16), 6525-6536, (1995).

[103] W.E. Thompson, and M.E. Jacox, J. Chem. Phys., 95(2), 735-745, (1991).

[104] A.A. Korkin, A. Balkova, R.J. Bartlett, R.J. Boyd, and P. Von Rague Schleyer, J. Phys. Chem., 100, 5702-5714, (1996).

[105] D. Sulzle, T. Weiske, and H. Schwarz, Int. J. Mass Spectrom. Ion Process.,125, 75-79, (1993).

[106] D. Schroder, C. Heinemann, H. Schwarz, J.N. Harvey, S. Dua, S.J. Blanksby, and J.H. Bowie, Chem. Eur. J., 4(12), 2550-2557, (1998).

[107] L. Pandolfo, G. Paiaro, S. Catinella, and P. Traldi, J. Mass Spectrom., 31, 209-212, (1996).

[108] H. Chen, and J.L. Holmes, Int. J. Mass Spectrom. Ion Process., 133, 111-119, (1994).

[109] D. Dawson, H. Chen, and J.L. Holmes, Eur. Mass Spectrom., 2, 373-375, (1996).

[110] D.A. Long, F.S. Murfin, and R.L. Williams, Proc. R. Soc. (London), Ser. A, 222, 251, (1954).

[111] A. Van der Pol, A. Van der Avoid, and P.E.S. Wermer, J. Chem. Phys., 92(12), 7498-7504, (1990).

[112] M. Havenith, M. Petri, C. Lubina, G. Hilpert, and W. Urban, J. Molecular Spectrosc., 167, 248-261, (1994).

[113] K. Norwood, J.H. Guo, and C.Y. Ng, J. Chem. Phys., 90(11), 6026-6033, (1989).

[114] L.S. Cederbaum, W. Domeke, and W. Von Niessen, Chem. Phys., 10, 459-470, (1975).

[115] J.P. Maier, J. Electron Spectrosc. Rel. Phenom., 40, 203-226, (1986).

Chapter 3 Tandem Mass Spectrometry of Perfluorinated Iodo, Oxo and Unsaturated Organics

3.1 Introduction

Over the past half-century, the gas-phase ion-chemistry of hydrogen containing organics has by far been the dominant species of choice for study, owing originally to the interest of the petroleum industry. A wealth of information on their reaction mechanisms, mass spectral characteristics, ion energetics and thermodynamic properties has been amassed on these compounds to the point that, generally, they are well understood and their behaviour well established. A recent compilation by Lias et. al. [1], provides a comprehensive reliable source of important thermodynamic data, namely the standard heats of formation, $\Delta_f H^0$, of the neutral and its radical-cation and its ionization energy, IE, of many chemical species. It acts not only as an invaluable tool in the analysis of ones' own mass spectral data, but also as a source of inspiration to the gas-phase ion-chemist for the design of experiments on new precursor molecules.

However, the information on the class of halogen (i.e., F, Cl, Br, I) containing compounds is not quite as extensive as those of the above. Their primary industrial interest was in their use as solvents and coolants, widely known as perfluorochlorocarbons. Due to their difficult syntheses, somewhat toxic qualities, and chemical instability, halogen containing compounds are generally more difficult to obtain and are less studied. As well, with the discovery in the 1970's of their ozone-depleting characteristics a new interest in their gas-phase ion-chemistry was created at the same time as their use began to be curtailed.

In the 1990's, the Montreal Protocols set out a timetable for the complete phasing out of many halogenated compounds by the early twenty-first century. Thus, a systematic study of some halogen containing compounds, prior to their possible future unavailability, is of interest and forms the subject of the next two thesis chapters.

The compounds of interest are those in which all of the hydrogens are replaced by fluorines, a term known as perfluorination. This study encompasses several isomeric perfluorinated iodo and oxo compounds, as well as some unsaturated perfluorocarbons.

As will be illustrated in the work to follow, the ion and neutral chemistry of perfluorinated compounds does in some instances closely parallel that of their hydrogen analogues and in other instances is a complete right unto its own. The differences stem from the so-called "perfluoro effect", first systematically studied by Brundle et. al. [2, 3]. The replacement of all the hydrogens in a compound by fluorine, the most electronegative of elements, results in the atomic-orbital overlap of the σ(C–F) molecular-orbitals to be much greater than that of the π(C–F) molecular-orbitals. The former are stabilized by ≈ 2–4 eV, whereas the latter are typically less affected and are stabilized by ≈ 0–1 eV. This results in not only a larger separation of σ and π orbital energies, but in a shortening (strengthening) of the σ–bonds with a concomitant slight lengthening (weakening) of the π–bonds in the neutral species.

However, whereas perfluorination generally stabilizes the neutral species (i.e., strongly lowers the heat of formation, $\Delta_f H^0$), there can be in some cases a very strong destabilization (dissociative) effect. While the ionization energies, IE, of most hydrogen compounds have values of ≈ 8–10 eV, their perfluorinated counterparts have IE's of typically ≈ 10–12 eV. In a recent study of Tuckett et. al. [4, 5] it was noted that in general the greater

effect of perfluorination is to shift the equilibrium geometry of the parent radical-cation, $M_1^{+\bullet}$, relative to the ground state of the neutral species, M_1, to longer bond lengths. This means that the formation of the radical-cation, $M_1^{+\bullet}$, in a perfluorinated system may involve a more dramatic change in bond lengths than would probably occur in the hydrogen analogue. This may result in a partial or a large shift in the bound part of the potential energy surface of $M_1^{+\bullet}$ out of the Franck-Condon region. In extreme cases, a complete shift out of the bound part of the Franck-Condon region may occur (e.g., perfluoromethane, CF_4, and perfluorocyclobutane, c-C_4F_8) and no stable parent radical-cation $M_1^{+\bullet}$ can be mass spectrometrically observed. As a rule of thumb, the presence of unsaturation (double, C=C, and triple, C≡C, bonds), conjugation (C=C=C , C=C=O), and other (less electronegative) halogens (e.g., I$^\bullet$) strongly encourage the production of a stable parent radical-cation $M_1^{+\bullet}$ (i.e., with an equilibrium geometry closely similar to the neutral M_1).

3.2 General Rationale for the Order of Stability and Dissociation of C_nF_mX / $C_nF_mX^+$

3.2.1 Electron-Withdrawing Properties of the F an CF_3 Groups

In general, a helpful illustration to keep in mind the differences in the physical properties due to perfluorination is the comparison of water and acetone with their fluorine analogues. Whereas OH_2 is an omnipresent chemical of life and $(CH_3)_2C{=}O$ is a common benign organic solvent, the strong electronegativity of fluorine reduces the intermolecular interactions to the point that they are no longer liquids, but OF_2 and $(CF_3)_2C{=}O$ are now corrosive and toxic gases, respectively.

Additionally, it is important to keep in mind the possibilities opened-up for unusual rearrangement and/or dissociation chemistry of perfluorinated $M_1^{+\bullet}$ due to the neutrals that are lost from such ions generally possessing a much more exothermic (stable) heat of formation (Δ_fH^0) than their hydrogen analogues. It is generally observed that common neutral losses in the gas-phase ion-chemistry of hydrogen compounds are $H^\bullet$, $CH_3^\bullet$, CH_4, $CH_2{=}CH_2$ and OH_2. A set of possible small neutral losses is presented in Table 3.1, and provides a comparison of the heats of formation Δ_fH^0 of the hydrogen and fluorine species. On inspection of Table 3.1, a few trends become evident. Due to their strongly negative Δ_fH^0 values, the $CF_3^\bullet$, CF_4, and $CF_2{=}CF_2$ losses will be greatly amplified in comparison to their hydrogen analogues. Most notably, the very strong exothermic $\Delta_fH^0[CF_2]$ and slightly endothermic $\Delta_fH^0[OF_2]$ values are the complete opposite of the hydrogen analogues and must manifest itself in a different rearrangement and/or dissociation chemistry.

As stated earlier, the heat of formation of the neutral species, $\Delta_fH^0[M_1]$, its ionization energy, $IE[M_1]$, (adiabatic, $IE_a[M_1]$, vertical, $IE_v[M_1]$) and thus the heat of formation of the cationic species, $\Delta_fH^0[M_1^{+\bullet}]$, for the hydrogen containing organic compounds are well known [1]. Thus, the order of stability of isomeric neutral and cationic hydrogen species are well-established [6], but such is not the case for their perfluoro analogues [1]. The recent reviews of Doliber et.al. [7], and Krespan et. al. [8], have dealt with the chemistry of fluorinated alkyl radicals and fluorinated carbocations. However, these reviews concentrated on their behaviour in solution, not in the gas-phase.

The neutral Δ_fH^0 values of most perfluoro species have not been experimentally (calorimetrically) determined. As well, the gas-phase ion-chemistry studies to determine their

Table 3.1 Comparison of Common Small Neutral Losses

Hydrogen Species	Heat of Formation $\Delta_f H^0$(kJ•mol^{-1})[a]	Fluorine Analogue	Heat of Formation $\Delta_f H^0$(kJ•mol^{-1})[a]
$H^•$	217.999	$F^•$	(79.4 ± 0.3)
$CH^•$	595.8	$CF^•$	(255.2 ± 8)
CH_2	390	CF_2	–(205 ± 12)
$CH_3^•$	(145.8 ± 1)	$CF_3^•$	–460
CH_4	–(74.5 ± 0.4)	CF_4	–(934.5 ± 0.4)
HC≡CH	(228.0 ± 1)	FC≡CF	(21 ± 21)
CH_2=CH_2	(52.2 ± 1)	CF_2=CF_2	–(659 ± 3)
OH_2	–241.83	OF_2	(24.5 ± 1.6)
HI	(26.4 ± 0.2)	FI	–(94.8 ± 3.8)

[a]Ref.[1].

(adiabatic) ionization energies, IE_a, and the appearance energies, AE, of their dissociation reactions, for the most part, have not been performed. For example, the iodoperfluoroalkane C_3F_7I and C_4F_9I isomers, which are discussed in this chapter, have not been systematically studied (e.g., via photoelectron spectroscopy). Their (adiabatic) ionization energies, $IE_a[M_1]$, and thus their cationic heats of formation heats of formation, $\Delta_fH^0[M_1^{+\bullet}]$, and their order of stability are unknown.

This being the case, one may use several qualitative arguments to rationalize their gas-phase ion-chemistry. As well, one may use Benson's Additivity Rules [9-11] for a quantitative estimate of their neutral heats of formation, $\Delta_fH^0[M_1]$, as discussed below.

According to Benson's Rules of Additivity [9-11], any additive property, such the heat of formation Δ_fH^0, may be estimated by dividing the molecule into its constituent parts, known as groups. Once one has assigned an empirical value to each group, based on the best available thermochemical data, the sum of the group values produces the estimated empirical value for the whole molecule. For example, $C–(H)_3(C)$, $C–(H)_2(C)_2$, and $C–(H)_2(I)(C)$, denote a methyl group bonded to a carbon, a methylene group bonded onto two carbons, and a terminal iodomethyl group, respectively. A series of Benson groups and their individual Δ_fH^0 values used in this chapter are presented in Table 3.2. Also, the Δ_fH^0 values of the relevant butyl neutrals, radicals and iodides and the propyl neutrals, radicals and iodides, and their perfluoro analogues are presented in Tables 3.3 and 3.4, respectively. The centre column contains their standard literature Δ_fH^0 values [1], and the first column presents the empirically estimated Benson's Additivity group Δ_fH^0 values [9-11]. The third column presents the stabilization energy per fluorine of the perfluoro series, resulting from the lower Δ_fH^0 values with respect to their hydrogen analogues. Thus, a compound such as 1-

Table 3.2 Benson's Additivity Terms for the Empirical Estimation of the Heats of Formation, $\Delta_f H^\circ$(kJ•mol^{-1})[a]

Hydrogen Series		Fluorine Series		$\Delta(\Delta_f H^\circ)$ (kJ•mol^{-1})
Benson's Group	Heat of Formation $\Delta_f H^\circ$(kJ•mol^{-1})	Benson's Group	Heat of Formation $\Delta_f H^\circ$(kJ•mol^{-1})	Stabilization Per Fluorine
Saturated Series				
$C-(C)_4$	0.42			
$C-(H)(C)_3$	−10.0	$C-(F)(C)_3$	−202.9	−192.9
$C-(H)_2(C)_2$	−20.9	$C-(F)_2(C)_2$	−405.8	−192.5
$C-(H)_3(C)$	−41.84	$C-(F)_3(C)$	−662.7	−207.0
Iodo Series				
$C-(I)(C)_3$	53.6			
$C-(H)(I)(C)_2$	43.9	$C-(F)(I)(C)_2$	(≈−142.7)[b]	(≈−186.6)[b]
$C-(H)_2(I)(C)$	33.5	$C-(F)_2(I)(C)$	−345.6	−189.5
Unsaturated Series				
$C_d-(C)_2$	42.63			
$C_d-(H)(C)$	35.8	$C_d-(F)(C)$	−136.0	−171.8
$C_d-(H)_2$	26.2	$C_d-(F)_2$	−327.2	−176.7
Radical Series				
$C^\bullet-(C)_3$	171.5			
$C^\bullet-(H)(C)_2$	171.5	$C^\bullet-(F)(C)_2$	(≈ −9.7)[b]	(≈−181.2)[b]
$C^\bullet-(H)_2(C)$	160.7	$C^\bullet-(F)_2(C)$	(≈−215.3)[b]	(≈−188.0)[b]

[a]Ref. [7-9], [b]Estimated, see text.

Table 3.3 Heats of Formation of Butyl Neutrals, Radicals and Iodides and Their Perfluoro Analogues

Species	Heat of Formation, $\Delta_f H^\circ$(kJ•mol^{-1}) Benson's Additivity[a]	Standard Literature[b]	$\Delta(\Delta_f H^\circ)$ (kJ•mol^{-1}) Stabilization Per Fluorine
Hydrogen Series			
$CH_3CH_2CH_2CH_2I$	−50.2	−52[c]	
$CH_3CH_2CHICH_3$	−60.7	−62[c]	
$(CH_3)_2CHCH_2I$	−60.2	−62[c]	
$(CH_3)_3CI$	−72.0	−(72.0 ± 2.2)	
$CH_3CH_2CH_2CH_2^\bullet$	77.0	74[c]	
$CH_3CH_2C^\bullet HCH_3$	67.0	(71.0 ± 1.6)	
$(CH_3)_2CHCH_2^\bullet$	67.0	70	
$(CH_3)_3C^\bullet$	46.0	(46.2 ± 2.5)	
$CH_2{=}CHCH_2CH_3$	−0.8	−(0.4 ± 0.5)	
$CH_2{=}C(CH_3)_2$	−14.8	−(16.9 ± 0.6)	
Perfluoro Series			
$CF_3CF_2CF_2CF_2I$	−1820.0		−196.4
$CF_3CF_2CFICF_3$	(≈−1874)[d]		(≈−201)[d]
$(CF_3)_2CFCF_2I$	−1874.0		−201.3
$(CF_3)_3CI$	−1934.7		−207.0
$CF_3CF_2CF_2CF_2^\bullet$	(−1694.0)[d]		(−196.8)[d]
$CF_3CF_2C^\bullet FCF_3$	(≈−1741)[d]		(≈−193)[d]
$(CF_3)_2CFCF_2^\bullet$	(−1742.0)[d]		(−193.5)[d]
$(CF_3)_3C^\bullet$	−1816.7		−196.7
$CF_2{=}CFCF_2CF_3$	−1531.8		−191.4
$CF_2{=}C(CF_3)_2$	−1610.0		−199.4

[a]Ref. [7-9], [b]Ref. [1], [c]Estimated by Ref. [1], [d]Estimated, see text.

Table 3.4 Heats of Formation of Propyl Neutrals, Radicals and Iodides and Their Perfluoro Analogues

Species	Heat of Formation, $\Delta_f H^\circ$ (kJ•mol^{-1}) Benson's Additivity[a]	Standard Literature[b]	$\Delta(\Delta_f H^\circ)$ (kJ•mol^{-1}) Stabilization Per Fluorine
Hydrogen Series			
$CH_3CH_2CH_2I$	−29.3	−(32.5 ± 1.7)	
$(CH_3)_2CHI$	−39.7	−(41.6 ± 1.7)	
$CH_3CH_2CH_2^\bullet$	97.9	(100.5 ± 2.1)	
$(CH_3)_2CH^\bullet$	87.9	(93.3 ± 2.5)	
$CH_2{=}CHCH_3$	20.2	(20.2 ± 0.4)	
Perfluoro Series			
$CF_3CF_2CF_2I$	−1414.2		−197.4
$(CF_3)_2CFI$	(≈−1468)[c]		(≈−210)[c]
$CF_3CF_2CF_2^\bullet$	(−1281.2)[c]	−1282[d]	(−197.4)[c]
$(CF_3)_2CF^\bullet$	(≈−1335)[c]		(≈−191)[c]
$CF_2{=}CFCF_3$	−1125.9	−1125	−190.9

[a]Ref. [7-9], [b]Ref. [1], [c]Estimated, see text, [d]Ref. [10].

iodobutane, $CH_3CH_2CH_2CH_2I$, may be broken down into the following groups, , $C–(H)_3(C)$, $C–(H)_2(C)_2$, $C–(H)_2(C)_2$,and $C–(H)_2(I)(C)$. Now, utilizing the Δ_fH^0 values for each of the Benson's groups shown in Table 3.2, one may estimate the $\Delta_fH^0[CH_3CH_2CH_2CH_2I]$ to be –50.2 $kJ•mol^{-1}$. (i.e., $\Delta_fH^0[C–(H)_3(C)] + 2\Delta_fH^0[C–(H)_2(C)_2] + \Delta_fH^0[C–(H)_2(I)(C)]$). On inspection of Tables 3.3 and 3.4, one may observe that the Δ_fH^0 values estimates by Benson Additivity are generally quite accurate.

At this point the assumptions concerning the estimation of the Benson's terms for the perfluoro groups and the perfluoro compounds deserve emphasis. The standard Δ_fH^0 literature of Lias et. al. [1] for the isomers $CH_3CH_2CHICH_3$ and $(CH_3)_2CHCH_2I$ in Tables 3.3 assign a common Δ_fH^0 value of –62 $kJ•mol^{-1}$. If one may assume a similar behaviour to be present in their perfluoro analogues, then one may set the Δ_fH^0 value of $CF_3CF_2CFICF_3$ to be –1874 $kJ•mol^{-1}$. Thus, now one may utilize the other Benson's group Δ_fH^0 values and estimate the Δ_fH^0 for the $C–(F)(I)(C)_2$ group to be $\approx$ –142.7 $kJ•mol^{-1}$. If one may now make a second assumption that the dissociation energy for the C–I bond, $D^0[C–I]$, in the hydrogen species (i.e., $D^0[C–I]$ is 239.8, 241.7, 232.8, 239.8, 238.8, and 225.2 $kJ•mol^{-1}$ for $CH_3CH_2CH_2I$ (n-C_3H_7I), $(CH_3)_2CHI$ (s-C_3H_7I), $CH_3CH_2CH_2CH_2I$ (n-C_4H_9I), CH_3CH_2CHI CH_3 (s-C_4H_9I), $(CH_3)_2CH$ CH_2I (i-C_4H_9I), and $(CH_3)_3CI$ (t-C_4H_9I), respectively) is the same value in their respective perfluoro analogues, one may estimate the perfluoro neutral radical heats of formation Δ_fH^0 in Tables 3.3 and 3.4. To illustrate the validity of this assumption one should consider the known $D^0[C–I]$ values for the $CH_3–I$ and $CF_3–I$ neutrals [1]. One may note that for the hydrogen species, $D^0[CH_3–I] = (\Delta_fH^0[CH_3^•] + \Delta_fH^0[I^•]) – (\Delta_fH^0[CH_3–I]) = ((145.8\ kJ•mol^{-1}) + (106.8\ kJ•mol^{-1}) – (15.4\ kJ•mol^{-1}) = 237.2\ kJ•mol^{-1}$,

whereas for the fluorine species, $D^0[CF_3–I] = (\Delta_fH^0[CF_3^\bullet] + \Delta_fH^0[I^\bullet]) – (\Delta_fH^0[CF_3–I]) =$ $((–460\ kJ\bullet mol^{-1}) + (106.8\ kJ\bullet mol^{-1}) – (–590\ kJ\bullet mol^{-1}) = 236.8\ kJ\bullet mol^{-1}$, i.e., a *small* difference of only 0.4 $kJ\bullet mol^{-1}$ [1]. Hence, the above assumption is indeed a reasonable one. Thus, on assigning Δ_fH^0 values for $CF_3CF_2C^\bullet FCF_3$ and $CF_3CF_2CF_2CF_2^\bullet$, one may estimate the Δ_fH^0 values for the $C^\bullet–(F)(C)_2$ and $C^\bullet–(F)_2(C)$ groups to be $\approx –9.7\ kJ\bullet mol^{-1}$ and $\approx$ $–215.3\ kJ\bullet mol^{-1}$, respectively.

On inspection of the third column of Table 3.2, one can see that the above assumptions are indeed quite reasonable and result in the stabilization energy per fluorine to be in the range of $\approx –170$ to $–210\ kJ\bullet mol^{-1}$. This results in the stabilization energy per fluorine in the range of $\approx –190$ to $–210\ kJ\bullet mol^{-1}$ for the perfluorobutyl and perfluoropropyl species illustrated in Tables 3.3 and 3.4. On inspection of Table 3.4, one can see that the experimental $\Delta_fH^0[CF_3CF_2CF_2^\bullet]$ value of Bryant [12], is very close to that estimated by Benson's Additivity. Thus, the trends in the Benson Δ_fH^0 values and the order of stability of the perfluoro neutral species are very likely to be reliable estimates of the presently unmeasured experimental Δ_fH^0 values.

Very few of the heats of formation Δ_fH^0 of the perfluorinated cations of interest are known [1]. However, recently Tuckett et. al. [4, 5] has measured the heats of formation of the perfluoro-n-propyl and the perfluoroallyl cations and determined their values to be $\Delta_fH^0[CF_3CF_2CF_2^+] = –(360 \pm 20)\ kJ\bullet mol^{-1}$ [4], and $\Delta_fH^0[(CF_2)_2C^+–F] = (84 \pm 20)\ kJ\bullet mol^{-1}$ [5], respectively. If one may take the ionization energy measurement of the perfluoroallyl radical, $IE[(CF_2)_2C^\bullet–F] = (8.44 \pm 0.05)$ eV, of Kagramanov et. al. [13] to be *adiabatic*, one can estimate the neutral heat of formation to be $\Delta_fH^0[(CF_2)_2C^\bullet–F] = –730.3\ kJ\bullet mol^{-1}$. On

consideration of the heat of formation of the respective hydrogen analogue, $\Delta_f H^0[(CH_2)_2C^{\bullet}-H] = 161$ kJ•mol^{-1}, one may obtain a stabilization per fluorine of −178.3 kJ•mol^{-1}, a value entirely within the range of the previously discussed perfluoro species. Thus, these heat of formation $\Delta_f H^0$ values for $CF_3CF_2CF_2^+$, $(CF_2)_2C^+-F$, and $(CF_2)_2C^{\bullet}-F$ will be used in the following sections to estimate the heat of formation $\Delta_f H^0$ of the dissociation products and in the construction of the probable energy level diagrams of the perfluorinated species studied here.

The issue of the order of stability of the neutral and cationic isomer needs to be discussed. On review of Tables 3.3 and 3.4 one can see that the behaviour of the saturated neutral hydrogen and fluorine species parallel each other. For the neutral parent iodo species C_nF_mI, and their radical-cations, $C_nF_mI^{+\bullet}$ (where $m = 2n+1$), the molecular orbital character of the frontier orbitals should be dominated by the lone-pair (p_x, p_y) iodine non-bonding atomic-like orbitals (where $IE_a[I^{\bullet}] = 10.45$ eV). Thus, the physical characteristics of both the neutral C_nF_mI and the radical-cation $C_nF_mI^{+\bullet}$ species should be dominated by the I atom itself. For the neutral species, C_nF_mI, the ranking of the $\Delta_f H^0$ values (i.e., the order of stability) should follow that of the hydrogen analogues C_nH_mI (i.e, tertiary > secondary > primary), as listed below,

$$(CF_3)_3CI > (CF_3)_2CFCF_2I > CF_3CF_2CFICF_3 > CF_3CF_2CF_2CF_2I$$

and

$$(CF_3)_2CFI > CF_3CF_2CF_2I$$

Additionally, upon ionization the IE_a values for each isomer should be dictated by the atomic I orbitals interacting with the molecular orbitals of the perfluoroalkyl moiety.

As will be discussed shortly, the IE_a values of both the parent species C_nF_mI and the fragment radical $C_nF_m^{\bullet}$ *increase* with CF_3 substitution. Thus, the order of IE_a values varies as follows; primary < secondary < tertiary (i.e., opposite to the order of the hydrogen analogues). However, since the characteristics of the I atom are proposed to dominate those of the C_nF_mI species, even with the reversal of the order of the IE_a values, the order of the corresponding $\Delta_fH^0[C_nF_mI^{+\bullet}]$ values should in most likelihood parallel that of the $C_nH_mI^{+\bullet}$ species. Therefore the order of stability should be as follows,

$$(CF_3)_3CI^{+\bullet} > (CF_3)_2CFCF_2I^{+\bullet} > CF_3CF_2CFICF_3^{+\bullet} > CF_3CF_2CF_2CF_2I^{+\bullet}$$

and

$$(CF_3)_2CFI^{+\bullet} > CF_3CF_2CF_2I^{+\bullet}$$

In regards to the neutral radical species $C_nF_m^{\bullet}$ produced via $I^{\bullet}$ loss from the parent neutral C_nF_mI, the order of stability (for both the H and F series) is as follows; (tertiary > secondary > primary),

$$R_3C^{\bullet} > R_2CX^{\bullet} > RCX_2^{\bullet}$$,when X = H, R =alkyl; when X = F, R =perfluoroalkyl

A qualitative rationalization for this trend is that as the radical site is surrounded progressively by more (bulky) R groups, it becomes less accessible to reaction (i.e., more stable). An extreme example of this stability occurs in the perfluorinated species,

$((CF_3)_2CF)_2C^{\bullet}-CF_2CF_3$, known as Scherer's radical, which is known to persist in a room temperature solution, even in the presence of dissolved O_2 [7].

However, in contrast to the neutral manifold, the behaviour of the hydrogen $C_nH_m^+$ and fluorine $C_nF_m^+$ analogues diverge in the cationic manifold. It is known that for hydrogen analogues, the order of stability of saturated fragment organic cations $C_nH_m^+$ is determined by the ability of the alkyl groups to *stabilize positive charge* in the sense that the IE_a value of the neutral radical is progressively *lowered* (i.e., the electron is *more* easily removed) as substitution at the charge-site is increased. Therefore, the known order of stability is as follows ; tertiary > secondary > primary,

$$R_3C^+ > R_2CH^+ > RCH_2^+, \text{ where R= alkyl}$$

However in the case of perfluorination, due to its strong electronegativity, fluorine possesses the ability to somewhat *destabilize positive charge* in the sense that the IE_a value of the neutral radical is progressively *raised* (i.e., the electron is *less* easily removed) as substitution about the charge-site is increased. Thus, the characteristics of the fragment cation $C_nF_m^+$ should be dominated by the interaction of the carbon atom charge-site with the surrounding (per)fluoro substituents. Therefore as discussed above, if the order of IE_a values of the $C_nF_m^{\bullet}$ is believed to be *opposite* to that of $C_nH_m^{\bullet}$, and such in contrast to the C_nF_mI parent (whose characteristics should be dominated by the I atom), it is proposed here that due to the very strong interaction of the charge-site with the perfluoroalkyl groups this may result in the $\Delta_fH^0[C_nF_m^+]$ of the various isomers to be close in value and may even result in a *reversed stability order* of the $C_nF_m^+$ species as follows, (primary > secondary > tertiary),

$RCF_2^+ > R_2CF^+ > R_3C^+$, where R= perfluoroalkyl

and specifically,

$CF_3CF_2CF_2CF_2^+ > CF_3CF_2C^+FCF_3 > (CF_3)_2CFCF_2^+ > (CF_3)_3C^+$

and

$CF_3CF_2CF_2^+ > (CF_3)_2CF^+$

To fully appreciate the factors involved in the proposed *reversal of the fragment cation stability order* of the perfluoro species $C_nF_m^+$ relative to the hydrogen species $C_nH_m^+$, the following points deserve emphasis. Firstly, the H and CH_3 groups are not as electronegative as their (per)fluoro analogues F and CF_3. The substitution of an F for an H will strongly stabilize (i.e. the raising of the IE_a's) the σ-orbitals compared to a mild stabilization of the π-orbitals (i.e., strongly electron- withdrawing for the σ-symmetry). However, due to the symmetry of the orbitals of the CF_3 group, the substitution of one CF_3 for an F results in the stabilization of both the σ and π-orbitals (i.e., the raising of their IE_a's) due to the strong electron withdrawing capacity for both σ, π-symmetry. Secondly, whereas CH_3 may be considered *electron-donating* and thus being able to *stabilize* positive charge, *lowering* the IE_a with the presence of each CH_3 group, the complete opposite must be said for the perfluoro analogue. The CF_3 group is extremely *electron-withdrawing* (both for σ and π-symmetry) and thus will strongly *destabilize* positive charge, *raising* the IE_a with each CF_3

Table 3.5 Comparison of the F and CF_3 Group Shifts on the IE_a Values

Species	Neutral Heat of Formation Δ_fH^0(kJ•mol^{-1}) Benson's Additivity[a]	Neutral Heat of Formation Δ_fH^0(kJ•mol^{-1}) Standard Literature[b]	Adiabatic Ionization Energy IE_a(eV)[b]	Ionic Heat of Formation Δ_fH^0(kJ•mol^{-1})[b]
Ethyne Series				
HC≡CH	226.8	(228.0 ± 1)	(11.400 ± 0.003)	1327.9
CH_3–C≡CH	185.8	(186.6 ± 2)	(10.36 ± 0.01)	1186.2
CH_3–C≡C–CH_3	144.8	(145.4 ± 0.8)	(9.562 ± 0.005)	1068
FC≡CF	21.0[d]	(21 ± 21)	11.18	1100
CF_3–C≡CF	−538.0[d]			
CF_3–C≡C–CF_3	−1097.0		12.35[h]	94.5[f]
Diethyne Series				
HC≡C–C≡CH	455.2	440	(10.180 ± 0.003)	1422
CH_3–C≡C–C≡C–H	414.2	425[c]	9.4	1332
CH_3–C≡C–C≡C–CH_3	373.2	377	(8.92 ± 0.05)	1238
FC≡C–C≡CF	249.4[d]		10.05[e]	1219.0[f]
CF_3–C≡C–C≡C–F	−309.6[d]		10.58[e]	711.2[f]
CF_3–C≡C–C≡C–CF_3	−868.6	−734	(10.99 ± 0.01)	326
Unsaturated (ene) Series				
CH_2=CH_2	52.5	(52.2 ± 1)	(10.507 ± 0.004)	1066
CH_2=$CHCH_3$	20.2	(20.2 ± 0.4)	(9.73 ± 0.02)	959
CH_2=$C(CH_3)_2$	−14.8	−(16.9 ± 0.6)	(9.239 ± 0.003)	874
CF_2=CF_2	−654.4	−(659 ± 3)	(10.12 ± 0.02)	316
CF_2=$CFCF_3$	−1125.9	−1125	(10.60 ± 0.03)	−102
CF_2=$C(CF_3)_2$	−1610.0			
Ketene Series				
CH_2=C=O	−47.8	−(47.7 ± 0.7)	(9.61 ± 0.02)	879.6
$(CH_3)_2$C=C=O	−115.1	−(134 ± 4)	8.45	681
CF_2=C=O	−401.2		≈11[g]	660.1[f]
$(CF_3)_2$C=C=O	−1356.9	−1427[c]	10.67	−398
Ketone Series				
CH_2=O	−116.3	−(108.7 ± 0.7)	(10.874 ± 0.002)	940.5
$(CH_3)_2$C=O	−216.3	−(217.2 ± 0.4)	9.705	719.2
CF_2=O	−644.3	−640	13.03	617
$(CF_3)_2$C=O	−1458.1	−1397	11.44	−293
Allene Series				
CH_2=C=CH_2	194.7	(190.6 ± 1)	(9.69 ± 0.01)	1126
CF_2=C=CH_2	−158.7	−202	(9.79 ± 0.03)	743
CF_2=C=CF_2	−512.1	−594	10.88	456

[a]Ref. [9-11], [b]Ref. [1], [c]Estimated by Ref. [1], [d]Estimated, see text, [e]Ref. [14], [f]Estimated Δ_fH^0[Ion] from Benson's Δ_fH^0[Neutral], [g]Estimated IE_a[CF_2=C=O],see text, [h]Ref. [15].

group. To clearly illustrate this trend, the relevant thermochemical data [1, 9-11, 14, 15] have been collected and are presented in Table 3.5 (where $\Delta_f H^0[C_t-(F)] = 10.5$ kJ•mol^{-1} is estimated from $\Delta_f H^0[FC{\equiv}CF]$). Contained within Table 3.5, there are subtly different effects of fluorination that require the definition of the following three separate cases known as (I) the "perfluoro" effect [2, 3, 15-17], (II) the "perfluorination" effect [15-17], and (III) the "negative-perfluorination" effect [16-17].

The first case, known as (I) the "perfluoro" effect results in (as stated earlier) the selective stabilization of the σ-orbitals over that of the π-orbitals. The type of molecules in which this occurs are those which possess some degree of symmetry, (e.g., linear, planar, aromatic, etc) so that their σ and π- molecular orbitals are separable.

The second case, known as (II) the "perfluorination" effect, results in the stabilization of all molecular orbitals and is due to the presence of CF_3 groups. This effect is very non-specific as it occurs in many types of molecules that possess both a high or low degree of symmetry (i.e., the σ and π character is. mixed, non-separable).

The third case, known as (III) the "negative-perfluorination" effect is anomalous and results in the lowering of the IE_a's of perfluoro species relative to the hydrogen analogues. Its occurrence is rare and not well understood. It is thought [16 ,17] to be a result of the repulsions of "through-bond" and "through-space" interactions (i.e. space-charge effects of the electron densities with the bonds) which destabilize the fluorinated species relative to that of the hydrogen species. On inspection of Table 3.5, one may see this effect in play on comparision of the IE_a's of the $HC{\equiv}CH/FC{\equiv}CF$, $HC{\equiv}C-C{\equiv}CH/\ FC{\equiv}C-C{\equiv}CF$, and $CH_2{=}CH_2/CF_2{=}CF_2$ pairs. An additional factor that qualitatively help to explain the phenomenon, and which should be considered, is the possible accessibility of the carbene

species (e.g., $CF_2{=}C{:}$, $CF_2{=}C{=}C{=}C{:}$, and $CF_3\bar{C}F$) in the cation manifold. If the carbene cation species are accessible and possess a common transition state structure of comparable symmetry, then a non-crossing situation may occur. An avoided-crossing could then take place which would push down the potential energy surface of the classical ($FC{\equiv}CF^{+\bullet}$, $FC{\equiv}C{-}C{\equiv}CF^{+\bullet}$, $CF_2{=}CF_2^{+\bullet}$) isomer and push up the potential energy surface of the carbene ($CF_2{=}C^{+\bullet}$, $CF_2{=}C{=}C{=}C^{+\bullet}$, $CF_3CF^{+\bullet}$) isomer. This would result in reduction in IE_a of the former (classical) series, whereas the latter (carbene) series would experience a corresponding rise in IE_a. In any event, the occurrence of this effect is difficult to predict and is the exception to the rule for the behavior of perfluorinated organics and will not discussed further.

There are six series of molecules presented in Table 3.5 as follows, $RC{\equiv}CR$, $RC{\equiv}C{-}C{\equiv}CR$, $CR_2{=}CR_2$, $CR_2{=}C{=}O$, $CR_2{=}O$, and $CR_2{=}C{=}CR_2$ and as known as the ethyne, diethyne, unsaturated (ene), ketene, ketone, and allene series respectively.

On inspection of the first three series (which do not contain O), one may note the following trends. For the hydrogen compounds, as each methyl group is added (CH_3 being electron-donating) there is a systematic *decrease* in IE_a. In contrast, for the fluorine compounds, as each perfluoromethyl group is added there is a systematic *increase* in the IE_a values. These opposing trends may be qualitatively explained if the charge and radical-site can be thought of to be primarily associated with the (unsaturated) π-system. Then the electron-donating character of the CH_3 group would increase the ease of ionization for the hydrogen species, whereas the electron-withdrawing character of the CF_3 would have the opposite effect. The effect of the CF_3 group relative to the F group on an IE_a may be more powerfully illustrated on examination of the C_4F_6 species. The $CF_3{-}C{\equiv}C{-}CF_3$ isomer

possesses a higher symmetry than the (cis) CF_2=CF–CF=CF_2 isomer [18]. For the hydrogen species, CH_3–C≡C–CH_3, CH_2=CH–CH=CH_2 with IE_a values of 9.56 and 9.06 eV [1, 18], and the fluorine species CF_3–C≡C–CF_3, CF_2=CF–CF=CF_2 with IE_a values of 12.35 and 9.5 eV [15, 18], respectively, one can see the perfluorination effect and the perfluoro effect increasing the IE_a's by 2.79 and 0.44 eV, correspondingly.

However, the presence of O in the molecule appears to alter this above rationale somewhat (due to the strong electronegativity of O). On inspection of the ketene (CR_2=C=O) and ketone (CR_2=O) series one may note that in both the hydrogen and fluorine analogues the IE_a of the non-(per)methylated species is higher the (per)methylated species. This implies the nature of the balance between the electron-donating and electron-withdrawing moieties of those oxygen containing species is somewhat more complex. A study on the stability of series of haloacetyl cations XCH_2CO^+ (X=Cl, Br, I) relative to CH_3CO^+ by Holmes et al., [19] measured the cationic Δ_fH^0 values. It was noted that the Δ_fH^0 values of the XCH_2CO^+ ions were considerably above that of CH_3CO^+, resulting from their higher $IE_a[XCH_2CO^{\bullet}]$ values. This was rationalized through the proposal that the halogen, not being located at the charge site, reduced the electron-donating character of the methyl group, thus raising the IE_a values. With this observation in mind, the following rationale for the trend in IE_a values of CR_2=O and CR_2=C=O species is proposed as follows. The CR_2=O molecule may be thought of as consisting of two moieties, namely CR_2 and O, the latter being the more electronegative (electron-withdrawing). Similar, the CR_2=C=O molecule may be thought of as consisting of two moieties namely, CR_2 and CO, the latter being more electronegative (electron-withdrawing). Therefore, the CR_2 moieties are always electron-donating, relatively speaking (i.e. the $(CH_3)_2C$ moiety is more electron-donating than the CH_2

moiety; and the $(CF_3)_2C$ moiety is more electron-donating than the CF_2 moiety). This implies that the charge site remains mainly associated with the unsaturated C=O and C=C=O groups, whereas the radical sites remain mainly associated with the saturated (per)methyl groups.

The $IE_a[CF_2=C=O]$ is estimated [20] and deserves comment. If on consideration of the allene series, the analogous species $CH_2=C=CH_2$ (IE_a = 9.69 eV) [1], and $CF_2=C=CF_2$ (IE_a = 10.88 eV) [1], can be used with $CH_2=C=O$ (IE_a = 9.61 eV) [1], a value of $IE_a[CF_2=C=O] \approx 11$eV [20] is obtained. This value, although approximate, is only slightly above the experimental value of IE $[(CF_3)_2C=C=O]$ = 10.67 eV [1]. Such a small difference in IE_a values may be put into perspective on consideration of the IE_a values for OH_2, CH_3OH and their perfluoroanalogues. The values are as follows, IE_a $[OH_2]$ = 12.61 eV [1], IE_a $[CH_3OH]$= 10.85 eV [1], IE_a $[OF_2]$ = 13.11 eV [1], IE_a $[CF_3OF]$ = 13.0 eV [1], resulting in the "perfluoro" effect and the "perfluorination" effect raising the IE_a's by 0.50 and 2.15 eV, respectively. As well, the stabilization within the hydrogen series on methylation (10.85 eV–12.61 eV = –1.76 eV) is appreciably higher (i.e. ≈ x 16 greater) than that present in the fluorine series on perfluoromethylation (13.0 eV–12.11 eV ≈ –0.11 eV). Thus, the estimated IE_a $[CF_2=C=O]$ appears to be of reasonable magnitude and serves to underscore the profoundly different physical characteristics of perfluorinated organics in relation to their hydrogen analogues.

The order of stability of the perfluorobutyl and perfluoropropyl iodides and radicals deserves further clarification. The central issue may be conveniently discussed in terms of substituent effects (i.e., a H group replaced by a CH_3, F, CF_3, etc.. group). However. the difference between a CH_3 and/or CF_3 moiety as a substituent group within a larger molecule

and $CH_3^\bullet$ and/or $CF_3^\bullet$ as an isolated species should be discussed. The IE_a values for the $CH_3^\bullet$ and $CF_3^\bullet$ species are (9.84 ± 0.01) eV [1] and 8.9 eV [1] (i.e, agreement with the recent value of (8.8 ± 0.1) eV of Tuckett. et. al. [4]), respectively. The reason for the (isolated species) IE_a value of 8.9 eV for the $CF_3^\bullet$ radical being (unexpectedly) *lower* than that of the corresponding hydrogen analogue is that the overall effect on the change in IE_a value on the substitution of F groups is the resultant of two opposing factors. The first factor is the high *inductive effect* of the F atoms which tends to *increase* the IE_a. The second factor is the *resonant effect* of ionic stabilization which tends to *decrease* the IE_a. Price et. al., [21,22] have discussed these two opposing effects and has stated that they have magnitudes of several eV and the resultant effect is difficult to predict with certainty. Nonetheless, it is clear that the resonant effect [21,22] is dominant over that of the inductive effect in determining the lower IE_a value of the $CF_3^\bullet$ species.

However, when the CF_3 moiety is present as a substituent within a larger molecule its behaviour is markedly different. As discussed, the overall effect of a CF_3 substituent group is that of a powerful inductive (*electron-withdrawing*) group which results in an *increase* in the IE_a value. This trend may discussed in a quantitative manner in terms of the Hammett equation of physical organic chemistry and will be discussed below.

The Hammett equation [23,24] arose from the observations in the 1930's that the substituent effects of reactions involving benzene derivatives may be correlated to the acid strengths of the respective benzoic acids. A general relation, known as the Hammett equation, was introduced to relate the nature of the substituent in the meta (m-) and para (p-) position and the reactivity of the benzene derivative and is as follows [23,24],

$$\ln\left(\frac{K_R}{K_H}\right) = \rho\sigma = \frac{(-\Delta(\Delta G^0))}{RT}$$

where K_R , K_H, ρ, σ, R, T, and $\Delta(\Delta G°)$ denote the rate constant for the substituted species, the rate constant for the unsubstituted species, the reaction parameter (a negative slope), the Hammett parameter of the substituent, the ideal gas constant, the Kelvin temperature, and the difference between the Gibbs free energy of reaction of the substituted species from that of the unsubstituted species, respectively.

The Hammett parameter, σ, [23, 24] is a unitless quantity that relates to the ratio K_R/K_H. If the substituted species undergoes ionization (in solution) at a slower rate than the unsubstituted species (i.e., $K_R/K_H < 0$) then $\sigma > 0$ (i.e., as $\rho < 0$). As well, if the opposite is true (i.e., $K_R/K_H > 0$) then the Hammett parameter has a value of $\sigma < 0$ (relative to the substituted hydrogen compound $\sigma = 0.00$).

The determining factor that governs the increase or decrease in the rate of ionization is the overall balance of the ability of the substituent to *inductively withdraw and resonantly stabilize positive charge* [23, 24]. If the substituent possesses a *lower* overall ability to "stabilize" positive charge (i.e., "electron-withdrawing") than that of hydrogen, then $\sigma > 0$, and the rate of ionization is *slower*. However, if the opposite is true and the substituent possesses a *greater* overall ability to "stabilize" positive charge (i.e., "electron donating") relative to hydrogen, the $\sigma < 0$, and the rate of ionization would *increase*.

Additionally, on consideration of the gas-phase, since $\Delta(\Delta G°)$ varies directly with IE, a plot of the negative of the IE value of a series of derivatized compounds versus their substituent σ values should yield a straight-line Hammett plot with a (negative) slope of ρ,

the reation parameter. This linear relationship was explored and confirmed in the gas-phase in a study by Harrison, Kebarle, and Lossing [25] of substituted benzyl radical-cations.

In the 1950's Taft et al. [26, 27] proposed that the overall Hammett parameter, σ, should be quantitatively separated into an inductive contribution, σ_I, and a resonance contribution, σ_R, defined below as follows;

$$\sigma = \sigma_I + \sigma_R$$

The inductive contribution, σ_I, may be considered as a measure of the $\Delta(\Delta G°)$ effect of the substituent (relative to the H atom) resulting from its power to attract or repel electrons through space and the σ-bonds [26,27]. The resonance contribution, σ_R, may be considered as a measure of the $\Delta(\Delta G°)$ effect resulting from the power of the substituent to attract or repel electrons through resonance interaction with the π-orbitals [26, 27]. For substituents of interest, they possess the following values as follows for the σ_I (inductive), σ_R (resonant), and overall σ, of – 0.05, – 0.13, – 0.18, for CH_3; 0.52, – 0.44, 0.08, for F; and 0.41, 0.09, 0.50, for CF_3 moities, respectively [26, 27]. Thus, on inspection of the above values one may see that CH_3, F, and CF_3 are overall electron-donating ($\sigma = -0.18$), near-zero electron-withdrawing ($\sigma = 0.08$), and strongly electron-withdrawing ($\sigma = 0.50$) substituents, respectively. Thus, one may generally expect a quantitative decrease in IE, a moderate increase in IE, and a strong increase in IE, with a substitution of each CH_3, F, and CF_3 respectively as will be discussed below.

A summary of the effects on the IE_a for CR_3 substitution and insertion of a CR_2 moiety into the chain is illustrated in Table 3.6 for the parent C_nR_mI and fragment $C_nR_m^{\bullet}$

Table 3.6 Adiabatic Ionization Energies of the Parent C_nH_mI / C_nF_mI and the Fragment Radical $C_nH_m^\bullet$ / $C_nF_m^\bullet$ Species

Hydrogen Series			Fluorine Series		
	Adiabatic Ionization Energy			Adiabatic Ionization Energy	
Species	IE_a(eV)[a]	ΔIE_a(eV)	Species	IE_a(eV)[a]	ΔIE_a(eV)
CH_3I	9.538		CF_3I	10.23	
CH_3CH_2I	9.346	–0.192	CF_3CF_2I		
$CH_3CH_2CH_2I$	9.269	–0.077	$CF_3CF_2CF_2I$	10.36[b]	
$CH_3CH_2CH_2CH_2I$	9.229	–0.050	$CF_3CF_2CF_2CF_2I$		
CH_3I	9.538		CF_3I	10.23	
CH_3CH_2I	9.346	–0.192	CF_3CF_2I		
$(CH_3)_2CHI$	9.175	–0.171	$(CF_3)_2CFI$		
$(CH_3)_3CI$	9.02	–0.155	$(CF_3)_3CI$		
$CH_3CH_2CH_2I$	9.269		$CF_3CF_2CF_2I$	10.36[b]	
$CH_3CH_2CHICH_3$	9.09	–0.179	$CF_3CF_2CFICF_3$		
$(CH_3)_2CHCH_2I$	9.202	–0.067[c]	$(CF_3)_2CFCF_2I$		
$CH_3^\bullet$	9.84		$CF_3^\bullet$	8.9	
$CH_3CH_2^\bullet$	8.13	–1.71	$CF_3CF_2^\bullet$	9.47[c]	0.57
$CH_3CH_2CH_2^\bullet$	8.09	–0.04	$CF_3CF_2CF_2^\bullet$	9.55[d]	0.08
$CH_3CH_2CH_2CH_2^\bullet$	8.02	–0.07	$CF_3CF_2CF_2CF_2^\bullet$	9.63[c]	0.08
$CH_3^\bullet$	9.84		$CF_3^\bullet$	8.9	
$CH_3CH_2^\bullet$	8.13	–1.71	$CF_3CF_2^\bullet$	9.47[c]	0.57
$(CH_3)_2CH^\bullet$	8.09	–0.77	$(CF_3)_2CF^\bullet$	9.97[c]	0.50
$(CH_3)_3C^\bullet$	8.02	–0.66	$(CF_3)_3C^\bullet$	10.47[c]	0.50
$CH_3CH_2CH_2^\bullet$	8.09		$CF_3CF_2CF_2^\bullet$	9.55[d]	
$CH_3CH_2C^\bullet HCH_3$	7.25	–0.84	$CF_3CF_2C^\bullet FCF_3$	10.05[c]	0.50
$(CH_3)_2CHCH_2^\bullet$	7.93	–0.16[f]	$(CF_3)_2CFCF_2^\bullet$		

[a]Ref. [1], [b]Ref. [28], [c]Estimated, see text, [d]Estimated from Ref. [4], [e]Relative to $CH_3CH_2CH_2I$, [f]Relative to $CH_3CH_2CH_2^\bullet$.

species. On inspection of this table which lists the ΔIE_a, the change in IE_a between each member of the series, the following trends become evident. Firstly, on consideration of the known C_nH_mI, and $C_nH_m^\bullet$ species, the substitution of CH_3 around the central C-I moiety and the $C^\bullet$ radical site generally changes the IE_a by increments of $\approx$ -0.2 eV, and $\approx$ -0.6 eV, respectively. As well for the insertion of CH_2 moiety to lengthen the straight chain of C_nH_mI and $C_nH_m^\bullet$ generally changes the IE_a values in increments of $\approx$ -0.06 eV, and –0.06 eV, respectively. Finally, for substitution of a CH_3 group at the first carbon (the α-position) and then at the second carbon (the β-position), it is observed that the effect of lowering the IE_a value is much stronger for the former process than the latter for both the C_nH_mI and $C_nH_m^\bullet$ species.

Now on turning to C_nF_mI and $C_nF_m^\bullet$ species, presented in the right-hand side of Table 3.6, one may see that there are only a few known IE_a values. The experimentally measured values for the C_nF_mI species are $IE_a[CF_3I] = 10.23$ eV of Lias et. al. [1], and $IE_a[CF_3CF_2CF_2I] = (10.36 \pm 0.01)$ eV of Watanabe et. al. [28]. Therefore, through the utilization of the Benson value of $\Delta_fH^0[CF_3CF_2CF_2I] = -1414.2$ kJ•mol^{-1} one may obtain for the cation a value of $\Delta_fH^0[CF_3CF_2CF_2I^{+\bullet}] = -414.6$ kJ•mol^{-1}. Thus the implied trend for the straight-chain C_nF_mI series is that of a small increase of IE with chain length (i.e., the reverse of the straight-chain C_nH_mI series.

In regards to the fragment radical $C_nF_m^\bullet$ series the following trends may be explored. For $CF_3^\bullet$ a value for IE_a of 8.9 eV [1] is known. Through the utilization of the Benson value of $\Delta_fH^0[CF_3CF_2CF_2^\bullet] = -1281.2$ kJ•mol^{-1} and the recent experimental value of $\Delta_fH^0[CF_3CF_2CF_2^+] = -(360 \pm 20)$ kJ•mol^{-1} of Tuckett et.al. [4], a value of $IE_a[CF_3CF_2CF_2^\bullet]$

= 9.55 eV may be calculated. However, in the case of $CF_3CF_2^+$ there is considerable uncertainty concerning the Δ_fH^0 value of the cation [1]. Of the several $\Delta_fH^0[CF_3CF_2^+]$ values listed (see p. 79 of ref. [1]) in Lias et.al. [1], for the interest of consistency the value of $\Delta_fH^0[CF_3CF_2^+] = 20.9$ kJ•mol^{-1}, derived from its appearance energy, AE, from CF_3CF_2I will be considered here. Using $\Delta_fH^0[CF_3CF_2^\bullet] = -(893 \pm 4)$ kJ•mol^{-1} [1], one may calculate a value of $IE_a[CF_3CF_2^\bullet] = 9.47$ eV. Thus, again a behaviour opposite to that of the $C_nH_m^\bullet$ case is illustrated here. The first substitution of CF_3 results in a *large increase* in the IE_a of 0.57 eV (i.e., 9.47 eV – 8.9 eV = 0.57 eV) at the radical-site, whereas there is a *smaller increase* in IE_a of 0.08 eV (i.e., 9.55 eV – 9.47 eV = 0.08 eV) for an insertion of CF_2 into the straight-chain radical.

For comparison, a study by Lossing et.al. [29] measured the *vertical* ionization values of several perfluorinated radicals of interest. The compounds of relevance were $(CF_3CF_2)_2N_2$, $(CF_3CF_2CF_2)_2N_2$, $((CF_3)_2CF)_2Hg$, and $((CF_3)_3C)_2Hg$ and were to serve as sources, on pyrolytic heating, for the $CF_3CF_2^\bullet$, $CF_3CF_2CF_2^\bullet$, $(CF_3)_2CF^\bullet$, and $(CF_3)_3C^\bullet$ radicals, respectively. The $CF_3CF_2^\bullet$ radical served (on increased heating) as a source of the $CF_3^\bullet$ radical. Of this group, the *vertical* ionization energy values of $IE_v[CF_3^\bullet] \approx 9.5$ eV, $IE_v[CF_3CF_2^\bullet] = 9.98$ eV, $IE_v[CF_3CF_2CF_2^\bullet] = 10.06$ eV, and $IE_v[(CF_3)_2CF^\bullet] = 10.50$ eV were sucessfully determined, however the value of the $(CF_3)_3C^\bullet$ species was *not*. It was proposed that the $((CF_3)_3C)_2Hg$ compound appeared to dissociate by a mechanism other than a simple C–Hg bond scission [29]. Thus, one may see that of the substitution of an F for a CF_3 group at the charge-site (the α–position) has a much stronger effect to raise the IE_v than does its subtitution one carbon away (the β–position) from the charge-site [29](i.e., $IE_v[(CF_3)_2CF^\bullet]$ –

$IE_v[CF_3CF_2^\bullet] = 0.52$ eV compared to $IE_v[CF_3CF_2CF_2^\bullet] - IE_v[CF_3CF_2^\bullet] = 0.08$ eV, a factor of 6.5x).

Additionally, on inspection of Table 3.5 of the FC≡CF, CF_3–C≡C–CF_3; FC≡C–C≡CF, CF_3–C≡C–C≡CF, CF_3–C≡C–C≡C–CF_3; and CF_2=CF_2, CF_2=$CFCF_3$ series one may note an increase in the IE_a values of ≈ 0.50 eV with the substitution of each CF_3 group. Thus, on consideration of the study of Lossing et. al. [29] and the patterns illustrated in Table 3.5, if one may propose an increase in IE_a value of ≈ 0.50 eV, and ≈ 0.08 eV for the substitution of a CF_3 group at the radical-site and for an insertion of a CF_2 group into the straight-chain species, then the IE_a values of the $C_nF_m^\bullet$ series may be estimated and are listed in Table 3.6

As pointed out by Lossing et. al. [29] and Majer [30], the stabilty of $CF_3CF_2CF_2^+$ relative to $(CF_3)_2CF^+$ merits further discussion. The observed [29] *reverse* order of the *vertical* ionization energies ofthe $C_nF_m^\bullet$ species is of importance in accounting for the observed differences in peak abundances in the normal mass spectra of alkanes and perfluoroalkanes [29, 30]. Majer [30] has pointed out that for perfluoroalkanes, the abundance of the $C_3F_7^+$ cations is *greater* in molecules containing $CF_3CF_2CF_2$ groups than in molecules that contain only $(CF_3)_2CF$ groups. This implies that the observed $C_3F_7^+$ cation is mainly the $CF_3CF_2CF_2^+$ isomer [30], and is consistent with $IE[CF_3CF_2CF_2^+] < IE[(CF_3)_2CF^+]$, [29]. Additionally, in the normal mass spectra of C_5 and C_6 perfluoroparaffins [30], the low abundance of the higher $C_nF_m^+$ cations compared to the CF_3^+ abundance also implies a *increasing* ionization energy along the $C_nF_m^\bullet$ series.

For further consideration, it is noted that the difference between the IE_a(9.55 eV) and IE_v(10.06 eV) values of $CF_3CF_2CF_2^\bullet$ is 0.51 eV. In comparison, the difference between the

IE_a(10.12 eV) and IE_v(10.52 eV) values of CF_2=CF_2 is 0.40 eV. Robin et. al. [31], has shown that the tetrakis(perfluoromethyl) substituted species $(CF_3)_2C$=$C(CF_3)_2$ possessed an IE_v value of 12.61 eV. This again implies an incremental increase in IE of ≈ 0.50 eV per CF_3 group substituted around a *unsaturated* moiety. Thus, the estimated IE_a values for the $C_nF_m^\bullet$ series listed in Table 3.6 are most likely quite reasonable.

However, for the case of the C_nF_mI series it should be remembered that the C–I moiety is considered to be *saturated*. Thus, any increase in IE_a values due to CF_3 substitution are most likely to be smaller than those which would occur in the corresponding radical species. As stated by Lossing et. al., [29] the conversion of a CF_3 moiety into a $C(CF_3)_3$ moiety involves the replacement of three C–F bonds, each capable of resonant stabilization (i.e., $\sigma_R < 0$) with three C–CF_3 bonds which possess very little resonant capability in that respect (i.e., $\sigma_R \approx 0$). Similarly, Taft et.al., [26,27] has stated the very strong inductive effect of the substituent $N(CH_3)_3^+$ moiety, which possessed σ_I, σ_R, and σ values of 0.86, 0.00, and 0.86, respectively. If one may suggest a similar behaviour for the $C(CF_3)_3$ moiety, a value of $IE_a[(CF_3)_3CI] > 10.62$ eV may be estimated (i.e., relative to IE_a[FI] = 10.62 eV) on the substitution of $C(CF_3)_3$ for F in the FI species. Thus, based on the strong electron-withdrawing characteristics of the CF_3 group one should expect the $(CF_3)_3CI^{+\bullet}$ species to possess the highest IE_a value of the C_4F_9I isomers as it should be very difficult to remove an electron from a CI moiety surrounded by three CF_3 groups.

3.2.2 Collision Gas Properites and the Collision Encounter Event

In the previous sub-section, one has discussed how the presence of the F and CF_3 groups influences the characteristics of the projectile-ion $M_1^{+\bullet}$. In this sub-section one will

discuss the interaction between $M_1^{+\bullet}$ and the collision gas G_1. Thus, another point on the accessing of the excited electronic states during the collision encounter between a fast moving projectile-ion in its ground electronic state and the stationary target gas deserves emphasis. During the collision encounter there are two major processes which tend to dominate the majority of the collision events. The first is known as collisional- excitation and the second is neutralization of the projectile-ion. Collisional-excitation of the ground state projectile ion occurs via a non-momentum transfer collision in which a portion of its translational kinetic energy is converted into internal excitation energy, E_{int}. The amount of E_{int} deposited in the projectile-ion determines which dissociation routes and their products may be accessed. The second process, neutralization of the projectile-ion, occurs via charge-exchange between the projectile-ion and the stationary target gas. As well to a lesser extent a third process, known as charge-stripping, resulting in the production of a doubly-charged projectile-ion may also occur.

The two main target gases that are used in this work are He and O_2. He is a small non-polarizable monoatomic gas with an IE_a of 24.587 eV [1]. As such it is seen to have a small collision parameter (diameter of interaction) and results in a "hard-collision" transfering large amounts of E_{int} into the projectile-ion and a high degree of fragmentation. Whereas O_2 is a larger polarizable diatomic molecule with a lower IE_a of 12.071 eV [1]. As such it is seen to have a larger (relative to He) collision parameter (diameter of interaction) and results in a "soft-collision" transferring slightly lower amounts of E_{int} into the projectile-ion. However, it should be remembered that the accessing of the excited electronic states via collisional-excitation (i.e, the degree of fragmentation) is generally considered to be collision gas *independent*. That is to say that generally the same dissociation routes are accessed

regardless of the target gas used. Experimentally this results in the same mass spectral peaks appearing in a CID mass spectrum whether He or O_2 is the target gas. However, the intensity of the peaks in the CID O_2 mass spectrum may be observed to be less than those of the corresponding CID He mass spectrum, but their relative intensities within each mass spectrum are preserved.

The major observed experimental difference between the utilization of He or O_2 as target gas in the production of a CID mass spectrum is the greater ability of O_2 to produce a doubly-charged (ie., charge-stripped) projectile-ion. Although, both He and O_2 target gases may produce a doubly-charged projectile-ion, the greater intensity of this peak when O_2 is used as a target may qualitatively result from the lower IE_a and larger collision interaction parameter (i.e., due to the linear O=O molecule).

As stated previously (see chapter 1), metastably generated fragment ions possess a lower E_{int} than the corresponding source generated ions. Thus, if the peak intensities in the CID mass spectra of a metastably generated and a source generated fragment ion are the same, then the same low energy structure ion has been accessed in the CID mass spectrum. For all the ions presented here in the following two thesis chapters, their CID mass spectra of the metastably and source generated ions are identical and thus represent the same ions. The only exception to this is the $C_2F_4^{+\bullet}$ (m/z 100) ion which possesses the following isomers, $CF_2{=}CF_2^{+\bullet}$, $CF_3CF^{+\bullet}$, and c-F_2(CFC)$F^{+\bullet}$. As will be discussed in the later section on $C_2F_4^{+\bullet}$ the mixing of these radical-cation structures is proposed to be rooted in the behaviour of the neutral manifold. The order of stability of the neutral manifold is as follows, $CF_2{=}CF_2$ > $CF_3\,\ddot{C}\,F$ > c-F_2(CFC)F, with the known values of $\Delta_f H^0[CF_2{=}CF_2] = -659$ kJ•mol^{-1} [1] and $\Delta_f H^0[CF_3\,\ddot{C}\,F] = -587.4$ kJ•mol^{-1} [32].

The cyclic c-F_2(CFC)F (where (CFC) denotes a three-membered ring) species facilitates the conversion between the classical structure and the carbene. This proposed cyclic, c-F_2(CFC)F, species is entirely in agreement with a similarly studied process by Chen et.al. [24], in which a metal-chelate, CF_3–M, underwent a process of CF_2 elimination. The CF_3–M species was converted into a cyclic c-F_2(CFM) structure (where (CFM) denotes a three-membered ring), which subsequently ring opened to produce a F_2C–M–F species. Finally, the C–M bond underwent direct scission, producing the metal fluoride, MF, and the CF_2 neutral was eliminated [24].

Thus, as will be presented in the following $C_2F_4^{+\bullet}$ (m/z 100) ion section, the radical-cation manifold is proposed to consist of a complex mixture of the three isomers which appear to be accessed in a slightly different manner by the He and O_2 target gases.

3.2.3 The Thermochemistry of FI and its Effect on Rearrangements

In this sub-section one will discuss the thermochemistry of fluorine iodide, FI, in relation to the opening of possible rearrangement routes which may be present in the perfluoroalkyl iodides, whilst inactive in the respective hydrogen analogues. Firstly, one should remember that the ionization energy (IE) of hydrogen and fluorine compounds typically cover a range of IE ≈ 8–10 eV, and IE ≈ 10–12 eV respectively [1]. Next, the heat of formation Δ_fH^0 (kJ•mol^{-1}) and the adiabatic ionization energy IE_a of $I^{\bullet}$, HI, and FI are 106.8 kJ•mol^{-1}, 26.4 kJ•mol^{-1}, –94.8 kJ•mol^{-1} and 10.45 eV, 10.39 eV, 10.62 eV, respectively [1]. Thus, a lowering of the Δ_fH^0 value upon fluorination (i.e., stabilization) is accompanyed by a very little increase in IE.

While keeping in mind the above information, the fragmentation of $M_1^{+\bullet} \rightarrow M_2^+ + M_3^\bullet$ is governed by the positive charge being carried by the $M_2^\bullet$ fragment having a lower IE than $M_3^\bullet$ (i.e., $IE_a[M_2^\bullet] < IE_a[M_3^\bullet]$). However, if they are close in value (i.e., $IE_a[M_2^\bullet] \approx IE_a[M_3^\bullet]$) then the sum of the heats of formation of the products are close in value, i.e,

$$(\Delta_f H^0[M_2^+] + \Delta_f H^0[M_3^\bullet]) \approx (\Delta_f H^0\,[M_2^\bullet] + \Delta_f H^0[M_3^+])$$

a competition of (metastable) dissociation pathways can be allowed. Thus, for hydrocarbon radicals, due to their IE_a's ≈ 8–10 eV, being below that of $IE_a[I^\bullet] = 10.45$ eV and $IE_a[HI] = 10.39$ eV, and with an $\Delta_f H^0[HI] = 26.4$ kJ•mol^{-1} [1], there is only one main dissociation route favoured as follows,

$R{-}I^{+\bullet} \rightarrow R^+ + I^\bullet$ **($I^\bullet$ loss)**, (R = alkyl)

with a direct C–I bond cleavage and the production of an unrearranged alkyl carbocation R^+.

However in contrast, fluorocarbon radicals with their higher IE_a's ≈ 9–11 eV open up the possibility, due to $\Delta_f H^0[FI] = -94.8$ kJ•mol^{-1} and $IE_a[FI] = 10.62$ eV, [1] of competing reactions and rearrangement FI loss, as follows,

$R{-}I^{+\bullet} \rightarrow R^+ + I^\bullet$ **($I^\bullet$ loss)**

$R{-}I^{+\bullet} \rightarrow I^+ + R^\bullet$ **($R^\bullet$ loss)**

$R{-}I^{+\bullet} \rightarrow (R'{-}F)^+ + FI$ **(Rearrangement with FI loss)**

$R{-}I^{+\bullet} \rightarrow FI^{+\bullet} + (R'{-}F)$ **(Rearrangement with (R'–F) loss)**

where R = perfluoroalkyl. Thus, instead of a simple $I^{\bullet}$ loss and the production of an unrearranged alkyl cation R^{+}, manifested as a single R^{+} peak in the metastable ion (MI) mass spectra of the hydrogen analogues; the metastable ion (MI) mass spectra of the perfluoro species may possess these four peaks, corresponding to the above actively competing processes.

The above thermochemistry of the perfluoro compounds results in the repeated appearance of the two following moieties in their mass spectra. The first species of importance is the perfluoroallylic moiety, $(CF_2)_2C^{+}–X$, shown below,

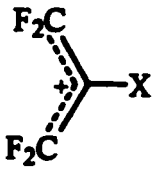

; X = I, CF_3, F

This results in the important perfluoroallyic cations $(CF_2)_2C^{+}–I$, $(CF_2)_2C^{+}–CF_3$, and $(CF_2)_2C^{+}–F$, with masses of m/z 239, 181, and 131, respectively. The second species of importance is the distonic "pseudo" perfluorotrimethylene moiety, $^{+}CF_2–(CFX)–^{\bullet}CF_2$, shown below,

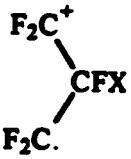

; X = I, CF_3, F

This results in the important "pseudo" perfluorotrimethylene distonic cations $^{+}CF_2–(CFI)–^{\bullet}CF_2$, $^{+}CF_2–(CFCF_3)–^{\bullet}CF_2$, and $^{+}CF_2–(CF_2)–^{\bullet}CF_2$, with masses of m/z 258, 200, and 150, respectively.

At this point one final source of information to aid in the rationalization of the gas-phase ion-chemistry deserves emphasis. It is the kinetic energy release (KER) measurement,

$T_{0.5}$, associated with the fragmentation of metastable ions (see Chapter 1). In every metastable dissociation some fraction of the internal energy of the fragment ion will be partitioned into translational degrees of freedom of the products. Generally, a simple bond cleavage involves very low excess internal energy and this manifests itself in a very narrow peak width a small $T_{0.5}$ value (e.g., ≈ 5 meV or less). When a rearrangement occurs, a larger amount of internal energy E_{int} will be required and a wider peak width and a larger $T_{0.5}$ value will result. Small rearrangements (i.e, the transfer of a small radical or atom) generally have $T_{0.5}$ values of ≈ 10–100 meV, whereas complex rearrangements (i.e., the transfer of large groups) generally have $T_{0.5}$ values of ≈ 100–500 meV.

For perfluoro compounds the general range of $T_{0.5}$ values are proposed to be as follows; (a) simple bond cleavages, ≈ 10 meV, (b) small rearrangements with $F^{\bullet}$ migration, ≈ 20 meV, (c) ring closures with $CF_3^{\bullet}$ loss, ≈ 30 meV, (d) $CF_3^{\bullet}$ migrations with CF_4 loss, ≈ 100–200 meV, and (e) $F^{\bullet}$ migrations about $F_2C{=}C{=}O^{+\bullet}$ resulting in $CF_3^+ + C{\equiv}O$ dissociation products, ≈ 400– 600 meV. As well, peak shape is a good qualitative aid to the elucidation of gas-phase ion-chemistry dissociations. Generally, a small (single component) Gaussian peak shape is an indication of a single species and/or transition state being accessed prior to dissociation. Whereas, a composite (e.g., two component) peak shape is an indication of several (e.g., two) species and/or transition states being accessed prior to dissociation. Such is the case in the dissociation of $C_2F_3O^+ \rightarrow CF_3^+ + C{\equiv}O$ resulting from $C_3F_6O^{+\bullet}$ isomers to be discussed later in the chapter. Finally, using the above rationale for the analysis of the gas-phase ion-chemistry of perfluoro compounds, some qualitative generalizations and first, for the perfluoroalkyl iodides C_4F_9I and C_3F_7I, then secondly the unsaturated perfluorocarbons

CF_3–C≡C–CF_3 and CF_2=CFCF_3, and finally on the perfluoro oxide C_3F_6O isomers and their relevant products will be discussed in this chapter.

The author wishes to express the hope that these observations will help encourage new work on perfluoro compounds by others, namely in the experimental (calorimetric) determination of the neutral heats of formation, $\Delta_f H^0[M_1]$, and the experimental (e.g., photoelectron spectra) determination of the (adiabatic and vertical) ionization energies, IE, which have been neglected in the past. They will be important quantitative aids in the systematic elucidation of the gas-phase ion-chemistry of this important class of perfluorinated organic compounds.

3.3 Perfluorobutyl Iodides C_4F_9I

There are four C_4F_9I isomers, namely, $CF_3CF_2CF_2CF_2I$, $CF_3CF_2CFICF_3$, $(CF_3)_2CFCF_2I$, and $(CF_3)_3CI$, named 1-iodoperfluorobutane (n-C_4F_9I), 2-iodoperfluorobutane (s-C_4F_9I), perfluoro-2-(iodomethyl)propane (i-C_4F_9I), and perfluoro-2-iodo-2-methyl-propane (t-C_4F_9I), respectively. On inspection of their structure, one can immediately view the $CF_3CF_2CF_2CF_2I$ and $CF_3CF_2CFICF_3$ isomers as being composed of two basic component groups, namely, $CF_2{=}CFCF_2CF_3$ and FI. Furthermore, the $(CF_3)_2CFCF_2I$ and $(CF_3)_3CI$ isomers may be seen to be composed of the two basic component groups $CF_2{=}C(CF_3)_2$ and FI. Thus, qualitatively the dissociation characteristics of these two sets of C_4F_9I isomers may be dictated by the interplay of the thermochemistry of the $CF_2{=}CFCF_2CF_3$ + FI and $CF_2{=}C(CF_3)_2$ + FI pairs. All the relevant Δ_fH^0 ($kJ{\bullet}mol^{-1}$) values of the neutral C_4F_9I species have been tabulated in Table 3.3.

We will now discuss the gas-phase ion-chemistry of the cationic manifold of the $C_4F_9I^{+\bullet}$ (m/z 346) isomers. The relevant cations that will be discussed are the following; the parent ,$C_4F_9I^{+\bullet}$ m/z 346, radical-cation and the fragment ions $C_3F_5I^{+\bullet}$, $C_3F_4I^+$, and $C_4F_8^{+\bullet}$ with m/z 258, 239, and 200, respectively. The other important perfluorobutyl cation, $C_4F_9^+$ m/z 219, fragment will be more closely examined in the next section.

$C_4F_9I^{+\bullet}$ (m/z 346)

Figure 3.1, illustrates the proposed energy levels of the $C_4F_9I^{+\bullet}$ (m/z 346) isomers with the known Δ_fH^0 ($kJ\bullet mol^{-1}$) of the dissociation products indicated in the brackets. The order of stability of the $C_4F_9I^{+\bullet}$ isomers illustrated there is based on the rationale that the frontier orbitals are dominated by the non-bonding (p_x , p_y) "pseudo-π" iodine orbitals, as per the hydrogen analogues. This follows the proposed (saturated) perfluoro order of ion stability (tertiary > secondary > primary), thus one has, $(CF_3)_3CI^{+\bullet} > (CF_3)_2CFCF_2I^{+\bullet} > CF_3CF_2CFICF_3^{+\bullet} > CF_3CF_2CF_2CF_2I^{+\bullet}$ (as per the effects of the σ-symmetry and σ,π-symmetry electron-withdrawing characteristics of F and CF_3, respectively, outlined in Section 3.2). Table 3.7 and Figure 3.2 illustrate the peak heights and the normal mass spectra of the (a) $CF_3CF_2CF_2CF_2I$ (n-C_4F_9I), (b) $CF_3CF_2CFICF_3$ (s-C_4F_9I), and (c) $(CF_3)_3CI$ (t-C_4F_9I); $C_4F_9I^{+\bullet}$ isomers, respectively. Table 3.8 presents the kinetic energy release, $T_{0.5}$ (meV), data for the metastable $C_4F_9I^{+\bullet}$ isomers. As well, Table 3.9, Figures 3.3 and 3.4, illustrate the peak heights, metastable ion (MI), and collision induced dissociation (CID) mass spectra of the (a) $CF_3CF_2CF_2CF_2I$ (n-C_4F_9I), (b) $CF_3CF_2CFICF_3$ (s-C_4F_9I), and (c) $(CF_3)_3CI$ (t-C_4F_9I); $C_4F_9I^{+\bullet}$ isomers, respectively.

On inspection of the peak heights of Table 3.7 and the normal mass spectra of Figure 3.2, the following qualitative observations can be made. First, all of the C_4F_9I isomers possess a molecular radical-cation $C_4F_9I^{+\bullet}$ m/z 346 of strong intensity, with peak abundances of 72.4, 100.0 , and 93.0 % for n-$C_4F_9I^{+\bullet}$, s-$C_4F_9I^{+\bullet}$, and t-$C_4F_9I^{+\bullet}$, respectively. Next, one can see that the base peak (100 %) is $C_4F_9^+$ m/z 219, $C_4F_9I^{+\bullet}$ m/z 346, and CF_3^+ m/z 69, for n-$C_4F_9I^{+\bullet}$, s-$C_4F_9I^{+\bullet}$, and t-$C_4F_9I^{+\bullet}$, respectively. As well, there is a concomitant decrease in the production of $C_4F_9^+$ m/z 219, via $I^\bullet$ loss (i.e., 100.0 %, 1.3 %, very weak) and an increase

Figure 3.1 Proposed Energy Levels of the $C_4F_9I^{+\bullet}$ (m/z 346) Isomers

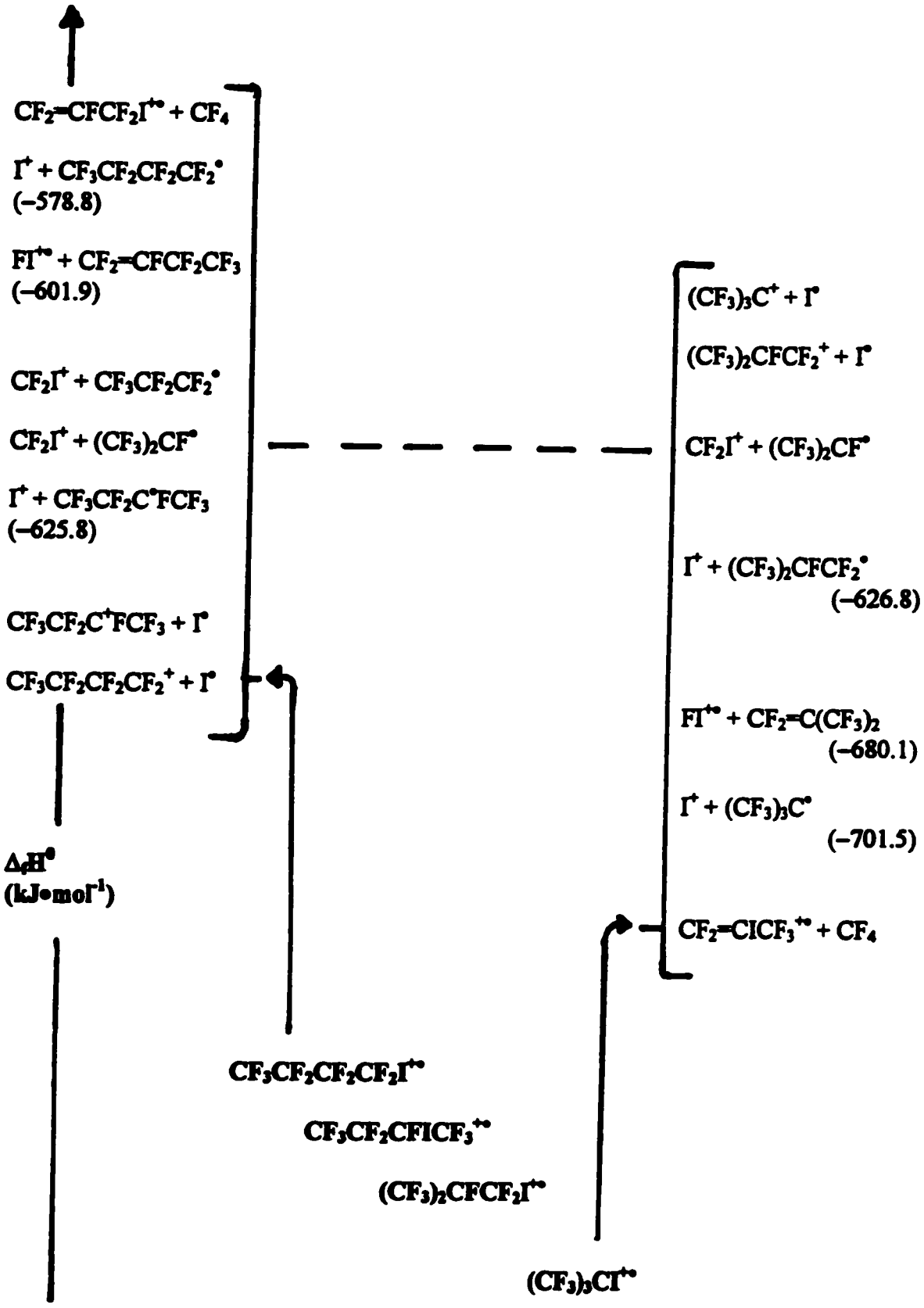

Table 3.7 Normal Mass Spectra of the C_4F_9I Isomers

Species	Mass (m/z)	Neutral Loss	Parent Ion n-C_4F_9I Height (%)	Parent Ion s-C_4F_9I Height (%)	Parent Ion t-C_4F_9I Height (%)
$C_4F_9I^{+\bullet}$	346		72.4	100.0	93.0
$C_4F_8I^+$	327	($-F^\bullet$)	5.5	0.7	7.3
$C_3F_6I^+$	277	($-CF_3^\bullet$)	<0.3	1.3	<0.3
$C_3F_5I^{+\bullet}$	258	($-CF_4$)	0.7	7.4	5.6
$C_2F_5I^{+\bullet}$	246	($-C_2F_4$)	<0.3	5.0	1.3
$C_3F_4I^+$	239		13.0	5.7	4.3
$C_2F_4I^{+\bullet}$	227		0.5	4.4	0.7
$C_4F_9^+$	219	($-I^\bullet$)	100.0	1.3	–[a]
$C_2F_3I^{+\bullet}$	208		0.6	2.7	1.3
$C_4F_8^{+\bullet}$	200	(–FI)	0.7	0.7	4.6
CF_2I^+	177		27.2	27.5	47.7
$C_3F_7^+$	169		37.5	8.1	2.0
$C_3F_6^{+\bullet}$	150		2.0	2.0	1.3
$FI^{+\bullet}$	146	($-C_4F_8$)	3.0	6.0	4.0
$C_3F_5^+$	131		35.2	37.9	5.6
I^+	127	($-C_4F_9^\bullet$)	31.2	48.7	91.1
$C_2F_5^+$	119		31.2	8.1	<0.3
$C_3F_4^{+\bullet}$	112		1.3	5.0	7.3
$C_2F_4^{+\bullet}$	100		30.6	14.8	7.0
$C_3F_3^+$	93		3.7	10.1	23.2
$C_2F_3^+$	81		1.0	1.3	2.6
$C_3F_2^{+\bullet}$	74		1.0	1.3	2.6
CF_3^+	69		65.8	94.6	100.0
$C_2F_2^{+\bullet}$	62		0.7	1.0	1.0
$CF_2^{+\bullet}$	50		1.7	8.1	3.3
CF^+	31		7.6	10.7	9.9

[a]Not observed.

Figure 3.2 Normal Mass Spectra of (a) $CF_3CF_2CF_2CF_2I$ (n-C_4F_9I), (b) $CF_3CF_2CFICF_3$ (s-C_4F_9I), and (c) $(CF_3)_3CI$ (t-C_4F_9I); $C_4F_9I^{+\bullet}$ (m/z 346) Isomers

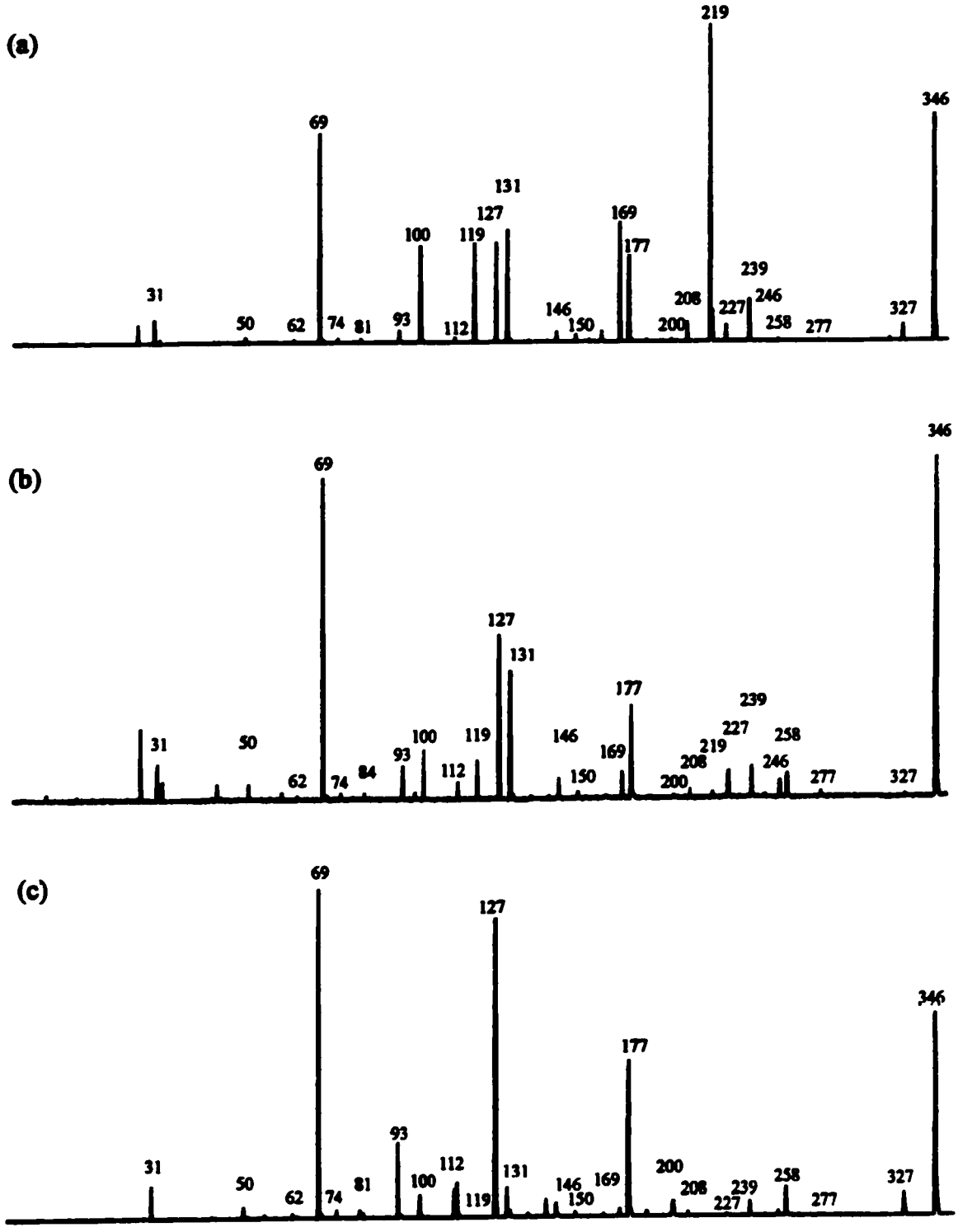

Table 3.8 Kinetic Energy Release $T_{0.5}$ Measurements of C_4F_9I Isomers

Mass (m/z)	Dissociation Process	Kinetic Energy Release, $T_{0.5}$(meV)
$CF_3CF_2CF_2CF_2I$		
(346 → 219)	$CF_3CF_2CF_2CF_2I^{+\bullet} \rightarrow CF_3CF_2CF_2CF_2^+ + I^\bullet$	13.4
(219 → 131)	$CF_3CF_2CF_2CF_2^+ \rightarrow (CF_2)_2C^+–F + CF_4$	149.3
$CF_3CF_2CFICF_3$		
(346 → 219)	$CF_3CF_2CFICF_3^{+\bullet} \rightarrow CF_3CF_2C^+FCF_3 + I^\bullet$	22.4
(219 → 131)	$CF_3CF_2C^+FCF_3 \rightarrow (CF_2)_2C^+–F + CF_4$	151.7
$(CF_3)_3CI$		
(346 → 258)	$(CF_3)_3CI^{+\bullet} \rightarrow CF_2{=}ClCF_3^{+\bullet} + CF_4$	–[a]
$(CF_3)_3C–C(CF_3)_3$		
	No Molecular Ion $(CF_3)_3C–C(CF_3)_3^{+\bullet}$	
(219 → 131)	$(CF_3)_3C^+ \rightarrow (CF_2)_2C^+–F + CF_4$	139.8

[a]Not measured.

Table 3.9 Metastable Ion (MI) 2FFR and Collision Induced Dissociation (CID) 2FFR $O_2 \approx 90$ %T Mass Spectra of the $C_4F_9I^{+\bullet}$ (m/z 346) Isomers

			Parent Ion					
			n-C_4F_9I		s-C_4F_9I		t-C_4F_9I	
	Mass	Neutral	Height (%)		Height (%)		Height (%)	
Species	(m/z)	Loss	MI	CID	MI	CID	MI	CID
$C_3F_6I^+$	277	($-CF_3^\bullet$)				3.0		6.6
$C_3F_5I^{+\bullet}$	258	($-CF_4$)				0.7	100.0	100.0
$C_3F_4I^+$	239					0.7		2.3
$C_2F_4I^+$	227	($-C_2F_5^\bullet$)			5.3	25.2		1.0
$C_4F_9^+$	219	($-I^\bullet$)	100.0	100.0	100.0	100.0	–[a]	–[a]
$C_2F_3I^{+\bullet}$	208					2.0		2.0
$C_4F_8^{+\bullet}$	200	(–FI)						1.0
$C_2F_2I^+$	189					<0.3		2.0
$C_4F_7^+$	181							11.9
CF_2I^+	177	($-C_3F_7^\bullet$)		0.7		4.6		3.3
$C_2FI^{+\bullet}$	170							1.3
$C_3F_7^+$	169			<0.3		0.7		
$CFI^{+\bullet}$	158			<0.3		2.3		4.6
$C_3F_6^{+\bullet}$	150			<0.3		2.0		4.0
$FI^{+\bullet}$	146	($-C_4F_8$)				0.7	6.6	14.6
CI^+	139					1.3		2.6
$C_3F_5^+$	131			1.3		17.2		
I^+	127	($-C_4F_9^\bullet$)		1.3		15.6	2.0	43.7
$C_2F_5^+$	119			<0.3		2.3		
$C_3F_4^{+\bullet}$	112					0.7		2.0
$C_2F_4^{+\bullet}$	100			<0.3		2.3		1.3
$C_3F_3^+$	93			<0.3		0.7		1.3
CF_3^+	69			<0.3		2.3		1.3

[a]Very weak, <0.1 %.

Figure 3.3 Metastable Ion (MI) 2FFR Mass Spectra of (a) $CF_3CF_2CF_2CF_2I$ (n-C_4F_9I), (b) $CF_3CF_2CFICF_3$ (s-C_4F_9I), and (c) $(CF_3)_3CI$ (t-C_4F_9I); $C_4F_9I^{+\bullet}$ (m/z 346) Isomers

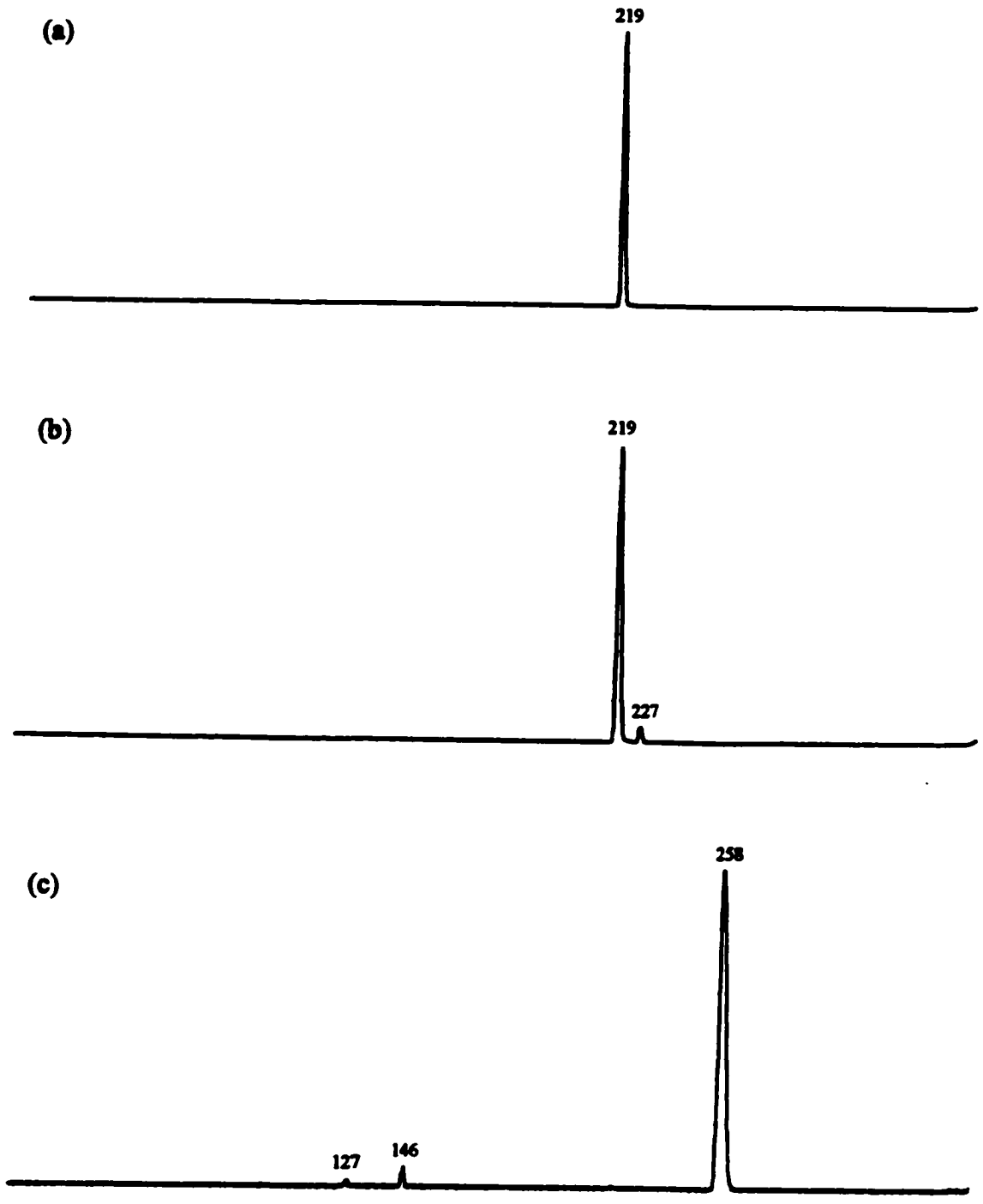

Figure 3.4 Collision Induced Dissociation (CID) 2FFR O_2 ≈ 90 %T Mass Spectra of (a) $CF_3CF_2CF_2CF_2I$ (n-C_4F_9I), (b) $CF_3CF_2CFICF_3$ (s-C_4F_9I), and (c) $(CF_3)_3CI$ (t-C_4F_9I); $C_4F_9I^{+\bullet}$ (m/z 346) Isomers

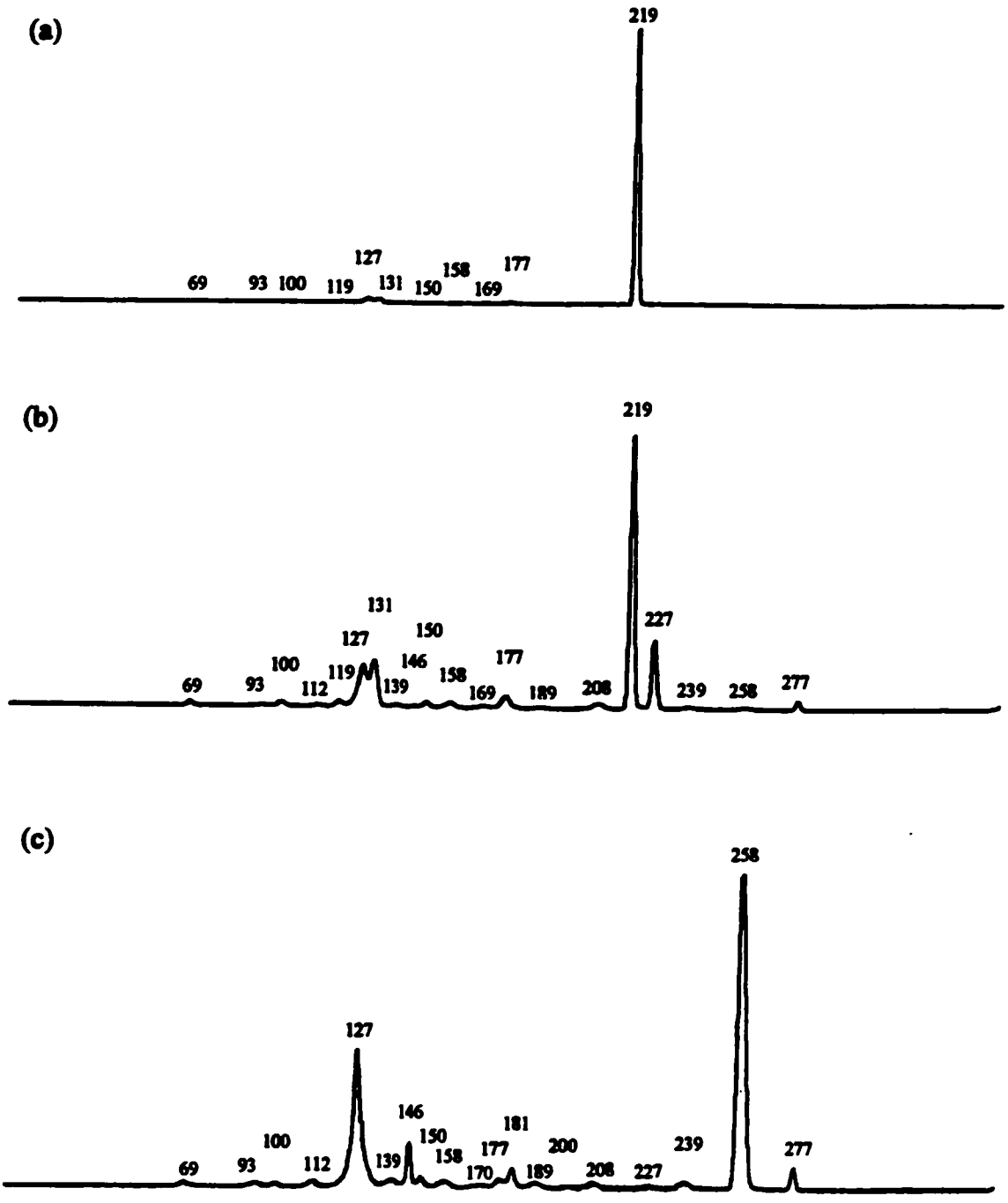

in the I^+ production (31.2 %, 48.7 %, 91.1 %), via $C_4F_9^\bullet$ loss, as one proceeds from the n-$C_4F_9I^{+\bullet}$, to the s-$C_4F_9I^{+\bullet}$, and to the t-$C_4F_9I^{+\bullet}$ isomer, respectively. Thus, it appears that while the n-$C_4F_9I^{+\bullet}$ and s-$C_4F_9I^{+\bullet}$ isomers have several fragment ions in their normal mass spectra of sizable intensity, such is not the case for the t-$C_4F_9I^{+\bullet}$ isomer whose main fragment ions are I^+ and CF_3^+.

Next, on inspection of the kinetic energy release values, $T_{0.5}$ (meV), one may note the following trends. Firstly, the $CF_3CF_2CF_2CF_2I^{+\bullet}$ and $CF_3CF_2CFICF_3^{+\bullet}$ isomers are similar in that they both have $I^\bullet$ loss as their primary metastable dissociation process. The $T_{0.5}$ values are 13.4 and 22.4 meV, respectively. The first $T_{0.5}$ value is indicative of a simple C–I bond cleavage producing an unrearranged $CF_3CF_2CF_2CF_2^+$ (m/z 219) cation and an $I^\bullet$ neutral. However, the higher magnitude of the latter $T_{0.5}$ value for the s-$C_4F_9I^{+\bullet}$ isomer (i.e., $\approx$ 2x the former $T_{0.5}$ value), is possibly indicative of a mixture of $CF_3CF_2CF_2CF_2^+$ and $CF_3CF_2C^+FCF_3$ (m/z 219) isomeric cations being produced as $I^\bullet$ loss is likely accompanied by simultaneous F migration. Thus, in contrast to the hydrogen analogues, it is proposed that the $CF_3CF_2CF_2CF_2^+$ (m/z 219) cation isomer possesses its own unique structure and its own potential well. The $CF_3CF_2C^+FCF_3$ (s-$C_4F_9^+$) isomer may possess a substantially smaller potential well and thereby may undergo a somewhat facile rearrangement to the more stable $CF_3CF_2CF_2CF_2^+$ (s-$C_4F_9^+$) isomer upon excitation during the metastable $I^\bullet$ loss process.

Now, turning ones' attention to the $(CF_3)_3CI^{+\bullet}$ (t-$C_4F_9I^{+\bullet}$) isomer, one may see that its primary metastable dissociation process is that of CF_4 loss and the production of the $C_3F_5I^{+\bullet}$ (m/z 258) cation. Thus its dissociation behaviour involves a completely different manifold (i.e., potential energy surface) than for the other n-$C_4F_9I^{+\bullet}$ and s-$C_4F_9I^{+\bullet}$ isomers. As stated previously, the rationalization for this radically different dissociation behaviour may be

qualitatively linked to the n-C_4F_9I and s-C_4F_9I isomers being governed by the CF_2=$CFCF_2CF_3$ + FI manifold; whereas the i-C_4F_9I and t-C_4F_9I isomers are governed by the CF_2=$C(CF_3)_2$ + FI manifold. Thus, one may infer that multiple branching of an isomer facilitates the elimination of a CF_4 neutral.

Next, on inspection of the peak heights, metastable ion (MI) and collision induced dissociation (CID) mass spectra of the $C_4F_9I^{+\bullet}$ (m/z 346) isomers, illustrated in Table 3.9, Figures 3.3, and 3.4, respectively, one may note the following trends. First, as previously stated the base peak (100 %) of the MI mass spectra of the n-$C_4F_9I^{+\bullet}$ and s-$C_4F_9I^{+\bullet}$ isomers is the $C_4F_9^+$ (m/z 219) peak, whereas it is the $C_3F_5I^{+\bullet}$ (m/z 258) peak for the t-$C_4F_9I^{+\bullet}$ isomer. Additionally, whereas the n-$C_4F_9I^{+\bullet}$ isomer possesses only one MI peak (i.e., $C_4F_9^+$ m/z 219), the s-$C_4F_9I^{+\bullet}$ isomer possesses a second minor MI peak for $C_2F_4I^+$ (m/z 227), corresponding to $^{\bullet}CF_2CF_3$ loss. The t-$C_4F_9I^{+\bullet}$ isomer has again a much more active metastable dissociation potential energy surface, manifested by the presence of four MI peaks for $C_3F_5I^{+\bullet}$, $C_4F_9^+$, $FI^{+\bullet}$, and I^+, at m/z 258, 219, 146, and 127, respectively.

It can be seen in Table 3.8, that the $FI^{+\bullet}$ m/z 146 cation, corresponding to C_4F_8 loss, is absent in the n-$C_4F_9I^{+\bullet}$ isomer, slightly present in the CID of the s-$C_4F_9I^{+\bullet}$ isomer, and strongly represented in the t-$C_4F_9I^{+\bullet}$ isomer. On inspection of Figure 3.1, the probable energy levels of the $C_4F_9I^{+\bullet}$ isomers, one may see that this trend is corresponds to the higher dissociation energy requirements for CF_2=$CFCF_2CF_3$ loss than for CF_2=$C(CF_3)_2$ loss (i.e., $FI^{+\bullet}$ + CF_2=$CFCF_2CF_3$ and $FI^{+\bullet}$ + CF_2=$C(CF_3)_2$ possess a $\Delta_f H^0$ of –601.9 and –680.1 kJ•mol^{-1}, respectively).

An increase in the intensity of the I^+ (m/z 127) cation, corresponding to $C_4F_9^\bullet$ loss, can be seen in Table 3.9 as one proceeds from the n-$C_4F_9I^{+\bullet}$, to the s-$C_4F_9I^{+\bullet}$, and to the t-$C_4F_9I^{+\bullet}$ isomer, respectively. This increase in ease of $C_4F_9^\bullet$ loss is governed the trend in the dissociation energy requirements as follows, $I^+ + CF_3CF_2CF_2CF_2^\bullet$, $I^+ + CF_3CF_2C^\bullet FCF_3$, $I^+ + (CF_3)_2CFCF_2^\bullet$, and $I^+ + (CF_3)_3C^\bullet$, each possess a Δ_fH^0 value of –578.8, –625.8, –626.8, and –701.5 kJ•mol^{-1}, respectively.

The largest difference in the fragment ions produced by the $C_4F_9I^{+\bullet}$ isomers occurs during the genesis of the $C_4F_9^+$ m/z 219. On inspection of Table 3.9, Figures 3.3 and 3.4, one may note that whilst being the base peak in the n-$C_4F_9I^{+\bullet}$ and s-$C_4F_9I^{+\bullet}$ isomers, the $C_4F_9^+$ m/z 219 fragment cation is exceptional weak in both the MI and CID mass spectra of the t-$C_4F_9I^{+\bullet}$ isomer. This is a direct result of the very different thermochemistry of the tert-butyl hydrogen and fluorine analogues. Whereas, in the hydrogen species the formation of the tert-butyl cation is favoured over that of the iodine cation (i.e., $(CH_3)_3C^+ + I^\bullet$, and $I^+ + (CH_3)_3C^\bullet$, possess a Δ_fH^0 value of 800.5, and 1161.4 kJ•mol^{-1} [1], respectively) it is proposed that for the perfluoro analogues this order is reversed. Therefore, the lower dissociation limit is that of $I^+ + (CF_3)_3C^\bullet$, with a Δ_fH^0 value of –701.5 kJ•mol^{-1}, compared to the $(CF_3)_3C^+ + I^\bullet$ dissociation limit, which must possess a higher Δ_fH^0 value.

Thus, to obtain a significant intensity of the $(CF_3)_3C^+$ (m/z 219) cation, as will be discussed later, one must utilize a different precusor ion, namely the $(CF_3)_3C–C(CF_3)_3^{+\bullet}$ species, with a different thermochemistry (i.e., via $(CF_3)_3C^\bullet$ loss) which favours its production.

Therefore, on going from the hydrogen compound manifold to the (per) fluoro compound manifold, an entire change in the thermochemistry (i.e., the $\Delta_f H^0$ order of the dissociation limits) can manifest itself resulting in completely different gas-phase ion-chemistry dissociation behaviour. To this end, one will now discuss the source generated $C_3F_5I^{+\bullet}$, $C_3F_4I^+$, and $C_4F_8^{+\bullet}$ fragments of the $C_4F_9I^{+\bullet}$ isomers to explore their perfluoro parent ion behaviour.

$C_3F_5I^{+\bullet}$ (m/z 258)

These isomeric fragment ions are generated from CF_4 loss by the $C_4F_9I^{+\bullet}$ radical-cation parent. There are three main $C_3F_5I^{+\bullet}$ isomers to be discussed here. They are as follows, CF_2=$CFCF_2I^{+\bullet}$, CF_2=$CICF_3^{+\bullet}$, and $^+CF_2$–(CFI) –$^\bullet CF_2$ and are known as the 3-iodoperfluoropropene, the 2-iodoperfluoropropene, and the distonic 2-iodoperfluorotrimethylene radical-cations, respectively. Figure 3.5 illustrates the proposed energy levels of the $C_3F_5I^{+\bullet}$ (m/z 258) isomers, with the known $\Delta_f H^0$ ($kJ \bullet mol^{-1}$) of the dissociation products indicated in the brackets. The order of stability of the $C_3F_5I^{+\bullet}$ isomers illustrated there is based on the rationale that the frontier orbitals are dominated by the unsaturated π–bond system which interacts with the non-bonding (p_x , p_y) "pseudo-π" iodine orbitals. As the fluorine atom is much more electronegative than the iodine atom, one may qualitatively say that a CF_2=CF–R moiety is better able to stabilize charge (i.e., more stable) than a CF_2=CI–R moiety. Thus, the proposed order of stability for the unsaturated $C_3F_5I^{+\bullet}$ isomers discussed here, and illustrated in Figure 3.5, is as follows, CF_2=$CFCF_2I^{+\bullet}$ > CF_2=$CICF_3^{+\bullet}$ > $^+CF_2$–(CFI) –$^\bullet CF_2$. Due to the precursors studied here, the cyclic iodoperfluorocyclopropane, c-$C_3F_5I^{+\bullet}$, isomer is not considered a participant in this manifold

and will not be discussed here. Table 3.10, Figures 3.6 and 3.7, illustrate the peak heights, the metastable ion (MI), and collision induced dissociation (CID) mass spectra of the $C_3F_5I^{+\bullet}$ (m/z 258) isomers source generated from (a) the n-C_4F_9I, (b) the s-C_4F_9I, and (c) the t-C_4F_9I isomers, respectively.

On inspection of the peak heights presented in Table 3.10 and the MI and CID mass spectra illustrated in Figures 3.6 and 3.7, one may note the following trends. First, for all of the $C_3F_5I^{+\bullet}$ isomers the following metastable peaks are present; $C_3F_4I^+$, $C_2F_3I^{+\bullet}$, $C_3F_5^+$, and $C_3F_4^{+\bullet}$, at m/z 239, 208, 131, and 112, each corresponding to $F^\bullet$, CF_2, $I^\bullet$, and FI loss, respectively. One may immediately see that the $C_3F_5I^{+\bullet}$ isomers produced from n-C_4F_9I and s-C_4F_9I exhibit similar behaviour, each possessing a base peak (100 %) at $C_3F_5^+$ m/z 131 (i.e., $-I^\bullet$); whilst the $C_3F_5I^{+\bullet}$ isomer produced from t-C_4F_9I possesses one at $C_3F_4I^+$ m/z 239 (i.e., $-F^\bullet$). The above observations are rationalized by the metastable CF_4 loss from the parent $C_4F_9I^{+\bullet}$ isomers producing the following $C_3F_5I^{+\bullet}$ species,

(a) $CF_3CF_2CF_2CF_2I^{+\bullet} \rightarrow CF_2{=}CFCF_2I^{+\bullet} + CF_4$

(b) $CF_3CF_2CFICF_3^{+\bullet} \rightarrow {}^+CF_2{-}(CFI){-}{}^\bullet CF_2 + CF_4$

(c) $(CF_3)_3CI^{+\bullet} \rightarrow CF_2{=}ClCF_3^{+\bullet} + CF_4$

Thus, the $C_3F_5I^{+\bullet}$ isomers produced from (a) the n-C_4F_9I, (b) the s-C_4F_9I, and (c) the t-C_4F_9I isomers are dominated by the $CF_2{=}CFCF_2I^{+\bullet}$, ${}^+CF_2{-}(CFI){-}{}^\bullet CF_2$, and $CF_2{=}ClCF_3^{+\bullet}$ cation structures, respectively. This being the case, on inspection of the probable energy levels of the $C_3F_5I^{+\bullet}$ isomers, illustrated in Figure 3.5, one may note that in order to generate the 2-iodoperfluoroallyl cation, $(CF_2)_2C^+{-}I$ (m/z 239), the $CF_2{=}CFCF_2I^{+\bullet}$ species must pass

Figure 3.5 Proposed Energy Levels of the $C_3F_5I^{+\bullet}$ (m/z 258) Isomers

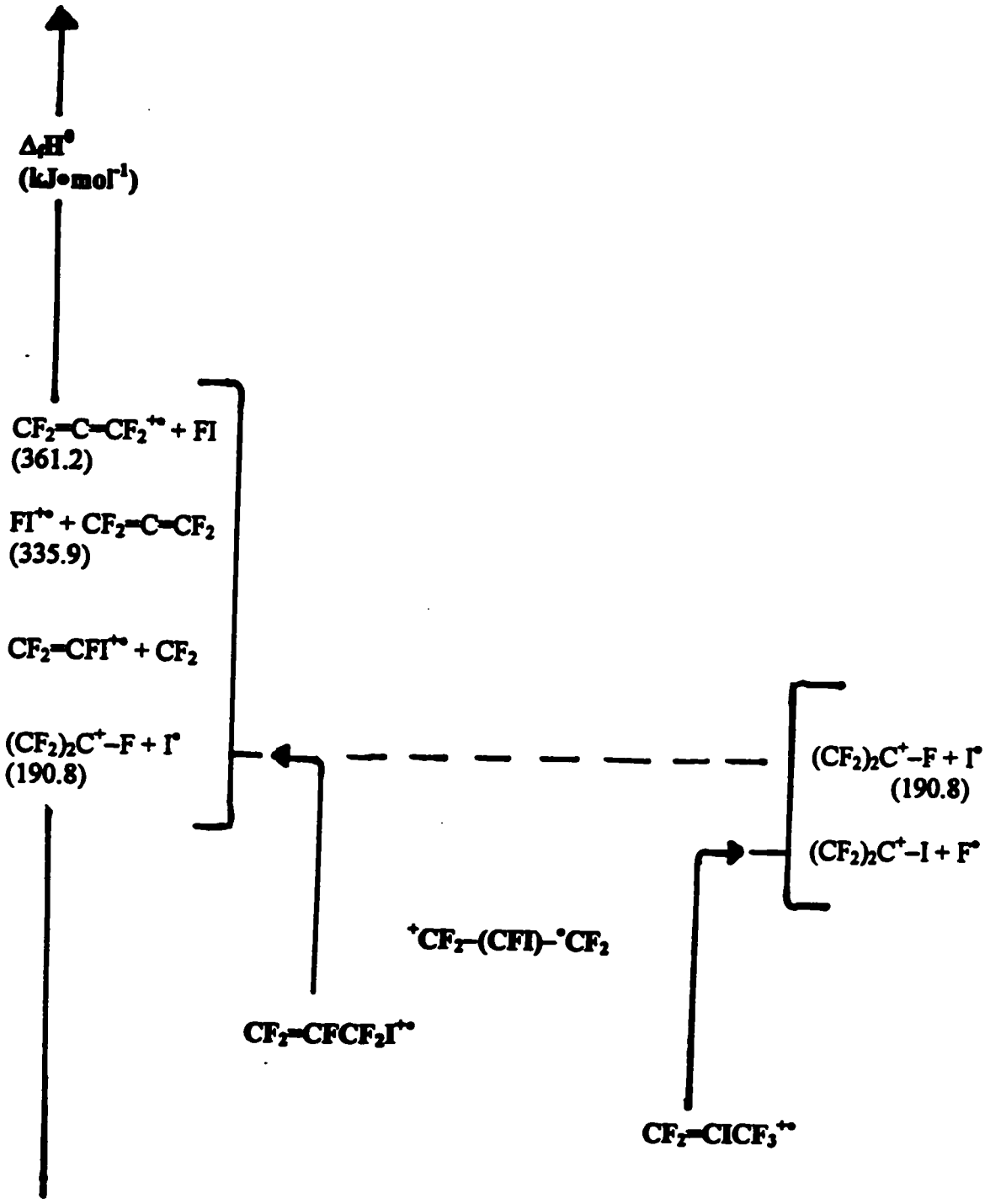

Table 3.10 Metastable Ion (MI) 2FFR and Collision Induced Dissociation (CID) 2FFR He ≈ 90 %T Mass Spectra of Source Generated $C_3F_5I^{+\bullet}$ (m/z 258) from the C_4F_9I Isomers

			Parent Ion					
			n-C_4F_9I		s-C_4F_9I		t-C_4F_9I	
	Mass	Neutral	Height (%)		Height (%)		Height (%)	
Species	(m/z)	Loss	MI	CID	MI	CID	MI	CID
$C_3F_4I^+$	239	($-F^\bullet$)	37.1	40.4	92.7	94.7	100.0	100.0
$C_2F_3I^{+\bullet}$	208	($-CF_2$)	79.5	96.0	34.4	36.4	14.2	14.2
$C_2F_2I^+$	189	($-CF_3^\bullet$)	2.0	9.3		10.6		5.0
$CF_2I^{+\bullet}$	177			1.3		0.7		<0.3
$C_2FI^{+\bullet}$	170	($-CF_4$)		4.0		2.6		1.3
$CFI^{+\bullet}$	158			4.6		4.0		2.0
$FI^{+\bullet}$	146			4.0		2.6		1.3
CI^+	139			4.6		3.0		1.3
$C_3F_5^+$	131	($-I^\bullet$)	100.0	100.0	100.0	100.0	27.2	27.2
I^+	127	($-C_3F_5^\bullet$)		26.2		19.9		7.3
$C_3F_4^{+\bullet}$	112	($-FI$)	6.0	52.3	8.6	54.0	2.3	13.2
$C_3F_3^+$	93			6.6		4.3		<0.3
$C_2F_3^+$	81			0.7		0.7		
CF_3^+	69			4.0		1.3		

Figure 3.6 Metastable Ion (MI) 2FFR Mass Spectra of Source Generated $C_3F_5I^{+\bullet}$ (m/z 258) from (a) n-C_4F_9I, (b) s-C_4F_9I, and (c) t-C_4F_9I.

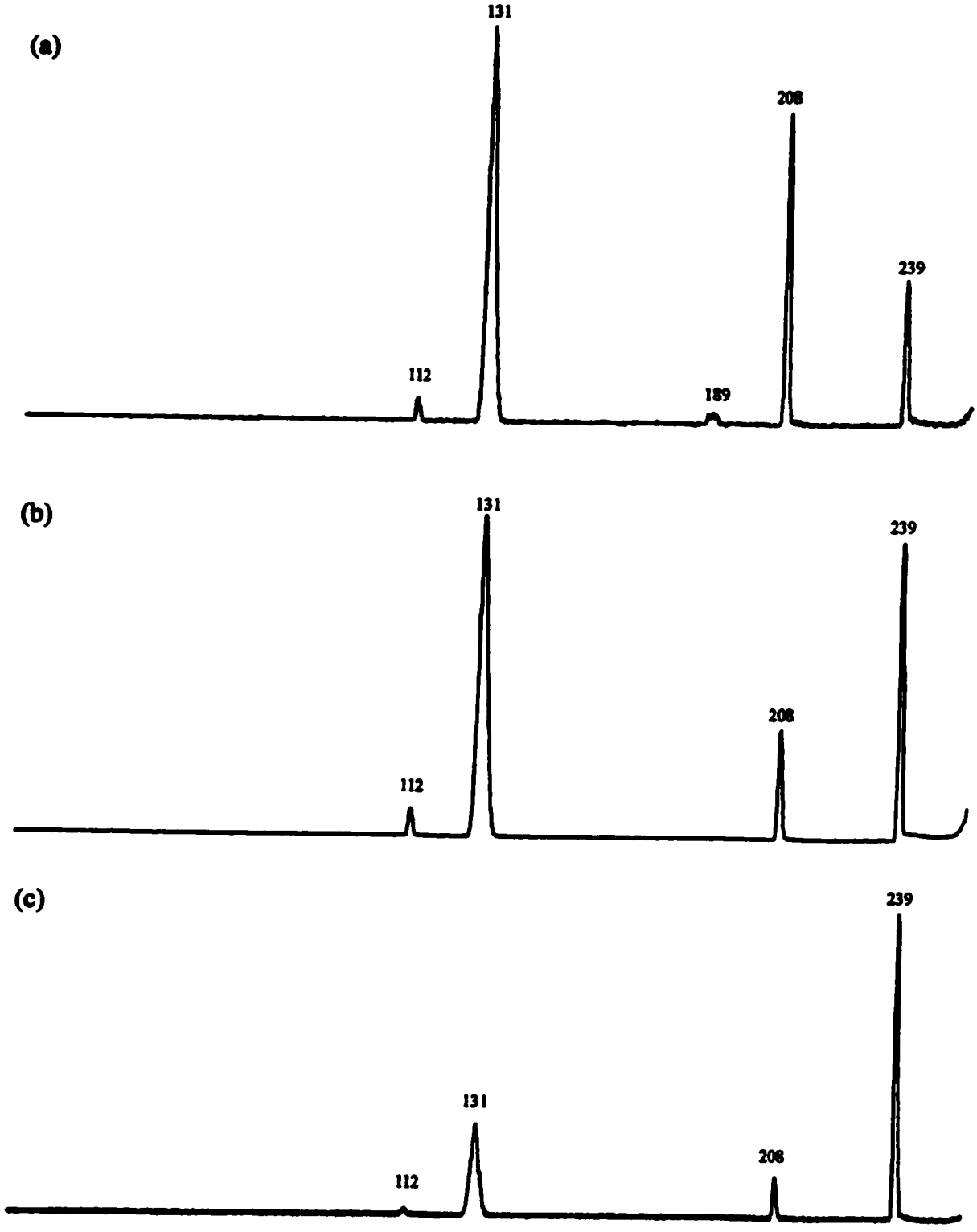

Figure 3.7 Collision Induced Dissociation (CID) 2FFR He ≈ 90 %T Mass Spectra of Source Generated $C_3F_5I^{+\bullet}$ (m/z 258) from (a) n-C_4F_9I, (b) s-C_4F_9I, and (c) t-C_4F_9I.

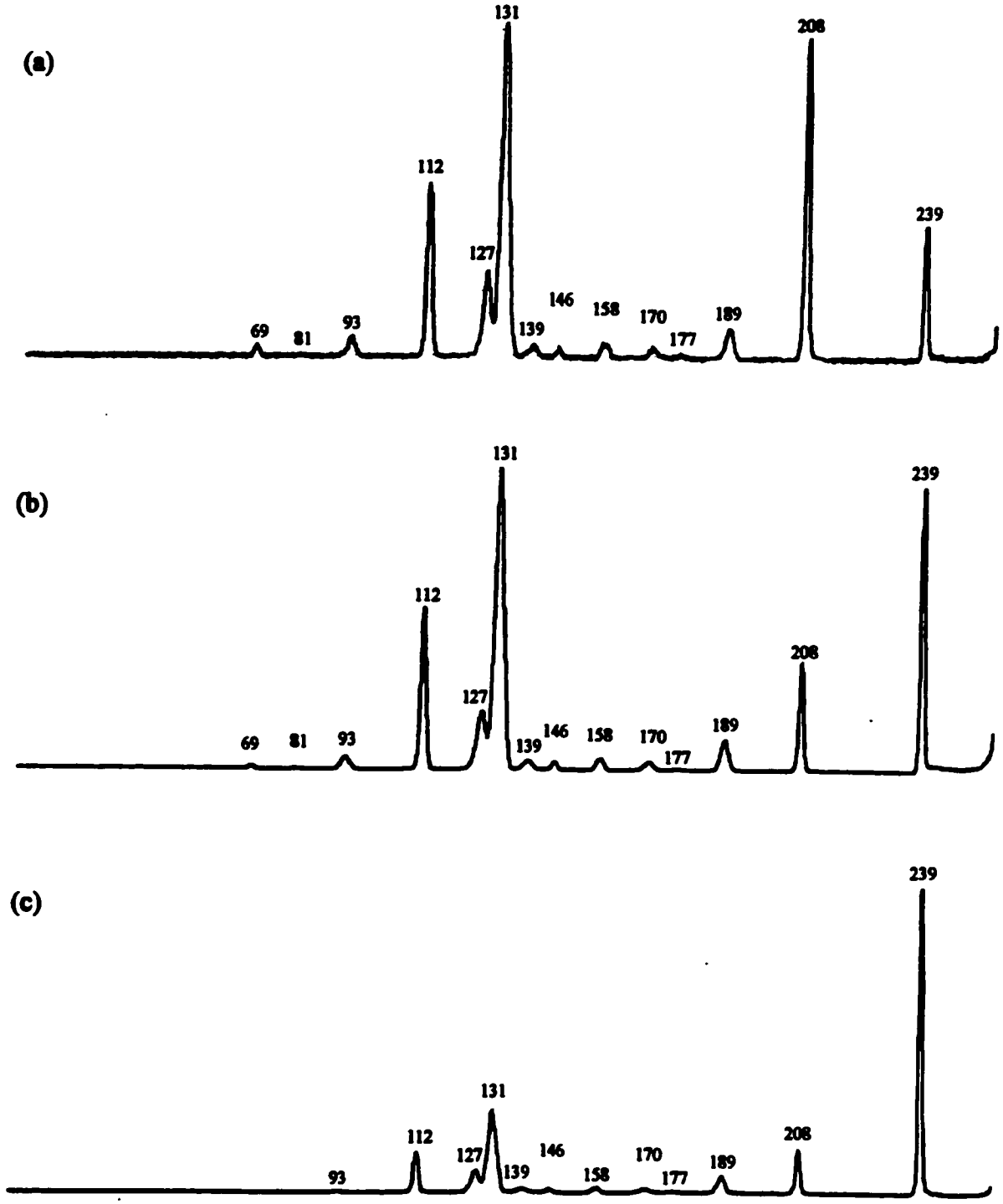

through the distonic $^{+}CF_2$–(CFI)–$^{\bullet}CF_2$ species to reach the lowest energy dissociation limit of $(CF_2)_2C^{+}$–I + $F^{\bullet}$.

$C_3F_4I^{+}$ (m/z 239)

These isomeric fragment ions are generated from $F^{\bullet}$ loss by the source generated $C_3F_5I^{+\bullet}$ fragment radical-cation. There are four main $C_3F_4I^{+}$ isomers to be discussed here. They are as follows, $(CF_2)_2C^{+}$–I, CF_2–$(CF)^{+}$–CFI, CF_2=C^{+}–CF_2I, and CF_3–$\ddot{C}$–CFI^{+} and are known as the 2-iodoperfluoroallyl, 1-iodoperfluoroallyl, the 2-iodoperfluoropropenyl, and the 1-iodoperfluoropropyl carbene cations, respectively. If one may assume that the most symmetric distribution of positive charge yields the lowest energy isomer, then one may propose the following order of stability; $(CF_2)_2C^{+}$–I > CF_2–$(CF)^{+}$–CFI > CF_2=C^{+}–CF_2I > CF_3–$\ddot{C}$–CFI^{+}. The proposed energy levels of the $C_3F_4I^{+}$ isomers are illustrated in Figure 3.8. The peak intensities of the MI and CID mass spectra of the $C_3F_4I^{+}$ isomers are listed in Table 3.11 and illustrated in Figures 3.9 and 3.10.

On inspection of Table 3.11 and Figures 3.9 and 3.10, one may see that the $C_3F_4I^{+}$ ions produced from n-C_4F_9I and s-C_4F_9I are probably the same and may be the $(CF_2)_2C^{+}$–I isomer. This structure is suggested due to the main MI peak of CF_2=C=$CF_2^{+\bullet}$ (m/z 112) and the minor MI peaks of c-$C_3F_3^{+}$ (m/z 93) and I^{+} (m/z 127). The presence of a doubly-charged $(CF_2)_2CI^{2+\bullet}$ (m/z 119.5) in the CID O_2 mass spectra of Figure 3.10 also supports this assignment.

The $C_3F_4I^{+}$ ions produced from t-C_4F_9I isomers appear to be different in nature and may have a CF_2–$(CF)^{+}$–CFI structure. This is suggested due to the main MI peak of CF_3–C≡$CF^{+\bullet}$ (m/z 112) (possibly mixed with a small amount of CF_2=C=$CF_2^{+\bullet}$) and minor

Figure 3.8 Proposed Energy Levels of the $C_3F_4I^+$ (m/z 239) Isomers

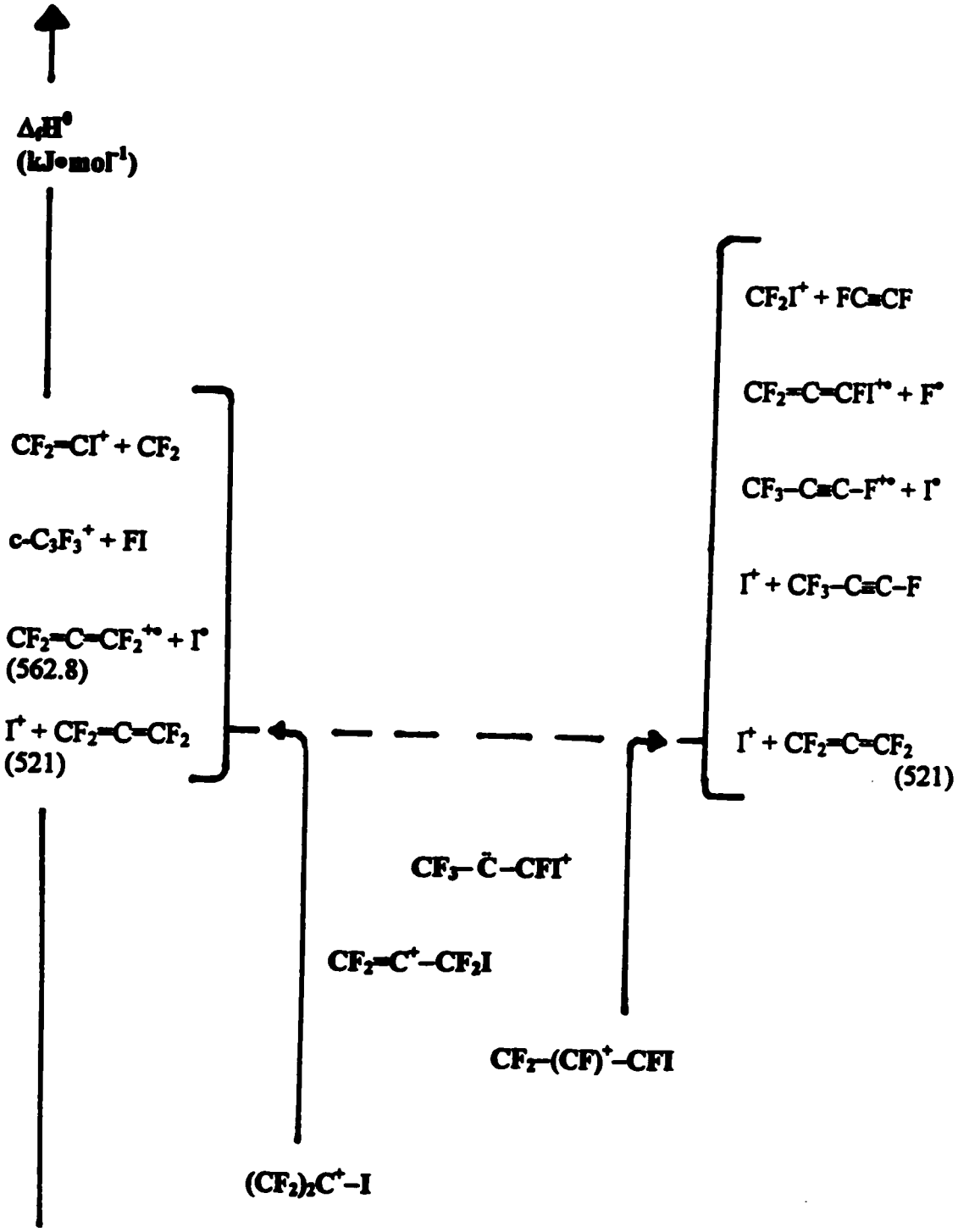

Table 3.11 Metastable Ion (MI) 2FFR and Collision Induced Dissociation (CID) 2FFR $O_2 \approx 90$ %T Mass Spectra of Source Generated $C_3F_4I^+$ (m/z 239) from the C_4F_9I Isomers

			Parent Ion					
			n-C_4F_9I		s-C_4F_9I		t-C_4F_9I	
	Mass	Neutral	Height (%)		Height (%)		Height (%)	
Species	(m/z)	Loss	MI	CID	MI	CID	MI	CID
$C_3F_3I^{+\bullet}$	220	($-F^\bullet$)					7.3	4.6
$C_3F_2I^+$	201	($-F_2$)						0.7
$C_2F_2I^+$	189	($-CF_2$)		2.0		4.0		9.6
$CF_2I^{+\bullet}$	177	($-C_2F_2$)					1.3	0.7
$C_2FI^{+\bullet}$	170	($-CF_3^\bullet$)		1.3		2.0		2.0
$CFI^{+\bullet}$	158			0.7		0.7		1.3
C_2I^+	151	($-CF_4$)		<0.3		0.7		
$FI^{+\bullet}$	146			<0.3		<0.3		
CI^+	139			4.0		5.3		5.3
I^+	127	($-C_3F_4$)	0.7	28.5	0.7	37.7		23.2
$C_3F_4I^{2+\bullet}$	119.5			2.6		3.3		0.7
$C_3F_4^{+\bullet}$	112	($-I^\bullet$)	100.0	100.0	100.0	100.0	100.0	100.0
$C_3F_3^+$	93	($-FI$)	2.6	17.2	2.6	18.5	1.3	6.0
$C_3F_2^{+\bullet}$	74			0.7		0.7		
CF_3^+	69			0.7		<0.3		
$C_2F_2^{+\bullet}$	62			<0.3		<0.3		

Figure 3.9 Metastable Ion (MI) 2FFR Mass Spectra of Source Generated $C_3F_4I^+$ (m/z 239) from (a) n-C_4F_9I, (b) s-C_4F_9I, and (c) t-C_4F_9I.

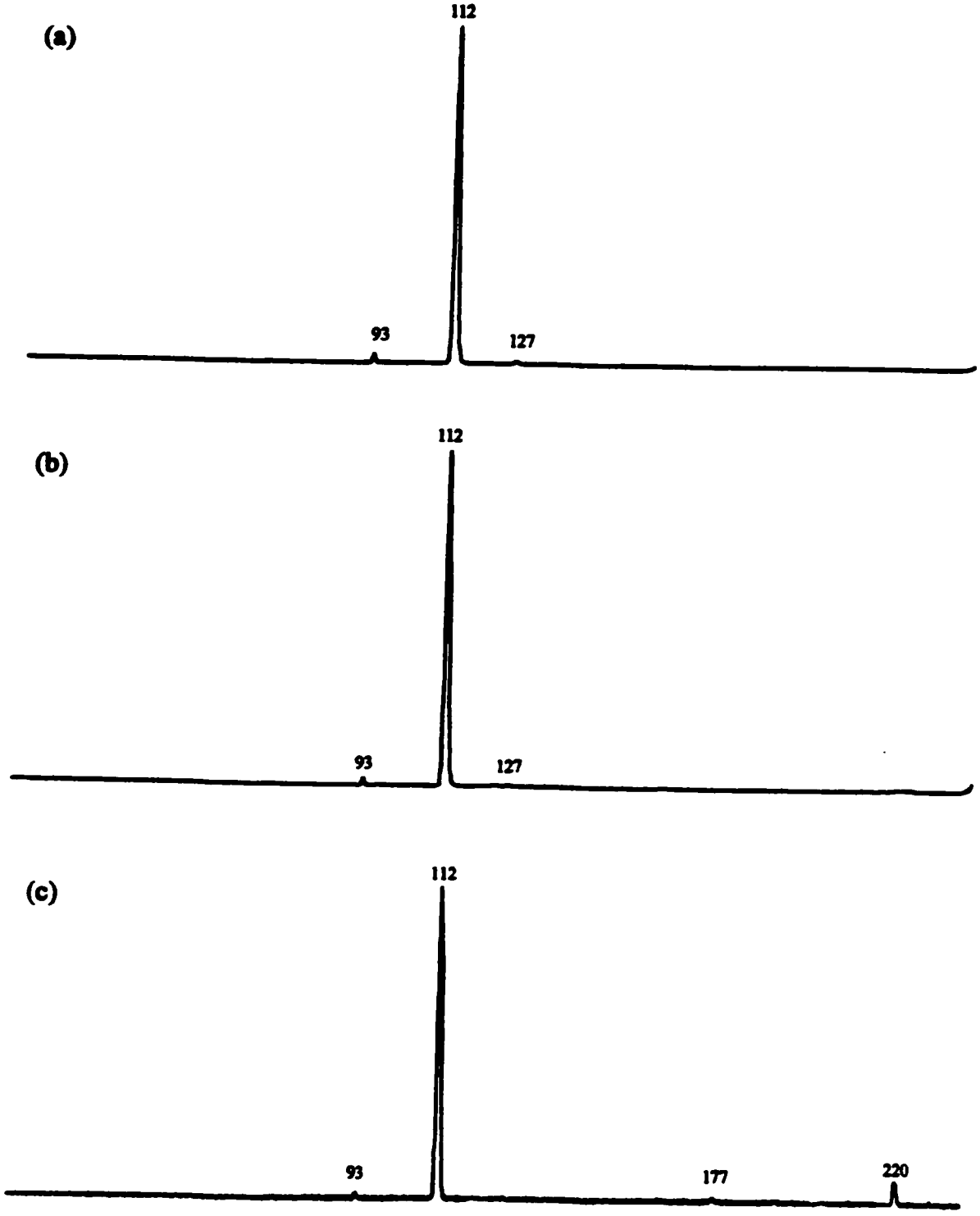

Figure 3.10 Collision Induced Dissociation (CID) 2FFR O_2 ≈ 90 %T Mass Spectra of Source Generated $C_3F_4I^+$ (m/z 239) from (a) n-C_4F_9I, (b) s-C_4F_9I, and (c) t-C_4F_9I

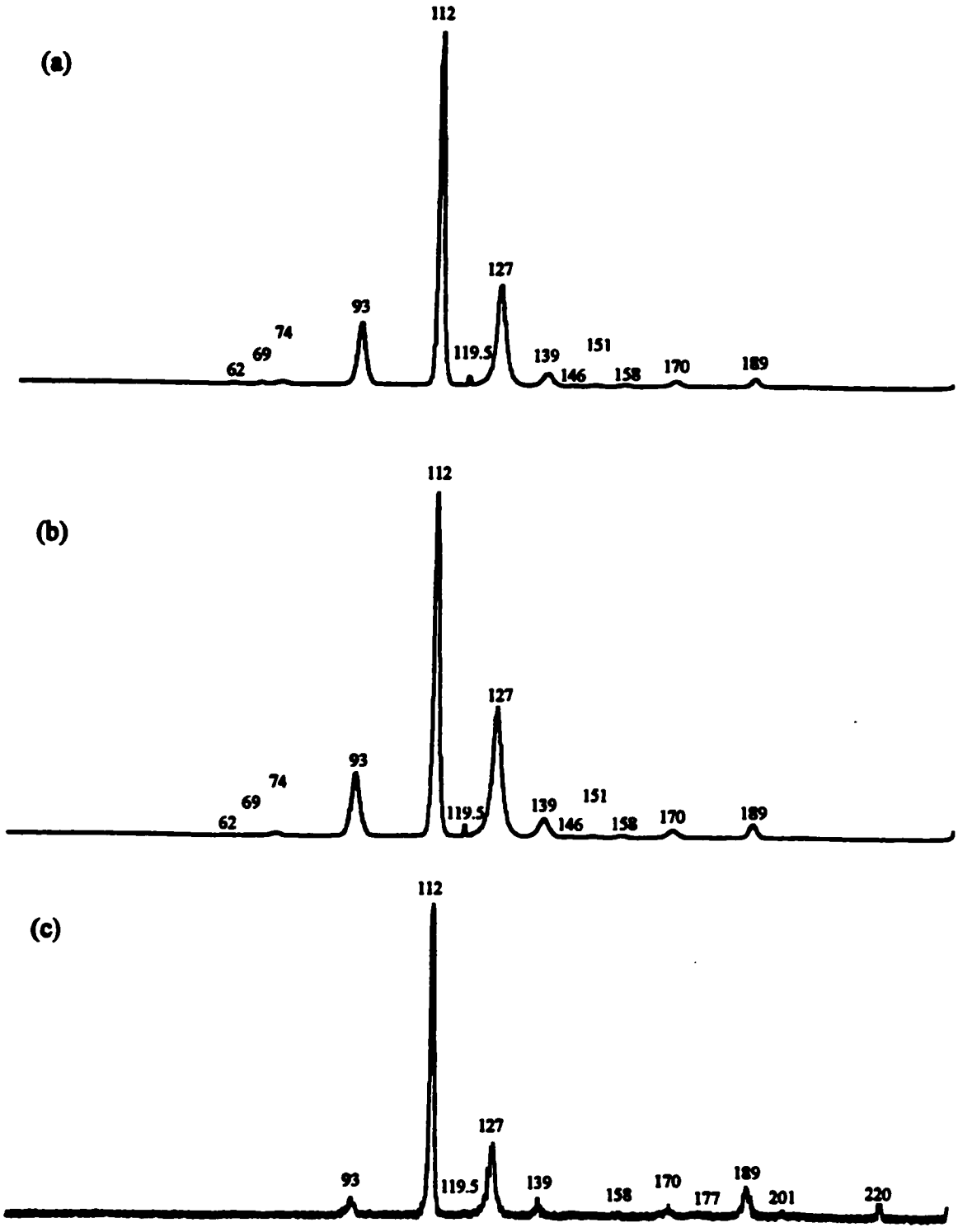

MI peaks of c-$C_3F_3^+$ (m/z 93), CF_2I^+ (m/z 177), and CF_2=C=$CFI^{+\bullet}$ (m/z 220). Additionally, the presence of a doubly-charged CF_2–(CF)–$CFI^{2+\bullet}$ (m/z 119.5) of a slightly lower intensity also supports this assignment.

$C_4F_8^{+\bullet}$ (m/z 200)

These isomeric fragment ions are generated by FI loss from the $C_4F_9I^{+\bullet}$ parent-ion. There are four main $C_4F_8^{+\bullet}$ isomers to be discussed here. They are CF_2=$CFCF_2CF_3^{+\bullet}$, CF_2=$C(CF_3)_2^{+\bullet}$, $^+CF_2$–(CFCF_3)–$^\bullet CF_2$, and $^+CF_2CF_2CF_2CF_2^\bullet$. The cyclic c-$C_4F_8^{+\bullet}$ isomer is not known to possess a stable ion and will not be discussed here. One should remember that the Benson values are $\Delta_fH^0[CF_2$=$CFCF_2CF_3] = -1531.8$ kJ•mol^{-1} and $\Delta_fH^0[CF_2$=$C(CF_3)_2] = -1610.0$ kJ•mol^{-1} (see Table3.3). Now remembering that $IE_a[CF_2$=$CFCF_3] = 10.60$ eV [1], thus using the proposed ≈ 0.08 eV and ≈ 0.50 eV increases in IE_a values for the insertion of CF_2 and CF_3 moieties (see Table 3.6), one may estimate the values of $IE_a[CF_2$=$CFCF_2CF_3] \approx$ 10.68 eV and $IE_a[CF_2$=$CFCF_3] \approx 11.10$ eV, respectively. Thus, this does result in the estimated cationic values of $\Delta_fH^0[CF_2$=$CFCF_2CF_3^{+\bullet}] \approx -501.3$ kJ•mol^{-1} and $\Delta_fH^0[CF_2$=$C(CF_3)_2^{+\bullet}] \approx -5400.0$ kJ•mol^{-1}, respectively. Thus, one may assume that the order of stability for CF_2=$CFCF_2CF_3^{+\bullet}$ and CF_2=$C(CF_3)_2^{+\bullet}$ parallels that of their perfluoro neutral counterparts, then one may propose the following order of stability; CF_2=$C(CF_3)_2^{+\bullet}$ > CF_2=$CFCF_2CF_3^{+\bullet}$ > $^+CF_2$–(CFCF_3)–$^\bullet CF_2$ > $^+CF_2CF_2CF_2CF_2^\bullet$. (One should note that this parallels the behaviour of CH_2=$C(CH_3)_2^{+\bullet}$ > CH_2=$CHCH_2CH_3^{+\bullet}$). The proposed energy levels of the $C_4F_8^{+\bullet}$ isomers are illustrated in Figure 3.11. The peak intensities of the MI and

Figure 3.11 Proposed Energy Levels of the $C_4F_8^{+\bullet}$ (m/z 200) Isomers

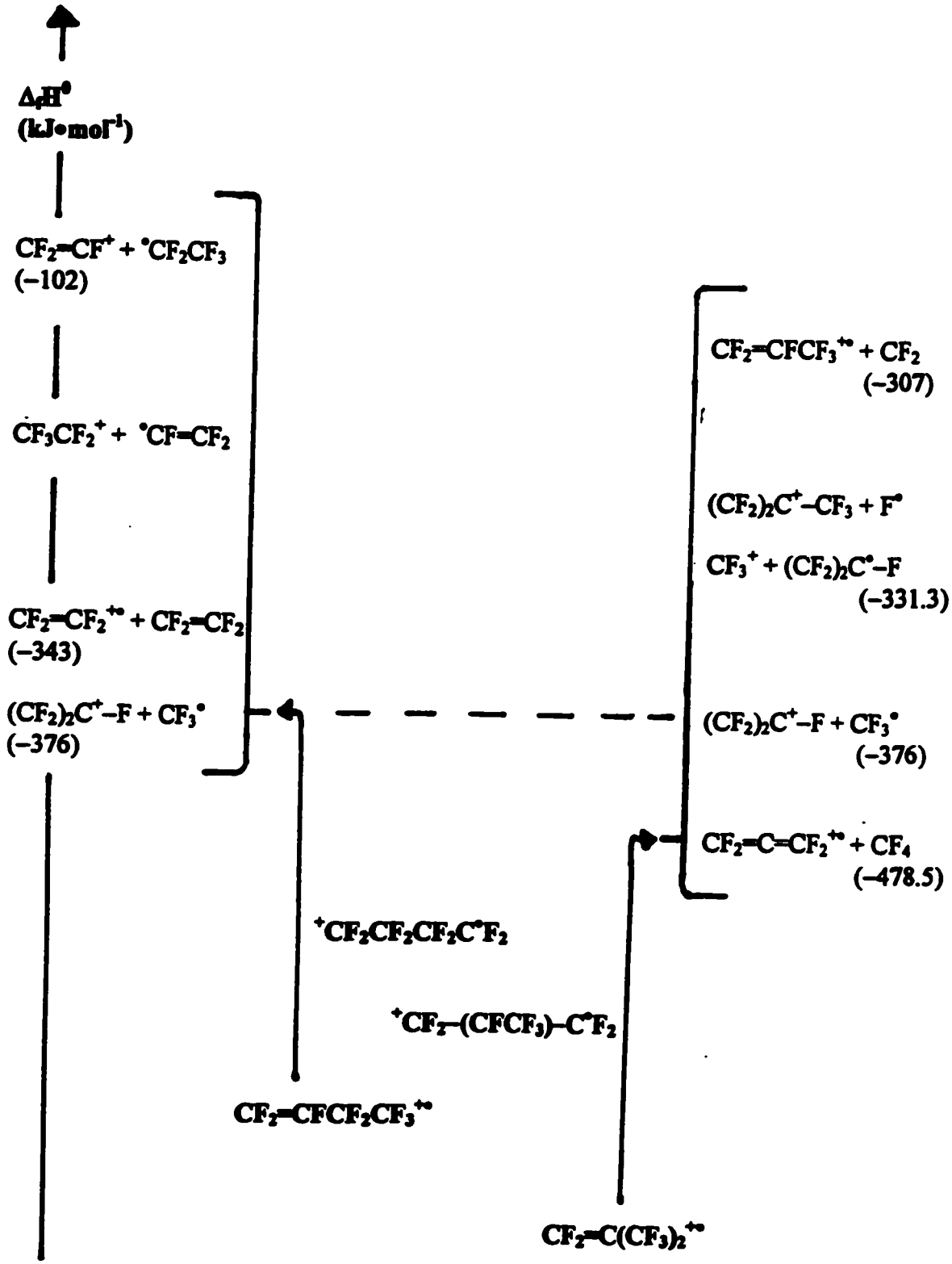

Table 3.12 Metastable Ion (MI) 2FFR and Collision Induced Dissociation (CID) 2FFR He ≈ 90 %T Mass Spectra of Source Generated $C_4F_8^{+\bullet}$ (m/z 200) from the C_4F_9I Isomers

			Parent Ion					
			n-C_4F_9I		s-C_4F_9I		t-C_4F_9I	
	Mass	Neutral	Height (%)		Height (%)		Height (%)	
Species	(m/z)	Loss	MI	CID	MI	CID	MI	CID
$C_4F_7^+$	181	($-F^\bullet$)					4.6	2.0
$C_3F_6^{+\bullet}$	150	($-CF_2$)		<0.3		0.7	2.0	1.3
$C_3F_5^+$	131	($-CF_3^\bullet$)	100.0	100.0	100.0	100.0	6.0	3.3
$C_2F_5^+$	119		0.7	0.7	<0.3	0.7		
$C_3F_4^{+\bullet}$	112	($-CF_4$)		<0.3	<0.3	0.7	100.0	100.0
$C_2F_4^{+\bullet}$	100	($-C_2F_4$)		<0.3		0.7		<0.3
$C_3F_3^+$	93			<0.3		0.7		0.7
$C_2F_3^+$	81			<0.3		<0.3		0.7
$C_3F_2^{+\bullet}$	74			<0.3		<0.3		<0.3
CF_3^+	69	($-C_3F_5^\bullet$)		0.7		0.7	2.0	4.0

Figure 3.12 Metastable Ion (MI) 2FFR Mass Spectra of Source Generated $C_4F_8^{+\bullet}$ (m/z 200) from (a) n-C_4F_9I, (b) s-C_4F_9I, and (c) t-C_4F_9I.

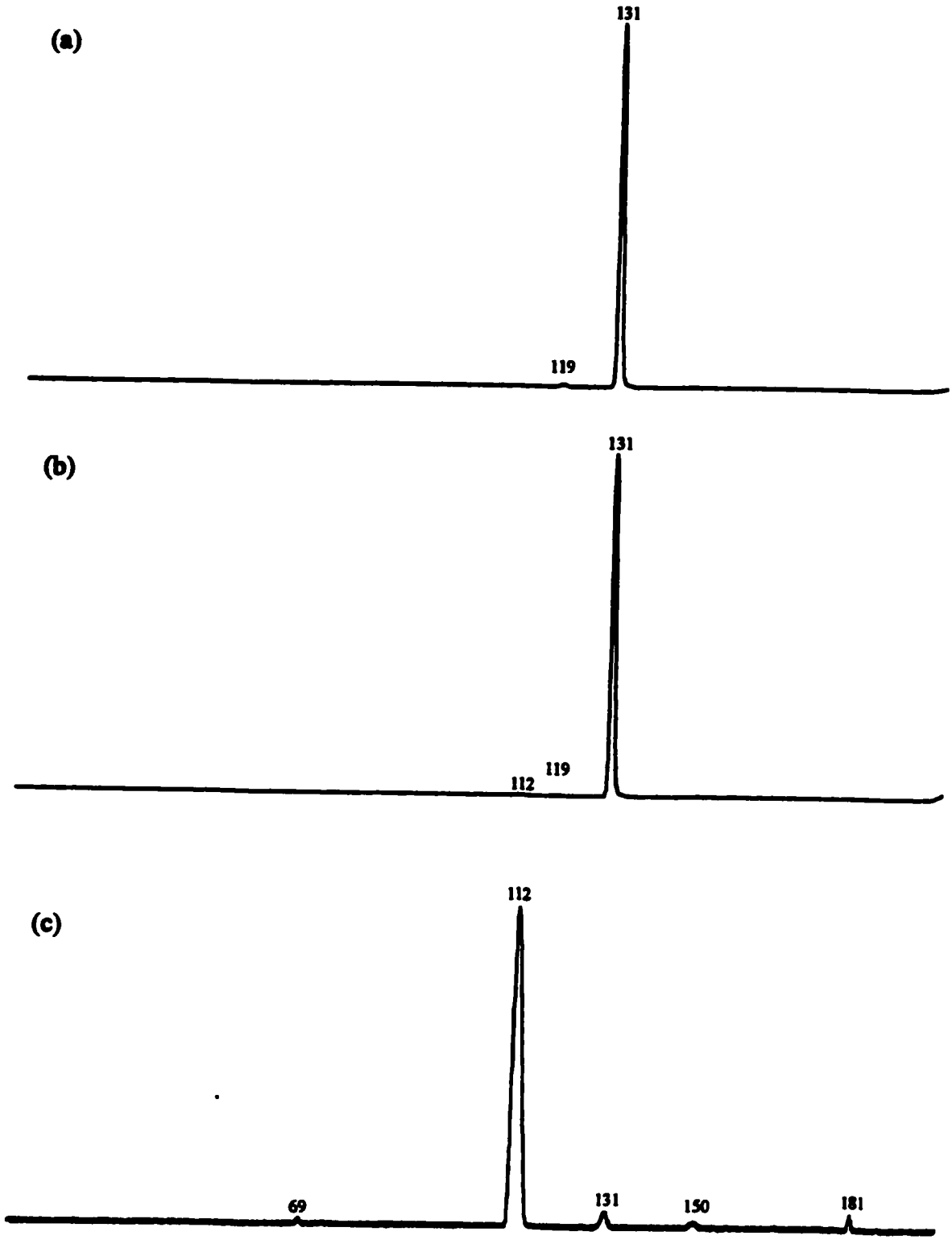

Figure 3.13 Collision Induced Dissociation (CID) 2FFR He ≈ 90 %T Mass Spectra of Source Generated $C_4F_8^{+\bullet}$ (m/z 200) from (a) n-C_4F_9I, (b) s-C_4F_9I, and (c) t-C_4F_9I

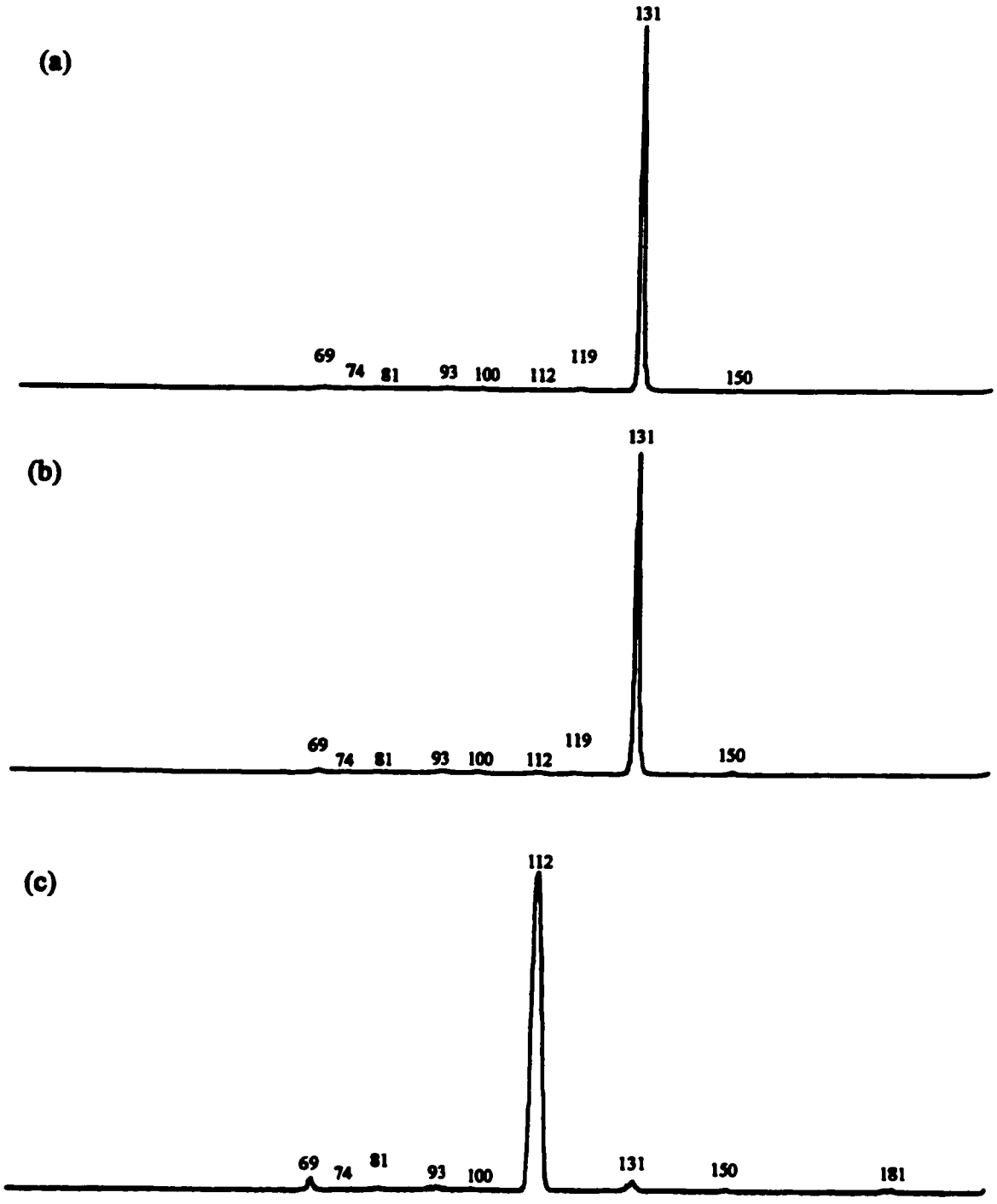

CID mass spectra of the $C_4F_8^{+\bullet}$ isomers are listed in Table 3.12 and illustrated in Figures 3.12 and 3.13.

On inspection of Table 3.12 and Figures 3.12 and 3.13, one may see that the $C_4F_8^{+\bullet}$ ions produced from n-C_4F_9I and s-C_4F_9I are probably similar and may be dominated by the CF_2=$CFCF_2CF_3^{+\bullet}$ isomer. This structure is suggested due to the main MI peak of $(CF_2)_2C^+$–F (m/z 131) and the minor MI peaks of $CF_3CF_2^+$ (m/z 119) and CF_2=C=$CF_2^{+\bullet}$ (m/z 112). The CID 2FFR He ≈ 90 %T mass spectra are also very similar indeed.

The $C_4F_8^{+\bullet}$ ion produced from t-C_4F_9I is clearly different in nature and may be proposed to have a CF_2=$C(CF_3)_2^{+\bullet}$ structure. This structure is suggested due to the main MI peak of CF_2=C=$CF_2^{+\bullet}$ (m/z 112) and the many minor MI peaks of CF_3^+ (m/z 69), $(CF_2)_2C^+$–F (m/z 131), CF_2=$CFCF_3^{+\bullet}$ (m/z 150), and $(CF_2)_2C^+$–CF_3 (m/z 147). This structure clearly possesses a very active potential energy surface with the facile ability to produce two vety stable perfluoroallyl moiety cations, namely $(CF_2)_2C^+$–F and $(CF_2)_2C^+$–CF_3. On review of the proposed energy levels of $C_4F_8^{+\bullet}$ presented in Figure 3.11, such ability is not surprising.

$C_4F_9^+$ (m/z 219)

These isomeric fragment ions are generated by $I^\bullet$ loss from the n-$C_4F_9I^{+\bullet}$ and s-$C_4F_9I^{+\bullet}$ parent-ions and by $(CF_3)_3C^\bullet$ loss from the $(CF_3)_3C$–$C(CF_3)_3^{+\bullet}$ parent-ion. As per the discussion in Section 3.2, the Δ_fH^0 values of the $C_4F_9^+$ isomers are very likely of similar value and may even possess a *reversed* order of stability with respect to the hydrogen analogues. Thus, the stability order is proposed to be as follows; $CF_3CF_2CF_2CF_2^+$ > $CF_3CF_2C^+FCF_3$ > $(CF_3)_2CFCF_2^+$ > $(CF_3)_3C^+$. The proposed energy levels of the $C_4F_9^+$ isomers are illustrated in Figure 3.14. As listed in Table 3.8, the kinetic energy release, $T_{0.5}$,

Figure 3.14 Proposed Energy Levels of the $C_4F_9^+$ (m/z 219) Isomers

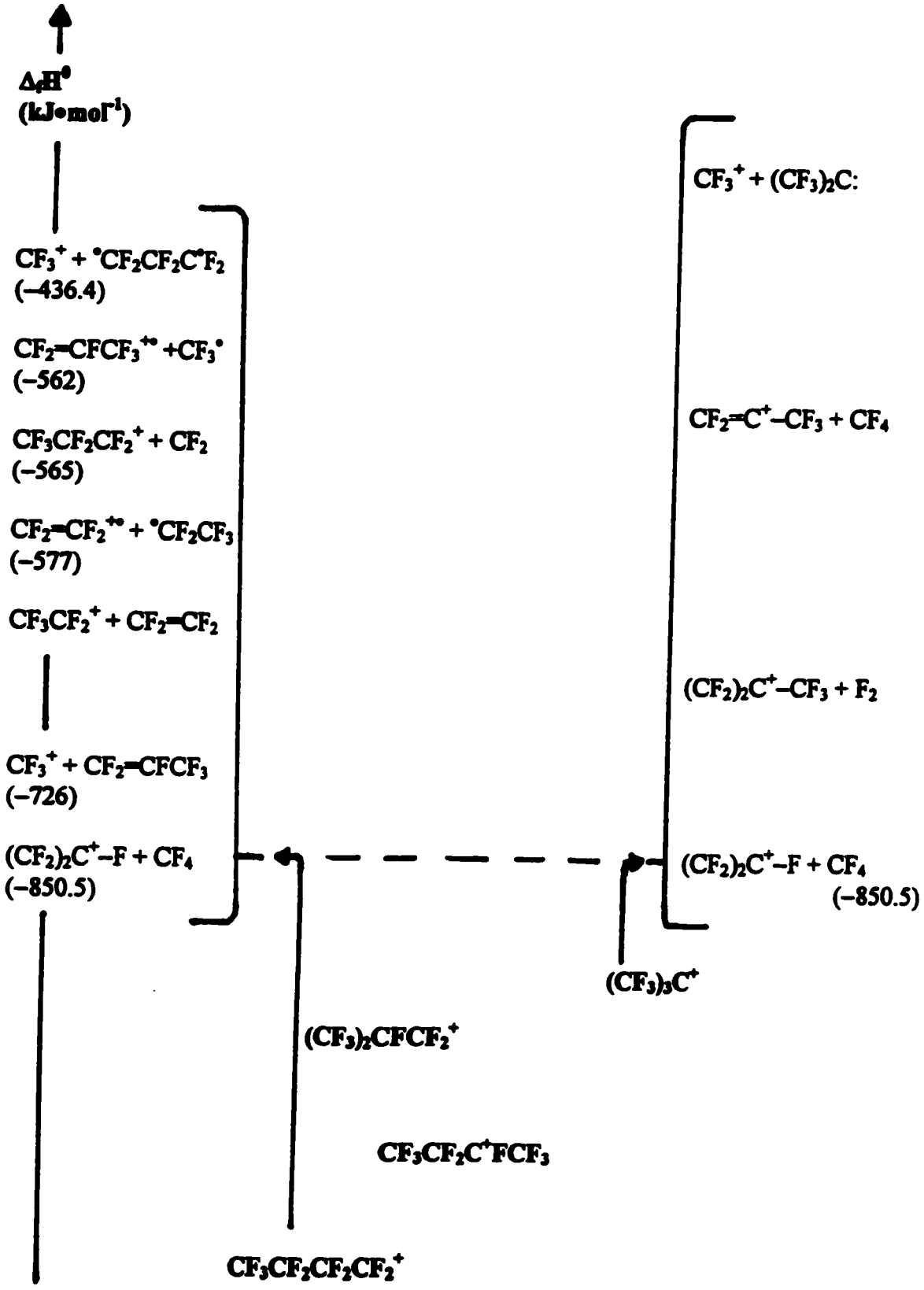

Table 3.13 Metastable Ion (MI) 2FFR and Collision Induced Dissociation (CID) 2FFR He ≈ 90 %T Mass Spectra of Source Generated $C_4F_9^+$ (m/z 219) from the C_4F_9I Isomers

			Parent Ion					
			n-C_4F_9I		s-C_4F_9I		$(CF_3)_3C$–$C(CF_3)_3$	
	Mass	Neutral	Height (%)		Height (%)		Height (%)	
Species	(m/z)	Loss	MI	CID	MI	CID	MI	CID
$C_4F_7^+$	181	($-F_2$)					2.0	2.0
$C_3F_7^+$	169	($-CF_2$)		3.3		0.7		
$C_3F_6^{+\bullet}$	150	($-CF_3^\bullet$)		3.0		0.7		2.0
$C_3F_5^+$	131	($-CF_4$)	100.0	100.0	100.0	100.0	100.0	100.0
$C_2F_5^+$	119	($-C_2F_4$)		7.9		1.3		
$C_3F_4^{+\bullet}$	112			<0.3				
$C_2F_4^{+\bullet}$	100			13.2		2.0		1.3
$C_3F_3^+$	93			1.3		<0.3		
$C_2F_3^+$	81			0.7				
$C_3F_2^{+\bullet}$	74			<0.3				
CF_3^+	69	($-C_3F_6$)	8.3	43.0	5.3	10.6	3.0	3.0
$CF_2^{+\bullet}$	50			<0.3				

Figure 3.15 Metastable Ion (MI) 2FFR Mass Spectra of Source Generated $C_4F_9^+$ (m/z 219) from (a) n-C_4F_9I, (b) s-C_4F_9I, and (c) $(CF_3)_3C–C(CF_3)_3$.

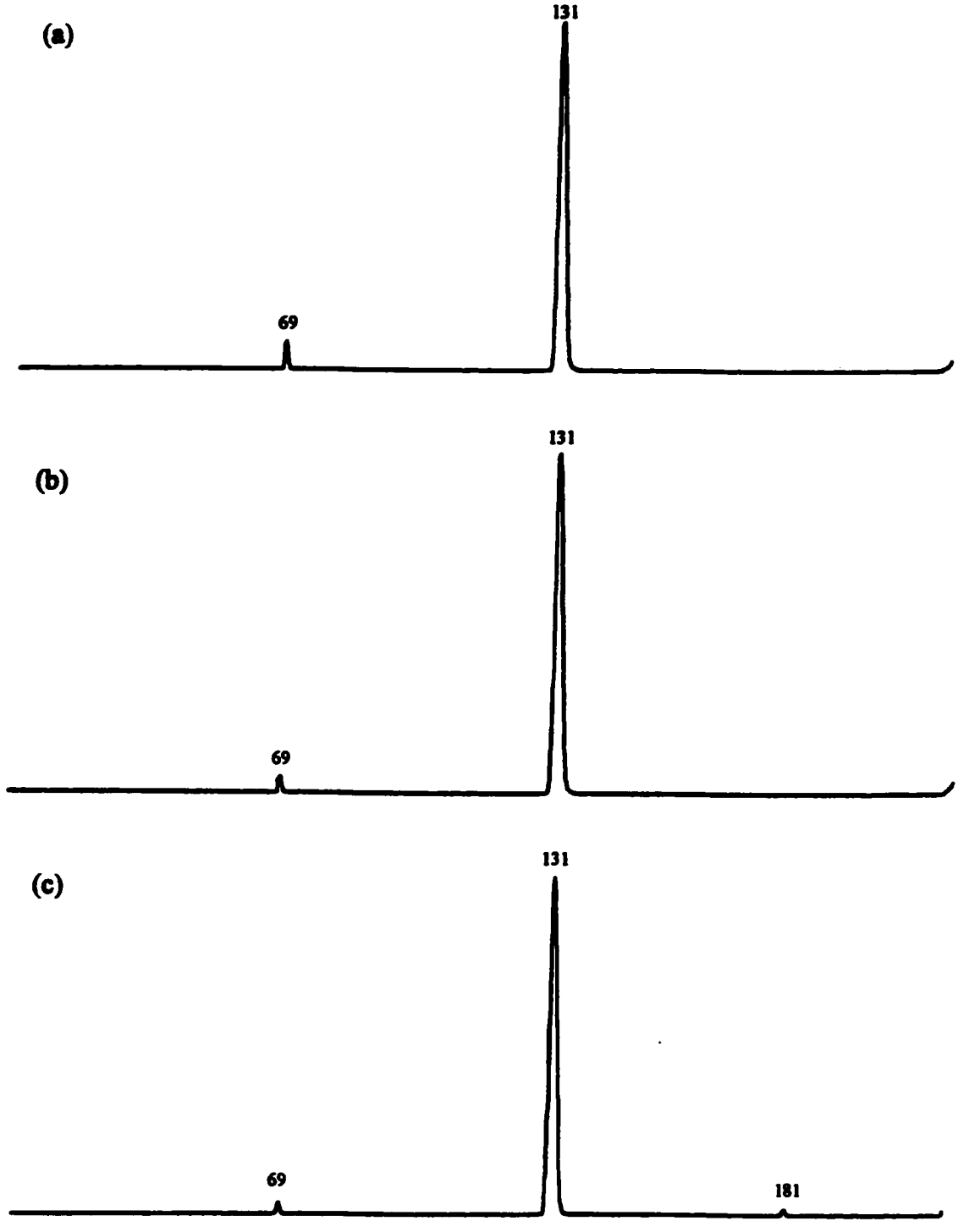

Figure 3.16 Collision Induced Dissociation (CID) 2FFR He ≈ 90 %T Mass Spectra of Source Generated $C_4F_9^+$ (m/z 219) from (a) n-C_4F_9I, (b) s-C_4F_9I, and (c) $(CF_3)_3C–C(CF_3)_3$.

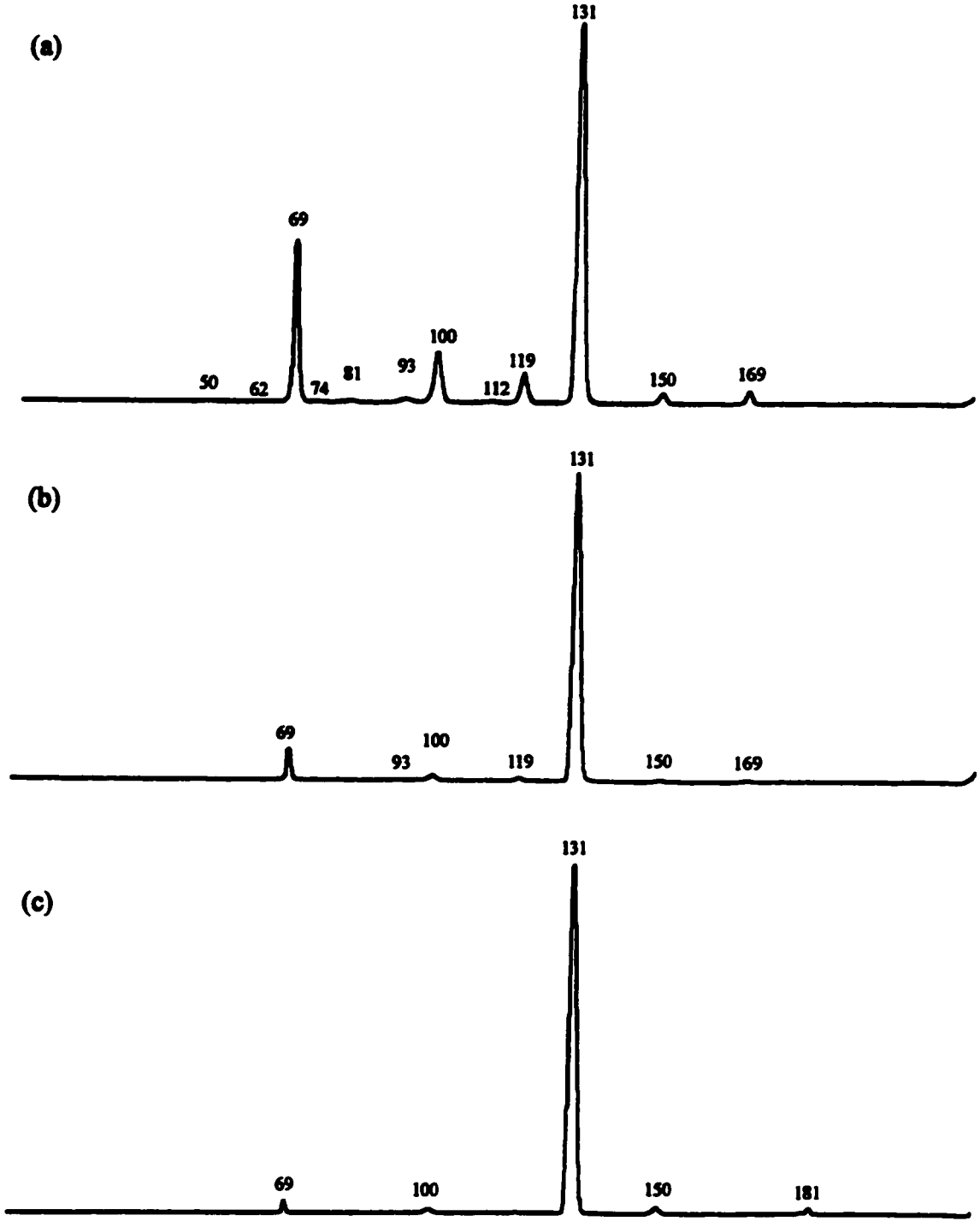

measurements for the metastably generated $CF_3CF_2CF_2CF_2^+$ and $CF_3CF_2C^+FCF_3$ isomers undergoing the unimolecular metastable dissociation of $(CF_2)_2C^+–F + CF_4$ have $T_{0.5}$ values of 150 and 152 meV, respectively, indicative of an identical process. However, the $(CF_3)_3CI^{+\bullet}$ isomer proved *not* to be a source of metastably generated $(CF_3)_3C^+$. The only practical precursor of the $(CF_3)_3C^+$ cation proved to be $(CF_3)_3C–C(CF_3)_3$. The normal mass spectrum of $(CF_3)_3C–C(CF_3)_3^{+\bullet}$ consisted of the following peaks CF_3^+ (m/z 69), $C_3F_5^+$ (m/z 131), and $C_4F_9^+$ (m/z 219) with intensities of 47.7 %, 100.0 %, and 43.0 %, respectively. Unfortunately, the molecular ion $C_8F_{18}^{+\bullet}$ (m/z 438) was *not* observed. As listed in Table 3.8, the source generated $(CF_3)_3C^+$ cation which undergoes the unimolecular metastabledissociation of $(CF_2)_2C^+–F + CF_4$ has a $T_{0.5}$ value of 140 meV. Therefore, within experimental limits all of the three isomers, n-$C_4F_9^+$, s-$C_4F_9^+$, and t-$C_4F_9^+$ possess the same $T_{0.5}$ value for CF_4 loss and thus they undergo the same unimolecular metastable dissociation process.

The peak intensities of the MI and CID mass spectra of the $C_4F_9^+$ isomers are listed in Table 3.13 and illustrated in Figures 3.15 and 3.16. On inspection of Table 3.13 and Figures 3.15 and 3.16, one may see that the $C_4F_9^+$ ions produced from n-$C_4F_9I^{+\bullet}$, s-$C_4F_9I^{+\bullet}$ and $(CF_3)_3C–C(CF_3)_3^{+\bullet}$ may possess their own unique potential wells for the $CF_3CF_2CF_2CF_2^+$, $CF_3CF_2C^+FCF_3$, $(CF_3)_3C^+$ isomers, respectively. Although the MI and CID mass spectra for the $CF_3CF_2CF_2CF_2^+$ and $CF_3CF_2C^+FCF_3$ are similar, their potential wells though close in energy are most probably unique. This suggestion is supported by the notably higher CID peak intensities for $(CF_3^+ + {}^\bullet CF_2CF_2CF_2{}^\bullet)$, $(CF_2{=}CF_2^{+\bullet} + {}^\bullet CF_2CF_3)$ and $(CF_3CF_2^+ + CF_2{=}CF_2)$ processes for $CF_3CF_2CF_2CF_2^+$, with respect to possible corresponding $(CF_3^+ +$

CF_2=$CFCF_3$), (CF_3CF^+ + $^{\bullet}CF_2CF_3$) and ($CF_3CF_2^+$ + $CF_3\check{C}F$) processes for $CF_3CF_2C^+FCF_3$, respectively.

As well, on inspection of the MI and CID mass spectra of $C_4F_9^+$ produced from $(CF_3)_3C$–$C(CF_3)_3^{+\bullet}$ via $(CF_3)_3C^{\bullet}$ loss is clearly of a different nature and most likely has the structure of the $(CF_3)_3C^+$ isomer. This structure is supported by the presence in both the MI and CID mass spectra of the $(CF_2)_2C^+$–CF_3 (m/z 181) cation (i.e., F_2 loss) and the complete *absence* of the $C_3F_7^+$ (m/z 169) and $C_2F_5^+$ (m/z 119) cations (i.e., CF_2 loss and C_2F_4 loss, respectively). Thus, in summary although there is likely to be some degree of communication between the $CF_3CF_2CF_2CF_2^+$ and $CF_3CF_2C^+FCF_3$ isomers, it appears that each of the $CF_3CF_2CF_2CF_2^+$, $CF_3CF_2C^+FCF_3$, and $(CF_3)_3C^+$ may possess their own distinct potential wells and can retain their respective structures.

3.4 Perfluoropropyl Iodides C_3F_7I

There are two known C_3F_7I isomeric neutral compounds, namely $CF_3CF_2CF_2I$, and $(CF_3)_2CFI$, and are called 1-iodoperfluoropropane (n-C_3F_7I), and 2-iodoperfluoropropane (s-C_3F_7I), respectively. On inspection of their structure, one may immediately view the $CF_3CF_2CF_2I$, and $(CF_3)_2CFI$ isomers as being composed of two basic component groups, namely CF_2=$CFCF_3$ and FI. Thus, qualitatively the dissociation characteristics of these C_3F_7I isomers may be dictated by the interplay of the thermochemistry of the CF_2=$CFCF_3$ + FI pair. All the relevant Δ_fH^0 ($kJ \bullet mol^{-1}$) values of the neutral C_3F_7I isomers have been tabulated in Table 3.4.

One will now discuss the gas-phase ion-chemistry of the cationic manifold of the C_3F_7I isomers. The relevant cations that will be discussed here are the following; the parent $C_3F_7I^{+\bullet}$ (m/z 296) radical-cation, and the fragment ions $C_3F_6I^+$ (m/z 277), $C_2F_4I^+$ (m/z 227), $C_3F_7^+$ (m/z 169),and lastly the perfluoroallylic $C_3F_5^+$ (m/z 131) species.

$C_3F_7I^{+\bullet}$ (m/z 296)

As per the previous discussion that centred on the perfluorobutyl iodides C_4F_9I and their fragmentation products, one will now turn the discussion towards the related perfluoropropyl iodide species C_3F_7I. The three cationic isomers that will be discussed here are $CF_3CF_2CF_2I^{+\bullet}$, $(CF_3)_2CFI^{+\bullet}$, and $(c\text{-}C_3F_6I^+)\bullet(F^\bullet)$. The latter species is proposed to be an ion-molecule complex composed of a four-membered cyclic moiety, c-$C_3F_6I^+$, (with the positive charge on the I atom) electrostatically associated with $F^\bullet$. Thus $(c\text{-}C_3F_6I^+)\bullet(F^\bullet)$ is proposed to act as an intermediary between $CF_3CF_2CF_2I^{+\bullet}$ and $(CF_3)_2CFI^{+\bullet}$. Such species as

$(c\text{-}C_3F_6I^+)\bullet(F^\bullet)$ generally possess significant association energies of at least on the order of ≈ 42 $kJ\bullet mol^{-1}$. However, with the $F^\bullet$ species as a participant, the association energy of the $(c\text{-}C_3F_6I^+)\bullet(F^\bullet)$ species may even be greater in magnitude. It should be remembered that the neutral counterpart, $(c\text{-}C_3F_6I^\bullet)\bullet(F^\bullet)$ should exist only as a (physically bound) Van der Waals complex with an association energy of ≈ 1 $kJ\bullet mol^{-1}$ (i.e., an extremely weakly associated neutral species).

As per the previous discussion of section 3.2, the proposed order of stability of the $C_3F_7I^{+\bullet}$ isomers is as follows; $(CF_3)_2CFI^{+\bullet} > CF_3CF_2CF_2I^{+\bullet} > (c\text{-}C_3F_6I^+)\bullet(F^\bullet)$. The proposed energy levels of the $C_3F_7I^{+\bullet}$ isomers are illustrated in Figure 3.17. The peak intensities of the normal mass spectra of the $C_3F_7I^{+\bullet}$ isomers are listed in Table 3.14 and illustrated in Figure 3.18. The kinetic energy release, $T_{0.5}$, measurements of the $C_3F_7I^{+\bullet}$ isomers are listed in Table 3.15. The peak intensities of the MI and CID mass spectra of the $C_3F_7I^{+\bullet}$ isomers are listed in Table 3.16, and illustrated in Figures 3.19, and 3.20, respectively.

On inspection of Table 3.14 and Figure 3.18, one may note the following points on the normal mass spectra of the $C_3F_7I^{+\bullet}$ isomers. In the case of the $CF_3CF_2CF_2I^{+\bullet}$ isomer, the main peaks of interest with the following intensities are 96.0 %, 49.7 %, 100.0 %, 43.4 %, and 92.1 %, corresponding to the CF_3^+ (m/z 69), I^+ (m/z 127), $CF_3CF_2CF_2^+$ (m/z 169), CF_2I^+ (m/z 177), and $CF_3CF_2CF_2I^{+\bullet}$ (m/z 296) ions, respectively. Now in the case of the $(CF_3)_2CFI^{+\bullet}$ isomer, the corresponding peaks of interest possess the following intensities 50.3 %, 23.8 %, 13.9 %, 10.6 %, and 100.0 % for the CF_3^+ (m/z 69), I^+ (m/z 127), $(CF_3)_2CF^+$ (m/z 169), CF_2I^+ (m/z 177), and $(CF_3)_2CFI^{+\bullet}$ (m/z 296) ions, respectively. It is interesting to note the drop in peak intensity of $CF_3CF_2CF_2^+$ from 100.0 % to that of 13.9 % for $(CF_3)_2CF^+$, which is in agreement with the discussion of section 3.2.

Figure 3.17 Proposed Energy Levels of the $C_3F_7I^{+\bullet}$ (m/z 296) Isomers

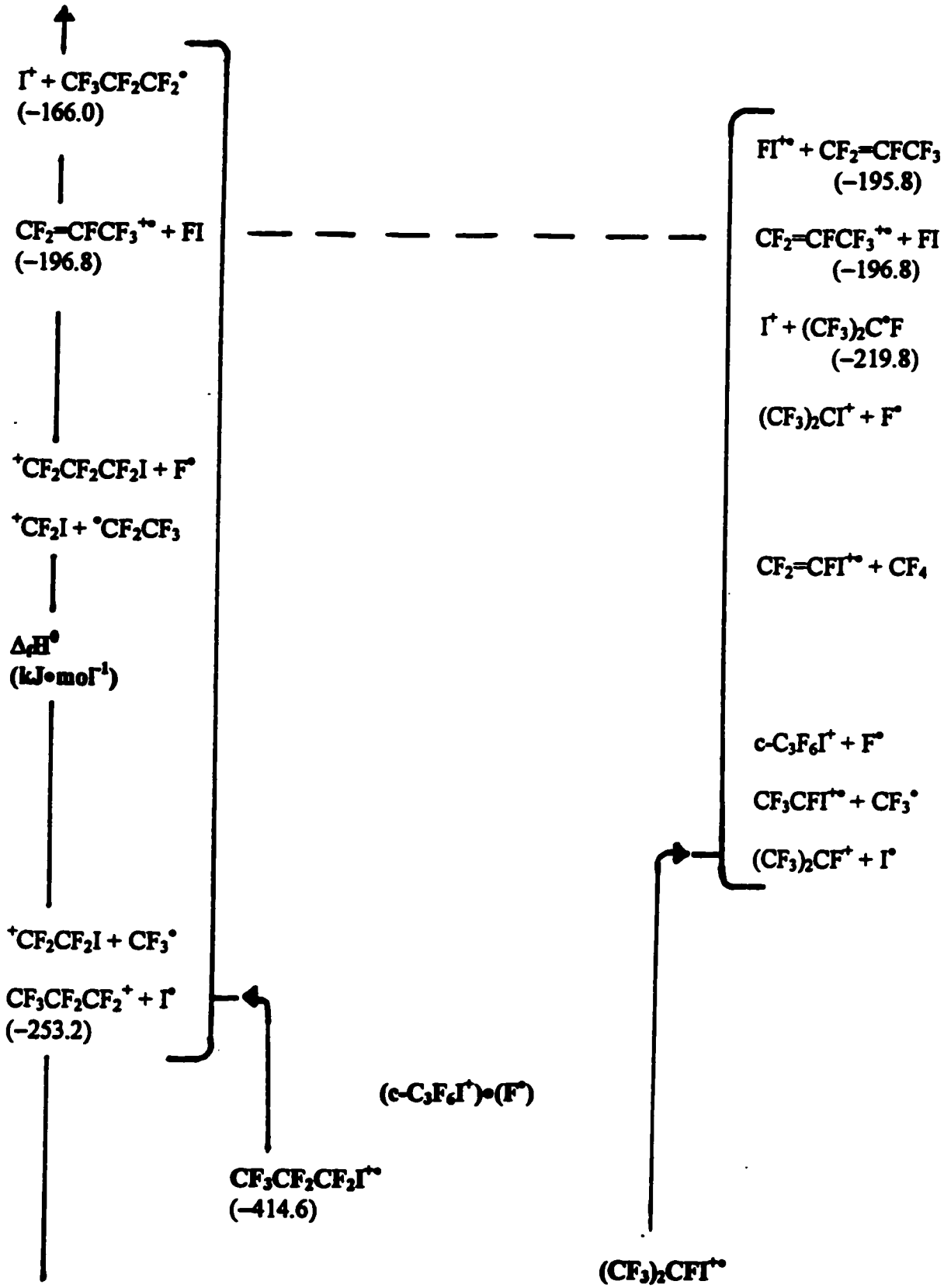

Table 3.14 Normal Mass Spectra of the C_3F_7I Isomers

Species	Mass (m/z)	Neutral Loss	Parent Ion n-C_3F_7I Height (%)	Parent Ion s-C_3F_7I Height (%)
$C_3F_7I^{+\bullet}$	296		92.1	100.0
$C_3F_6I^+$	277	($-F^\bullet$)	10.3	14.6
$C_3F_5I^{+\bullet}$	258	($-F_2$)		0.7
$C_2F_5I^{+\bullet}$	246	($-CF_2$)		<0.3
$C_3F_4I^+$	239			<0.3
$C_2F_4I^+$	227	($-CF_3^\bullet$)	2.6	4.3
$C_2F_3I^{+\bullet}$	208	($-CF_4$)	5.6	1.3
CF_2I^+	177	($-C_2F_5^\bullet$)	43.4	10.6
$C_3F_7^+$	169	($-I^\bullet$)	100.0	13.9
$CFI^{+\bullet}$	158		5.3	1.3
$FI^{+\bullet}$	146	($-C_3F_6$)	11.3	11.3
$C_3F_5^+$	131		17.2	14.6
I^+	127	($-C_3F_7^\bullet$)	49.7	23.8
$C_2F_5^+$	119		17.2	5.6
$C_3F_4^{+\bullet}$	112			1.3
$C_2F_4^{+\bullet}$	100		39.1	13.9
$C_3F_3^+$	93		2.3	2.0
$C_2F_3^+$	81		1.3	0.7
$C_3F_2^{+\bullet}$	74		0.7	<0.3
$CF_3^{+\bullet}$	69		96.0	50.3
$C_2F_2^{+\bullet}$	62		1.3	<0.3
$CF_2^{+\bullet}$	50		7.3	0.7
CF^+	31		21.2	6.6

Figure 3.18 Normal Mass Spectra of (a) $CF_3CF_2CF_2I$ (n-C_3F_7I) and (b) $(CF_3)_2CFI$ (s-C_3F_7I) ; $C_3F_7I^{+\bullet}$ (m/z 296) Isomers

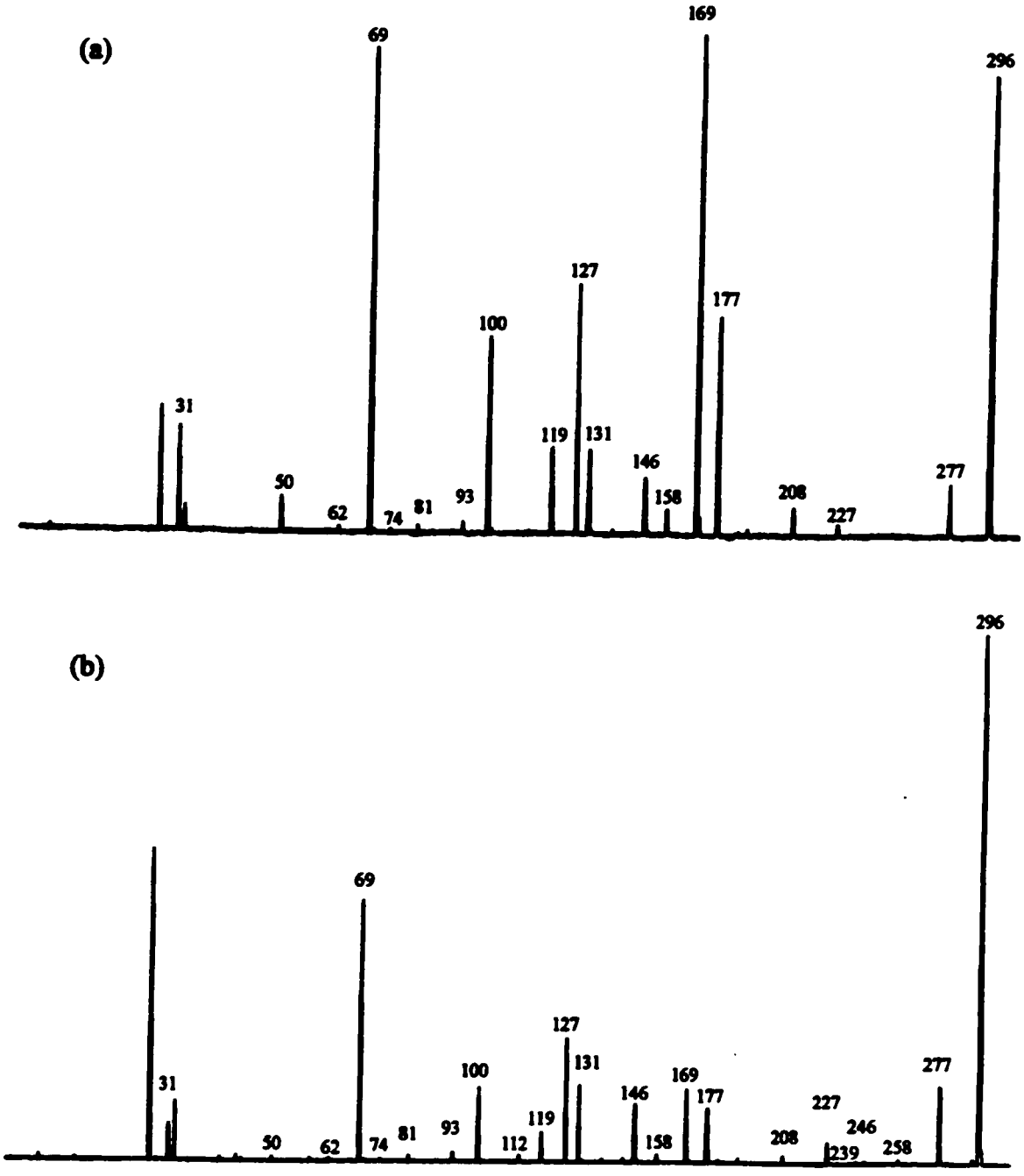

Table 3.15 Kinetic Energy Release $T_{0.5}$ Measurements of C_3F_7I Isomers

Mass (m/z)	Dissociation Process	Kinetic Energy Release, $T_{0.5}$ (meV)	Collision Sensitivity[b]
$CF_3CF_2CF_2I$			
(296 → 169)	$CF_3CF_2CF_2I^{+\bullet} \rightarrow CF_3CF_2CF_2^+ + I^\bullet$	9.1	2
(277 → 177)	$c\text{-}C_3F_6I^+ \rightarrow CF_2I^+ + CF_2{=}CF_2$	15.9	1.1
(277 → 131)	$c\text{-}C_3F_6I^+ \rightarrow (CF_2)_2C^+{-}F + FI$	17.4	1.1
(169 → 69)	$CF_3CF_2CF_2^+ \rightarrow CF_3^+ + CF_2{=}CF_2$	12.2	6.0
(131 → 69)	$(CF_2)_2C^+{-}F \rightarrow CF_3^+ + FC{\equiv}CF$	31.0	3.3
$(CF_3)_2CFI$			
(296 → 277)	$(CF_3)_2CFI^{+\bullet} \rightarrow c\text{-}C_3F_6I^+ + F^\bullet$	–[a]	17
(296 → 227)	$(CF_3)_2CFI^{+\bullet} \rightarrow C_2F_4I^+ + CF_3^\bullet$	11.3	28
(296 → 169)	$(CF_3)_2CFI^{+\bullet} \rightarrow (CF_3)_2CF^+ + I^\bullet$	15.8	10
(277 → 177)	$c\text{-}C_3F_6I^+ \rightarrow CF_2I^+ + CF_2{=}CF_2$	16.8	1.2
(277 → 131)	$c\text{-}C_3F_6I^+ \rightarrow (CF_2)_2C^+{-}F + FI$	16.6	1.2
(169 → 69)	$(CF_3)_2CF^+ \rightarrow CF_3^+ + CF_2{=}CF_2$	13.0	1.5
(131 → 69)	$(CF_2)_2C^+{-}F \rightarrow CF_3^+ + FC{\equiv}CF$	29.0	3.0

[a]Too weak to measure, [b]Peak Height Increase (Collision Gas/ No Gas) with Δ relative to 2×10^{-7} Torr for He collision gas.

Table 3.16 Metastable Ion (MI) 2FFR and Collision Induced Dissociation (CID) 2FFR He ≈90 %T Mass Spectra of the $C_3F_7I^{+\bullet}$ (m/z 296) Isomers

			Parent Ion			
			n-C_3F_7I		s-C_3F_7I	
	Mass	Neutral	Height (%)		Height (%)	
Species	(m/z)	Loss	MI	CID	MI	CID
$C_3F_6I^+$	277	($-F^\bullet$)			–[a]	<0.3
$C_3F_5I^{+\bullet}$	258	($-F_2$)				<0.3
$C_3F_4I^+$	239					<0.3
$C_2F_4I^+$	227	($-CF_3^\bullet$)		<0.3	4.6	10.6
$C_2F_3I^{+\bullet}$	208	($-CF_4$)		<0.3		1.3
$C_2F_2I^+$	189					0.7
CF_2I^+	177	($-C_2F_5^\bullet$)		1.3		5.3
$C_3F_7^+$	169	($-I^\bullet$)	100.0	100.0	100.0	100.0
$CFI^{+\bullet}$	158			0.7		1.3
$C_3F_6^{+\bullet}$	150			<0.3		2.0
$FI^{+\bullet}$	146	($-C_3F_6$)				0.7
CI^+	139					0.7
$C_3F_5^+$	131					1.3
I^+	127	($-C_3F_7^\bullet$)		2.0		9.3
$C_2F_5^+$	119			0.7		1.3
$C_3F_4^{+\bullet}$	112					0.7
$C_2F_4^{+\bullet}$	100			0.7		4.6
$C_3F_3^+$	93					<0.3
$C_2F_3^+$	81					<0.3
CF_3^+	69			2.3		6.6

[a]Very weak.

Figure 3.19 Metastable Ion (MI) 2FFR Mass Spectra of (a) $CF_3CF_2CF_2I$ (n-C_3F_7I) and (b) $(CF_3)_2CFI$ (s-C_3F_7I); $C_3F_7I^{+\bullet}$ (m/z 296) Isomers

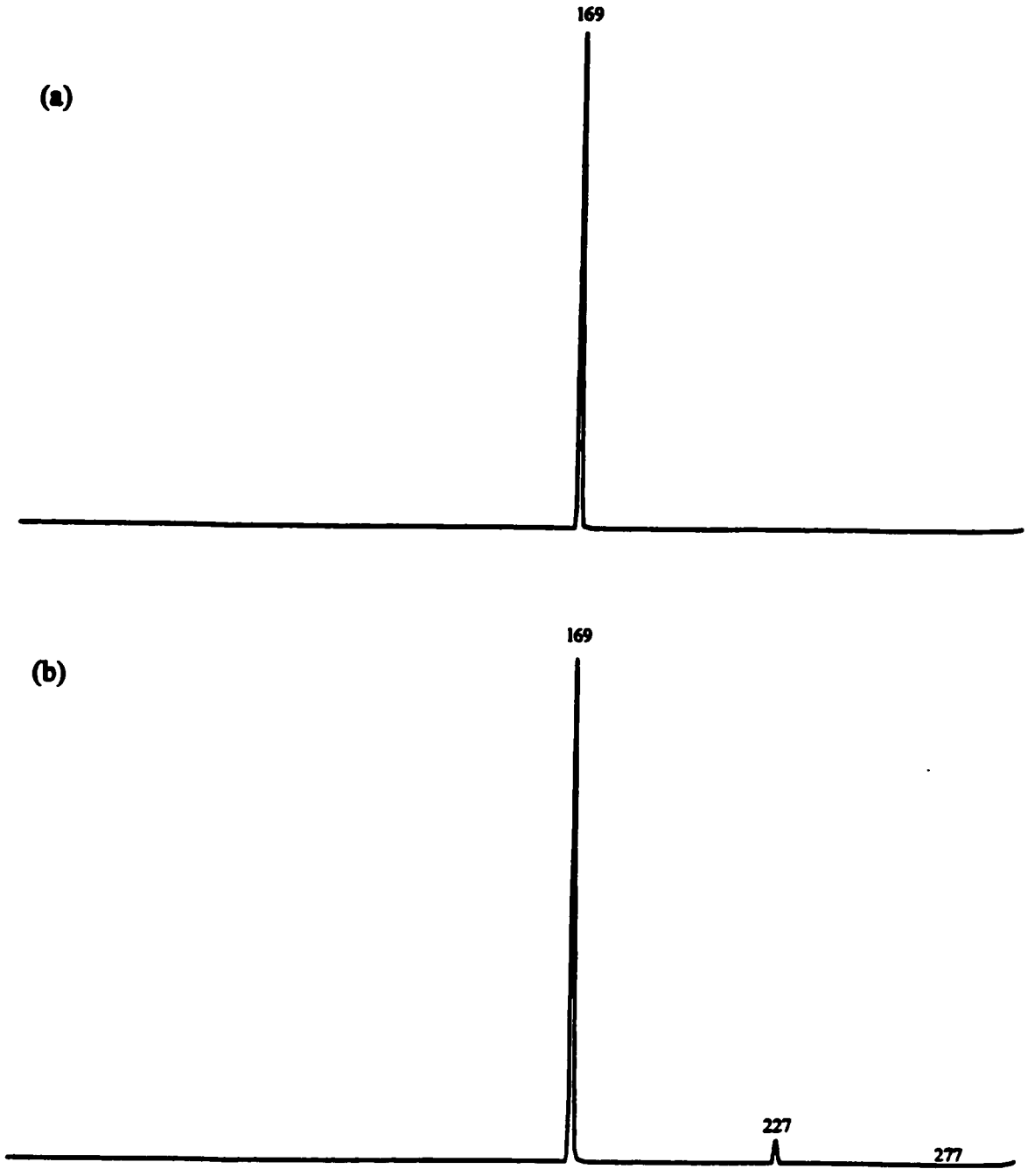

Figure 3.20 Collission Induced Dissociation (CID) 2FFR He ≈ 90 %T Mass Spectra of (a) $CF_3CF_2CF_2I$ (n-C_3F_7I) and (b) $(CF_3)_2CFI$ (s-C_3F_7I); $C_3F_7I^{+\bullet}$ (m/z 296) Isomers

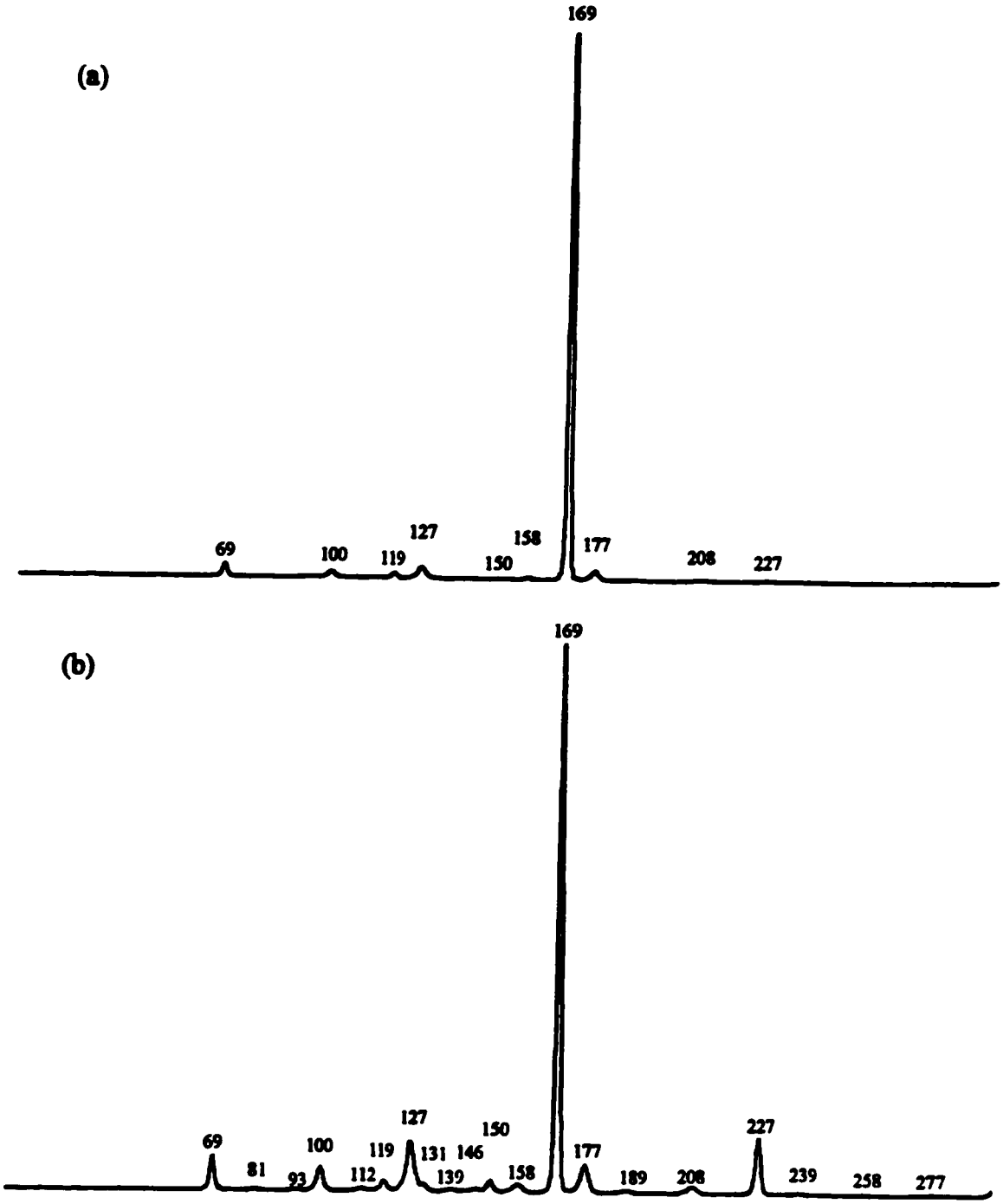

On inspection of the $T_{0.5}$ measurements listed in Table 3.15, one may see immediately the differences between the $CF_3CF_2CF_2I^{+\bullet}$ and $(CF_3)_2CFI^{+\bullet}$ isomers. Whereas the former isomer possesses only one unimolecular metastable dissociation process, namely $CF_3CF_2CF_2I^{+\bullet} \rightarrow CF_3CF_2CF_2^{+} + I^{\bullet}$, the latter isomer possesses three unimolecular metastable dissociation processes as follows, $(CF_3)_2CFI^{+\bullet} \rightarrow c\text{-}C_3F_6I^{+} + F^{\bullet}$, $(CF_3)_2CFI^{+\bullet} \rightarrow CF_3CFI^{+} + CF_3^{\bullet}$, $(CF_3)_2CFI^{+\bullet} \rightarrow (CF_3)_2CF^{+} + I^{\bullet}$. Furthermore, the fourth column of Table 3.15 lists the collision sensitivities of the dissociation routes. The collision sensitivity of a peak is defined as the peak height increase on the introduction of a collision gas in the collision cell relative to its peak height without any collision gas present (under the agreed upon reproducible collision gas pressure, see footnote of Table 3.15). The useful experimental aid this measurement provides is it is generally accepted that a *collision insensitive MI peak* has communication with and/or undergoes a *rearrangement* prior to reaching the dissociation limit. Whereas, in contrast a very *collision sensitive MI peak* is generally thought to be indicative of a *direct unrearranged path* (i.e., a simple bond cleavage) to reach the dissociation limit.

Thus, on inspection of Table 3.15 one may note the following trends. Firstly, in the $CF_3CF_2CF_2I^{+\bullet}$ case, the only MI process possesses a small $T_{0.5}$ value of 9.1 meV but is relativelv collision insensitive. Thus, on one hand one would predict a simple C–I bond cleavage (i.e., due to the low $T_{0.5}$ value), and on the other hand one would expect the dissociating species $C_3F_7I^{+\bullet}$ to be in communication with with or rearranging to another species prior to reaching the dissociation limit of $CF_3CF_2CF_2^{+} + I^{\bullet}$. As will be discussed shortly, it is believed that the $CF_3CF_2CF_2I^{+\bullet}$ and $(CF_3)_2CFI^{+\bullet}$ isomers each possess their own independent potential wells in which they live. The communication between these two

potential wells is proposed to be facilitated via the intermediate $(c\text{-}C_3F_6I^+)\bullet(F^\bullet)$ ion-molecule complex. Thus, if one propose that such an interaction is the case, then one may suggest that the $CF_3CF_2CF_2I^{+\bullet}$ isomer is in communication with the $(c\text{-}C_3F_6I^+)\bullet(F^\bullet)$ species en-route to the $CF_3CF_2CF_2^+ + I^\bullet$ dissociation limit.

The second case of the $(CF_3)_2CFI^{+\bullet}$ isomer is somewhat different. On inspection of Table 3.15 one may see that the $(CF_3)_2CFI^{+\bullet}$ isomer possesses a slightly larger $T_{0.5}$ value of 15.8 meV, but is very collision sensitive for the $(CF_3)_2CF^+ + I^\bullet$ dissociation process. Thus, one may propose a direct C–I bond cleavage. This may then result in the production of $(CF_3)_2CF^+ + I^\bullet$ that is accompanied by a concomitant communication between the $CF_3CF_2CF_2^+$ and the $(CF_3)_2CF^+$ isomers creating a mixture of a portion of their populations (i.e., $(CF_3)_2CF^+$ is mainly produced with a small amount of $CF_3CF_2CF_2^+$). Additionally, there are two other unimolecular dissociation routes for the $(CF_3)_2CFI^{+\bullet}$ isomer. On review of their high collision sensitivities and $T_{0.5}$ values, one may propose the isomerization of $(CF_3)_2CFI^{+\bullet}$ to $(c\text{-}C_3F_6I^+)\bullet(F^\bullet)$ prior to $F^\bullet$ loss; and the direct bond cleavage of $(CF_3)_2CFI^{+\bullet}$ to produce CF_3CFI^+ during $CF_3^\bullet$ loss, respectively.

For the sake of clarity, the other MI dissociations listed in Table 3.15 will be discussed fully here and later referred back to in the following sections for the particular cationic species. The next MI dissociations of interest for the source generated $c\text{-}C_3F_6I^+$ species are the following $CF_2I^+ + CF_2{=}CF_2$, and $(CF_2)_2C^+{-}F + FI$. One may note that regardless of the $n\text{-}C_3F_7I$ or $s\text{-}C_3F_7I$ precursor, the $c\text{-}C_3F_6I^+$ species undergoes rearrangements in both MI processes due to their common $T_{0.5}$ values (i.e., all $\approx$ 16.5 meV) and their collision insensitivities.

Next on consideration of the behaviour of the source generated $C_3F_7^+$ species, one may note their precursor dependant behaviour. In the case of the $C_3F_7^+$ ion produced from $CF_3CF_2CF_2I^{+\bullet}$, it is most likely that $CF_3CF_2CF_2^+$ is produced. This is based on the $T_{0.5}$ value (i.e., ≈ 12 meV) and the strong collision sensitivity of the $CF_3CF_2CF_2^+ \rightarrow CF_3^+ + CF_2{=}CF_2$ dissociation process. In the case of $C_3F_7^+$ ion produced from $(CF_3)_2CFI^{+\bullet}$, it is most likely dominated by the $(CF_3)_2CF^+$ isomer. This is based on the a similar $T_{0.5}$ value (i.e., ≈ 12 meV) and a weak collision in the $(CF_3)_2CF^+ \rightarrow CF_3^+ + CF_2{=}CF_2$ dissociation process (i.e., an indication of a rearrangement). These observations may lead one to propose the participation of a third species, a cyclic c-$C_3F_7^+$ isomer, composed of a $CF_2CF_2CF_2$ moiety bridged by an F^+ ion, closing the four-membered ring. Such a c-$C_3F_7^+$ species (or transition state) may act act as an intermediary between the $CF_3CF_2CF_2I^{+\bullet}$ and $(CF_3)_2CFI^{+\bullet}$ isomers.

Lastly, one may now turn to the source generated $C_3F_5^+$ species produced from the C_3F_7I isomers. On inspection of the common $T_{0.5}$ values (i.e., ≈ 30 meV) and relative collision insensitivities, one may propose that regardless of the precursor the perfluoroallylic $(CF_2)_2C^+$–F cation is produced. It then may then undergo a rearrangement (a concomitant F migration and a C–C bond clevage) en-route to the $CF_3^+ + FC{\equiv}CF$ dissociation limit.

Now one will now return to the discussion of the $C_3F_7I^{+\bullet}$ parent-ions. As stated previously, the peak intensities of the MI and CID mass spectra of the $C_3F_7I^{+\bullet}$ isomers are listed in Table 3.16 and illustrated in Figures 3.19 and 3.20. On inspection of Table 3.16 and Figures 3.19 and 3.20, one may note the following trends. Firstly, both isomers possess the same base peak at (m/z 169) for $CF_3CF_2CF_2^+$ and $(CF_3)_2CF^+$, respectively. Secondly, as previously stated the $(CF_3)_2CFI^{+\bullet}$ isomer possess two extra MI peaks for CF_3CFI^+ (m/z 227), and c-$C_3F_6I^+$ (m/z 277), corresponding to $CF_3^\bullet$, and $F^\bullet$ losses, respectively. Therefore it is

proposed here, as it was similarly proposed for the $C_4F_9I^{+\bullet}$ isomers, that the $CF_3CF_2CF_2I^{+\bullet}$ and $(CF_3)_2CFI^{+\bullet}$ isomers possess their own independent potential wells in which they live. Thus, as was similarly proposed for the $C_4F_9I^{+\bullet}$ isomers, it is proposed here that the $CF_3CF_2CF_2I^{+\bullet}$ and $(CF_3)_2CFI^{+\bullet}$ isomers retain their own structure.

$C_3F_6I^+$ (m/z 277)

These isomeric fragment ions are generated by $F^\bullet$ loss from the parent $C_3F_7I^{+\bullet}$ radical-cation. There are three main $C_3F_6I^+$ isomers to be discussed here. They are as follows; the cyclic c-$C_3F_6I^+$, the open-chain $^+CF_2CF_2CF_2I$, and the branched $(CF_3)_2CI^+$ isomers. The proposed order of stability is as follows; c-$C_3F_6I^+$ > $^+CF_2CF_2CF_2I$ > $(CF_3)_2CI^+$. The proposed energy levels of the $C_3F_6I^+$ isomers are illustrated in Figure 3.21. The peak intensities of the MI and CID mass spectra of the $C_3F_6I^+$ isomers are listed in Table 3.17 and illustrated in Figures 3.22 and 3.23.

On inspection of Table 3.17 and Figures 3.22 and 3.23, one may see that the $C_3F_6I^+$ ions produced from n-$C_3F_7I^{+\bullet}$ and s-$C_3F_7I^{+\bullet}$ are probably the same and may be the c-$C_3F_6I^+$ isomer. This common structure is suggested due to the striking commonality of both the MI and CID mass spectra (i.e., they are superimposable upon one another). The most outstanding feature is the almost equivalent losses of FI and CF_2=CF_2 producing the corresponding $(CF_2)_2C^+$–F (m/z 131), and CF_2I^+ (m/z 177) ions, respectively. The most useful visualization of the potential surface of the reacting species is one of a "puckered" four-membered c-$C_3F_6I^+$ ring structure in which the simultaneous dissociation routes of CF_2I^+ + CF_2=CF_2 and $(CF_2)_2C^+$–F + FI (via the bisected extraction of the F atom by the juxtpositioned I atom) are almost equal facility. It is interesting (and somewhat surprising)

Figure 3.21 Proposed Energy Levels of the $C_3F_6I^+$ (m/z 277) Isomers

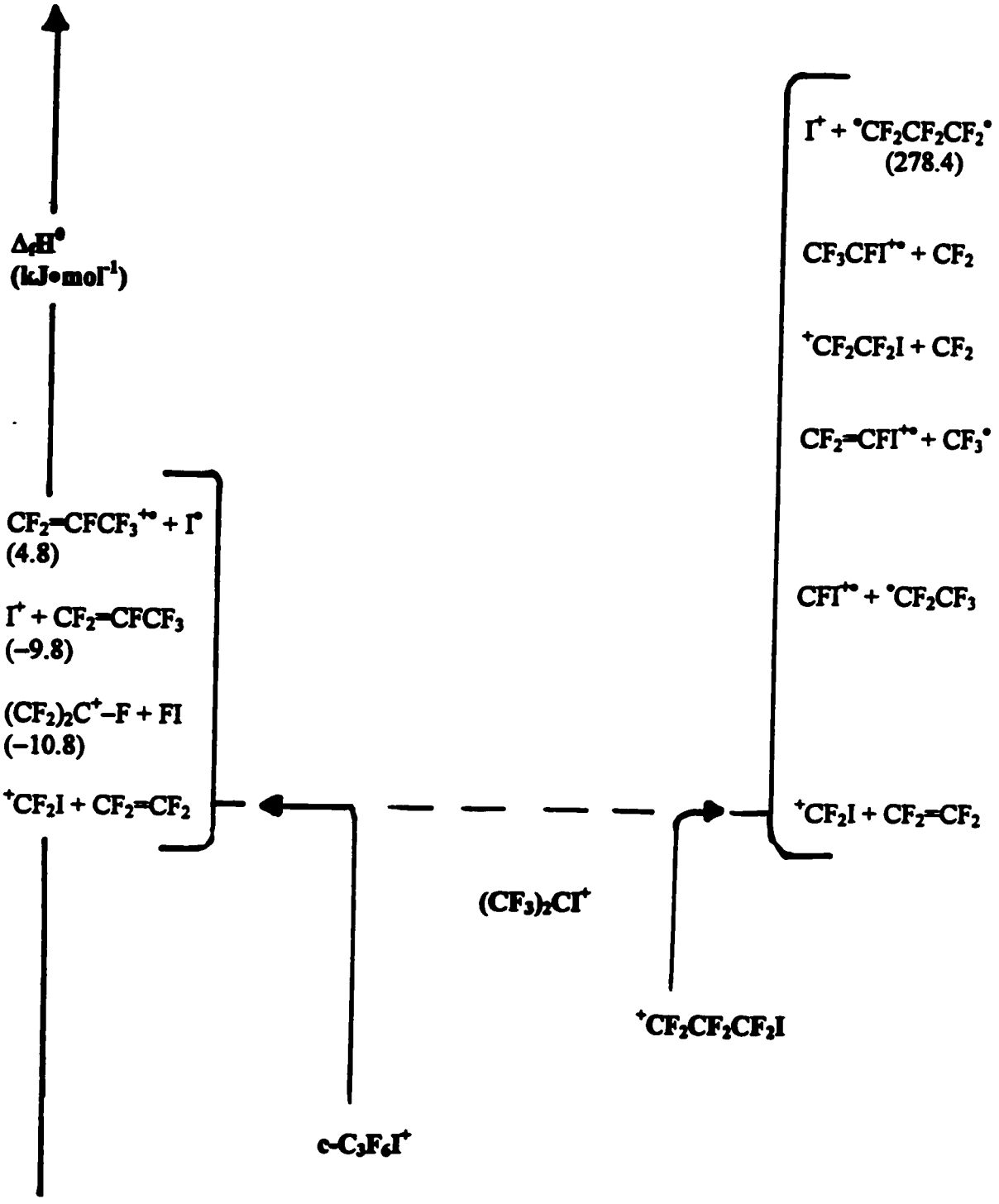

Table 3.17 Metastable Ion (MI) 2FFR and Collision Induced Dissociation (CID) 2FFR He ≈90 %T Mass Spectra of Source Generated $C_3F_6I^+$ (m/z 277) from the C_3F_7I Isomers

			Parent Ion			
			n-C_3F_7I Height (%)		s-C_3F_7I Height (%)	
Species	Mass (m/z)	Neutral Loss	MI	CID	MI	CID
$C_2F_4I^+$	227	($-CF_2$)		0.7		0.7
$C_2F_3I^{+\bullet}$	208	($-CF_3^\bullet$)		2.3		1.3
$C_2F_2I^+$	189	($-CF_4$)		0.7		<0.3
CF_2I^+	177	($-C_2F_4$)	100.0	100.0	100.0	100.0
$CFI^{+\bullet}$	158	($-C_2F_5^\bullet$)	1.3	2.0		1.3
$C_3F_6^{+\bullet}$	150	($-I^\bullet$)		4.6		4.0
CI^+	139			<0.3		<0.3
$C_3F_5^+$	131	(–FI)	81.8	89.1	86.8	88.7
I^+	127	($-C_3F_6$)	6.0	13.2	4.0	10.6
$C_2F_5^+$	119			<0.3		
$C_3F_4^{+\bullet}$	112			<0.3		<0.3
$C_2F_4^{+\bullet}$	100			1.3		1.3
$C_3F_3^+$	93			<0.3		
$C_2F_3^+$	81			<0.3		
CF_3^+	69			1.3		1.3

Figure 3.22 Metastable Ion (MI) 2FFR Mass Spectra of Source Generated $C_3F_6I^+$ (m/z 277) from (a) n-C_3F_7I and (b) s-C_3F_7I

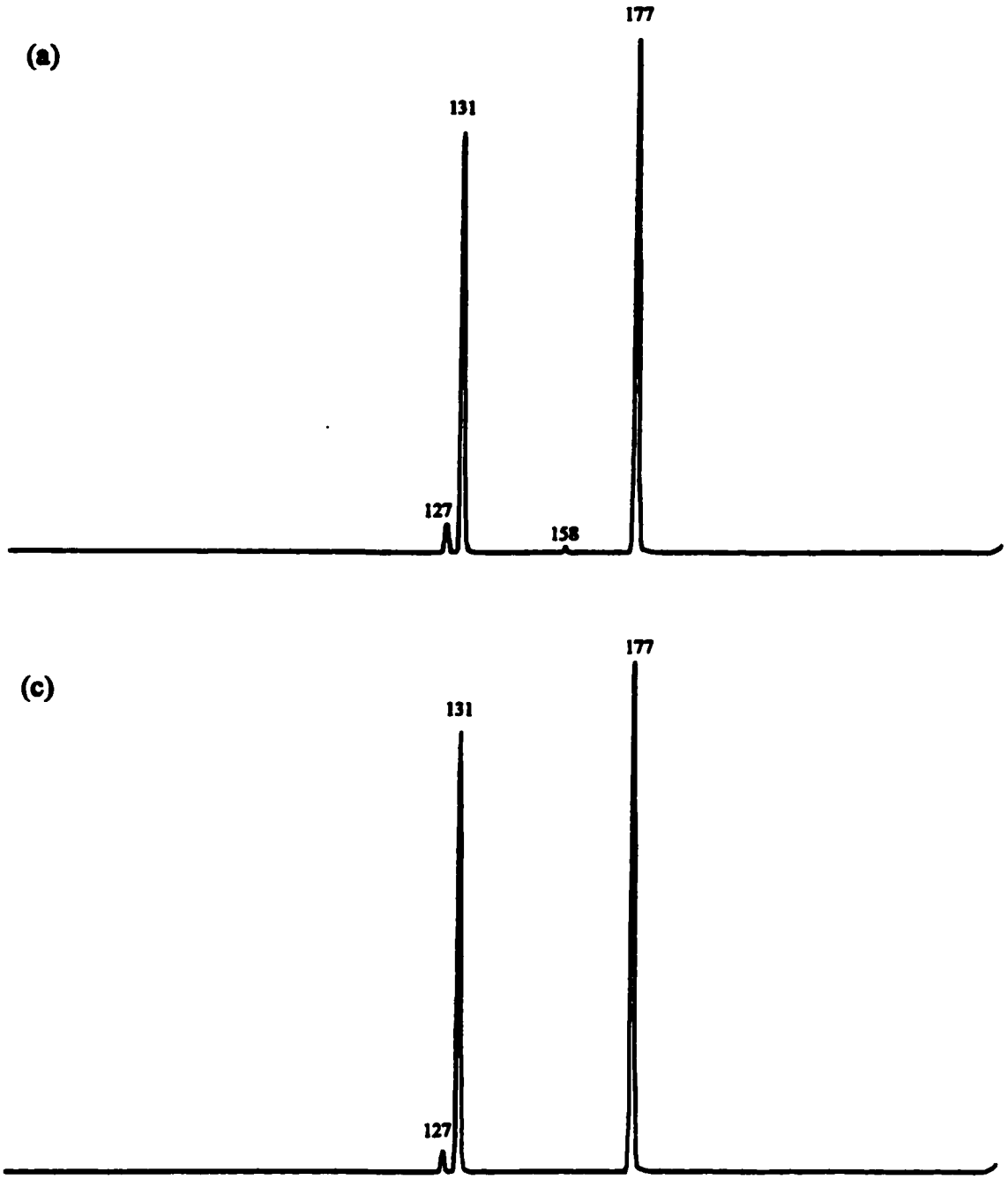

Figure 3.23 Collision Induced Dissociation (CID) 2FFR He ≈ 90 %T Mass Spectra of Source Generated $C_3F_6I^+$ (m/z 277) from (a) n-C_3F_7I and (b) s-C_3F_7I

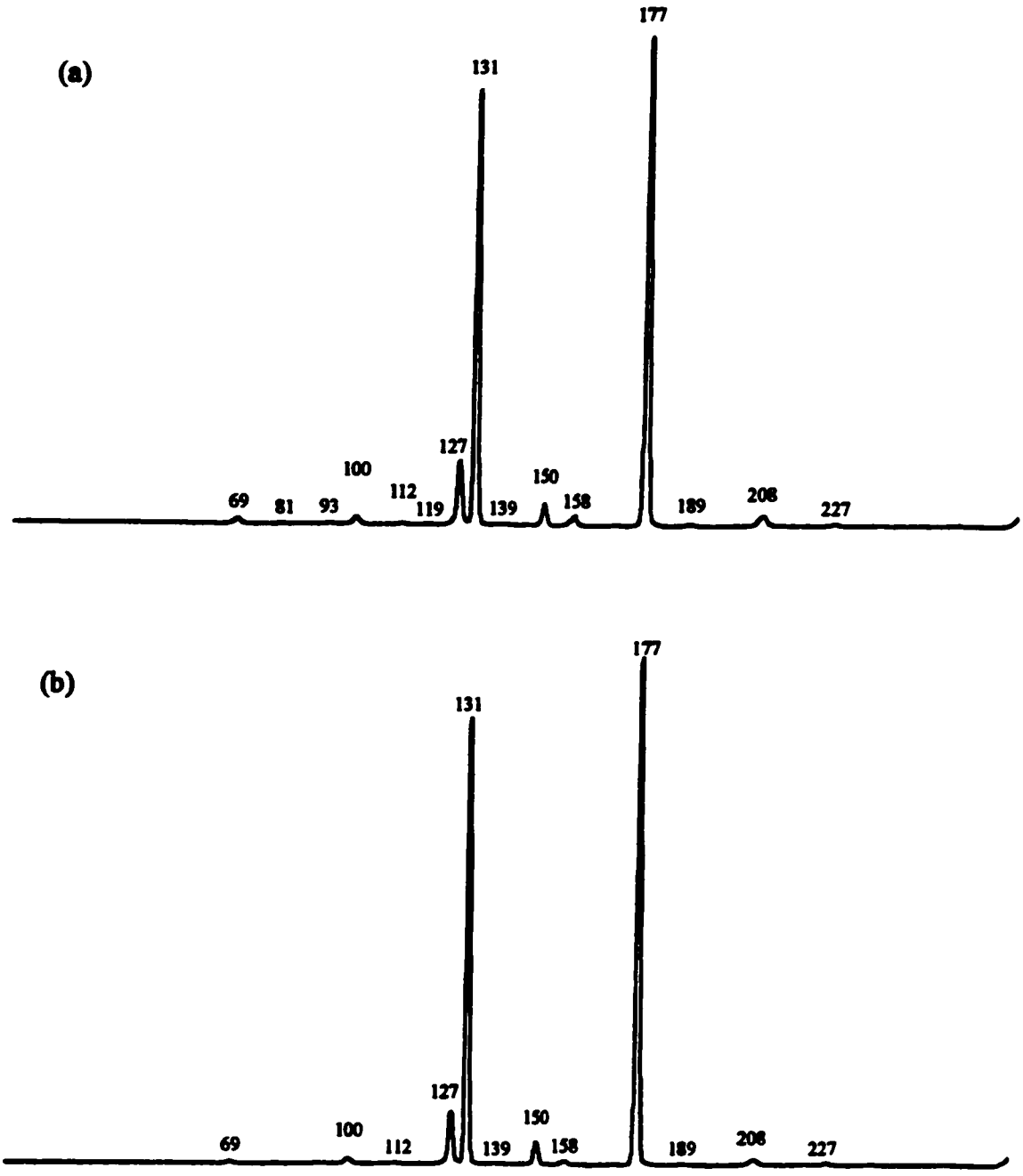

that the analogous c-$C_4F_8^{+\bullet}$ species, whilst possessing a known (and fully analyzed) photoelectron spectrum, presented by Tuckett et. al. [5], it does not possess the Franck-Condon Factors that grant the observation of a stable parent radical-cation species mass spectrometrically. This would seem to suggest for the c-$C_3F_6I^+$ species a very interesting, important, and hitherto computational-chemically unexplored stabilizing interaction between the F (the most electronegative) and I (one of the least electronegative) atomic-orbitals which compose the molecular-orbitals of this (proposed) observed species, analogous to the (unstable) unobserved c-$C_4F_8^{+\bullet}$ species.

$C_2F_4I^+$ (m/z 227)

These isomeric fragment ions are generated by $CF_3^\bullet$ loss from the parent $C_3F_7I^{+\bullet}$ radical-cation. There are three main $C_2F_4I^+$ isomers to be discussed here. They are as follows; $^+CF_2CF_2I$, CF_3CFI^+, and c-F_2(CFC)FI^+ (i.e., a cyclic structure with a three-membered fluorine bridged (CFC) ring). The proposed order of stability (as per section 3.2) is as follows; $^+CF_2CF_2I > CF_3CFI^+ >$ c-F_2(CFC)FI^+. The proposed energy levels of the $C_2F_4I^+$ isomers are illustrated in Figure 3.24. The peak intensities of the MI and CID mass spectra of the $C_2F_4I^+$ isomers are listed in Table 3.18 and illustrated in Figures 3.25 and 3.26.

On inspection of Table 3.18 and Figures 3.25 and 3.26, one may see that the $C_2F_4I^+$ ions produced from n-$C_3F_7I^{+\bullet}$ and s-$C_3F_7I^{+\bullet}$ are different. The $^+CF_2CF_2I$ isomer is most likely produced from the $CF_3CF_2CF_2I^{+\bullet}$ parent radical-cation. Whereas, the CF_3CFI^+ isomer is most likely produced from the $(CF_3)_2CFI^{+\bullet}$ parent radical-cation. These structures are suggested due to the presence of the single MI peak of $CF_2{=}CF_2^{+\bullet}$ (m/z 100) for the $^+CF_2CF_2I$ isomer; and the two MI peaks of $CF_3CF^{+\bullet}$ (m/z 100), and CF_2I^+ (m/z 177) for the

Figure 3.24 Proposed Energy Levels of the $C_2F_4I^+$ (m/z 227) Isomers

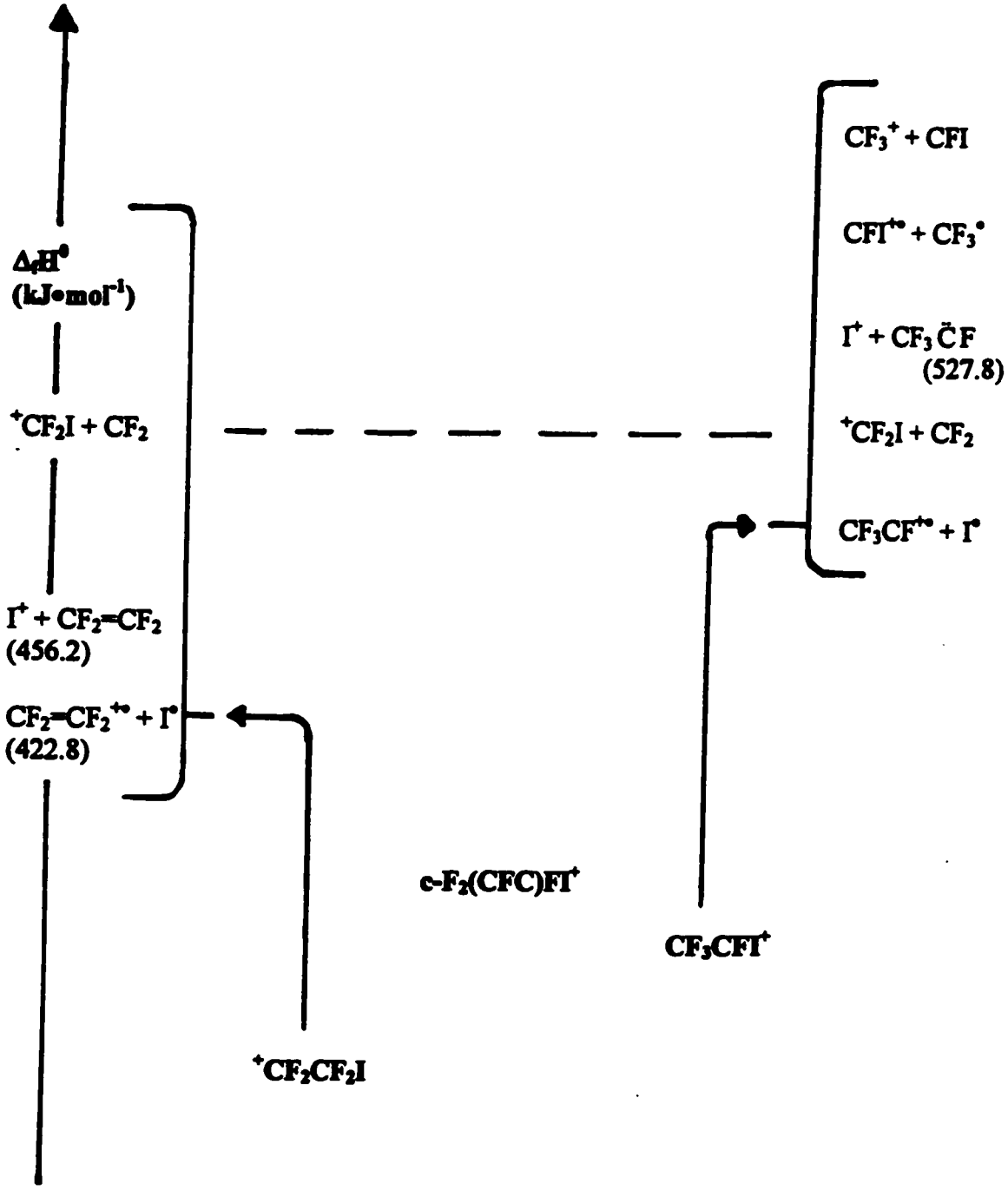

Table 3.18 Metastable Ion (MI) 2FFR and Collision Induced Dissociation (CID) 2FFR He ≈90 %T Mass Spectra of Source Generated $C_2F_4I^+$ (m/z 227) from the C_3F_7I Isomers

			Parent Ion			
			n-C_3F_7I Height (%)		s-C_3F_7I Height (%)	
Species	Mass (m/z)	Neutral Loss	MI	CID	MI	CID
$C_2F_3I^{+\bullet}$	208	($-F^\bullet$)		0.7		1.3
$C_2F_2I^+$	189	($-F_2$)				<0.3
CF_2I^+	177	($-CF_2$)		21.2	6.2	33.8
$C_2FI^{+\bullet}$	170			<0.3		<0.3
$CFI^{+\bullet}$	158	($-CF_3^\bullet$)		4.0		7.9
$FI^{+\bullet}$	146	($-C_2F_3^\bullet$)		<0.3		<0.3
CI^+	139	($-CF_4$)		0.7		1.3
I^+	127	($-C_2F_4$)		5.3		7.9
$C_2F_4^{+\bullet}$	100	($-I^\bullet$)	100.0	100.0	100.0	100.0
$C_2F_3^+$	81	($-FI$)		<0.3		0.7
CF_3^+	69			1.3		2.0
CF^+	31			<0.3		<0.3

Figure 3.25 Metastable Ion (MI) 2FFR Mass Spectra of Source Generated $C_2F_4I^+$ (m/z 227) from (a) n-C_3F_7I and (b) s-C_3F_7I

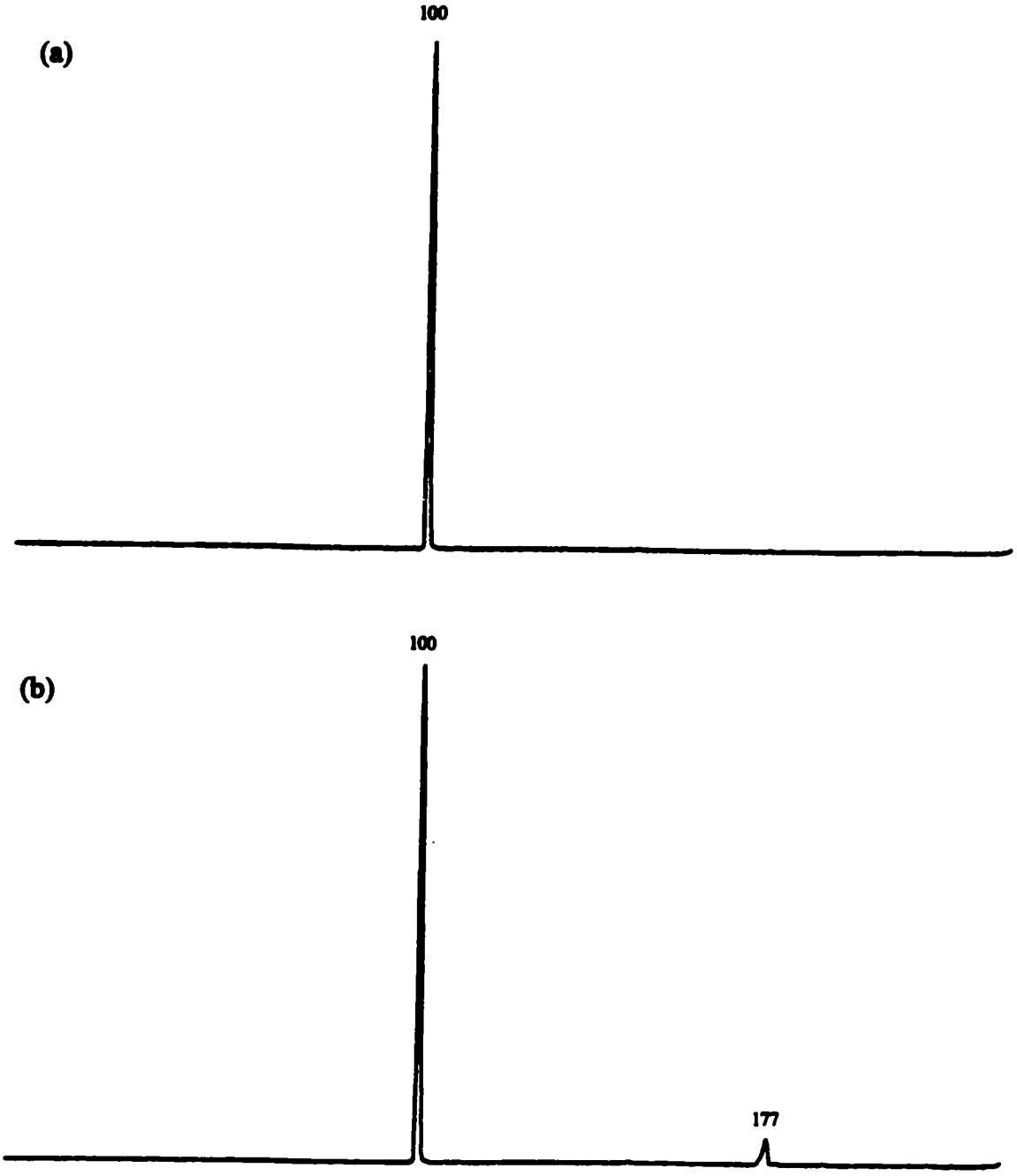

Figure 3.26 Collision Induced Dissociation (CID) 2FFR He ≈ 90 %T Mass Spectra of Source Generated $C_2F_4I^+$ (m/z 227) from (a) n-C_3F_7I and (b) s-C_3F_7I

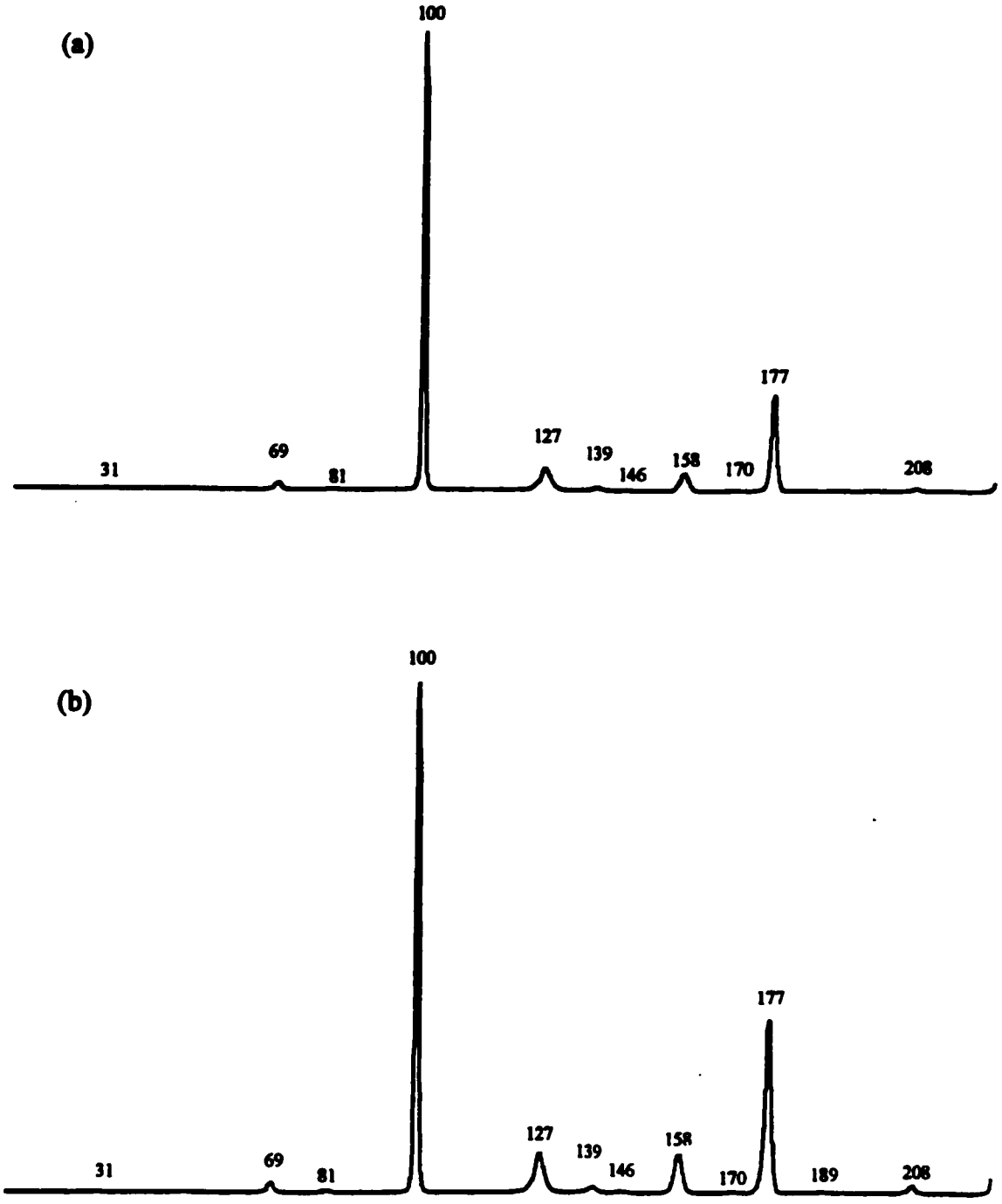

CF_3CFI^+ isomer. The (unexpected) presence of the second MI peak of CF_2I^+ (m/z 177) for the CF_3CFI^+ isomer suggests that this isomer is in communication with the cyclic fluorine bridged c-F_2(CFC)FI^+ isomer. Additionally, this may lead one to suggest that the CF_3CFI^+ and c-F_2(CFC)FI^+ isomers may have close Δ_fH^0 values.

$C_3F_7^+$ (m/z 169)

These isomeric fragment ions are generated by $I^\bullet$ loss from the parent $C_3F_7I^{+\bullet}$ radical-cation. There are three main $C_3F_7^+$ isomers to be discussed here. They are as follows; $CF_3CF_2CF_2^+$, $(CF_3)_2CF^+$, and the (proposed) cyclic structure c-$C_3F_7^+$. The proposed order of stability (as per section 3.2) is as follows; $CF_3CF_2CF_2^+ > (CF_3)_2CF^+ >$ c- $C_3F_7^+$. The proposed energy levels of the $C_3F_7^+$ isomers are illustrated in Figure 3.27. The peak intensities of the MI and CID mass spectra of the $C_3F_7^+$ isomers are listed in Table 3.19 and illustrated in Figures 3.28 and 3.29.

On inspection of Table 3.19 and Figures 3.28 and 3.29, one may see that the $C_3F_7^+$ ions produced from n-$C_3F_7I^{+\bullet}$ and s-$C_3F_7I^{+\bullet}$ are different. The $CF_3CF_2CF_2^+$ isomer is likely produced from n-$C_3F_7I^{+\bullet}$, and the $(CF_3)_2CF^+$ isomer is likely produced from s-$C_3F_7I^{+\bullet}$. As previously discussed in the C_3F_7I section, the $T_{0.5}$ values and collision sensitivities of the $CF_3CF_2CF_2^+$ and $(CF_3)_2CF^+$ isomers undergoing the unimolecluar metastable dissociation to $CF_3^+ + CF_2{=}CF_2$ are listed in Table 3.15. Both of the $CF_3CF_2CF_2^+$ and $(CF_3)_2CF^+$ isomers possess a common $T_{0.5}$ value (i.e., $\approx$ 12 meV). However, the former isomer exhibited a strong collision sensitivity (i.e., suggestive of a simple bond cleavge), whereas the latter isomer exhibited a collision insensitivity (i.e., suggestive of a rearrangement). Such behaviour is expected given the lower Δ_fH^0 value for the $CF_3^+ + CF_2{=}CF_2$ dissociation limit

Figure 3.27 Proposed Energy Levels of the $C_3F_7^+$ (m/z 169) Isomers

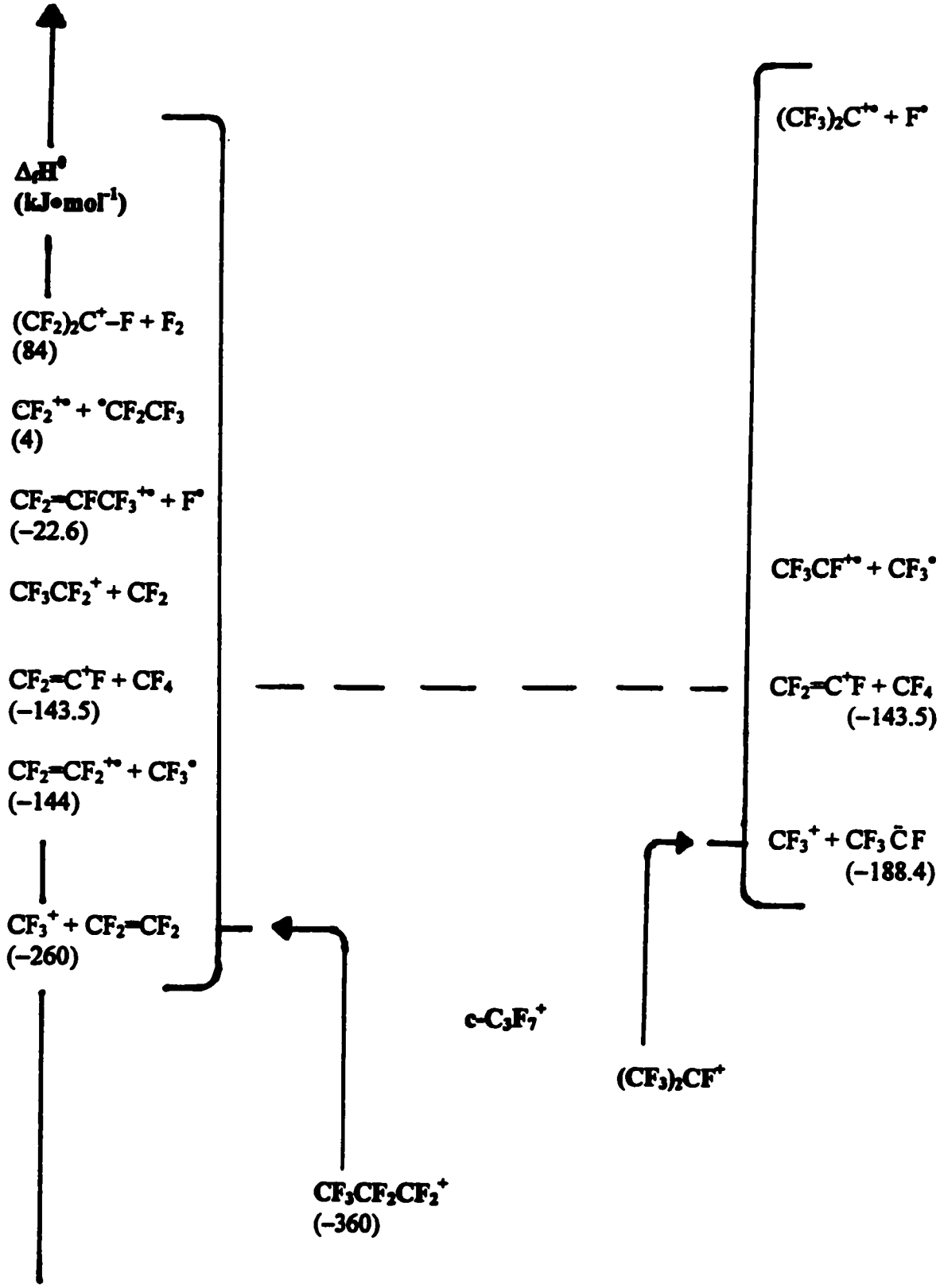

Table 3.19 Metastable Ion (MI) 2FFR and Collision Induced Dissociation (CID) 2FFR He ≈90 %T Mass Spectra of Source Generated $C_3F_7^+$ (m/z 169) from the C_3F_7I Isomers

			Parent Ion			
			n-C_3F_7I Height (%)		s-C_3F_7I Height (%)	
Species	Mass (m/z)	Neutral Loss	MI	CID	MI	CID
$C_3F_6^{+\bullet}$	150	($-F^\bullet$)		1.3		
$C_3F_5^+$	131	($-F_2$)		0.7		<0.3
$C_2F_5^+$	119	($-CF_2$)		13.9		2.6
$C_2F_4^{+\bullet}$	100	($-CF_3^\bullet$)		30.5		2.6
$C_3F_3^+$	93			0.7		<0.3
$C_2F_3^+$	81	($-CF_4$)		1.3		<0.3
$C_3F_2^{+\bullet}$	74			<0.3		
CF_3^+	69	($-C_2F_4$)	100.0	100.0	100.0	100.0
$C_2F_2^{+\bullet}$	62			<0.3		
$CF_2^{+\bullet}$	50	($-C_2F_5^\bullet$)		3.3		<0.3
CF^+	31			2.0		<0.3

Figure 3.28 Metastable Ion (MI) 2FFR Mass Spectra of Source Generated $C_3F_7^+$ (m/z 169) from (a) n-C_3F_7I and (b) s-C_3F_7I

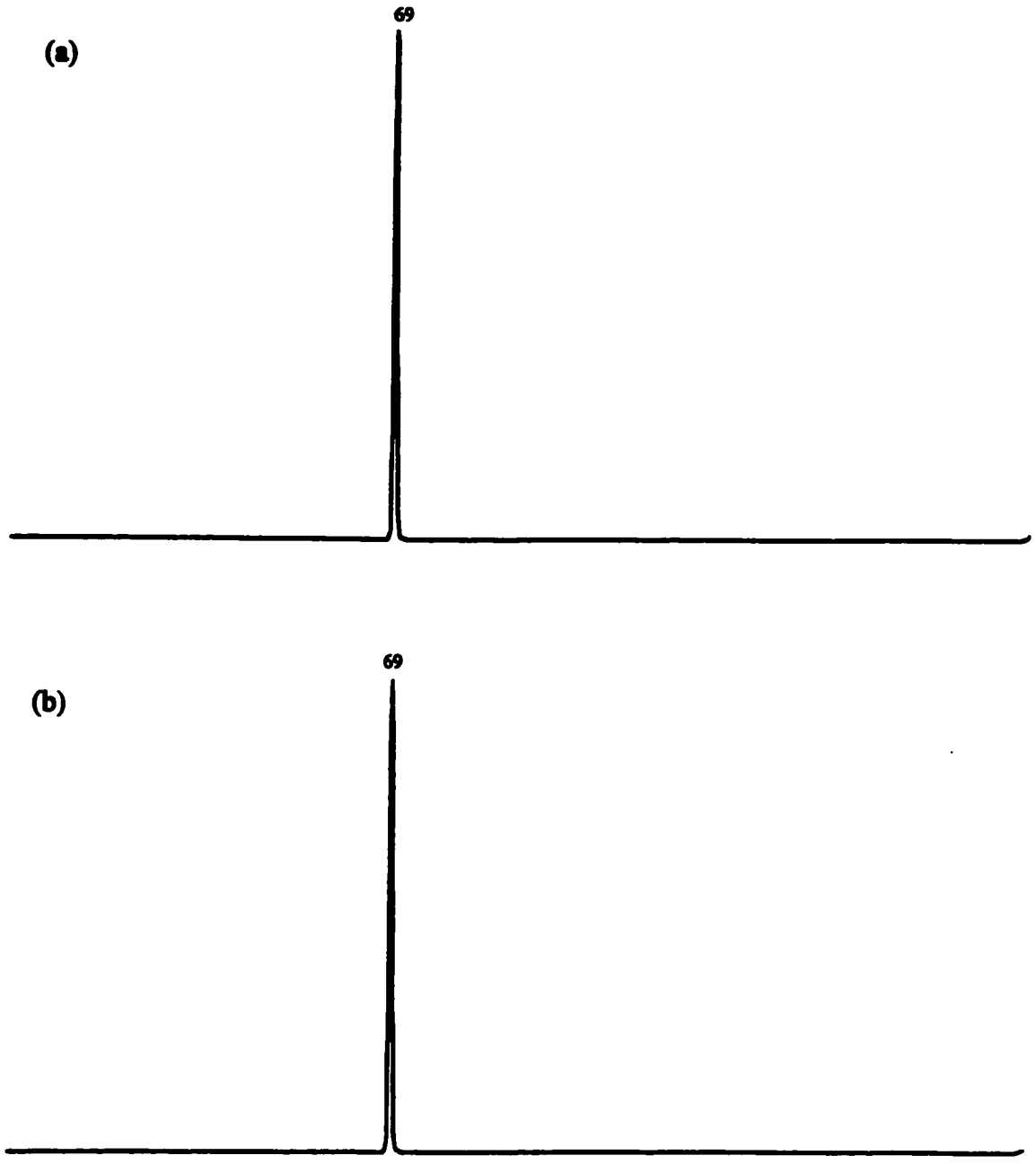

Figure 3.29 Collision Induced Dissociation (CID) 2FFR He ≈ 90 %T Mass Spectra of Source Generated $C_3F_7^+$ (m/z 169) from (a) n-C_3F_7I and (b) s-C_3F_7I

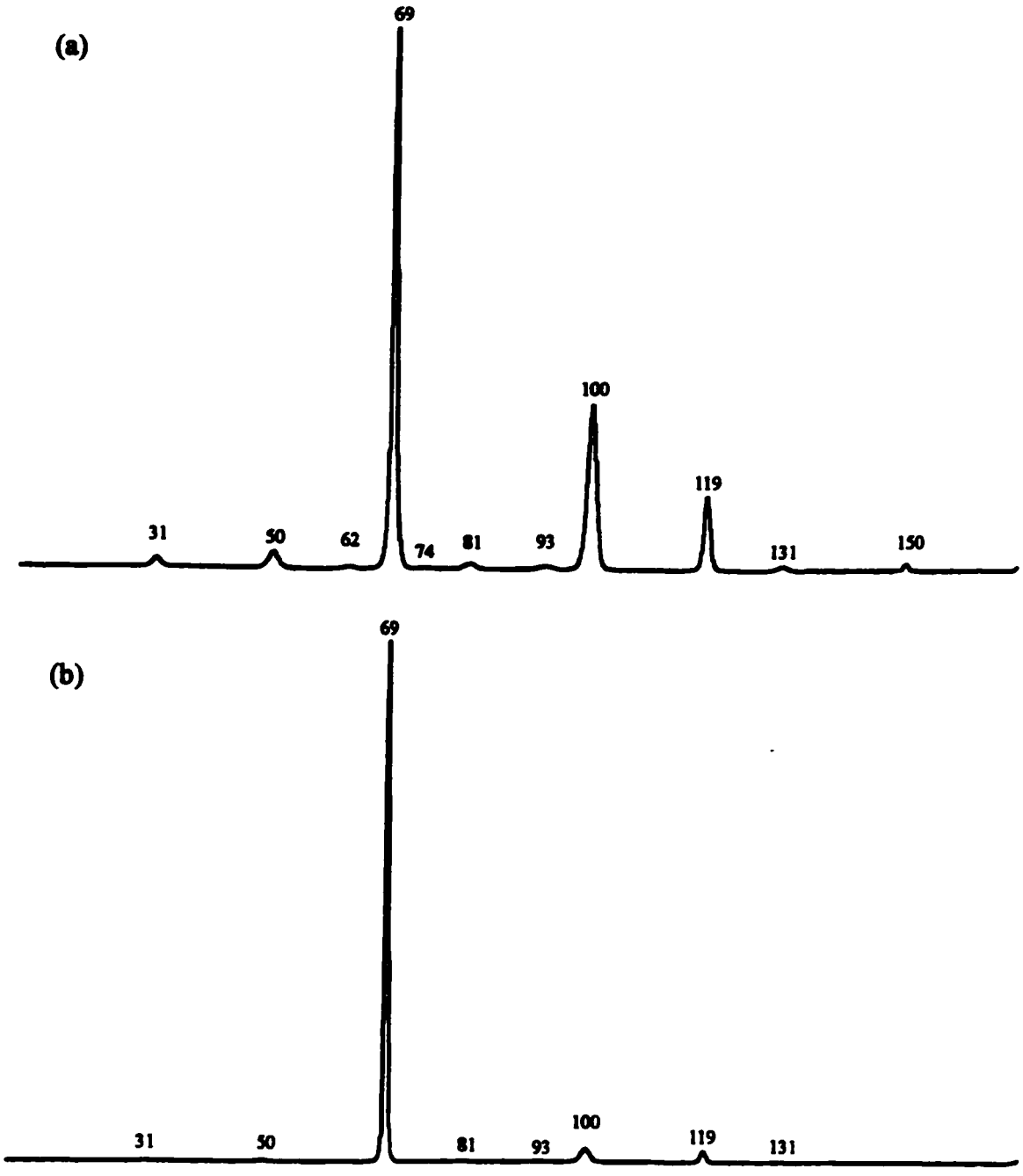

relative to the $\Delta_f H^0$ value for the $CF_3^+ + CF_3\ddot{C}F$ dissociation limit. Additionally, the difference in the peak intensities of the $C_2F_4^{+\bullet}$ (m/z 100), and $C_2F_5^+$ (m/z 119) ions are helpful. Whereas, for the $\subset F_3CF_2CF_2^+$ isomer their peak intensities are 30.5 % and 13.9 %, and for the $(CF_3)_2CF^+$ isomer they are of much lower value of 2.6 % and 2.6 %, respectively. This is to be expected as whilst very facile for the $CF_3CF_2CF_2^+$ isomer, the CF_2 and $CF_3^\bullet$ losses are much more energy demanding for $(CF_3)_2CF^+$ isomer. Thus, it is proposed here that the $CF_3CF_2CF_2^+$ and $(CF_3)_2CF^+$ isomers possess their own unique potential wells in which they live and that they retain their respective structures.

$C_3F_5^+$ (m/z 131)

These isomeric fragment ions are most likely generated by FI loss from the source generated c-$C_3F_6I^+$ fragment-cation. There are three main $C_3F_5^+$ isomers to be discussed here. They are as follows; the symmetric allylic species $(CF_2)_2C^+–F$, the less symmetric $CF_2=C^+–CF_3$, and the $CF_3–CF=CF^+$ species. The proposed order of stability is as follows; $(CF_2)_2C^+–F > CF_2=C^+–CF_3 > CF_3–CF=CF^+$. The proposed energy levels of the $C_3F_5^+$ isomers are illustrated in Figure 3.30. The peak intensities of the MI and CID mass spectra of the $C_3F_7^+$ isomers are listed in Table 3.20 and illustrated in Figures 3.31 and 3.32.

On inspection of Table 3.20 and Figures 3.31 and 3.32, one may see that the $C_3F_5^+$ ions produced from n-C_3F_7I and s-C_3F_7I are very similar and most plausibly the same structure. As previously discussed in the C_3F_7I section, both of the $C_3F_5^+$ isomers produced possess identical $T_{0.5}$ value (i.e., $\approx$ 30 meV) for their metastable $C_3F_5^+ \rightarrow CF_3^+ + FC\equiv CF$ reaction and they are both only moderately collision sensitive. This would be indicative of a rearrangement process, namely a F transfer from the $(CF_2)_2C^+–F$ to the $CF_3–CF=CF^+$

Figure 3.30 Proposed Energy Levels of the $C_3F_5^+$ (m/z 131) Isomers

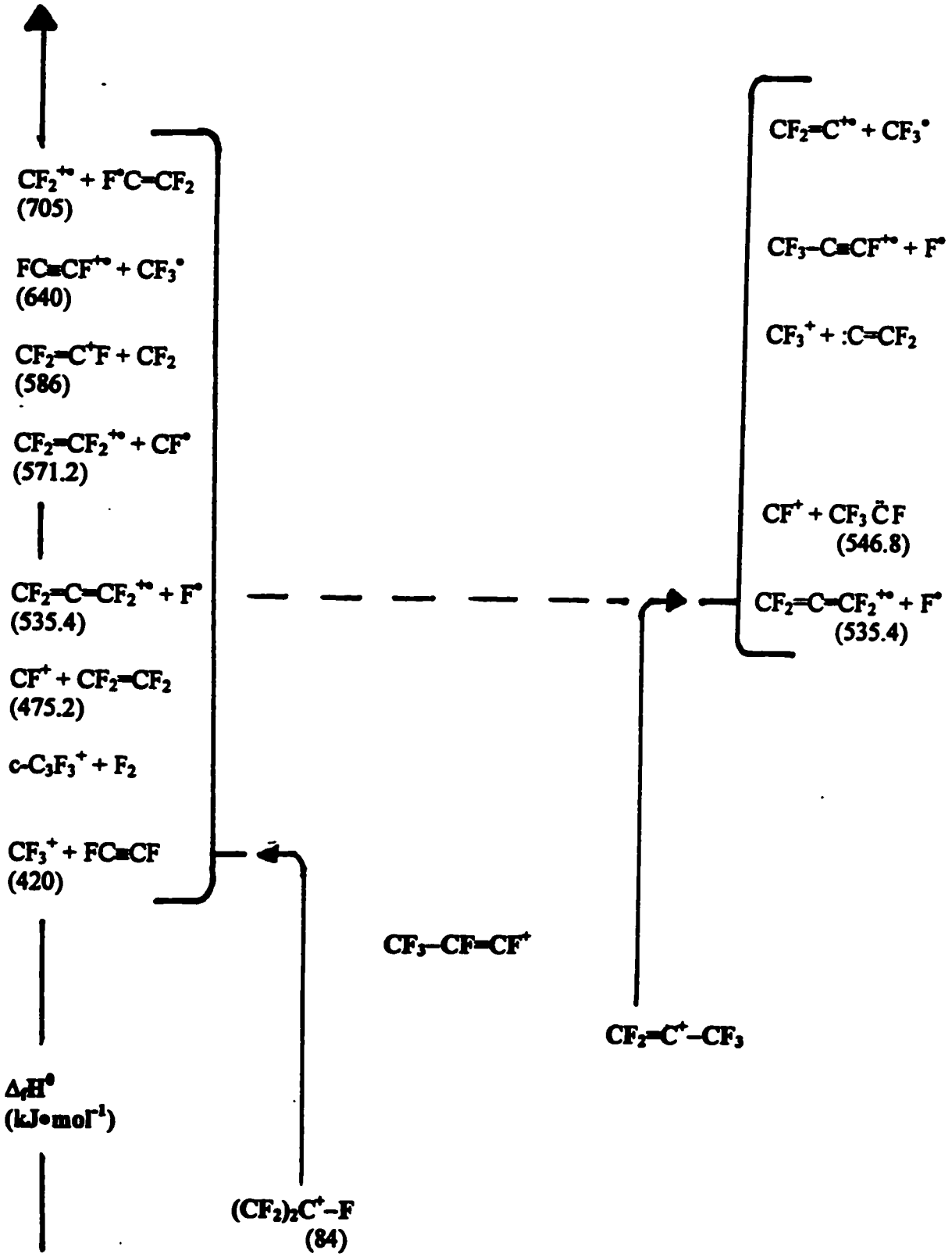

Table 3.20 Metastable Ion (MI) 2FFR and Collision Induced Dissociation (CID) 2FFR O_2 ≈90 %T Mass Spectra of Source Generated $C_3F_5^+$ (m/z 131) from the C_3F_7I Isomers

Species	Mass (m/z)	Neutral Loss	Parent Ion n-C_3F_7I Height (%) MI	n-C_3F_7I Height (%) CID	s-C_3F_7I Height (%) MI	s-C_3F_7I Height (%) CID
$C_3F_4^{+\bullet}$	112	($-F^\bullet$)		2.6		9.3
$C_2F_4^{+\bullet}$	100	($-CF^\bullet$)		<0.3		0.7
$C_3F_3^+$	93	($-F_2$)		7.3		35.8
$C_2F_3^+$	81	($-CF_2$)		6.0		25.8
$C_3F_2^{+\bullet}$	74			0.7		6.0
CF_3^+	69	($-C_2F_2$)	100.0	100.0	100.0	100.0
$C_3F_5^{2+\bullet}$	65.5			2.0		6.6
$C_2F_2^{+\bullet}$	62	($-CF_3^\bullet$)		1.3		7.9
C_3F^+	55			<0.3		1.3
$CF_2^{+\bullet}$	50	($-C_2F_3^\bullet$)		1.3		9.9
C_2F^+	43	($-CF_4$)		<0.3		2.0
CF^+	31	($-C_2F_4$)		3.3		17.2

Figure 3.31 Metastable Ion (MI) 2FFR Mass Spectra of Source Generated $C_3F_5^+$ (m/z 131) from (a) n-C_3F_7I and (b) s-C_3F_7I

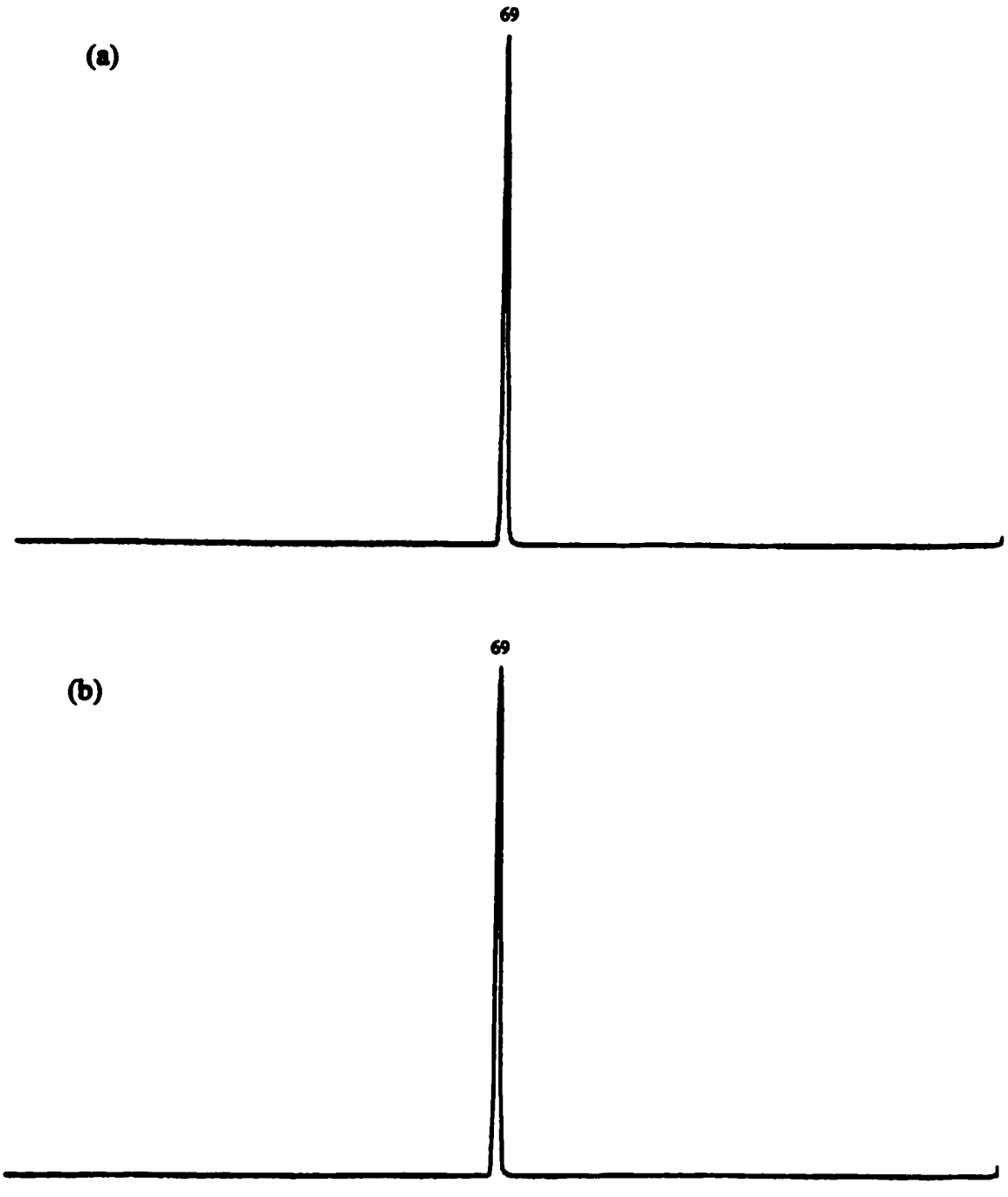

Figure 3.32 Collision Induced Dissocaition (CID) 2FFR O_2 ≈ 90 %T Mass Spectra of Source Generated $C_3F_5^+$ (m/z 131) from (a) n-C_3F_7I and (b) s-C_3F_7I

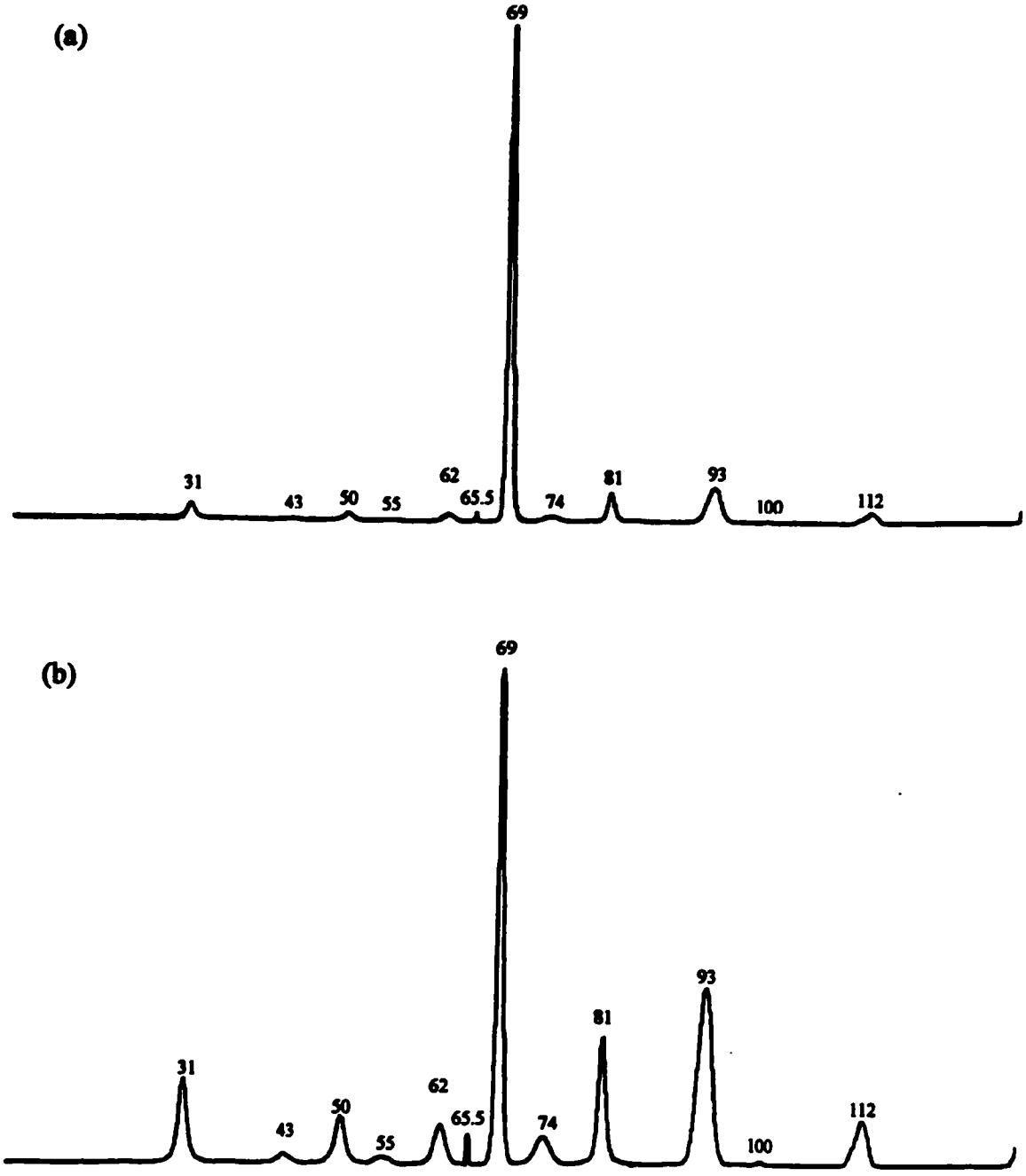

structure followed by a direct bond cleavage en-route to the $CF_3^+ + FC{\equiv}CF$ dissociation limit. The presence of the doubly-charged allylic $[(CF_2)_2C{-}F]^{2+}$ (m/z 65.5) species in both of the CID mass spectra is supportive of a common structure. In regards to the $C_3F_5^+$ species produced from s-C_3F_7I the CID peak intensities of the CF^+ (m/z 31), $CF_2{=}C^+F$ (m/z 81), and c-$C_3F_3^+$ (m/z 93) ions, their high intensities of 17.2 %, 25.8 %, and 35.8 % , respectively are indicative of the allylic $(CF_2)_2C^+{-}F$ structure. The first process of the $CF_2{=}CF_2$ loss is suggestive of a ring closure followed by CF^+ ejection. The second process of the CF_2 loss is a result of the scission of the allylic system. The third process of the F_2 loss is indicative of the production of the ring closed aromatic c-$C_3F_3^+$ ion. However, in the case of the $C_3F_5^+$ species produced from n-C_3F_7I, the above processes have much lower CID peak intensities of 3.3 %, 6.0 %, and 7.3 %, respectively. Notwithstanding this, their intensities are of significant magnitude and are supportive of the $(CF_2)_2C^+{-}F$ structure. Their lower CID peak intensities may suggest the presence of a communication with the smaller populations of $CF_3{-}CF{=}CF^+$ and $CF_2{=}C^+{-}CF_3$, with however the population of $(CF_2)_2C^+{-}F$ being the dominant isomer.

3.5 Unsaturated Perfluorocarbons C_nF_m

This section will deal with the gas-phase ion-chemistry of the perfluorocarbons C_nF_m. As will be seen the C_nF_m behaviour is rich. Whereas, the previously discussed C_nF_mI species and the soon to be discussed C_nF_mO species, have their thermochemical behaviour dominated by the heteroatom (i.e., the I and the O atom), the presence of only C and F atoms results in relatively more predictable dissociation behaviour.

There are two sources for the seven ions which be discussed here. The unsaturated perfluorocarbons are perfluoro-2-butyne, CF_3–C≡C–CF_3, and perfluoropropene, CF_2=$CFCF_3$. The former compound serves as the source for the $C_4F_6^{+\bullet}$, $C_4F_4^{+\bullet}$, $C_3F_4^{+\bullet}$, $C_3F_3^{+}$, and $C_3F_2^{+\bullet}$ ions, whereas the latter compound serves as the source of the $C_3F_6^{+\bullet}$, and $C_2F_4^{+\bullet}$ ions, respectively.

$C_4F_6^{+\bullet}$ (m/z 162)

These isomeric ions are generated the ionization of CF_3–C≡C–CF_3. There are five main $C_4F_6^{+\bullet}$ isomers to be discussed here. They are perfluoro-1,3-butadiene CF_2=CF–CF=$CF_2^{+\bullet}$, perfluoro-2-butyne CF_3–C≡C–$CF_3^{+\bullet}$, CF_2=$CFCCF_3^{+\bullet}$, CF_2=C^+–$^\bullet CFCF_3$, and the highly delocalized "pseudo-allylic" $(CF_2)_3C^{+\bullet}$ species. The proposed order of stability is as follows; CF_2=CF–CF=$CF_2^{+\bullet}$ > CF_3–C≡C–$CF_3^{+\bullet}$ > CF_2=$CFCCF_3^{+\bullet}$ > CF_2=C^+–$^\bullet CFCF_3$ > $(CF_2)_3C^{+\bullet}$. One should note there is no observed experimental evidence for the presence of the CF_3CF_2–C≡$CF^{+\bullet}$ isomer. The proposed energy levels of the $C_4F_6^{+\bullet}$ isomers are illustrated in Figure 3.33. The peak intensities of the normal mass spectrum of CF_3–C≡C–$CF_3^{+\bullet}$ are listed in Table 3.34. The kinetic energy release $T_{0.5}$ measurements for

Figure 3.33 Proposed Energy Levels of the $C_4F_6^{+\bullet}$ (m/z 162) Isomers

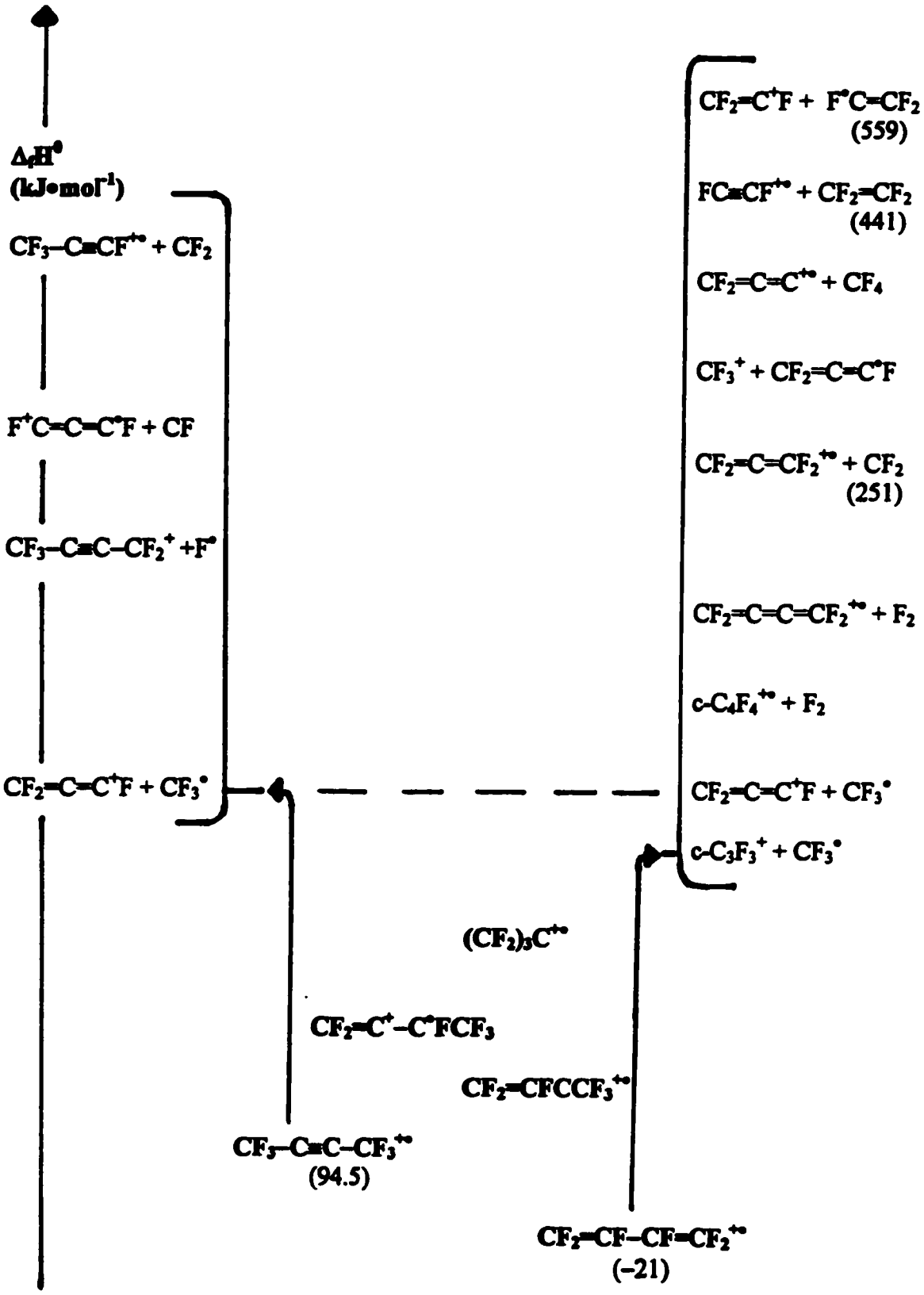

Table 3.21 Normal Mass Spectra of Perfluoro-2-butyne CF_3–C≡C–CF_3

Species	Mass (m/z)	Neutral Loss	Height (%)
$C_4F_6^{+\bullet}$	162		81.5
$C_4F_5^{+}$	143	($-F^{\bullet}$)	94.0
$C_3F_5^{+}$	131	($-CF^{\bullet}$)	0.7
$C_4F_4^{+\bullet}$	124	($-F_2$)	15.2
$C_3F_4^{+\bullet}$	112	($-CF_2$)	15.9
$C_4F_3^{+}$	105		<0.3
$C_2F_4^{+\bullet}$	100	($-C_2F_2$)	3.3
$C_3F_3^{+}$	93	($-CF_3^{\bullet}$)	100.0
$C_4F_2^{+\bullet}$	86		<0.3
$C_2F_3^{+}$	81		<0.3
$C_3F_2^{+\bullet}$	74	($-CF_4$)	15.2
CF_3^{+}	69	($-C_3F_3^{\bullet}$)	32.5
$C_2F_2^{+\bullet}$	62	($-C_2F_4$)	1.3
C_3F^{+}	55		6.6
$CF_2^{+\bullet}$	50		3.3
C_2F^{+}	43		<0.3
$C_3^{+\bullet}$	36		0.7
CF^{+}	31		11.9

Figure 3.34 Normal Mass Spectrum of Perfluoro-2-butyne
CF_3–C≡C–$CF_3^{+\bullet}$ (m/z 162)

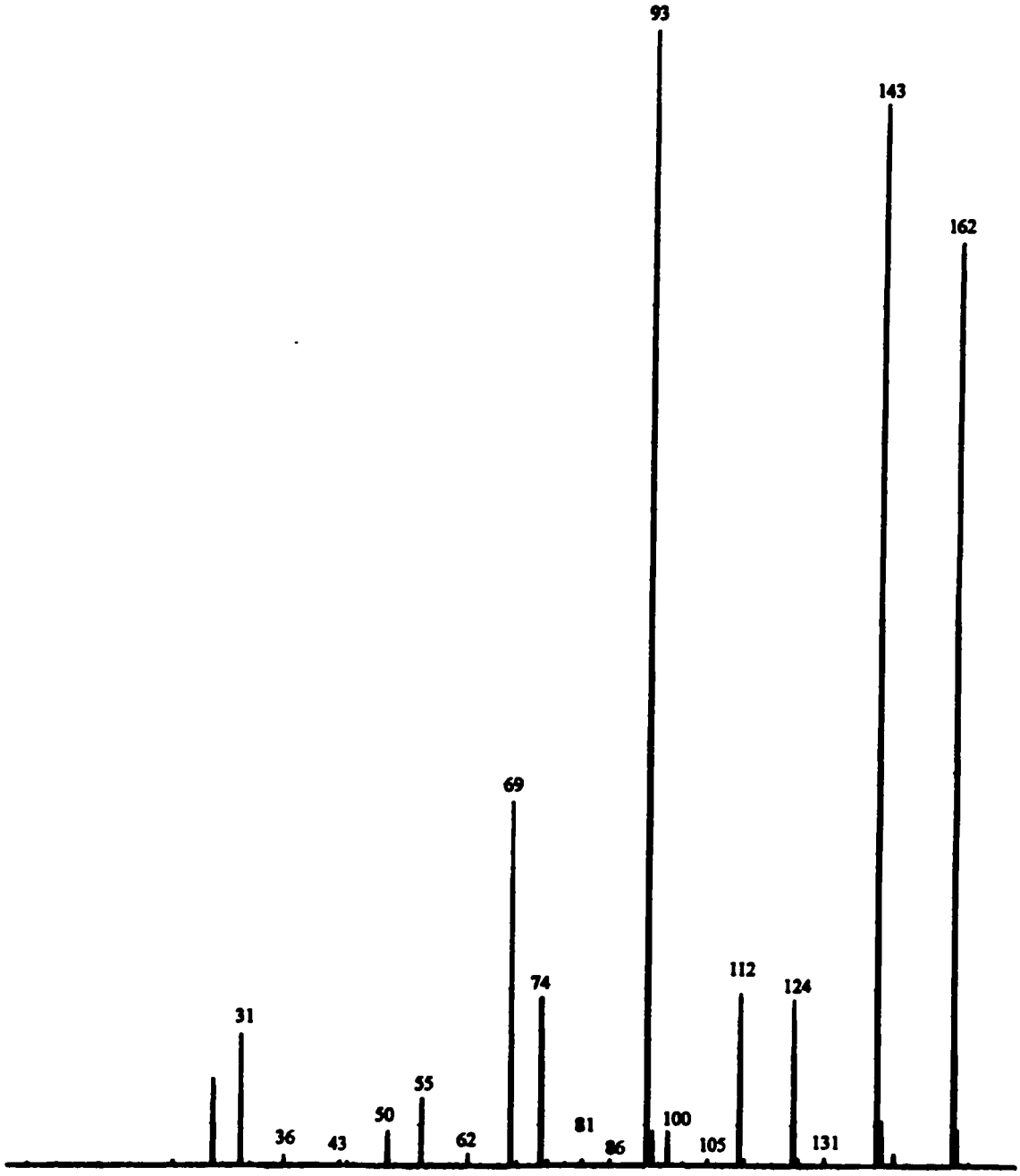

Table 3.22 Kinetic Energy Release $T_{0.5}$ Measurements of Unsaturated Perfluorocarbons

Mass (m/z)	Dissociation Process	Kinetic Energy Release, $T_{0.5}$ (meV)
$CF_3–C{\equiv}C–CF_3$		
$(162 \rightarrow 93)^a$	$CF_3–C{\equiv}C–CF_3^{+\bullet} \rightarrow c\text{-}C_3F_3^+ + CF_3^\bullet$	30.1
$CF_2{=}CFCF_3$		
$(150 \rightarrow 100)$	$CF_2{=}CFCF_3^{+\bullet} \rightarrow CF_3CF^{+\bullet} + CF_2$	11.7
$(100 \rightarrow 69)$	$CF_2{=}CF_2^{+\bullet} \rightarrow CF_3^+ + CF^\bullet$	5.0

[a]Rearrangement of $CF_3–C{\equiv}C–CF_3^{+\bullet}$ to $CF_2{=}CF–CF{=}CF_2^{+\bullet}$ is favoured.

Table 3.23 Metastable Ion (MI) 2FFR and Collision Induced Dissociation (CID) 2FFR He ≈ 90 %T Mass Spectra of Perfluoro-2-butyne $CF_3–C{\equiv}C–CF_3^{+\bullet}$ (m/z 162)

Species	Mass (m/z)	Neutral Loss	Height (%) MI	CID
$C_4F_5^+$	143	($-F^\bullet$)		2.0
$C_4F_4^{+\bullet}$	124	($-F_2$)		2.0
$C_3F_4^{+\bullet}$	112	($-CF_2$)		11.9
$C_3F_3^+$	93	($-CF_3^\bullet$)	100.0	100.0
$C_2F_3^+$	81	($-CF_3^\bullet$)		<0.3
$C_3F_2^{+\bullet}$	74	($-CF_4$)		2.6
CF_3^+	69	($-C_3F_3^\bullet$)		5.3
$C_2F_2^{+\bullet}$	62	($-C_2F_4$)		<0.3
C_3F^+	55			0.7
$CF_2^{+\bullet}$	50			<0.3
CF^+	31			<0.3

Figure 3.35 Metastable Ion (MI) 2FFR Mass Spectrum of Perfluoro-2-butyne $CF_3–C{\equiv}C–CF_3^{+\bullet}$ (m/z 162)

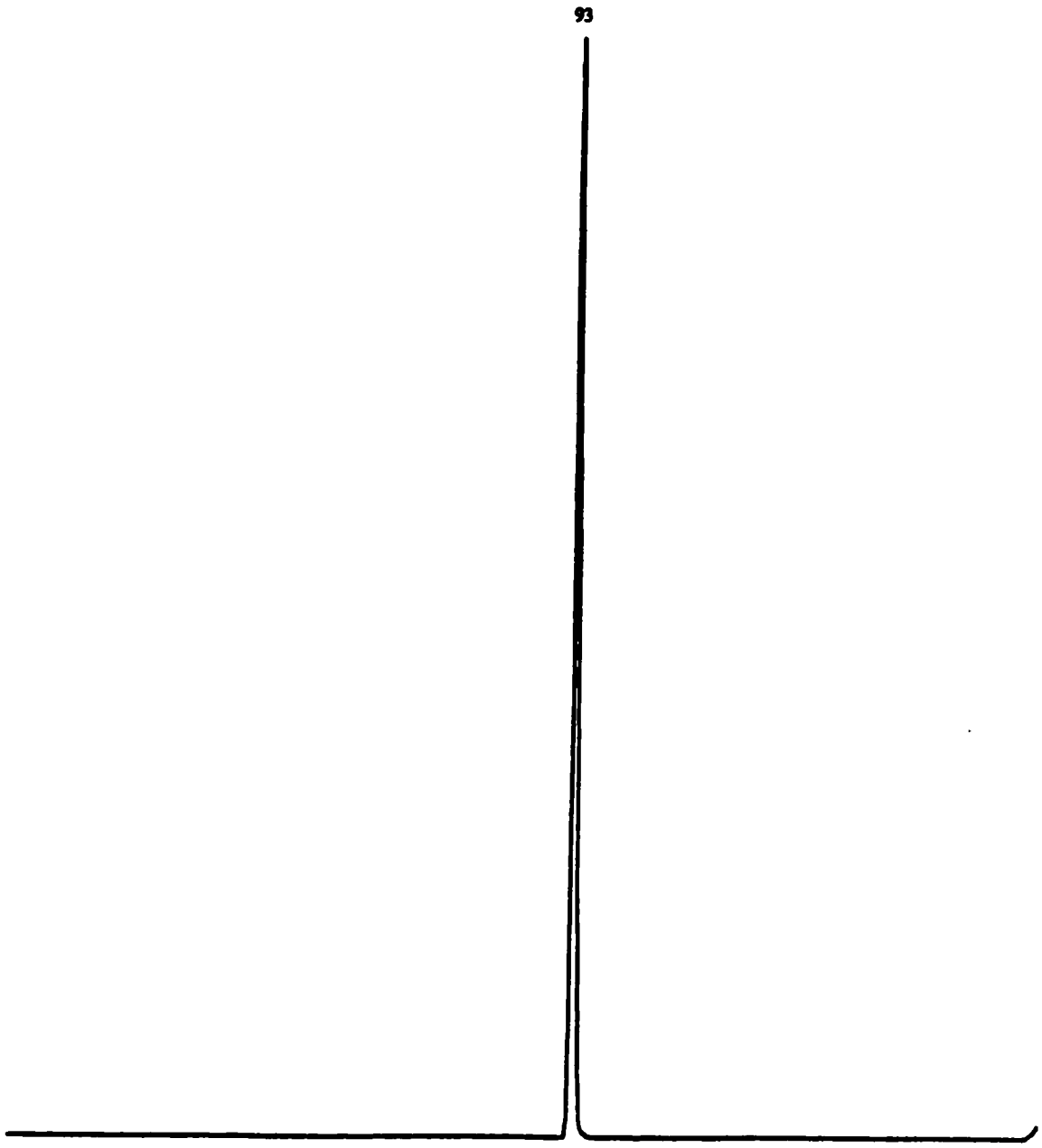

Figure 3.36 Collision Induced Dissociation (CID) 2FFR He ≈ 90 %T Mass Spectrum of Perfluoro-2-butyne CF_3–C≡C–$CF_3^{+\bullet}$ (m/z 162)

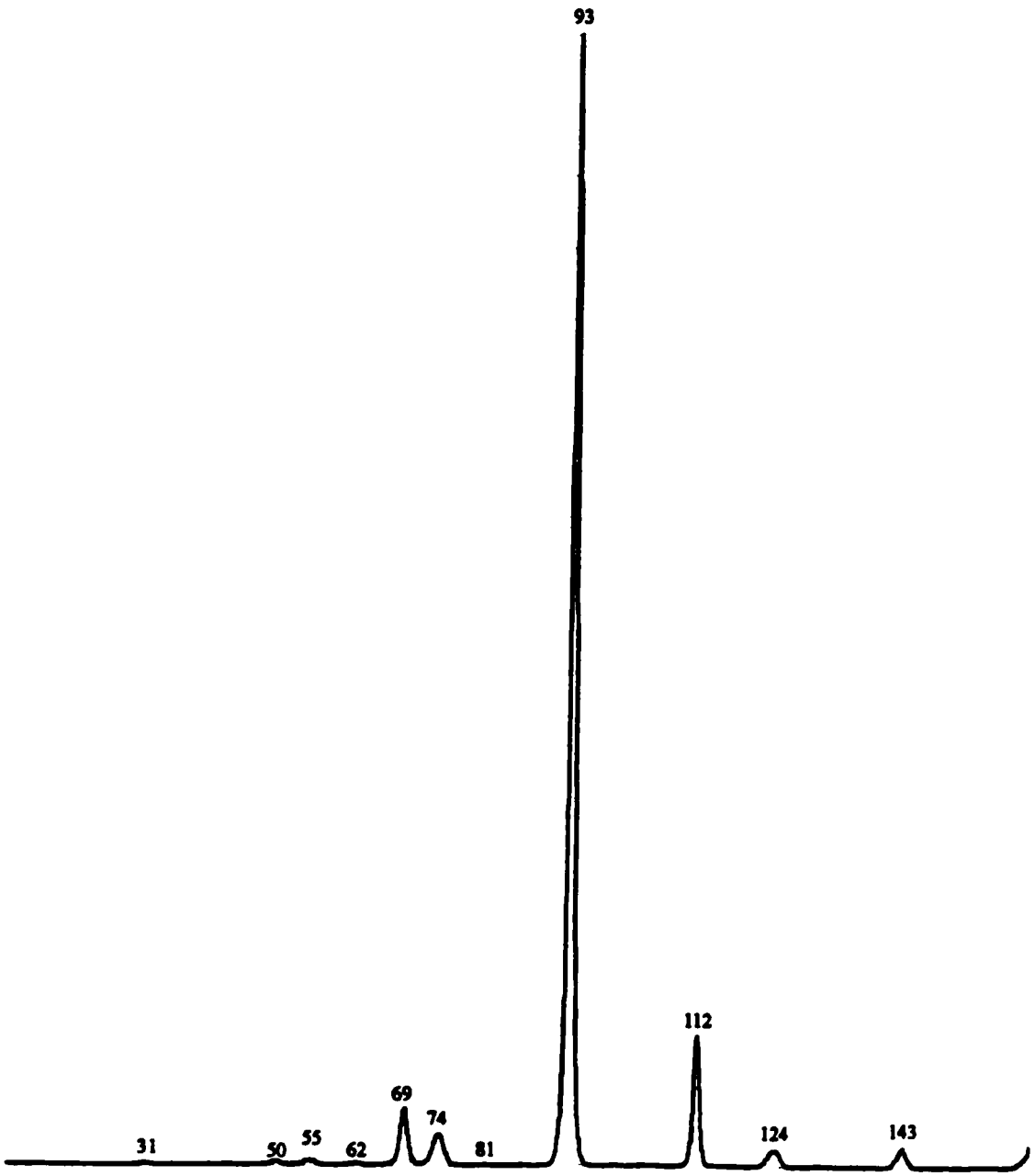

the unsaturated perfluorocarbons are illustrated in Table 3.22. The peak intensities of the MI and CID mass spectra are listed in Table 3.23 and illustrated in Figures 3.35 and 3.36, respectively.

On inspection of Figure 3.33, the proposed energy levels of the $C_4F_6^{+\bullet}$ isomers, one may plainly see that the Δ_fH^0 value of CF_3–C≡C–$CF_3^{+\bullet}$ (94.5 kJ•mol^{-1}) is proposed to be much higher (over 100 kJ•mol^{-1}) than that of the CF_2=CF–CF=$CF_2^{+\bullet}$ (–21 kJ•mol^{-1}), whereas the latter species possesses an experimental Δ_fH^0 value [1]. The Δ_fH^0 value for former was derived from Benson's Additivity [9-11] for the neutral and its experimentally measured IE_a value [15] (see Table 3.5). It is proposed here that it is this great difference in Δ_fH^0 values which results in the very strong tendency for CF_3–C≡C–$CF_3^{+\bullet}$ to rearrange to CF_2=CF–CF=$CF_2^{+\bullet}$.

On inspection of Table 3.21 and Figure 3.34, one may note a few main features of the normal mass spectrum of CF_3–C≡C–$CF_3^{+\bullet}$. Firstly, there are intense of 32.5 %, 100.0 %, 94.0 %, and 81.5 % for the CF_3^+(m/z 69), $C_3F_3^+$(m/z 93), and $C_4F_5^+$(m/z 143), fragment ions, and the $C_4F_6^{+\bullet}$ (m/z 162) parent ion, respectively. The first three fragment ions correspond to the neutral losses of $C_3F_3^\bullet$, $CF_3^\bullet$, and $F^\bullet$, respectively. Secondly, there are some significant peaks of smaller intensity of 15.2 %, 15.9 %, and 15.2 % for the $C_3F_2^{+\bullet}$ (m/z 74), $C_3F_4^{+\bullet}$ (m/z 112),and $C_4F_4^{+\bullet}$ (m/z 124) ions, respectively. These fragment ions correspond to the neutral losses of CF_4, CF_2, and F_2, respectively.

On inspection of the kinetic energy release $T_{0.5}$ measurements listed in Table 3.22, one may see that CF_3–C≡C–$CF_3^{+\bullet}$ possesses only one MI process whose products are $C_3F_3^+$ + $CF_3^\bullet$ and has a $T_{0.5}$ value of 30.1 meV. It is proposed here that the direct bond cleavage process of CF_3–C≡C–$CF_3^{+\bullet}$ → CF_3–C≡C^+ + $CF_3^\bullet$ is *not* occuring. The proposed process

occurring here is a rearrangement of CF_3–C≡C–$CF_3^{+\bullet}$ into CF_2=CF–CF=$CF_2^{+\bullet}$. Then, with the CF_2=CF–CF=$CF_2^{+\bullet}$ species in a cis configuration, an F atom from an opposite CF_2 moiety is transferred to the other CF_2 moiety resulting in a concomitant ejection of $CF_3^{\bullet}$ and a ring closure that forms the aromatic c- $C_3F_3^+$ ion.

The above propose favoured rearrangement of CF_3–C≡C–$CF_3^{+\bullet}$ to CF_2=CF–CF=$CF_2^{+\bullet}$ is further supported on inspection of the peak intensities of the MI and CID mass spectra of CF_3–C≡C–$CF_3^{+\bullet}$ listed in Table 3.23 and illustrated in Figures 3.35 and 3.36, respectively. As stated previously, there is only one MI peak, for c-$C_3F_3^+$ production. In regards to the CID mass spectrum, one may see that there are few peaks of sizable intensity. Two peaks of interest are those of CF_3^+(m/z 69), and CF_2=C=$CF_2^{+\bullet}$ (m/z 112) of 5.3 %, and 11.9% in intensity, and they correspond to the neutral losses of $C_3F_3^{\bullet}$, and CF_2, respectively. The latter process, involving the dissociation limit of CF_2=C=$CF_2^{+\bullet}$ + CF_2 is suggestive of the being a communication between the CF_2=CF–CF=$CF_2^{+\bullet}$ isomer and the "pseudo-allylic" $(CF_2)_3C^{+\bullet}$ isomer en-route to the neutral CF_2 loss.

$C_4F_4^{+\bullet}$ (m/z 124)

These isomeric fragment ions are generated by F_2 loss from the CF_3–C≡C–$CF_3^{+\bullet}$ (and/or isomerized CF_2=CF–CF=$CF_2^{+\bullet}$) parent radical-cation. There are six main $C_4F_4^{+\bullet}$ isomers to be discussed here. They are c-$C_4F_4^{+\bullet}$, CF_2=C=C=$CF_2^{+\bullet}$, CF_2=CF–C≡$CF^{+\bullet}$, CF_2=C^+–CF=$C^{\bullet}$F, $^+$CFCFCFCF$^{\bullet}$, and CF_3–C^+=C=$C^{\bullet}$F. The distonic $^+$CFCFCFCF$^{\bullet}$ species represents a ring-opened form of the aromatic cyclic c-$C_4F_4^{+\bullet}$ species. One may see that both of the c-$C_4F_4^{+\bullet}$ and CF_2=C=C=$CF_2^{+\bullet}$ isomers may be able to produce a doubly-charged

species c-$C_4F_4^{2+}$. However, due to the proposed extra stability afforded an aromatic species, the c-$C_4F_4^{+\bullet}$ ion is believed to possess a lower $\Delta_f H^0$ value and a greater ability to delocalize a 2+ charge than does the CF_2=C=C=$CF_2^{+\bullet}$ isomer. Hence, the proposed order of stability is listed as follows; c-$C_4F_4^{+\bullet}$ > CF_2=C=C=$CF_2^{+\bullet}$ > CF_2=CF–C≡$CF^{+\bullet}$ > CF_2=C^+–CF=C$^\bullet$F > $^+$CFCFCF$^\bullet$ > CF_3–C^+=C=C$^\bullet$F. The proposed energy levels of the $C_4F_4^{+\bullet}$ isomers are illustrated in Figure 3.37. The peak intensities of the MI and CID mass spectra of the $C_4F_4^{+\bullet}$ isomers are listed in Table 3.24 and illustrated in Figures 3.38 and 3.39, respectively.

On inspection of Table 3.24 and Figures 3.38 and 3.39, one may see that the $C_4F_4^{+\bullet}$ ions produced from CF_3–C≡C–$CF_3^{+\bullet}$ are mainly those of the (proposed) c-$C_4F_4^{+\bullet}$ species. This structure is suggested due to the three MI peaks of F^+C=C=C$^\bullet$F (m/z 74), CF_2=C^+F (m/z 81), and c-$C_3F_3^+$ (m/z 93), each corresponding to the neutral losses of CF_2, $C_2F^\bullet$, and $CF^\bullet$, respectively. Their peak intensities are of the same magnitude both in the MI and CID mass spectra and are 100.0 %, 0.7 %, and 49.7 %, respectively. All of these neutral losses are consistent with the c-$C_4F_4^{+\bullet}$ ring structure. For the CF_2 loss, the four-membered ring puckers and an opposite F atom is taken by the CF group and a CF_2 group is ejected. For the $C_2F^\bullet$ loss, again the four-membered ring puckers and transfers an F atom to the opposite CF moiety. The ring then opens and ejects a $^\bullet$C≡CF group. Lastly, the four-membered ring undergoes undergoes a concomitant $CF^\bullet$ ejection and a ring closure to form the three-membered aromatic c-$C_3F_3^+$ ion. One should note that a small amount of the CF_2=C=C=$CF_2^{+\bullet}$ isomer is likely to be accessed in the CID mass spectrum by the presence of the peak for CF_2=C=C=C^+F (m/z 143) of 6.6 % intensity, corresponding to the neutral $F^\bullet$

Figure 3.37 Proposed Energy Levels of the $C_4F_4^{+\bullet}$ (m/z 124) Isomers

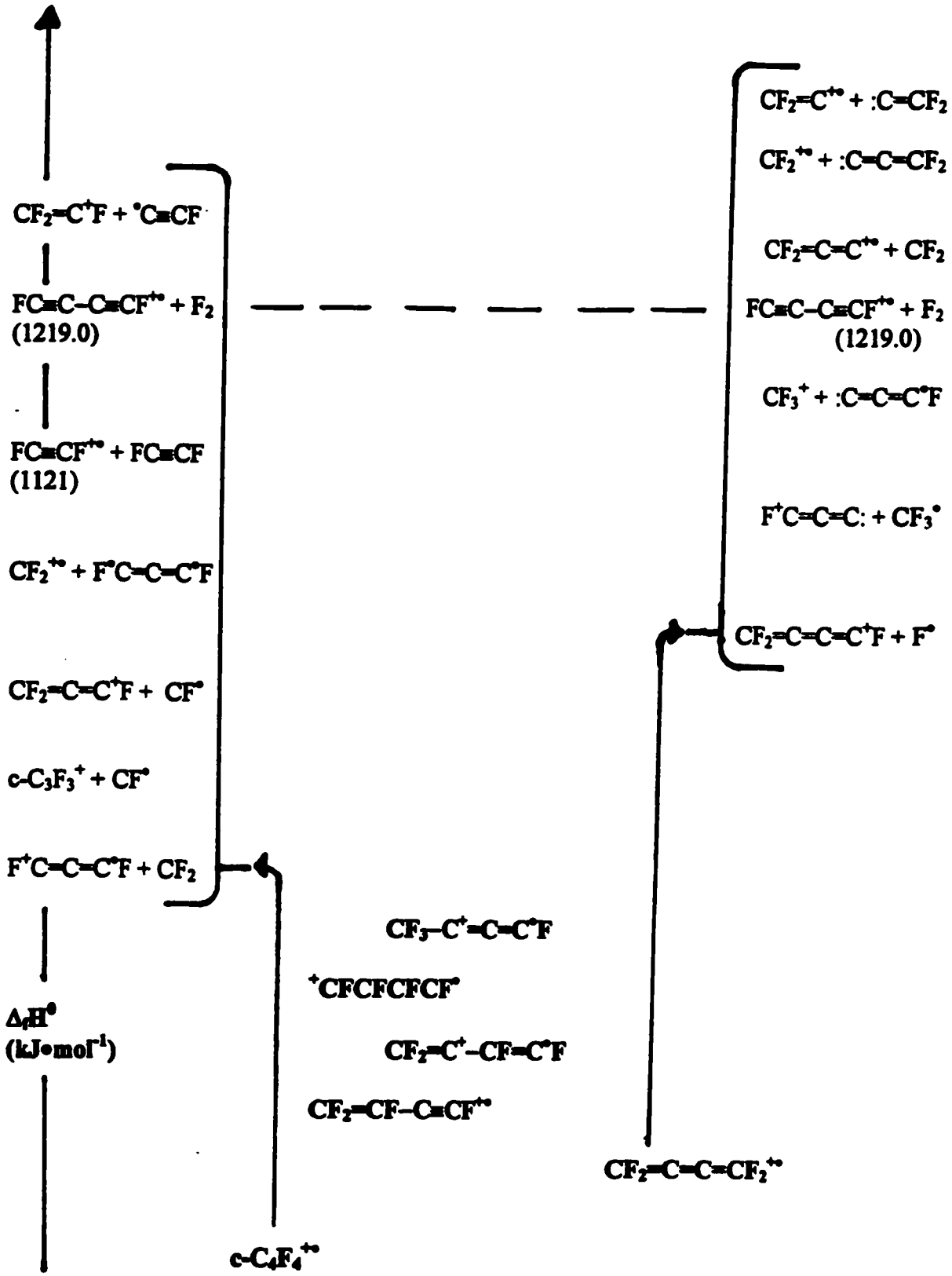

Table 3.24 Metastable Ion (MI) 2FFR and Collision Induced Dissociation (CID) 2FFR $O_2 \approx 90$ %T Mass Spectra of Source Generated $C_4F_4^{+\bullet}$ (m/z 124) from CF_3–C≡C–CF_3

Species	Mass (m/z)	Neutral Loss	Height (%) MI	CID
$C_4F_3^+$	105	($-F^\bullet$)		6.6
$C_3F_3^+$	93	($-CF^\bullet$)	49.7	49.7
$C_4F_2^{+\bullet}$	86	($-F_2$)		1.3
$C_2F_3^+$	81	($-C_2F^\bullet$)	0.7	0.7
$C_3F_2^{+\bullet}$	74	($-CF_2$)	100.0	100.0
CF_3^+	69			2.6
$C_4F_4^{2+}$	62			2.0
$C_2F_2^{+\bullet}$	62	($-C_2F_2$)		0.7
C_3F^+	55	($-CF_3^\bullet$)		7.3
$CF_2^{+\bullet}$	50			2.6
C_2F^+	43			<0.3
$C_3^{+\bullet}$	36	($-CF_4$)		<0.3
CF^+	31			1.3

Figure 3.38 Metastable Ion (MI) 2FFR Mass Spectrum of Source Generated $C_4F_4^{+\bullet}$ (m/z 124) from CF_3–C≡C–CF_3

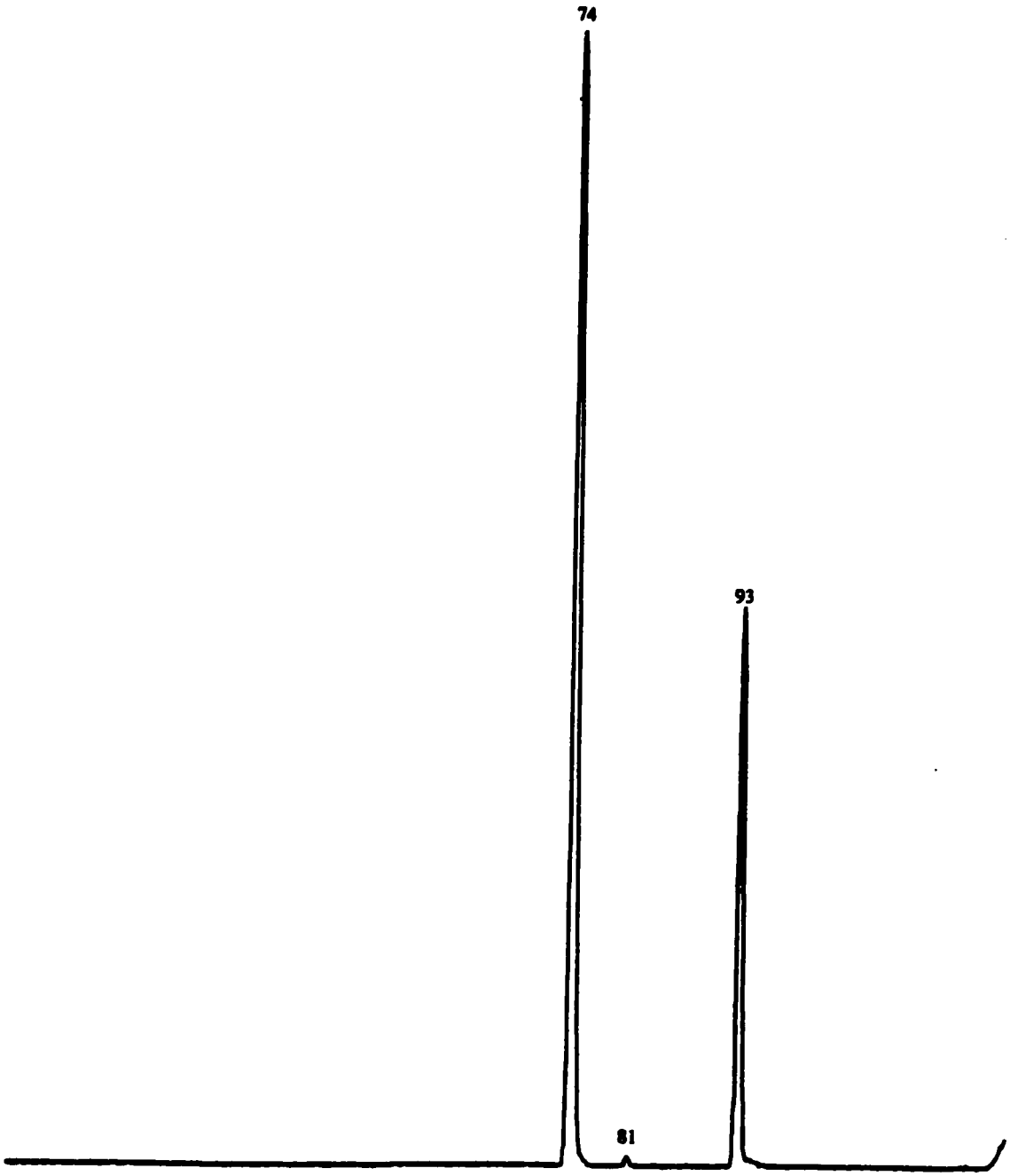

Figure 3.39 Collision Induced Dissociation (CID) 2FFR O_2 ≈ 90 %T Mass Spectrum of Source Generated $C_4F_4^{+\bullet}$ (m/z 124) from CF_3–C≡C–CF_3

loss. Additionally, one should note the significant doubly-charged peak for $C_4F_4^{2+}$ (m/z 62) with an intensity of 2.0 %. It is believed here to be mainly due to the cyclic aromatic c-$C_4F_4^{+\bullet}$ species, however there may be as well some $CF_2{=}C{=}C{=}CF_2^{+\bullet}$ present as well.

$C_3F_4^{+\bullet}$ (m/z 112)

These isomeric fragment ions are generated by CF_2 loss from the $CF_3{-}C{\equiv}C{-}CF_3^{+\bullet}$ parent-ion. There are three main isomers to be discussed here. They are, perfluoroallene $CF_2{=}C{=}CF_2^{+\bullet}$, perfluoropropyne $CF_3{-}C{\equiv}CF^{+\bullet}$, and the distonic $^{+}CF_2{-}CF{=}C^{\bullet}F$ species. The $CF_2{=}C{=}CF_2^{+\bullet}$ ion has an experimentally known Δ_fH^0 value of 456 kJ•mol^{-1}, whereas the $CF_3{-}C{\equiv}CF^{+\bullet}$ isomer does not. However as previously stated in section 3.2 and illustrated in Table 3.5, the replacement of an F atom by a CF_3 group (unsaturated) molecule and/or radical tends to *systematically raise* the IE_a value by an increment of ≈ 0.50 eV. If one may take the midpoint between the known IE_a values of $FC{\equiv}CF$ and $CF_3{-}C{\equiv}C{-}CF_3$ to be a reasonable estimate of $IE_a[CF_3{-}C{\equiv}CF]$, thus upon utilization of the Benson value (see Table 3.5) of $\Delta_fH^0[CF_3{-}C{\equiv}CF]$ = –538.0 kJ•mol^{-1} one may arrive at a value of $\Delta_fH^0[CF_3{-}C{\equiv}CF^{+\bullet}]$ ≈ 597 kJ•mol^{-1}. Therefore, the proposed order of stability of the $C_3F_4^{+\bullet}$ isomers is listed as follows; $CF_2{=}C{=}CF_2^{+\bullet} > CF_3{-}C{\equiv}CF^{+\bullet} > {}^{+}CF_2{-}CF{=}C^{\bullet}F$. The proposed energy levels of the $C_3F_4^{+\bullet}$ isomers are illustrated in Figure 3.40. The peak intensities of the MI and CID peaks of the $C_3F_4^{+\bullet}$ isomers are listed in Table 3.25 and illustrated in Figures 3.41 and 3.42, respectively.

Figure 3.40 Proposed Energy Levels of the $C_3F_4^{+\bullet}$ (m/z 112) Isomers

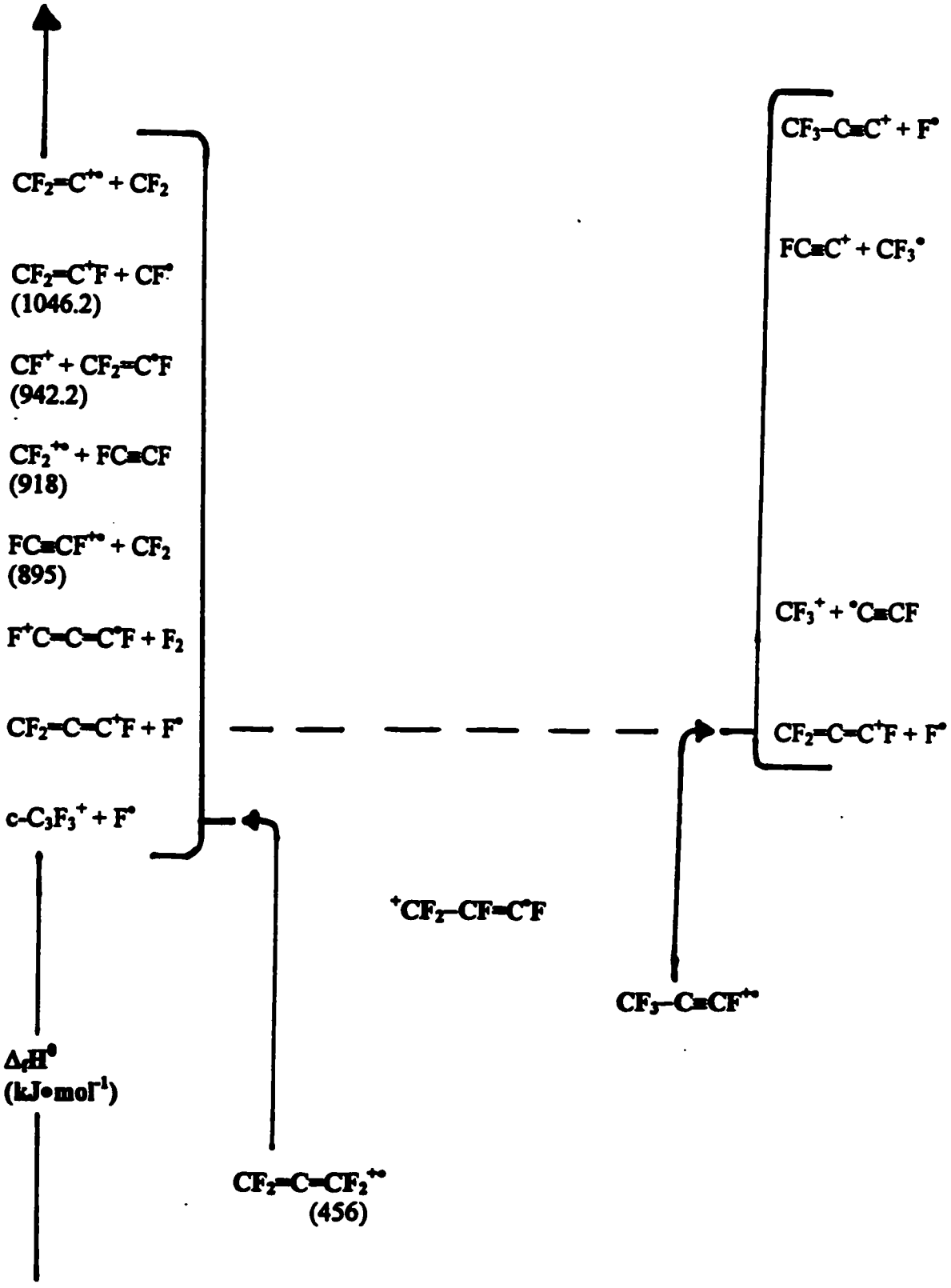

Table 3.25 Metastable Ion (MI) 2FFR and Collision Induced Dissociation (CID) 2FFR He ≈ 90 %T Mass Spectra of Source Generated $C_3F_4^{+\bullet}$ (m/z 112) from CF_3–C≡C–CF_3

Species	Mass (m/z)	Neutral Loss	Height (%) MI	CID
$C_3F_3^+$	93	(–F$^\bullet$)	100.0	100.0
$C_2F_3^+$	81	(–CF$^\bullet$)		0.7
$C_3F_2^{+\bullet}$	74	($-F_2$)		19.2
CF_3^+	69	($-C_2F^\bullet$)		2.0
$C_2F_2^{+\bullet}$	62	($-CF_2$)		9.3
C_3F^+	55			2.6
$CF_2^{+\bullet}$	50	($-C_2F_2$)		5.3
C_2F^+	43	($-CF_3^\bullet$)		2.0
$CF^{+\bullet}$	31	($-C_2F_3^\bullet$)		10.6

Figure 3.41 Metastable Ion (MI) 2FFR Mass Spectrum of Source Generated $C_3F_4^{+\bullet}$ (m/z 112) from CF_3–C≡C–CF_3

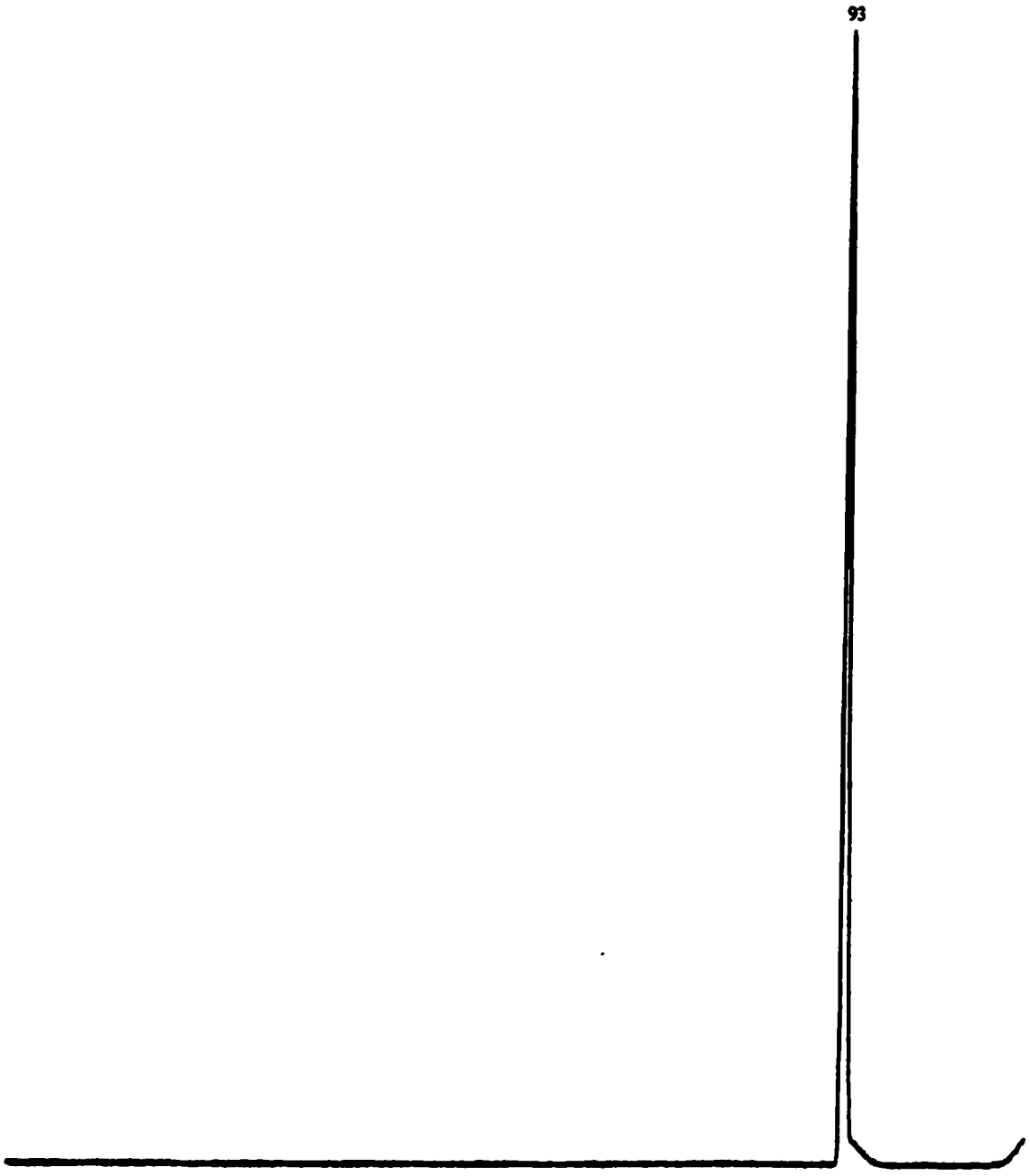

Figure 3.42 Collision Induced Dissociation (CID) 2FFR He ≈ 90 %T Mass Spectrum of Source Generated $C_3F_4^{+\bullet}$ (m/z 112) from $CF_3–C{\equiv}C–CF_3$

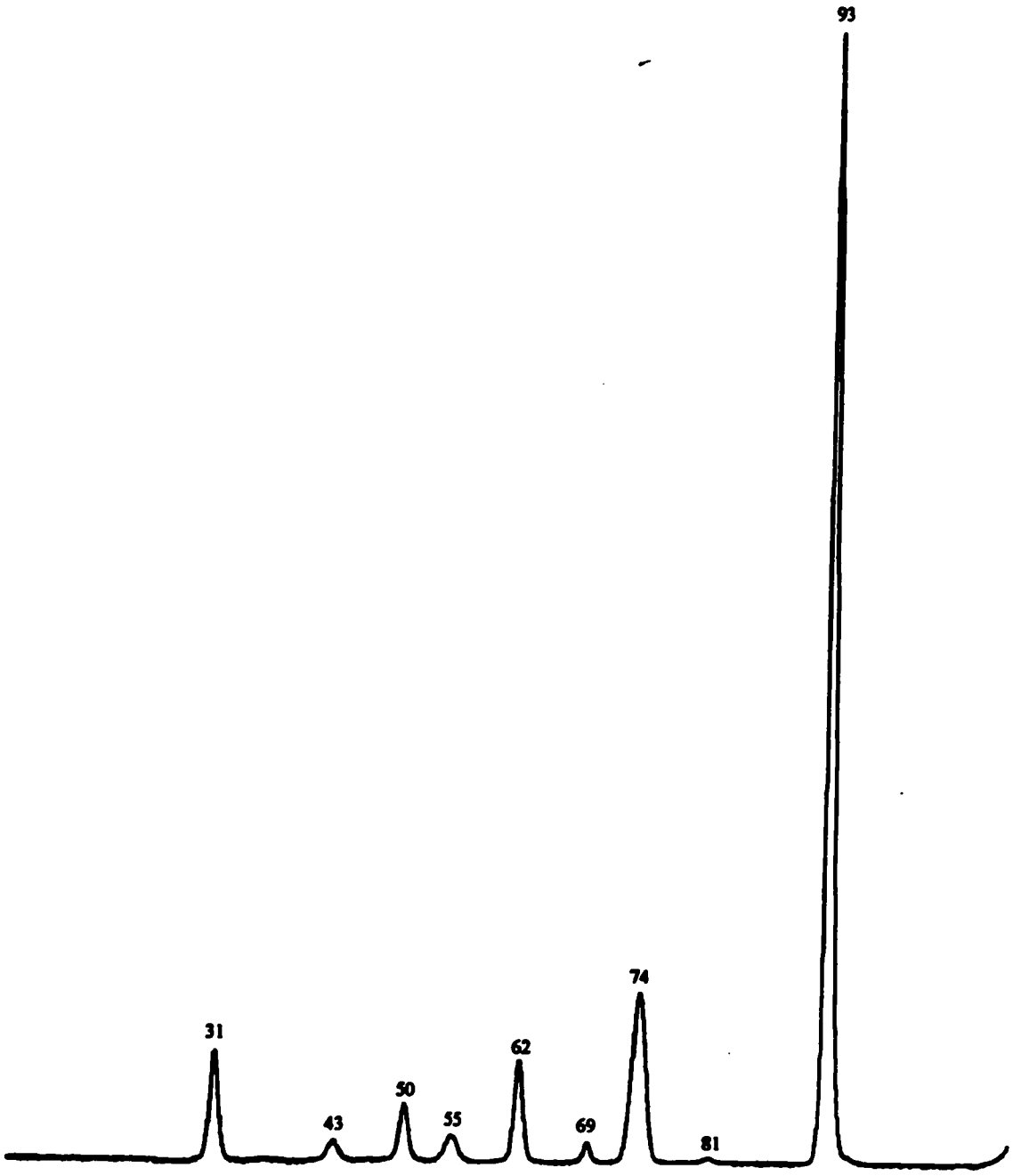

On inspection of Table 3.25 and Figures 3.41 and 3.42, one may see that the $C_3F_4^{+\bullet}$ ions produced from CF_3–C≡C–$CF_3^{+\bullet}$ are most likely dominated by the CF_2=C=$CF_2^{+\bullet}$ isomer. As well, there is only one MI peak for the c-$C_3F_3^+$ (m/z 93) ion. This suggests that the CF_2=C=$CF_2^{+\bullet}$ isomer is in communication with the $^+CF_2$–CF=C$^\bullet$F isomer en-route to the dissociation limit c-$C_3F_3^+$ + $F^\bullet$. In regards to the CID mass spectrum, the peaks of significant intensity are those of 10.6 %, 9.3 %, and 19.2 % for the CF^+ (m/z 31), FC≡$CF^{+\bullet}$ (m/z 62), and F^+C=C=C$^\bullet$F (m/z 74) ions, corresponding to neutral losses of CF_2=C$^\bullet$F, CF_2, and F_2, respectively. This again supports the suggestion of a CF_2=C=$CF_2^{+\bullet}$ isomer undergoing dissociations in communication with the distonic $^+CF_2$–CF=C$^\bullet$F isomer. However, it should be noted that some of the CF_3–C≡$CF^{+\bullet}$ isomer is accessed in the CID mass spectrum because of the presence of the peaks of intensity of 2.0 %, and 2.0 % for the FC≡C^+ (m/z 43), and CF_3^+ (m/z 69) ions, corresponding ot the neutral losses of $CF_3^\bullet$ and $^\bullet$C≡CF, respectively. Thus it is believed here that the dominant isomer produced here is CF_2=C=$CF_2^{+\bullet}$, which is in communication with the distonic $^+CF_2$–CF=C$^\bullet$F isomer en-route to dissociation.

$C_3F_3^+$ (m/z 93)

These isomeric fragment ions are generated by $CF_3^\bullet$ loss from the CF_3–C≡C–$CF_3^{+\bullet}$ parent-ion. There are four main $C_3F_3^+$ isomers to be discussed here. They are c-$C_3F_3^+$, CF_2=C=C$^+$F, $^+$CFCFC$F^\bullet$, and CF_3–C≡C^+. The distonic $^+$CFCFC$F^\bullet$ species denotes a ring opened c-$C_3F_3^+$ ion. As stated previously, the natural expectation for the production of a $C_3F_3^+$ ion from the CF_3–C≡C–$CF_3^{+\bullet}$ parent-ion may be taken to be that of a simple bond cleavage yielding the CF_3–C≡C^+ + $CF_3^\bullet$ dissociation products. However, it is proposed here

Figure 3.43 Proposed Energy Levels of the $C_3F_3^+$ (m/z 93) Isomers

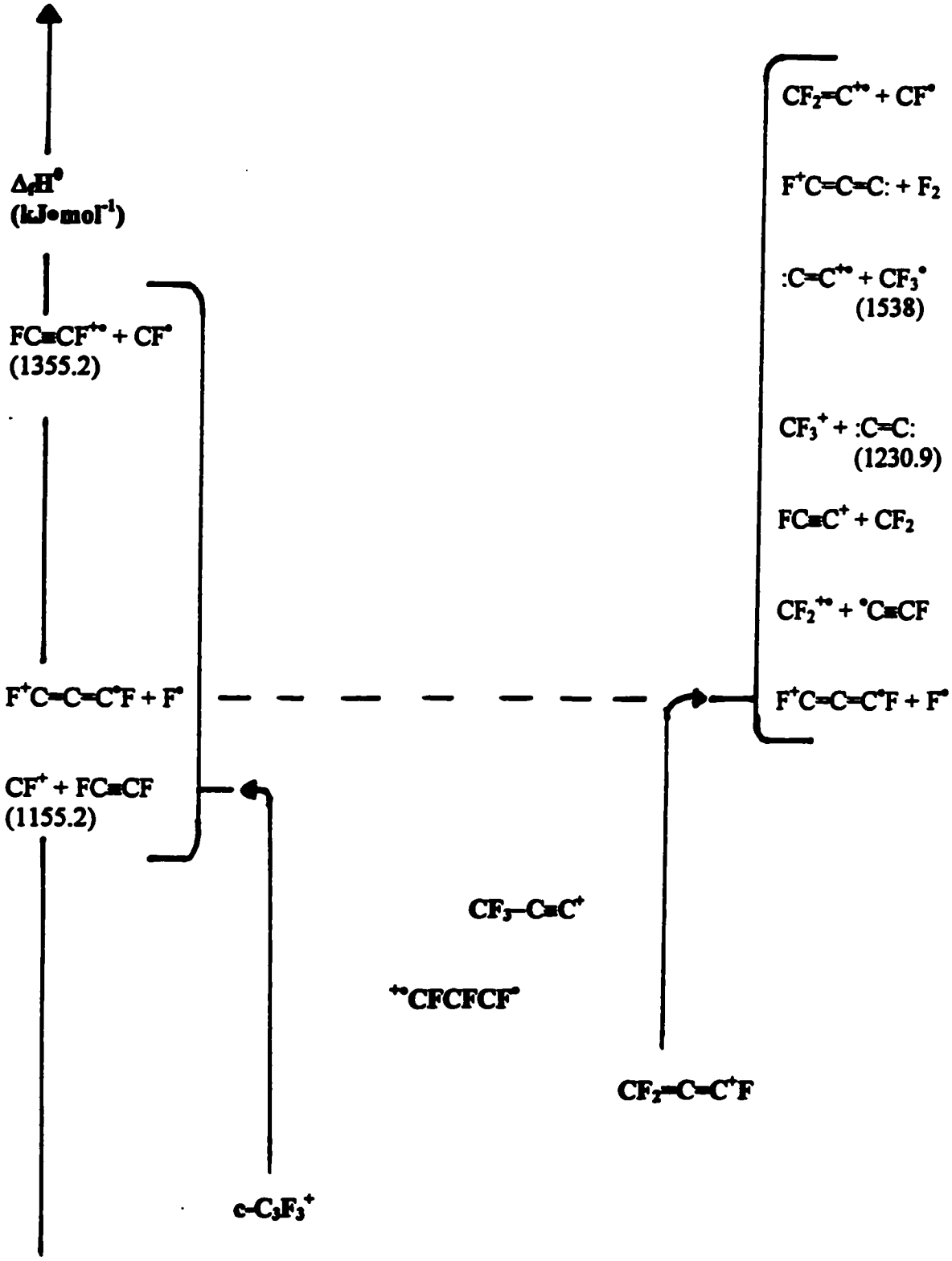

Table 3.26 Metastable Ion (MI) 2FFR and Collision Induced Dissociation (CID) 2FFR O_2 ≈ 90 %T Mass Spectra of Source Generated $C_3F_3^+$ (m/z 93) from CF_3–C≡C–CF_3

Species	Mass (m/z)	Neutral Loss	Height (%) MI	CID
$C_3F_2^{+\bullet}$	74	(–F$^\bullet$)	2.0	100.0
CF_3^+	69	(–C_2)		2.0
$C_2F_2^{+\bullet}$	62	(–CF$^\bullet$)		11.9
C_3F^+	55	(–F_2)		15.9
$CF_2^{+\bullet}$	50	(–$C_2F^\bullet$)		13.9
$C_3F_3^{2+\bullet}$	46.5			11.3
C_2F^+	43	(–CF_2)		15.9
$C_3F_2^{2+}$	37			2.6
$C_3^{+\bullet}$	36			1.3
CF^+	31	(–C_2F_2)	100.0	84.8
$C_2^{+\bullet}$	24	(–$CF_3^\bullet$)		0.7

Figure 3.44 Metastable Ion (MI) 2FFR Mass Spectrum of Source Generated $C_3F_3^+$ (m/z 93) from CF_3–C≡C–CF_3

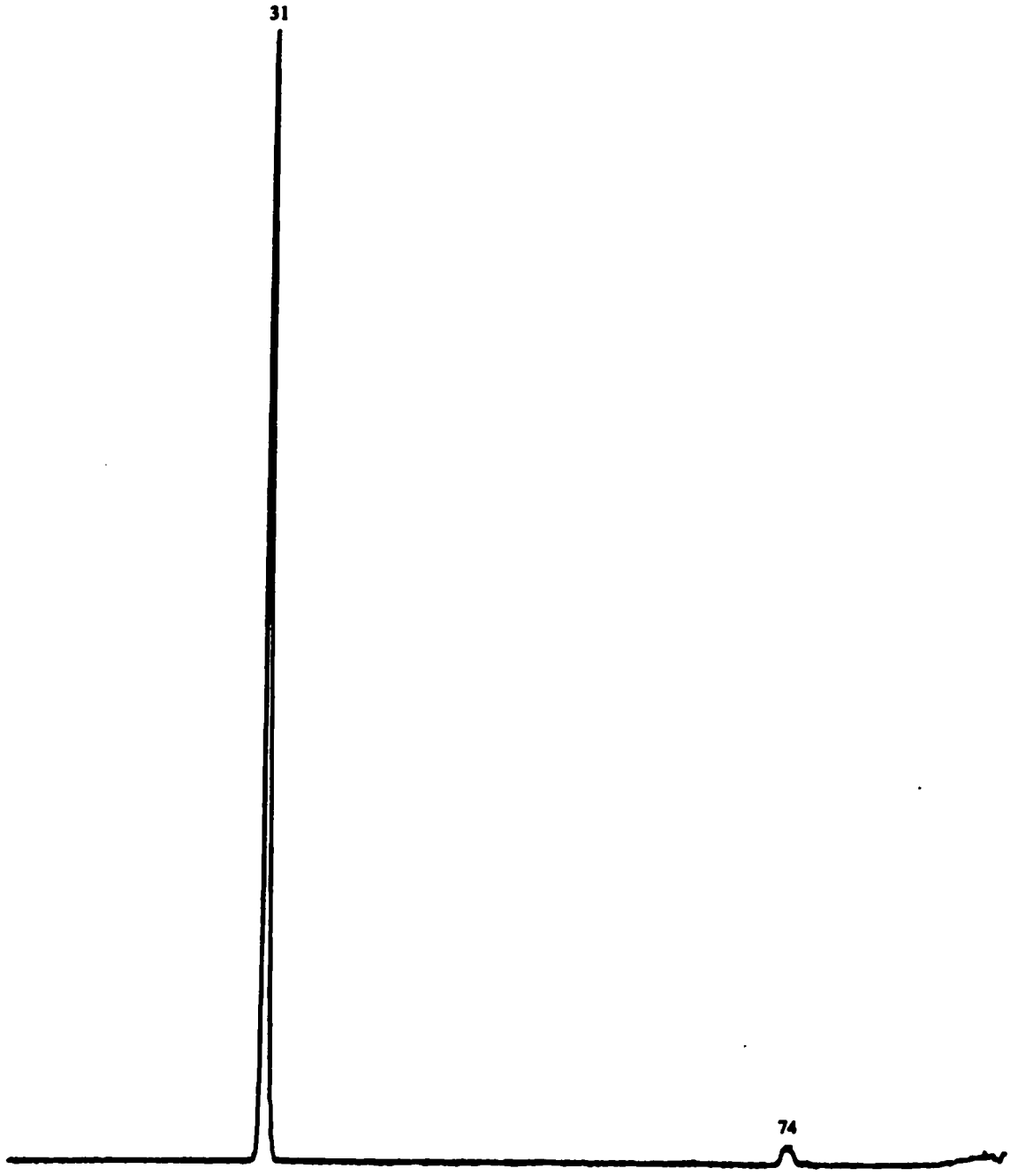

Figure 3.45 Collision Induced Dissociation (CID) 2FFR O_2 ≈ 90 %T Mass Spectrum of Source Generated $C_3F_3^+$ (m/z 93) from CF_3–C≡C–CF_3

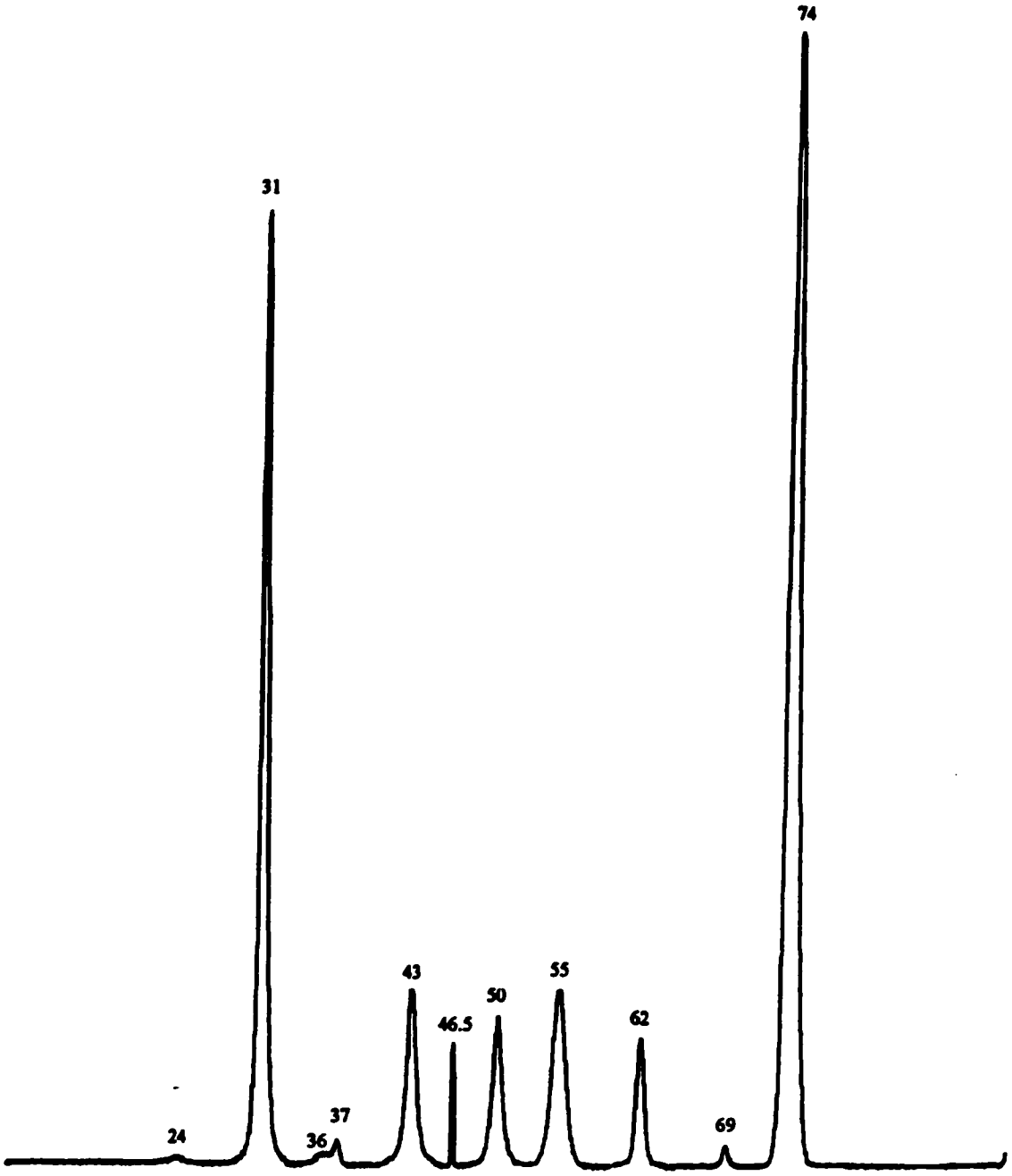

that CF_3–C≡C–$CF_3^{+\bullet}$ undergoes a favoured rearrangement to CF_2=CF–CF=$CF_2^{+\bullet}$, which in the cis configuration undergoes a concomitant $CF_3^{\bullet}$ ejection and ring-closure to from the dissociation products c-$C_3F_3^+$ + $CF_3^{\bullet}$. The proposed order of stability is listed as follows; c-$C_3F_3^+$ > CF_2=C=C^+F > $^+$CFCFC$F^{\bullet}$ > CF_3–C≡C^+. The proposed energy levels of the $C_3F_3^+$ isomers are illustrated in Figure 3.43. The peak intensities of the MI and CID mass spectra of the $C_3F_3^+$ isomers are listed in Table 3.26 and illustrated in Figures 3.44 and 3.45, respectively.

On inspection of Table 3.26 and Figures 3.34 and 3.45, one may see that the $C_3F_3^+$ ions produced from CF_3–C≡C–$CF_3^{+\bullet}$ are likely dominated by the c-$C_3F_3^+$ isomer. There are two MI peaks of intensity of 100.0 %, and 2.0 % for the CF^+ (m/z 31), and F^+C=C=C$^{\bullet}$F (m/z 74) ions, corresponding to the neutral losses of FC≡CF, and $F^{\bullet}$, respectively. In regards to the CID mass spectrum, there are two doubly-charged peaks for c-$C_3F_3^{2+\bullet}$ (m/z 46.5) and F^+C=C=C^+F (m/z 37) with intensities of 11.3 % and 2.6%, respectively. These two peaks are linked through the ring-opening process of c-$C_3F_3^{2+\bullet}$ → F^+C=C=C^+F + $F^{\bullet}$. It should be noted that the F^+C=C=C^+F species is isoelectronic with the neutral species carbon suboxide, O=C=C=C=O.

Additionally, along with the FC≡$CF^{+\bullet}$ + $CF^{\bullet}$ dissociation limit related to the c-$C_3F_3^+$ isomer, one may see that the CF_2=C=C^+F isomer and to a lesser extent the CF_3–C≡C^+ isomer are accessed in the CID mass spectrum due to the activation of the $CF_2^{+\bullet}$ + $^{\bullet}$C≡CF, FC≡C^+ + CF_2; and the CF_3^+ + :C=C:, :C=$C^{+\bullet}$ + $CF_3^{\bullet}$, pairs of dissocaition limits, correspondingly.

$C_3F_2^{+\bullet}$ (m/z 74)

These isomeric fragment ions are generated by CF_4 loss from the CF_3–C≡C–$CF_3^{+\bullet}$ parent-ion. There are three main $C_3F_2^{+\bullet}$ isomers to be discussed here. They are $F^+C{=}C{=}C^\bullet F$, $CF_2{=}C{=}C^{+\bullet}$, and the cyclic c-F(C C̈ C)$F^{+\bullet}$ where (C C̈ C) denotes a three-membered ring consisting of a C̈ carbene atom astride a FC=CF moiety. The proposed order of stability of the $C_3F_2^{+\bullet}$ isomers is listed as follows; $F^+C{=}C{=}C^\bullet F > CF_2{=}C{=}C^{+\bullet} >$ c-F(C C̈ C)$F^{+\bullet}$. The proposed energy levels of the $C_3F_2^{+\bullet}$ isomers are illustrated in Figure 3.46. The peak intensities of the MI and CID mass spectra of the $C_3F_2^{+\bullet}$ isomers are listed in Table 3.27 and illustrated in Figures 3.47 and 3.48, respectively.

On inspection of Table 3.27 and Figures 3.47 and 3.48, one may see that the $C_3F_2^{+\bullet}$ ions produced from CF_3–C≡C–$CF_3^{+\bullet}$ are likely dominated by the $F^+C{=}C{=}C^\bullet F$ isomer. There are two MI peaks of intensity of 0.7 %, and 100.0 % for the CF^+ (m/z 31), and $F^+C{=}C{=}C$: (m/z 55) ions, corresponding to the neutral losses of $^\bullet C{\equiv}CF$ and $F^\bullet$, respectively. In regards to the CID mass spectrum, there is a doubly-charged peak for $F^+C{=}C{=}C^+F$ (m/z 37) with an intensity of 1.3%. As stated previously, the $F^+C{=}C{=}C^+F$ species is isoelectronic with the O=C=C=C=O neutral. Additionally, it should be noted that both of the isomers $CF_2{=}C{=}C^{+\bullet}$ and c-F(C C̈ C)$F^{+\bullet}$ are also accessed to an extent in the CID mass spectra. For the $CF_2{=}C{=}C^{+\bullet}$ isomer, the $CF_2^{+\bullet}$ + :C=C: and :C=$C^{+\bullet}$ + CF_2 dissociation limits are observed to active. For the c-F(C C̈ C)$F^{+\bullet}$ isomer to a lesser extent, the FC≡$CF^{+\bullet}$ + C dissociation limit is observed to be active. Thus, although to some smaller extent $CF_2{=}C{=}C^{+\bullet}$ and c-F(C C̈ C)$F^{+\bullet}$ are both accessed in the CID mass spectra, the dominant structure is proposed to be that of the $F^+C{=}C{=}C^\bullet F$ isomer.

Figure 3.46 Proposed Energy Levels of the $C_3F_2^{+\bullet}$ (m/z 74) Isomers

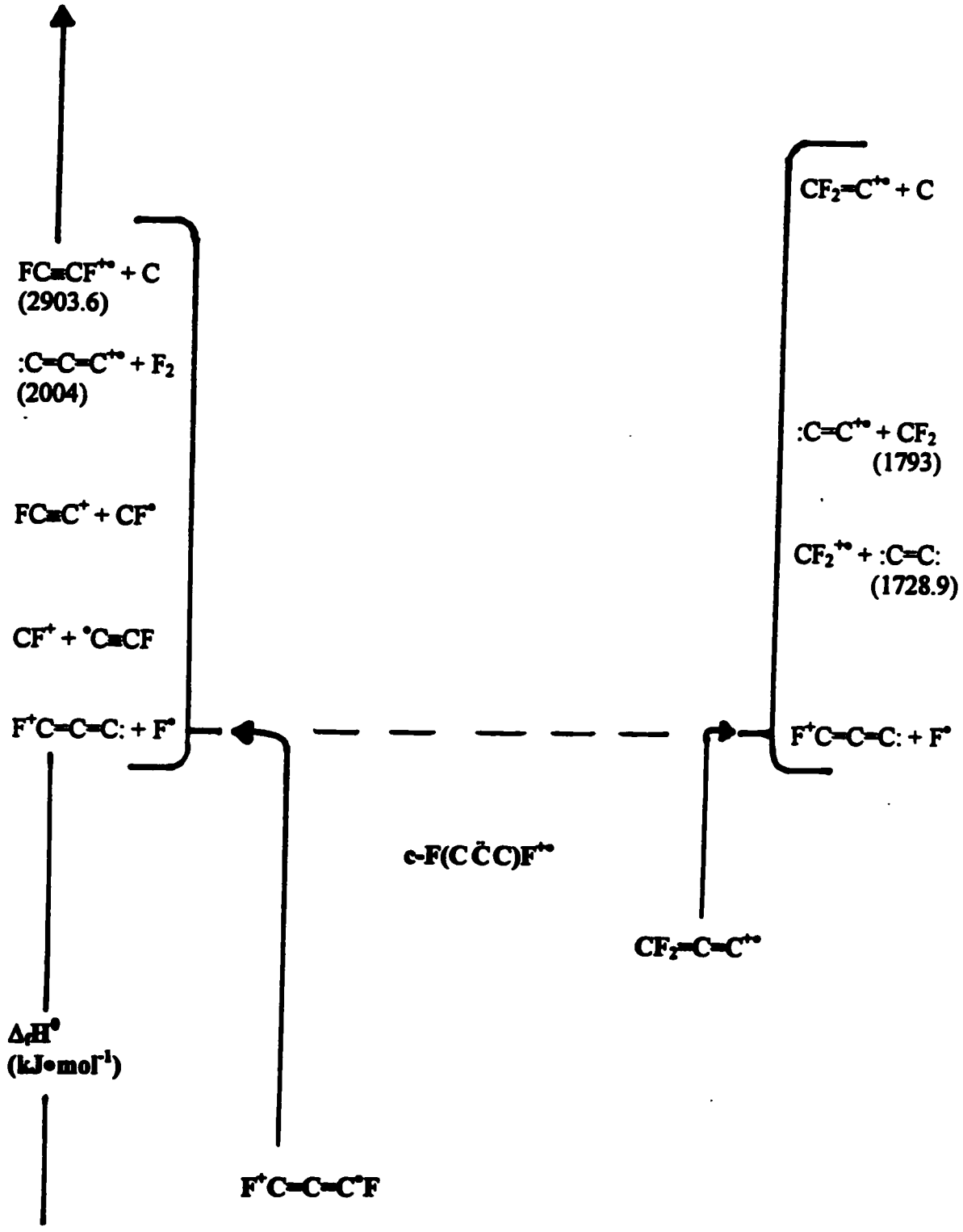

Table 3.27 Metastable Ion (MI) 2FFR and Collision Induced Dissociation (CID) 2FFR $O_2 \approx 90$ %T Mass Spectra of Source Generated $C_3F_2^{+\bullet}$ (m/z 74) from CF_3–C≡C–CF_3

Species	Mass (m/z)	Neutral Loss	Height (%) MI	CID
$C_2F_2^{+\bullet}$	62	(–C)		0.7
C_3F^+	55	(–F$^\bullet$)	100.0	100.0
$CF_2^{+\bullet}$	50	(–C_2)		3.3
C_2F^+	43	(–CF$^\bullet$)		3.3
$C_3F_2^{2+}$	37			1.3
$C_3^{+\bullet}$	36	(–F_2)		0.3
$CF^{+\bullet}$	31	(–$C_2F^\bullet$)	0.7	14.6
$C_2^{+\bullet}$	24	(–CF_2)		0.7

Figure 3.47 Metastable Ion (MI) 2FFR Mass Spectrum of Source Generated $C_3F_2^{+\bullet}$ (m/z 74) from $CF_3–C{\equiv}C–CF_3$

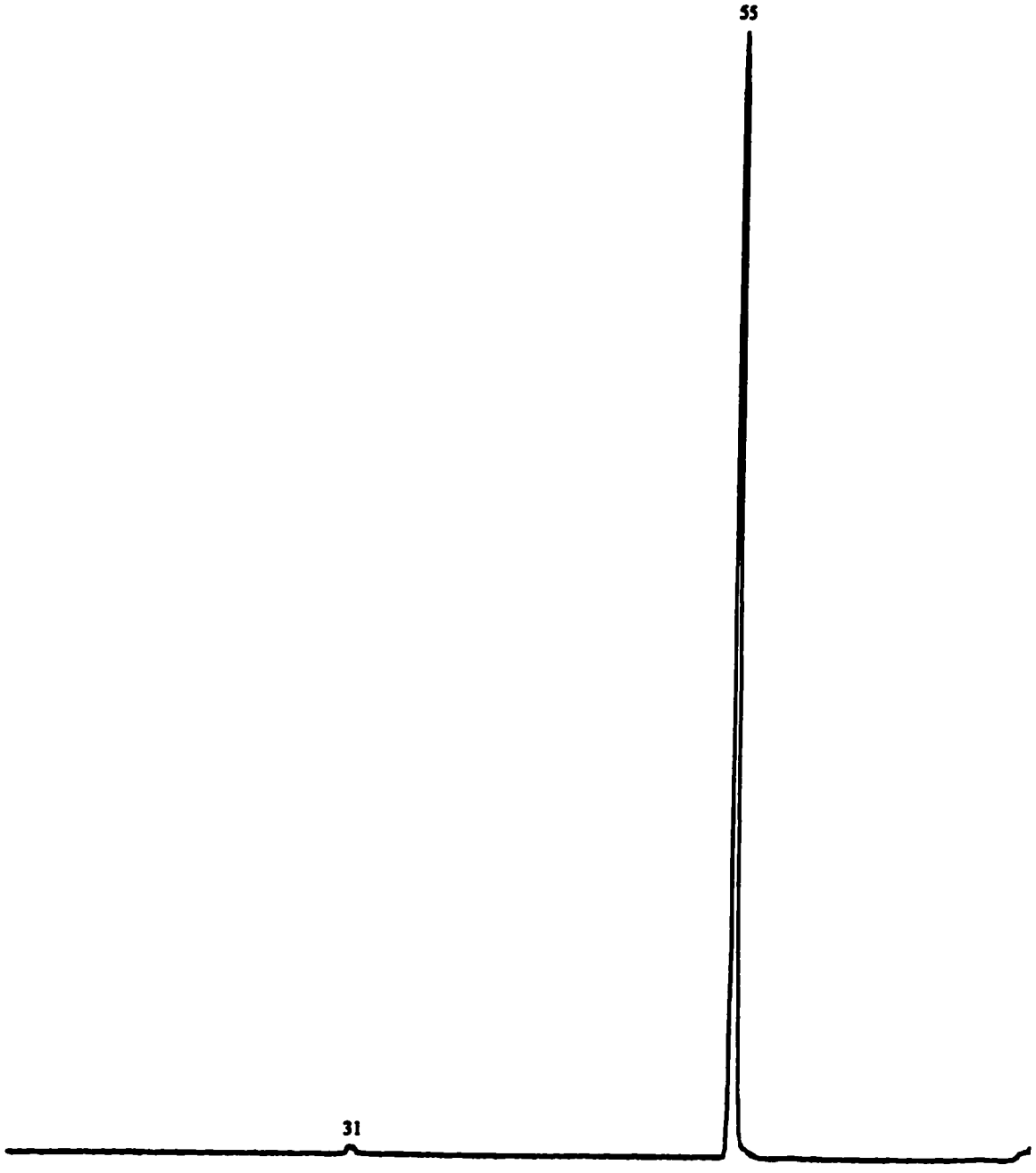

Figure 3.48 Collision Induced Dissociation (CID) 2FFR O_2 ≈ 90 %T Mass Spectrum of Source Generated $C_3F_2^{+\bullet}$ (m/z 74) from CF_3–C≡C–CF_3

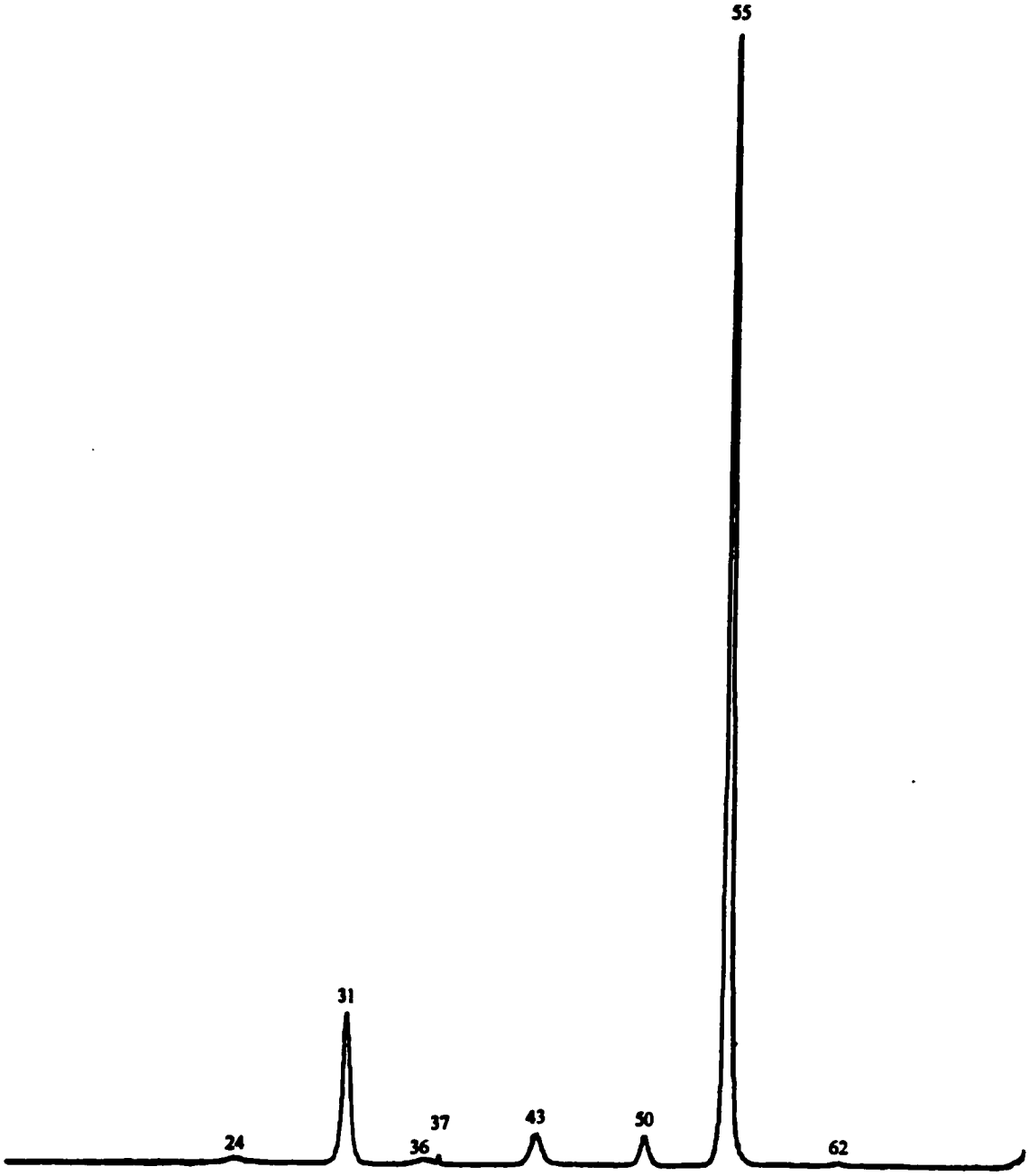

$C_3F_6^{+\bullet}$ (m/z 150)

The precursor molecule that will be used here is perfluoropropene, CF_2=$CFCF_3$. There are four main $C_3F_6^{+\bullet}$ isomers to be discussed here. They are perfluoropropene CF_2=$CFCF_3^{+\bullet}$, perfluorocyclopropane, c-$C_3F_6^{+\bullet}$, the distonic perfluorotrimethylene, $^{+}CF_2CF_2CF_2^{\bullet}$, and the perfluorodimethylcarbene $(CF_3)_2C^{+\bullet}$ ions, respectively. There are known values of $\Delta_fH^0[CF_2$=$CFCF_3^{+\bullet}] = -102$ kJ•mol^{-1}, and $\Delta_fH^0[c\text{-}C_3F_6^{+\bullet}] = 101$ kJ•mol^{-1} available in the literature [1]. The distonic $^{+}CF_2CF_2CF_2^{\bullet}$ species represents an open-chain form of c-$C_3F_6^{+\bullet}$. The $(CF_3)_2C^{+\bullet}$ isomer, due to the presence of the two CF_3 groups which are known to be strongly electron-withdrawing, is proposed here to have the highest Δ_fH^0 value. Thus, the proposed order of stability is listed as follows; CF_2=$CFCF_3^{+\bullet}$ > c-$C_3F_6^{+\bullet}$ > $^{+}CF_2CF_2CF_2^{\bullet}$ > $(CF_3)_2C^{+\bullet}$. The proposed energy levels of the $C_3F_6^{+\bullet}$ isomers are illustrated in Figure 3.49. The peak intensities of the normal mass spectrum of CF_2=$CFCF_3^{+\bullet}$ are listed in Table 3.28 and illustrated in Figure 3.50. The kinetic energy release $T_{0.5}$ values for CF_2=$CFCF_3^{+\bullet}$ are listed in Table 3.22. The peak intensities of the MI and CID mass spectra of the $C_3F_6^{+\bullet}$ isomers are listed in Table 3.29 and illustrated in Figures 3.51 and 3.52, respectively.

On inspection of Table 3.28 and Figure 3.50, one may note the following trends in the normal mass spectra of CF_2=$CFCF_3^{+\bullet}$. The major peaks of intensity of 61.6 %, 49.0 %, 100.0 %, and 63.6 % for the CF_3^+ (m/z 69), $C_2F_4^{+\bullet}$ (m/z 100), $C_3F_5^+$ (m/z 131), and CF_2=$CFCF_3^{+\bullet}$ (m/z 150) ions, correspond for the first three fragment-ions to the neutral losses of CF_2=$C^{\bullet}F$, CF_2, and $F^{\bullet}$, respectively. The minor peaks of smaller intensities of 16.0

Figure 3.49 Proposed Energy Levels of the $C_3F_6^{+\bullet}$ (m/z 150) Isomers

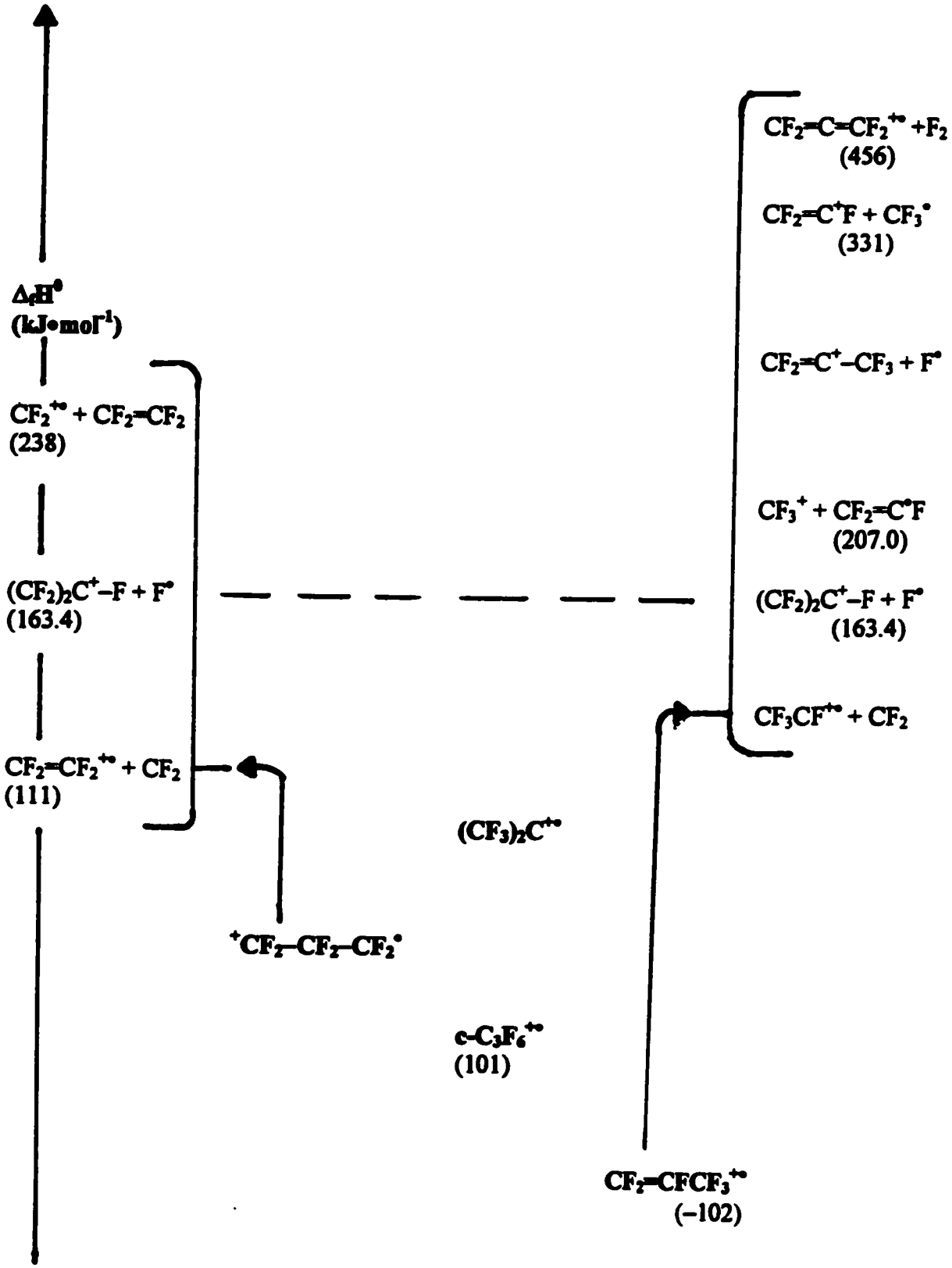

Table 3.28 Normal Mass Spectra of Perfluoropropene CF_2=$CFCF_3$

Species	Mass (m/z)	Neutral Loss	Height (%)
$C_3F_6^{+\bullet}$	150		63.6
$C_3F_5^{+}$	131	($-F^{\bullet}$)	100.0
$C_3F_4^{+\bullet}$	112	($-F_2$)	1.3
$C_2F_4^{+\bullet}$	100	($-CF_2$)	49.0
$C_3F_3^{+}$	93		4.0
$C_2F_3^{+}$	81	($-CF_3^{\bullet}$)	11.9
$C_3F_2^{+\bullet}$	74		0.7
CF_3^{+}	69	($-C_2F_3^{\bullet}$)	61.6
$C_2F_2^{+\bullet}$	62	($-CF_4$)	2.6
C_3F^{+}	55		0.7
$CF_2^{+\bullet}$	50	($-C_2F_4$)	4.0
C_2F^{+}	43		0.7
CF^{+}	31	($-C_2F_5^{\bullet}$)	16.0

Figure 3.50 Normal Mass Spectrum of Perfluoropropene CF_2=$CFCF_3^{+\bullet}$ (m/z 150)

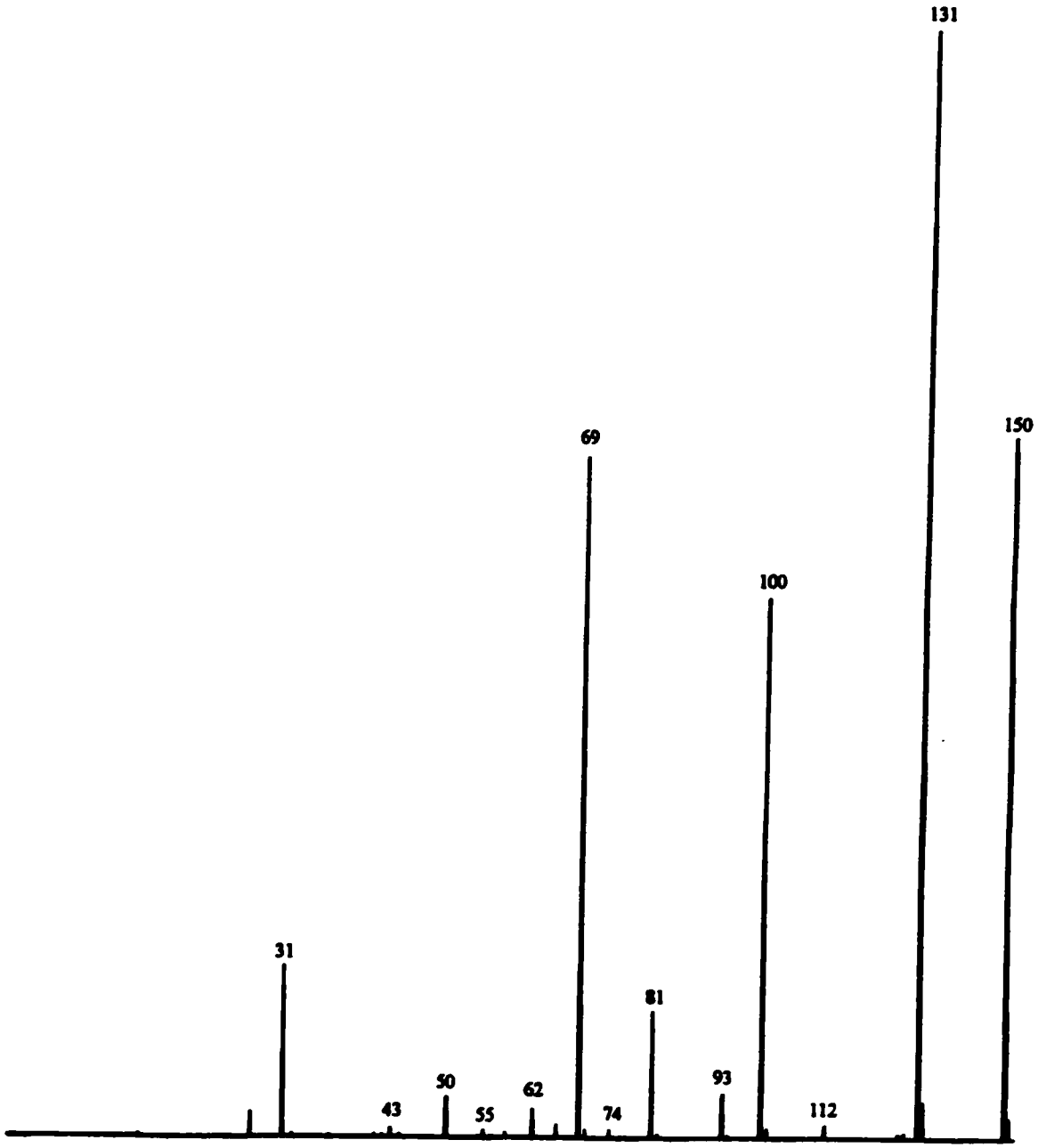

Table 3.29 Metastable Ion (MI) 2FFR and Collision Induced Dissociation (CID) 2FFR He ≈ 90 %T Mass Spectra of Perfluoropropene $CF_2{=}CFCF_3^{+\bullet}$ (m/z 150)

Species	Mass (m/z)	Neutral Loss	Height (%) MI	CID
$C_3F_5^+$	131	($-F^\bullet$)		6.0
$C_3F_4^{+\bullet}$	112	($-F_2$)		0.7
$C_2F_4^{+\bullet}$	100	($-CF_2$)	100.0	100.0
$C_3F_3^+$	93			6.0
$C_2F_3^+$	81	($-CF_3^\bullet$)		9.3
$C_3F_4^{+\bullet}$	74			1.3
CF_3^+	69	($-C_2F_3^\bullet$)		48.3
$C_3F_5^{2+\bullet}$	65.5			0.7
$C_2F_2^{+\bullet}$	62	($-CF_4$)		2.6
C_3F^+	55			0.7
$CF_2^{+\bullet}$	50	($-C_2F_4$)		3.3
C_2F^+	43			0.7
CF^+	31	($-C_2F_5^\bullet$)		5.3

Figure 3.51 Metastable Ion (MI) 2FFR Mass Spectrum of Perfluoropropene CF_2=$CFCF_3^{+\bullet}$ (m/z 150)

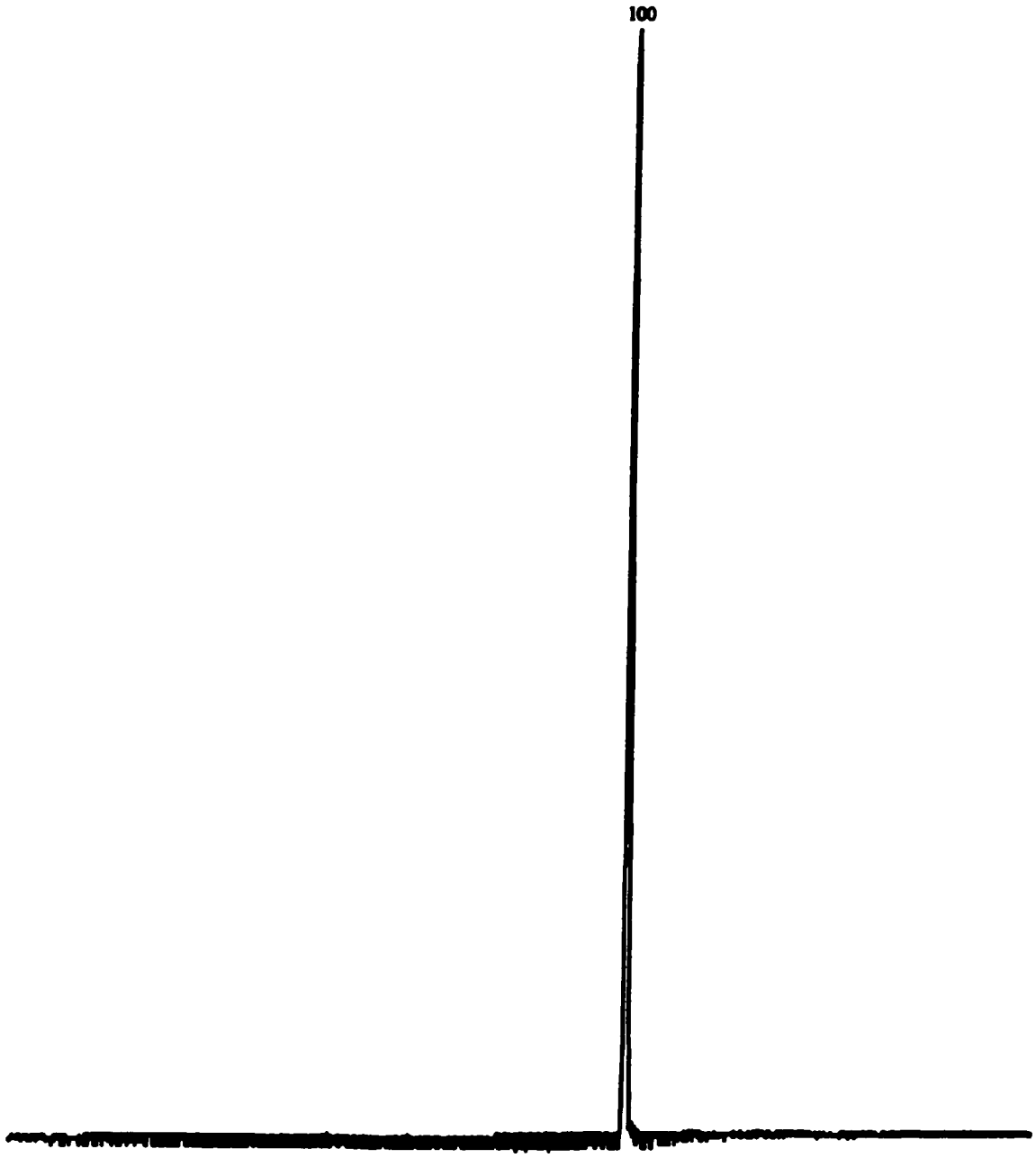

Figure 3.52 Collision Induced Dissociation (CID) 2FFR He ≈ 90 %T Mass Spectrum of Perfluoropropene CF_2=$CFCF_3^{+\bullet}$ (m/z 150)

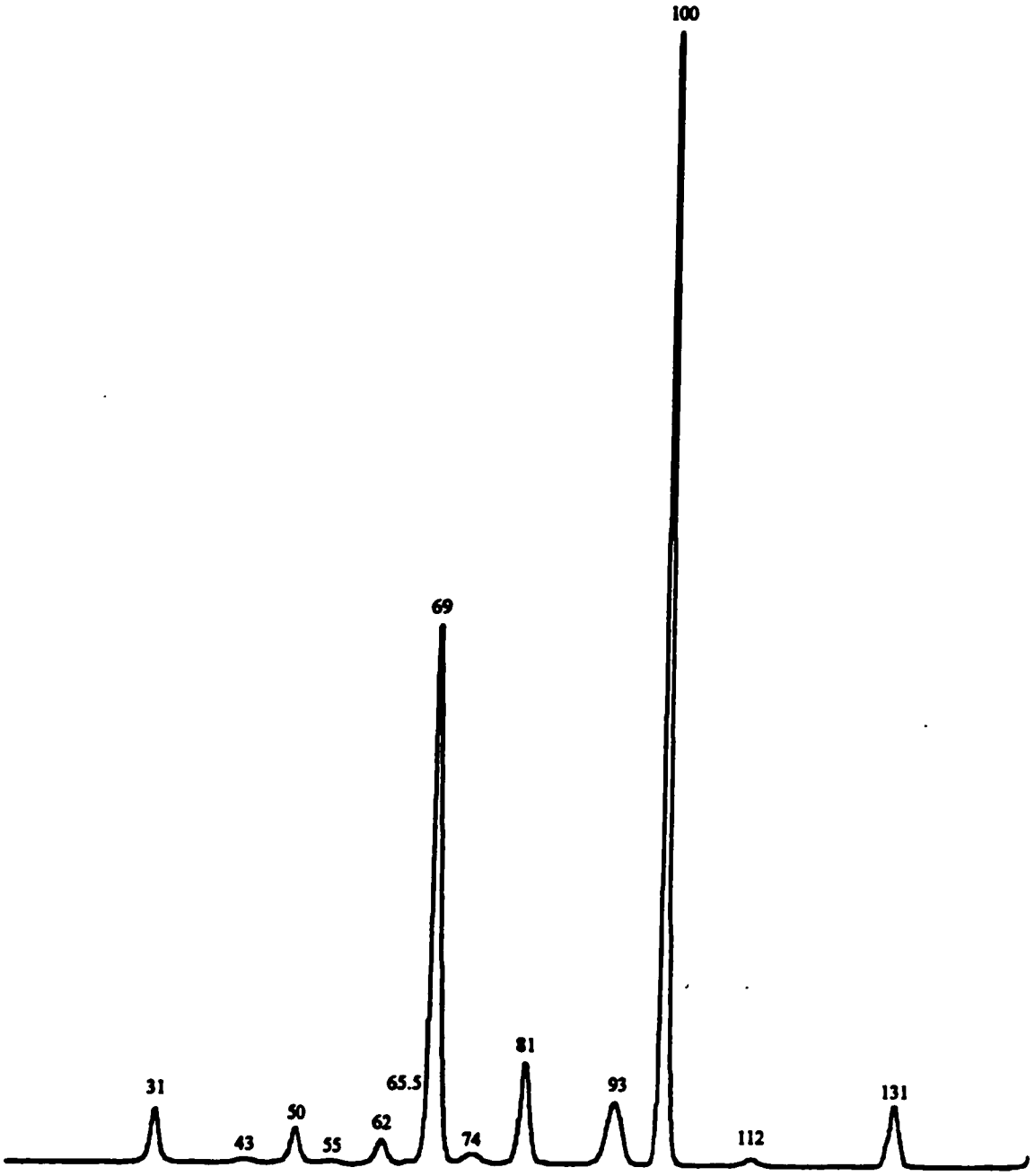

%, 4.0 %, 2.6 %, 11.9 %, and 1.3 % are for the CF^+ (m/z 31), $CF_2^{+\bullet}$ (m/z 50), $FC{\equiv}CF^{+\bullet}$ (m/z 62), $CF_2{=}C^+F$ (m/z 81), and $CF_2{=}C{=}CF_2^{+\bullet}$ (m/z 112), corresponding to the neutral losses of $^\bullet CF_2CF_3$, $CF_2{=}CF_2$, CF_4, $CF_3^\bullet$, and F_2, respectively.

Now in regards to the kinetic energy release $T_{0.5}$ measurements for $CF_2{=}CFCF_3^{+\bullet}$ listed in table 3.22, one may note that there is only one MI process present, namely $CF_2{=}CFCF_3^{+\bullet} \rightarrow CF_3CF^{+\bullet} + CF_2$, with a $T_{0.5}$ value of 11.7 meV (i.e., generally indicative of a direct bond cleavage). Its magnitude may be due to the (higher) energy requirements involved in the scission of a double bond as compared to the (lower) energy requirements involved in the scission of a single bond. As will be discussed shortly, (in the following $C_2F_4^{+\bullet}$ section) the $C_2F_4^{+\bullet}$ ion generated metastably from the $CF_2{=}CFCF_3^{+\bullet}$ parent-ion is proposed to be the carbene $CF_3CF^{+\bullet}$ isomer, whereas the source generated species is the classical $CF_2{=}CF_2^{+\bullet}$ isomer.

In regards to the MI and CID mass spectra of $CF_2{=}CFCF_3^{+\bullet}$, on inspection of Table 3.29 and Figures 3.51 and 3.52, one may note the following trends. Firstly as previously stated, there is only one MI peak for the $CF_3CF^{+\bullet}$ (m/z 100) ion, corresponding to the neutral loss of CF_2. In the CID mass spectrum the major peaks are of intensity 48.3 %, and 100.0 % for the CF_3^+ (m/z 69), and $CF_3CF^{+\bullet}$ (m/z 100) ions, corresponding to the neutral losses of $CF_2{=}C^\bullet F$ and CF_2, respectively. The other significant CID peaks are of smaller intensity of 9.3 %, and 6.0% for the $CF_2{=}C^+F$ (m/z 81), and $(CF_2)_2C^+{-}F$ (m/z 131), corresponding to the neutral losses of $CF_3^\bullet$ and $F^\bullet$, respectively. Additionally, one should note the peak for the doubly-charged $(^+CF_2)_2C{-}F$ (m/z 65.5) species with the small intensity of 0.7%. The acccesing in the CID mass spectra of $C_3F_6^{+\bullet}$ isomers other than that of $CF_2{=}CFCF_3^{+\bullet}$ is

suggested by the two following peaks. Firstly, the peak with the intensity of 3.3 % for the $CF_2^{+\bullet}$ (m/z 50) ion, most likely corresponds to the neutral loss of CF_2=CF_2 (rather than $CF_3\check{C}F$). This is suggestive of the occurrence of the dissociation process for the distonic species, $^{+}CF_2$–CF_2–$CF_2^{\bullet} \rightarrow CF_2^{+\bullet} + CF_2$=$CF_2$. Secondly, the peak with the intensity of 0.7 % for the CF_2=C=$CF_2^{+\bullet}$ (m/z 112) ion, most likely corresponds to the neutral loss of F_2. This is suggestive of the occurrence of the dissociation process for the perfluorodimethylcarbene species, $(CF_3)_2C^{+\bullet} \rightarrow CF_2$=C=$CF_2^{+\bullet} + F_2$. In any event, even with the indication of the presence of small amounts the $^{+}CF_2$–CF_2–$CF_2^{\bullet}$ and $(CF_3)_2C^{+\bullet}$ isomers which were possibly accessed in the CID mass spectrum, the dominant species present is clearly the CF_2=$CFCF_3^{+\bullet}$ isomer. One should note that even if a small amount of the c-$C_3F_6^{+\bullet}$ isomer were present, it is unlikely to have been a significant participant in the $C_3F_6^{+\bullet}$ manifold (due its expected high ring-strain energy, which in its neutral c-C_3F_6 is 266.1 kJ•mol^{-1} [34]).

$C_2F_4^{+\bullet}$ (m/z 100)

These isomeric fragment ions are generated by CF_2 loss form the CF_2=$CFCF_3^{+\bullet}$ parent-ion. There are two main $C_2F_4^{+\bullet}$ isomers to be discussed here. They are CF_2=$CF_2^{+\bullet}$, and $CF_3CF^{+\bullet}$. The cyclic [c-F_2(CFC)$F^{+\bullet}$]‡ transition state, denoted by TS1 where (CFC) represents a three-membered ring with the F atom astride a F_2C–CF moiety, is proposed to act as an intermediary between the classical CF_2=$CF_2^{+\bullet}$ and carbene type $CF_3CF^{+\bullet}$ isomers. Thus, the proposed order of stability of the $C_2F_4^{+\bullet}$ isomers is listed as follows; CF_2=$CF_2^{+\bullet}$ > $CF_3CF^{+\bullet}$. The proposed energy levels are illustrated in Figure 3.53. The kinetic energy release $T_{0.5}$ measurement for the source generated CF_2=$CF_2^{+\bullet}$ ion is listed in Table 3.22. The

peak intensities for the MI 2FFR mass spectrum; the CID 2FFR He and O_2 mass spectra of the source generated and metastably MI(*) 1FFR generated; and the neutralization-reionization (NR) 2FFR Xe/O_2 mass spectrum of the source generated $C_2F_4^{+\bullet}$ (m/z 100) ions from CF_2=$CFCF_3$ are listed in Table 3.30 and illustrated in Figures 3.54, 3.55, 3.56, and 3.57, respectively.

The proposed potential energy surface for the $C_2F_4^{+\bullet} \rightarrow CF_3^+ + CF^\bullet$ and $CF_2^{+\bullet} + CF_2$ dissociations are illustrated in Figure 3.58 and deserves further comment. Thus, as stated above it is proposed here that the cyclic $[c\text{-}F_2(CFC)F^{+\bullet}]^\ddagger$ transition state, TS1, acts as a bridge between the CF_2=$CF_2^{+\bullet}$ and $CF_3CF^{+\bullet}$ isomers. The CF_2=$CF_2^{+\bullet}$ isomer has a known Δ_fH^0 value of 316 kJ•mol^{-1} and it has a dissociation limit of $CF_2^{+\bullet} + CF_2$ with a *high* Δ_fH^0 value of 692 kJ•mol^{-1}. In contrast, Δ_fH^0 value for the $CF_3CF^{+\bullet}$ isomer is unknown, and it has a dissociation limit of $CF_3^+ + CF^\bullet$ with a *low* Δ_fH^0 value of 654.2 kJ•mol^{-1}. However, the $\Delta_fH^0[CF_3CF^{+\bullet}]$ may estimated in the following manner. If one may assume that upon the substitution of an F by a CF_3 group the effect is that of a systematic *lowering* of $\Delta_fH^0[M_1^{+\bullet}]$, then the difference, $\Delta_fH^0[CF_2$=$CFCF_3^{+\bullet}] - \Delta_fH^0[CF_2$=$CF_2^{+\bullet}] = (-102$ kJ•mol$^{-1}) - (316$ kJ•mol$^{-1}) = -418$ kJ•mol^{-1} may be utilized on $\Delta_fH^0[CF_2^{+\bullet}]$ to predict $\Delta_fH^0[CF_3CF^{+\bullet}]$. Therefore, one may estimate that $\Delta_fH^0[CF_3CF^{+\bullet}] \leq \Delta_fH^0[CF_2^{+\bullet}] + (-418$ kJ•mol$^{-1}) \leq (897$ kJ•mol$^{-1}) + (-418$ kJ•mol$^{-1}) \leq 479$ kJ•mol^{-1}. Additionally, if one may suggest that the energy difference between the $CF_3CF^{+\bullet}$ isomer and the cyclic $[c\text{-}F_2(CFC)F^{+\bullet}]^\ddagger$ transition state is at least on the order of ≈ 42 kJ•mol^{-1} (i.e., 10 kcal•mol^{-1}), then one may estimate the Δ_fH^0 value of $[c\text{-}F_2(CFC)F^{+\bullet}]^\ddagger$ to be ≤ 521 kJ•mol^{-1}. At this point it is interesting to note the proposed drop in $\Delta_fH^0[M_1^{+\bullet}]$ upon substitution of an F by a CF_3 group in regards to the

$CF_2{=}CF_2^{+\bullet}$ and $CF_2{=}CFCF_3^{+\bullet}$ cations (i.e., the drop of ≈ –418 kJ•mol^{-1}) is comparable to the Benson $\Delta_fH^0[M_1]$ for the difference in $CFCF_3$ and CF_2 neutral *moieties* (see Table 3.2). Thus, on inspection one has for the *Benson neutral moieties*, $\Delta_fH^0[CFCF_3] - \Delta_fH^0[CF_2] = (\Delta_fH^0[C\text{–}(F)(C)] + \Delta_fH^0[C\text{–}(F)_3(C)]) - (\Delta_fH^0[C_d\text{–}(F)_2]) = ((-136.0\ kJ\bullet mol^{-1}) + (-662.7\ kJ\bullet mol^{-1})) - (-327.2\ kJ\bullet mol^{-1}) = -471.5\ kJ\bullet mol^{-1}$, indicative of the proposed $\Delta_fH^0[CF_3CF^{+\bullet}]$ from $\Delta_fH^0[CF_2^{+\bullet}]$ being a reasonable estimate indeed. Additionally, one should note the expected trend of $IE_a[CF_2{=}CF_2] < IE_a[CF_3\ddot{C}F]$ is implicit in Figure 3.58.

As stated previously in section 3.2, all of the CID mass spectra (regardless of target gas) of the ions which were either *source generated* or *metastably MI(*) generated* were *identical* and represented the accessing of the *same ion structure*. However as will be discussed shortly, the $C_2F_4^{+\bullet}$ ion represented the only observed *exception* to this trend in all of the compounds studied here in this thesis and thus deserves a more thorough discussion presented below.

Thus, it will be clearly reemphasized here that the *source generated* $C_2F_4^{+\bullet}$ ion produced from $CF_2{=}CFCF_3$ is the *classical* $CF_2{=}CF_2^{+\bullet}$ isomer. Whereas, the *metastably MI(*) generated* $C_2F_4^{+\bullet}$ ion produced from $CF_2{=}CFCF_3$ is the *carbene* type $CF_3CF^{+\bullet}$ isomer. This caveat is the unifying basis for the interpretation of the following mass spectral experiments summarized in Table 3.30 and illustrated in Figures 3.54, 3.55, 3.56, and 3.57.

Firstly, the kinetic energy release $T_{0.5}$ measurement of the source generated $CF_2{=}CF_2^{+\bullet}$ ion listed in Table 3.22 is for the (*unexpected*) MI process of $CF_2{=}CF_2^{+\bullet} \rightarrow CF_3^+ + CF^\bullet$ and possesses a small $T_{0.5}$ value of 5.0 meV (i.e., indicative of a direct bond cleavage). This should suggest that diversion (i.e., a rearrangement of $CF_2{=}CF_2^{+\bullet}$ to $CF_3CF^{+\bullet}$) occurs en-route towards the *expected* dissociation process of $CF_2{=}CF_2^{+\bullet} \rightarrow CF_2^{+\bullet} + CF_2$, whose

Figure 3.53 Proposed Energy Levels of the $C_2F_4^{+\bullet}$ (m/z 100) Isomers

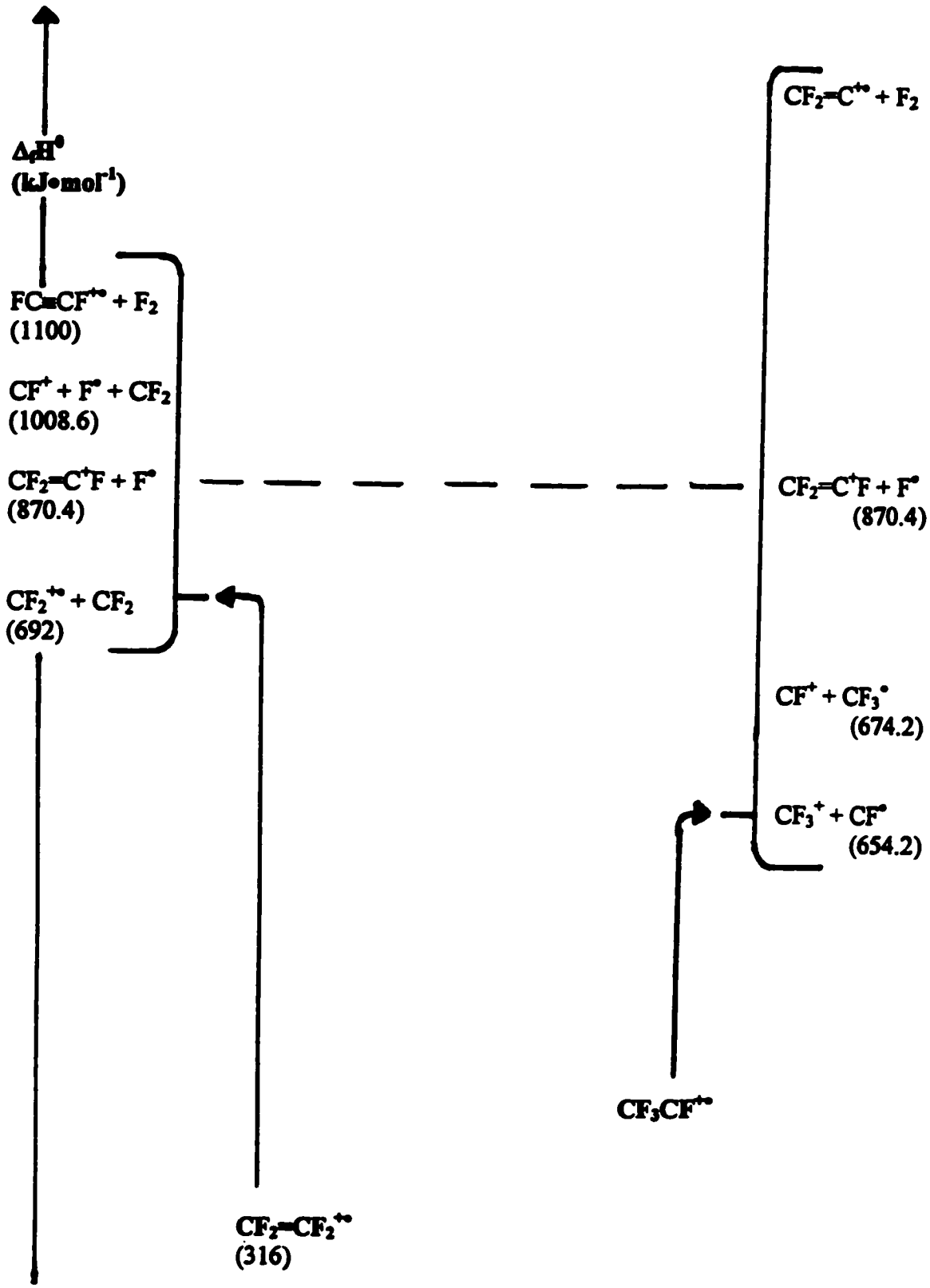

Table 3.30 Metastable Ion (MI) 2FFR, Collision Induced Dissociation(CID) 2FFR He ≈ 90 %T and O_2 ≈ 90 %T Mass Spectra of Source Generated and Metastable MI (*) 1FFR Generated, and Neutralization-Reionization (NR) 2FFR Xe ≈ 90 %T / O_2 ≈ 90 %T of Source Generated $C_2F_4^{+\bullet}$ (m/z 100) from CF_2=$CFCF_3$

			MI	CID				NR
				Source Generated		MI (*) Generated		
Species	Mass (m/z)	Neutral Loss		He	O_2	He	O_2	
$C_2F_4^{+\bullet}$	100							100.0
$C_2F_3^+$	81	($-F^\bullet$)		23.2	13.2	100.0	100.0	5.3
CF_3^+	69	($-CF^\bullet$)	100.0	100.0	100.0	50.3	29.3	26.5
$C_2F_2^{+\bullet}$	62	($-F_2$)		1.3	1.3	2.6	2.6	4.6
$CF_2^{+\bullet}$	50	($-CF_2$)		21.8	16.6	2.6	20.5	68.5
C_2F^+	43			<0.3	<0.3			3.3
CF^+	31	($-CF_3^\bullet$)		1.3	1.3			82.8
$C_2^{+\bullet}$	24							1.3
F^+	19							0.7

Figure 3.54 Metastable Ion (MI) 2FFR Mass Spectrum of Source Generated $C_2F_4^{+\bullet}$ (m/z 100) from CF_2=$CFCF_3$

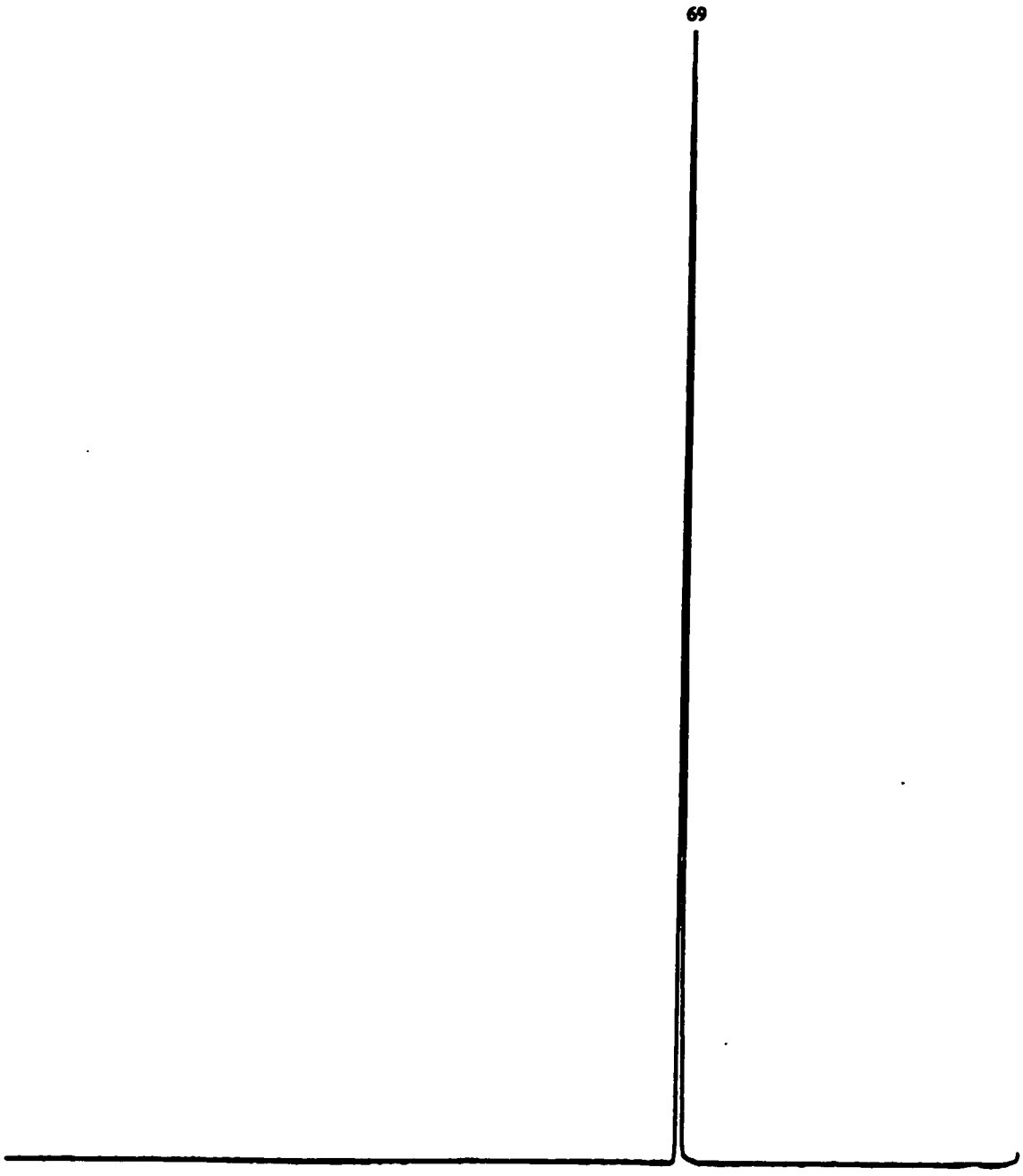

Figure 3.55 Collision Induced Dissociation (CID) 2FFR (a) He ≈ 90 %T and (b) O_2 ≈ 90 %T Mass Spectra of Source Generated $C_2F_4^{+\bullet}$ (m/z 100) from CF_2=$CFCF_3$

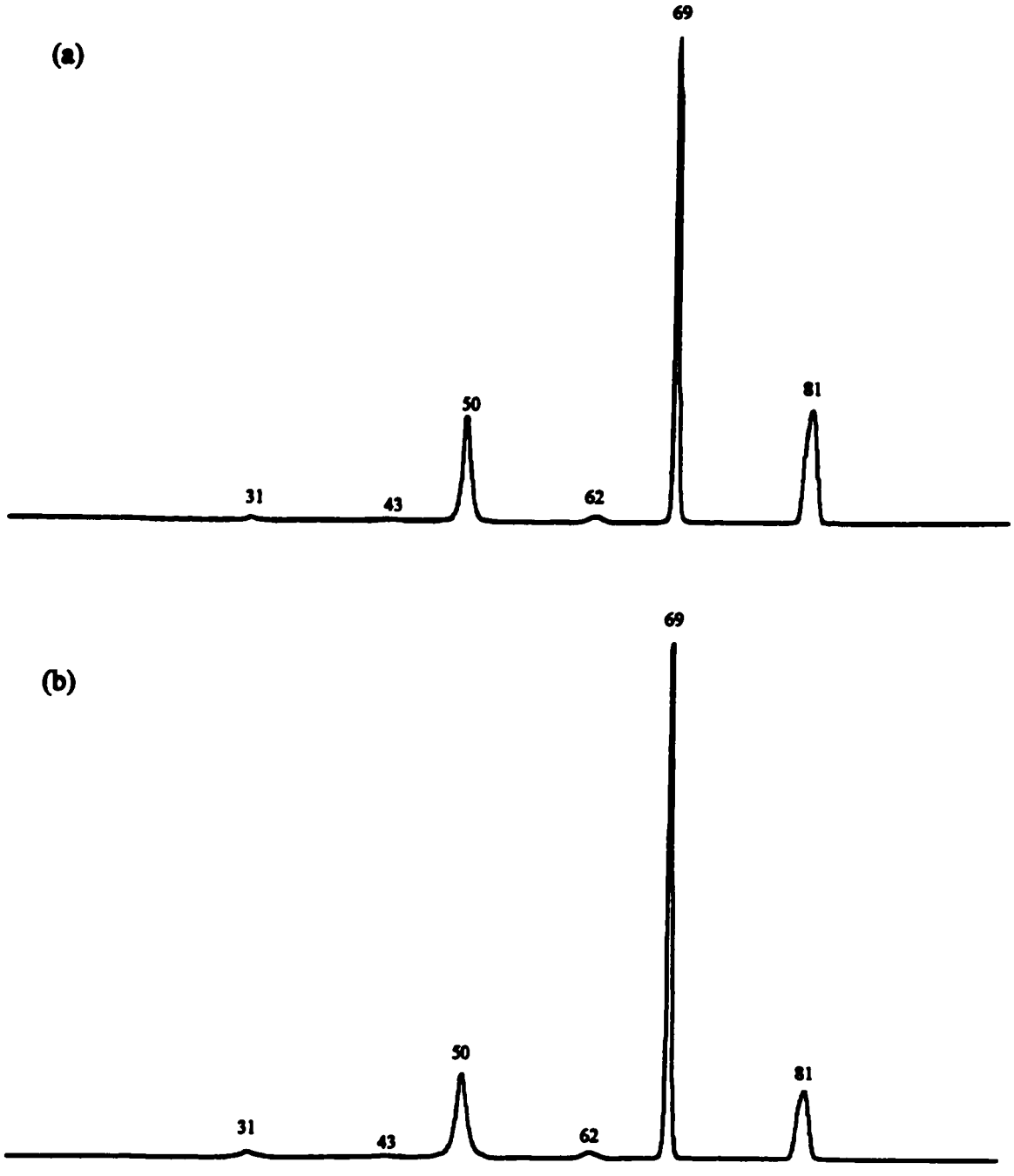

Figure 3.56 Collision Induced Dissociation (CID) 2FFR (a) He ≈ 90 %T and (b) O_2 ≈ 90 %T Mass Spectra of Metastably Generated MI(*) 1FFR (at m/z 66.7) of $C_2F_4^{+\bullet}$ (m/z 100) from CF_2=$CFCF_3$

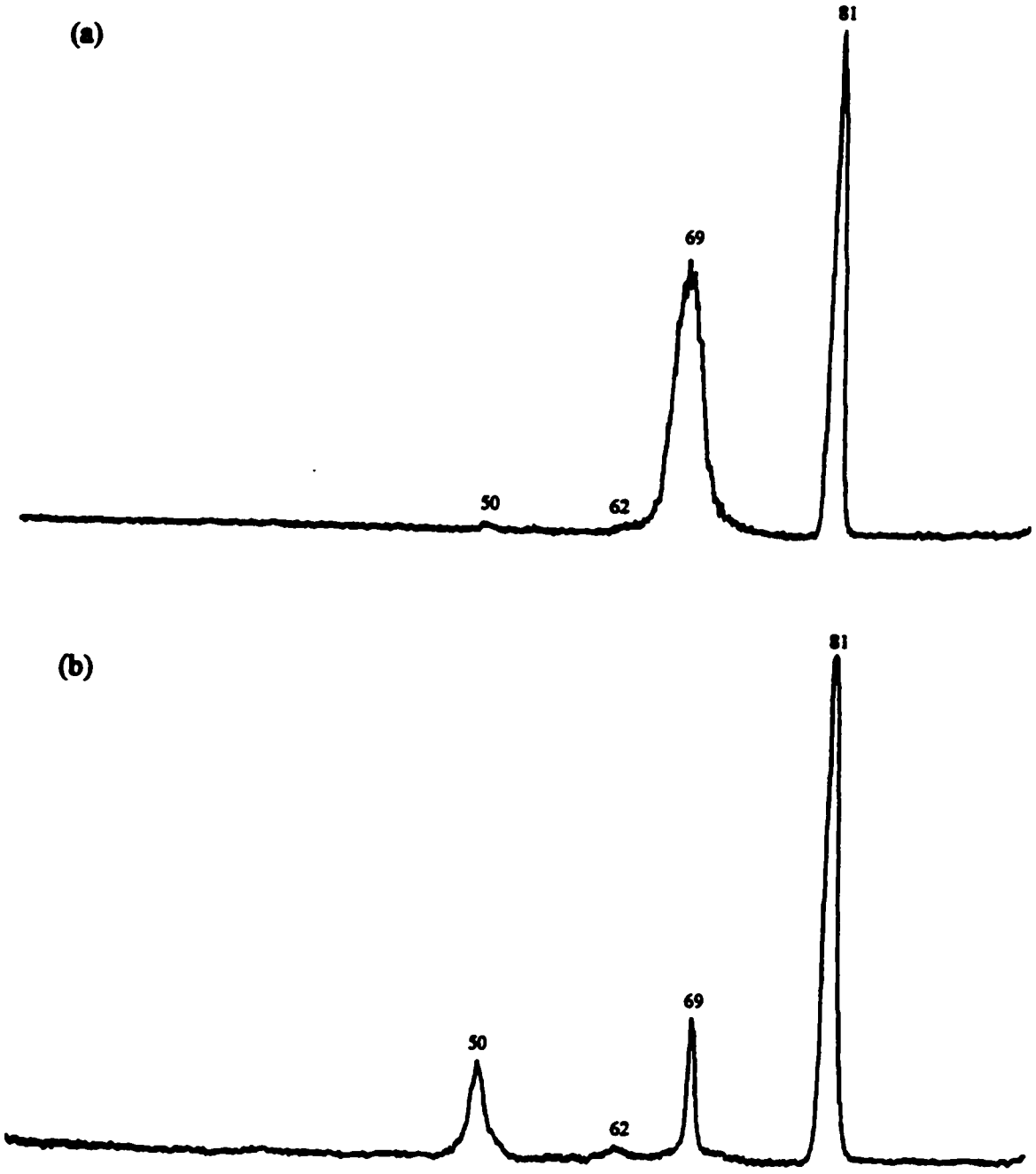

Figure 3.57 Neutralization-Reionization (NR) 2FFR Xe ≈ 90 %T / O_2 ≈ 90 %T Mass Spectrum of Source Generated $C_2F_4^{+\bullet}$ (m/z 100) from CF_2=$CFCF_3$

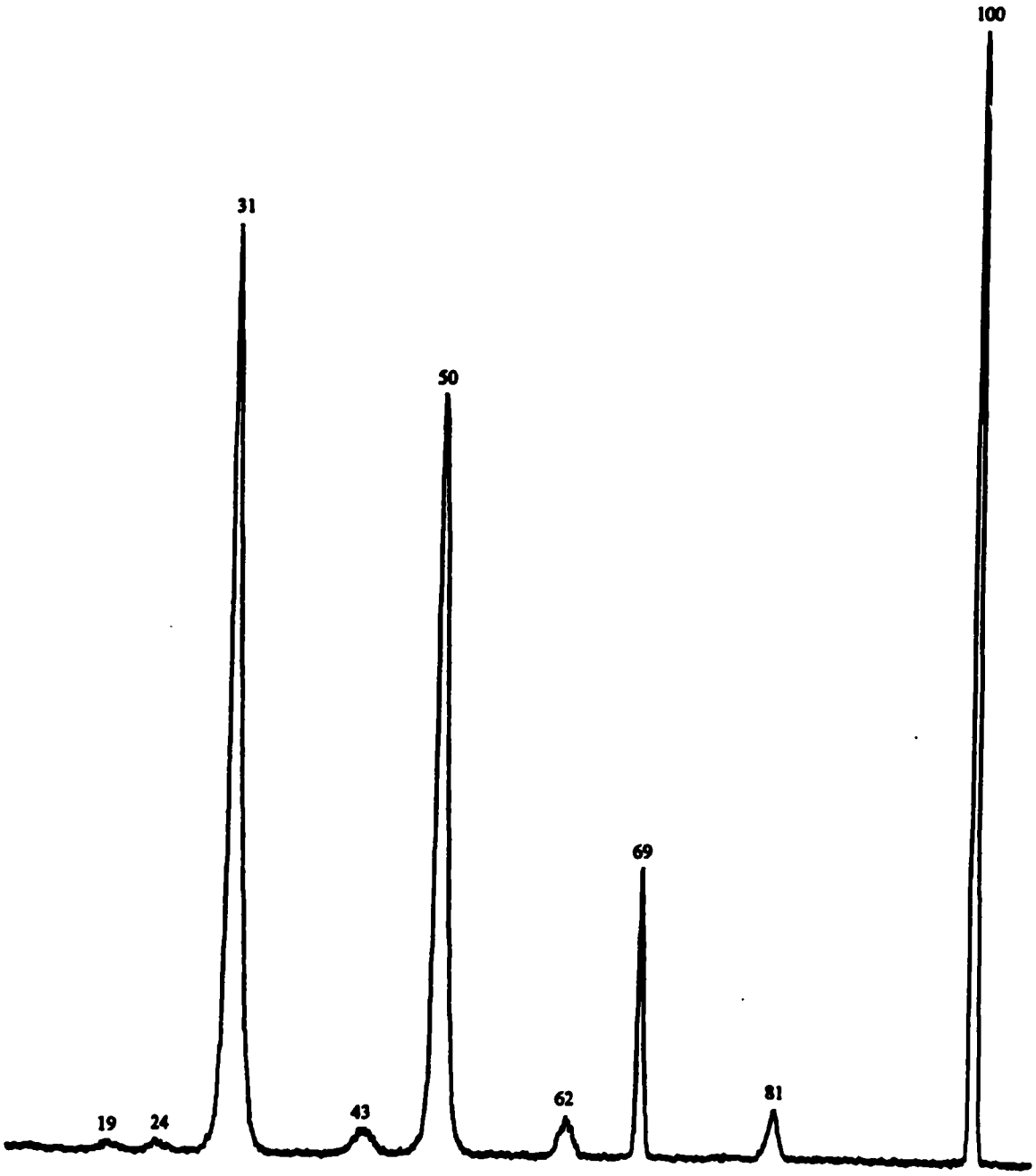

Figure 3.58 Proposed Potential Energy Surface of the $C_2F_4^{+\bullet} \rightarrow CF_3^+ + CF^\bullet$ and $CF_2^{+\bullet} + CF_2$ Dissociations

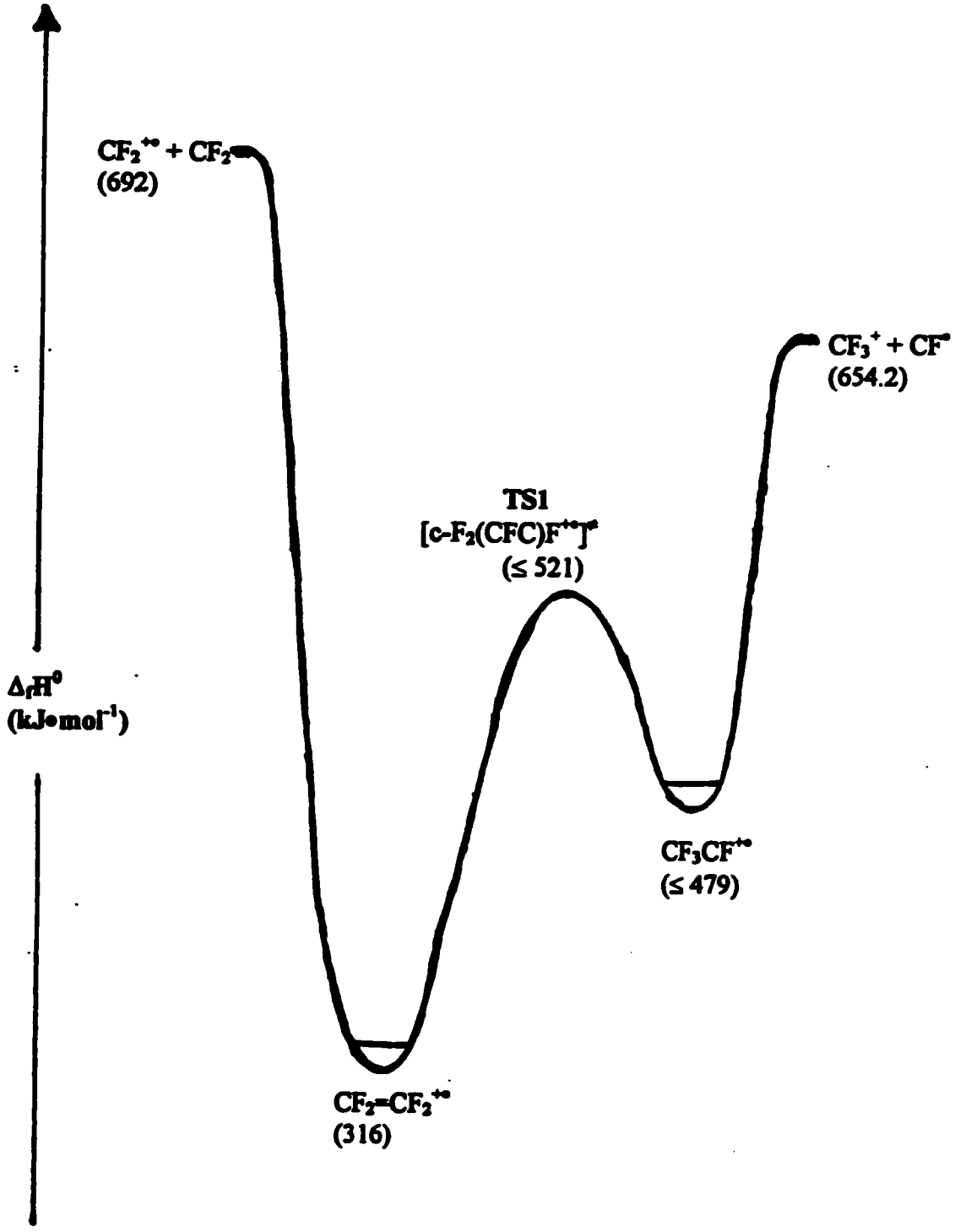

dissociation products have a *high* $\Delta_f H^0$ value of 692 kJ•mol^{-1}. However, on inspection of Figure 3.53, one may note that there are two alternate dissociation paths present, namely $CF_3^+ + CF^\bullet$ and $CF^+ + CF_3^\bullet$, with *lower* $\Delta_f H^0$ values of 654.2 kJ•mol^{-1} and 674.2 kJ•mol^{-1}, respectively. Thus, the presence of these two alternative dissociation paths of lower $\Delta_f H^0$ value, is proposed to be the driving force here behind the rearrangement of the source generated CF_2=$CF_2^{+\bullet}$ isomer into the $CF_3CF^{+\bullet}$ isomer, via the cyclic $[c\text{-}F_2(CFC)F^{+\bullet}]^\ddagger$ transition state, just prior to reaching the lowest dissociation limit of $CF_3^+ + CF^\bullet$. The low $T_{0.5}$ value (i.e., 5.0 meV) is indicative of the facile nature of the communication between the potential wells of CF_2=$CF_2^{+\bullet}$ and $CF_3CF^{+\bullet}$ (see Figure 3.58).

On inspection of Table 3.30 and Figures 3.54, 3.55, 3.56, 3.57, and 3.58, one may note the following trends. Firstly in regards to the *source generated* CF_2=$CF_2^{+\bullet}$ MI and CID mass spectra the following trends may be observed. In the MI mass spectrum (see Figure 3.54), there is only one peak for the CF_3^+ (m/z 69) ion, corresponding to the neutral loss of $CF^\bullet$. Now in the CID mass spectra (see Figure 3.55), the peak intensities appear to be nearly identical *regardless* of whether He or O_2 were used as the target gas. The major peaks in both the CID 2FFR He and O_2 mass spectra are for the $CF_2^{+\bullet}$ (m/z 50), CF_3^+ (m/z 69) (*base peak*), and CF_2=C^+F (m/z 81) ions, corresponding to the neutral losses of CF_2, $CF^\bullet$, and $F^\bullet$, respectively.

Now on inspection of the *metastably generated* $CF_3CF^{+\bullet}$ isomer CID 2FRR He and O_2 mass spectra (see Figure 3.56), one may certain *differences*, not only between the CID 2FFR mass spectra of the *source generated* CF_2=$CF_2^{+\bullet}$ isomer (whose peak intensities are target gas independent), but additionally between the peak intensities of the CID 2FFR He and the CID 2FFR O_2 mass spectra of the $CF_3CF^{+\bullet}$ isomer (whose peak intensities are target

gas dependant). For the CID 2FFR He mass spectrum of $CF_3CF^{+\bullet}$ the peak intensities of *2.6 %*, 2.6 %, 50.3 %, and 100.0 % are for the *$CF_2^{+\bullet}$ (m/z 50)*, CF_3^+ (m/z 69), and $CF_2{=}C^+F$ (m/z 81) ions, corresponding to the neutral losses of CF_2, $CF^\bullet$, and $F^\bullet$, respectively. In contrast, for the CID 2FFR O_2 mass spectrum of $CF_3CF^{+\bullet}$ the peak intensities of *20.5 %*, 2.6 %, 29.3 %, and 100.0 % are for the *$CF_2^{+\bullet}$ (m/z 50)*, CF_3^+ (m/z 69), and $CF_2{=}C^+F$ (m/z 81) ions, corresponding to the neutral losses of CF_2, $CF^\bullet$, and $F^\bullet$, respectively. The common feature in both of the CID 2FFR mass spectra of metastably generated $CF_3CF^{+\bullet}$ is the *new* base peak of the $CF_2{=}C^+F$ (m/z 81) ion, whereas for *source generated* $CF_2{=}CF_2^{+\bullet}$ the base was the CF_3^+ (m/z 69) ion. This may suggest that the $CF_3CF^{+\bullet}$ isomer is in communication with the cyclic $[c\text{-}F_2(CFC)F^{+\bullet}]^{\ddagger}$ transition state en-route to the $CF_2{=}C^+F + F^\bullet$ dissociation limit. It is also noteworthy that for $CF_3CF^{+\bullet}$ the other $CF^+ + CF_3$ dissociation limit is *not* accessed by either target gas.

The next two major differences in the CID 2FFR He and O_2 mass spectra of the metastably generated $CF_3CF^{+\bullet}$ are those of the peak intensities of the $CF_2^{+\bullet}$ (m/z 50), and CF_3^+ (m/z 69) ions, which are 2.6 % and 50.0 % in the case of the He target gas, however they are 20.5 % and 29.3 % in the case of the O_2 target gas, respectively. As well, one should note that the CF_3^+ peak in the CID 2FFR He case is quite wide compared to the thin CF_3^+ peak in the CID 2FFR O_2 case. Thus, one may propose that when He is the target gas the dissociation route of $CF_3CF^{+\bullet} \rightarrow CF_3^+ + CF^\bullet$ is accessed, whereas when O_2 is the target as the dissociation route of $CF_3CF^{+\bullet} \rightarrow CF_2^{+\bullet} + CF_2$ is more favourably accessed than in the He case. There are two main rationales for this (rarely) observed collision gas dependence and they will be discussed below.

The first rationale for the observed target gas dependence in the CID 2FFR He and O_2 mass spectra of metastably generated $CF_3CF^{+\bullet}$ is one of the difference in the physical properties of the target gas, namely their IE values, and the nature in which they interact with the projectile-ion. As previously stated in Chapter 1, during the charge-exchange process between the target gas, G_1, and the projectile-ion, $M_1^{+\bullet}$, the neutralization energy balance, Q_N, is given by,

$$Q_N = IE_v[G_1] - NE_v[M_1^{+\bullet}]$$

where $IE_v[G_1]$, and $NE_v[M_1^{+\bullet}]$ denote the vertical ionization energy of G_1, and the vertical neutralization energy of $M_1^{+\bullet}$ ($NE_v[M_1^{+\bullet}] \leq IE_v[G_1]$), respectively. The Q_N value provides a measure of the internal energy, E_{int}, required (endothermic $Q_N < 0$), not required (thermoneutral $Q_N \approx 0$), or deposited (exothermic $Q_N > 0$) in the neutralized $M_1^{+\bullet}$ (i.e., M_1) during the collision event.

Now, in the case of the $C_2F_4^{+\bullet}$ isomers the IE_a values (assuming $IE_a \approx IE_v$) of the relevant neutrals $F^{\bullet}$, $:C{=}C:$, $CF^{\bullet}$, CF_2, $FC{\equiv}CF$, $CF_3^{\bullet}$, $CF_2{=}C^{\bullet}F$, and the parent $CF_2{=}CF_2$ are, 17.42 eV, 12.11 eV, 9.11 eV, 11.42 eV, 11.18 eV, 8.9 eV, 10.2 eV, and 10.12 eV, respectively [1]. Unfortunately, there is on known IE value for the $^{\bullet}C{\equiv}CF$ species. In addition as previously stated in section 3.2, He possesses a high IE and is a non-polarizable moniatomic species, whereas O_2 posseses a lower IE value and is a relatively polarizable diatomic species. Thus for O_2, one may view it as possessing a facile ability to *neutralize* and *(re)ionize* a cation and its neutral species, respectively, where the He species does *not*.

Thus, for He with an IE_a of 24.59 eV [1], the Q_N values for the *neutralization* processes are 7.17 eV, 12.48 eV, 15.48 eV, 13.17 eV, 13.41 eV, 15.69 eV, 14.39 eV, and 14.47 eV, corresponding to the F^+, $:C{=}C^{+\bullet}$, CF^+, $CF_2^{+\bullet}$, $FC{\equiv}CF^{+\bullet}$, CF_3^+, $CF_2{=}C^+F$, and $CF_2{=}CF_2^{+\bullet}$ species, respectively. Note that all of these neutralization processes are endothermic ($Q_N > 0$).

Now, in regards to O_2 with an IE_a of 12.07 eV [1], the Q_N values for the *neutralization* processes are –5.35 eV, –0.04 eV, 2.96 eV, 0.65 eV, 0.89 eV, 3.17 eV, 1.89 eV, and 1.95 eV, corresponding to the F^+, $:C{=}C^{+\bullet}$, CF^+, $CF_2^{+\bullet}$, $FC{\equiv}CF^{+\bullet}$, CF_3^+, $CF_2{=}C^+F$, and $CF_2{=}CF_2^{+\bullet}$ species, respectively. Note that in contrast ot the He case, the neutralization processes span the range from endothermic ($Q_N > 0$), nearly thermoneutral ($Q_N \approx 0$), and exothermic ($Q_N < 0$), in nature.

Thus, in regards to the opposite processes, namely that *(re)ionization*, the O_2 target gas will be considered as active. However, due its characteristics, the He target gas will be considered of less utility.

Therefore, on consideration of the possible *(re)ionization* procesess which may be present in the CID 2FFR O_2 mass spectra of metastably generated $CF_3CF^{+\bullet}$ (and it is not likely to be significant in the He case), one may propose the for O_2 (with its IE_a of 12.07 eV), the most facile *(re)ionization* processes may occur with the encounters with those species with relatively low IE_a values. Thus, one may propose that the (re)ionization of the $CF^\bullet$ and $CF_3^\bullet$ neutrals should be believed to be facile compared to that of CF_2.

Now with the above rationale in mind, on inspection of Table 3.30 and Figure 3.56, the CID 2FFR mass spectra of MI(*) generated $CF_3CF^{+\bullet}$, the following may be observed. Firstly, with the conspicuous absence of the CF^+ (m/z 31) peak in either case of target gas

utilized, its possible origin due to the (re)ionization process of the $CF^{\bullet}$ species from the $CF_3^+ + CF^{\bullet}$ dissociation limit (with $\Delta_f H^0$ value of 654.2 kJ•mol^{-1}), *is not observed.* Secondly, the CF_3^+ (m/z 69) peak (whose $CF_3^{\bullet}$ neutral possesses a similar IE_a value to that of $CF^{\bullet}$) *is observed* for both target gases. Thus, if the $CF^+ + CF_3^{\bullet}$ dissociation limit (with $\Delta_f H^0$ value of 674.2 kJ•mol^{-1}) *were the sole source* of the proposed (re)ionized CF_3^+ ion, one should expect a similar presence of both the CF^+ and CF_3^+ ions in the CID 2FFR O_2 mass spectrum of metastably generated $CF_3CF^{+\bullet}$. Additionally, the large intensity (i.e., 20.5 %) of the less favoured (i.e., higher IE_a) (re)ionization product of $CF_2^{+\bullet}$ (m/z 50) ion in the CID 2FFR O_2 mass spectrum of metastably generated $CF_3CF^{+\bullet}$, should lead one to conclude that there may be *other factor* at work to aid in the explanation of the observed collision gas dependence.

The *other factor* which can be proposed to be responsible for the observed differences in the He and O_2 CID 2FFR mass spectra of metastably generated $CF_3CF^{+\bullet}$ is the *electronic states* of O_2 and their possible interaction with the $CF_3CF^{+\bullet}$ isomer. As previously discussed in the emission chapter (Chapter 2), the lowest valence electron configuration of O_2 is, $\ldots(3\sigma_g)^2(1\pi_u)^4(1\pi_g)^2$, and results in the electronic states of $\tilde{X}\,^3\Sigma_g^-$, $\tilde{a}\,^1\Delta_g$, and $\tilde{b}\,^1\Sigma_g^+$. The next highest energy electron configuration results from the $(1\pi_u) \leftarrow (1\pi_g)$ excitation that produces the valence electron configuration of, $\ldots(3\sigma_g)^2(1\pi_u)^3(1\pi_g)^3$. The resulting electronic states are the following, $\tilde{c}\,^1\Sigma_u^-$, $\tilde{C}\,^3\Delta_u$, $\tilde{A}\,^3\Sigma_u^+$, and $\tilde{B}\,^3\Sigma_u^-$. These electronic states of O_2 may be separated into two sets.

The first set is as follows; $\tilde{X}\,^3\Sigma_g^-$, $\tilde{a}\,^1\Delta_g$, $\tilde{b}\,^1\Sigma_g^+$, $\tilde{c}\,^1\Sigma_u^-$, $\tilde{C}\,^3\Delta_u$, and $\tilde{A}\,^3\Sigma_u^+$ which have $\Delta_f H^0$ values [35. 36] of 0.0 kJ•mol^{-1} (0.0 eV), 94.3 kJ•mol^{-1} (0.977 eV), 157.0 kJ•mol^{-1} (1.627 eV), 390.7 kJ•mol^{-1} (4.050 eV), 410.6 kJ•mol^{-1} (4.255 eV), and 418.8 kJ•mol^{-1} (4.340

eV), respectively. These electronic states possess the common dissociation limit of $O[(2p)^3P] + O[(2p)^3P]$, which has the Δ_fH^0 value of 498.4 kJ•mol^{-1} (5.165 eV).

The second set consists of $\tilde{B}\,^3\Sigma_u^-$ which has a Δ_fH^0 value [35. 36] of 590.5 kJ•mol^{-1} (6.120 eV) and has a dissociation limit of $O[(2p)^3P] + O[(2p)^1D]$, with a the Δ_fH^0 value of 688.2 kJ•mol^{-1} (7.133 eV).

Now, one must remembered there are two main types of transitions. An *optically allowed* transition possesses a high degree of probability, whereas an *optically forbidden* transition a low (or near-zero) degree of probability. As previously discussed, (see Chapter 2), the only optically (photon) allowed excited state of O_2 is $\tilde{B}\,^3\Sigma_u^-$ (due to the allowed electric-dipole transition-moment). However, as opposed to the mechanism of optical excitation, the process of *collisional-excitation*, via a non-momentum transfer of internal energy, E_{int}, from the fast moving projectile-ion $M_1^{+\bullet}$ into the stationary target gas G_1 (i.e., a radiationless vibrational excitation) is *not* bound by the same restrictive transition rules [16, 17]. Thus, one may propose that there is a significant *non-zero* transition probability for the build-up of collisionally-excited steady-state populations of the first electronic set of $\tilde{a}\,^1\Delta_g$, $\tilde{b}\,^1\Sigma_g^+$, $\tilde{c}\,^1\Sigma_u^-$, $\tilde{C}\,^3\Delta_u$, and $\tilde{A}\,^3\Sigma_u^+$ and the $O[(2p)^3P] + O[(2p)^3P]$ dissociation products; as well as the second electronic set of $\tilde{B}\,^3\Sigma_u^-$ and the $O[(2p)^3P] + O[(2p)^1D]$ dissociation products.

Now, the Δ_fH^0 value for the $CF_2{=}CF_2^{+\bullet}$ is known to be 316 kJ•mol^{-1}, however that of $CF_3CF^{+\bullet}$ is *not*, thus it is proposed here the $\Delta_fH^0[CF_3CF^{+\bullet}]$ value may be in the range of 410.3 kJ•mol^{-1} to 1004.2 kJ•mol^{-1} (i.e., 0.977 to 7.133 eV *above* the $\Delta_fH^0[CF_2{=}CF_2^{+\bullet}]$ value). Then, it is believed here that an *energy-resonance* between the $\Delta_fH^0[CF_3CF^{+\bullet}]$ value and the collisionally-excited O_2 species and/or products may exist which would favour the

dissociation route of $CF_3CF^{+\bullet} \rightarrow CF_2^{+\bullet} + CF_2$, which would not exist in the He target case. Therefore, it is believed here that this proposed *energy-resonance* is the major factor at work here to explain the peak intensity *differences* observed in the MI(*) generated CID 2FFR mass spectra of $CF_3CF^{+\bullet}$ when the He and O_2 target gases are utilized.

One should note that in contrast to $CF_3CF^{+\bullet}$ discussed above, this is not the case for the *source generated* $CF_2{=}CF_2^{+\bullet}$ isomer. Thus, a further experiments was carried out on the *source generated* $CF_2{=}CF_2^{+\bullet}$ isomer to further examine its behaviour (However, one should note that the intensity of the MI(*) generated $CF_3CF^{+\bullet}$ was too weak for the following experiments to be carried out on that isomer). The neutralization-reionization (NR) mass spectrometry technique was the experiment that was performed on the source generated $CF_2{=}CF_2^{+\bullet}$ isomer.

As previously discussed in Chapter 1, the NR technique provides the following information. In the NR technique, there are two collision cells used and they are separated by a repeller with a positive charge so that only the neutral species are transmitted form the first collision cell to the second one. The first collision cell is known as the *neutralization* cell, whereas the second collision cell is known as the *reionization* cell. The incoming cationic species are neutralized (by the encounter with the collision gas) in the neutralization cell and then the transmitted neutral species are reionized (by the encounter with the collision gas) in the reionization cell and are then detected as ions. This technique is utilized for the production and characterization of (elusive) neutral species in the gas-phase that have a lifetime of at least the transit time (i.e., ≈ 1 μs) between the neutralization and reionization cells.

As will be discussed later in Chapter 4, the NR technique was sucessful in the first *direct* experiment gas-phase observation of the elusive neutral species known as perfluoroketene, CF_2=C=O, [20]. Now, turning to the NR mass spectrum of source generated CF_2=$CF_2^{+\bullet}$, on inspection Table 3.30 and Figure 3.57, one may see the following trends. Firstly, one should note that the neutralization gas is Xe, with IE_a = 12.13 eV [1], and the reionization gas is O_2, with IE_a = 12.13 eV [1]. Secondly, the $\Delta_f H^0$ values for CF_2=CF_2, $CF_3\check{C}F$, and $[c\text{-}F_2(CFC)F]^{\ddagger}$ are –659 kJ•mol^{-1}, –587.4 kJ•mol^{-1}, and unknown, respectively. Thus, in the neutralization step *only* the lower energy CF_2=CF_2 neutral will be produced any possible residual $CF_3\check{C}F$ isomer will collapse to CF_2=CF_2, whereas the $[c\text{-}F_2(CFC)F]^{\ddagger}$ transition state is most likely revert to CF_2=CF_2 as well, or dissociate into CF_2=$C^{\bullet}F$ + $F^{\bullet}$. Thus, the CF_2=CF_2 isomer is proposed to be the only significant participant in the neutral manifold.

Now, after the transmission of the produced neutrals (past the positively charged repeller) in to the reionization cell, one may note the major NR peaks of intensity 82.8 %, 68.5 %, 26.5 %, and 100.0 %, correspond to CF^+ (m/z 31), $CF_2^{+\bullet}$ (m/z 50), CF_3^+ (m/z 69), and the recovery peak CF_2=$CF_2^{+\bullet}$, respectively. Each of these three first NR peaks correspond to the accessing of the following dissociation limits of $CF^+ + F^{\bullet} + CF_2$, $CF_2^{+\bullet} + CF_2$, and $CF_3^+ + CF^{\bullet}$, with $\Delta_f H^0$ values of 1008.6 kJ•mol^{-1}, 692 kJ•mol^{-1}, and 654.2 kJ•mol^{-1}, respectively. As well, the large peak of 82.8 % for CF^+ results mainly from the pre-existing $CF^{\bullet}$ neutral species originating from the MI process CF_2=$CF_2^{+\bullet} \rightarrow CF_3^+ + CF^{\bullet}$ that had taken place before entering the neutralization cell. In addition, some may also result from the secondary reaction of $CF_2^{+\bullet} \rightarrow CF^+ + F^{\bullet}$. Thus, in regards to the two purely NR peaks, namely those of (the *higher*) 68.5 % intensity of the $CF_2^{+\bullet}$ peak (*relative* to the *lower*) 26.5 %

intensity of the CF_3^+ peak are indicative of a very *direct* transition along the potential energy surface of $CF_2{=}CF_2^{+\bullet}$ towards its major dissociation products $CF_2^{+\bullet} + CF_2$ (i.e., see the left-hand side of Figure 3.53, the proposed energy levels of the $C_2F_4^{+\bullet}$ isomers, and the left-hand side of Figure 3.58, the proposed potential energy surface of the $C_2F_4^{+\bullet} \rightarrow CF_3^+ + CF^\bullet$ and $CF_2^{+\bullet} + CF_2$ dissociations).

3.6 Perfluorocarbon Oxides C_3F_6O

This section will deal with the gas-phase ion-chemistry of the perfluorocarbon oxides, C_3F_6O and their various products. As will be seen in the three series of isomeric ions $C_3F_6O^{+\bullet}$ (m/z 166), $C_3F_5O^+$ (m/z 147), and $C_2F_3O^+$ (m/z 97) presented here, the thermochemical behaviour of these species is dominated by the "tug-of-war" between the electronegative O and F atomic-orbitals and how they dictate the composition of the molecular-orbitals of the C_nF_mO species.

There will be three sources of the C_3F_6O precursors and they are perfluoroacetone, $(CF_3)_2C{=}O$, perfluoromethylvinyl ether, $CF_2{=}CFOCF_3$, and perfluoromethyl oxirane, c-$F_2(COC)FCF_3$. The only precursor of the recently observed stable neutral perfluroroketene, $CF_2{=}C{=}O$, is $CF_2{=}CFOCF_3$ and this will be the subject of the following separate chapter, Chapter 4 Perfluoroketene $CF_2{=}C{=}O$. Thus, for the final section of this chapter one will now explore the behaviour of the $C_3F_6O^{+\bullet}$, $C_3F_5O^+$, and $C_2F_3O^+$ ions.

$C_3F_6O^{+\bullet}$ (m/z 166)

The three commercially available isomers of the C_3F_6O compounds utilized here are perfluoroacetone, $(CF_3)_2C{=}O$, perfluoromethylvinyl ether, $CF_2{=}CFOCF_3$, and perfluoromethyl oxirane, c-$F_2(COC)FCF_3$. In the radical-cation manifold there are five main $C_3F_6O^{+\bullet}$ isomers to be discussed. They are $(CF_3)_2C{=}O^{+\bullet}$, $CF_2{=}C(OF)CF_3{}^{+\bullet}$, $CF_2{=}CFOCF_3{}^{+\bullet}$, $CF_3CF_2CF{=}O^{+\bullet}$, and c-$F_2(COC)FCF_3{}^{+\bullet}$. The first of the $C_3F_6O^{+\bullet}$ isomers has a known value of $\Delta_fH^0[(CF_3)_2C{=}O^{+\bullet}] = -293$ kJ•mol^{-1} [1], and will be considered to the lowest isomer in the order of stability. Thus, the proposed order of stability is listed as follows; $(CF_3)_2C{=}O^{+\bullet}$ >

CF_2=C(OF)$CF_3^{+\bullet}$ > CF_2=CFO$CF_3^{+\bullet}$ > CF_3CF_2CF=$O^{+\bullet}$ > c-F_2(COC)F$CF_3^{+\bullet}$. Here, the isomer c-F_2(COC)F$CF_3^{+\bullet}$ is placed at the highest Δ_fH^0 value due to the proposed ring-strain of the (COC) three-membered ring and the lack of an observed c-F_2(COC)F$CF_3^{+\bullet}$ molecular ion. The proposed energy levels of the $C_3F_6O^{+\bullet}$ isomers are illustrated in Figure 3.59. The peak intensities of the normal mass spectra of the $C_3F_6O^{+\bullet}$ isomers are listed in Table 3.31 and illustrated in Figure 3.60. The kinetic energy release measurement $T_{0.5}$ values of $C_3F_6O^{+\bullet}$ isomers are listed in Table 3.32. The peak intensities of the MI and CID mass spectra of the $C_3F_6O^{+\bullet}$ isomers are listed in Table 3.33 and illustrated in Figure 3.61 and 3.62, respectively.

On inspection of Table 3.31 and Figure 3.60 one may note the following trends in the normal mass spectra of the $C_3F_6O^{+\bullet}$ isomers. Firstly, the c-F_2(COC)F$CF_3^{+\bullet}$ isomer does not have a molecular ion. Secondly, all three $C_3F_6O^{+\bullet}$ isomers possess the same base peak of CF_3^+ (m/z 69) due to $C_2F_3O^\bullet$ loss. As well, the peak intensities of the $CF_2^{+\bullet}$ (m/z 50) ion due to C_2F_4O loss, and the $CF_3CF_2^+$ (m/z 119) ion due to C=O loss progressively increase as one goes across the $(CF_3)_2C$=$O^{+\bullet}$, CF_2=CFO$CF_3^{+\bullet}$, and c-F_2(COC)F$CF_3^{+\bullet}$ isomers. The $(CF_3)_2C$=$O^{+\bullet}$ and CF_2=CFO$CF_3^{+\bullet}$ isomers both possess molecular-ions of peak intensities of 4.6 % and 9.3 %, respectively. The $(CF_3)_2C$=$O^{+\bullet}$ isomer has the largest intensity of $CF_3^\bullet$ loss of 5.5 % for the $C_2F_3O^+$ (m/z 97) ion. The CF_2=CFO$CF_3^{+\bullet}$ isomer has the largest intensity of CF_4 of 11.9 % for the $C_2F_2O^{+\bullet}$ (m/z 78) ion.

Next turning to the matter of the kinetic energy release measurement $T_{0.5}$ values of the $C_3F_6O^{+\bullet}$ isomers, on inspection of Table 3.32 the following trends may be observed. The $(CF_3)_2C$=$O^{+\bullet}$ isomer the major unimolecular metastable dissociation $(CF_3)_2C$=$O^{+\bullet}$ → CF_3–C≡O^+ + $CF_3^\bullet$ with a tiny $T_{0.5}$ value of 0.2 meV. This peak is composite in shape with a

Figure 3.59 Proposed Energy Levels of the $C_3F_6O^{+\bullet}$ (m/z 166) Isomers

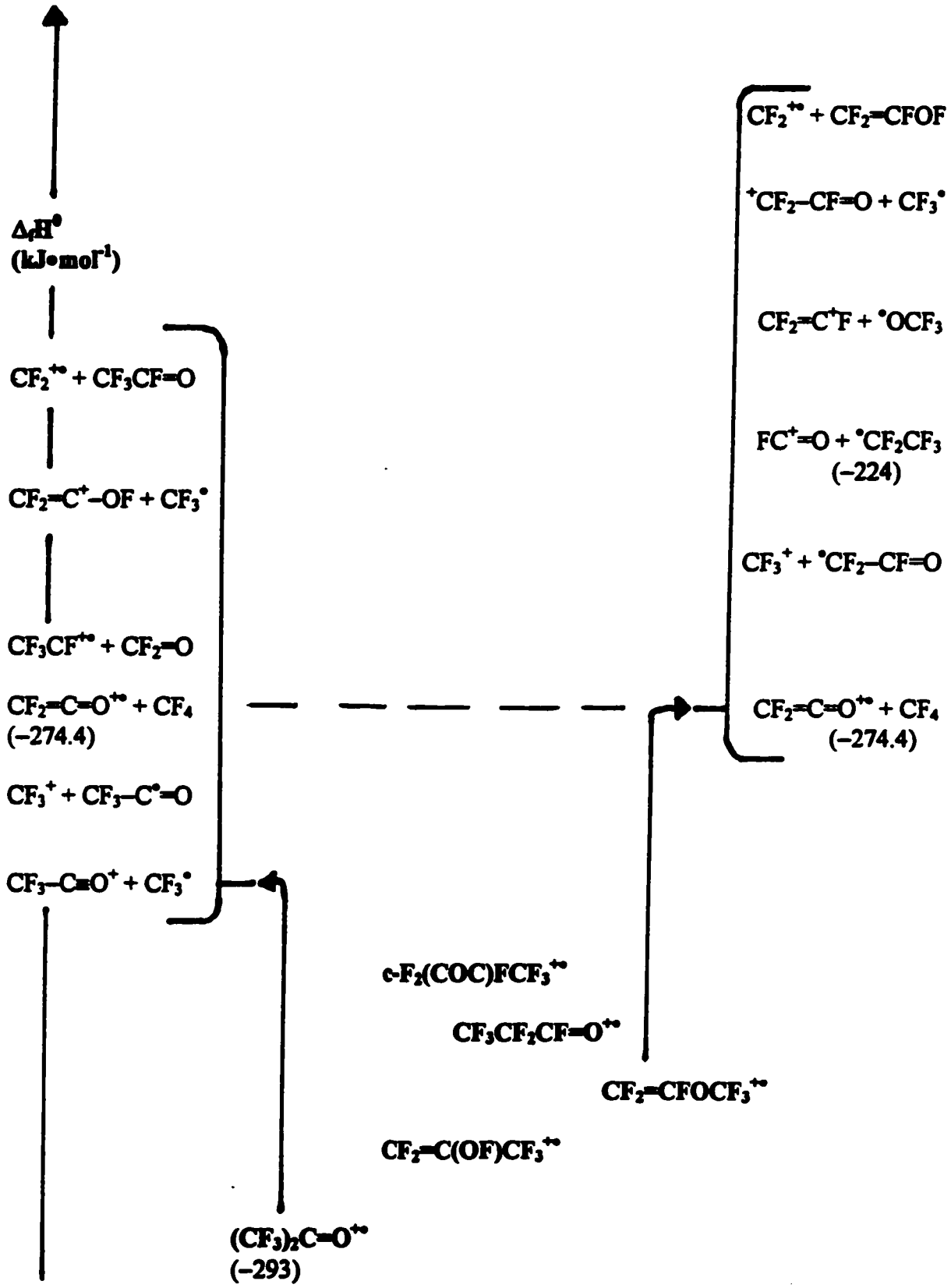

Table 3.31 Normal Mass Spectra of the C_3F_6O Isomers

Species	Mass (m/z)	Neutral Loss	Parent Ion $(CF_3)_2C{=}O$ Height (%)	Parent Ion $CF_2{=}CFOCF_3$ Height (%)	Parent Ion c-F_2(COC)FCF_3 Height (%)
$C_3F_6O^{+\bullet}$	166		4.6	9.3	
$C_3F_5O^+$	147	($-F^\bullet$)	24.5	4.6	4.0
$C_3F_5^+$	131	($-OF^\bullet$)			1.3
$C_2F_5^+$	119	(–CO)	3.3	6.6	20.5
$C_3F_4^{+\bullet}$	112	($-OF_2$)	<0.3		
$C_2F_4^{+\bullet}$	100	($-CF_2O$)	2.0		21.2
$C_2F_3O^+$	97	($-CF_3^\bullet$)	55.0	1.3	9.3
$C_3F_3^+$	93		0.7		1.3
$C_2F_3^+$	81		<0.3	18.5	25.8
$C_2F_2O^{+\bullet}$	78	($-CF_4$)	5.3	11.9	2.6
CF_3^+	69	($-C_2F_3O^\bullet$)	100.0	100.0	100.0
$C_2F_2^{+\bullet}$	62		<0.3	0.7	0.7
$CF_2^{+\bullet}$	50	($-C_2F_4O$)	14.6	14.6	37.1
CFO^+	47		0.7	11.9	19.2
C_2F^+	43		<0.3	<0.3	<0.3
CF^+	31		5.3	20.5	25.8

Figure 3.60 Normal Mass Spectra of (a) $(CF_3)_2C{=}O^{+\bullet}$ (b) $CF_2{=}CFOCF_3^{+\bullet}$ and (c) c-F_2(COC)$FCF_3^{+\bullet}$; $C_3F_6O^{+\bullet}$ (m/z 166) Isomers

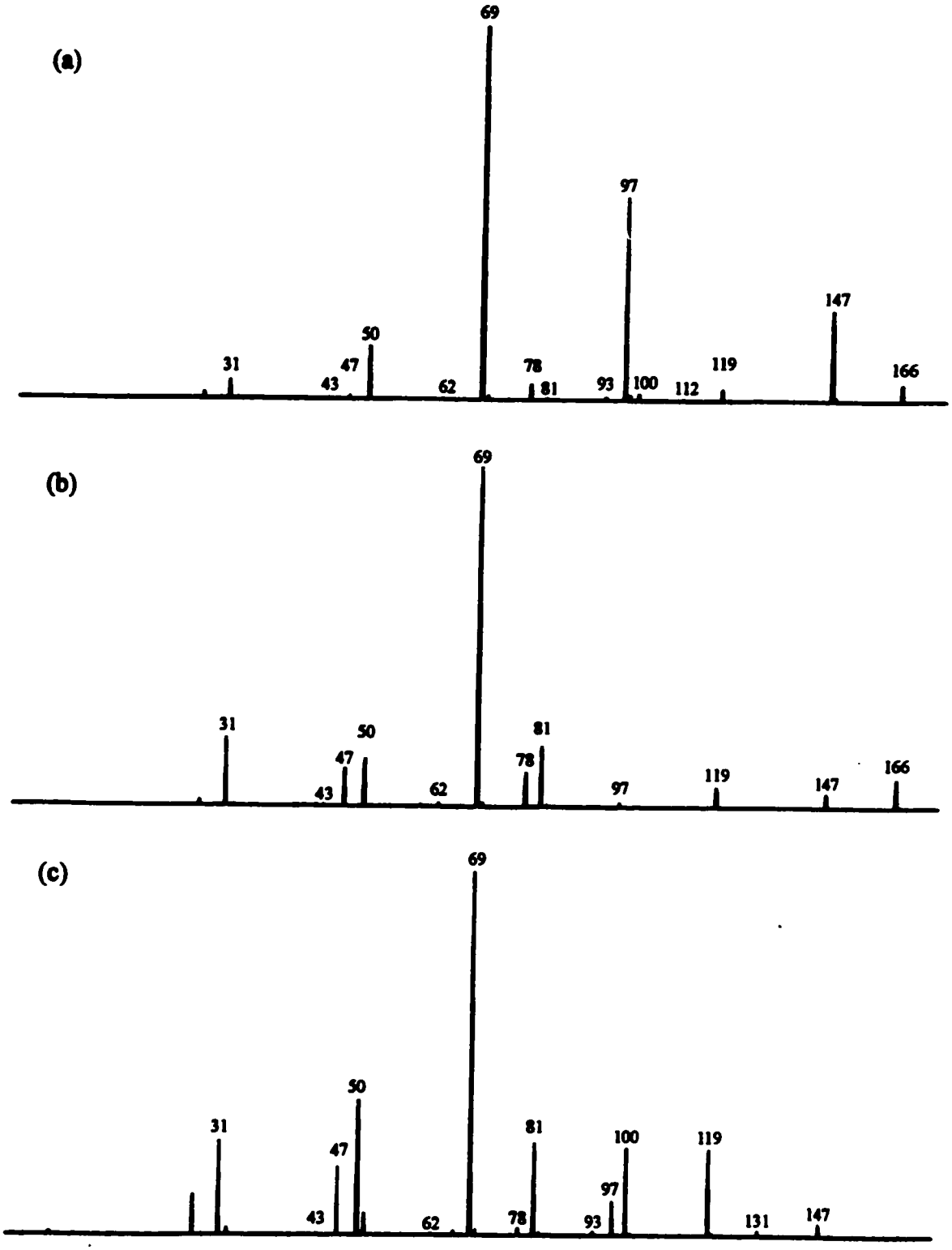

Table 3.32 Kinetic Energy Release $T_{0.5}$ Measurements of C_3F_6O Isomers

Mass (m/z)	Dissociation Process		Kinetic Energy Release, $T_{0.5}$ (meV)
$(CF_3)_2C{=}O$			
(166 → 97)	$(CF_3)_2C{=}O^{+\bullet}$	→ $CF_3{-}C{\equiv}O^+ + CF_3^\bullet$	0.2
	$CF_2{=}C(OF)CF_3^{+\bullet}$	→ $CF_3{-}C{\equiv}O^+ + CF_3^\bullet$	6.4
(147 → 119)	$C_3F_5O^+$	→ $CF_3CF_2^+ + C{\equiv}O$	31.8
(147 → 97)	$C_3F_5O^+$	→ $CF_3{-}C{\equiv}O^+ + CF_2$	7.9
(97 → 69)[a]	$CF_3{-}C{\equiv}O^+$	→ $CF_3^+ + C{\equiv}O$	1.9
	$CF_2{=}COF^+$	→ $CF_3^+ + C{\equiv}O$	606.7
(97 → 50)[b]	$CF_2{=}COF^+$	→ $CF_2^{+\bullet} + F^\bullet C{=}O$	–[b]
$CF_2{=}CFOCF_3$			
(166 → 78)	$CF_2{=}CFOCF_3^{+\bullet}$	→ $CF_2{=}C{=}O^{+\bullet} + CF_4$	84.7
(78 → 50)	$CF_2{=}C{=}O^{+\bullet}$	→ $CF_2^{+\bullet} + C{\equiv}O$	2.1
(147 → 119)	$C_3F_5O^+$	→ $CF_3CF_2^+ + C{\equiv}O$	6.0
(147 → 97)	$C_3F_5O^+$	→ $CF_3{-}C{\equiv}O^+ + CF_2$	24.6
(147 → 69)[b]	$C_3F_5O^+$	→ $CF_3^+ + CF_2{=}C{=}O$	–[b]
(97 → 69)[a]	$CF_3{-}C{\equiv}O^+$	→ $CF_3^+ + C{\equiv}O$	1.8
	$F_2C^+{-}CF{=}O$	→ $CF_3^+ + C{\equiv}O$	491.5
c-F_2(COC)FCF_3			
	No Molecular Ion	c-F_2(COC)$FCF_3^{+\bullet}$	
(147 → 119)	$C_3F_5O^+$	→ $CF_3CF_2^+ + C{\equiv}O$	78.5
(147 → 69)[b]	$C_3F_5O^+$	→ $CF_3^+ + CF_2{=}C{=}O$	–[b]
(97 → 69)[a]	$CF_3{-}C{\equiv}O^+$	→ $CF_3^+ + C{\equiv}O$	2.2
	$F_2C^+{-}CF{=}O$	→ $CF_3^+ + C{\equiv}O$	487.2
(131 → 69)	$(CF_2)_2C^+{-}F$	→ $CF_3^+ + FC{\equiv}CF$	23.2

[a]Two components, a thin spike on a wide hump, [b]Too weak to measure.

Table 3.33 Metastable Ion (MI) 2FFR and Collision Induced Dissociation (CID) 2FFR He ≈ 90 %T Mass Spectra of the $C_3F_6O^{+\bullet}$ (m/z 166) Isomers

			Parent Ion					
			$(CF_3)_2C{=}O$		$CF_2{=}CFOCF_3$		c-F_2(COC)FCF_3	
	Mass	Neutral	Height (%)		Height (%)		Height (%)	
Species	(m/z)	Loss	MI	CID	MI	CID	MI	CID
$C_2F_4^{+\bullet}$	100	($-CF_2O$)		0.7			–[a]	–[a]
$C_2F_3O^+$	97	($-CF_3^\bullet$)	100.0	100.0		0.7		
$C_2F_3^+$	81	($-CF_3O^\bullet$)				2.0		
$C_2F_2O^{+\bullet}$	78	($-CF_4$)		0.7	100.0	100.0		
CF_3^+	69	($-C_2F_3O^\bullet$)		17.9		23.2		
$CF_2^{+\bullet}$	50	($-C_2F_4O$)		1.3		0.7		
CFO^+	47	($-C_2F_5^\bullet$)				<0.3		

[a] c-F_2(COC)FCF_3 possesses no molecular ion (m/z 166).

Figure 3.61 Metastable Ion (MI) 2FFR Mass Spectra of (a) $(CF_3)_2C{=}O^{+\bullet}$ and (b) $CF_2{=}CFOCF_3^{+\bullet}$; $C_3F_6O^{+\bullet}$ (m/z 166) Isomers

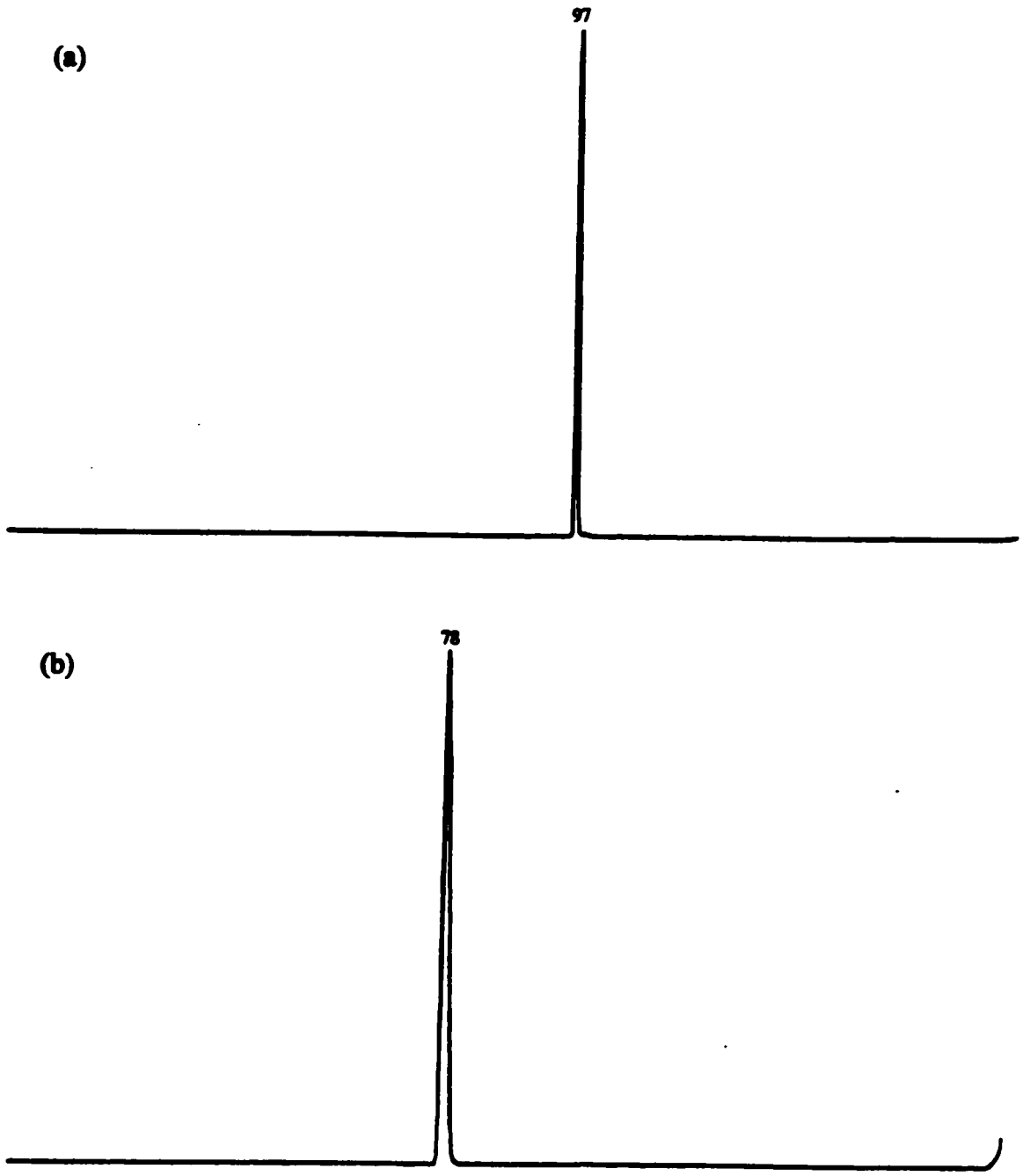

Figure 3.62 Collision Induced Dissociation (CID) 2FFR He ≈ 90 %T Mass Spectra of (a) $(CF_3)_2C{=}O^{+\bullet}$ and (b) $CF_2{=}CFOCF_3^{+\bullet}$; $C_3F_6O^{+\bullet}$ (m/z 166) Isomers

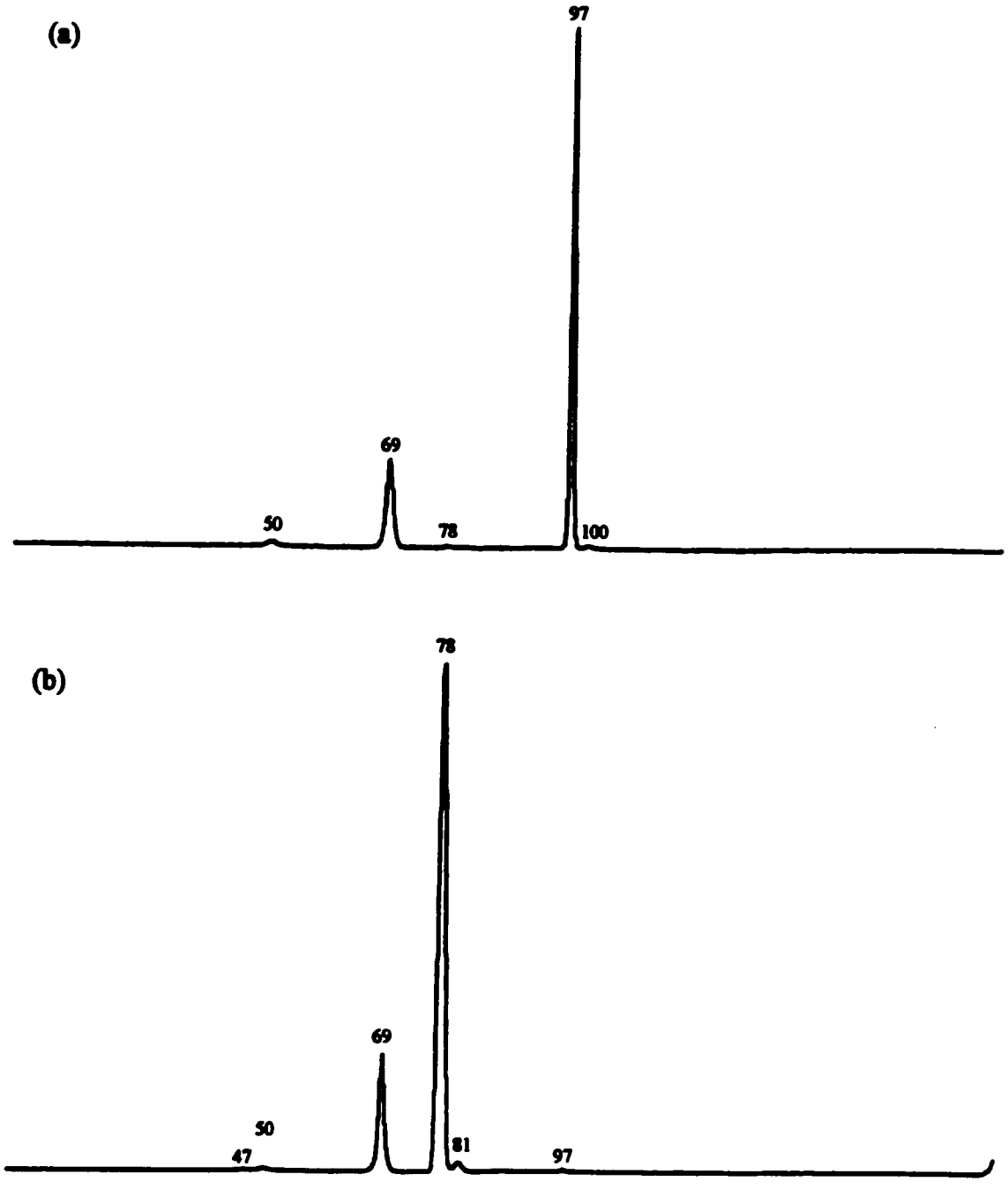

wide-foot component of $T_{0.5}$ value of 6.4 meV fro the parallel MI process of $CF_2{=}C(OF)CF_3^{+\bullet} \rightarrow CF_2{=}C^+{-}OF + CF_3^{\bullet}$. In contrast, for the $CF_2{=}CFOCF_3^{+\bullet}$ isomer the major unimolecular metastable dissociation is $CF_2{=}CFOCF_3^{+\bullet} \rightarrow CF_2{=}C{=}O^{+\bullet} + CF_4$ with a larger $T_{0.5}$ value of 84.7 meV, indicative of an energy barrier and/or a rearrangement. As previously stated, there was no c-$F_2(COC)FCF_3^{+\bullet}$ molecular ion observed.

Now for the sake of clarity, the other kinetic energy release measurement $T_{0.5}$ values of the other species produced from the $C_3F_6O^{+\bullet}$ parent-ions will be discussed here together and then briefly referred back to in their own upcoming sections.

For the $(CF_3)_2C{=}O^{+\bullet}$ isomer the source generated $C_3F_5O^+$ (m/z 147) isomer, via $F^{\bullet}$ loss, has two MI processes. The first MI process $C_3F_5O^+ \rightarrow CF_3CF_2^+ + C{\equiv}O$ with a $T_{0.5}$ value of 31.8 meV may be indicative of a rearrangement process. Thus, it is proposed that the $^+CF_2(C{=}O)CF_3$ isomer undergoes a CF_3 transfer to form the $CF_3CF_2{-}C{\equiv}O^+$ isomer, which then undergoes C≡O loss. The second MI process $C_3F_5O^+ \rightarrow CF_3{-}C{\equiv}O^+ + CF_2$ with a lower $T_{0.5}$ value of 7.9 meV is indicative of a direct bond-cleavage. Thus, it is proposed that the $^+CF_2(C{=}O)CF_3$ isomer undergoes a direct CF_2 loss. The next peak, for $C_2F_3O^+$ (m/z 97) is complex and it is one of the few species which is observed to have a composite (i.e., non-Gaussian) peak shape. For the $C_2F_3O^+ \rightarrow CF_3^+ + C{\equiv}O$ dissociation process, the MI peak of CF_3^+ (m/z 69) consists of a thin-spike component atop a wide-hump component background. It is proposed that there are two $C_2F_3O^+$ isomers present, the $CF_3{-}C{\equiv}O^+$ and the $CF_2{=}C^+{-}OF$ isomers giving $T_{0.5}$ values of 1.9 meV (i.e., the thin-spike) and 607 meV (i.e., the wide-hump), respectively. In addition the $C_2F_3O^+$ ion undergoes another MI process producing the $CF_2^{+\bullet} + CFO^{\bullet}$ products. However, its intensity is too weak to measure its $T_{0.5}$ value. It is

proposed here that the CF_2=C^+–OF species dissociates to $CF_2^{+\bullet}$ + F$^\bullet$C=O, via a high energy cyclic [c-CF_2=(CFO)$^+$]‡ transition state.

For the CF_2=CFO$CF_3^{+\bullet}$ isomer, there is an another MI process present, absent for the $(CF_3)_2$C=$O^{+\bullet}$ isomer mentioned above. Through the metastable loss of CF_4, the resultant $C_2F_2O^{+\bullet}$ isomer undergoes the MI process of CF_2=C=$O^{+\bullet}$ → $CF_2^{+\bullet}$ + C≡O with a $T_{0.5}$ value of 2.1 meV, indicative of a direct bond-clevage. This newly observed CF_2=C=$O^{+\bullet}$ species and its stable neutral CF_2=C=O will be explored in chapter 4. The next source generated $C_3F_5O^+$ (m/z 147) ion , via F$^\bullet$ loss, has three MI processes. The first MI process $C_3F_5O^+$ → $CF_3CF_2^+$ + C≡O with a $T_{0.5}$ value of 6.0 meV is indicative of a direct bond-cleavage process. Thus, it is proposed here that the CF_2=C^+–OCF_3 species isomerizes to the CF_3CF_2–C≡O^+ ion, which then undergoes C≡O loss. The second MI process $C_3F_5O^+$ → CF_3–C≡O^+ + CF_2 with a $T_{0.5}$ value of 24.6 meV is indicative of a rearrangement process. Thus, it is proposed here that the CF_2=CFOCF_2^+ isomer undergoes a not only CF_2 loss, but a concomitant rearrangement of $^+CF_2$–CF=O to CF_3–C≡O^+. The third MI process $C_3F_5O^+$ → CF_3^+ + CF_2=C=O was too weak in intensity to measure its $T_{0.5}$ value. Again, it is proposed here that the CF_2=C^+–OCF_3 species undergoes direct bond-cleavage yielding CF_3^+ and the stable neutral CF_2=C=O. The next source generated $C_2F_3O^+$ (m/z 97) species undergoing the dissociation to CF_3^+ + C≡O exhibits a similar CF_3^+ peak-shape as that produced previously from $(CF_3)_2$C=$O^{+\bullet}$. However, here the thin-spike component with a $T_{0.5}$ value of 1.8 meV ,atop the wide-hump component with a $T_{0.5}$ value of 492 meV, is of much smaller intensity. The thin-spike component is assigned to the CF_3–C≡O^+ → CF_3^+ + C≡O dissociation,

whereas the wide-hump component is assigned to the $F_2C^+–CF=O \rightarrow CF_3^+ + C\equiv O$ dissociation.

For the c-$F_2(COC)FCF_3^{+\bullet}$ isomer, as stated previously there is no molecular ion. For the source generated $C_3F_5O^+$ (m/z 147) fragment-ion, in contrast to the two previous isomers, there are only two MI processes. The first MI process $C_3F_5O^+ \rightarrow CF_3CF_2^+ + C\equiv O$ with a very high $T_{0.5}$ value of 78.5 meV is indicative of an energy barrier and/or a rearrangement process. Thus, it is proposed here that the c-$F_2(COC)^+–CF_3$ isomer undergoes a concomitant (COC) ring-opening and CF_3 transfer to produce the $CF_3CF_2–C\equiv O^+$ species. This species then undergoes C≡O loss, resulting in the largest $T_{0.5}$ value observed in any $C_3F_5O^+$ dissociation. The second MI process $C_3F_5O^+ \rightarrow CF_3^+ + CF_2=C=O$ was too weak in intensity to measure its $T_{0.5}$ value, and it is proposed to be simple bond-cleavage of the $CF_2=C^+–OCF_3$ species. It is believed that the presence of the (COC) ring and the energy released in its opening is the driving force at work here behind these two MI processes. The next source generated $C_2F_3O^+$ (m/z 97) species undergoing the dissociation to $CF_3^+ + C\equiv O$ exhibits a CF_3^+ peak-shape similar to that produced previously from $CF_2=CFOCF_3^{+\bullet}$, except that the thin-spike component is of slightly higher intensity. Once again, the thin-spike component with a $T_{0.5}$ value of 2.2 meV is assigned to the $CF_3–C\equiv O^+ \rightarrow CF_3^+ + C\equiv O$ dissociation , whereas the wide-hump component with a $T_{0.5}$ value of 487 meV is assigned to the $F_2C^+–CF=O \rightarrow CF_3^+ + C\equiv O$ dissociation.

One should note here that the extra measurement dissociation of $(CF_2)_2C^+–F \rightarrow CF_3^+ + FC\equiv CF$ yielded a $T_{0.5}$ value, within experimental error, that was in agreement with the previously measured process listed in Table 3.15.

Now on inspection of Table 3.33 and Figures 3.61 and 3.62, one may note the following trends in th CID mass spectra of the $C_3F_6O^{+\bullet}$ isomers, which are significantly different from each other. The only MI process for the $(CF_3)_2C{=}O^{+\bullet}$ is the $C_2F_3O^+ + CF_3^\bullet$ dissociation. For the $CF_2{=}CFOCF_3^{+\bullet}$ isomer the only MI process is the $CF_2{=}C{=}O^{+\bullet} + CF_4$ dissociation, whereas the c-F_2(COC)$FCF_3^{+\bullet}$ possesses no observable molecular ion. In regards to the CID mass spectra, both of the $(CF_3)_2C{=}O^{+\bullet}$ and $CF_2{=}CFOCF_3^{+\bullet}$ isomers possess a CF_3^+ (m/z 69), corresponding to $C_2F_3O^\bullet$ loss, of similar intensity. The $CF_2{=}CFOCF_3^{+\bullet}$ isomer possesses a CID peak for $CF_2{=}C^+F$ corresponding to $^\bullet OCF_3$, and this is absent in the $(CF_3)_2C{=}O^{+\bullet}$ case. In contrast, the $(CF_3)_2C{=}O^{+\bullet}$ isomer possesses a CID peak for $C_2F_4^{+\bullet}$ (m/z 100), corresponding to $CF_2{=}O$ loss, which is absent in the $CF_2{=}CFOCF_3^{+\bullet}$ case. The most likely route for its production is a cyclic transition state leading to the $CF_3CF^{+\bullet} + CF_2{=}O$ dissociation limit. In addition, the slightly higher peak intensity of the $CF_2^{+\bullet}$ (m/z 50) ion in the $(CF_3)_2C{=}O^{+\bullet}$ isomer as opposed to the $CF_2{=}CFOCF_3^{+\bullet}$ isomer is proposed to be due to the lower Δ_fH^0 value of the $CF_2^{+\bullet} + CF_3CF{=}O$ dissociation limit of the former isomer in comparison with the $CF_2^{+\bullet} + CF_2{=}CFOF$ dissociation limit of the latter isomer.

$C_3F_5O^+$ (m/z 147)

These isomeric fragment ions are generated by $F^\bullet$ loss from the $C_3F_6O^{+\bullet}$ parent-ion. There are seven main $C_3F_5O^+$ isomers to be discussed here. They are the following, $^+CF_2(C{=}O)CF_3$, $(CF_2)_2C^+{-}OF$, $CF_3CF_2{-}C{\equiv}O^+$, $CF_2{=}CFOCF_2^+$, $CF_2{=}C^+{-}OCF_3$, c-F_2(COC)$^+{-}CF_3$, and c-F_2(COC)FCF_2^+. The proposed order of stability is listed as follows;

$^{+}CF_2(C{=}O)CF_3 > (CF_2)_2C^{+}{-}OF > CF_3CF_2{-}C{\equiv}O^{+} > CF_2{=}CFOCF_2^{+} > CF_2{=}C^{+}{-}OCF_3 >$ c-$F_2(COC)^{+}{-}CF_3 >$ c-$F_2(COC)FCF_2^{+}$. The proposed energy level of the $C_3F_5O^{+}$ isomers are illustrated in Figure 3.63. The peak intensities of the MI and CID mass spectra of the $C_3F_5O^{+}$ isomers listed in Table 3.34 and illustrated in Figures 3.64 and 3.65, respectively.

On inspection of Table 3.34 nad Figures 3.64 and 3.65, one may see the following trends in the MI and CID mass spectra of the $C_3F_5O^{+}$ isomers. For the $^{+}CF_2(C{=}O)CF_3$ and $CF_3CF_2{-}C{\equiv}O^{+}$ isomers produced from the $(CF_3)_2C{=}O^{+\bullet}$ parent, the two MI peaks of intensity of 100.0 % and 66.2 % for the $CF_3{-}C{\equiv}O^{+}$ (m/z 97) and $CF_3CF_2^{+}$ (m/z 119) ions, correspond to the neutral losses of CF_2 and C≡O, respectively. On inspection of its CID mass one may see that the $CF_2{=}C{=}O^{+\bullet} + CF_3^{\bullet}$ dissociation limit (with a $\Delta_f H^0$ value of 200.1 kJ•mol^{-1}) is only slightly accessed (i.e., 2.0 %), whilst the $CF_3^{+} + CF_2{=}C{=}O$ dissociation limit (with a $\Delta_f H^0$ value of –2.2 kJ•mol^{-1}) is more strongly accessed (i.e., 21.2 %). One should note that the $^{+}CF_2(C{=}O)CF_3$ isomer is proposed to undergo a *barrierless* (1,2) CF_3-shift to generate $CF_3CF_2{-}C{\equiv}O^{+}$ prior to dissociation. Additionally, the small peak intensity of 0.7% for the $C_3F_3^{+}$ (m/z 93) ion is proposed to be a result of the accessing of the $CF_2{=}C^{+}F + OF_2$ dissociation limit of a small population of the allylic $(CF_2)_2C^{+}{-}OF$ species.

For the $CF_2{=}C^{+}{-}OCF_3$ and $CF_2{=}CFOCF_2^{+}$ isomers produced from the $CF_2{=}CFOCF_3^{+\bullet}$ parent, there are three MI peaks of intensity 0.7 %, 1.3 %, and 100.0 % for the CF_3^{+} (m/z 69), $CF_3{-}C{\equiv}O^{+}$ (m/z 97), and $CF_3CF_2^{+}$ (m/z 119) ions, which correspond to the neutral losses of $CF_2{=}C{=}O$, CF_2, and C≡O, respectively. On inspection of the CID mass spectra one may note that there are only peaks of very weak intensity and thus they appear to be very collision insensitive. One should note that this is proposed to be the $CF_2{=}C^{+}{-}OCF_3$ isomer going over a *barrier* for a (1,3) CF_3-shift to generate the $CF_3CF_2{-}C{\equiv}O^{+}$ isomer

Figure 3.63 Proposed Energy Levels of the $C_3F_5O^+$ (m/z 147) Isomers

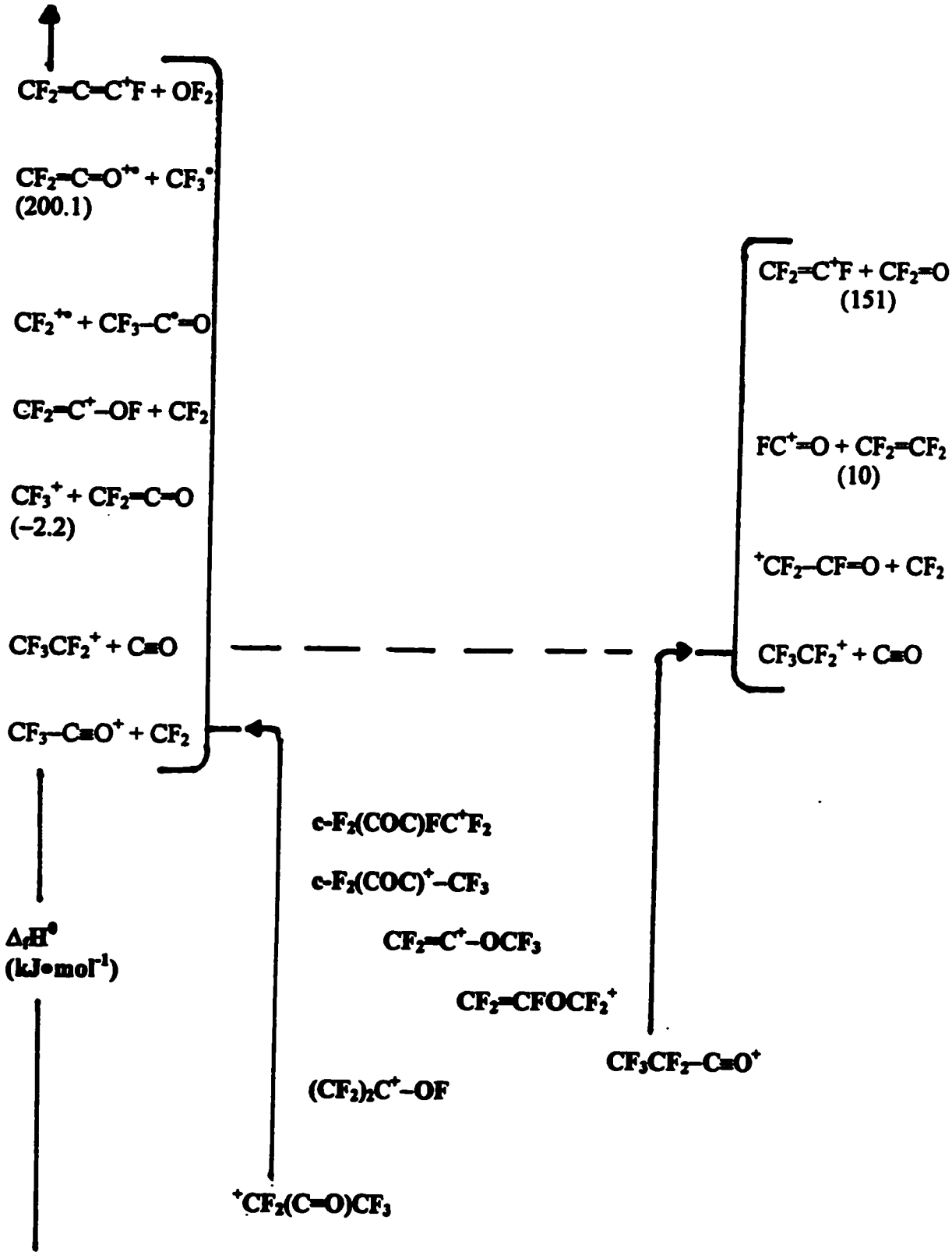

Table 3.34 Metastable Ion (MI) 2FFR and Collision Induced Dissociation (CID) 2FFR He ≈ 90 %T Mass Spectra of Source Generated $C_3F_5O^+$ (m/z 147) from the C_3F_6O Isomers

			Parent Ion					
			$(CF_3)_2C{=}O$		$CF_2{=}CFOCF_3$		c-F_2(COC)FCF_3	
	Mass	Neutral	Height (%)		Height (%)		Height (%)	
Species	(m/z)	Loss	MI	CID	MI	CID	MI	CID
$C_2F_5^+$	119	(–CO)	66.2	21.2	100.0	100.0	100.0	100.0
$C_2F_3O^+$	97	(–CF_2)	100.0	100.0	1.3	1.3		0.7
$C_3F_3^+$	93	(–OF_2)		0.7				
$C_2F_3^+$	81	(–CF_2O)				2.0		3.3
$C_2F_2O^{+\bullet}$	78	(–$CF_3^\bullet$)		2.0		<0.3		<0.3
CF_3^+	69	(–C_2F_2O)		21.2	0.7	2.6	<0.3	3.3
$C_2F_2^{+\bullet}$	62					<0.3		<0.3
$CF_2^{+\bullet}$	50	(–$C_2F_3O^\bullet$)		4.0		<0.3		0.7
CFO^+	47	(–C_2F_4)				<0.3		<0.3
CF^+	31			<0.3		<0.3		<0.3

Figure 3.64 Metastable Ion (MI) 2FFR Mass Spectra of Source Generated $C_3F_5O^+$ (m/z 147) from (a) $(CF_3)_2C{=}O^{+\bullet}$ (b) $CF_2{=}CFOCF_3^{+\bullet}$ and (c) c-F_2(COC)$FCF_3^{+\bullet}$

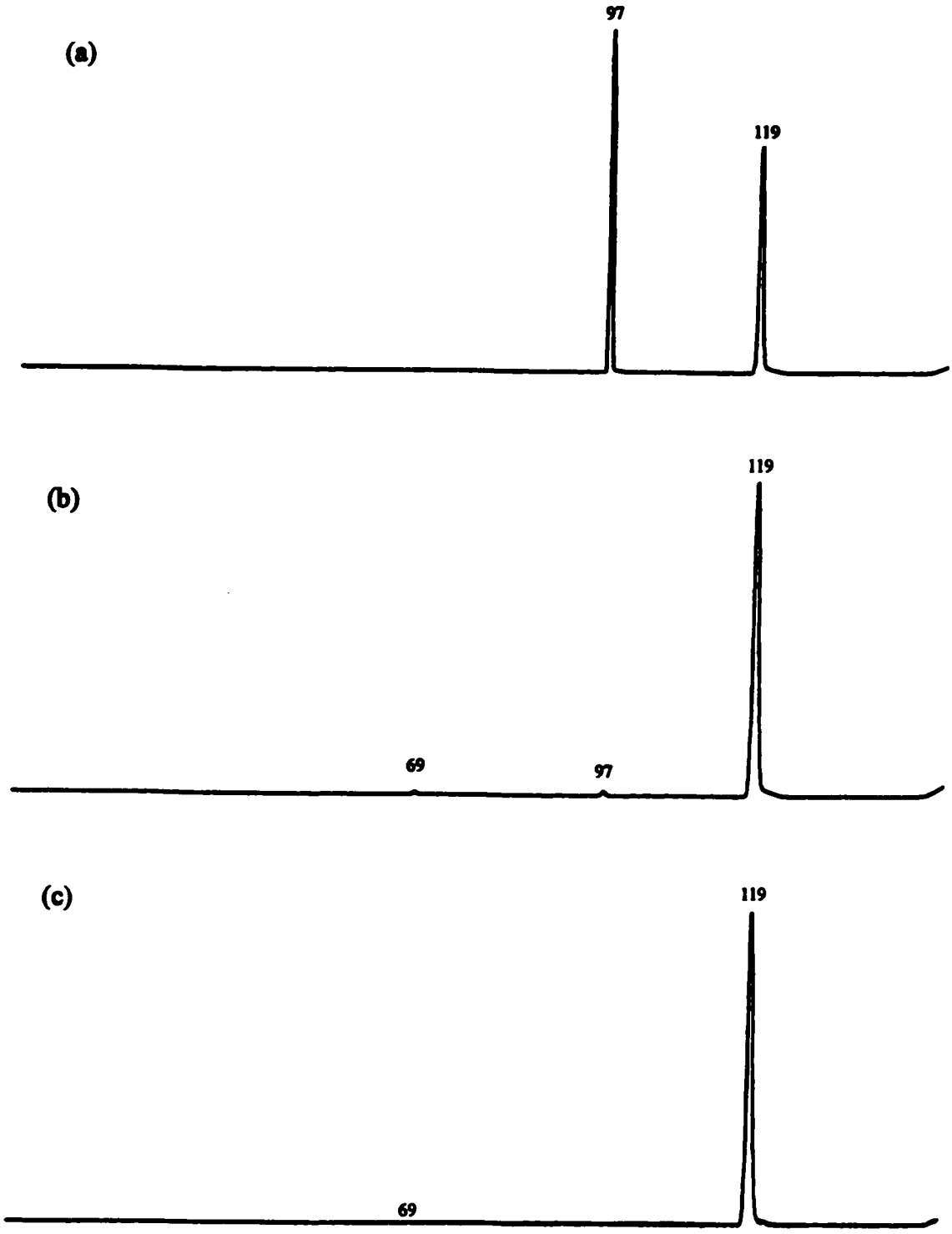

Figure 3.65 Collision Induced Dissociation (CID) 2FFR He ≈ 90 %T Mass Spectra of Source Generated $C_3F_5O^+$ (m/z 147) from (a) $(CF_3)_2C{=}O^{+\bullet}$ (b) $CF_2{=}CFOCF_3^{+\bullet}$ and (c) c-F_2(COC)$FCF_3^{+\bullet}$

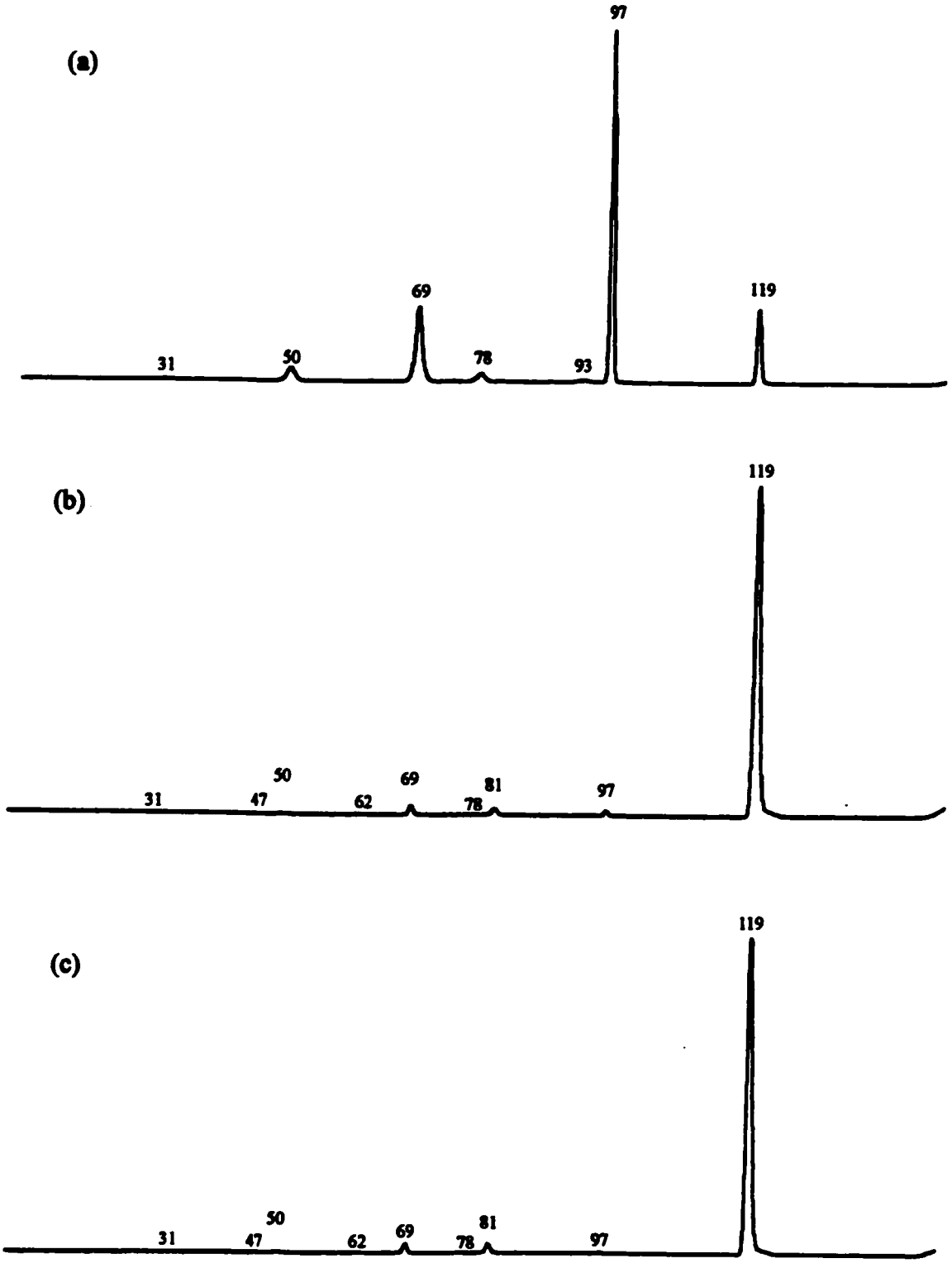

which then dissociates. However, the CF_2=$CFOCF_2^+$ isomer is likely to be a thermochemical "dead-end" to dissociation.

For the c-F_2(COC)$^+$–CF_3 and possibly the c-F_2(COC)FCF_2^+ isomers produced from the (dissociative) c-F_2(COC)$FCF_3^{+\bullet}$ parent, the two MI peaks of intensity <0.3 %, and 100.0 % for the CF_3^+ (m/z 69), and $CF_3CF_2^+$ (m/z 119) ions, correspond to the neutral losses of CF_2=C=O, and C≡O, respectively. One may note here that the MI peak for $C_2F_3O^+$ (m/z 97) via CF_2 loss is *not* observed here. Again on inspection of the CID mass spectra one may note that there are only peaks of very weak intensity and thus they appear to be very collision insensitive. Thus, one may propose that the majority of of the active processes present here are those of high energy rearrangements.

$C_2F_3O^+$ (m/z 97)

These isomeric fragment ions are generated by $CF_3^\bullet$ loss from the $C_3F_6O^{+\bullet}$ parent-ion. There are three main $C_2F_3O^+$ isomers to be discussed here. They are the following, CF_3–C≡O^+, $^+CF_2$–CF=O, $^+$, and CF_2=C^+–OF. The proposed order of stability is listed as follows; CF_3–C≡O^+ > $^+CF_2$–CF=O > CF_2=C^+–OF. The proposed energy levels of the $C_2F_3O^+$ isomers are illustrated in Figure 3.66. The peak intensities of the MI and CID mass spectra of the $C_2F_3O^+$ isomers listed in Table 3.35 and illustrated in Figures 3.67 and 3.68, respectively. A close-up of the MI peak shape of the CF_3^+ (m/z 69) ion from the $C_3F_6O^{+\bullet}$ isomers for the $C_2F_3O^+ \rightarrow CF_3^+ + C{\equiv}O$ dissociation and its proposed potential energy surface are illustrated in Figures 3.69 and 3.70, respectively.

On inspection of Table 3.35 and Figures 3.67 and 3.68, one may see the following trends in the MI and CID mass spectra of the $C_2F_3O^+$ isomers. Firstly, all of the $C_2F_3O^+$

Figure 3.66 Proposed Energy Levels of the $C_2F_3O^+$ (m/z 97) Isomers

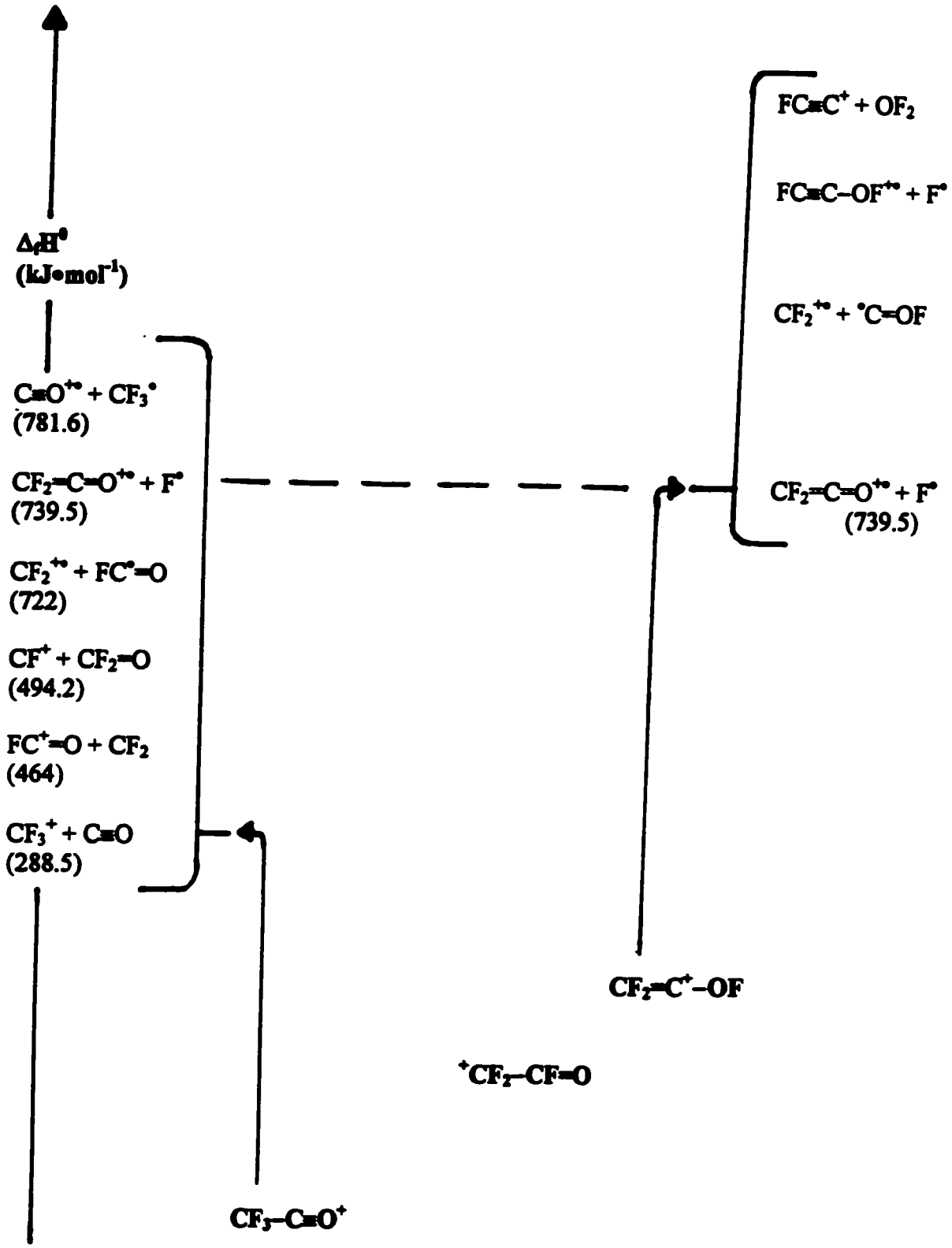

Table 3.35 Metastable Ion (MI) 2FFR and Collision Induced Dissociation (CID) 2FFR He ≈ 90 %T Mass Spectra of Source Generated $C_2F_3O^{+\bullet}$ (m/z 97) from the C_3F_6O Isomers

			Parent Ion					
			$(CF_3)_2C{=}O$		$CF_2{=}CFOCF_3$		c-F_2(COC)FCF_3	
	Mass	Neutral	Height (%)		Height (%)		Height (%)	
Species	(m/z)	Loss	MI	CID	MI	CID	MI	CID
CF_3^+	69	(–CO)	100.0	100.0	100.0	100.0	100.0	100.0
$CF_2^{+\bullet}$	50	(–CFO$^\bullet$)	1.6	6.0		11.0		9.3
CFO^+	47	(–CF_2)		<0.3		11.0		7.9
C_2F^+	43	(–OF_2)						<0.3
CF^+	31	(–CF_2O)		1.3		5.6		3.3
$CO^{+\bullet}$	28	(–$CF_3^\bullet$)		1.3				1.3

Figure 3.67 Metastable Ion (MI) 2FFR Mass Spectra of Source Generated $C_2F_3O^+$ (m/z 97) from (a) $(CF_3)_2C{=}O^{+\bullet}$ (b) $CF_2{=}CFOCF_3^{+\bullet}$ and (c) c-F_2(COC)$FCF_3^{+\bullet}$

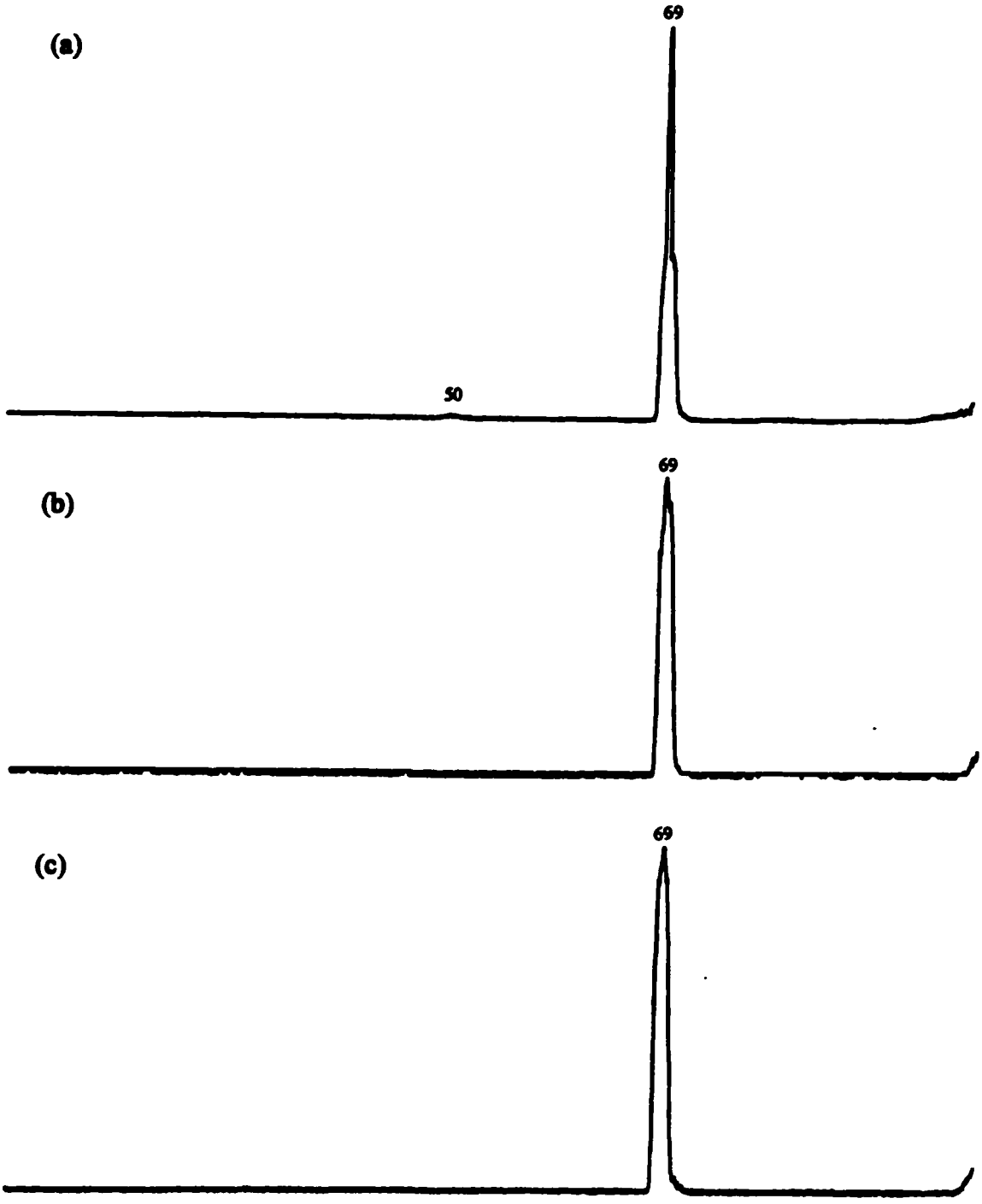

Figure 3.68 Collision Induced Dissociation (CID) 2FFR He ≈ 90 %T Mass Spectra of Source Generated $C_2F_3O^+$ (m/z 97) from (a) $(CF_3)_2C{=}O^{+\bullet}$ (b) $CF_2{=}CFOCF_3^{+\bullet}$ and (c) c-F_2(COC)$FCF_3^{+\bullet}$

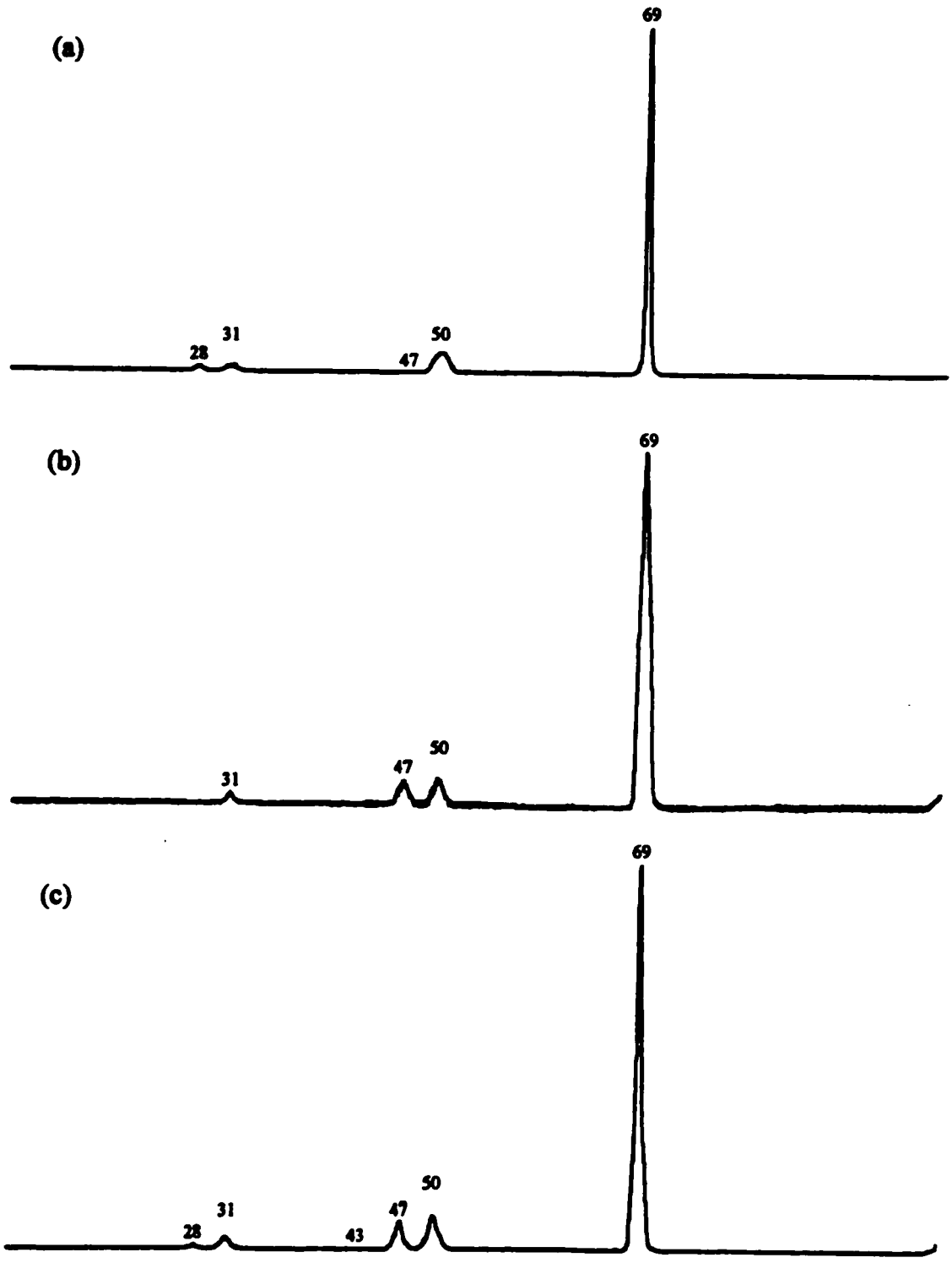

Figure 3.69 Close-Up of the Metastable Peak CF_3^+ (m/z 69) from the Source Generated $C_2F_3O^+$ (m/z 97) from (a) $(CF_3)_2C{=}O^{+\bullet}$ (b) $CF_2{=}CFOCF_3^{+\bullet}$ and (c) c-F_2(COC)$FCF_3^{+\bullet}$

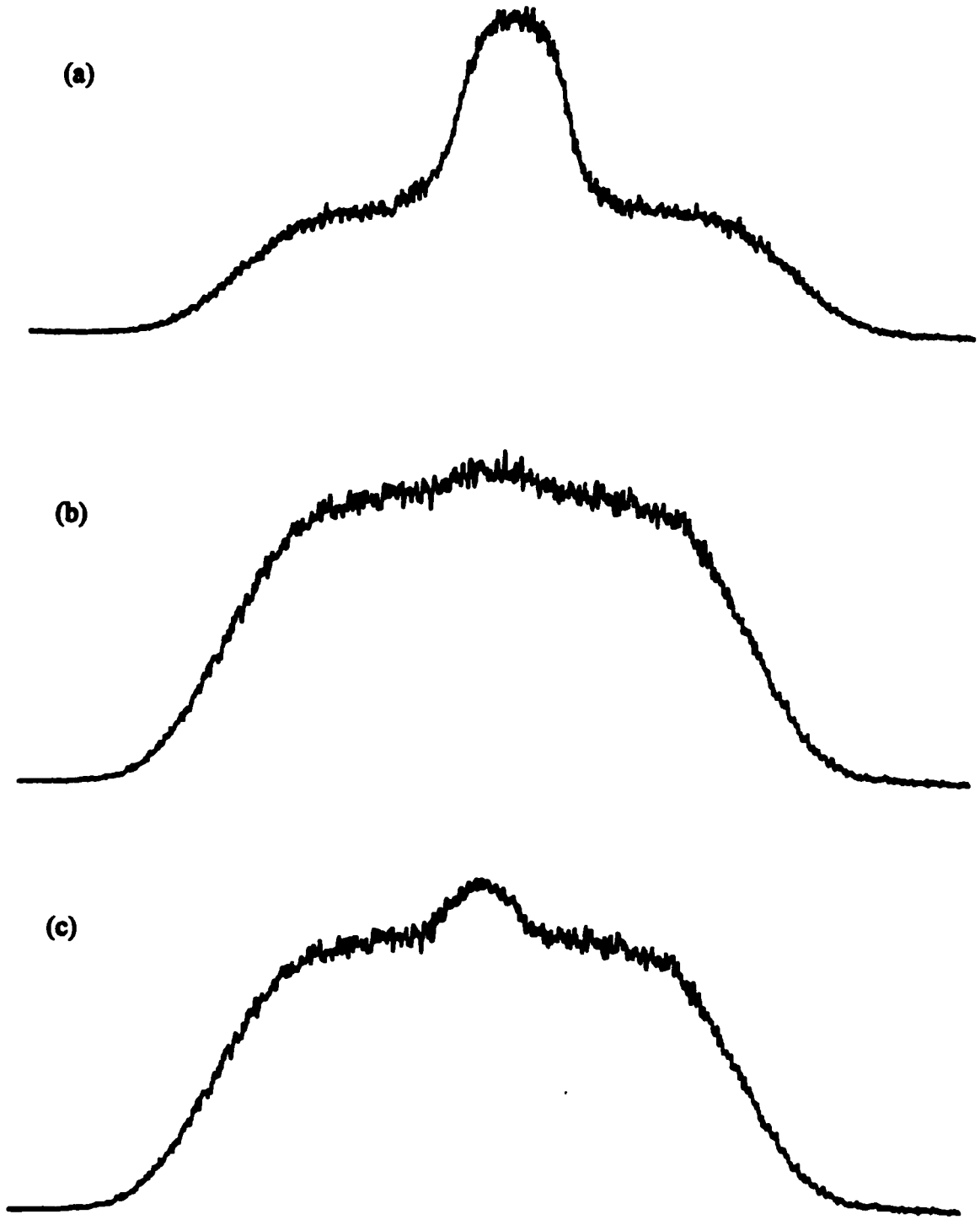

Figure 3.70 Proposed Potential Energy Surface of the $C_2F_3O^+ \rightarrow CF_3^+ + C{\equiv}O$ Dissociation Process

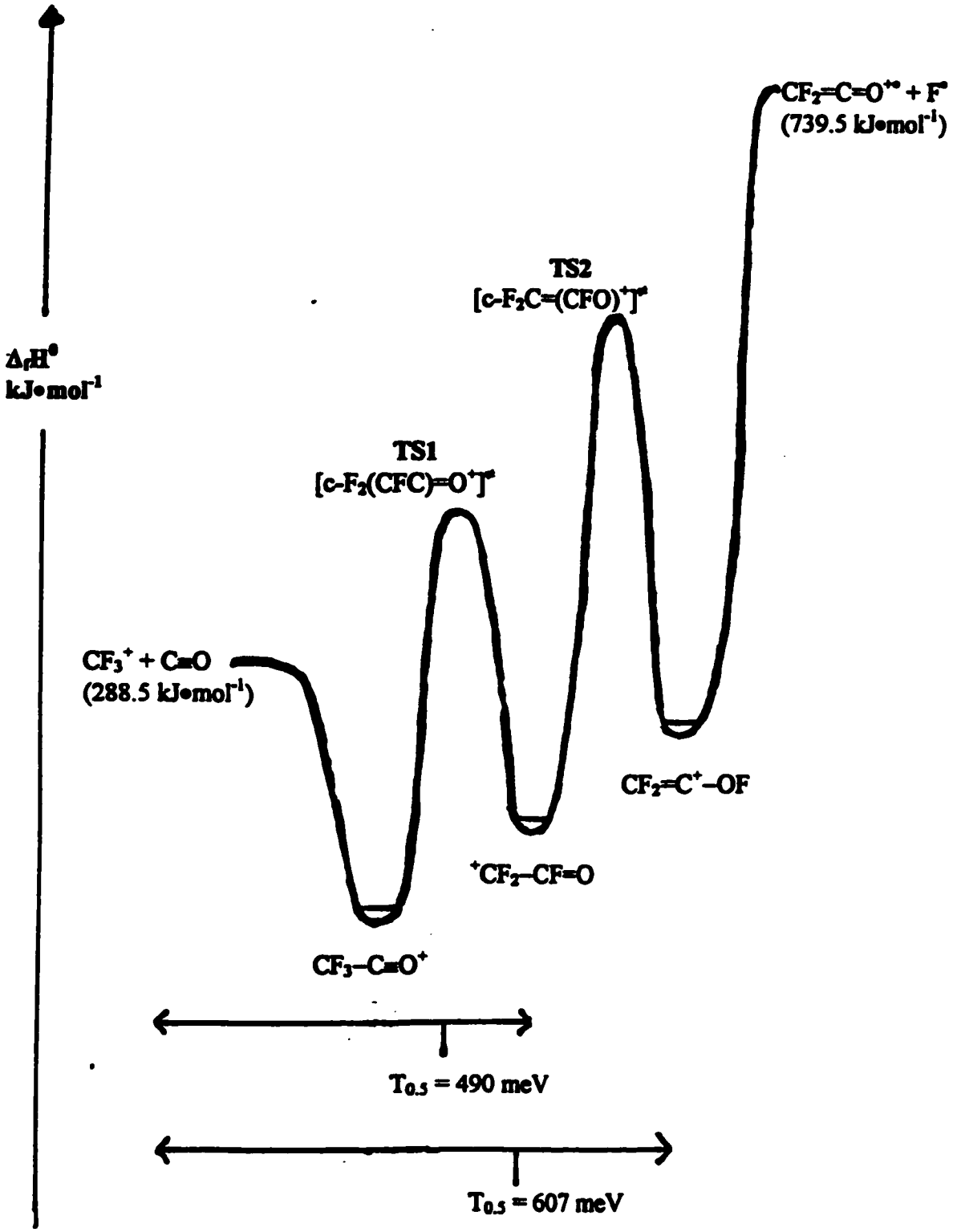

isomers have as their main MI peak, and the base peak in their CID mass spectra that of the CF_3^+ (m/z 69) ion, corresponding to C≡O loss. Additionally illustrated in Figure 3.69, the close-up of the MI peak for CF_3^+ clearly shows that all of the $C_2F_3O^+$ isomers produce a composite peak shape. As previously stated, it consists of a thin-spike component atop a wide-hump component background. For all of the thin-spike components their $T_{0.5}$ value is ≈ 2 meV and it is assigned to the common $CF_3–C{\equiv}O^+ \rightarrow CF_3^+ + C{\equiv}O$ dissociation process (see Table 3.32). However, the wide-hump component possesses a larger $T_{0.5}$ value (i.e., ≈ 607 meV) for the $(CF_3)_2C{=}O^{+\bullet}$ precursor than for the two other $CF_2{=}CFOCF_3^{+\bullet}$ and c-F_2(COC)$FCF_3^{+\bullet}$ precursors which have a lower common $T_{0.5}$ value (i.e., ≈ 490 meV). As well, the collision sensitivities of the thin-spike components are markedly different. For the $(CF_3)_2C{=}O^{+\bullet}$ precursor, the admission a of tiny amount of collision gas resulted in the thin-spike component to grow so rapidly that it "swamped" all the rest of the peak. However, for the $CF_2{=}CFOCF_3^{+\bullet}$ and c-F_2(COC)$FCF_3^{+\bullet}$ precursors, the admission of collision gas to near single-collision conditions (see Table 3.32) results in the former isomer products being very collision insensitive (i.e, the thin-spike component grew only ≈ 2x), and the latter isomer products being moderatedly collision insensitive (i.e, the thin-spike component grew only ≈ 5x).

The above observations can be rationalized as follows. On inspection of Figure 3.70, the proposed potential energy surface of the $C_2F_3O^+ \rightarrow CF_3^+ + C{\equiv}O$ dissociation process, it is proposed here that there is a cyclic transition state, [c-F_2(CFC)=O^+]‡ (denoted as TS1), which acts as a bridge between the $CF_3–C{\equiv}O^+$ and $F_2C^+–CF{=}O$ isomers. As well, it is proposed there is another cyclic transition state, [c-$F_2C{=}(CFO)^+$]‡ (denoted as TS2),which acts as a bridge between the $F_2C^+–CF{=}O$ and $CF_2{=}C^+–OF$ isomers. For the $CF_3–C{\equiv}O^+$

isomer, its $CF_3^+ + C{\equiv}O$ dissociation limit has a $\Delta_f H^0$ value of 288.5 kJ•mol^{-1}. For the $F_2C^+{-}CF{=}O$ isomer, its $CF_2^{+\bullet} + F^\bullet C{=}O$ dissociation limit has a $\Delta_f H^0$ value of 722 kJ•mol^{-1}. For the $CF_2{=}C^+{-}OF$ isomer, its $CF_2{=}C{=}O^{+\bullet} + F^\bullet$ dissociation limit is proposed to have a $\Delta_f H^0$ value of 739.5 kJ•mol^{-1}.

Now with the above information in mind, one may now clearly analyze the behaviour $C_2F_3O^+$ species from each $C_3F_6O^{+\bullet}$ precursor. For the $C_2F_3O^+$ species produced from the $(CF_3)_2C{=}O^{+\bullet}$ precursor, it is proposed that they are the $CF_3{-}C{\equiv}O^+$ and $CF_2{=}C^+{-}OF$ isomers. The $CF_3{-}C{\equiv}O^+$ isomer is extremely collision sensitive and undergoes direct bond-cleavage, $CF_3{-}C{\equiv}O^+ \rightarrow CF_3^+ + C{\equiv}O$, with a small $T_{0.5}$ value (i.e., $\approx$ 2 meV) to the dissociation products with a very low $\Delta_f H^0$ value (i.e., 288.5 kJ•mol^{-1}). Now, the $CF_2{=}C^+{-}OF$ isomer may undergo two MI processes. The first MI process, $CF_2{=}C^+{-}OF \rightarrow CF_2^{+\bullet} + F^\bullet C{=}O$, is proposed to proceed via the $[c\text{-}F_2C{=}(CFO)^+]^\ddagger$ transition state (unfortunately too weak in intensity to measure its $T_{0.5}$ value) to the dissociation products with a higher $\Delta_f H^0$ value (i.e., 722 kJ•mol^{-1}). In order to reach the lowest dissociation limit (i.e., $CF_3^+ + C{\equiv}O$), the second MI process of $CF_2{=}C^+{-}OF \rightarrow CF_3^+ + C{\equiv}O$ must proceed on through a second transition state, $[c\text{-}CF_2{=}(CFO)^+]^\ddagger$. Thus, for the $CF_2{=}C^+{-}OF$ isomer to reach $CF_3^+ + C{\equiv}O$ it must transverse through $[c\text{-}CF_2{=}(CFO)^+]^\ddagger$ to $F_2C^+{-}CF{=}O$ then to $[c\text{-}F_2(CFC){=}O^+]^\ddagger$ en-route to the lowest $\Delta_f H^0$ dissociation limit. Thus, this would account for the large $T_{0.5}$ value of $\approx$ 607 meV assigned to this entire process.

For the $C_2F_3O^+$ species produced from the $CF_2{=}CFOCF_3^{+\bullet}$ precursor it is proposed that they are the $^+CF_2{-}CF{=}O$, and a small amount of $CF_3{-}C{\equiv}O^+$. However, the only observed MI products are $CF_3^+ + C{\equiv}O$ and *not* any $CF_2^{+\bullet} + F^\bullet C{=}O$. Thus, it is proposed here

that the $^{+}CF_2$–CF=O isomer proceeds through the [c-F_2(CFC)=O^{+}]‡ transition state to the lowest Δ_fH^0 value dissociation limit of CF_3^{+} + C≡O with a lower $T_{0.5}$ value of ≈ 490 meV.

For the $C_2F_3O^{+}$ species produced from the c-F_2(COC)$FCF_3^{+\bullet}$ precursor, it is proposed that they again are the $^{+}CF_2$–CF=O, and a small amount of CF_3–C≡O^{+}. As well, the only observed MI dissociation products are just CF_3^{+} + C≡O. Thus, as it was proposed for the CF_2=CF$OCF_3^{+\bullet}$ precursor, the [c-F_2(CFC)=O^{+}]‡ transition state is accessed en-route to the CF_3^{+} + C≡O dissociation limit.

One should note here that the CF_2=C=$O^{+\bullet}$ + $F^{\bullet}$ dissociation limit (see Figure 3.70), with it possessing the (proposed) highest Δ_fH^0 value (i.e., 739.5 kJ•mol^{-1}) was *not* observed to be accessed by *any* of the precursors studied here.

3.7 Conclusions

Thus, in this chapter it may be observed that with the high electron density of the F atoms and somewhat different Δ_fH^0 values of their species compared to their hydrogen analogues (see Table 3.1), a rich and different (rearrangement) gas-phase ion-chemistry of the perfluorinated organics is exhibited. This behaviour sometimes parallels that of its well studied hydrogen cousins, and sometimes it exhibits the completely unexpected.

A case in point is the behaviour of CF_2=CF$OCF_3^{+\bullet}$ in the production of the CF_2=C=$O^{+\bullet}$ species, and subsequently its neutral CF_2=C=O. The next chapter will deal with this newly observed important species, which was first directly experimentally observed by our group to possess a stable gas-phase neutral, namely that of perfluoroketene, CF_2=C=O.

3.7 References

[1] S.G. Lias, J.E. Bartmess, J.F. Liebman, J.L. Holmes, R.D. Levin, and W.G. Mallard, Gas-Phase Ion and Neutral Thermochemistry, J. Phys. Ref. Data, 17(1), (1988).

[2] C.R. Brundle, M.B. Robin, N.A. Kuebler, and H. Basch, J. Amer. Chem. Soc., 94(5), 1451-1465, (1972).

[3] C.R. Brundle, M.B. Robin, and N.A. Kuebler, J. Amer. Chem. Soc., 94(5), 1466-1475, (1972).

[4] G.K. Jarvis, K.J. Boyle, C.A. Mayhew, and R.P. Tuckett, J. Phys. Chem. A, 102(19), 3219-3229, (1998).

[5] G.K. Jarvis, K.J. Boyle, C.A. Mayhew, and R.P. Tuckett, J. Phys. Chem. A, 102(19), 3230-3237, (1998).

[6] C. Aubry, and J.L. Holmes, J. Phys. Chem. A, 102(32), 6441-6447, (1998).

[7] W.R. Dolbier, Jr., Chem. Rev., 96, 1557-1584, (1996).

[8] C.G. Krespan, and V.A. Petrov, Chem. Rev., 96, 3269-3301, (1996).

[9] S.W. Benson, F.R. Cruickshank, D.M. Golden, G.R. Haugen, H.E. O'Neil, A.S. Rodgers, R. Shaw, and R. Walsh, Chem. Rev., 69, 279-324, (1969).

[10] S.W. Benson, Thermochemical Kinetics, 2nd Ed., John Wiley and Sons, New York, New York, USA, pp. 24-28, (1976).

[11] N. Cohen, and S.W. Benson, Chem. Rev., 93, 2419-2438, (1993).

[12] W.M. Bryant, J. Polym. Sci., 56, 278, (1962).

[13] N.D. Kagramanov, K. Ujszaszy, J. Tamas, A.K. Maltsev, and O.M. Nefedov, Bull. Acad. Sci. USSR, Div. Chem., 7, 1531, (1983).

[14] G. Bieri, L. Asbrink, and W. Von Niessen, J. Electron Spectros. Rel. Phenom., 23, 281-332, (1981).

[15] J.P. Delwiche, M-TH. Praet, G. Caprace, M-J. Hubin-Franskin, P. Natalis, and J.E. Collin, J. Electron Spectros. Rel. Phenom., 12, 395-403, (1977).

[16] J.H.D. Eland, Photoelectron Spectroscopy. An Introduction to Ultraviolet Photoelectron Spectroscopy in the Gas Phase, Butterworths, London, U.K., (1974).

[17] J.H.D. Eland, Photoelectron Spectroscopy. An Introduction to Ultraviolet Photoelectron Spectroscopy in the Gas Phase, 2nd Ed., Butterworths, London, U.K., (1984).

[18] C.R. Brundle, and M.B. Robin, J. Am. Chem. Soc., 92(19), 5550-5555, (1970).

[19] J.L. Holmes, and M. Dakubu, Org. Mass Spectrom., 24, 461-464, (1989).

[20] D.F. Dawson, and J.L. Holmes, J. Phys. Chem. A, 103(26), 5217-5220, (1999).

[21] R. Bralsfold, P.V. Harris, and W.C. Price, Proc. Royal Soc. London A, 258, 459-469, (1960).

[22] W.C. Price, T.R. Passmore, and D.M. Roessler, Discuss. Faraday Soc., 35, 201-211, (1963).

[23] L.P. Hammett, Physical Organic Chemistry. Reaction Rates, Equilibria, and Mechanism, 2nd Ed., McGraw-Hill, Inc., New York, New York, USA, pp. 355-373, (1970).

[24] E.M. Kosover, An Introduction to Physical Organic Chemistry, John Wiley and Sons, Inc., New York, New York, USA, pp. 45-62, (1968).

[25] A.G. Harrison, P. Kebarle, and F.P. Lossing, J. Amer. Chem. Soc., 83, 777-780, (1961).

[26] R.W. Taft, Jr., J. Amer. Chem. Soc., 79, 1045-1049, (1957).

[27] R.W. Taft, Jr., N.C. Deno, and P.S. Skull, Ann. Rev. Phys. Chem., 9, 287, (1958).

[28] K. Watanabe, T. Nakayama, and J. Mottl, J. Quant. Spectrosc. Radiat. Transfer, 2, 369-382, (1962).

[29] I.P. Fisher, J.B. Homer, and F.P. Lossing, J. Am. Chem. Soc., 87(5), 957-960, (1965).

[30] J.R. Majer, Advan. Fluorine Chem., 2, 1, (1961).

[31] M.R. Robin, G.N. Taylor, and N.A. Kuebler, J. Org. Chem., 38(5), 1049-1051, (1973).

[32] C.A. Longfellow, L.A. Smeliar, Y.T. Lee, Y.R. Lee, C.Y. Yeh, and S.M. Lin, J. Phys. Chem. A, 101, 338-344, (1997).

[33] Q. Chen, and B.S. Freiser, J. Phys. Chem. A, 102, 3343-3351, (1998).

[34] H.E. O'Neal, and S.W. Benson, J.Phys. Chem., (6)72, 1866-1887, (1968).

[35] P.H. Krupenie, "The Spectrum of Molecular Oxygen", J. Phys. Chem. Ref. Data, 1(2), 423-534, (1972).

[36] S. Bashkin, and J.O. Stoner, Jr., Atomic Energy and Grotrian Diagrams 1. Hydrogen I -Phosphorous XV, Amreican Elsevier Publishing Company Inc., New York, NY, USA, (1975).

Chapter 4 Tandem Mass Spectrometry of CF_2=C=O. The First Experimental Observation of Gas-Phase Neutral Perfluoroketene.

4.1 Introduction

Until recently, perfluoroketene [1-3] had not been experimentally identified as a stable species in any phase. However, Kotting et. al. [4] has proposed the generation of neutral perfluoroketene, F_2C=C=O, from a reaction of perfluorovinylidene F_2C=C: with carbon dioxide O=C=O, via the elimination of C≡O, in a 1 % CO_2 doped Ar matrix at 30 K. The matrix isolated F_2C=C=O was characterized utilizing IR difference spectroscopy, isotopic labeling, and density functional theory (DFT) calculations. The $\nu_2(A_1)$; ν(CO) stretch, $\upsilon_4(A_1)$; ν(CC) stretch, $\nu_7(B_2)$; $\nu_{as}(CF_2)$ asymmetric stretching vibrations were identified and assigned values of 2161.6 cm^{-1}, 1426.8 cm^{-1}, 1274.4 cm^{-1}, respectively. The DFT calculations [4] also proposed a planar stable C_{2v} structure for perfluoroketene F_2C=C=O with bond angles and lengths similar to that of ketene H_2C=C=O and possessing a small *endothermic* barrier for the dissociation CF_2=C=O → CF_2 + C≡O.

Concurrent with the above observations of Kotting et.al. [4], a recent high-level calculation by Zachariah et.al. [5] showed F_2C=C=O to be species with a heat of formation $\Delta_f H^0[CF_2=C=O] = -(290.4 \pm 13.2)$ kJ•mol^{-1} thus possessing an *exothermic* dissociation with respect to the dissociation products CF_2 + C≡O (i.e., $\Delta_f H^0[CF_2] = -(203.3 \pm 16.5)$ kJ•mol^{-1} [5], and $\Delta_f H^0[C\equiv O] = -110.5$ kJ•mol^{-1} [6-8]). In addition, the earlier report on CF_2=C=O by Dailey III [9] gave the neutral and the radical-cation forms closely similar planar geometries with an *endothermic* dissociation barrier of ≈ 42 kJ•mol^{-1} (i.e., 10 kcal•mol^{-1}) for the CF_2=C=O → CF_2 + C≡O process. Thus, this makes vertical neutralization of CF_2=C=$O^{+\bullet}$ by

Neutralization-Reionization Mass Spectrometry (NRMS) an attractive technique [10] for the first production of gas-phase neutral CF_2=C=O.

Presented here in this chapter is a study which was carried out in our group that led to the first experimental identification of *stable gas-phase* CF_2=C=O *neutral*. Recently, Dawson and Holmes [11] presented an NR study on CF_2=C=O$^{+\bullet}$ produced from ionized CF_2=CFOCF$_3$ which was shown to produce *stable neutral perfluoroketene* following neutralization via electron-transfer from Xe followed by collisional-reionization by O_2 target gases. An intense recovery signal for $C_2F_2O^{+\bullet}$ (m/z 78) was obtained for both the source and metastably generated perfluoroketene ions and which was unequivocally assigned to the CF_2=C=O$^{+\bullet}$ structure [11]. The perfluoroketene molecules were metastable in the microsecond time frame (i.e., the transit time between the neutralization and the reionization cells) with respect to their dissociation CF_2=C=O → CF_2 + C≡O.

It is proposed here that CF_2=C=O is indeed a genuinely (endothermically bound) stable molecule that is difficult to isolate in the solution-phase, as well as in high concentrations in the gas-phase due to its high chemical reactivity. It is asserted here that the most reasonable estimate of the heat of formation the perfluoroketene neutral is $\Delta_fH^0[CF_2=C=O] = -401.3$ kJ•mol^{-1}; this value being derived through the use of Benson's Rules of Additivity [12-16]. Thus, with the lowest dissociation limit CF_2 + C≡O possessing a Δ_fH^0 value [6] of –315.5 kJ•mol^{-1}, one obtains an *endothermic* dissociation energy of 85.8 kJ•mol^{-1}. Additionally, through the use of the Wigner-Witmer Correlation Rules [17-21], one may predict the direct unimolecular dissociation of the C_{2v} planar CF_2=C=O[$\tilde{X}\,^1A_1$] neutral via a C_{2v} planar transition state into the spin and symmetry allowed dissociation products of CF_2[$\tilde{X}\,^1A_1$] + C≡O[$\tilde{X}\,^1A_1(^1\Sigma^+)$]. Therefore, one may qualitatively propose a

smooth (i.e., without a hump) potential energy surface en-route for the CF_2=C=O[$\tilde{X}\,^1A_1$] → CF_2[$\tilde{X}\,^1A_1$] + C≡O[$\tilde{X}\,^1A_1(^1\Sigma^+)$] dissociation process. This process would hence possess little or no reverse activation energy barrier of any significant magnitude (i.e., a near threshold process).

As well, on the matter of the adiabatic ionization energies and cationic heats of formations of perfluoroketene it will be proposed in the following chapter that one may, via (semi)-quantitative means, estimate a value of $IE_a[CF_2=C=O] \approx 11$ eV, and consequently $\Delta_f H^0[CF_2=C=O^{+\bullet}] = 660.1$ kJ•mol^{-1}. The rationale for the estimation of the above mentioned and previously "unknown" (experimentally and theoretically unstudied) thermodynamic quantities for CF_2=C=O will be discussed in the following sections. Therefore, it is proposed here that the following values of *$\Delta_f H^0[CF_2=C=O] = -401.3$ kJ•mol^{-1}, $IE_a[CF_2=C=O] \approx 11$ eV, and $\Delta_f H^0[CF_2=C=O^{+\bullet}] = 660.1$ kJ•mol^{-1}* represent (in the absence of reliable, systematic experimental and theoretical studies) the *best approximation* of these hitherto previously undetermined thermodynamic quantities for the perfluoroketene CF_2=C=O species.

In the exploration of the properties of CF_2=C=O frequent analogies with the previously studied CH_2, CH_2=C=O, CF_2, and other related species will be drawn upon. The areas that will be dealt with are the following; the electronic and optical spectroscopic properties [1, 22-34]; the photoelectron spectroscopic properties [1, 35-51]; and the mass spectrometric properties [1, 52-63] of CH_2, CH_2=C=O, CF_2, CF_2=C=O and related species.

Now in regards to the production of CF_2=C=O, there are relatively few precursor perfluoro molecules available. Fortunately, two possible precursors for ionized perfluoroketene can be obtained, namely, the C_3F_6O isomers $(CF_3)_2$C=O and CF_2=CFOCF$_3$. In the case of their hydrogen analogues, with the aid of the low $\Delta_f H^0[CH_4] = -74.5$ kJ•mol^{-1}

[6, 7] value ionized acetone produces predominantly $CH_2{=}C{=}O^{+\bullet}$ ions by loss of CH_4 in its metastable ion mass spectrum, where it competes with $CH_3{-}C{\equiv}O^+$ for the lowest energy fragmentation process [52, 53]. In contrast, metastable methylvinylether ($CH_2{=}CHOCH_3$) ions produce mainly $CH_3{-}C{\equiv}O^+$ fragments via an isomerization to energy-rich acetone ions [52]. Consequently, the *very* low $\Delta_f H^0[CF_4] = -934.5$ kJ•mol^{-1} [6, 7] value promised to make the formation of $CF_2{=}C{=}O^{+\bullet}$ from $(CF_3)_2C{=}O$ a likely process. However, as will be discussed later in this chapter, this expectation was not realized and instead it was metastable $CF_2{=}CFOCF_3^{+\bullet}$ that produced $CF_2{=}C{=}O^{+\bullet}$ via the loss of CF_4 [11].

Thus, the organisation of the characteristics of $CF_2{=}C{=}O$ to be discussed in this chapter are entitled as follows; Section 4.1.1 The Electron Configurations and Electronic States of $CF_2{=}C{=}O$ and Related Species, Section 4.1.2 The Heat of Formation of Neutral $CF_2{=}C{=}O$ and Related Species, Section 4.1.3 The Ionization Energy of $CF_2{=}C{=}O$ and Related Species, Section 4.1.4 The Dissociation of $CF_2{=}C{=}O$ and Related Species; Section 4.2 Experimental Mass Spectra of $CF_2{=}C{=}O^{+\bullet}$; Section 4.3 Conclusions; and Section 4.4 References. Thus to re-emphasize, the guiding axiom throughout this entire chapter is that $CF_2{=}C{=}O$ is a genuinely bound (although highly reactive) neutral species with an *endothermic* dissociation energy of ≈ 86 kJ•mol^{-1} to reach the CF_2 + $C{\equiv}O$ dissociation products.

4.1.1 The Electron Configurations and Electronic States of $CF_2{=}C{=}O$ and Related Species

In this section many qualitative comparisons with the related hydrogen CH_2, $CH_2{=}O$, $CH_2{=}C{=}O$, and the perfluoro CF_2, $CF_2{=}O$ species will be utilized to propose the properties of the relatively unstudied $CF_2{=}C{=}O$ molecule. The ordering of the molecular orbital types of

the CH_2, CH_2=O, CH_2=C=O, CF_2, CF_2=O, and the proposed CF_2=C=O are listed in Table 4.1. The qualitative pictorial representations of the molecular orbitals of CH_2 and CF_2 are illustrated in Figures 4.1 and 4.2, respectively. Additionally, the neutral and cationic electronic states of CH_2 compared to CF_2, CH_2=C=O compared to CF_2=C=O, are listed in Tables 4.2, and 4.3, respectively.

Now to set out the qualitative rationale that will be utilized to illustrate the material presented in the above mentioned Tables 4.1, 4.2, 4.3, and Figures 4.1, 4.2, one should discuss briefly the characteristics of the atoms and their atom-orbitals that when assembled into a molecular framework make up their respective molecular orbitals. The atoms of interest with their ground state electron configuration are as follows; $H^{\bullet}$, $(1s)^2$; C, $(1s)^2(2s)^2(2p)^2$; O, $(1s)^2(2s)^2(2p)^4$; and $F^{\bullet}$, $(1s)^2(2s)^2(2p)^5$. They possess IE_a values of 13.598 eV, 11.260 eV, 13.618 eV, and 17.422 eV for $H^{\bullet}$, C, O, $F^{\bullet}$ and correspond to the removal of an electron from a (1s) atomic-orbital in the former, and the (2p) atomic-orbital in the three latter cases, respectively. These are known as valence atomic-orbitals and have spherical symmetry. Any atomic-orbitals (i.e., (ns), (np), (nd),...) composed of higher principal quantum numbers, n, (e.g., (3s), (3p), (3d), (4s),...) are known as Rydberg atomic-orbitals [17-22, 24-26, 30].

Thus, on inspection of the above atomic IE_a values, one may qualitatively see that on the combination of the individual atoms into a molecular framework one may expect molecular IE_a values for hydrogen compounds $C_nH_mO_p$ and perfluoro compounds $C_nF_mO_p$ to be in the ranges of ≈ 8-10 eV, and ≈ 10-12 eV, respectively. Thus, the physical characteristics (e.g., its IE_a value, Δ_fH^0 value, etc...) of a molecule are dictated by the symmetry of the molecular framework and the identity of the atoms in it. The atomic-

Table 4.1 Classes of Molecular Orbitals for the Hydrogen CH_2, CH_2=O, CH_2=C=O and the Fluorine CF_2, CF_2=O, CF_2=C=O Series

Hydrogen Compounds	
	(1s)-type Core Orbitals
CH_2	$(1a_1)^2$
CH_2=O	$(1a_1)^2(2a_1)^2$
CH_2=C=O	$(1a_1)^2(2a_1)^2(3a_1)^2$
	(2s)-type Valence Orbitals
CH_2	$(2a_1)^2$
CH_2=O	$(3a_1)^2(4a_1)^2$
CH_2=C=O	$(4a_1)^2(5a_1)^2(6a_1)^2$
	(2p)-type Valence Orbitals
CH_2	$(1b_2)^2(3a_1)(1b_1)$
CH_2=O	$(1b_2)^2(5a_1)^2(1b_1)^2(2b_2)^2$
CH_2=C=O	$(7a_1)^2(1b_2)^2(1b_1)^2(2b_2)^2(2b_1)^2$
	Unoccupied (2p)-type Valence Orbitals
CH_2	–
CH_2=O	$(2b_1)^0(6a_1)^0$
CH_2=C=O	$(3b_2)^0(3b_1)^0(8a_1)^0(9a_1)^0$
Perfluorinated Compounds	
	(1s)-type Core Orbitals
CF_2	$(1a_1)^2(1b_2)^2(2a_1)^2$
CF_2=O	$(1a_1)^2(1b_2)^2(2a_1)^2(3a_1)^2$
CF_2=C=O	$(1a_1)^2(1b_2)^2(2a_1)^2(3a_1)^2(4a_1)^2$
	(2s)-type Valence Orbitals
CF_2	$(3a_1)^2(2b_2)^2(4a_1)^2$
CF_2=O	$(4a_1)^2(2b_2)^2(5a_1)^2(6a_1)^2$
CF_2=C=O	$(5a_1)^2(2b_2)^2(6a_1)^2(7a_1)^2(8a_1)^2$
	(2p)-type Valence Orbitals
CF_2	$(1b_1)^2(5a_1)^2(3b_2)^2(1a_2)^2(4b_2)^2(6a_1)^2$
CF_2=O	$(3b_2)^2(1b_1)^2(7a_1)^2(1a_2)^2(4b_2)^2(8a_1)^2(2b_1)^2(5b_2)^2$
CF_2=C=O	$(1b_1)^2(3b_2)^2(9a_1)^2(2a_2)^2(10a_1)^2(4b_2)^2(2b_1)^2(5b_2)^2(3b_1)^2$
	Unoccupied (2p)-type Valence Orbitals
CF_2	$(2b_1)^0(7a_1)^0(5b_2)^0$
CF_2=O	$(3b_1)^0(9a_1)^0$
CF_2=C=O	$(6b_2)^0(4b_1)^0(11a_1)^0$

Figure 4.1 Qualitative Molecular Orbitals of CH_2

$CH_2[\tilde{X}^3B_1]$

(1s)–Core	$(1a_1)^2$
(2s)–Valence	$(2a_1)^2$
(2p)–Valence	$(1b_2)^2(3a_1)(1b_1)$

$(1a_1)^2$

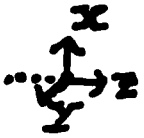

$(2a_1)^2$

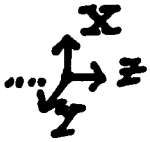

$(1b_2)^2$ $(3a_1)$ $(1b_1)$

Figure 4.2 Qualitative Molecular Orbitals of CF_2

$CF_2[\tilde{X}\,^1A_1]$

(1s)–Core	$(1a_1)^2(1b_2)^2(2a_1)^2$
(2s)–Valence	$(3a_1)^2(2b_2)^2(4a_1)^2$
(2p)–Valence	$(1b_1)^2(5a_1)^2(3b_2)^2(1a_2)^2(4b_2)^2(6a_1)^2$
(2p)–Unoccupied	$(2b_1)^0(7a_1)^0(5b_2)^0$

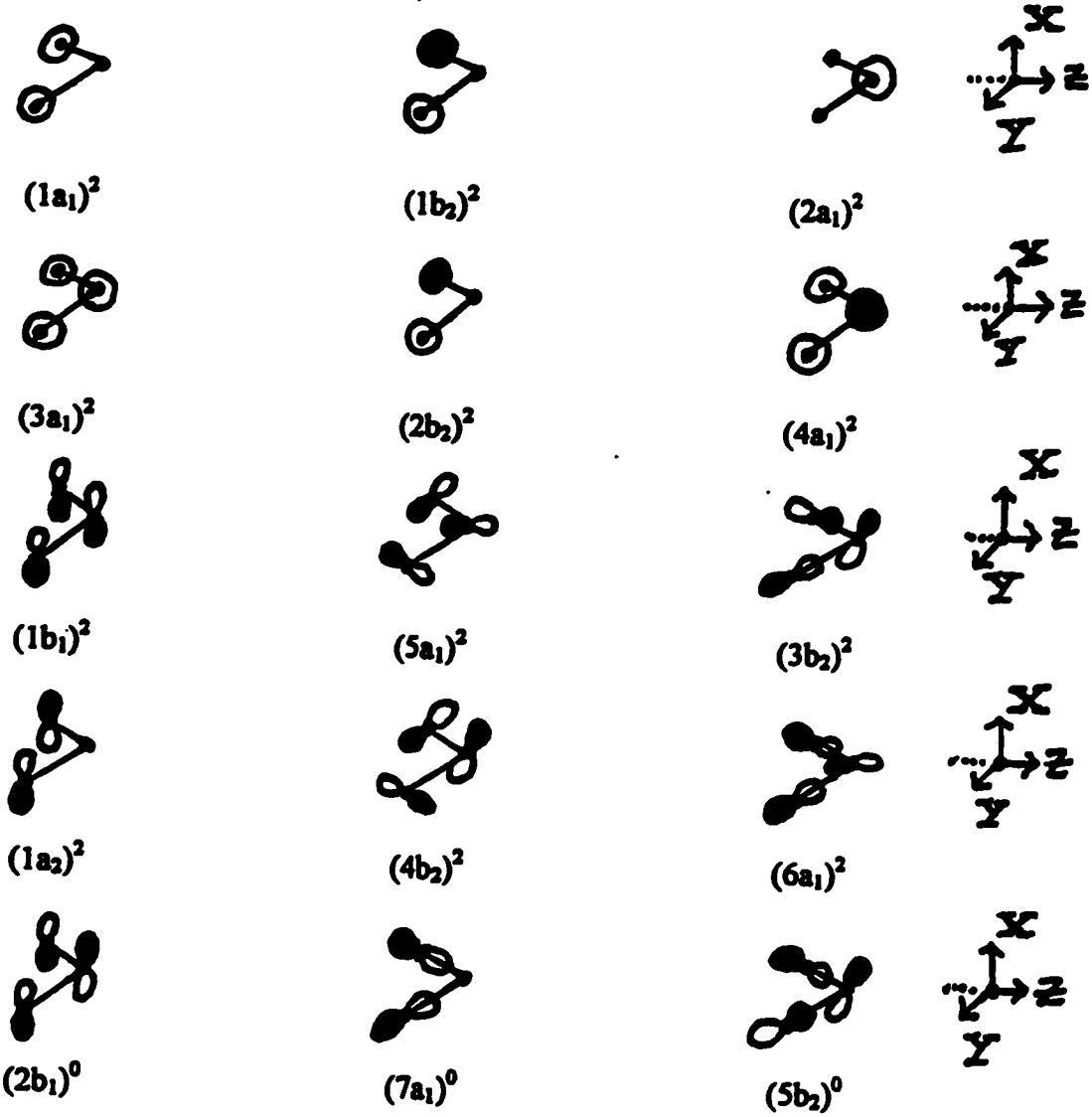

Table 4.2 The Neutral and Cationic Electronic States of CH_2 and CF_2

Valence Electron Configuration	Electronic States
CH_2	
$(2a_1)^2(1b_2)^2(3a_1)(1b_1)$	$\tilde{X}\,^3B_1$, $\tilde{a}\,^1B_1$
$(2a_1)^2(1b_2)^2(3a_1)^2$	$\tilde{b}\,^1A_1$
$(2a_1)^2(1b_2)(3a_1)^2(1b_1)$	$\tilde{A}\,^3A_2$, $\tilde{c}\,^1A_2$
$(2a_1)^2(1b_2)(3a_1)(1b_1)^2$	$\tilde{B}\,^3B_2$, $\tilde{d}\,^1B_2$
$(2a_1)^2(1b_2)^2(1b_1)^2$	$^1A_1$
$(2a_1)^2(1b_2)^2(3a_1)(3sa_1)$	$(3s)^3A_1$, $(3s)^1A_1$ (Rydberg)
$CH_2^{+\bullet}$	
$(2a_1)^2(1b_2)^2(3a_1)$	$\tilde{X}\,^2A_1$
$(2a_1)^2(1b_2)^2(1b_1)$	$\tilde{A}\,^2B_1$
$(2a_1)^2(1b_2)(3a_1)(1b_1)$	$\tilde{a}\,^4A_2$, $^2A_2$
$(2a_1)^2(1b_2)(3a_1)^2$	$^2B_2$
$(2a_1)(1b_2)^2(3a_1)(1b_1)$	$^4B_1$, $^2B_1$
$(2a_1)(1b_2)(3a_1)^2(1b_1)$	$^4A_2$, $^2A_2$
CF_2	
$(1a_2)^2(4b_2)^2(6a_1)^2$	$\tilde{X}\,^1A_1$
$(1a_2)^2(4b_2)^2(6a_1)(2b_1)$	$\tilde{a}\,^3B_1$, $\tilde{A}\,^1B_1$
$(1a_2)^2(4b_2)^2(6a_1)(3sa_1)$	$(3s)^3A_1$, $(3s)^1A_1$ (Rydberg)
$CF_2^{+\bullet}$	
$(1a_2)^2(4b_2)^2(6a_1)$	$\tilde{X}\,^2A_1$
$(1a_2)^2(4b_2)(6a_1)^2$	$\tilde{A}\,^2B_2$
$(1a_2)(4b_2)^2(6a_1)^2$	$\tilde{B}\,^2A_2$
$(1a_2)^2(4b_2)(6a_1)(2b_1)$	$^4A_2$, $^2A_2$
$(1a_2)(4b_2)^2(6a_1)(2b_1)$	$^4B_2$, $^2B_2$
$(1a_2)(4b_2)(6a_1)^2(7a_1)$	$^4B_1$, $^2B_1$

Table 4.3 The Neutral and Cationic Electronic States of CH_2=C=O and CF_2=C=O

Valence Electron Configuration	Electronic States
CH_2=C=O	
$(7a_1)^2(1b_2)^2(1b_1)^2(2b_2)^2(2b_1)^2$	$\tilde{X}\,^1A_1$
$(7a_1)^2(1b_2)^2(1b_1)^2(2b_2)^2(2b_1)(3b_2)$	$\tilde{a}\,^3A_2$, $\tilde{A}\,^1A_2$
$(7a_1)^2(1b_2)^2(1b_1)^2(2b_2)^2(2b_1)(3b_1)$	$\tilde{b}\,^3A_1$, $\tilde{B}\,^1A_1$
$(7a_1)^2(1b_2)^2(1b_1)^2(2b_2)^2(2b_1)(8a_1)$	$^3B_1$, $^1B_1$
$(7a_1)^2(1b_2)^2(1b_1)^2(2b_2)^2(2b_1)(3sa_1)$	$(3s)^3B_1$, $(3s)^1B_1$ (Rydberg)
CH_2=C=O$^{+\bullet}$	
$(7a_1)^2(1b_2)^2(1b_1)^2(2b_2)^2(2b_1)$	$\tilde{X}\,^2B_1$
$(7a_1)^2(1b_2)^2(1b_1)^2(2b_2)(2b_1)^2$	$\tilde{A}\,^2B_2$
$(7a_1)^2(1b_2)^2(1b_1)(2b_2)^2(2b_1)^2$	$\tilde{B}\,^2B_1$
$(7a_1)^2(1b_2)(1b_1)^2(2b_2)^2(2b_1)^2$	$\tilde{C}\,^2B_2$
$(7a_1)(1b_2)^2(1b_1)^2(2b_2)^2(2b_1)^2$	$\tilde{D}\,^2A_1$
$(7a_1)^2(1b_2)^2(1b_1)^2(2b_2)(2b_1)(3b_2)$	$^4B_1$, $^2B_1$
$(7a_1)^2(1b_2)^2(1b_1)^2(2b_2)(2b_1)(3b_1)$	$^4B_2$, $^2B_2$
$(7a_1)^2(1b_2)^2(1b_1)^2(2b_2)(2b_1)(8a_1)$	$^4A_1$, $^2A_1$
CF_2=C=O	
$(10a_1)^2(4b_2)^2(2b_1)^2(5b_2)^2(3b_1)^2$	$\tilde{X}\,^1A_1$
$(10a_1)^2(4b_2)^2(2b_1)^2(5b_2)^2(3b_1)(6b_2)$	$\tilde{a}\,^3A_2$, $\tilde{A}\,^1A_2$
$(10a_1)^2(4b_2)^2(2b_1)^2(5b_2)^2(3b_1)(4b_1)$	$\tilde{b}\,^3A_1$, $\tilde{B}\,^1A_1$
$(10a_1)^2(4b_2)^2(2b_1)^2(5b_2)^2(3b_1)(11a_1)$	$^3B_1$, $^1B_1$
$(10a_1)^2(4b_2)^2(2b_1)^2(5b_2)^2(3b_1)(3sa_1)$	$(3s)^3B_1$, $(3s)^1B_1$ (Rydberg)
CF_2=C=O$^{+\bullet}$	
$(10a_1)^2(4b_2)^2(2b_1)^2(5b_2)^2(3b_1)$	$\tilde{X}\,^2B_1$
$(10a_1)^2(4b_2)^2(2b_1)^2(5b_2)(3b_1)^2$	$\tilde{A}\,^2B_2$
$(10a_1)^2(4b_2)^2(2b_1)(5b_2)^2(3b_1)^2$	$\tilde{B}\,^2B_1$
$(10a_1)^2(4b_2)(2b_1)^2(5b_2)^2(3b_1)^2$	$\tilde{C}\,^2B_2$
$(10a_1)(4b_2)^2(2b_1)^2(5b_2)^2(3b_1)^2$	$\tilde{D}\,^2A_1$
$(10a_1)^2(4b_2)^2(2b_1)^2(5b_2)(3b_1)(6b_2)$	$^4B_1$, $^2B_1$
$(10a_1)^2(4b_2)^2(2b_1)^2(5b_2)(3b_1)(4b_1)$	$^4B_2$, $^2B_2$
$(10a_1)^2(4b_2)^2(2b_1)^2(5b_2)(3b_1)(3a_1)$	$^4A_1$, $^2A_1$

orbitals merge together within the molecular framework to form the molecular-orbitals. There are two general types of molecular orbitals and they are known as core and valence orbitals.

Core-orbitals are basically the (1s)-type atomic-orbitals associated only with the atom on which it is centred (i.e., it is essentially an isolated atomic-orbital unassociated with the rest of the molecular framework). The (1s)-type core-orbitals of all atoms (save that of $H^{\bullet}$) possess very high ionization energies in the range of ≈ 100-700 eV and require X-ray sources of X-ray photoelectron spectroscopy (XPS) to remove them [20, 21, 30, 39]. Thus, they are considered non-participants in determining the unique physical characteristics of the molecule. This task is considered to be left that of the valence-orbitals which may be accessed via ultraviolet photoelectron spectroscopy (UPS) [20, 21, 30, 40].

The valence orbitals may be generally separated into two types known as inner-valence and outer-valence orbitals. Inner-valence orbitals possess higher IE_a values generally in the range of ≈ 20-50 eV, and whose molecular orbitals are usually composed of only of (2s)-type atomic-orbitals. Outer-valence orbitals possess lower IE_a values generally in the range of ≈ 5-20 eV, and whose molecular-orbitals are usually composed of (2s)-type and (2p)-type atomic-orbitals.

The molecular Rydberg-orbitals [25] are those which are composed of higher principle quantum numbers, n, (e.g., (3s), (3p), (3d), (4s),...) and are atomic-like in shape (i.e., s, p, d-like), very diffuse in nature (i.e., large) and may extend over large regions of the molecular framework. Rydberg-orbitals act as intermediaries between the neutral M_i and its radical-cation $M_i^{+\bullet}$ (see Chapter 2).

All of the molecules discussed in this chapter possess what is known as planar C_{2v} symmetry. The C_{2v} point group posesses a principal rotational axis, centred on the Z-axis of the right-handed (X,Y,Z) Cartesian-coordinate system. This axis is known as C_2, as the molecule can rotate onto (the positive or negative of) itself through a rotation of 180^0. Additionally, there are two mutually perpendicular reflection planes, σ_v, centred on the C_2 (Z-axis). One is the ZX-plane, $\sigma_v(ZX)$, and transforms as the X-axis. The other is the ZY-plane, $\sigma_v(ZY)$, and transforms as the Y-axis [17-19, 22, 30].

As previously discussed in chapter 2, there are two types of electric-dipole transitions that are governed by the Laporte Rules [17-19, 22, 30], they are known as allowed (i.e., high non-zero intensity), and forbidden (i.e., zero, very-low near-zero intensity). For a transition to be allowed, the direct-product of the upper and lower electronic states (i.e., (upper state)$\otimes$(lower state)) must contain at least one of the X, Y, or Z-coordinates, and thus be polarized along the X, Y, or Z-axes. To determine the symmetry of the orbitals, the electron configurations, and the electronic states of the C_{2v} molecules illustrated in Tables 4.1, 4.2, 4.3, and Figures 4.1, 4.2, one should keep in mind the following axioms.

Orbitals that have electron density of positive-amplitude are drawn white in colour, whereas those that have electron density of negative-amplitude are drawn black in colour. The s-orbitals are drawn as spheres centred on each atom, whereas the p-orbitals are drawn as double-lobes, one lobe of positive-amplitude, one lobe of negative-amplitude, with zero amplitude (i.e., a node) at the centre of the atom.

A molecular-orbital that is rotated about C_2 (i.e., through 180^0) and goes onto the positive of itself it is denoted as, a, whereas if it goes onto the negative of itself it is denoted as, b. Secondly, a molecular-orbital that is reflected through the ZX-plane and goes onto the

positive of itself it is assigned a subscript of, 1, whereas if it goes onto the negative of itself it is assigned a subscript of, 2. Thus, in C_{2v} there are molecular-orbital of a_1, a_2, b_1, b_2, symmetry, and electronic states of A_1, A_2, B_1, B_2. All of the C_{2v} molecular-orbitals may occupy up to two electrons each, this if all of the orbitals are fully occupied the corresponding electronic state label is A_1. The direct-product rules for the C_{2v} group [17-19, 22, 30] are listed as follows; $A \otimes A = A$, $B \otimes B = A$, $A \otimes B = B$, $B \otimes A = B$, and for the subscripts one has; $1 \otimes 1 = 1$, $2 \otimes 2 = 1$, $1 \otimes 2 = 2$, $2 \otimes 1 = 2$. Now since in C_{2v} symmetry A_1, B_1, and B_2 transform as Z, X, and Y, respectively, the *only forbidden transitions* are those where (upper state)$\otimes$(lower state) = A_2 symmetry. Thus, in C_{2v} all electronic transitions between electronic states are allowed save those of $A_1 \leftrightarrow A_2$, and $B_1 \leftrightarrow B_2$, on the basis of *overall symmetry* alone. Thus, the *overall symmetry* of the C_{2v} electronic states are composed of the direct-product of all of the *half-filled* (i.e., one-electron) molecular-orbitals (as all full orbitals are consider A_1).

Another quantity that must be considered to determine if a transition is electric-dipole allowed or forbidden is that of *total-spin*, S, of the upper and lower electronic states involved (see Chapter 2). Briefly restated here, the total-spin, S, of an electronic state is the sum of the individual spin, s, of each electron present [17-19, 22, 30]. Each individual electron may have an up spin (α), with $s = \frac{1}{2}$, or a down spin (β), with $s = -\frac{1}{2}$. Thus for a full orbital (in C_{2v} that is one with two electrons) it has a value of $s = 0$, whereas for a half-full orbital $|s| = \frac{1}{2}$. The total spin, $S = (s_1 + s_2 + s_3 + \ldots)$, is by convention expressed as a term known as *multiplicity*, having a value of $(2S + 1)$. Thus, when the total spin S = 0, 1/2, 1, 3/2, 2,... one has a multiplicity of $(2S + 1) = 1, 2, 3, 4, 5, \ldots$, known as a singlet, doublet, triplet, quartet, and quartet, respectively. The multiplicity is displayed as an upper-left superscript in the

term symbol of the electronic state (e.g, $^1A_1$, $^2A_1$, $^3A_1$, $^4A_1$, or $^5A_1$). Now, the *Spin Selection Rule* [17-19, 22, 30] states that an *electric-dipole allowed electronic transition is one were the total spin*, S,(i.e., the multiplicity) *of the initial and final electronic states are the same* (i.e., $\Delta S = 0$). Thus, when $\Delta S = 0$ such as, singlet ↔ singlet, doublet ↔ doublet, and so on, the electronic transitions are *allowed* (i.e., non-zero, high intensity). In contrast, when $\Delta S \neq 0$, such as, singlet ↔ triplet, doublet ↔ quartet, and so on, electronic transitions are *forbidden* (i.e., zero, near-zero intensity) and may only transpire through the mechanism of spin-orbit coupling [17-19, 22, 30] (see Chapter 2).

Next at this point, one should discuss types of bonding in the molecular-orbitals. The qualitative types of molecular-orbital are *bonding*, *anti-bonding*, and *non-bonding*. Additionally, there are two main types of bonds to be discussed here, they are σ-, and π-bonds. For, σ-bonds, the electron density is centred along the axis that joins the two adjacent atoms in the molecular framework. For, π-bonds, the electron density is located above and below, but not along, the axis joining the two adjacent atoms in the molecular framework. Now, these individual bond types are combined to make up the bonding, anti-bonding, and non-bonding molecular orbitals. For a *bonding-molecular-orbital*, there are constructive (i.e., additive) overlaps of electron density of positive-amplitude (denoted by white lobes) with another of positive-amplitude, or alternatively overlaps of electron density of negative-amplitude (denoted by black lobes) with another of negative-amplitude (i.e., increased electron-density), thus forming an increased overlap of electron-density (i.e., a bond). In contrast, for an *anti-bonding molecular-orbital*, there are destructive (i.e., subtractive) overlaps of electron-density of positive-amplitude with that of negative-amplitude, thus forming an overall absence of electron-density (i.e., a node, or anti-bond). Finally, for a *non-*

bonding molecular-orbital, there is a gap of electron-density somewhere in the molecular framework that completely separates any two regions of electron-density (i.e., of positive and/or negative amplitude). This results in there being no interaction (i.e., no additive or subtractive overlap) at all between the regions of electron-density (i.e., a non-bond).

Now, with above information in mind, on inspection of Tables 4.1, 4.2, and 4.3, as well as Figures 4.1, and 4.2, one may note the following trends. Firstly, on inspection of Table 4.1, one may clearly see the following analogies in the core and valence orbitals as follows. The (1s)-type core-orbitals of CH_2, CH_2=O, and CH_2=C=O, are listed as, $(1a_1)^2$, $(1a_1)^2(2a_1)^2$, and $(1a_1)^2(2a_1)^2(3a_1)^2$, respectively, and correspond to $(C1s)^2$, $(O1s)^2(C1s)^2$, and $(O1s)^2(C1s)^2(C1s)^2$. Similarly, the (1s)-type core-type of CF_2, CF_2=O, and CF_2=C=O, are listed as $(1a_1)^2(1b_1)^2(2a_1)^2$, $(1a_1)^2(1b_1)^2(2a_1)^2(3a_1)^2$, and $(1a_1)^2(1b_1)^2(2a_1)^2(3a_1)^2(4a_1)^2$, respectively, and correspond to $(F1s)^2(F1s)^2(C1s)^2$, $(F1s)^2(F1s)^2(O1s)^2(C1s)^2$, and $(F1s)^2(F1s)^2(O1s)^2(C1s)^2(C1s)^2$. Now, via the utilization of the remaining (2s) and (2p) atomic-orbitals of H$^\bullet$ (and (H1s) as well), C, and O, for the hydrogen compounds and that of F$^\bullet$, C, and O, for their perfluoro analogues, one may build an entire set of (2s)-type, (2p)-type, and unoccupied (2p)-type valence molecular-orbitals for the CH_2, CH_2=O, CH_2=C=O and CF_2, CF_2=O, CF_2=C=O compounds listed in Table 4.1. All of these valence orbitals are known and have been studied [31-45], save those of the latter species CF_2=C=O. The molecular-orbitals of CF_2=C=O are proposed here are by analogy to the other five known species, and will serve to aid in the discussion of the proposed electronic states and dissociation characteristics of the neutral and radical-cation perfluoroketene species.

Now, on inspection of Figures 4.1, and 4.2, which illustrate the qualitative molecular-orbitals of CH_2 and CF_2, respectively, one may note the following trends. Firstly, one shall see the different ground electronic states of $CH_2[\tilde{X}\,^3B_1]$ and $CF_2[\tilde{X}\,^1A_1]$, and the larger amount of molecular-orbitals which occur upon the perfluorination of a species. Thus, on inspection of Figure 4.1, the qualitative molecular-orbitals of CH_2 and CF_2, one may see that $(1a_1)^2$ is a (C1s) core-orbital; $(2a_1)^2$ is a (2s)-type σ-bonding valence-orbital; $(1b_2)^2(3a_1)(1b_1)$ are (2p)-type σ-bonding, σ-bonding, and π-non-bonding valence-orbitals, respectively.

Thus, to illustrate the analogy of going from a hydrogen species to its perfluorinated analogue one should now inspect Figure 4.2, the qualitative molecular orbitals of CF_2. One shall clearly see that the molecular-orbitals illustrated here are much more complex and they will be discussed as follows. One may see that there are three core-orbitals $(1a_1)^2(1b_2)^2(2a_1)^2$ which are $(F1s)^2(F1s)^2(C1s)^2$, respectively. Next the $(3a_1)^2(2b_2)^2(4a_1)^2$ are (2s)-type σ-bonding, σ-non-bonding, and σ-anti-bonding valence-orbitals, respectively. Then, the $(1b_1)^2(5a_1)^2(3b_2)^2$ are (2p)-type π-non-bonding, σ-anti-bonding, and σ-anti-bonding valence-orbitals, respectively. The last three illustrated unoccupied orbitals are $(2b_1)^0(7a_1)^0(5b_2)^0$ and are (2p)-type π-anti-bonding, σ-non-bonding, and σ-anti-bonding valence-orbitals, respectively

Thus, after inspection of the above illustrated molecular-orbitals of CH_2 and CF_2, one may qualitatively see by analogy, via the appropriate mixing of the corresponding CO molecular-orbitals, the construction and symmetry of the respective resultant CH_2=C=O and CF_2=C=O molecular-orbitals listed in Table 4.1.

At this point, now that the order of the molecular-orbitals (MO) of the CH_2, CF_2, CH_2=C=O, and CF_2=C=O species have been proposed and explored, the electronic states and transitions of their neutrals and radical-cations shall be discussed. (One should remember the caveat that in C_{2v} only transitions where (upper state)$\otimes$(lower state) = A_2 are forbidden). The neutral and cationic electronic state of CH_2 and CF_2 are illustrated in Figure 4.2 [31, 32, 38-41] and their outer-valence orbitals are considered. The ground electronic states of the species listed are $CH_2[\tilde{X}\,^3B_1]$, $CF_2[\tilde{X}\,^1A_1]$, $CH_2^{+\bullet}[\tilde{X}\,^2A_1]$, and $CF_2^{+\bullet}[\tilde{X}\,^2A_1]$.

For CH_2 [31], the lowest energy electronic transitions $\tilde{A}\,^3A_2 \rightarrow \tilde{X}\,^3B_1$ and $\tilde{b}\,^1A_1 \rightarrow \tilde{a}\,^1B_1$ are both electric-dipole allowed. As well, the $(3s)^{1,3}A_1$ Rydberg state(s) [25] are proposed to possess the capacity to act as an intermediary between the CH_2 and $CH_2^{+\bullet}$ species.

Similarly, for CF_2 [32, 38], the lowest energy electronic transitions $\tilde{A}\,^1B_1 \rightarrow \tilde{X}\,^1A_1$ and $\tilde{a}\,^3B_1 \rightarrow \tilde{X}\,^1A_1$ are electric-dipole allowed and spin-forbidden (i.e., occurring via spin-orbit coupling), respectively, and were observed by Koda [32], to possess many banded optical emission structures in the wavelength, λ, ranges of 250-350 nm and 470-720 nm, respectively. In addition, the $(3s)^{1,3}A_1$ Rydberg state(s) [25] are proposed to possess the capacity to act as an intermediary between the CF_2 and $CF_2^{+\bullet}$ species.

Now that one has discussed the neutrals, radical-cations $CH_2^{+\bullet}$ and $CF_2^{+\bullet}$ will be dealt with. For $CH_2^{+\bullet}$, the lowest electronic transitions $^2A_2 \rightarrow \tilde{X}\,^2A_1$, $\tilde{A}\,^2B_1 \rightarrow \tilde{X}\,^2A_1$, and $^4B_1 \rightarrow \tilde{a}\,^4A_2$ are each electric-dipole forbidden, allowed, and allowed, respectively. Similarly, for $CF_2^{+\bullet}$ [37], the lowest electronic transitions $\tilde{B}\,^2A_2 \rightarrow \tilde{X}\,^2A_1$, $\tilde{A}\,^2B_2 \rightarrow \tilde{X}\,^2A_1$, and $^4B_2 \rightarrow {}^4A_2$

are electric-dipole forbidden, allowed, and allowed, respectively. Notably, these above mentioned electronic states of the CH_2 and CF_2 neutral and radical-cation species are informative and essential to bear in mind as one considers the electronic states and dissociation routes of their CH_2=C=O and CF_2=C=O neutral and radical-cation relatives. The dissociation routes of the CH_2=C=O and CF_2=C=O neutral and radical-cations will be the subject of a later section, with the caveat that the carbon monoxide neutral fragment is consider to always come off "cold"(i.e., in its ground electronic state CO[$\tilde{X}\,^1A_1(^1\Sigma^+)$] (see section 4.1.4).

At this point, one will discuss the electronic states and transitions of CH_2=C=O and (the proposed) CF_2=C=O neutral and radical-cations that are listed in Table 4.3. For CH_2=C=O [1, 33, 34], the electronic states and vibrational energies have been well established. Turner et. al., [35], and Maier et.al., [36], have established the electronic states and vibrational energies via photoelectron spectroscopy. The previous comparison of the CH_2 and CF_2 neutral and radical-cations, combined with the established properties of the CH_2=C=O neutral and radical-cations will be utilized to propose, by analogy, the properties of the CF_2=C=O neutral and radical-cations.

Firstly, for CH_2=C=O[$\tilde{X}\,^1A_1$] the outer-valence orbitals are $(7a_1)^2(1b_2)^2(1b_1)^2(2b_2)^2(2b_1)^2$. Thus, one has the lowest energy electronic transitions $\tilde{B}\,^1A_1 \rightarrow \tilde{X}\,^1A_1$, $\tilde{A}\,^1A_2 \rightarrow \tilde{X}\,^1A_1$, and $\tilde{b}\,^3A_1 \rightarrow \tilde{a}\,^3A_2$ are electric-dipole allowed, forbidden, and forbidden, respectively. The C_{2v} planar $\tilde{a}\,^3A_2$ electronic state (in concert with the higher energy $^3B_1$) has the facility to distort into the in-plane $^3A'$, and the out-of-plane $^3A''$ [1], that are paramount to the lowest energy CH_2=C=O $\rightarrow$ CH_2 + C≡O dissociation process to be

discussed later (see section 4.1.4). Additionally, the $(3s)^{1,3}B_1$ Rydberg state(s) (pp. 83, 84, 100 of [25]) possess the capacity to act as an intermediary between the CH_2=C=O and CH_2=C=O$^{+\bullet}$ species.

Now, for the CF_2=C=O[$\tilde{X}\,^1A_1$] the (proposed) outer-valence are $(10a_1)^2(4b_2)^2(2b_1)^2(5b_2)^2(3b_1)^2$. Similarly, one has the (proposed) lowest energy electronic transitions $\tilde{B}\,^1A_1 \rightarrow \tilde{X}\,^1A_1$, $\tilde{A}\,^1A_2 \rightarrow \tilde{X}\,^1A_1$, and $\tilde{b}\,^3A_1 \rightarrow \tilde{a}\,^3A_2$ are electric-dipole allowed, forbidden, and forbidden, respectively. As will be discussed later (see section 4.1.4) due to the different nature of CF_2=C=O, the $\tilde{a}\,^3A_2$ (i.e., the distorted $^3A'$, $^3A''$) is a (proposed) non-participant in the lowest energy CF_2=C=O $\rightarrow$ CF_2 + C≡O dissociation process. Additionally, the $(3s)^{1,3}B_1$ Rydberg state(s) [25] are proposed to possess the capacity to act as an intermediary between the CF_2=C=O and CF_2=C=O$^{+\bullet}$ species.

Now that one has discussed the neutrals, the radical-cations CH_2=C=O$^{+\bullet}$ and CF_2=C=O$^{+\bullet}$ will be dealt with and are illustrated in Table 4.3. For CH_2=C=O$^{+\bullet}$, the UPS studies [35, 36] have established the IE_a values for the $\tilde{X}\,^2B_1$, $\tilde{A}\,^2B_2$, $\tilde{B}\,^2B_1$, $\tilde{C}\,^2B_2$, $\tilde{D}\,^2A_1$ electronic states and illustrated all of them to possess a many lined structured progression of peaks (save the $\tilde{A}\,^2B_2$ state which showed a disruption due to predissociation [36]). Thus with the above established information for CH_2=C=O$^{+\bullet}$, the lowest energy electronic transitions $\tilde{D}\,^2A_1 \rightarrow \tilde{X}\,^2B_1$, $\tilde{C}\,^2B_2 \rightarrow \tilde{X}\,^2B_1$, $\tilde{B}\,^2B_1 \rightarrow \tilde{X}\,^2B_1$, $\tilde{A}\,^2B_2 \rightarrow \tilde{X}\,^2B_1$ are electric-dipole allowed, forbidden, allowed, and forbidden, respectively. Similarly, for CF_2=C=O$^{+\bullet}$, it is propose that one shall have the lowest energy electronic transitions $\tilde{D}\,^2A_1 \rightarrow \tilde{X}\,^2B_1$, $\tilde{C}\,^2B_2 \rightarrow \tilde{X}\,^2B_1$, $\tilde{B}\,^2B_1 \rightarrow \tilde{X}\,^2B_1$, $\tilde{A}\,^2B_2 \rightarrow \tilde{X}\,^2B_1$ which possess the same electri-dipole results. Thus, if a possible source of sufficiently high concentrations of CF_2=C=O neutral

could be produced and then introduced into a suitable sampling system of a photoelectron spectrometre, one should propose the production of a UPS spectra for CF_2=C=O analogous to that of the previously observed CH_2=C=O species [35, 36], and it would be amenable to the systematic perfluoro effects observed by Brundle el. al., [40, 41]. Additionally and of utmost importance, a successful production of an UPS spectrum of CF_2=C=O would represent another piece of experimental evidence to confirm the existence of the neutral.

Thus, with the conclusion of this section on the electronic states of CF_2=C=O and its related species, one final point deserves emphasis. This analysis was based on the qualitative discussion of the separability of the symmetry of the symmetry of the (2s)-type and (2p)-type molecular-orbitals and the *single-electron configurations* that may be produced from them. The addition of *multiple-electron configuration interaction* (used in quantum-mechanical ab initio studies [21, 43-45]) into the previous analysis of this section *does not appreciably alter* the conclusions proposed here. Additionally, the ab initio calculation method utilized on UPS spectra, known as hydrogen-atoms-in-molecules (HAM/3), has been very successful in the accurate quantitative prediction of the position and analysis of photoelectron peaks in the data banks of Absrink, Bieri, and Von Neissen [43-45].

4.1.2 The Heat of Formation of Neutral CF_2=C=O and Related Species

Now that one has thoroughly explored the proposed molecular-orbitals, electron configurations, and electronic states of the neutral and radical-cation CF_2=C=O species, in a manner that which should convince the reader of the validity of its actual existence, one will now turn to the question of the estimation of $\Delta_f H^0[CF_2=C=O]$. The hydrogen analogue ketene, CH_2=C=O, can exist as a monomer (vacuum distilled and kept at low temperature [1,

36]), or as a dimer. Its dimeric form, upon pyrolytic heating, can serve as a convenient source for the monomer, CH_2=C=O. As stated previously, the perfluoro compound CF_2=C=O until recently was not thought to be stable in any phase [1] (although, now Kotting et.al., have proposed its existence in an Ar matrix at 30 K [4]). In contrast, the dimeric forms for both of the hydrogen and fluorine cases are known to exist [1, 50, 51]; c-(CH_2–C=O)$_2$ as a colourless liquid [50, 51], possessing a known photoelectron spectrum with an IE_a = 9.92 eV; whereas c-(CF_2–C=O)$_2$ is a blue coloured liquid [51], possessing a known photoelectron spectrum with an IE_a = 10.05 eV. Thus, it can be seen that the dimerization of CX_2=C=O into c-(CX_2–C=O)$_2$ exerts a stabilizing effect that changes the gaseous monomer into a liquid dimer. (However, one should note that to the knowledge of this author, there is no literature to show the production of gaseous CF_2=C=O monomer upon pyrolytic heating of the liquid c-(CF_2–C=O)$_2$ dimer).

For the hydrogen species the $\Delta_fH^0[CH_2=C=O] = -(47.7 \pm 2.5)$ kJ•mol^{-1} [6] value is well established. Additionally, one may empirically estimate, via Benson's Additivity [12-16], a value of $\Delta_fH^0[CH_2=C=O] = \Delta_fH^0[C_d–(H)_2] + \Delta_fH^0[CO_{ketone}] = (26.2$ kJ•mol^{-1}) + (-74.1 kJ•mol^{-1}) = -47.9 kJ•mol^{-1}, which is in excellent agreement with experiment. However, for the perfluoro species there is *no experimental* $\Delta_fH^0[CF_2=C=O]$ listed in the standard literature [6-8]. In order to reasonably estimate and support the rationale for the proposal of the empirically estimated value of $\Delta_fH^0[CF_2=C=O] = -401.3$ kJ•mol^{-1} being *the most reasonable one to date*, one shall consult the data presented in Tables 4.4, and 4.5.

Table 4.4 presents all of the relevant Benson's Additivity Terms for the empirical estimation of the Δ_fH^0 value of CF_2=C=O and its related species. Thereupon, Table 4.5

Table 4.4 Relevant Benson's Additivity Terms for the Empirical Estimation of the Heats of Formation $\Delta_f H^0$(kJ•mol^{-1})[a] for CF_2=C=O, its Dimer c-(CF_2–C=O)$_2$ and Related Species

Benson's Group	Heat of Formation $\Delta_f H^0$(kJ•mol^{-1})[a]	Stabilization Per Fluorine $\Delta(\Delta_f H^0)$(kJ•mol^{-1})
Allene Series		
C_a	142.3	
Carbonyl Series		
$[CO]_{ketone}$	–74.1	
$CO–(C)_2$	–132.6	
$CO–(H)$[b]	–58.2	
$CO–(H)_2$	–116.4	
$CO–(F)$[b]	–322.2	–264.4
$CO–(F)_2$	–644.4	–264.4
Unsaturated Series		
$C_d–(H)_2$	26.2	
$C_d–(F)(H)$	–146.9	–173.1
$C_d–(F)_2$	–327.2	–176.7
Saturated Series		
$C–(H)_2(C)_2$	–20.9	
$C–(H)_3(C)$	–41.84	
$C–(F)_2(C)_2$	–405.8	–192.5
$C–(F)_3(C)$	–662.7	–207.0
Ring-Strain Series		
c-(CH_2–CH_2)$_2$	109.6	
c-(CH_2–C=O)$_2$	–[c]	
c-(CF_2–CF_2)$_2$	117.2	
c-(CF_2–C=O)$_2$	–[c]	

[a]Ref. [12-16], [b]Estimated, see Ref. [15] p. 25, [c]Unknown.

Table 4.5 Relevant Thermochemical Data of Related Unsaturated Species for the Estimation of $\Delta_f H^\circ[CF_2{=}C{=}O]$

Species	Heat of Formation, $\Delta_f H^\circ$ (kJ•mol^{-1})		
	Benson's Additivity[a]	Standard Literature[b]	Ab Initio Theory[c]
Ethene Series			
$CH_2{=}CH_2$	52.5	(52.2 ± 1.0)	(51.5 ± 4.2)
$CFH{=}CH_2$	−120.7	−(138.8 ± 1.7)	−(139.2 ± 6.5)
$CF_2{=}CH_2$	−301.2	−(345 ± 10)	−(340.1 ± 11.0)
$CFH{=}CF_2$	−474.1	−(491 ± 8)	−(485.6 ± 14.0)
$CF_2{=}CF_2$	−654.4	−(659 ± 3)	−(653.7 ± 16.9)
Ketone Series			
$CH_2{=}O$	−116.4	−(108.7 ± 0.7)	−(108.5 ± 4.2)
$CFH{=}O$	−380.4	−377[d]	−(382.3 ± 4.4)
$CF_2{=}O$	−644.4	−640	−(598.4 ± 7.0)
Allene Series			
$CH_2{=}C{=}CH_2$	194.7	(190.6 ± 1.0)	
$CFH{=}C{=}CH_2$	21.6		
$CF_2{=}C{=}CH_2$	−158.7	−202	
$CFH{=}C{=}CF_2$	−331.8		
$CF_2{=}C{=}CF_2$	−516.1	−594	
Ketene Series			
$CH_2{=}C{=}O$	−47.9	−(47.7 ± 2.5)	−(40.6 ± 7.2)
$CFH{=}C{=}O$	−221.0		−(147.2 ± 9.8)
$CF_2{=}C{=}O$	−401.3		−(290.3 ± 13.2)

[a]Ref. [12-16], [b]Ref. [6], [c]Ref. [5], [d]Esitimated by Ref. [6].

presents all of the relevant thermochemical data of the unsaturated species for the estimation of $\Delta_f H^0[CF_2{=}C{=}O]$. The dissociation of the neutral $CF_2{=}C{=}O$ now deserves attention as shown below'

$$CF_2{=}C{=}O \xrightarrow{\bullet} CF_2 + C{\equiv}O$$

The product energies are $\Delta_f H^0[CF_2] = -(205 \pm 12)$ kJ•mol^{-1} [6], and $\Delta_f H^0[C{\equiv}O] = -110.5$ kJ•mol^{-1} [6], a sum of -315.5 kJ•mol^{-1}. Therefore, for $CF_2{=}C{=}O$ to be a stable species with an *endothermic* dissociation energy (i.e., $(\Delta_f H^0[CF_2] + \Delta_f H^0[C{\equiv}O]) - (\Delta_f H^0[CF_2{=}C{=}O]) > 0$ kJ•mol^{-1}) one *must propose* that $\Delta_f H^0[CF_2{=}C{=}O] < -315.5$ kJ•mol^{-1}. Thus, it is useful to review the present state of the available neutral heats of formation of the related fluorine substituted ethene, ketone, allene, and ketene series which one may see on inspection of Table 4.5.

In Table 4.5, the first column contains the $\Delta_f H^0$ values estimated using Benson's Additivity Scheme [12-16], whereas the last column contains the ab initio theoretical values of Zachariah et.al., [5]. The centre column gives the values from the compilation of Lias et. al., [6]. The limitations of the ab initio results are dictated by the characteristics of the model used and by the size of the basis set (i.e., to minimize the calculation time and the round-off error). The Benson's Additivity results are derived from the fixed differences between the constituent groups (e.g., $C_d{-}(H)_2$ to $C_d{-}(F)(H)$ and $C_d{-}(F)(H)$ to $C_d{-}(F)_2$ possess a stabilization energy of -173.1 kJ•mol^{-1} and -180.3 kJ•mol^{-1}, respectively). Thus, via Benson's Additivity [12-16] one may calculate $\Delta_f H^0[CF_2{=}C{=}O] = \Delta_f H^0[C_d{-}(F)_2] +$

$\Delta_f H^0[CO_{ketene}] = (-327.2\ kJ \bullet mol^{-1}) + (-74.1\ kJ \bullet mol^{-1}) = -401.3\ kJ \bullet mol^{-1}$, and will be taken to be the *best available estimate, and thus will be used in all the following discussions.*

In support of this proposition, on inspection of Table 4.5 one can see that Benson's Additivity is either reasonably accurate or consistently underestimates the $\Delta_f H^0$ values; although generally reliable, the ab initio results have difficulty with the presence of oxygen in the species (e.g., $CF_2{=}O$, $CH_2{=}C{=}O$). On consideration of the data presented in Table 4.5, the difference between the experimental value of $\Delta_f H^0[CH_2{=}C{=}O] = -(47.7 \pm 2.5)\ kJ \bullet mol^{-1}$ [6], and that presented by Zachariah et. al., [5] for the ab initio calculated value of $\Delta_f H^0[CF_2{=}C{=}O] = -(290.3 \pm 13.2)\ kJ \bullet mol^{-1}$, namely, $-242.6\ kJ \bullet mol^{-1}$ (i.e., the effect of two fluorine substitutions), appears to be anomalously low. It seems that a revised $\Delta_f H^0[CF_2{=}C{=}O]$ value may be *significantly lower* than the above ab initio value [5].

Previously, Kotting et. al., [4], and Dailey III et. al., [9] calculated the $CF_2{=}C{=}O \rightarrow CF_2 + C{\equiv}O$ dissociation energy barrier to be *endothermic* and in the range of $\approx$ 24 to 42 $kJ \bullet mol^{-1}$, respectively. Now, if one may accept the Benson's $\Delta_f H^0[CF_2{=}C{=}O] = -401.3\ kJ \bullet mol^{-1}$ proposed here, one should obtain a *larger endothermic* dissociation energy of $\approx$ 86 $kJ \bullet mol^{-1}$. At first glance, this value of $\approx$ 86 $kJ \bullet mol^{-1}$ may seem to be a somewhat significant divergence from the aforementioned ab initio results [4, 9]. However, it is not entirely unreasonable, as it is $\approx$ 26 % of the analogous $CH_2{=}C{=}O \rightarrow CH_2 + C{\equiv}O$ dissociation (see section 4.1.4). In fact, one may indeed propose that this is indicative of $CF_2{=}C{=}O$ being a genuinely (endothermically) bound entity that is just difficult to isolate in solution and/or in very high concentrations at ambient conditions in the gas-phase due to its facile chemical reactivity (which is duly mollified via dimerization, i.e., the formation of c-$(CF_2{-}C{=}O)_2$).

4.1.3 The Ionization Energy and Cationic Heat of Formation of CF_2=C=O and Related Species

Thus, having in the last section dealt with the rationale that proposed that Benson's $\Delta_fH^0[CF_2{=}C{=}O] = -401.3$ kJ•mol^{-1} is the best estimate to date, one will now turn ones attention to the estimation of $IE_a[CF_2{=}C{=}O]$ and $\Delta_fH^0[CF_2{=}C{=}O^{+\bullet}]$. To this end, Table 4.6 presents the relevant thermochemical data of the related unsaturated species for the estimation of $IE_a[CF_2{=}C{=}O]$ and $\Delta_fH^0[CF_2{=}C{=}O^{+\bullet}]$ in which the ethene, ketone, allene, and cyclic series are tabulated. The first two columns contain the neutral heats of formation, the former derived from Benson's Additivity [12-16] (with the aid of the values in Table 4.4), and the latter gives the values from the compilation of Lias et. al., [6]. The third and fourth columns give the adiabatic ionization energies and heats of formation of the corresponding species [6], respectively. On inspection of Table 4.6, one should note the following trends.

For the neutral heats of formation (i.e., the first two columns) one may note that generally Benson's Additivity is either reasonably accurate or underestimates the Δ_fH^0 value. Additionally, the Benson's Δ_fH^0 values for the cyclic species; $\Delta_fH^0[c\text{-}(CH_2{-}CH_2)_2] = 4\ \Delta_fH^0[C{-}(H)_2(C)_2] + E_{strain}(c\text{-}C_4H_8) = 4(-20.9\ kJ{\bullet}mol^{-1}) + (109.6\ kJ{\bullet}mol^{-1}) = 26.0\ kJ{\bullet}mol^{-1}$; and $\Delta_fH^0[c\text{-}(CF_2{-}CF_2)_2] = 4\ \Delta_fH^0[C{-}(F)_2(C)_2] + E_{strain}(c\text{-}C_4F_8) = 4(-405.8\ kJ{\bullet}mol^{-1}) + (117.2\ kJ{\bullet}mol^{-1}) = -1506.0\ kJ{\bullet}mol^{-1}$; can be seen to be reasonable estimates of experimental values of $\Delta_fH^0[c\text{-}(CH_2{-}CH_2)_2] = (28.4 \pm 0.5)\ kJ{\bullet}mol^{-1}$, and $\Delta_fH^0[c\text{-}(CF_2{-}CF_2)_2] = -1515\ kJ{\bullet}mol^{-1}$, respectively. (Unfortunately the ring strain energies, E_{strain}, for the dimer $c\text{-}(CH_2{-}C{=}O)_2$ and $c\text{-}(CF_2{-}C{=}O)_2$ species are unknown).

Table 4.6 Relevant Thermochemical Data of Related Unsaturated Species for the Estimation of $IE_a[CF_2{=}C{=}O]$ and $\Delta_fH^\circ[CF_2{=}C{=}O]$

Species	Neutral Heat of Formation, Δ_fH°(kJ•mol^{-1}) Benson's Additivity[a]	Standard Literature[b]	Adiabatic Ionization Energy IE_a(eV)[b]	Ionic Heat Of Formation Δ_fH°(kJ•mol^{-1})[b]
Ethene Series				
$CH_2{=}CH_2$	52.5	(52.2 ± 1.0)	(10.507 ± 0.004)	1066
$CFH{=}CH_2$	−120.7	−(138.8 ± 1.7)	(10.363 ± 0.015)	861.1
$CF_2{=}CH_2$	−301.2	−(345 ± 10)	(10.29 ± 0.01)	648
$CFH{=}CF_2$	−474.1	−(491 ± 8)	10.14	487
$CF_2{=}CF_2$	−654.4	−(659 ± 3)	(10.12 ± 0.02)	316
Ketone Series				
$CH_2{=}O$	−116.4	−(108.7 ± 0.7)	(10.874 ± 0.002)	940.5
$(CH_3)_2C{=}O$	−216.4	−(217.2 ± 0.4)	9.705	719.2
$CF_2{=}O$	−644.4	−640	13.03	617
$(CF_3)_2C{=}O$	−1458.1	−1397	11.44	−293
Allene Series				
$CH_2{=}C{=}CH_2$	194.7	(190.6 ± 1)	(9.69 ± 0.01)	1126
$CF_2{=}C{=}CH_2$	−158.7	−202	(9.79 ± 0.03)	743
$CF_2{=}C{=}CF_2$	−516.1	−594	10.88	456
Ketene Series				
$CH_2{=}C{=}O$	−47.9	−(47.7 ± 2.5)	(9.61 ± 0.02)	879.6
$(CH_3)_2C{=}C{=}O$	−115.1	−(134 ± 4)	8.45	681
$CF_2{=}C{=}O$	−401.3		≈11[g]	660.1[f]
$(CF_3)_2C{=}C{=}O$	−1356.9	−1427[c]	10.67	−398
Cyclic Series				
c-$(CH_2{-}CH_2)_2$	26.0	(28.4 ± 0.5)	(9.92 ± 0.05)	985
c-$(CH_2{-}C{=}O)_2$		−163[c]	9.4	745
c-$(CF_2{-}CF_2)_2$	−1506.0	−1515[d]	(11.6 ± 0.2)[e]	−396[h]
c-$(CF_2{-}C{=}O)_2$		−771[e]	(10.05 ± 0.1)	199

[a]Ref. [12-16], [b]Ref. [6], [c]Estimated by Ref. [6], [d]Ref. [8, 16], [e]Ref. [49], [f]Estimated Δ_fH°[Ion] from Benson's Δ_fH°[Neutral], [g]Estimated $IE_a[CF_2{=}C{=}O]$, see text, [h]Estimated Upper Limit of Δ_fH°[Ion], see text.

At this point, the effects of the replacement of all H atoms in a molecule by F atoms deserves reemphasis (see section 3.1.1). There are three effects listed as follows, (I) the "perfluoro-effect", (II) the "perfluorination effect", and (III) the "negative perfluorination effect". Briefly, (I) the "perfluoro-effect" preferentially stabilizes the σ-orbitals over those of the π-orbitals which results in a strong in a strong increase and mild increase in IE_a values, respectively. Next, (II) the "perfluorination effect" results from the replacement of the H atoms and/or the CH_3 groups by the CF_3 groups. Due to the symmetry of the CF_3 group, both the σ- and π-orbitals are strongly stabilized and both of their IE_a values are raised. Lastly, (III) the "negative perfluorination effect" is anomalous and results in the reduction of the IE_a values. (For a full discussion of these effects see section 3.1.1, and a comparison of Tables 3.5 and 4.6).

Now, for the ethene series one may observe the negative perfluorination effect in action as $IE_a[CH_2{=}CH_2] = (10.507 \pm 0.004)$ eV [6] drops systematically to $IE_a[CF_2{=}CF_2] = (10.12 \pm 0.02)$ eV [6]. This effect is anomalous and may possibly be a result of the strong polarization and weakening of the C=C bond which was proposed to result in the facile isomerization of the classical $CF_2{=}CF_2^{+\bullet}$ structure into the carbene $CF_3CF^{+\bullet}$ structure (see the $C_2F_4^{+\bullet}$ section of Chapter 3). This above behaviour is *atypical* and should not lead the reader astray in the qualitative estimation of $IE_a[CF_2{=}C{=}O]$.

Now, for the ketone series one may see the following trends. Firstly, one may see that as normally expected, $IE_a[CF_2{=}O] > IE_a[CH_2{=}O]$ and $IE_a[(CF_3)_2C{=}O] > IE_a[(CH_3)_2C{=}O]$. As well, as discussed in section 3.1.1, the presence of the O atom alters the

distribution of the electron-density and results in $IE_a[CH_2{=}O] > IE_a[(CH_3)_2C{=}O]$ and $IE_a[CF_2{=}O] > IE_a[(CF_3)_2C{=}O]$.

Now, for the allene series one may see the expected increase of IE_a values with the degree of fluorination as follows; $IE_a[CH_2{=}C{=}CH_2] < IE_a[CF_2{=}C{=}CH_2] < IE_a[CF_2{=}C{=}CF_2]$. It is noteworthy that the photoelectron vibrational peak intensity envelopes of the $\tilde{X}$ and $\tilde{A}$ electronic states of $CF_2{=}C{=}CH_2$ [46] and $CF_2{=}C{=}CF_2$ [47] both exhibit strikingly similar, long structured vibrational progressions. Due to the clear structural similarity of these two species to that of $CF_2{=}C{=}O$, one may propose that it is very likely that the $\tilde{X}$ and $\tilde{A}$ electronic states of $CF_2{=}C{=}O^{+\bullet}$ may be of similar character.

Next, for the ketene series one may observe the following trends. Firstly, one may see that $IE_a[CH_2{=}C{=}O] > IE_a[(CH_3)_2C{=}O]$. Now, as was proposed in Dawson, and Holmes [11], if the analogous species $CH_2{=}C{=}CH_2$ (IE_a = 9.69 eV) [6, 7] and $CF_2{=}C{=}CF_2$ (IE_a = 10.88 eV) [6, 7] can be used with $CH_2{=}C{=}O$ (IE_a = 9.61 eV) [6, 7] one should estimate an $IE_a[CF_2{=}C{=}O] \approx 11$ eV value. This is in indeed an entirely reasonable estimate since it is known that $IE_a[(CF_3)_2C{=}O] = 10.67$ eV (i.e., $IE_a[CF_2{=}C{=}O] > IE_a[(CF_3)_2C{=}O]$, which is analogous to the hydrogen case). In additional support, on inspection of Table 4.6 one may see that with dimerization, $IE_a[CH_2{=}C{=}O] > IE_a[c\text{-}(CH_2{-}C{=}O)_2]$ and analogously $IE_a[CF_2{=}C{=}O] > IE_a[c\text{-}(CF_2{-}C{=}O)_2]$. As well, one shall also note the complimentary trends of $IE_a[c\text{-}(CH_2{-}CH_2)_2] > IE_a[CH_2{=}C{=}O] > IE_a[c\text{-}(CH_2{-}C{=}O)_2]$, as well as $IE_a[c\text{-}(CF_2{-}CF_2)_2$ $IE_a[CF_2{=}C{=}O]] > IE_a[c\text{-}(CF_2{-}C{=}O)_2]$.

Therefore, now that $IE_a[CF_2{=}C{=}O] \approx 11$ eV may be seen to be a reasonable estimate, consequently one may estimate $\Delta_f H^0[CF_2{=}C{=}O^{+\bullet}] = 660.1$ kJ•mol^{-1}. Therefore, on

consideration of the $CF_2^{+\bullet}$ + C≡O dissociation products $\Delta_f H^0$ value of 786.5 kJ•mol^{-1}, one may calculate an *endothermic* dissociation energy of 126.4 kJ•mol^{-1} for the CF_2=C=O$^{+\bullet}$ → $CF_2^{+\bullet}$ + C≡O dissociation process. However, it may be seen that this value is not entirely unreasonable, as it is ≈ 32 % of the analogous CH_2=C=O$^{+\bullet}$ → $CH_2^{+\bullet}$ + C≡O dissociation energy (see section 4.1.4). It is noteworthy that this (i.e., ≈ 32 %) is in line with that of the proposed neutral dissociation CF_2=C=O → CF_2 + C≡O being ≈ 26 % of the dissociation energy of its analogous hydrogen species (see section 4.1.4).

4.1.4 The Dissociation of CF_2=C=O and Related Species

Now that the previous sections have adequately discussed the electron configurations, electronic states and transitions, the estimates of the thermodynamic quantities $\Delta_f H^0$[CF_2=C=O], IE$_a$[CF_2=C=O], and $\Delta_f H^0$[CF_2=C=O$^{+\bullet}$], one will now discuss the particulars of the neutral CX_2=C=O → CX_2 + C≡O and radical-cation CX_2=C=O$^{+\bullet}$ → $CX_2^{+\bullet}$ + C≡O dissociation processes, as governed by the Wigner-Witmer Correlation Rules [17-21] and in the following section how they relate to the observed mass spectral spectrometric properties of CF_2=C=O$^{+\bullet}$ [11], later presented in section 4.2.

The direct (unrearranged) dissociation of small symmetric molecules (i.e., a molecule with less than about 12 atoms) is generally governed by the Wigner-Witmer Correlation Rules [17-21]. There are two rules known as follows, (I) the spin-allowed, and (II) symmetry-allowed dissociations (see Chapter 2). Briefly restated here, (I) the spin-allowed dissociation is one in which the sum of the spins of the fragments contains the spin of the parent. Next, (II) the symmetry-allowed dissociation is one in which the direct product of the symmetries of the fragments must contain that of the parent.

In this section, Table 4.7 lists the vibrational modes of CH_2=C=O and CF_2=C=O, whereas Figures 4.3, and 4.4, illustrate the proposed potential energy surfaces of CH_2=C=O and CH_2=C=$O^{+\bullet}$, and CF_2=C=O and CF_2=C=$O^{+\bullet}$, respectively. The CX_2=C=O species is of C_{2v} planar symmetry, and thus has (3(5) – 6) = 9 vibrational modes. They are listed in Table 4.7 as follows; $\nu_1(A_1)$, $\nu_s(CX_2)$ sym. str.; $\nu_2(A_1)$, ν(CO) str.; $\nu_3(A_1)$, $\delta(CX_2)$ def.; $\nu_4(A_1)$, ν(CC) str.; $\nu_5(B_1)$, γ(CCO) oop. skl. bend.; $\nu_6(B_1)$, $\gamma(CX_2)$ wag.; $\nu_7(B_2)$, $\nu_{as}(CX_2)$ asym. str.; $\nu_8(B_2)$, $\rho(CX_2)$ rock.; and $\nu_9(B_2)$, δ(CCO) ip. skl. bend. On inspection of Table 4.7, one can see that for the vibrational energy $\tilde{\upsilon}\,(cm^{-1})$ columns, the first lists the gas-phase $\tilde{\upsilon}\,(cm^{-1})$ for CH_2=C=O [34, 35], whereas the second and third lists Kotting et. al., [4] experimentally determined values in a solid Ar matrix, and Dailey III et. al., [9] ab initio values, respectively, for the $\tilde{\upsilon}\,(cm^{-1})$ of the CF_2=C=O neutrals. (In regards to the third column, it is noteworthy that the *older lower level* MP/6-31G* calculations of Dailey III et. al., [9], yielded *closely similar values* to the *recent two higher level* MP2/6-311G(d) (scaled by 0.97) and B3LYP/6-311G(d) calculations of Kotting et. al., [4]).

Therefore, one should expect, according to the Wigner-Witmer Correlations, the most facile dissociation occur when *both* rules (I) and (II) are observed, and the ground electronic state parent may then produce ground electronic state fragments. If this is not the case, the molecule may resort to the mixing of its vibrational and electronic states, known as vibronic mixing, to attain the dissociation route and fragments of lowest energy.

Now, for the neutral CX_2=C=O if it is required, a *vibrational resonance* of a lower energy electronic state (e.g., the ground state $\tilde{X}$) may occur (in concert with a higher energy electronic state) to change its C_{2v} planar $\tilde{X}\,^1A_1$ structure into a bent in-plane $^3A'$, and out-of-

Table 4.7 Vibrational Modes of CH_2=C=O and CF_2=C=O

Vibrational Mode[a]	Vibrational Energy CH_2=C=O Observed[b] $\tilde{\upsilon}$ (cm^{-1})	CF_2=C=O Observed[c] $\tilde{\upsilon}$ (cm^{-1})	Calculated[d] $\tilde{\upsilon}$ (cm^{-1})
$\nu_1(A_1)$; $\nu_s(CX_2)$ sym.str.	3070		782.0
$\nu_2(A_1)$; ν(CO) str.	2152	2161.6	2177.0
$\nu_3(A_1)$; $\delta(CX_2)$ def.	1388		435.6
$\nu_4(A_1)$; ν(CC) str.	1118	1426.8	1429.6
$\nu_5(B_1)$; γ(CCO) oop. skl. bend	592		372.9
$\nu_6(B_1)$; $\gamma(CX_2)$ wag.	525		269.7
$\nu_7(B_2)$; $\nu_{as}(CX_2)$ asym.str.	3166	1274.4	1296.0
$\nu_8(B_2)$; $\rho(CX_2)$ rock.	977		203.7
$\nu_9(B_2)$; δ(CCO) ip. skl. bend	438		663.3

[a] ν_s–symmetric stretch, ν_{as}–asymmetric stretch, δ–in-plane bend, γ–out-of-plane bend, ρ–in-plane rock. [b] Ref. [34, 36]. [c] Ref. [4]. [d] Ref. [9].

Figure 4.3 Proposed Potential Energy Surfaces of CH_2=C=O and CH_2=C=O$^{+\bullet}$

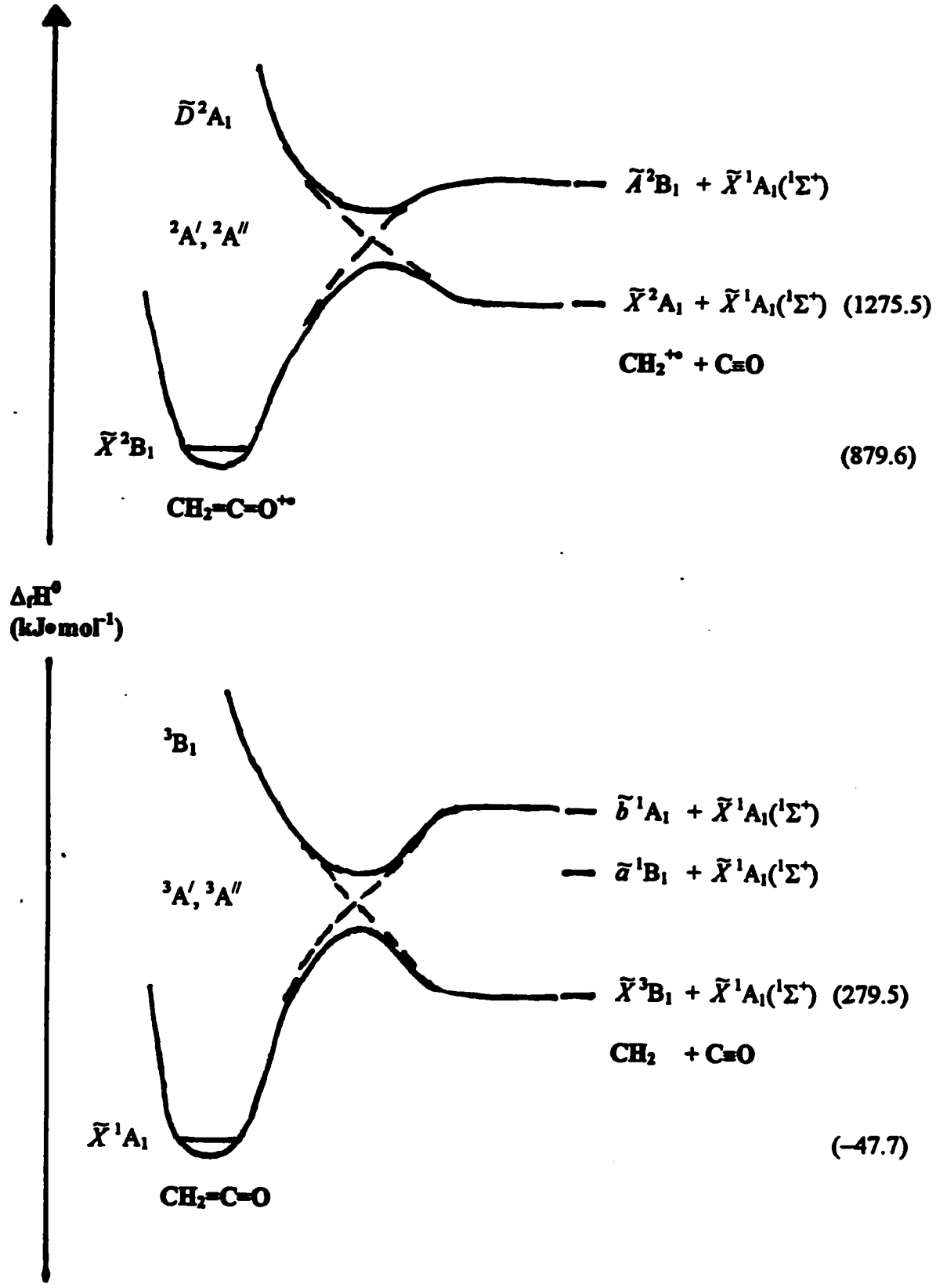

Figure 4.4 Proposed Potential Energy Surfaces of CF_2=C=O and CF_2=C=$O^{+\bullet}$

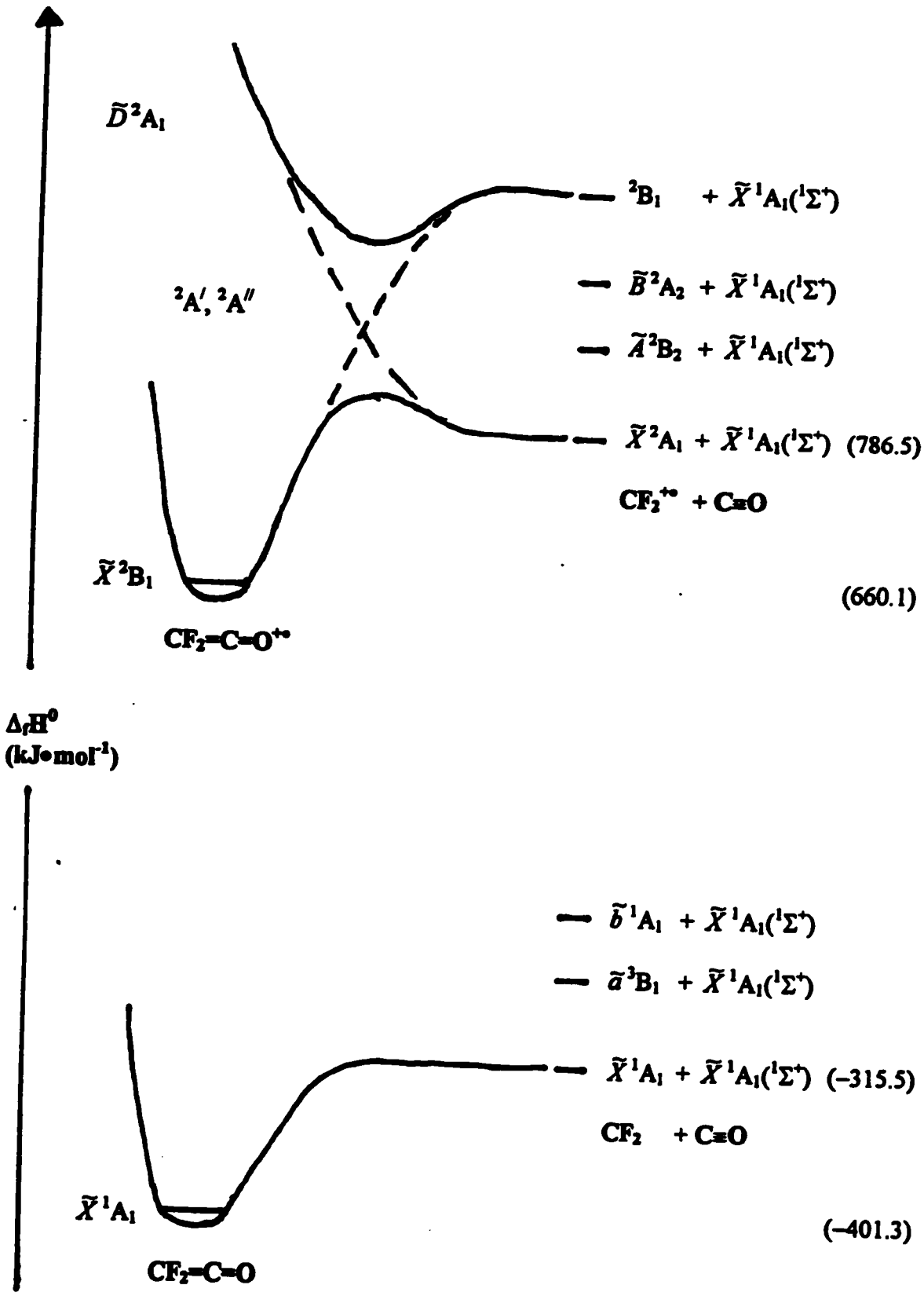

plane $^3A''$, C_s structure, respectively. The C_s bent in-plane $^3A'$ structure may be proposed to be composed of a vibrational resonance of the in-plane $\nu_8(B_2)$, $\rho(CX_2)$ rock.; $\nu_9(B_2)$, $\delta(CCO)$ ip. skl. bend.; and the $\nu_4(A_1)$, $\nu(CC)$ str. modes. Likewise, the alternate C_s bent out-of-plane $^3A''$ structure may be proposed to be composed of a vibrational resonance of the out-of-plane $\nu_6(B_1)$, $\gamma(CX_2)$ wag.; $\nu_5(B_1)$, $\gamma(CCO)$ oop. skl. bend.; and the $\nu_4(A_1)$, $\nu(CC)$ str. modes. Therefore, the lower and higher electronic states may now *vibronically mix* and thus undergo an *avoided crossing* to arrive at their different dissociation limits.

Additionally, for the radical-cation $CX_2{=}C{=}O^{+\bullet}$, if it is required, the C_{2v} planar $\tilde{X}\,^2A_1$ structure may adopt the bent $^2A'$, and $^2A''$ structures composed of the same (neutral) vibrational modes in order to vibronically mix with a higher electronic state and achieve an avoided crossing.

On inspection of Figure 4.3, one may note that for both $CH_2{=}C{=}O$ and $CH_2{=}C{=}O^{+\bullet}$, their lowest energy dissociations involve the above-mentioned vibronic mixing to create the $^3A'$, $^3A''$ and $^2A'$, $^2A''$ bent in-plane and out-of-plane structures, respectively. For the $CH_2{=}C{=}O$ manifold, the $CH_2{=}C{=}O[\tilde{X}\,^1A_1]$ and $CH_2{=}C{=}O[^3B_1]$ species vibronically mix, via the bent $^3A'$, $^3A''$ structures. Thus, an avoided crossing takes place in which the *spin-forbidden* $CH_2{=}C{=}O[\tilde{X}\,^1A_1] \rightarrow CH_2[\tilde{X}\,^3B_1] + C{\equiv}O[\tilde{X}\,^1A_1(^1\Sigma^+)]$ direct dissociation occurs in concert with the $CH_2{=}C{=}O[^3B_1] \rightarrow CH_2[\tilde{b}\,^1A_1] + C{\equiv}O[\tilde{X}\,^1A_1(^1\Sigma^+)]$ dissociation. Likewise, for the $CH_2{=}C{=}O^{+\bullet}$ manifold, the $CH_2{=}C{=}O^{+\bullet}[\tilde{X}\,^2B_1]$ and the $CH_2{=}C{=}O^{+\bullet}[\tilde{D}\,^2A_1]$ species vibronically mix, via the bent $^2A'$, $^2A''$ structures. Thus, an avoided crossing takes place in which the *symmetry-forbidden* $CH_2{=}C{=}O^{+\bullet}[\tilde{X}\,^2B_1] \rightarrow CH_2^{+\bullet}[\tilde{X}\,^2A_1] +$

$C{\equiv}O[\tilde{X}\,^1A_1(^1\Sigma^+)]$ direct dissociation occurs in concert with the $CH_2{=}C{=}O^{+\bullet}[\tilde{D}\,^2A_1] \rightarrow$ $CH_2^{+\bullet}[\tilde{A}\,^2B_1] + C{\equiv}O[\tilde{X}\,^1A_1(^1\Sigma^+)]$ dissociation.

The invoking of vibronic mixing of a ground electronic state of a species with a higher excited state species is a common mechanism frequently utilized during the dissociation of some symmetric molecules (via the Wigner-Witmer Correlation Rules). Such underlying behaviour may be implicitly present in the NRMS study of $O{=}C{=}C{=}O^{+\bullet}$ and $O{=}C{=}C{=}C{=}O^{+\bullet}$ of Chen, and Holmes [62], as well as was explicitly explored by Dawson, and Holmes [63], in the production of $O{=}C{=}C{=}O^{+\bullet}$ from $O{=}C{=}C{=}C{=}O^{+\bullet}$, [63].

At this point, it is noteworthy to emphasize the disrupted vibrational spectral pattern in the $\tilde{A}\,^2B_2$ electronic state in the photoelectron spectrum of $CH_2{=}C{=}O^{+\bullet}$ observed by Hall, and Maier [36]. Hall, and Maier attributed this observation being due the proposed predissociation interaction with the $\tilde{D}\,^2A_1$ state that "indicates that the $\tilde{A}\,^2B_2$ state ketene is already probably predissociated" [36]. As well, they state that "a short lifetime (of the $\tilde{A}\,^2B_2$ state) is also implied by the *lack of detectable (optical) emission from this state, and higher states*; decaying radiatively to the ground electronic state $\tilde{X}\,^2B_1$ of the ketene radical-cation" (p. 377 of [36]). Additionally, McCulloh, and Dibeler [60] attribute the above observation to the predissociation of $\tilde{A}\,^2B_2$, via an interaction (presumably) with the auto-ionizing $(ns)^{1,3}B_2$ Rydberg state(s) of $CH_2{=}C{=}O$. (Thus, the $CH_2{=}C{=}O^{+\bullet}$ species *should not* be expected to an amenable candidate to study with the collision induced emission (CIE) technique utilized in Chapter 2).

It is noteworthy that the dissociation energy of the neutral (CH_2=C=O → CH_2 + C≡O) and that of the radical-cation (CH_2=C=O$^{+\bullet}$ → $CH_2^{+\bullet}$ + C≡O) are 327.2 kJ•mol^{-1}, and 395.9 kJ•mol^{-1}, respectively. Thus, the neutral lives in a *smaller* potential energy well (i.e., ≈ 83 %) than that of its respective radical-cation. At this point, it is important to emphasize that with all of the mass spectral and ab initio studies [55-61], the CH_2=C=O$^{+\bullet}$ → $CH_2^{+\bullet}$ + C≡O dissociation process occurs at/or near threshold (i.e., with no appreciable reverse activation energy barrier) with an extremely small, $T_{0.5}$ = 2.6 meV value, and the energy partitioning is consistent with simple quasi-equilibrium theory (QET) [55, 56] (i.e., the "hump" in the neutral dissociation of Figure 4.3 is exaggerated for visual effect). Thus, one should expect the following *above characteristics to be exhibited in its perfluoro analogue* CF_2=C=O.

Indeed, on inspection of Figure 4.4, the proposed potential energy surfaces of CF_2=C=O and CF_2=C=O$^{+\bullet}$, one shall note many similarities and contrasts to that of Figure 4.3. Firstly, for the CF_2=C=O manifold, via the Wigner-Witmer Correlation Rules [17-21], the direct dissociation of the C_{2v} planar CF_2=C=O species is *both spin and symmetry allowed.* Therefore, the CF_2=C=O[$\tilde{X}\,^1A_1$] → CF_2[$\tilde{X}\,^1A_1$] + C≡O[$\tilde{X}\,^1A_1(^1\Sigma^+)$] direct dissociation may be proposed to proceed through a C_{2v} planar transition state (i.e., it is drawn here to have a zero reverse activation energy).

However, it is a different matter for the CF_2=C=O$^{+\bullet}$ manifold. The dissociation of the ground electronic state CF_2=C=O$^{+\bullet}$[$\tilde{X}\,^2B_1$], via the Wigner-Witmer Correlation Rules [17-21], is *symmetry forbidden.* Thus, as with what occurred with the analogous CH_2=C=O$^{+\bullet}$ case, the bent $^2A'$, $^2A''$ structures are invoked, via a vibrational resonance and a vibronic mixing of the $\tilde{X}\,^2B_1$ and $\tilde{D}\,^2A_1$ electronic states of CF_2=C=O$^{+\bullet}$. Therefore, this facilitates an

avoided crossing resulting in the concomitant $CF_2{=}C{=}O^{+\bullet}[\tilde{X}\,^2B_1] \rightarrow CF_2^{+\bullet}[\tilde{X}\,^2A_1] + C{\equiv}O[\tilde{X}\,^1A_1(^1\Sigma^+)]$ and $CF_2{=}C{=}O^{+\bullet}[\tilde{D}\,^2A_1] \rightarrow CF_2^{+\bullet}[^2B_1] + C{\equiv}O[\tilde{X}\,^1A_1(^1\Sigma^+)]$ dissociations.

As well, it is noteworthy that similar to its hydrogen analogue, the proposed dissociation energy of the perfluoro neutral ($CF_2{=}C{=}O \rightarrow CF_2 + C{\equiv}O$) and that of the radical-cation ($CF_2{=}C{=}O^{+\bullet} \rightarrow CF_2^{+\bullet} + C{\equiv}O$) are proposed to be 85.8 $kJ{\bullet}mol^{-1}$, and 126.4 $kJ{\bullet}mol^{-1}$, respectively. Thus similarly, the neutral is proposed to live in a *smaller* potential energy well (i.e., $\approx$ 68 %) than that of its respective radical-cation. Therefore, one may propose that $CH_2{=}C{=}O$ and $CF_2{=}C{=}O$ share certain similarities and differences, however, on the whole they are very close cousins indeed; the latter, like the former, being a genuinely stable species. It is simply that $CF_2{=}C{=}O$ is more reactive (i.e., more difficult to isolate) as its *endothermic* dissociation energies for its neutral and radical-cation are proposed to be $\approx$ 26 % and $\approx$ 32 %, respectively, that of the former.

4.2 Experimental Mass Spectra of CF_2=C=O$^{+\bullet}$

In this section the experimental mass spectral data of Dawson, and Holmes [11] on the CF_2=C=O$^{+\bullet}$ species will be presented and discussed. At this point it is important to emphasize that the mass spectral characteristics of CF_2=C=O$^{+\bullet}$ are *entirely similar and compatible* with the previous studies of Hop, Holmes, and Terlouw, on the CID, NR mass spectra of CH_2=C=O$^{+\bullet}$ [56], and of Bouma, Gill, and Radom, on the ab initio calculation of the potential energy surfaces and transition states of CF_2=C=O$^{+\bullet}$ and its isomers [58].

The information will be presented as follows; Table 4.8, and 4.9 illustrate the kinetic energy release, $T_{0.5}$, measurements of CF_2=C=O; and the peak intensities of the metastable ion (MI) 2FFR, collision induced dissociation (CID) 2FFR, and neutralization-reionization (NR) 2FFR mass spectra of source generated CF_2=C=O$^{+\bullet}$ (m/z 78) from CF_2=CFOCF$_3$; respectively. Additionally, Figures 4.5, 4.6, 4.7, 4.8, 4.9, 4.10, and 4.11, illustrate the following; the proposed energy levels of the $C_2F_2O^{+\bullet}$ (m/z 78) isomers; the metastable ion (MI) 2FFR mass spectrum of source generated CF_2=C=O$^{+\bullet}$ (m/z 78) from CF_2=CFOCF$_3$; (a) collision induced dissociation (CID) 2FFR mass spectrum of source generated $C_2F_2O^{+\bullet}$ (m/z 78) , (b) collision induced dissociation (CID) 3FFR mass spectrum of 2FFR metastably generated $C_2F_2O^{+\bullet}$ (m/z 78) from CF_2=CFOCF$_3$; the close-up of the neutralization-reionization (NR) 2FFR mass spectrum signal for $CO^{+\bullet}$ and $CF_2^{+\bullet}$ of source generated $C_2F_2O^{+\bullet}$ (m/z 78); and the proposed potential energy surfaces of the $C_2F_2O^{+\bullet}$ isomers, respectively.

Figure 4.5 Proposed Energy Levels of the $C_2F_2O^{+\bullet}$ (m/z 78) Isomers

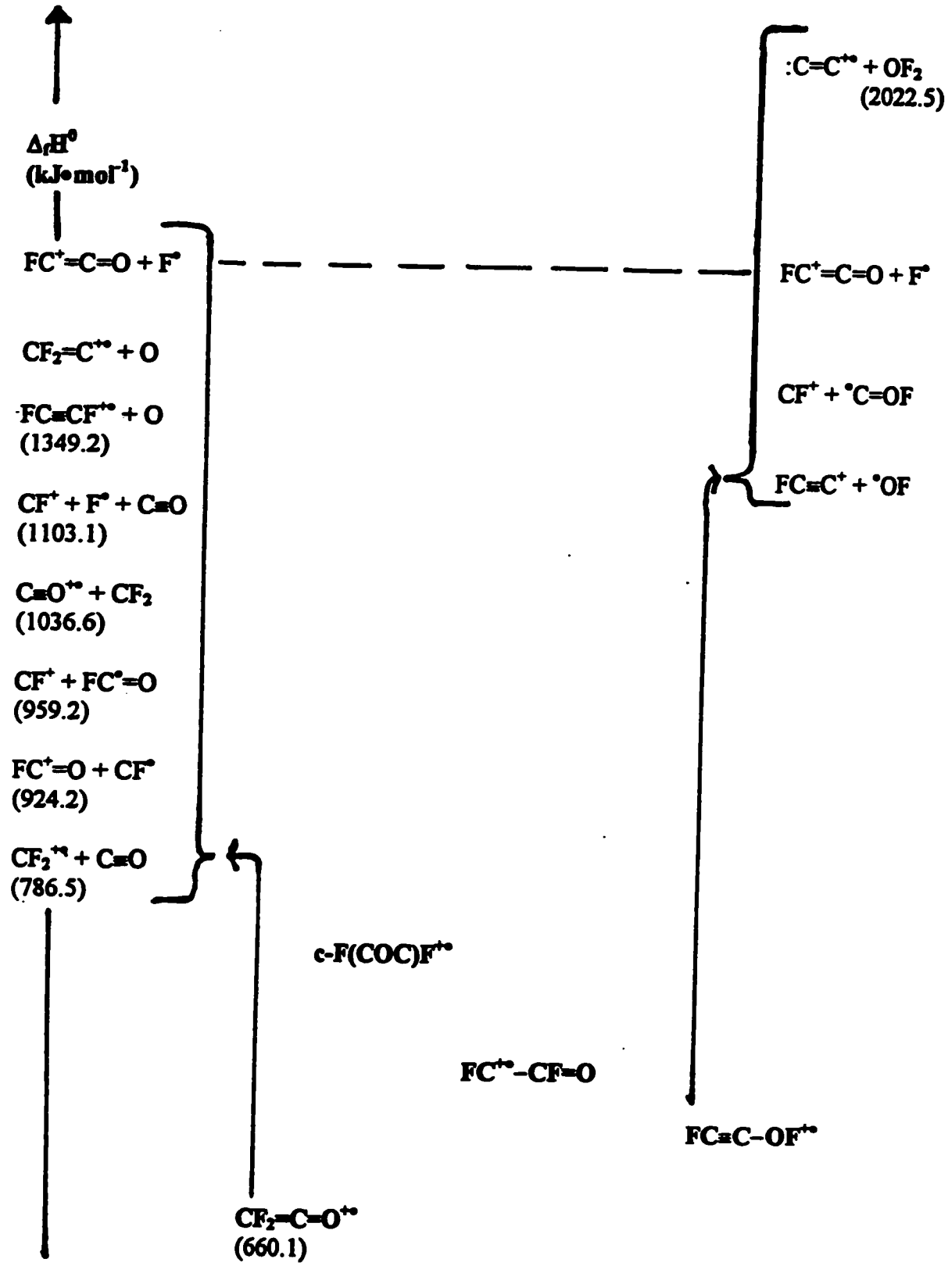

Table 4.8 Kinetic Energy Release $T_{0.5}$ Measurements of CF_2=C=O

Mass (m/z)	Dissociation Process and Target Gases	Kinetic Energy Release, $T_{0.5}$ (meV)
MI Processes		
(78 → 50)	$CF_2{=}C{=}O^{+\bullet} \rightarrow CF_2^{+\bullet} + C{\equiv}O$	2.1
CID Processes		
(78 → 50)	$CF_2{=}C{=}O^{+\bullet} \rightarrow CF_2^{+\bullet} + C{\equiv}O$; He	84.4
	; O_2	82.7
(78 → 31)	$FC^{+\bullet}{-}CF{=}O \rightarrow CF^{+} + FC{=}O^{\bullet}$; O_2	439.5
(78 → 28)	$CF_2{=}C{=}O^{+\bullet} \rightarrow C{\equiv}O^{+\bullet} + CF_2$; O_2	245.2
NR Processes		
(78 → 78)	$CF_2{=}C{=}O^{+\bullet}$ Recovery Peak ; Xe/O_2	
(78 → 50)[a]	$CF_2{=}C{=}O^{+\bullet} \rightarrow CF_2^{+\bullet} + C{\equiv}O$; Xe/O_2	554.2
(78 → 31)	$FC^{+}{-}CF{=}O \rightarrow CF^{+} + FC{=}O^{\bullet}$; Xe/O_2	499.5
(78 → 28)[a]	$CF_2{=}C{=}O^{+\bullet} \rightarrow C{\equiv}O^{+\bullet} + CF_2$; Xe/O_2	554.2

[a]Composite Peak Shape

Table 4.9 Metastable Ion (MI) 2FFR, Collision Induced Dissociation (CID) 2FFR He ≈ 90 %T and Neutralization-Reionization (NR) 2FFR Xe ≈ 90 %T / O_2 ≈ 90 %T Mass Spectra of Source Generated CF_2=C=$O^{+\bullet}$ (m/z 78) from CF_2=CFOCF_3

Species	Mass (m/z)	Neutral Loss	Height (%) MI	CID	NR
$C_2F_2O^{+\bullet}$	78				81.5
$C_2F_2^{+\bullet}$	62	(–O)		2.6	2.6
$CF_2^{+\bullet}$	50	(–CO)	100.0	100.0	100.0
CFO^+	47	(–$CF^\bullet$)		0.7	0.7
C_2F^+	43	(–$OF^\bullet$)		1.3	1.3
$C_2O^{+\bullet}$	40	(–F_2)		0.7	0.7
$C_2F_2O^{2+}$	39			2.6	0.7
CF^+	31	(–$CFO^\bullet$)		13.9	61.6
$CO^{+\bullet}$	28	(–CF_2)		6.6	23.3
$C_2^{+\bullet}$	24	(–OF_2)		<0.3	0.7
F^+	19				2.0
$C^{+\bullet}$	12				<0.3

Figure 4.6 Metastable Ion (MI) 2FFR Mass Spectrum of Source Generated $CF_2{=}C{=}O^{+\bullet}$ (m/z 78) from $CF_2{=}CFOCF_3$

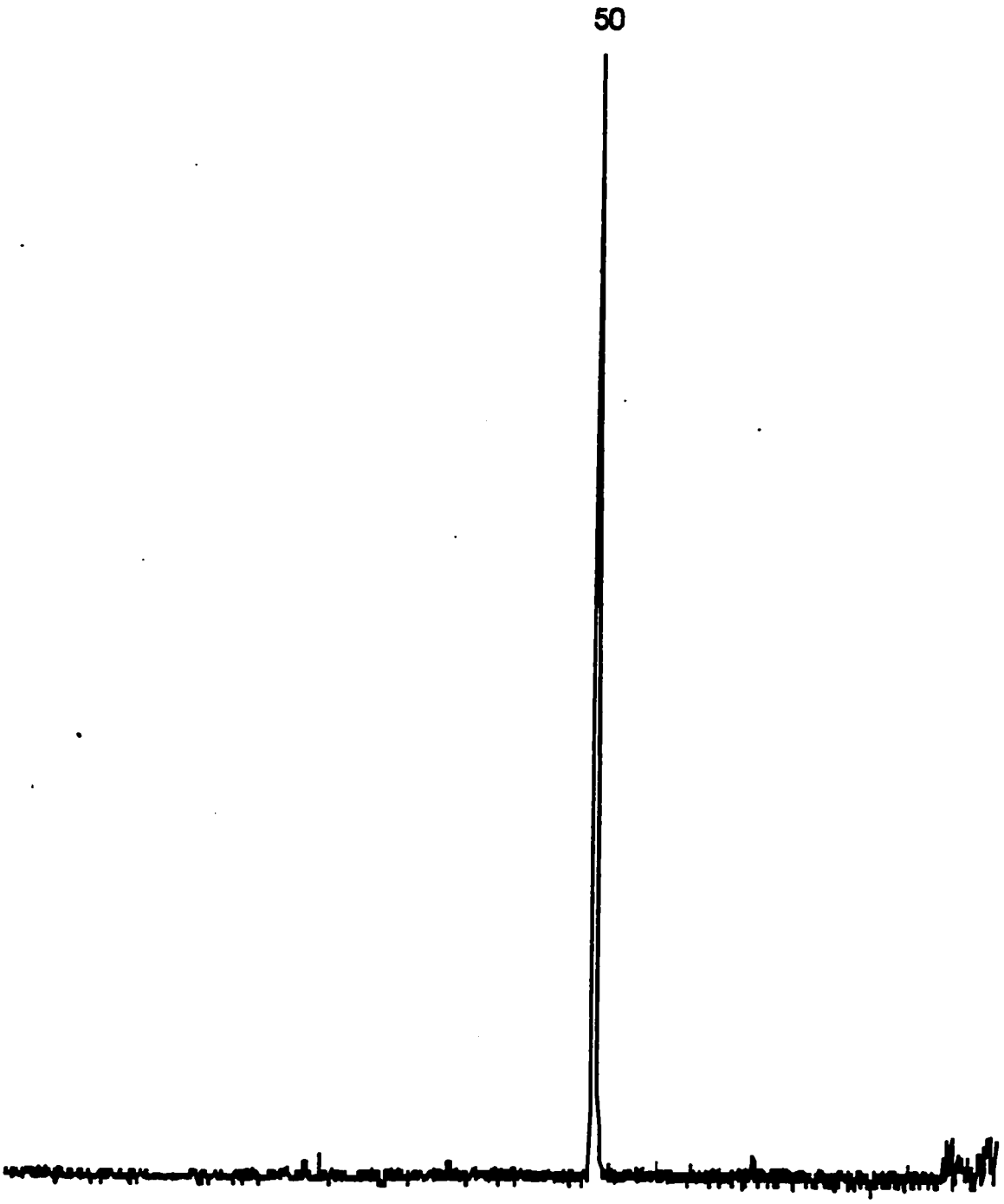

Figure 4.7 (a) Collision Induced Dissociation (CID) 2FFR He ≈ 90 %T Mass Spectrum of Source-Generated $C_2F_2O^{+\bullet}$ (m/z 78). (b) Collision Induced Dissociation (CID) 3FFR He ≈ 90 %T Mass Spectrum of Metastably Generated $C_2F_2O^{+\bullet}$ (m/z 78) from CF_2=$CFOCF_3^{+\bullet}$.

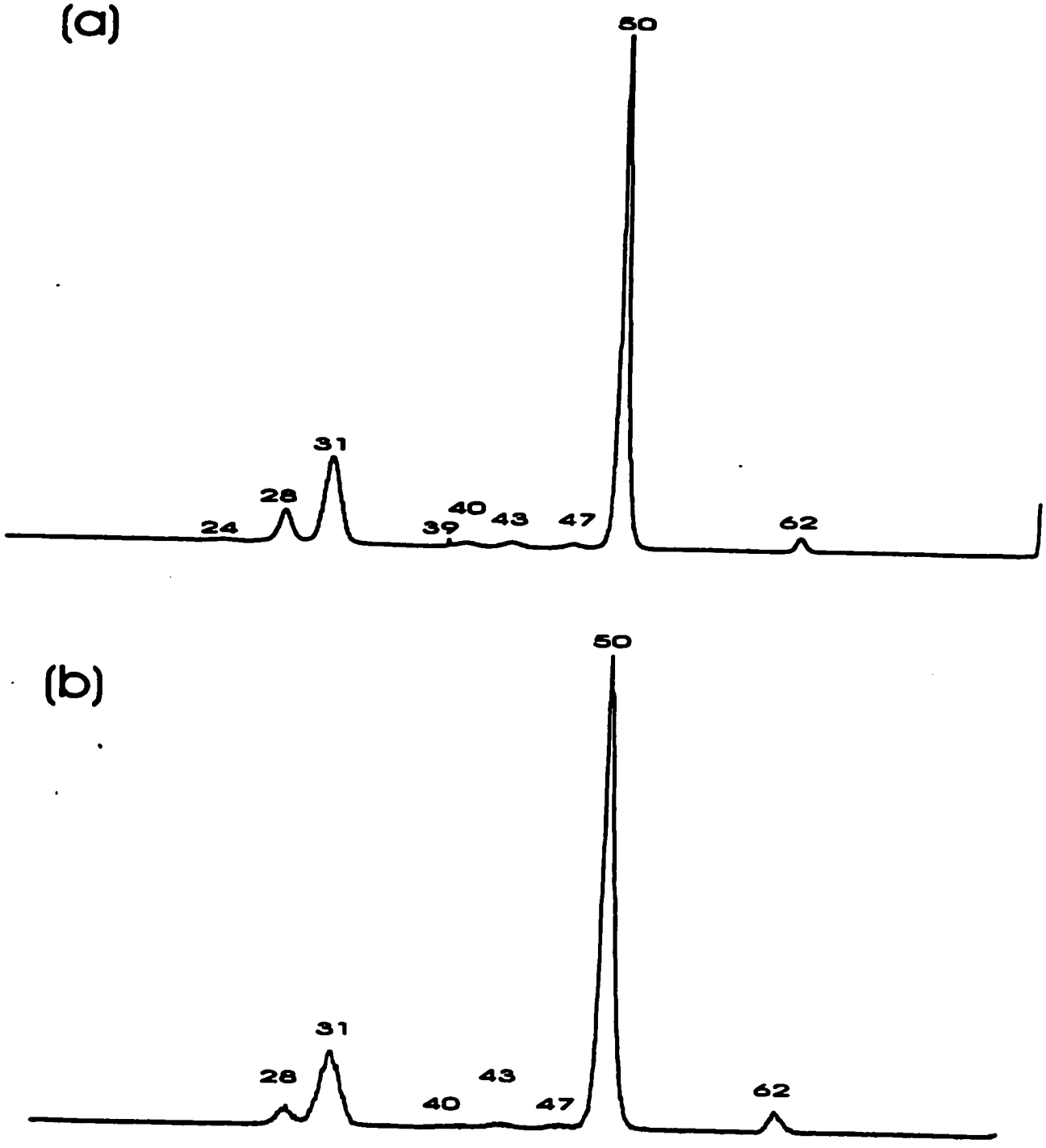

Figure 4.8 Neutralization-Reionization (NR) 2FFR Xe ≈ 90 %T / O_2 ≈ 90 %T Mass Spectrum of Source-Generated $C_2F_2O^{+\bullet}$ (m/z 78)

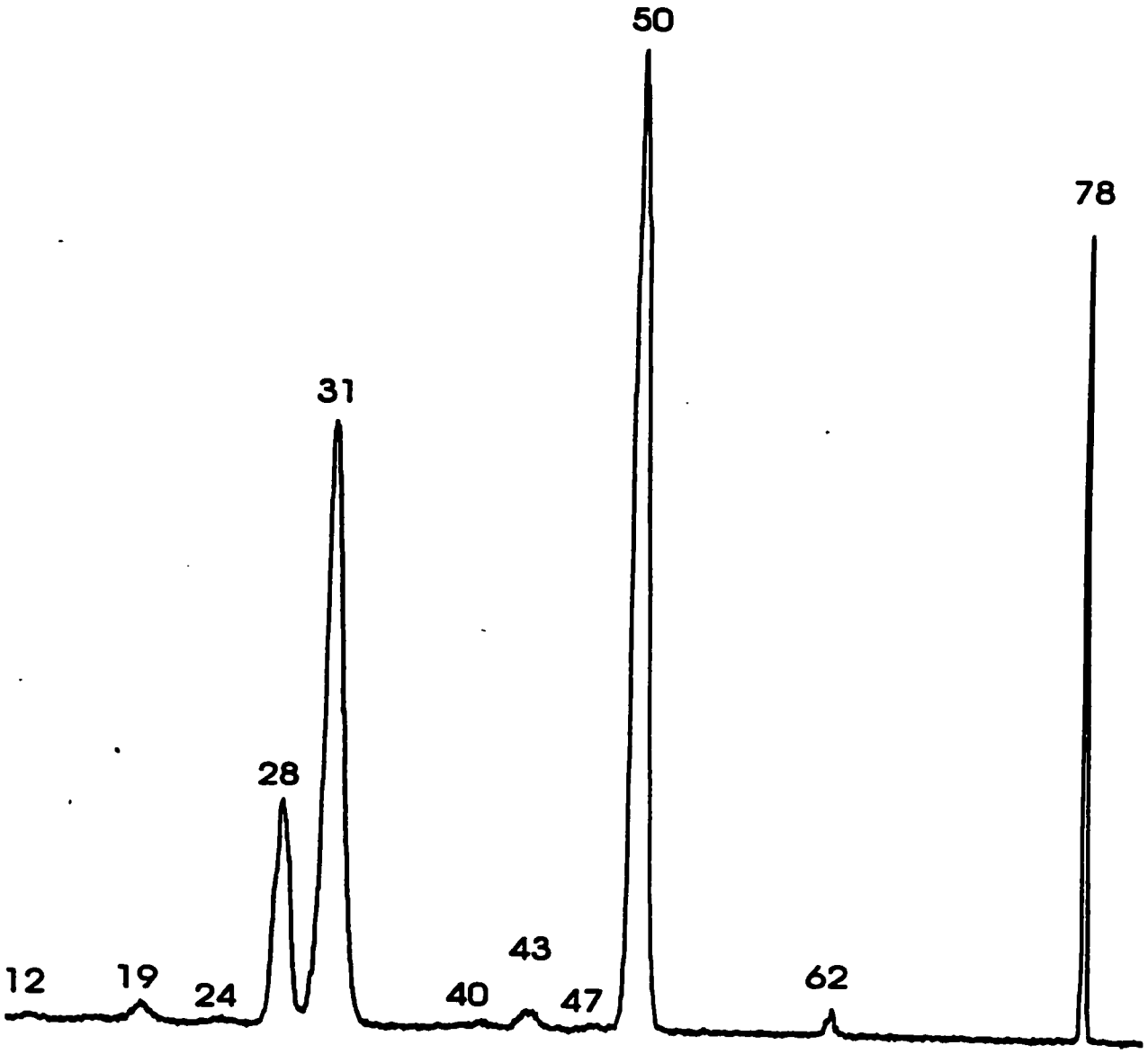

Figure 4.9 Neutralization-Reionization (NR) 3FFR Xe ≈ 90 %T / O_2 ≈ 90 %T Mass Spectrum of 2FFR Metastably Generated $C_2F_2O^{+\bullet}$ (m/z 78) from CF_2=$CFOCF_3^{+\bullet}$

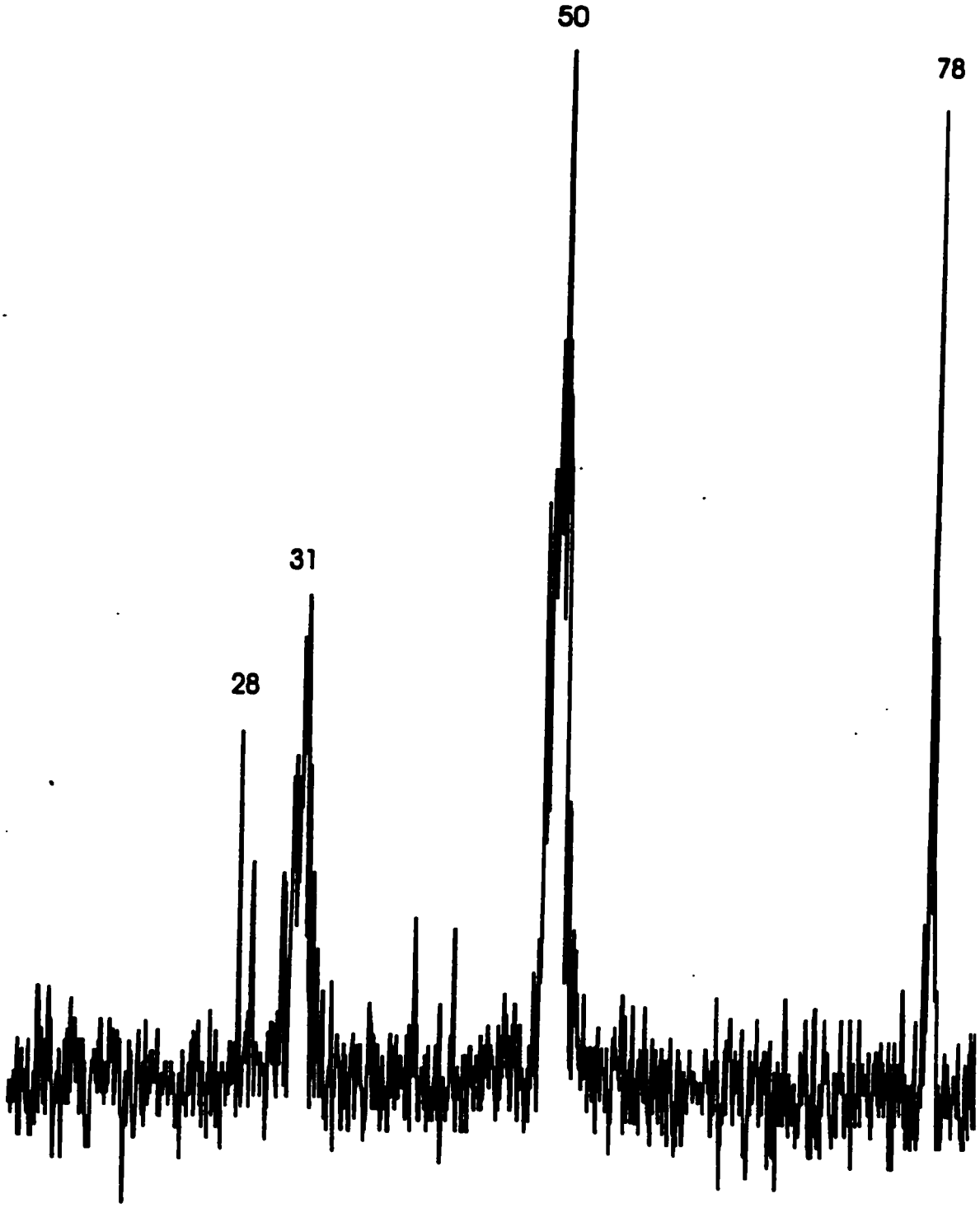

Figure 4.10 Close-Up of the Neutralization-Reionization (NR) 2FFR Xe ≈ 90 %T / O_2 ≈ 90 %T Mass Spectrum Signal for $CO^{+\bullet}$ and $CF_2^{+\bullet}$ of Source-Generated $C_2F_2O^{+\bullet}$ (m/z 78)

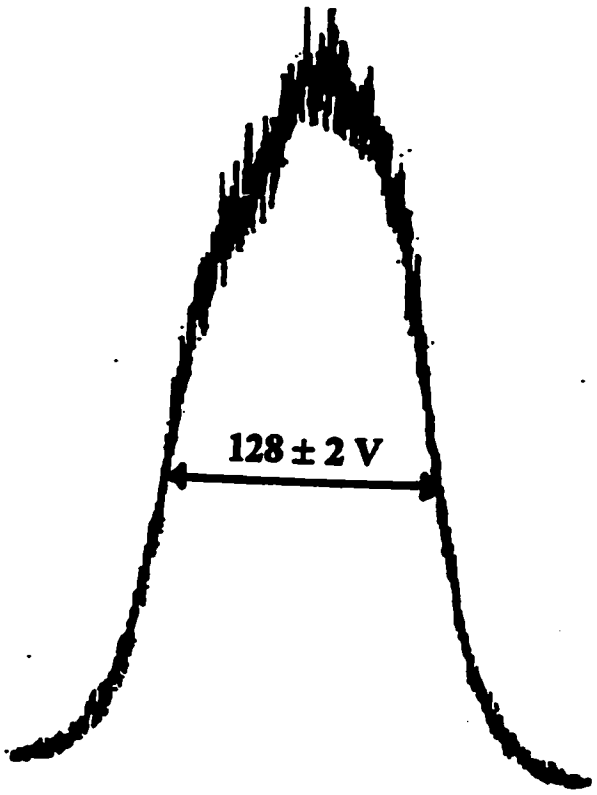

Figure 4.11 Proposed Potential Energy Surfaces of the $C_2F_2O^{+\bullet}$ Isomers

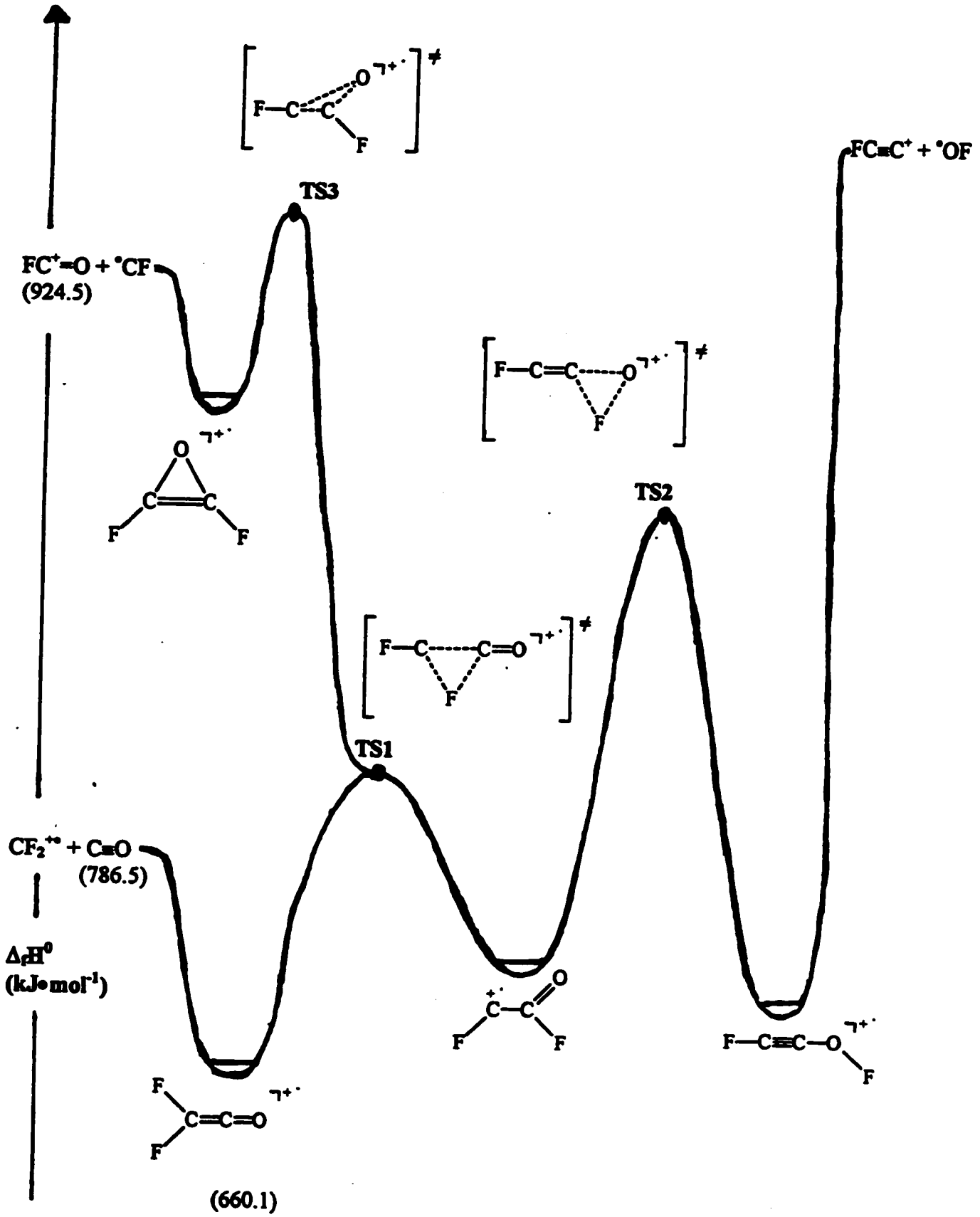

On inspection of Figure 4.5, the proposed energy levels of the $C_2F_2O^{+\bullet}$ (m/z 78) isomers, one may note that the proposed order of stability is as follows; $CF_2{=}C{=}O^{+\bullet}$ > $FC{\equiv}C{-}OF^{+\bullet}$ > $FC^{+\bullet}{-}CF{=}O$ > c-F(C ÖC)F$^{+\bullet}$ (the latter species is proposed to have the highest Δ_fH^0 value due to its proposed high ring-strain). The left-hand side of the $C_2F_2O^{+\bullet}$ dissociation manifold illustrates the proposed dissociation products predominantly from the $CF_2{=}C{=}O^{+\bullet}$ isomer. Its lowest energy dissociation is $CF_2^{+\bullet}$ + C≡O with a Δ_fH^0 value of 786.5 kJ•mol^{-1}. The right-hand side of the $C_2F_2O^{+\bullet}$ dissociation manifold illustrates the proposed dissociation products predominantly form the $FC{\equiv}C{-}OF^{+\bullet}$ isomer. Its lowest energy dissociation is proposed to be $FC{\equiv}C^+$ + $^\bullet$OF. The $FC^+{=}C{=}O$ + F$^\bullet$ dissociation products are proposed to be common to both of the left- and right-hand manifolds.

At this point, there are certain previous observations from past studies on the hydrogen analogue, $CH_2{=}C{=}O^{+\bullet}$, that deserve emphasis here, as there are certain parallels and contrasts in the behaviour to that of the perfluoro $CF_2{=}C{=}O^{+\bullet}$ species which will soon be made evident. Firstly, as previously stated, via the aid of the *low value* of $\Delta_fH^0[CH_4]$ = –74.5 kJ•mol^{-1} [6], the $(CH_3)_2C{=}O^{+\bullet}$ dissociation favoured the $CH_2{=}C{=}O^{+\bullet}$ + CH_4 products over those of $CH_3{-}C{\equiv}O^+$ + $CH_3^\bullet$ [52, 53]. In contrast, the $CH_2{=}CHOCH_3^{+\bullet}$ dissociation favours the $CH_3{-}C{\equiv}O^+$ + $CH_3^\bullet$ products, via the isomerization of energy rich acetone ions [52, 53]. Once again, the *extremely low value* $\Delta_fH^0[CH_4]$ = –934.5 kJ•mol^{-1} [6, 7] promised to make the formation of $CF_2{=}C{=}O^{+\bullet}$, from $(CF_3)_2C{=}O^{+\bullet}$ as a likely process, but in contrast it was actually the $CF_2{=}CFOCF_3^{+\bullet}$ species that favoured the $CF_2{=}C{=}O^{+\bullet}$ + CF_4 dissociation products.

The normal mass spectrum of both $(CF_3)_2C{=}O^{+\bullet}$ and $CF_2{=}CFOCF_3^{+\bullet}$ each contained molecular ions of about 4 %, and 20 %, respectively (see the $C_3F_6O^{+\bullet}$ section of Chapter 3). For the perfluoroacetone ion, the major fragment ions were CF_3^+ (100 %), CF_3CO^+ (50 %), $CF_3(C{=}O)CF_2^+$ (26 %), and $CF_2^{+\bullet}$ (15 %). The $C_2F_2O^{+\bullet}$ (m/z 78) ion was of similar abundance to the molecular ion. The MI mass spectrum contained only the $CF_3{-}C{\equiv}O^+$ (m/z 97) ion and the *extremely weak* $C_2F_2O^{+\bullet}$ (m/z 78) [11].

In contrast, the perfluorovinylether molecular ion, produced a dissimilar mass spectrum; base peak CF_3^+(100 %), $C_2F_3^+$ (15 %), $C_2F_2O^{+\bullet}$ (15%), $CF_2^{+\bullet}$ (10 %), CFO^+ (9 %), and $C_2F_6^{+\bullet}$(6 %). The MI mass spectrum (see Figure 4.6) contained a *single* broad Gaussian peak for CF_4 loss to produce $C_2F_2O^{+\bullet}$ (m/z 78). The kinetic energy release (KER) was $T_{0.5}$ =80 meV; the peak was *very insensitive* to collision gas, in keeping with a rearrangement preceding fragmentation [11].

Now, on returning to the $CH_2{=}C{=}O^{+\bullet}$ studies of Hijazi, Holmes, and Terlouw [55], and Hop, Holmes, and Terlouw [56], one may note the following trends. The $CH_2{=}C{=}O^{+\bullet} \rightarrow CH_2^{+\bullet} + C{\equiv}O$ dissociation process has a very small, $T_{0.5}$ = 2.6 meV value and proceeds at/or near threshold (i.e., no reverse activation energy barrier) [55, 56]. As was stated in section 4.1.4, by Lorquet [59], this was proposed by *ab initio calculations*, to be due to the *bent* $CH_2{=}C{=}O^{+\bullet}[^2A', ^2A'']$ electronic states acting as *"premonitional-modes"* acting to *lower* (i.e., to near zero) the *"hump"* in the $CH_2{=}C{=}O^{+\bullet}[\tilde{X}\,^2B_1] \rightarrow CH_2^{+\bullet}[\tilde{X}\,^2A_1] + C{\equiv}O[\tilde{X}\,^1A_1(^1\Sigma^+)]$ dissociation potential energy surface. Additionally, an *ab initio study* by Bouma, Gill, and Radom [58], proposed the cyclic-transition states; $[c\text{-}H(CHC){=}O^{+\bullet}]^{\ddagger}$, $[c\text{-}HC{=}(CHO)^{+\bullet}]^{\ddagger}$, and $[c\text{-}H(C\ddot{O}C)H^{+\bullet}]^{\ddagger}$, to have the facility to act as intermediaries between the $CH_2{=}C{=}O^{+\bullet} \rightarrow$

$HC^{+\bullet}$–CH=O; $HC^{+\bullet}$–CH=O → HC≡C–$OH^{+\bullet}$; and $HC^{+\bullet}$–CH=O → c-H(C ÖC)$H^{+\bullet}$ isomerizations, respectively.

Next, one should consider the *experimental mass spectral results* of Hop, Holmes, and Terlouw [56]. The CID 2FFR ≈ O_2 90 %T mass spectrum of CH_2=C=$O^{+\bullet}$, illustrated in Figure 1(a) of [56], showed the expected major mass spectral peaks of $CH_2^{+\bullet}$ (m/z 14), and $CO^{+\bullet}$ (m/z 28). There was also the observation of the $C_2H_2^{+\bullet}$ (m/z 26), and CHO^+ (m/z 29) peaks, that were proposed by Holmes et. al., [56] to be a result of the accessing of the other $C_2H_2O^{+\bullet}$ isomers, via the production of the *excited* electronic states of CH_2=C=$O^{+\bullet}$, *not considered by Radom et. al.. [58].*

One should note that Holmes et. al., [56] were successful in the production of the oxirene radical-cation, c-H(C ÖC)$H^{+\bullet}$, however, upon neutralization in the NR experiment, the neutral c-H(C ÖC)H *isomerized* into the more stable CH_2=C=O isomer (p. 444 of [56]). Additionally, the NR 2FFR Xe ≈ 90 %T / O_2 ≈ 90 %T mass spectrum of CH_2=C=$O^{+\bullet}$, illustrated in Figure 3(a) of [56], possessed the *expected major peaks* of $CH_2^{+\bullet}$ (m/z 14), $CO^{+\bullet}$(m/z 28), and a *large recovery peak* for the CH_2=C=$O^{+\bullet}$ (m/z 42) isomer. As will be shown in the following experimental data presented in Tables 4.8, and 4.9, and Figures 4.6 to 4.10, and the rationale proposed by the potential energy surfaces of the $C_2F_2O^{+\bullet}$ isomers illustrated in Figure 4.11, the CF_2=C=$O^{+\bullet}$ species is proposed to *mimic very closely* the behaviour of its CH_2=C=$O^{+\bullet}$ analogue.

Firstly, on inspection of Table 4.8, the kinetic energy release, $T_{0.5}$, measurements of CF_2=C=O, (which were conducted under *single collision conditions*, i.e., ≈ 90 %T), one may note the following trends. The MI process, CF_2=C=$O^{+\bullet}$ → $CF_2^{+\bullet}$ + C≡O has been measured

by Dawson, and Holmes [11] to possess a $T_{0.5}$ = 2.1 meV value and a peak shape *extremely similar* that of its hydrogen analogue (i.e., $T_{0.5}$ = 2.6 meV [56]). There are three CID processes studied here for the source generated CF_2=C=O$^{+\bullet}$. The first is the CF_2=C=O$^{+\bullet}$ → $CF_2^{+\bullet}$ + C≡O dissociation process. The signal is composite with a very narrow MI signal (i.e., probably $T_{0.5}$ ≈ 2.1 meV) atop the much broader peak of $T_{0.5}$ = 83 meV, and it was target gas *independent*. The second, is the FC$^{+\bullet}$–CF=O → $CF_2^{+\bullet}$ + C≡O dissociation process, with a very large $T_{0.5}$ ≈ 440 meV value. This is most likely indicative of a CF_2=C=O$^{+\bullet}$ rearrangement into FC$^{+\bullet}$–CF=O, as the final C–C bond scission occurs. Thirdly, is the CF_2=C=O$^{+\bullet}$ → C≡O$^{+\bullet}$ + CF_2 dissociation process, with a large $T_{0.5}$ ≈ 245 meV value. On inspection of Figure 4.5, this large value is expected for the high $\Delta_f H^0$ value of 1036.6 kJ•mol^{-1} for the C≡O$^{+\bullet}$ + CF_2 dissociation limit.

Next, one has the $T_{0.5}$ values for the NR (2FFR) Xe ≈ 90 %T / O_2 ≈ 90 %T mass spectrum of source generated CF_2=C=O$^{+\bullet}$. As indicated, there is a very intense (see Table 4.9, and Figure 4.8 and 4.9) recovery peak for CF_2=C=O$^{+\bullet}$ (m/z 78). Both of the $CF_2^{+\bullet}$(m/z 50) and C≡O$^{+\bullet}$ (m/z 28) peaks are *have the same peak shape*; they are *composite* with a *very narrow signal* (i.e., probably $T_{0.5}$ ≈ 2.1 meV) atop a *much broader peak* (see Figure 4.10). The broader peak components for *both* $CF_2^{+\bullet}$ (m/z 50) and C≡O$^{+\bullet}$ (m/z 28) are the same and give $T_{0.5}$ ≈ 550 meV. This is entirely expected (as previously stated in Chapter 1) as is the case for any unimolecular dissociation reaction,

$$M_1^{+\bullet} \rightarrow M_2^{+} + M_3^{\bullet}$$

where, m_1, m_2, and m_3 are the masses of the, $M_1^{+\bullet}$, M_2^{+}, and $M_3^{\bullet}$ species, respectively, the kinetic energy release, $T_{0.5}$, in units of meV, is expressed as follows,

$$T_{0.5} = \frac{1}{16}\left(\frac{(m_1)^2}{(m_2)(m_3)}\right)\left(\frac{(\Delta E_2)^2 - (\Delta E_1)^2}{V_{acc}}\right)$$

where, V_{acc}, ΔE_1, and ΔE_2 denote the accelerating voltage, in V, the main beam full-width at half-height, in V, the fragment ion beam full-width at half-height, in V, respectively. Therefore, in accordance with their common ΔE_1 and *NRMS* ΔE_2 (i.e., (128 ± 2) V, see Figure 4.10) values, it is plain for one to see the shared value for the $[(m_1)^2]/[(m_2)^2(m_3)^2]$ component for the respective $CF_2{=}C{=}O^{+\bullet} \rightarrow CF_2^{+\bullet} + C{\equiv}O$, and $CF_2{=}C{=}O^{+\bullet} \rightarrow C{\equiv}O^{+\bullet} + CF_2$ dissociations (during the NRMS process).

Thus, it is proposed here that the *excited electronic states of unstable* neutral $CF_2{=}C{=}O$ molecules dissociate readily ($CF_2{=}C{=}O \rightarrow CF_2 + C{\equiv}O$) to produce (after collisional ionization) the *very broad components* of the $CF_2^{+\bullet}$ and $C{\equiv}O^{+\bullet}$ ion peaks (i.e., $T_{0.5} \approx 550$ meV). The *narrow components* are compatible with the dissociation of *excited electronic state reionized stable* neutral $CF_2{=}C{=}O$ (i.e., $T_{0.5} \approx 2.1$ meV) [11].

On inspection of Table 4.9, one may note that the base peak in all of the mass spectra (i.e., MI, CID, and NR) is the $CF_2^{+\bullet}$ (m/z 50) peak. The other major peaks are the CF^+ (m/z 31) and $C{\equiv}O^{+\bullet}$ (m/z 28) peaks that correspond to $FC^{\bullet}{=}O$ and CF_2 losses, respectively. In both of the CID and NR mass spectra there is a doubly-charged $C_2F_2O^{2+}$ (m/z 39) peak, and the previously mentioned NR recovery peak of $C_2F_2O^{+\bullet}$ (m/z 78) has a strong intensity of ≈ 81.5 %.

Thus, on inspection of Figure 4.6, one may note the single MI peak of $CF_2^{+\bullet}$ (m/z 50) that corresponds to the $C{\equiv}O$ loss from the $CF_2{=}C{=}O^{+\bullet}$ parent.

Now, on inspection of Figure 4.7, where (a) illustrates the CID 2FFR mass spectrum of source generated $CF_2{=}C{=}O^{+\bullet}$, and (b) illustrates the CID 3FFR mass spectrum of 2FFR

metastably generated CF_2=C=O$^{+\bullet}$ from CF_2=CFOCF$_3$, one may see that they are consistent with a single ion structure, namely, CF_2=C=O$^{+\bullet}$. Note that the doubly-charged $C_2F_2O^{2+}$ (m/z 39) is weak in 4.7 (b), 4.8, and 4.9, but nonetheless clearly present upon magnification [11]. In the study of Holmes et. al., [56], the CID mass spectrum of ketene (CH_2=C=O$^{+\bullet}$) ions also contained a doubly-charged ion.

Next, on inspection of Figures 4.8 and 4.9, the neutralization-reionization (NR) 2FFR mass spectra of source generated $C_2F_2O^{+\bullet}$ (m/z 78), and the neutralization-reionization (NR) 3FFR mass spectra of 2FFR metastably generated $C_2F_2O^{+\bullet}$ (m/z 78) from CF_2=CFOCF$_3$, respectively, one may clearly see that they represent a *single ion structure, namely, perfluoroketene*, CF_2=C=O$^{+\bullet}$. The base peak in both Figures 4.8 and 4.9 is that of $CF_2^{+\bullet}$ (m/z 50), as well as an intense recovery peak (≈ 80 %) for CF_2=C=O$^{+\bullet}$ (m/z 78). Additionally, the major peaks of CF^+ (m/z 31) and C≡O$^{+\bullet}$ (m/z 28) are clearly present in both Figures 4.8 and 4.9 (although weaker in Figure 4.9). Due to the much weaker signal intensity of the 2FFR metastably generated CF_2=C=O$^{+\bullet}$ species in Figure 4.9, the smaller intensity NR peaks are only distinguishable in the source generated CF_2=C=O$^{+\bullet}$ species in Figure 4.8. The lower intensity peaks in Figure 4.8 are listed as follows; FC≡CF$^{+\bullet}$ (m/z 62), FC$^+$=O (m/z 47), FC≡C$^+$ (m/z 43), C=C=O$^{+\bullet}$ (m/z 40), :C=C$^{+\bullet}$ (m/z 24), F^+ (m/z 19), and $C^{+\bullet}$ (m/z 12).

All of the above experimental observations strongly support the dominant $C_2F_2O^{+\bullet}$ isomer being that of the perfluoroketene (CF_2=C=O$^{+\bullet}$) ion, and the production of a stable neutral CF_2=C=O species (with an *endothermic* dissociation energy) during the neutralization step of the NR experiments. All other isomeric C_2F_2O neutral and radical-cation structures are not compatible with the observations. The cyclic perfluorooxirene, c-F(C$\breve{O}$C)F, neutral

has been predicted by the ab initio calculations of Schaefer III et. al., [57], only to be a *saddle point* on the C_2F_2O potential energy surface. As well, even if c-F(C$\tilde{O}$C)F were indeed by some other precursor to be experimental produced in the gas-phase, *it is very likely to befall the same fate of its hydrogen analogue*, proposed by Holmes et. al., [56] (i.e., an isomerization of c-F(C$\tilde{O}$C)F $\rightarrow$ CF_2=C=O, followed by a dissociation, upon collisional excitation, into CF_2 + C≡O). Additionally, the carbene, F$\tilde{C}$–CF=O, by all accounts should surely collapse to the most stable isomer, CF_2=C=O. Lastly, perfluoromethynol, FC≡C–OF, is highly unlikely to be responsible for the above mass spectra [11].

Thus, on inspection of Figure 4.11, the proposed potential energy surfaces of the $C_2F_2O^{+\bullet}$ isomers, one may see presented here, a *qualitatively unifying scheme* of their behaviour. The *caveat* being that although *none of the proposed transition states* illustrated here *have been the subject of any ab initio calculations* in the literature, to the knowledge of this author, *they do parallel those proposed by Radom et. al.*,[58], for the analogous hydrogen $C_2H_2O^{+\bullet}$ isomers.

Therefore, one may see that CF_2=C=$O^{+\bullet}$, c-F(C$\tilde{O}$C)$F^{+\bullet}$, and FC≡C–$OF^{+\bullet}$ may undergo direct fragmentation into the dissociation products of $CF_2^{+\bullet}$ + C≡O; FC^+=O + $^\bullet$CF; and FC≡C^+ + $^\bullet$OF; respectively. The isomerization of CF_2=C=$O^{+\bullet}$ into $FC^{+\bullet}$–CF=O, and $FC^{+\bullet}$–CF=O into FC≡C–$OF^{+\bullet}$ are proposed to be facilitated by the cyclic transition states [c-F(CFC)=$O^{+\bullet}$]‡, TS1, and by [c-FC=(CFO)$^{+\bullet}$]‡, TS2, respectively. However, at this point the transition state [c-F(CFC)=$O^{+\bullet}$]‡ deserves special emphasis. This transition state, TS1, is proposed to further distort into another transition state [c-F(C$\tilde{O}$C)$F^{+\bullet}$]‡, TS3, which then drops into the potential well of the perfluorooxirene ion, c-F(C$\tilde{O}$C)$F^{+\bullet}$. Therefore, on

careful inspection of Figure 4.11, one may see the special nature of the [c-F(CFC)=O$^{+\bullet}$]‡ transition state; *as it serves as the nexus that intimately links the* CF_2=C=O$^{+\bullet}$, FC$^{+\bullet}$–CF=O and c-F(C$\breve{O}$C)F$^{+\bullet}$, isomers.

Thus, on a thorough consideration of the above experimental data presented in Figures 4.6-4.10, and the proposed potential energy surfaces of the $C_2F_2O^{+\bullet}$ isomers illustrated in Figure 4.11, one may confidently state that the $C_2F_2O^{+\bullet}$ ion structure examined here is that of the perfluoroketene ion, CF_2=C=O$^{+\bullet}$, and that the stable CF_2=C=O neutral is indeed produced.

4.3 Conclusions

Therefore, in the previous sections of this chapter the following theses have been *thoroughly explored and adequately justified.* Firstly, the combined tandem mass spectrometric techniques of MI, CID, and NR indicate that the $C_2F_2O^{+\bullet}$ (m/z 78) ion produced from ionized CF_2=$CFOCF_3$ is that of a single structure, namely, the perfluoroketene, CF_2=C=$O^{+\bullet}$ [11]. The proposed thermodynamic values for perfluoroketene are $\Delta_f H^0[CF_2{=}C{=}O] = -401.3$ kJ•mol^{-1}, $IE_a[CF_2{=}C{=}O] \approx 11$ eV, and $\Delta_f H^0[CF_2{=}C{=}O^{+\bullet}] = 660.1$ kJ•mol^{-1}. The ground electronic states of the neutral and radical-cation species are proposed to be $\tilde{X}\,^1A_1$ and $\tilde{X}\,^2B_1$, respectively. The *endothermic* dissociation energies for the lowest energy fragmentations for the neutral (i.e., $CF_2{=}C{=}O \rightarrow CF_2 + C{\equiv}O$) and the radical-cation (i.e., $CF_2{=}C{=}O^{+\bullet} \rightarrow CF_2^{+\bullet} + C{\equiv}O$) are proposed to be ≈ 86 kJ•mol^{-1} and ≈ 126 kJ•mol^{-1}, respectively. They are asserted to be reasonable estimates as they are ≈ 26 % and ≈ 32 % of the analogous hydrogen species dissociation energies, respectively. This therefore serves to emphasize the proposal that $CF_2{=}C{=}O$ is a stable species (i.e., in its neutral and radical-cation) that is simply difficult to isolate due to its high reactivity (e.g., dimerization, polymerization, and/or dissociation, etc...) in solution and/of at ambient conditions in high concentrations in the gas-phase.

Most importantly, the presence of the neutral $CF_2{=}C{=}O$ as a stable species, possessing a lifetime (of at least 1μs) on the order of the transit time between the neutralization cell and the reionization cell in the NR mass spectra presented here (see Figures 4.8, and 4.9), *represents the first direct experimental gas-phase observation* of this elusive primary member of the perfluorinated ketenes [11].

4.4 References

[1] T.T. Tidwell, Ketenes, John Wiley and Sons, New York, New York, USA, pp. 1-57, 321-336, 445-458,(1995).

[2] S. Patai, Ed., The Chemistry of Ketenes, Allenes and Related Compounds. Part 1, John Wiley and Sons, New York, New York, USA, (1980).

[3] S. Patai, Ed., The Chemistry of Ketenes, Allenes and Related Compounds. Part 2, John Wiley and Sons, New York, New York, USA, (1980).

[4] C. Kotting, W. Sander, M. Senzlober, and H. Burger, Eur. Chem. J., 4(9), 1611- 1615, (1998).

[5] M.R. Zachariah, P.R. Westmoreland, D.R. Burgess, Jr., W. Tsang, and C.F. Melius, J. Phys. Chem., 100, 8737-8747, (1996).

[6] S.G. Lias, J.F. Liebman, J.L Holmes, R.D. Levin, and W.G. Malland, J. Phys. Chem. Ref. Data , 17, (1988).

[7] M.W. Chase, Jr., NIST–JANAF Thermochemical Tables, 4th Ed., J. Phys. Ref. Data Monogr., 9, (1998).

[8] H.E. O'Neal, and S.W. Benson, Natl. Stand. Ref. Data Ser. Natl. Bur. Stand., 21, (1970).

[9] J.A. Berson, D.M. Dirney, W.P. Dailey III, and J.F. Liebman, Molecules Structure and Energies, Springer-Verlag, New York, New York, USA, Vol. 6, pp. 391-441, (1987).

[10] (a) C. Wesdemiotis, and F.W. McLafferty, Chem. Rev., 87, 405, (1987).
(b) J.K. Terlouw, and H. Schwarz, Angew. Chem. Int. Ed. Engl., 26, 805, (1987).
(c) J.L. Holmes, Mass Spectrom. Rev., 8, 513, (1989).

(d) C.A. Shalley, G. Horning, D. Schroder, and H. Schwarz, Chem. Soc. Rev., 27, 91, (1998).

[11] D.F. Dawson, and J.L. Holmes, J. Phys. Chem. A., 103, 5217-5220, (1999).

[12] S.W. Benson, and J.H. Buss, J. Chem. Phys., 29(3), 546-572, (1958).

[13] N. Cohen, and S.W. Benson, Chem. Rev., 2419-2438, (1993).

[14] S.W. Benson, F.R. Cruickshank, D.M. Golden, G.R. Haugen, H.E. O'Neal, A.S. Rogers, R. Shaw, and R. Walsh, Chem. Rev., 29, 279-324, (1969).

[15] S.W. Benson, Thermochemical Kinetics, 2nd Ed., John Wiley and Sons, New York, New York, USA, pp. 24-28, (1976).

[16] H.E. O'Neal, and S.W. Benson, J. Phys. Chem., (6)72, 1866-1877, (1968).

[17] G. Herzberg, Molecular Spectra and Molecular Structure I. Spectra of Diatomic Molecules., Van Nostrand Reinhold Company, New York, New York, USA, pp. 315-322, (1950).

[18] G. Herzberg, Molecular Spectra and Molecular Structure II. Infrared and Raman Spectra of Polyatomic Molecules., D. Van Nostrand Company Inc., New York, New York, USA, (1945).

[19] G. Herzberg, Molecular Spectra and Molecular Structure III. Electron Spectra and Electronic Structure of Polyatomic Molecules., Van Nostrand Company, New York, New York, USA, pp. 281-287, (1966).

[20] J.H.D. Eland, Photoelectron Spectroscopy. An Introduction to Ultraviolet Photoelectron Spectroscopy in the Gas Phase, Butterworths, London, U.K., (1974).

[21] J.H.D. Eland, Photoelectron Spectroscopy. An Introduction to Ultraviolet Photoelectron Spectroscopy in the Gas Phase, 2nd Ed., Butterworths, London, U.K., (1984).

[22] P.F. Bernath, Spectra of Atoms of Molecules, Oxford University Press Inc., New York, New York, USA, (1995).

[23] T.A. Miller, Ed., and V.E. Bondybey, Ed., Molecular Ions: Spectroscopy, Structure and Chemistry, North-Holland Publishing Company, New York, New York, USA, (1983).

[24] G. Herzberg, Atomic Spectra and Atomic Structure, Dover Publications, New York, New York, USA, (1944).

[25] A.B.F. Duncan, Rydberg Series in Atoms and Molecules, Academic Press Inc., New York, New York, USA, (1971).

[26] R.W.B. Pearse, and A.G. Gaydon, The Identification of Molecular, 4th Ed., John Wiley and Sons, New York, New York, USA, (1976).

[27] S. Bashkin, and J.O. Stoner, Jr., Atomic Energy Levels and Grotrian Diagrams 1. Hydrogen I – Phosphorous XV, American Elsevier Publishing Company Inc., New York, New York, USA, (1975).

[28] S. Bashkin, and J.O. Stoner, Jr., Atomic Energy Levels and Grotrian Diagrams 1. Hydrogen I – Phosphorous XV, Addenda, North-Holland Publishing Company Inc., New York, New York, USA, (1978).

[29] M.T. Bowers, Ed., Gas Phase Ion Chemistry, Ions and Light, Vol. 3, Academic Press Inc., New York, New York, USA, (1984).

[30] F.A. Cotton, Chemical Applications of Group Theory, 3rd Ed., John Wiley and Sons, New York, New York, USA, (1990).

[31] S.V. O'Neil, H.F. Schaefer III, and C.F. Bender, J. Chem. Phys., 55(1), 162-169, (1971).

[32] S. Koda, Chem. Phys. Lett., 55(2), 353-357, (1978).

[33] L.B. Harding, and W.A. Goddard III, J. Amer. Chem. Soc., 98(20), 6093-6099, (1976).

[34] C.B. Moore, and G.C. Pimentel, J. Chem. Phys., 38(12), 2816-2829, (1963).

[35] D.W. Turner, C. Baker, A.D. Baker, and C.R. Brundle, Molecular Photoelectron of Molecules, John Wiley and Sons, New York, New York, USA, (1970).

[36] D. Hall, and J.P. Maier, Chem. Phys., 24, 373-378, (1977).

[37] J.M. Dyke, L. Golab, N. Jonathan, A. Morris, M. Okuda, J. Chem. Soc. Faraday Trans. 2, 70, 1828-1836, (1974).

[38] K.K. Murray, D.G. Leopold, T.M. Miller and W.C. Lineburger, J. Chem. Phys., 89,(9), 5442-5453, (1988).

[39] F.C. Tompkins, Ed., The Photoelectron Spectroscopy of Molecules, Faraday Discuss. Chem. Soc., 54, 1-306, (1972).

[40] C.R. Brundle, M.B. Robin, N.A. Kuebler, and H. Basch, J. Amer. Chem. Soc., 94(5), 1451-1465, (1972).

[41] C.R. Brundle, M.B. Robin, and N.A. Kuebler, J. Amer. Chem. Soc., 94(5), 1466-1475, (1972).

[42] M.R. Robin, G.N. Taylor, and N.A. Kuebler, J. Org. Chem., 38(5), 1049-1051, (1973).

[43] G. Bieri, and L. Asbrink, J. Electron Spectrosc. Rel. Phenom., 20, 149-167, (1980).

[44] W. Von Niessen, G. Bieri, and L. Asbrink, J. Electron Spectrosc. Rel. Phenom., 21, 175-191, (1980).

[45] G. Bieri, L. Asbrink, and W. Von Niessen, J. Electron Spectrosc. Rel. Phenom., 23, 281-322, (1981).

[46] L.N. Domelsmith, K.N. Houk, C. Predrahita, and W.J. Dolbier, Jr., J. Amer, Chem Soc, 100(22), 6908-6911, (1978).

[47] R.K. Thomas, and H. Thompson, Proc. R. Soc. London Ser. A, 339, 29, (1974).

[48] G.K. Jarvis, K.J. Boyle, C.A. Mayhew, and R.P. Tuckett, J. Phys. Chem. A, 102(19), 3219-3229, (1998).

[49] G.K. Jarvis, K.J. Boyle, C.A. Mayhew, and R.P. Tuckett, J. Phys. Chem. A, 102(19), 3230-3237, (1998).

[50] P. Schang, R. Gleuther, and A. Pieker, Ber. Bunsenges. Phys. Chem., 82, 629-633, (1978).

[51] R. Gleiter, P. Schang, M. Bloch, E. Heilbrouner, J.C. Bunzli, D.C. Frost, and L. Weiler, Chem. Ber., 118, 2127-2133, (1985).

[52] C. Lifshitz, Org. Mass Spectrom., 23, 303-306, (1988).

[53] N. Heinrich, F. Louage, C. Lifshitz, and H. Schwarz, J. Am. Chem. Soc., 110, 8183-8192, (1988).

[54] J.L. Holmes, and J.K. Terlouw, Org. Mass Spectrom., 15, 383, (1980).

[55] N.H. Hijazi, J.L. Holmes, and J.K. Terlouw, Org. Mass Spectrom., 119-120, (1979).

[56] C.E.C.A. Hop, J.L. Holmes, and J.K. Terlouw, J. Amer. Chem. Soc., 111, 441-445, (1989).

[57] J.E. Fowler, J.M. Galbraith, G. Vacek, H.E. Schaefer III, J. Amer. Chem. Soc., 116, 9311-9319, (1994).

[58] W.J. Bouma, P.M.W. Gill, and L. Radom., Org. Mass Spectrom., 19(12), 610-616, (1984).

[59] J.C. Lorquet, Int. J. Mass Spectrom. Ion Phys., 38, 343-350, (1981).

[60] K.E. McCulloh, and V.H. Dibeler, J. Chem. Phys., 64(11), 4445-4450, (1976).

[61] R. Stockbauer, Int. J. Mass Spectrom. Ion Phys., 25, 401-410, (1977).

[62] H. Chen, and J.L. Holmes, Int. J. Mass Spectrom. Ion Process., 133, 111-119, (1994).

[63] D. Dawson, H. Chen, and J.L. Holmes, Eur. Mass Spectrom., 2, 373-375, (1996).

Appendix A. The Atomic and Molecular Term Symbols, Electronic Transitions and the Wigner-Witmer Rules

This appendix will discuss the following topics; atomic and molecular term symbols and electronic transitions [1-5], the Wigner-Witmer Correlation Rules [6-10], and Rydberg series [11].

Table A.1 illustrates the quantum numbers and they are n, l, m_l, and m_s, which denote the principal quantum number, the orbital angular momentum quantum number, the magnetic quantum number, and the spin quantum number, respectively. For example for l = 0, 1, 2,and 3, one has the s, p, d, and f orbitals, respectively. Thus, for the s, p, d, and f orbitals one has m_l = (0), (1, 0, −1), (2, 1, 0, −1, −2), and (3, 2, 1, 0, −1, −2, −3), respectively, and combined with m_s = (1/2, −1/2) the full orbitals are denoted as $(s)^2$, $(p)^6$, $(d)^{10}$, and $(f)^{14}$, respectively. Similarly, for the linear molecule (or the local symmetry of the specific bond) one has $\lambda = 0$, 1, 2, and 3, that correspond to the σ, π, δ, and ϕ orbitals, respectively. Thus, for the σ, π, δ, and ϕ orbitals one has m_λ = (0), (1, −1), (2, −2), and (3, −3), respectively, and combined with m_s = (1/2, −1/2) the full orbitals are denoted as $(\sigma)^2$, $(\pi)^4$, $(\delta)^4$, and $(\phi)^4$, respectively.

Table A.2 illustrates the atomic term symbols governed by the Russell-Saunders LS coupling scheme, and are denoted by $(nl)\ ^{(2S+1)}L_J$.

Table A.3 illustrates the atomic term symbols governed by the j–l, coupling scheme and are denoted by $(nl)\ [K]_J$.

Table A.4 illustrates the molecular term symbols governed by the Russell-Saunders ΛS coupling scheme, and are denoted by $^{(2S+1)}\Lambda_\Omega$.

Table A.6 illustrates the link between the atomic electronic states to those of the respective linear molecular electronic states.

Tables A.7-A.11 illustrate the Wigner-Witmer Correlation Rules that govern which parent molecular electronic states may be formed from the respective fragments. Briefly, the direct unimolecular dissociations of *small symmetric* molecules are governed by the Wigner-Witmer Correlation Rules as follows; (I) *conservation of symmetry*, i.e., the direct product of the electronic states of the dissociation products must contain that of the parent; and (II) *conservation of spin*, i.e., the sum of the spins of the dissociation products must contain that of the parent. Table A.7 illustrates the Wigner-Witmer Correlation Rules for the multiplicities of the separated groups. Tables A.8, and A.9 illustrate the Wigner-Witmer Correlation Rules for the molecular electronic states resulting from the identical states of the separated like atoms, and from the given states of the unlike atoms, respectively. Tables A.10, and A.11 illustrate the Wigner-Witmer Correlation Rules for the molecular electronic states resulting from the identical states of the separated equal groups, and from the given states of the unequal groups, respectively.

Now, as an illustrative example, Figure A.1 presents the potential energy curves and the lower dissociation limits of O=O [4]. Thus, the $\tilde{X}\,^3\Sigma_g^-$, $\tilde{a}\,^1\Delta_g$, $\tilde{b}\,^1\Sigma_g^+$, and $\tilde{A}\,^3\Sigma_u^+$ electronic states are shown to be related to the O[(2p) ^{3}P] + O[(2p) ^{3}P] dissociation limit, whereas the $\tilde{B}\,^3\Sigma_u^-$ electronic state is shown to be related to the O[(2p) ^{3}P] + O[(2p) ^{1}D] dissociation limit, respectively.

Lastly, a brief mention of the Rydberg orbitals [11] is merited. Rydberg orbitals, on atoms and molecules, are composed of an orbital (nl), where the principal quantum number, n, is greater than those present (either partially or fully occupied) in the ground state species.

For an atomic example, consider the $C^{+\bullet}$ that possesses an electron configuration of $(1s)^2(2s)^2(2p)$ for the ground electronic state of $(2p)\ ^2P^0$. The "ordinary" excited electronic state of $(2p)\ ^2S$ corresponds to an electron configuration $(1s)^2(2s)(2p)^2$. Whereas, the Rydberg excited electronic states of $(3s)\ ^2S$, $(3p)\ ^2P^0$, and $(3p)\ ^2D$, correspond to the electron configurations of $(1s)^2(2s)^2(3s)$, $(1s)^2(2s)^2(3p)$, and $(1s)^2(2s)^2(3d)$, respectively.

For a molecular example, consider the diatomic N≡N species possesses an electron configuration of $(1\sigma_g)^2(1\sigma_u)^2(2\sigma_g)^2(2\sigma_u)^2(1\pi_u)^4(3\sigma_g)^2$ for the ground electronic of $\tilde{X}\ ^1\Sigma_g^+$. The "ordinary" excited electronic states of $\tilde{c}\ ^3\Pi_u$, and $\tilde{b}\ ^3\Pi_g$ correspond to the electron configurations, $\ldots(2\sigma_g)^2(2\sigma_u)(1\pi_u)^4(3\sigma_g)^2(1\pi_g)$, and $\ldots(2\sigma_g)^2(2\sigma_u)^2(1\pi_u)^4(3\sigma_g)(1\pi_g)$, respectively. Whereas, the Rydberg excited electronic state of $(3s\sigma_g)\tilde{e}\ ^3\Sigma_g^+$ corresponds to the electron configuration of $\ldots(2\sigma_g)^2(2\sigma_u)^2(1\pi_u)^4(3\sigma_g)^2(3s\sigma_g)$. Thus, one should remember that a Rydberg state may act (either radiatively and/or non-radiatively) as an intermediary between the radical-cation $M_1^{+\bullet}$ and its neutral M_1 (e.g., $N{\equiv}N^{+\bullet}[\tilde{X}\ ^2\Sigma_g^+] + e^- \rightarrow N{\equiv}N[(3s\sigma_g)\tilde{e}\ ^3\Sigma_g^+] \rightarrow N{\equiv}N[\tilde{c}\ ^3\Pi_u]$).

Table A.1 The Quantum Numbers

Atomic Species

In the spherical symmetry of an atom, the atomic electron configuration quantum numbers are as follows;

n, the principal quantum number
l, the orbital angular momentum quantum number
m_l, the magnetic quantum number
m_s, the spin quantum number

where, $n = 1, 2, 3, \ldots, \infty$
$l = 0, 1, 2, \ldots, n-1$
$m_l = \{l, l-1, l-2, \ldots, 2-l, 1-l, -l\}$, i.e., there are $(2l+1)$ values
$m_s = \pm \frac{1}{2}$, (up) $\alpha = +\frac{1}{2}$, (down) $\beta = -\frac{1}{2}$, i.e., there are only two values

and, l	0	1	2	3	...
Symbol	s	p	d	f	

Molecular Species

Similarly, in the cylindrical symmetry of a linear molecule, the molecular electron configuration quantum numbers have the same designation as that of the above atomics (except l is exchanged for λ) and value save the following;

$m_\lambda = 0$, when $\lambda = 0$
$m_\lambda = (\lambda, -\lambda)$, when $\lambda \neq 0$, i.e., there are only two values

and, λ	0	1	2	3	...
Symbol	σ	π	δ	ϕ	

Table A.2 The Atomic Term Symbols I. Russell-Saunders LS Coupling

Term Symbols

For the atomic electronic states, via Russell-Saunders LS coupling, the term symbols are as follows;

$$(nl)^{(2S+1)}L_J$$

that possesses (2L + 1)(2S + 1) microstates with (2S + 1) spin components where;

L, the magnitude of the total angular momentum
S, the magnitude of the total spin
J, the magnitude of the sum of L and S projected onto the Z-axis (spherical)

and,

L	0	1	2	3	...
Symbol	S	P	D	F	

when, $L \geq S$, $J = L + S, \ldots, |L - S|$
$S > L$, $J = S + L, \ldots, |S - L|$

Selection Rules

Thus, for a single photon, the Laporte electric-dipole selection rules in hydrogenic atoms for allowed transitions are as follows;

Δn = any integer
$\Delta l = \pm 1$
$\Delta m_l = 0, \pm 1$

$\Delta L = 0, \pm 1$
$\Delta S = 0$
$\Delta J = 0, \pm 1$ (save $J' = 0 \rightarrow J'' = 0$)

Determination of Gerade (Even) and Ungerade (Uneven)

Upon reflection through the origin;
(i) an odd number of odd l, goes onto the negative of itself, thus ungerade, denoted by ^{0}
(ii) an even number of odd l, goes onto the positive of itself, thus gerade

Table A.3 The Atomic Term Symbols II. The j–l Coupling

Term Symbols

For the atomic electronic states, primarily for the *excited* electronic states of the neutral noble gases (Ne, Ar, Kr, Xe), they *can not* be described in terms of the standard Russell-Saunders LS coupling, where the excited electron strongly interacts with the inner electrons thus allowing the derivation of unique values for its quantized spin. For the neutral, the *ground* state electron configuration is full, i.e., $(ns)^2(np)^6$, and the *ground* electronic state may be classified, via Russell-Saunders LS coupling, as $^1S_0$.

Upon ionization, the radical-cation species has a ground state electron configuration of $(ns)^2(np)^5$, and a ground electronic state of $^2P^0_{3/2,\ 1/2}$ (that may as well be classified, along with their excited states, via Russell-Saunders LS coupling). However, the *difference* in the IE_a values of the $^2P^0_{3/2}$ and $^2P^0_{1/2}$ states is *not negligible* and increases with atomic number.

Therefore, when one deals with the *excited* electronic configuration of the neutral atom, $(ns)^2(np)^5(nl)$, and the resultant excited electronic states, the excited outer electron is viewed to be only loosely associated with an inner ionic core, of either $^2P^0_{3/2}$ or $^2P^0_{1/2}$ (i.e., $^2P^0_J$ were max J =3/2 or 1/2) and the concept of a unique spin is lost. Thus, another coupling scheme, known as j–l coupling, must be used. A new quantum number, known as K, is introduced and the Racah term symbols are defined as follows;

	Even l	Odd l	Coupled Core
$(ns)^2(np)^5(nl)$	$(nl)\ [K]_J$	$(nl)\ [K]^0_J$	$^2P^0_{3/2}$

$$K = \{j + l, j + l - 1, \ldots, |\, j - l \,|\}$$
$$J = \{K + 1/2\ , K - 1/2\},\ \text{e.g.,}\ (1,0)\ ,\ (2,1)$$

$(ns)^2(np)^5(nl')$	$(nl')\ [K]_J$	$(nl')\ [K]^0_J$	$^2P^0_{1/2}$

$$K = \{j + l, j + l - 1, \ldots, |\, j - l \,|\}$$
$$J = \{K - 1/2\ , K + 1/2\},\ \text{e.g.,}\ (0,1)\ ,\ (1,2)$$

Selection Rules

The selection rules and quantum numbers here have the same designation (except there is no S) and values as those of Russell-Saunders coupling (see previous table), save that of K as follows;

$$K = 0, \pm 1, \pm 2$$

Table A.4 The Molecular Term Symbols I. Russell-Saunders ΛS Coupling

Term Symbols

For the linear molecular electronic states, via Russell-Saunders ΛS coupling, the term symbols are as follows;

$$^{(2S+1)}\Lambda_{\Omega}$$

that possess (1)(2S + 1) for Σ, and (2)(2S + 1) for Π, Δ, Φ, ..., microstates, with (2S + 1) spin components where,

Λ, the magnitude of the total orbital angular monentum
S, the magnitude of the total spin
Ω, the magnitude of the sum of Λ and S projected onto the Z-axis (Cylindrical, molecular axis)

and,

Λ	0	1	2	3	...
Symbol	Σ	Π	Δ	Φ	

when, $\Lambda \geq S$, $\Omega = \Lambda + S, \ldots, |\Lambda - S|$
$\Lambda = 0$, $\Omega = S$
$S > \Lambda$, $\Omega = \Lambda + S, \ldots, \Lambda - S$

Selection Rules

Thus, the Laporte electric-dipole allowed transitions among the energy levels are determined via the following selection rules;

$\Delta\Lambda = 0, \pm 1$, i.e., Σ–Σ, Π–Σ, Δ–Π
$\Delta S = 0$
$\Delta\Omega = 0, \pm 1$
$+ \Leftrightarrow +, - \Leftrightarrow -$, i.e., Σ^-–Σ^-, Σ^+–Σ^+, Π–Σ^-, Π–Σ^+, (reflection in the ZX-plane) due to μ_Z being Σ^+
$g \Leftrightarrow u$, gerade (even) ⇔ ungerade (uneven)

Determination Gerade (Even), Ungerade (Uneven); and Σ^+, Σ^-

Upon inversion ($i = \sigma_h C_2$) along the molecular Z-axis;
(i) an orbital that goes onto the positive of itself, thus a subscript g denotes gerade
(ii) an orbital that goes onto the negative of itself, thus a subscript u denotes ungerade

Upon reflection (σ_v(ZX)) in the ZX-plane[a];
(i) a π-orbital that goes onto the positive of itself, thus is denoted by Σ^+
(ii) a π-orbital that goes onto the negative of itself, thus is denoted by Σ^-

[a]All σ-orbitals have a symmetry of Σ^+.

Table A.5 The Molecular Term Symbols II. Non-Linear Polyatomics

Term Symbols[a]

The Mulliken term symbols for the polyatomic molecules are determined as follows;

(I) All one-dimensional (i.e., a 1x1 matrix, $\chi(E)=1$) representations are designated A or B; two-dimensional (i.e., a 2x2 matrix, $\chi(E)=2$) representations are designated E; and three-dimensional (i.e., a 3x3 matrix, $\chi(E)=3$) representations are designated T.

For the one-dimensional representations (i.e., the sum of the diagonal elements, known as the trace of the identity matrix, $\chi(E)=1$) the following applies,

(II) One-dimensional representations that are symmetric with respect to rotation by $(2\pi)/n$ about the principal C_n axis (symmetric meaning $\chi(C_n)=1$) are designated A, whilst those antisymmetric in this respect ($\chi(C_n)=-1$) are designated B.

(III) Subscripts 1 and 2 are usually attached to the A and B representations to designate those which are ,respectively, symmetric and antisymmetric with respect to a C_2 (i.e., a rotation by 180^0) perpendicular to the principal axis or, if such a C_2 axis is lacking, to a vertical plane of symmetry, σ_v.

(IV) Primes, /, and double primes, //, are superscripted to all letters, when appropriate, to indicate those which are, respectively, symmetric and antisymmetric with respect to σ_h (i.e., a reflection in the plane perpendicular to C_n).

(V) In a group with a centre of inversion (i.e., $i=\sigma_h C_2$, a rotation by 180^0 about C_n and then a reflection through as plane perpendicular to C_n), the subscript g (from the German gerade meaning even) is attached to the symbols for representations which are symmetric with to inversion, and the subscript u (from the German ungerade, meaning uneven) is used for those which are antisymmetric to inversion.

(VI) The use of numerical subscripts for the E and the T representations also follow certain rules, but these can not be easily stated precisely without some further mathematical development. It will be satisfactory here to regard them as arbitrary labels.

Selection Rules

The Laporte electric-dipole allowed transitions (with $\Delta S=0$) in a point group are governed by the direct product (from the character table) of the upper and lower electronic states as follows;

(upper state)$\otimes$(lower state) = representation that transforms as X, Y, or Z

[a]Ref. [5], pp. 90-91.

Table A.6 The Link Between the Atomic and Linear Molecular States

Atomic Electronic State	Linear Molecular Electronic States
S	Σ^+
S^0	Σ^-
P	Π, Σ^-
P^0	Π, Σ^+
D	Δ, Π, Σ^+
D^0	Δ, Π, Σ^-
F	$\Phi, \Delta, \Pi, \Sigma^-$
F^0	$\Phi, \Delta, \Pi, \Sigma^+$

Table A.7 The Wigner-Witmer Correlation Rules for the Multiplicities (2S + 1) of the Molecular Electronic States Resulting from the Given Multiplicities of the Separated Atoms and/or Groups[a]

Separated Atoms and/or Groups	Resultant Molecule
1 + 1	1
1 + 2	2
1 + 3	3
2 + 2	1, 3
2 + 3	2, 4
2 + 4	3, 5
3 + 3	1, 3, 5
3 + 4	2, 4, 6
4 + 4	1, 3, 5, 7

[a]Multiplicities are (2S + 1) where, 1, 2, 3, 4, 5, 6, and 7 denote a singlet, doublet, triplet, quartet, sextet, and septet, repectively, and S is the total spin.

Table A.8 The Wigner-Witmer Correlation Rules for the Molecular Electronic States Resulting from Identical States of the Separated Like Atoms

Electronic States of the Separated Atoms	Electronic States of the Linear Molecule
$^1S + {}^1S$ or $^1S^0 + {}^1S^0$	$^1\Sigma_g^+$
$^2S + {}^2S$ or $^2S^0 + {}^2S^0$	$^3\Sigma_u^+$, $^1\Sigma_g^+$
$^3S + {}^3S$ or $^3S^0 + {}^3S^0$	$^5\Sigma_g^+$, $^3\Sigma_u^+$, $^1\Sigma_g^+$
$^4S + {}^4S$ or $^4S^0 + {}^4S^0$	$^7\Sigma_u^+$, $^5\Sigma_g^+$, $^3\Sigma_u^+$, $^1\Sigma_g^+$
$^1P + {}^1P$ or $^1P^0 + {}^1P^0$	$^1\Delta_g$, $^1\Pi_g$, $^1\Pi_u$, $^1\Sigma_g^+(2)$, $^1\Sigma_u^-$
$^2P + {}^2P$ or $^2P^0 + {}^2P^0$	$^3\Delta_u$, $^1\Delta_g$, $^3\Pi_g$, $^3\Pi_u$, $^1\Pi_g$, $^1\Pi_u$, $^3\Sigma_u^+(2)$, $^3\Sigma_g^-$, $^1\Sigma_g^+(2)$, $^1\Sigma_u^-$
$^3P + {}^3P$ or $^3P^0 + {}^3P^0$	$^5\Delta_g$, $^3\Delta_u$, $^1\Delta_g$, $^5\Pi_g$, $^5\Pi_u$, $^3\Pi_g$, $^3\Pi_u$, $^1\Pi_g$, $^1\Pi_u$, $^5\Sigma_g^+(2)$, $^5\Sigma_u^-$, $^3\Sigma_u^+(2)$, $^3\Sigma_g^-$, $^1\Sigma_g^+(2)$, $^1\Sigma_u^-$
$^1D + {}^1D$ or $^1D^0 + {}^1D^0$	$^1\Gamma_g$, $^1\Phi_g$, $^1\Phi_u$, $^1\Delta_g(2)$, $^1\Delta_u$, $^1\Pi_g(2)$, $^1\Pi_u(2)$, $^1\Sigma_g^+(3)$, $^1\Sigma_u^-(2)$
$^2D + {}^2D$ or $^2D^0 + {}^2D^0$	$^3\Gamma_u$, $^1\Gamma_g$, $^3\Phi_g$, $^3\Phi_u$, $^1\Phi_g$, $^1\Phi_u$, $^3\Delta_u(2)$, $^3\Delta_g$, $^1\Delta_g(2)$, $^1\Delta_u$, $^3\Pi_g(2)$, $^3\Pi_u(2)$, $^1\Pi_g(2)$, $^1\Pi_u(2)$, $^3\Sigma_u^+(3)$, $^3\Sigma_g^-(2)$, $^1\Sigma_g^+(3)$, $^1\Sigma_u^-(2)$
$^3D + {}^3D$ or $^3D^0 + {}^3D^0$	$^5\Gamma_g$, $^3\Gamma_u$, $^1\Gamma_g$, $^5\Phi_g$, $^5\Phi_u$, $^3\Phi_g$, $^3\Phi_u$, $^1\Phi_g$, $^1\Phi_u$, $^5\Pi_g(2)$, $^5\Pi_u(2)$, $^3\Pi_g(2)$, $^3\Pi_u(2)$, $^1\Pi_g(2)$, $^1\Pi_u(2)$, $^5\Sigma_g^+(3)$, $^3\Sigma_u^-(2)$, $^3\Sigma_u^+(3)$, $^3\Sigma_g^-(2)$, $^1\Sigma_g^+(3)$, $^1\Sigma_u^-(2)$

Table A.9 The Wigner-Witmer Correlation Rules for the Molecular Electronic States Resulting from the Given States of Separated Unlike Atoms

Electronic States of the Separated Atoms	Electronic States of the Linear Molecule
$S + S$ or $S^0 + S^0$	Σ^+
$S + S^0$	Σ^-
$S + P$ or $S^0 + P^0$	Π, Σ^-
$S + P^0$ or $S^0 + P$	Π, Σ^+
$S + D$ or $S^0 + D^0$	Δ, Π, Σ^+
$S + D^0$ or $S^0 + D$	Δ, Π, Σ^-
$S + F$ or $S^0 + F^0$	$\Phi, \Delta, \Pi, \Sigma^-$
$S + F^0$ or $S^0 + F$	$\Phi, \Delta, \Pi, \Sigma^+$
$P + P$ or $P^0 + P^0$	$\Delta, \Pi(2), \Sigma^+(2), \Sigma^-$
$P + P^0$	$\Delta, \Pi(2), \Sigma^+, \Sigma^-(2)$
$P + D$ or $P^0 + D^0$	$\Phi, \Delta(2), \Pi(3), \Sigma^+, \Sigma^-(2)$
$P + D^0$ or $P^0 + D$	$\Phi, \Delta(2), \Pi(3), \Sigma^+(2), \Sigma^-$
$P + F$ or $P^0 + F^0$	$\Gamma, \Phi(2), \Delta(3), \Pi(3), \Sigma^+(2), \Sigma^-$
$P + F^0$ or $P^0 + F$	$\Gamma, \Phi(2), \Delta(3), \Pi(3), \Sigma^+, \Sigma^-(2)$
$D + D$ or $D^0 + D^0$	$\Gamma, \Phi(2), \Delta(3), \Pi(4), \Sigma^+(3), \Sigma^-(2)$
$D + D^0$	$\Gamma, \Phi(2), \Delta(3), \Pi(4), \Sigma^+(2), \Sigma^-(3)$
$D + F$ or $D^0 + F^0$	$H, \Gamma(2), \Phi(3), \Delta(4), \Pi(5), \Sigma^+(3), \Sigma^-(2)$
$D + F^0$ or $D^0 + F$	$H, \Gamma(2), \Phi(3), \Delta(4), \Pi(5), \Sigma^+(2), \Sigma^-(3)$

Table A.10 The Wigner-Witmer Correlation Rules for the Electronic States of the Linear Molecules Resulting from the Identical States of the Separated Equal Groups

Electronic States of the Separated Groups	Electronic States of the Linear Molecule
$^1\Sigma^+ + {}^1\Sigma^+$ or $^1\Sigma^- + {}^1\Sigma^-$	$^1\Sigma_g^+$
$^2\Sigma^+ + {}^2\Sigma^+$ or $^2\Sigma^- + {}^2\Sigma^-$	$^3\Sigma_u^+, {}^1\Sigma_g^+$
$^3\Sigma^+ + {}^3\Sigma^+$ or $^3\Sigma^- + {}^3\Sigma^-$	$^5\Sigma_g^+, {}^3\Sigma_u^+, {}^1\Sigma_g^+$
$^4\Sigma^+ + {}^4\Sigma^+$ or $^4\Sigma^- + {}^4\Sigma^-$	$^7\Sigma_u^+, {}^5\Sigma_g^+, {}^3\Sigma_u^+, {}^1\Sigma_g^+$
$^1\Pi + {}^1\Pi$	$^1\Delta_g, {}^1\Sigma_g^+, {}^1\Sigma_u^-$
$^2\Pi + {}^2\Pi$	$^3\Delta_u, {}^1\Delta_g, {}^3\Sigma_u^+, {}^3\Sigma_g^-, {}^1\Sigma_g^+, {}^1\Sigma_u^-$
$^3\Pi + {}^3\Pi$	$^5\Delta_g, {}^3\Delta_u, {}^1\Delta_g, {}^5\Sigma_g^+, {}^5\Sigma_u^-, {}^3\Sigma_u^+, {}^3\Sigma_g^-, {}^1\Sigma_g^+, {}^1\Sigma_u^-$
$^1\Delta + {}^1\Delta$	$^1\Gamma_g, {}^1\Sigma_g^+, {}^1\Sigma_u^-$
$^2\Delta + {}^2\Delta$	$^3\Gamma_u, {}^1\Gamma_g, {}^3\Sigma_u^+, {}^3\Sigma_g^-, {}^1\Sigma_g^+, {}^1\Sigma_u^-$
$^3\Delta + {}^3\Delta$	$^5\Gamma_g, {}^3\Gamma_u, {}^1\Gamma_g, {}^5\Sigma_g^+, {}^5\Sigma_u^-, {}^3\Sigma_u^+, {}^3\Sigma_g^-, {}^1\Sigma_g^+, {}^1\Sigma_u^-$

Table A.11 The Wigner-Witmer Correlation Rules for the Electronic States of the Linear Molecules Resulting from the Given States of the Separated Unequal Groups

Electronic States of the Separated Groups	Electronic States of the Linear Molecule
$S + \Sigma^+$ or $S^0 + \Sigma^-$	Σ^+
$S + \Sigma^-$ or $S^0 + \Sigma^+$	Σ^-
$S + \Pi$ or $S^0 + \Pi$	Π
$S + \Delta$ or $S^0 + \Delta$	Δ
$P + \Sigma^+$ or $P^0 + \Sigma^-$	Π, Σ^-
$P + \Sigma^-$ or $P^0 + \Sigma^+$	Π, Σ^+
$P + \Pi$ or $P^0 + \Pi$	$\Delta, \Pi, \Sigma^+, \Sigma^-$
$P + \Delta$ or $P^0 + \Delta$	Φ, Δ, Π
$D + \Sigma^+$ or $D^0 + \Sigma^-$	Δ, Π, Σ^+
$D + \Sigma^-$ or $D^0 + \Sigma^+$	Δ, Π, Σ^-
$D + \Pi$ or $D^0 + \Pi$	$\Phi, \Delta, \Pi(2), \Sigma^+, \Sigma^-$
$D + \Delta$ or $D^0 + \Delta$	$\Gamma, \Phi, \Delta, \Pi, \Sigma^+, \Sigma^-$
$\Sigma^+ + \Sigma^+$ or $\Sigma^- + \Sigma^-$	Σ^+
$\Sigma^+ + \Sigma^-$	Σ^-
$\Sigma^+ + \Pi$ or $\Sigma^- + \Pi$	Π
$\Sigma^+ + \Delta$ or $\Sigma^- + \Delta$	Δ
$\Pi + \Pi$	$\Delta, \Sigma^+, \Sigma^-$
$\Pi + \Delta$	Φ, Π
$\Delta + \Delta$	$\Gamma, \Sigma^+, \Sigma^-$

Figure A.1 The Potential Energy Curves and Lower Dissociation Limits of O_2

O=O

$(2\sigma_g)^2(2\sigma_u)^2(3\sigma_g)^2(1\pi_u)^4(1\pi_g)^2$

$(2\sigma_g)^2(2\sigma_u)^2(3\sigma_g)^2(1\pi_u)^3(1\pi_g)^3$

Electronic States

$\tilde{X}\,^3\Sigma_g^-$, $\tilde{a}\,^1\Delta_g$, $\tilde{b}\,^1\Sigma_g^+$
$\tilde{A}\,^3\Sigma_u^+$, $\tilde{B}\,^3\Sigma_u^-$, $^3\Delta_u$
$^1\Sigma_u^+$, $^1\Sigma_u^-$, $^1\Delta_u$

Dissociation Products	**Possible Species**
$O[(2p)\,^3P] + O[(2p)\,^3P]$	$^5\Delta_g$, $^3\Delta_u$, $\tilde{a}\,^1\Delta_g$, $^5\Pi_g$, $^5\Pi_u$, $^3\Pi_g$, $^3\Pi_u$ $^1\Pi_g$, $^1\Pi_u$, $^5\Sigma_g^+(2)$, $^5\Sigma_u^-$, $\tilde{A}\,^3\Sigma_u^+$, Σ_u^+ $\tilde{X}\,^3\Sigma_g^-$, $\tilde{b}\,^1\Sigma_g^+$, $^1\Sigma_g^+$, $^1\Sigma_u^-$
$O[(2p)\,^3P] + O[(2p)\,^1D]$	$^3\Phi_g$, $^3\Phi_u$, $^3\Delta_g(2)$, $^3\Delta_u(2)$, $^3\Pi_g(3)$, $^3\Pi_u(3)$, $^3\Sigma_g^+$, $^3\Sigma_u^+$, $^3\Sigma_g^-(2)$, $\tilde{B}\,^3\Sigma_u^-$ $^3\Sigma_u^-$

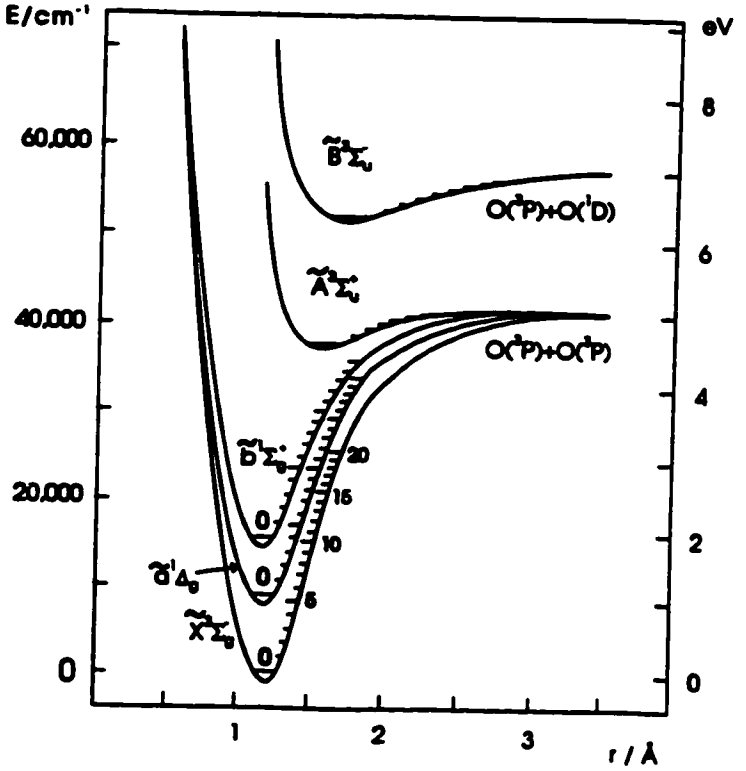

The low-lying electronic states of the O_2 molecule.

A.2 References

[1] G. Herzberg, Atomic Spectra and Atomic Structure, Dover Publishing, New York, New York, USA, (1944)

[2] W.L. Wiese, M.W. Smith, and B.N. Miles, Atomic Transition Probabilites, Vol. II, NSRDS-NRS 22, Washington DC, USA, (1969).

[3] W.C. Martin, R. Zalubbas, and L. Hagan, Atomic Energy Levels-The Rare Earth Elements, NSRDS-NRS 60, US Government Printing Office, Washington DC, USA, (1978).

[4] P.F. Bernath, The Spectra of Atoms and Molecules, Oxford University Press Inc., New York, New York, USA, (1995).

[5] F.A. Cotton, Chemical Applications of Group Theory, 3rd Ed., John Wiley and Sons, New York, New York, USA, (1990).

[6] G. Herzberg, Molecular Spectra and Molecular Structure I. Spectra of Diatomic Molecules, Van Nostrand Reinhold Company, New York, New York, USA, (1950).

[7] G. Herzberg, Molecular Spectra and Molecular Structure II. Infrared and Raman Spectra of Polyatomic Molecules, D. Van Nostrand Company, New York, New York, USA, (1945).

[8] G. Herzberg, Molecular Spectra and Molecular Structure III. Electronic Spectra and Electronic Structure of Polyatomic Molecules, Van Nostrand Company, New York, New York, USA, (1966).

[9] J.H.D. Eland, Photoelectron Spectroscopy. An Introduction to Ultraviolet Photoelectron Spectroscopy in the Gas Phase, Butterworths, London, UK, (1974).

[10] J.H.D. Eland, Photoelectron Spectroscopy. An Introduction to Ultraviolet Photoelectron Spectroscopy in the Gas Phase, 2nd, Butterworths, London, UK, (1984).

[11] A.B.F. Duncan, Rydberg Series in Atoms and Molecules, Academic Press Inc., New York, New York, USA, (1971).

Appendix B. The Non-Crossing Rule, Walsh's Rules, and the Renner-Teller Theorem

This appendix will discuss the following topics; the Non-Crossing rule [1-7], Walsh's Rules [1-8], and the Renner-Teller Theorem [1-9]. Additionally, two illustrative examples, namely O=C=O, and O=C=C=O [10, 11], will be presented here to explore the forces at work that govern the interaction between their linear and bent forms.

Figure B.1 illustrates the Non-Crossing Rules that states it is forbidden for the potential energy curves/surfaces of two electronic states of the same symmetry to cross. There will always be a mixing of the wavefunctions of the two electronic states such that they undergo an avoided crossing. For example, the $\tilde{X}\,^2\Sigma^+$ and $\tilde{B}\,^2\Sigma^+$ electronic states of $C{\equiv}O^{+\bullet}$ are of the same symmetry and thus can not cross each-other. Therefore, this results in the separate dissociation processes of $C{\equiv}O^{+\bullet}[\,\tilde{X}\,^2\Sigma^+] \rightarrow C^{+\bullet}[(2p)\,^2P^0] + O[(2p)\,^3P]$ of lower energy, and $C{\equiv}O^{+\bullet}[\,\tilde{B}\,^2\Sigma^+] \rightarrow C^{+\bullet}[(2p)\,^2P^0] + O[(2p)\,^1D]$ of higher energy, respectively. Additionally, one should consider the $O{=}C{=}C{=}O[\,\tilde{X}\,^3\Sigma_g^-] \rightarrow C{\equiv}O[\,\tilde{a}\,^3\Pi] + C{\equiv}O[\,\tilde{X}\,^1\Sigma^+]$ dissociation process. Through the application of the Wigner-Witmer Correlation Rules [3-7], the *linear* dissociation process is spin allowed but symmetry forbidden. One would predict that both the $\tilde{X}\,^3\Sigma_g^-$ and $\tilde{B}\,^3\Sigma_u^-$ electronic states of O=C=C=O should dissociate into $C{\equiv}O[\,\tilde{e}\,^3\Sigma^-] + C{\equiv}O[\,\tilde{X}\,^1\Sigma^+]$ (and $\tilde{B}\,^3\Sigma_u^-$ in fact does). Now, to circumvent this situation, the ground electronic state species $O{=}C{=}C{=}O[\,\tilde{X}\,^3\Sigma_g^-]$ can trans-bend (setting up a vibrational resonance) and undergo vibronic mixing (i.e., the mixing of the vibrational and electronic states) with an excited state species $O{=}C{=}C{=}O[^3\Pi_g]$. Therefore, an avoided crossing between $O{=}C{=}C{=}O[\,\tilde{X}\,^3\Sigma_g^-]$ and $O{=}C{=}C{=}O[^3\Pi_g]$ may occur, resulting in concomitant

dissociation processes of O=C=C=O[$\tilde{X}\,^3\Sigma_g^-$] → C≡O[$\tilde{a}\,^3\Pi$] + C≡O[$\tilde{X}\,^1\Sigma^+$] of lower energy, and O=C=C=O[$^3\Pi_g$] → C≡O[$\tilde{e}\,^3\Sigma^-$] + C≡O[$\tilde{X}\,^1\Sigma^+$] of higher energy, respectively.

Figure B.2 illustrates Walsh's Rules which state that a molecule will distort from a geometry of higher symmetry (e.g., linear, planar) to one of lower symmetry (e.g., non-linear, non-planar) to maximize its molecular orbital overlap in order to minimize its total energy (bonding, non-bonding, anti-bonding). On inspection of Figure B.2, one may see the following; the (I) bonding orbitals are stabilizing (i.e., repulsive to bending), due to them possessing maximum positive (additive) overlap, and thus favour high symmetry; the (II) non-bonding orbitals are localized and non-interacting (i.e., no change to bending), due to them possessing no overlap; and the (III) anti-bonding orbitals are destabilizing (i.e., attractive to bending), due to them possessing negative (subtractive) overlap, and thus favour low symmetry.

Figure B.3 illustrates the bending of the O=C=O frontier π-orbitals. Generally, on going for a linear $D_{\infty h}$ to a bent $C_{\infty v}$ symmetry, the orbital symmetries transform as follows; $(\sigma_g)^2 \rightarrow (a_1)^2$, $(\sigma_u)^2 \rightarrow (b_2)^2$, $(\pi_u)^4 \rightarrow (a_1)^2(b_1)^2$, and $(\pi_g)^4 \rightarrow (a_2)^2(b_2)^2$. Thus, one may see that the $(1\pi_u)^4(1\pi_g)^4$ electron configuration of O=C=O[$\tilde{X}\,^1\Sigma_g^+$] is destabilized by bending and thus retains its linear symmetry [10]. However, one may see that the $(1\pi_u)^4(1\pi_g)^3(2\pi_u)$ electron configuration of O=C=O[$^3\Delta_u$] is stabilized by bending and in fact may be proposed to undergo *rapid* dissociation into C≡O[$\tilde{a}\,^3\Pi$] + O[(2p) ^{3}P] and/or C≡O[$\tilde{d}\,^3\Delta$] + O[(2p) ^{3}P].

Figure B.4 illustrates the trans-bending of the O=C=C=O frontier π-orbitals. Generally, on going for a linear $D_{\infty h}$ to a trans-bent C_{2h} symmetry, the orbital symmetries transform as follows; $(\sigma_g)^2 \rightarrow (a_g)^2$, $(\sigma_u)^2 \rightarrow (b_u)^2$, $(\pi_u)^4 \rightarrow (a_u)^2(b_u)^2$, and $(\pi_g)^4 \rightarrow (a_g)^2(b_g)^2$.

Thus, one may see that the $(1\pi_u)^4(1\pi_g)^4(2\pi_u)^2$ electron configuration of O=C=C=O[$\tilde{X}\,^3\Sigma_g^-$] is destabilized by (either trans C_{2h}, or cis C_{2v}) bending and thus retains its linear symmetry [11] (via the balancing effect of the $(2a_u)(6b_u)$ components of $(2\pi_u)^2$). However, upon ionization, the $(1\pi_u)^4(1\pi_g)^4(2\pi_u)$ electron configuration of O=C=C=O$^{+\bullet}$[$\tilde{X}\,^2\Pi_u$] may be somewhat (transitorily) stabilized by the trans-bending of $(6b_u)$. This may result in a rapid "flip-flop" between the linear ($^2\Pi_u$) and the trans-bent (^2B_u) geometries. Thus, one may regard the presence of these rapid bending and straightening processes to impart a *dynamically-linear* (momentarily bent) quasi-linear O=C=C=O$^{+\bullet}$[$\tilde{X}\,^2\Pi_u(^2B_u)$] structure. This dynamically-linear (i.e., quasi-linear) terminology is a result of the barrier height to bending and results in the discussion of the Renner-Teller Theorem presented below.

Figure B.5 illustrates the Renner-Teller Theorem which states that a linear molecule (i.e., $D_{\infty h}$, $C_{\infty v}$) which possesses a non-zero (i.e., not a single component Σ) orbital angular momentum (i.e., a double component Π, Δ, Φ, Γ,...) will experience dynamic (momentary) and/or dynamic (permanent) distortions in an effort to reduce this degeneracy. On inspection of Figure B.5, one may see present the three general cases of low (static-linear), moderate (*dynamic* linear-bent) and strong (static-bent) Renner-Teller distortions. In all three cases, the vibrational energy $\tilde{\upsilon}\,(cm^{-1})$ of lower potential energy curve component, V^-, and the higher energy potential energy component, V^+, are of similar or the same value [9].

For the low Renner-Teller Distortion case, both of the V^-, and V^+ components are repulsive to bending and there is a single potential well, both components are undistorted, and the species is statically linear (e.g., O=C=O$^{+\bullet}$[$\tilde{X}\,^2\Pi_g$]).

For the moderate Renner-Teller distortion case, one (or both) of the V^-, and V^+ components is (are) slightly attractive to bending. Here, the V^- component exhibits a slight

distortion producing a double potential well with a *small barrier*. The V^+ component is undistorted and exhibits a single potential well. Since the barrier between the double wells of V^- is small, the molecule rapidly "hops" between the two, and its considered to be dynamically-linear (i.e., quasi-linear, e.g., $OH_2^{+\bullet}[\,\tilde{A}\,^2A_1(^2\Pi_u)]$, $O{=}C{=}C{=}O^{+\bullet}[\,\tilde{X}\,^2\Pi_u(^2B_u)]$, and $O{=}C{=}C{=}O^{-\bullet}[\,\tilde{X}\,^2\Pi_u(^2A_u)]$).

Lastly, for the strong Renner-Teller distortion case, both of the V^-, and V^+ components are strongly attractive to bending. Thus, they both exhibit strong distortions and each possess a double potential well with a *large barrier*, and is considered to be statically bent (e.g., $CF_2^{+\bullet}[\,\tilde{X}\,^2A_1]$).

Therefore, in conclusion one should consider the qualitative aids of Walsh's Rules and the Renner-Teller Theorem when one critically reviews the quantitative results of quantum-mechanical ab initio calculation studies that attempt to determine the equilibrium geometry of a species (e.g., linear or bent, planar or non-planar).

Figure B.1 The Non-Crossing Rule

It is forbidden for the potential energy curves/surfaces of two electronic states of the same symmetry to cross. There will always be a mixing of the wavefunctions of the two electronic states such that they undergo an avoided-crossing.

An Avoided-Crossing of Two Bound Electronic States

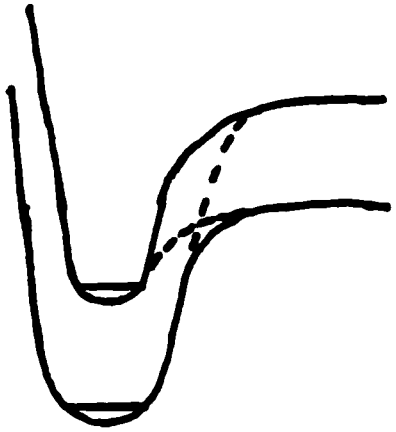

An Avoided-Crossing of a Bound and an Unbound Electronic State

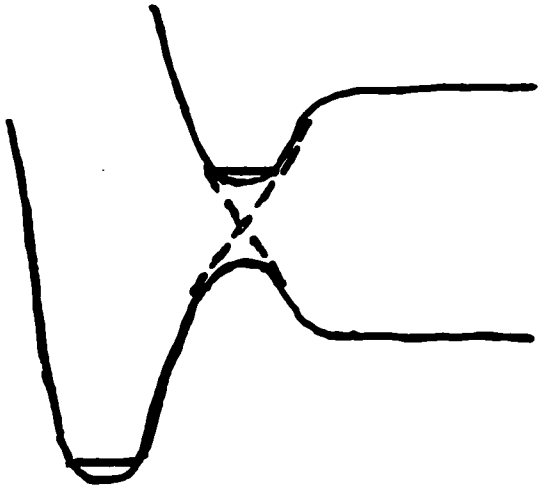

Figure B.2 Walsh's Rules

A molecule will distort from a geometry of high symmetry (e.g., linear, planar) to one of lower symmetry (e.g., non-linear, non-planar) to maximize its molecular-orbital overlap in order to minimize its total energy (bonding, non-bonding, anti-bonding).

(I) **Bonding Orbitals** are stabilizing, favour high symmtery

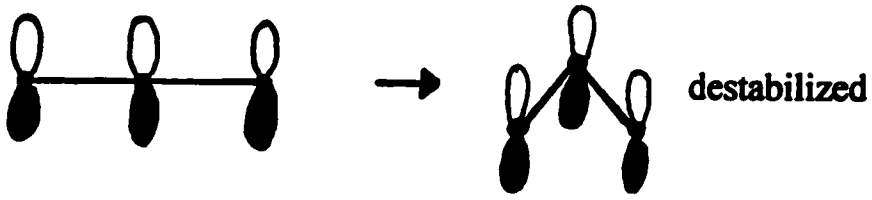

(II) **Non-Bonding Orbitals** are localized, non-interacting

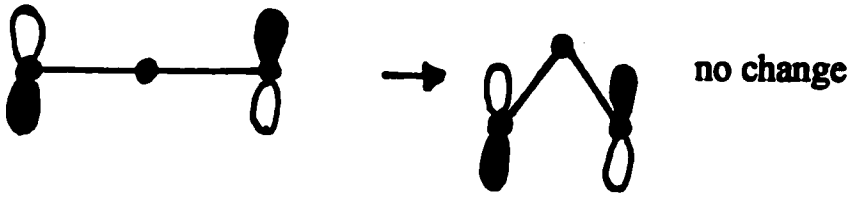

(III) **Anti-Bonding Orbitals** are destabilizing, favour low symmetry

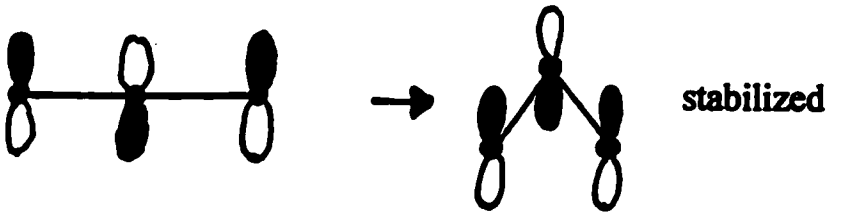

Figure B.3 The Bending of the O=C=O Frontier π-Orbitals

$\ldots(4\sigma_g)^2(3\sigma_u)^2(1\pi_u)^4(1\pi_g)^4(2\pi_u)^0$ $\quad\quad$ $\tilde{X}\,^1\Sigma_g^+$

Linear, $D_{\infty h}$		**Bent, C_{2v}**
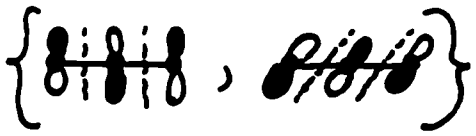		
$(2\pi_u)$	$(2b_1)$	$(6a_1)$
		
$(1\pi_g)$	$(1a_2)$	$(4b_2)$
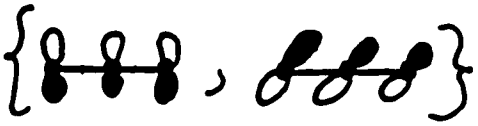		
$(1\pi_u)$	$(1b_1)$	$(5a_1)$

Figure B.4 The Trans-bending of the O=C=C=O Frontier Orbitals

$\cdots(4\sigma_u)^2(5\sigma_g)^2(1\pi_u)^4(1\pi_g)^4(2\pi_u)^2(2\pi_g)^0$ $\quad \tilde{X}\,^3\Sigma_g^-$

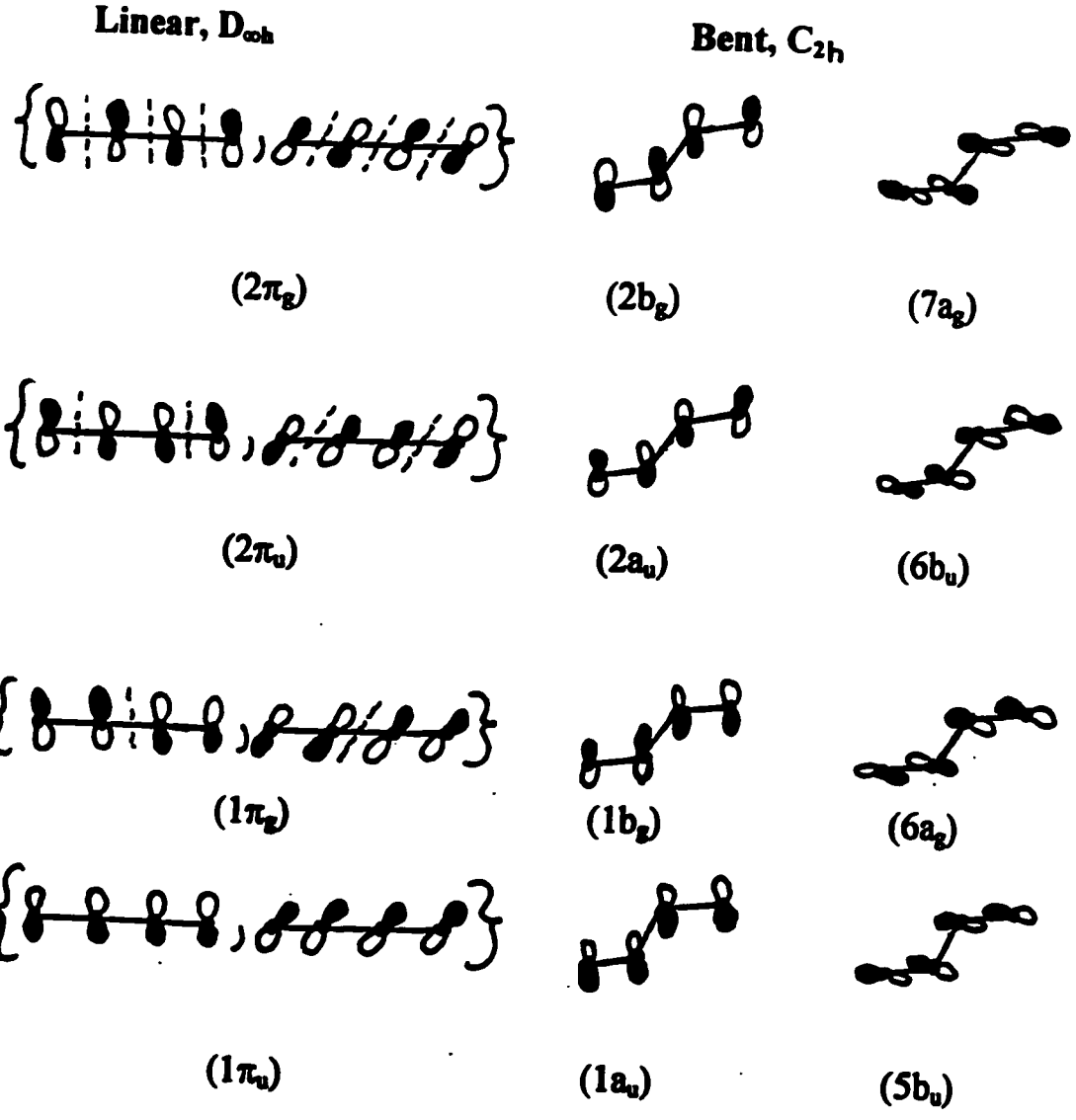

Figure B.5 The Renner-Teller Theorem

A linear molecule (i.e., $D_{\infty h}$, $C_{\infty v}$), which possesses a non-zero (i.e., not Σ) orbital angular momentum (i..e., Π, Δ, Φ, Γ, ...) will experience dynamic (momentary) and/or static (permanent) distortions in its geometry in an effort to reduce this degeneracy.

Low Renner-Teller Distortion (Static-linear)

–single potential well.

–both components undistorted.

–e.g., $O{=}C{=}O^{+\bullet}[\tilde{X}\,^2\Pi_g]$

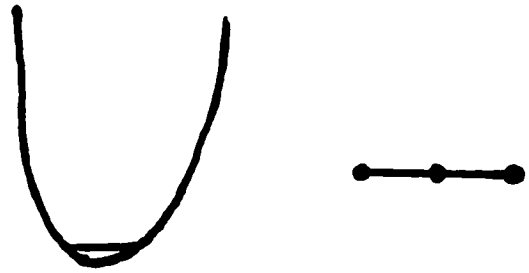

Moderate Renner-Teller Distortion (Dynamic-Linear/Bent)

–double potential well.

–one or both components distorted.

–*small* barrier between double wells.

–e.g., $OH_2^{+\bullet}[\tilde{A}\,^2A_1(^2\Pi_u)]$
, $O{=}C{=}C{=}O^{+\bullet}[\tilde{X}\,^2\Pi_u(^2B_u)]$
, $O{=}C{=}C{=}O^{-\bullet}[\tilde{X}\,^2\Pi_u(^2A_u)]$

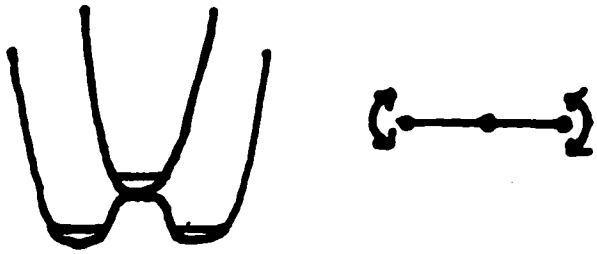

Strong Renner-Teller Distortion (Static- Bent)

–double potential well.

–both components distorted.

–*large* barrier between double wells.

–e.g., $CF_2^{+\bullet}[\tilde{X}\,^2A_1]$

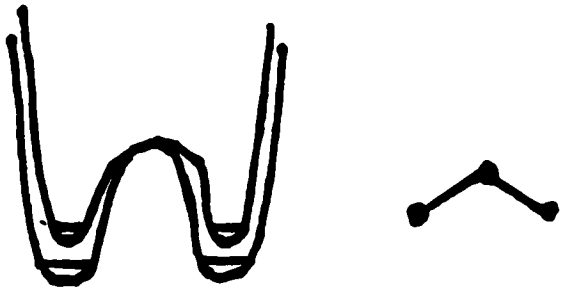

B.2 References

[1] P.F. Bernath, The Spectra of Atoms and Molecules, Oxford University Press Inc., New York, New York, USA, (1995).

[2] F.A. Cotton, Chemical Applications of Group Theory, 3rd Ed., John Wiley and Sons, New York, New York, USA, (1990).

[3] G. Herzberg, Molecular Spectra and Molecular Structure I. Spectra of Diatomic Molecules, Van Nostrand Reinhold Company, New York, New York, USA, (1950).

[4] G. Herzberg, Molecular Spectra and Molecular Structure II. Infrared and Raman Spectra of Polyatomic Molecules, D. Van Nostrand Company, New York, New York, USA, (1945).

[5] G. Herzberg, Molecular Spectra and Molecular Structure III. Electronic Spectra and Electronic Structure of Polyatomic Molecules, Van Nostrand Company, New York, New York, USA, (1966).

[6] J.H.D. Eland, Photoelectron Spectroscopy. An Introduction to Ultraviolet Photoelectron Spectroscopy in the Gas Phase, Butterworths, London, UK, (1974).

[7] J.H.D. Eland, Photoelectron Spectroscopy. An Introduction to Ultraviolet Photoelectron Spectroscopy in the Gas Phase, 2nd, Butterworths, London, UK, (1984).

[8] A.D. Walsh, "The Electronic Orbitals, Shapes and Spectra of Polyatomic Molecules Part(s) I-X", J. Chem. Soc., 2260-2331, (1953).

[9] T.J. Lee, D.J. Lee, H.F. Schaefer III, and P.M. Pitzer, "Analytic Second Derivatives for Renner-Teller Potential Energy Surfaces. Examples of Five Distinct Cases", J. Chem. Phys., 81(1), 356-361, (1984).

[10] S.V. Filseth, "Vapour Phase Photochemistry of the Neutral Oxides and Sulphides of Carbon", Adv. Photochem., 10, 1-57, (1977).

[11] R.C. Haddon, D. Poppinger, and L. Radom, "An Ab Initio Molecular Orbital Study of Ethenedione", J. Am. Chem. Soc., 97(7), 1645-1649, (1975).

Appendix C. Comments on Benson's Rules of Additivity and the Proposed Cation Order of Stability.

This appendix will discuss the following topics; Benson's Rules of Additivity, and the proposed cation order of stability.

As well, the purpose of this appendix is to present, in one location for the reader, a collection of the most relevant literature sources of the compilations of thermochemical data [1-3], Benson's Rules of Additivity [4-8], the perfluoro, perfluorination, and negative perfluorination effects [9-13], and other pertinent supporting (photoelectron spectroscopy) adiabatic ionization energy IE_a values [14-17]; necessary for the brief discussion presented here to act as an aid to prevent any confusion on the part of the layman, upon reading the main body of text presented in Chapters 3 and 4.

Benson's Rules of Additivity [4-8] state that, any additive property, such as $\Delta_f H^0$, may be estimated by dividing the molecule into its constituent parts known as groups. Once one has assigned an empirical value to each group, based on the best available thermochemical data, the sum of the group values produces the estimated empirical value for the whole molecule. Thus, one may use Benson's Rules of Additivity for a quantitative estimate of the neutral heats of formation, $\Delta_f H^0[M_1]$.

Traditionally, gas-phase ion-chemists have used experimental data, Benson's Rules, and more recently ab initio calculations, to reach a *consensus* on a $\Delta_f H^0[M_1]$ value. *In the absence of experimental $\Delta_f H^0[M_1]$ value, it is generally accepted to use Benson's Rules to suggest an estimate of $\Delta_f H^0[M_1]$.* However, a gas-phase ion-chemist experienced in

Benson's Rules, must always keep in mind that they are by their nature based upon the best available experimental data of the related groups. Collected here in Tables C.1 and C.2, are the relevant thermochemical and Benson's Rules values.

For example, upon utilization of the terms in Table C.2, one may estimate the following neutral heats of formation;

$\Delta_f H^0[CF_3–C\equiv C–CF_3] = 2(\Delta_f H^0[C–(F)_3(C)] + \Delta_f H^0[C_t–(C)]) = -1097.0\ kJ\bullet mol^{-1}$

and

$\Delta_f H^0[CF_2=CF–CF=CF_2] = 2(\Delta_f H^0[C_d–(F)_2] + \Delta_f H^0[C_d–(F)(C)]) = -926.3\ kJ\bullet mol^{-1}$

In a series of species under consideration, the species with the lowest $\Delta_f H^0$ value may be considered to be the most stable, and similarly the species with the highest $\Delta_f H^0$ value may be considered to be the least stable. Thus, the *order of stability* may be expressed as a listing of species, going from the most stable to the least stable. Therefore, one may suggest an *order of stability of the above neutrals* listed below as follows;

$$CF_3–C\equiv C–CF_3 > CF_2=CF–CF=CF_2$$

On inspection of Table C.1, one may note that there is no experimental $\Delta_f H^0$ value for $CF_3–C\equiv C–CF_3$, and the Benson's $\Delta_f H^0$ value for $CF_2=CF–CF=CF_2$ is close to the known experimental value. Thus, upon utilization of their known experimental adiabatic ionization energy IE_a values, one may propose a *cation order of stability* as follows;

Table C.1 Relevant Thermochemical Data for the Unsaturated C_nH_m and C_nF_m Series.

Species	Neutral Heat of Formation, Δ_fH° (kJ•mol^{-1}) Benson's Additivity[a]	Standard Literature[b]	Adiabatic Ionization Energy IE$_a$(eV)[b]	Ionic Heat of Formation Δ_fH° (kJ•mol^{-1})[b]
HC≡CH	226.8	(228.0 ± 1)	(11.400 ± 0.001)	1327.9
CH_3–C≡CH	185.8	(186.6 ± 2)	(10.36 ± 0.01)	1186.2
CH_3–C≡C–CH_3	144.8	(145.4 ± 0.8)	(9.562 ± 0.006)	1068
CH_2=CH–CH=CH_2	124.0		9.03[i]	995.2[d]
CH_2=C=C•H				
H_2C•–C≡CH	388.3	343	8.68	1179
c-C_3H_3•		(440 ± 17)	6.6	1075
CH_2=C=CH_2	194.7	(190.6 ± 1)	(9.69 ± 0.01)	1126
CH_2=C=C=CH_2		349	9.15	1232
c-C_4H_4	280.3		(8.16 ± 0.03)[j]	1067.6[d]
c-(CH_2–CH_2)$_2$	26.0	(28.4 ±0.5)	(9.92 ± 0.05)	985
FC≡CF	21.0[c]	(21 ± 21)	11.18	1100
CF_3–C≡CF	−538.0[c]			
CF_3–C≡C–CF_3	−1097.0		12.35[e]	94.5[d]
CF_2=CF–CF=CF_2	−926.3	−938	9.5	−21
CF_2=C=C•F				
F_2C•–C≡CF	115.1			
c-C_3F_3•				
CF_2=C=CF_2	−516.1	−594	10.88	456
CF_2=C=C=CF_2				
c-C_4F_4	−1171.5			
c-(CF_2–CF_2)$_2$	−1506.0	−1515[f]	(11.6 ± 0.2)[g]	−396[h]

[a]Ref. [4-8], [b]Ref. [1], [c]Estimated, see Table 3.5 and corresponding text, [d]Estimated Δ_fH^0[Ion] from Benson's Δ_fH^0[Neutral], [e]Ref. [11], [f]Ref. [3, 8], [g]Ref. [14], [h]Estimated Upper Limit of Δ_fH^0[Ion] , see Table 4.6 and corresponding text, [i]Ref. [15], [j]Ref.[16, 17].

Table C.2 Relevant Benson's Additivity Terms

Benson's Group	Benson's Heat of Formation, $\Delta_f H^\circ$ Term[a] (kcal•mol^{-1})	(kJ•mol^{-1})	Benson's Group	Benson's Heat of Formation, $\Delta_f H^\circ$ Term[a] (kcal•mol^{-1})	(kJ•mol^{-1})
C–(H)$_3$(C)	–10.00	–41.82	C–(F)$_3$(C)	–158.4	–662.7
C–(H)$_2$(C)$_2$	–5.00	–20.9	C–(F)$_2$(C)$_2$	–97.0	–405.8
C–(H)(C)$_3$	–2.40	–10.0	C–(F)(C)$_3$	–48.5	–202.9
C–(C)$_4$	0.10	0.42			
C$_d$–(H)$_2$	6.27	26.2	C$_d$–(F)$_2$	–78.2	–327.2
C$_d$–(H)(C)	8.55	35.8	C$_d$–(F)(C)	–32.5	–136.0
C$_d$–(C)$_2$	10.19	42.63			
C$_t$–(H)	27.1	113.4	C$_t$–(F)	(2.5)[b]	(10.5)[b]
C$_t$–(C)	27.3	114.2			
C$_a$	34.0	142.3			
CO–(H)	–13.9	–58.2	CO–(F)	–77	–322.2
[CO]$_d$-ketene	–17.7	–74.1			
CO–(C)$_2$	–31.7	–132.6			
C$^\bullet$–(H)$_2$(C)	38.4	160.7	C$^\bullet$–(F)$_2$(C)	(≈–51.5)[c]	(≈–215.3)[c]
C$^\bullet$–(H)(C)$_2$	41.0	171.5	C$^\bullet$–(F)(C)$_2$	(≈–2.3)[c]	(≈–9.7)[c]
C$^\bullet$–(C)$_3$	41.0	171.5			
Ring Strain (RS)					
c-C$_4$H$_8$	26.8		c-C$_4$F$_8$	28.0	117.2
c-C$_4$H$_6$	29.8		c-C$_4$F$_6$		
c-C$_4$H$_4$	(32.8)[d]	(137.2)[d]	c-C$_4$F$_4$	(≈32.8)[d]	(≈137.2)[d]

[a]Ref.[4-8], [b]Estimated, see Table 3.5 and corresponding text, [c]Estimated, see Table 3.2 and corresponding text, [d]Estimated ring strain (linearly interpolated).

$$CF_2{=}CF{-}CF{=}CF_2^{+\bullet} > CF_3{-}C{\equiv}C{-}CF_3^{+\bullet}$$

(i.e., as $\Delta_f H^0[CF_2{=}CF{-}CF{=}CF_2^{+\bullet}] = -21$ kJ•mol^{-1} (exp. value), and $\Delta_f H^0[CF_3{-}C{\equiv}C{-}CF_3^{+\bullet}] =$ 94.5 kJ•mol^{-1} (est. value), thus about 115.5 kJ•mol^{-1} apart). Thus, by keeping in mind the above context and meaning of the term *order of stability*, the reader shall avoid any future confusion, and gain a further appreciation for the utility, clarity and compactness of the ideas expressed in this short form notation.

At this point, one final topic deserves emphasis. It is that the basis for the *proposed cation order of stability* of the series of isomeric species discussed in Chapters 3 and 4, was a combination of the application of Benson's Rules and intuition. The rationale utilized was that *the cations that can be seen to best share the positive charge (i.e., a delocalized cyclic structure) were proposed to be the most stable species*, and this was the foundation upon which the (qualitative) proposed energy level diagrams were constructed.

In conclusion, it is the author's hope that this thesis will in the future generate new interest in these perfluorinated species, this being the original underlying motivation for its writing.

C.2 References

[1] S.G. Lias, J.F. Liebman, J.L. Holmes, R.D. Levin, and W.G. Mallard, J. Phys. Chem. Ref. Data, 17, (1988).

[2] M.W. Chase, Jr., NIST-JANAF Thermochemical Tables, 4th Ed., J. Phys. Ref. Data Monogr., 9, (1998).

[3] H.E. O'Neal, and S.W. Benson, Natl. Stand. Ref. Data Ser. Natl. Bur. Stand., 21, (1970).

[4] S.W. Benson, and J.H. Buss, J. Chem. Phys. 29(3), 546-572, (1958).

[5] N. Cohen, and S.W. Benson, Chem. Rev., 2419-2438, (1993).

[6] S.W. Benson, F.R. Cruickshank, D.M. Golden, G.R. Haugen, H.E. O'Neal, A.S. Rodgers, R. Shaw, and R. Walsh, Chem. Rev., 29, 279-324, (1969).

[7] S.W. Benson, Thermochemical Kinetics, 2nd,John Wiley and Sons, New York, New York, USA, (1976).

[8] H.E. O'Neal, and S.W. Benson, J. Phys. Chem., (6)72, 1866-1877, (1968).

[9] C.R. Brundle, M.B. Robin, N.A. Kuebler, and H. Basch, J. Amer. Chem. Soc., 94(5), 1451-1465, (1972).

[10] C.R. Brundle, M.B. Robin, and N.A. Kuebler, J. Amer. Chem. Soc., 94(5), 1466-1475, (1972).

[11] J.P. Delwiche, M-TH. Praet, G. Caprace, M-J. Hubin-Franskin, P. Natalis, and J.E. Collin, J. Electron Spectros. Rel. Phenom., 12, 395-403, (1977).

[12] J.H.D. Eland, Photoelectron Spectroscopy. An Introduction to Ultraviolet Photoelectron Spectroscopy in the Gas Phase, Butterworths, London, U.K., (1974).

[13] J.H.D. Eland, Photoelectron Spectroscopy. An Introduction to Ultraviolet Photoelectron Spectroscopy in the Gas Phase, 2nd Ed., Butterworths, London, U.K., (1984).

[14] G.K. Jarvis, K.J. Boyle, C.A. Mayhew, and R.P. Tuckett, J. Phys. Chem. A, 102(19), 3230-3237, (1998).

[15] G. Bieri, F. Burger, E. Heilbronner, and J.P. Maier, Helv. Chim. Acta, 60, 2213-2233, (1977).

[16] D.W. Kohn, and P. Chen, J. Am. Chem. Soc., 115, 2844-2848, (1993).

[17] J. Kreile, N. Munzel, A. Schweig, and H. Specht, Chem. Phys. Lett., 124(2), 140-146, (1986).

Claims to Original Research

Collision-Induced Emission (CIE) Spectroscopy

A collision-induced emission (CIE) spectroscopy study of a series of small and larger polyatomic molecules was carried out with the motivation to utilize the resultant optical emissions of the intact-parent species and its corresponding fragments as an aid to compliment their mass spectrometric structural information. The series of small polyatomics studied was that of the linear N≡N, C≡O, O=C=O, and O=C=C=O species. The series of larger polyatomics studied was that of the aromatic C_6H_6, C_6F_6, and C_4H_4O species.

The monochromated collision-induced (CIE) spectra for the fast moving 8 keV projectile-ion, $M_1^{+\bullet}$, and the stationary target gas, G_1, encounter event, under single collision conditions, was observed over the UV-VIS-NIR 190-1020 nm wavelength range, via a liquid nitrogen cooled charge-coupled device (CCD) camera. This represented a CIE study, for the first time ever, which was extended into the NIR wavelength region of 700-1020 nm.

For the $N{\equiv}N^{+\bullet}$, $C{\equiv}O^{+\bullet}$, $O{=}C{=}O^{+\bullet}$, and $O{=}C{=}C{=}O^{+\bullet}$ projectile-ions, the intact-parent radical-cation emissions were observed save that of the latter. As well, the intact-parent neutral emissions for N≡N and C≡O were observed, however not those of O=C=O and O=C=C=O, which underwent fragmentation. The Wigner-Witmer Correlation Rules were used to correlate the fragmentation products to those of the proposed respective neutral and radical-cation parent species.

The aromatic species benzene, C_6H_6, perfluorobenzene, C_6F_6, and furan C_4H_4O were also studies by the CIE technique, however they yielded no observable intact-parent radical-cation emissions. This may be interpreted as the dominance of quasi-equilibrium dissociation over emission as the size of the system under consideration is increased. It is proposed that if

the present CIE experimental apparatus were to be modified to include a "deceleration-zone" just prior to $M_1^{+\bullet}$ entering the observation cell, it may in the future be possible to extend the CIE to larger polyatomic species.

Tandem Mass Spectrometry of Perfluorinated Organics

For the first time ever and collected in one location, a comprehensive systematic tandem mass spectrometry study of the series of perfluorinated iodo, oxo, and unsaturated organics has been presented here. Its original intent was to bring the somewhat self-contained field of fluorine chemistry more into the mainstream milieu of gas-phase ion-chemistry. Their gas-phase ion-chemistry behaviour has been qualitatively rationalized to be due to the extreme electronegativity of F compared to H, via the perfluoro and perfluorination effects.

The study of the perfluoro iodo compounds served as a vivid illustration of the differences between the behaviour of the perfluorinated compounds and that of their hydrogen analogues. There exists a delicately balanced competition between the $I^{\bullet}$ and FI neutral losses from the $C_nF_mI^+$ parent-cation during the genesis of the resultant perfluorocarbocation fragment. In particular, for the perfluorobutyl carbocations studied here, there was proposed a *reversed order of cation stability (i.e.,primary > secondary > tertiary)*; $CF_3CF_2CF_2CF_2^+ > (CF_3)_2CFCF_2^+ > (CF_3)_3C^+$, that was in complete contrast to their hydrogen analogues.

As well, *the perfluoroketene neutral* $CF_2{=}C{=}O$ *deserves special emphasis.* The $CF_2{=}CFOCF_3^{+\bullet}$ species possessed a sole metastable process; the loss of CF_4 and the production of $CF_2{=}C{=}O^{+\bullet}$. The NR study of $CF_2{=}C{=}O^{+\bullet}$ exhibited a strong recovery peak at m/z 78, which thus supports the existence of neutral $CF_2{=}C{=}O$ as a stable species with a lifetime on the order of the transit time between the neutralization and reionization cells (i.e., $\approx 1\mu s$). *This*

represented the first direct experimental evidence for the existence of the long sought after elusive CF_2=C=O *neutral.*